

Physiology and breeding of cereals

Edited by

Gustavo A. Slafer, Iker Aranjuelo, Roxana Savin
and Ignacio Romagosa

Published in

Frontiers in Plant Science



FRONTIERS EBOOK COPYRIGHT STATEMENT

The copyright in the text of individual articles in this ebook is the property of their respective authors or their respective institutions or funders. The copyright in graphics and images within each article may be subject to copyright of other parties. In both cases this is subject to a license granted to Frontiers.

The compilation of articles constituting this ebook is the property of Frontiers.

Each article within this ebook, and the ebook itself, are published under the most recent version of the Creative Commons CC-BY licence. The version current at the date of publication of this ebook is CC-BY 4.0. If the CC-BY licence is updated, the licence granted by Frontiers is automatically updated to the new version.

When exercising any right under the CC-BY licence, Frontiers must be attributed as the original publisher of the article or ebook, as applicable.

Authors have the responsibility of ensuring that any graphics or other materials which are the property of others may be included in the CC-BY licence, but this should be checked before relying on the CC-BY licence to reproduce those materials. Any copyright notices relating to those materials must be complied with.

Copyright and source acknowledgement notices may not be removed and must be displayed in any copy, derivative work or partial copy which includes the elements in question.

All copyright, and all rights therein, are protected by national and international copyright laws. The above represents a summary only. For further information please read Frontiers' Conditions for Website Use and Copyright Statement, and the applicable CC-BY licence.

ISSN 1664-8714
ISBN 978-2-8325-6010-5
DOI 10.3389/978-2-8325-6010-5

About Frontiers

Frontiers is more than just an open access publisher of scholarly articles: it is a pioneering approach to the world of academia, radically improving the way scholarly research is managed. The grand vision of Frontiers is a world where all people have an equal opportunity to seek, share and generate knowledge. Frontiers provides immediate and permanent online open access to all its publications, but this alone is not enough to realize our grand goals.

Frontiers journal series

The Frontiers journal series is a multi-tier and interdisciplinary set of open-access, online journals, promising a paradigm shift from the current review, selection and dissemination processes in academic publishing. All Frontiers journals are driven by researchers for researchers; therefore, they constitute a service to the scholarly community. At the same time, the *Frontiers journal series* operates on a revolutionary invention, the tiered publishing system, initially addressing specific communities of scholars, and gradually climbing up to broader public understanding, thus serving the interests of the lay society, too.

Dedication to quality

Each Frontiers article is a landmark of the highest quality, thanks to genuinely collaborative interactions between authors and review editors, who include some of the world's best academicians. Research must be certified by peers before entering a stream of knowledge that may eventually reach the public - and shape society; therefore, Frontiers only applies the most rigorous and unbiased reviews. Frontiers revolutionizes research publishing by freely delivering the most outstanding research, evaluated with no bias from both the academic and social point of view. By applying the most advanced information technologies, Frontiers is catapulting scholarly publishing into a new generation.

What are Frontiers Research Topics?

Frontiers Research Topics are very popular trademarks of the *Frontiers journals series*: they are collections of at least ten articles, all centered on a particular subject. With their unique mix of varied contributions from Original Research to Review Articles, Frontiers Research Topics unify the most influential researchers, the latest key findings and historical advances in a hot research area.

Find out more on how to host your own Frontiers Research Topic or contribute to one as an author by contacting the Frontiers editorial office: frontiersin.org/about/contact

Physiology and breeding of cereals

Topic editors

Gustavo A. Slafer — Catalan Institution for Research and Advanced Studies (ICREA), Spain

Iker Aranjuelo — Institute of Agrobiotechnology, Spanish National Research Council (CSIC), Spain

Roxana Savin — Universitat de Lleida, Spain

Ignacio Romagosa — Agrotecnio Center, Spain

Citation

Slafer, G. A., Aranjuelo, I., Savin, R., Romagosa, I., eds. (2025). *Physiology and breeding of cereals*. Lausanne: Frontiers Media SA. doi: 10.3389/978-2-8325-6010-5

Table of contents

- 05 **Impact of rising temperatures on historical wheat yield, phenology, and grain size in Catalonia**
Davide Gulino, Roser Sayeras, Joan Serra, Josep Betbese, Jordi Doltra, Adrian Gracia-Romero and Marta S. Lopes
- 16 **CRISPR/Cas9-mediated enhancement of semi-dwarf glutinous traits in elite Xiangdaowan rice (*Oryza sativa* L.): targeting *SD1* and *Wx* genes for yield and quality improvement**
Quanxiu Wang, Haolin Gao, Ke Liu, Honglin Wang, Fan Zhang, Lanmeng Wei, Kaijing Lu, Mengmeng Li, Yiming Shi, Jinhui Zhao, Wei Zhou, Bo Peng and Hongyu Yuan
- 30 **Thermal imaging can reveal variation in stay-green functionality of wheat canopies under temperate conditions**
Jonas Anderegg, Norbert Kirchgessner, Helge Aasen, Olivia Zumsteg, Beat Keller, Radek Zenkl, Achim Walter and Andreas Hund
- 45 **Integration of molecular breeding and multi-resistance screening for developing a promising restorer line Guihui5501 with heavy grain, good grain quality, and endurance to biotic and abiotic stresses**
Minyi Wei, Qun Yan, Dahui Huang, Zengfeng Ma, Shen Chen, Xiaoting Yin, Chi Liu, Yuanyuan Qin, Xiaolong Zhou, Zishuai Wu, Yingping Lu, Lihui Yan, Gang Qin and Yuexiong Zhang
- 61 **Does late water deficit induce root growth or senescence in wheat?**
Kanwal Shazadi, John T. Christopher and Karine Chenu
- 75 **The trade-off between grain weight and grain number in wheat is explained by the overlapping of the key phases determining these major yield components**
Lucas Vicentin, Javier Canales and Daniel F. Calderini
- 89 **Dissecting the effect of heat stress on durum wheat under field conditions**
Eder Licieri Groli, Elisabetta Frascaroli, Marco Maccaferri, Karim Ammar and Roberto Tuberosa
- 108 **Development and characterisation of novel durum wheat–*H. chilense* 4H^{ch} chromosome lines as a source for resistance to *Septoria tritici* blotch**
Zuny Cifuentes, Maria-Carmen Calderón, Cristina Miguel-Rojas, Josefina C. Sillero and Pilar Prieto
- 119 **Stem traits promote wheat climate-resilience**
Simeon Ntawuguranayo, Michael Zilberberg, Kamal Nashef, David J. Bonfil, Naresh Kumar Bainsla, Francisco J. Piñera-Chavez, Matthew Paul Reynolds, Zvi Peleg and Roi Ben-David

- 134 **Modeling QTL-by-environment interactions for multi-parent populations**
Wenhao Li, Martin P. Boer, Ronny V. L. Joosen, Chaozhi Zheng, Lawrence Percival-Alwyn, James Cockram and Fred A. Van Eeuwijk
- 148 **Dynamics of apex and leaf development in barley as affected by *PPD-H1* alleles in two contrasting *PHYC* backgrounds under short or long photoperiod**
Jorge D. Parrado, Roxana Savin and Gustavo A. Slafer
- 161 **Impact of irrigation, nitrogen fertilization, and plant density on stay-green and its effects on agronomic traits in maize**
Nadia Chibane, Pedro Revilla, Venkata Rami Reddy Yannam, Purificación Marcet, Emma Fernández Covelo and Bernardo Ordás
- 174 **Validation of QTLs associated with corn borer resistance and grain yield: implications in maize breeding**
Ana López-Malvar, Zoila Reséndiz-Ramírez, Ana Butrón, Jose Cruz Jiménez-Galindo, Pedro Revilla and Rosa Ana Malvar
- 187 **Genetic control of root/shoot biomass partitioning in barley seedlings**
Alejandra Cabeza, Ana M. Casas, Beatriz Larruy, María Asunción Costar, Vanesa Martínez, Bruno Contreras-Moreira and Ernesto Igartua



OPEN ACCESS

EDITED BY

Roxana Savin,
Universitat de Lleida, Spain

REVIEWED BY

Daniel Julio Miralles,
University of Buenos Aires, Argentina
John Foulkes,
University of Nottingham, United Kingdom

*CORRESPONDENCE

Marta S. Lopes

✉ marta.dasilva@irta.cat

RECEIVED 23 June 2023

ACCEPTED 18 September 2023

PUBLISHED 11 October 2023

CITATION

Gulino D, Sayeras R, Serra J, Betbese J,
Doltra J, Gracia-Romero A and Lopes MS
(2023) Impact of rising temperatures on
historical wheat yield, phenology,
and grain size in Catalonia.
Front. Plant Sci. 14:1245362.
doi: 10.3389/fpls.2023.1245362

COPYRIGHT

© 2023 Gulino, Sayeras, Serra, Betbese,
Doltra, Gracia-Romero and Lopes. This is an
open-access article distributed under the
terms of the [Creative Commons Attribution
License \(CC BY\)](#). The use, distribution or
reproduction in other forums is permitted,
provided the original author(s) and the
copyright owner(s) are credited and that
the original publication in this journal is
cited, in accordance with accepted
academic practice. No use, distribution or
reproduction is permitted which does not
comply with these terms.

Impact of rising temperatures on historical wheat yield, phenology, and grain size in Catalonia

Davide Gulino¹, Roser Sayeras², Joan Serra², Josep Betbese¹,
Jordi Doltra², Adrian Gracia-Romero¹ and Marta S. Lopes^{1*}

¹Sustainable Field Crops Program, IRTA (Institute of Agrifood Research and Technology), Lleida, Spain,

²Sustainable Field Crops Program, IRTA (Institute of Agrifood Research and Technology), Girona, Spain

Introduction: Climate change poses significant challenges to agriculture, impacting crop yields and necessitating adaptive strategies in breeding programs. This study investigates the genetic yield progress of wheat varieties in Catalonia, Spain, from 2007 to 2021, and examines the relationship between genetic yield and climate-related factors, such as temperature. Understanding these dynamics is crucial for ensuring the resilience of wheat crops in the face of changing environmental conditions.

Methods: Genetic yield progress was assessed using a linear regression function, comparing the average yield changes of newly released wheat varieties to benchmark varieties. Additionally, a quadratic function was employed to model genetic yield progress in winter wheat (WW). The study also analyzed correlations between genetic yield (GY) and normalized values of hectoliter weight (HLW) and the number of grains (NG) for both spring wheat (SW) and WW. Weather data were used to confirm climate change impacts on temperature and its effects on wheat growth and development.

Results: The study found that genetic yield was stagnant for SW but increased linearly by 1.31% per year for WW. However, the quadratic function indicated a possible plateau in WW genetic yield progress in recent years. Positive correlations were observed between GY and normalized values of HLW and NG for both SW and WW. Climate change was evident in Catalonia, with temperatures increasing at a rate of 0.050 °C per year. This rise in temperature had detrimental effects on days to heading (DH) and HLW, with reductions observed in both SW and WW for each °C increase in annual minimum and average temperature.

Discussion: The findings highlighted the urgent need to address the impact of climate change on wheat cultivation. The stagnation of genetic yield in SW and the potential plateau in WW genetic yield progress call for adaptive measures. Breeding programs should prioritize phenological adjustments, particularly sowing date optimization, to align with the most favorable months of the year.

Moreover, efforts should be made to enhance HLW and the number of grains per unit area in new wheat varieties to counteract the negative effects of rising temperatures. This research underscores the importance of ongoing monitoring and adaptation in agricultural practices to ensure yield resilience in the context of a changing climate.

KEYWORDS

wheat, yield progress, climate change, genetic gain, temperature

1 Introduction

Wheat is the most cultivated crop in the world covering 220.76 million ha, followed by maize (205.87 million ha), and rice (165.25 million ha), and represents a third of the total grain production with an estimated value of 770 million tons, following rice (787 million tons) and maize (1,210 million tons) (FAOSTAT, 2021). In Europe, it is also the most cultivated cereal with 62.82 million ha followed by barley with 22.52 million ha, while in Spain, barley is first with 2.51 million ha followed by wheat with 2.12 million ha (FAOSTAT, 2021). The same pattern was observed in Catalonia, NE of Spain, where this study was performed: barley covers 154,574 ha, as the first cultivated cereal, while wheat covers 103,149 ha (Statistical Institute of Catalonia, 2021). Based on the importance of wheat at both the local and global scales among staple food crops, massive breeding efforts are required to support challenges in food security, considering the consistent increase in the world population. Currently, climate change represents an additional challenge to provide high-yield varieties that may adapt to extreme environmental conditions. Climate change is projected to decrease the global wheat yield by approximately 1.9% by 2050, affecting mostly developing countries, such as in Africa and Southern Asia, where food security is already a problem (Pequeno et al., 2021). Furthermore, the co-occurrence of extremely hot and dry events from 1980 to 2009 had a global negative impact on the yield of major cereal crops, and its probability increased by up to six times in wheat-specific growing regions (Heino et al., 2023). In addition, Asseng et al. (2015) used 30 different wheat crop models to demonstrate a 6% decrease in yield for each degree Celsius increase in most wheat-growing regions. Considering these predictions, periodic evaluation of the rate of genetic gain in grain yield is crucial to estimate how breeding efforts effectively contribute to satisfying the increasing global food demand and to identify new potential avenues for future improvement. Crop yield progress is defined as the slope of the linear regression function between the average yield and time (Sayre et al., 1997), which provides information on the impact of breeding on yield or other traits of interest. Long-term check varieties (the most widely grown in the region) are included every year in post-registration trials, allowing for the estimation of yield gain, which is calculated as the yield percentage of new varieties against the yield of long-term check varieties every year. Thus, it is possible to evaluate the rate of grain

yield increase across years in such trials (Graybosch and Peterson, 2010; Crespo-Herrera et al., 2018). Moreover, yield progress can be internally assessed in wheat breeding programs to track the impact of breeding on new varieties. However, to evaluate progress in the yield available to farmers, all new wheat varieties released by the private and public sectors in a certain region over time must be assessed. Using this evaluation, the potential variety portfolio available to farmers in any given year can be evaluated. In this study, progress in yield was assessed using a set of all available varieties between 2007 and 2021 (from all public and private breeding programs). Specifically, this study aimed to (1) determine the extent of genetic yield progress (if any) in the last 15 years (2007–2021) in both spring wheat (SW) and winter wheat (WW) varieties; (2) explain which agronomic traits contribute to yield progress or stagnation using correlation analysis; and (3) evaluate the extent of climate change by analyzing weather trends across time and their impact on yield, yield components, phenology, and other agronomic traits.

2 Materials and methods

2.1 Experimental data

The Institute of Agrifood Research and Technology (IRTA) coordinates a field trial network (post-registration variety testing trials, <https://extensius.cat/xarxes-de-varietats/>) in the Catalonia region to provide farmers with information on the most adapted varieties of various arable crops annually. These trials evaluate an approximate annual average of 20 new SW and 38 WW varieties, regardless of their potential adoption by farmers, as detailed in Supplementary Table 1. These evaluations are conducted against established benchmark check varieties (“Artur Nick” for SW and “Nogal” for WW) widely cultivated in the region. The varieties available in the Catalonia market are annually evaluated, reporting data on agronomic traits and adaptation to the various wheat-growing regions. These replicated trials were conducted using experimental micro-plots (8 m × 1.2 m) located in the most representative production areas distributed throughout the different agroclimatic zones of Catalonia. These areas are all characterized by a Mediterranean climate, with hot summers and mild winters. The post-registration variety testing trials for WW

TABLE 1 Long-term weather data for experimental trial locations of spring wheat (SW) and winter wheat (WW) in Catalonia: from 2007 to 2021 for La Tallada, Lleida, and Vilobí d'Onyar, from 2013 to 2021 for Solsona and Vic.

Location	Growth habit	WV [†]	J	F	M	A	M	J	J	O	N	D	Year
La Tallada	SW	TM [‡]	14	15	17	19	23	27	30	22	17	15	21
		TA [±]	7	8	10	13	17	21	24	16	11	8	15
		Tm [‡]	1	2	4	7	11	15	17	11	6	2	9
		p	48	38	58	73	50	29	34	80	80	29	602
		SR [§]	7	10	14	18	22	24	24	11	7	6	15
Lleida	SW	TM	10	14	17	20	25	30	32	22	15	10	21
		TA	5	7	10	13	17	22	24	15	9	5	14
		Tm	1	1	4	7	10	14	17	9	4	1	8
		P	27	18	32	51	39	30	27	39	42	16	364
		SR	6	11	16	20	25	27	27	13	8	5	17
Vic	WW	TM	10	13	16	18	23	28	31	21	14	11	20
		TA	4	6	9	11	15	20	23	14	8	4	13
		Tm	-1	0	2	5	8	13	15	9	3	0	7
		P	38	30	39	72	69	63	54	66	64	15	668
		SR											
Solsona	WW	TM	10	12	15	18	22	28	32	21	14	11	20
		TA	4	6	8	11	14	19	23	14	8	5	13
		Tm	0	1	2	5	7	12	15	8	3	0	7
		P	38	33	54	76	59	45	38	79	80	11	600
		SR	8	11	16	19	23	25	26	13	8	7	17
Vilobí d'Onyar	WW	TM	14	15	17	20	24	28	31	23	18	15	22
		TA	6	7	9	12	16	20	23	15	10	6	14
		Tm	-1	0	2	5	8	12	15	8	3	0	7
		P	43	38	58	71	66	48	35	74	83	25	645
		SR											

WV[†], weather variables; TM[‡], average maximum temperature (°C); TA[±], average mean temperature (°C); Tm[‡], average minimum temperature (°C); p^{||}, average of cumulative precipitation (mm); SR[§], average solar radiation (MJ m⁻²).

were conducted at three rainfed locations representative of areas with cooler winters from West to East counties: Solsona (county Solsonès), Vic (county of Osona), and Vilobí d'Onyar (county of La Selva). For SW, the locations were Lleida (county of Segrià), irrigated trial, and La Tallada d'Empordà (county of Baix Empordà), rainfed, representatives respectively of the West and East warmer wheat production areas of Catalonia. Table 1 shows the average long-term weather data at each location. The varieties tested in these trials were not treated with pesticides. For each variety and year of trial, agronomic traits were determined using the following methods: grain yield (GY) at 13% humidity was determined by machine harvesting the whole plot; days to heading (DH) as the number of days from 1 January to when 50% of the spikes have emerged on 50% of all stems (Pask et al., 2012); plant height (PH) after flowering, when plants have reached their maximum height; hectoliter weight (HLW) by weighing a 550-

mL volume of grains; thousand kernel weight (TKW) taking three random samples of 200 whole grains (removing all aborted and broken grains); and number of grains (NG) was calculated from GY and TKW. All agronomic traits were analyzed and expressed for each wheat variety as absolute values and as the percentage of a long-term check variety (a widely grown variety in the country) grown in the same trial and year: “Artur Nick” and “Nogal” for SW and WW, respectively (normalized values). Utilizing Artur Nick and Nogal as reference lines for estimating genetic gain in both SW and WW presents potential limitations: (1) Model Variability: the models employed in calculating yield progress (as depicted in Figures 1C, D) and their corresponding equations might exhibit variations when different reference varieties are used. These variations can influence the slopes and statistical significance of the models, potentially impacting the accuracy of the assessment. (2) Temporal variability in disease resistance of check varieties: the

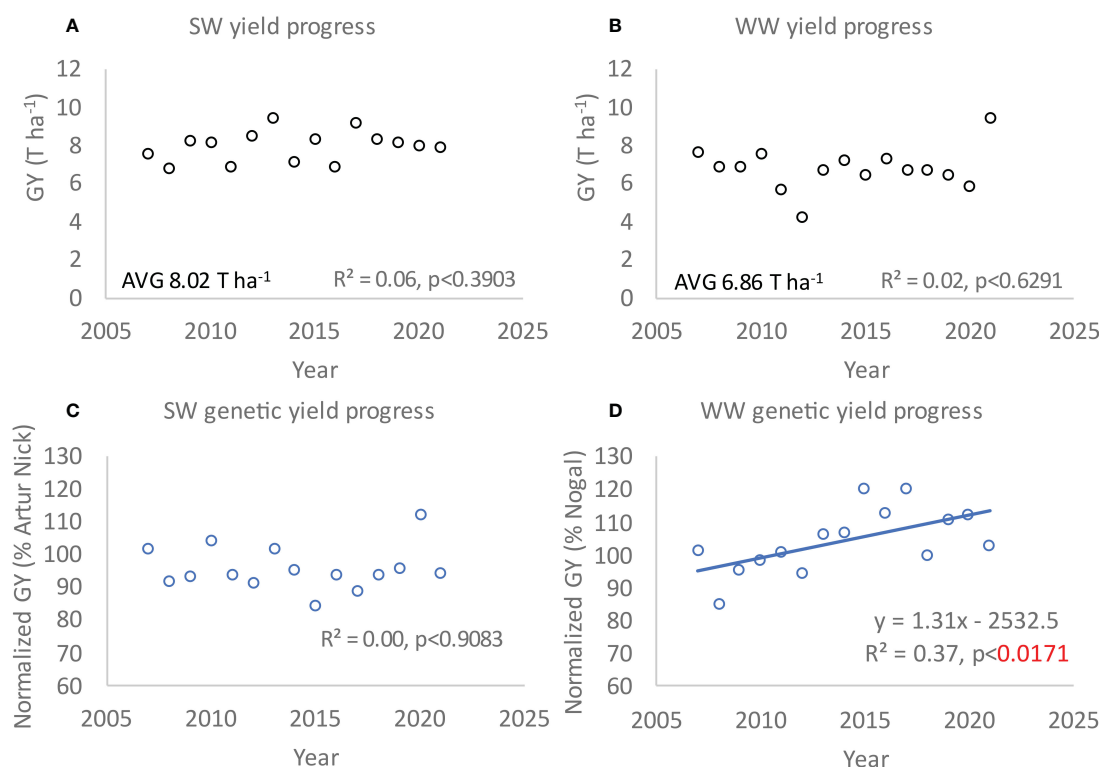


FIGURE 1

(A, B) Spring wheat (SW) and winter wheat (WW) yield progress in Catalonia between 2007 and 2021 in absolute values. (C, D) Normalized yield expressed as the percentage of GY variation against a check spring wheat variety “Artur Nick” and a check winter wheat variety “Nogal”. Spring and winter wheat GY was obtained from experimental untreated (no pesticides applied) trials conducted in the regions of La Tallada (rainfed) and Lleida (irrigated), Vic, Solsona, and Vilobi d’Onyar, respectively. Means of all the varieties tested each year in each location are plotted and regression equations are shown with coefficients of determination (R^2) and associated probability ($p < 0.05$ in red).

analysis exclusively relies on data from “non-treated” trials. In such trials, the use of check varieties to gauge susceptibility may introduce inaccuracies due to the varying impact of diseases. However, disease affected both check and test varieties simultaneously, as evidenced by the significant positive correlation between check variety yield and the average yield of all tested varieties over the years ($y = 1.05x + 2.1$, $R^2 = 0.69$, $p < 0.0001$ for Artur Nick and $y = 0.95x + 70.9$, $R^2 = 0.74$, $p < 0.0001$ for Nogal). These correlations indicated environmental consistency: over the 15-year period, the trials likely occurred in relatively consistent environmental conditions, including soil type, climate, and other environmental factors, and in non-treated trials, the impact of diseases and environmental stressors may have been relatively consistent across varieties, leading to a uniform performance pattern. These correlations indicate that both Artur Nick and Nogal are adequate check varieties to calculate yield progress of newly released varieties over the years. Weather variables were provided by the local meteorological services at “Servei Meteorològic de Catalunya” and collected from the reference weather stations for the cultivation sites: maximum temperature (TM), average temperature (TA), and minimum temperature (Tm) expressed in °C, precipitation per day (P), and global solar radiation per day (SR), in mm and MJ m⁻², respectively. The annual averages of weather variables were calculated. Correlations in SW regions were calculated using data from 2007

to 2021, and for WW regions, between 2013 and 2021 (according to weather data availability in each location).

2.2 Statistical analysis

For each trial and season, the effects between varieties were tested using an analysis of variance (ANOVA). Absolute and normalized trait value means were obtained by averaging all the varieties per trial, year, and repetitions. Simple regression analysis was performed between (a) annual and monthly weather variable means and years; (b) absolute trait means and years, normalized trait means and years, and among each other; and (c) absolute trait means and annual and monthly weather variables. Regression analyses were performed using absolute and normalized trait means.

Linear, quadratic, and cubic fits were tested using absolute and normalized means against the years. Regression analyses were conducted for 2007–2021. The slope, observed through regression equations, was used to determine the estimated rate of genetic gain, expressed as the percentage yield (or other agronomic traits) above the check varieties per year. Slopes with probability levels < 0.05 were considered statistically significant, as well as p -values of $0.05 < p < 0.10$. The statistical software package SAS-JMP Pro 16 (SAS Institute Inc., Cary, NC, USA, 1989–2019) was used to perform all reported statistical analyses. Graphs reporting the correlations and

TABLE 2 Significant historical changes of annual and monthly weather variables in spring wheat (SW) (La Tallada and Lleida) and winter wheat (WW) locations (Vic, Solsona, and Vilobí d'Onyar) in Catalonia, Spain.

Growth habit	WV	Regression equation	R^2	p -value	Years
SW	TM ¹	$y = 0.086\text{Year} - 152.8$	0.47	0.0048	15
	TA [±]	$y = 0.050\text{Year} - 86.9$	0.34	0.0218	15
	SR [§]	$y = 0.043\text{Year} - 71.3$	0.20	0.0926	15
	May P	$y = -2.41\text{Year} + 4,905.7$	0.20	0.0969	15
	Jul TM	$y = 0.170\text{Year} - 310.4$	0.32	0.0274	15
	Jul TA	$y = 0.102\text{Year} - 182.4$	0.19	0.0983	15
	Dec TM	$y = 0.114\text{Year} - 216.5$	0.25	0.0542	15
	Dec TA	$y = 0.104\text{Year} - 202.7$	0.22	0.0723	15
WW	Feb TM	$y = 0.547\text{Year} - 1,089.7$	0.38	0.0740	9
	Oct TA	$y = -0.281\text{Year} + 581.0$	0.40	0.0634	9
	Oct Tm	$y = -0.356\text{Year} + 726.1$	0.53	0.0247	9

WV, weather variables; TM¹, annual average maximum temperature (°C); TA[±], annual average mean temperature (°C); Tm[±], annual average minimum temperature (°C); P^{||}, annual average of cumulative precipitation (mm); SR[§], annual average solar radiation (MJ m⁻²).

Weather variables with significant changes over time are shown with regression equations, R^2 , and probability values ($p < 0.05$, in bold with $0.05 < p < 0.10$). The number of years (years) with available meteorological stations close to the wheat growing regions are shown.

regression equations were plotted using Microsoft Excel 365 (Version 2304, Redmond, WA, USA).

3 Results

3.1 Climate change characterization in the major SW and WW growing regions of Catalonia

SW is grown in locations with higher average minimum temperatures (La Tallada and Lleida with yearly Tm of 9°C and 8°C, as shown in Table 1) whereas WW is grown in cooler locations (Vic, Solsona, and Vilobí d'Onyar) with yearly Tm of 7°C. The long-term average cumulative annual precipitation was higher than 600 mm at most locations, except for Lleida (364 mm) (Table 1), where SW is grown with irrigation. January to March were the coolest months with temperatures frequently lower than 0 in all three WW regions (Table 1). June and July represented the hottest months at all locations, with maximum temperatures above 30°C (Table 1).

Temperature in the main SW and WW locations of Catalonia (since 1990) exhibited an overall increase with a stable linear rate of 0.042–0.045°C per year, respectively, representing a total increase of 1.34°C in La Tallada in the past 32 years (Supplementary Table 2). Historical weather data analysis indicated significant changes in the SW area, with maximum (TM) and average temperatures (TA) increasing at rates of 0.086°C and 0.050°C per year, respectively. However, significant weather changes for WW regions have not been found (only nine years of averaged data are available; Table 2). Moreover, analysis per location indicated consistent increases of average and maximum temperatures, for both winter and spring cultivated area: annually, the TA in Vilobí increased at a rate of

0.042, TM in La Tallada at 0.042, and in Lleida at 0.043°C, in the last 23, 32, and 25 years, respectively (Supplementary Table 2). For SW, July and December temperatures were significantly increased: for TM at a rate of 0.170°C and 0.114°C, and for TA at a rate of 0.102 and 0.104 per year, respectively. Moreover, May P decreased at –2.41 mm per year. For WW, a significant increase in February TM was reported at a rate of 0.547°C per year. October TA and Tm decreased significantly at –0.281 and –0.356°C per year, respectively.

3.2 Historical wheat grain yield progress in Catalonia and associated traits

To evaluate the GY progress associated with wheat breeding (for SW and WW varieties), the GY variation of new varieties released annually was calculated against the check varieties (normalized GY, Figure 1).

SW GY was significantly higher than WW by more than 1 T ha⁻¹ ($p < 0.0001$; Figures 1A, B). Moreover, when considering each WW location, yield progress was significant in Vic and Solsona ($y = 1.08x - 2068.9$, $R^2 = 0.23$, $p < 0.0796$ for Vic and $y = 1.46x - 2,845.1$, $R^2 = 0.25$, $p < 0.0682$). However, SW GY progress due to breeding has been stagnant for the past 15 years, as indicated by a nonsignificant linear regression across time (Figure 1C) and nonsignificant yield progress by location (p -value = 0.4 and 0.3 for La Tallada and Lleida, respectively). Moreover, the quadratic and cubic fits were not significant for SW. With regard to WW, the absolute GY changes in the rainfed WW regions of Catalonia were stagnant (Figure 1B). However, normalized GY showed a significant positive trend with significant linear, quadratic, and cubic fits (Figure 1D; Supplementary Figure 1D). To contrast this regional information, historical FAO GY data were also analyzed (including

TABLE 3 Average, minimum (Min), maximum (Max), and standard deviation (Std. Dev) of grain yield (GY), days to heading (DH), date of heading (expressed as a date: “day –month”) plant height (PH), hectoliter weight (HLW), thousand kernel weight (TKW), and number of grains (NG) in spring wheat (SW) and winter wheat (WW).

Trait	Average		Min		Max		Std. Dev	
Growth Habit	SW	WW	SW	WW	SW	WW	SW	WW
GY (T ha ⁻¹)	8.02	6.86	3.89	1.96	13.15	12.86	1.58	2.00
GDD (°C)	1,209	1,003	982	819	1,557	1,181	87	71
Date of heading	19–4	6–5	1–4	9–4	9–5	3–6		
PH (cm)	90.0	82.5	60.0	55.0	119.5	128.5	10.6	9.7
HLW (kg hL ⁻¹)	79.5	73.9	64.1	50.5	88.3	87.3	3.9	5.4
TKW (g)	40.1	38.2	24.0	19.3	59.8	56.8	6.3	6.4
NG (grains m ⁻²)	20,443.5	17,794.6	8,207.3	5,378.4	35,822.8	32,598.0	4,781.3	5,039.3

SW area included average data collected at La Tallada and Lleida; WW included average data collected at Vic, Solsona, and Vilobí d'Onyar.

bread and durum wheat grain yields in Spain), showing nonsignificant yield progress in Spain (Supplementary Figure 2).

Average values of the analyzed traits for both SW and WW are shown in Table 3. GY, PH, HLW, TKW, and NG average values are higher for spring varieties. Simple linear regressions for normalized GY and traits across time indicated that in SW, PH decreased (at a -0.3 cm year⁻¹ rate), whereas in WW, both HLW and NG increased over time (Table 4, see also results by location in Supplementary Table 3). The correlations of GY with HLW and NG were significant for both SW and WW (Table 4).

3.3 Weather impact on historical wheat yield and associated agronomic traits

The means of absolute traits and annual weather variables were used in correlation analysis (Table 5). The HLW for SW and the DH for WW decreased over time at a rate of -0.382 and -0.815 per year, respectively (Table 5). In addition, DH was negatively correlated with Tm and TA in SW and WW, respectively. Moreover, in SW, HLW was negatively correlated with TM and TA. In WW, HLW negatively correlated with Tm and cumulative annual precipitation

TABLE 4 Significant ($p < 0.10$) correlations between normalized traits (% of check varieties “Artur Nick” and “Nogal” in spring and winter wheat, respectively), including grain yield (GY), days to heading (DH), plant height (PH), hectoliter weight (HLW), thousand kernel weight (TKW), and numbers of grains (NG) for both spring (SW) and winter wheat (WW) across time (years) and with GY.

Normalized trait or time	Growth habit	Normalized trait	Correlation	% norm change/year	abs change/year	R ²	p-value
Years	SW	GY	0.03	0.05%	0.004 T ha ⁻¹	0.00	0.9083
(15)		DH	0.19	0.03%	0.042 days	0.04	0.4998
		HLW	-0.10	-0.05%	-0.043 kg/hL ⁻¹	0.01	0.7147
		TKW	-0.40	-0.36%	-0.098 g/1,000 seeds	0.16	0.1383
		PH	-0.45	-0.32%	-0.292 cm	0.20	0.0952
		NG	-0.04	-0.06%	12.59 grains m ²	0.00	0.8750
	WW	GY	0.60	1.31%	0.086 T ha ⁻¹	0.36	0.0171
		DH	0.33	0.04%	0.080 days	0.11	0.2261
		HLW	0.51	0.23%	0.173 kg/hL	0.26	0.0513
		TKW	0.25	0.36%	0.271 g/1,000 seeds	0.06	0.3646
		NG	0.54	1.04%	184.1 grains m ²	0.29	0.0381
GY	SW	HLW	0.53			0.28	0.0426
		NG	0.78			0.61	0.0006
	WW	HLW	0.74			0.55	0.0014
		NG	0.83			0.69	0.0001

The colors reported in the table indicate the sign of correlations (Pearson values), either positive or negative, with shades of green and red, respectively; Non significant correlations are shown in grey. Probability values are shown in bold with $0.05 < p < 0.10$.

TABLE 5 Significant correlations ($p < 0.10$) of agronomic traits with time (Year) and between traits and annual weather variables, for spring wheat (SW) and winter wheat (WW).

Trait or time	Growth habit	WV* or Trait	Regression equation	Slope (units)	SE [~]	R ²	p-value	Years
Year	SW	HLW	$y = -0.382\text{Year} + 849.6$	$-0.382 \text{ (kg hL}^{-1}\text{)}$	0.11	0.48	0.0041	15
	WW	DH	$y = -0.815\text{Year} + 1845.9$	-0.815 (days)	0.29	0.27	0.0153	15
HLW	SW	TM	$y = -1.932\text{TM} + 120.6$	$-1.932 \text{ (kg hL}^{-1}\text{)}$	1.09	0.19	0.0995	15
		TA	$y = -3.129\text{TA} + 125.5$	$-3.129 \text{ (kg hL}^{-1}\text{)}$	1.55	0.23	0.0647	15
	WW	Tm	$y = -6.977\text{Tm} + 121.1$	$-6.977 \text{ (kg hL}^{-1}\text{)}$	2.41	0.55	0.0229	9
		P	$y = -5.728\text{P} + 84.3$	$-5.728 \text{ (kg hL}^{-1}\text{)}$	1.51	0.67	0.0069	9
DH	SW	Tm	$y = -8.145\text{Tm} + 196.1$	-8.145 (days)	3.47	0.30	0.0355	15
	WW	TA	$y = -12.490\text{TA} + 305.7$	-12.490 (days)	3.72	0.62	0.0122	9

* , weather variables; ~, standard error.

HLW, Hectoliter weight; and DH, days to heading; Tm, minimum temperature; TA, average temperature; TM, maximum temperature and P, rainfall.

Probability values in bold with $0.05 < p < 0.10$.

(P) (Table 5; Supplementary Figure 3). Regarding the correlations among traits for absolute values (indicative of the environmental and agronomic effects), positive correlations were observed in SW of yield with DH, PH, and NG. Moreover, significant positive correlations were depicted in WW for GY with PH and NG (Supplementary Table 4).

To better understand the impact of weather variables, a correlation analysis was performed between agronomic traits and monthly weather variables (Table 6). The overall analysis indicated that agronomic traits were particularly influenced by weather in February and May (Table 6 shows significant correlations with various agronomic traits). February temperatures negatively affected DH in both SW and WW. However, the May temperatures were negatively correlated with PH, HLW, and TKW. For SW, a negative correlation between GY and Tm in January and April and between GY and solar radiation (SR) in June and November were observed. For WW, GY was negatively correlated with TA and Tm in October (Table 6). The GY components showed negative correlations for both SW and WW with rainfall in January and June (for WW, also moderately in December), affecting HLW. In addition, for WW, a negative effect of Tm in May, Tm and TA in April, and TM in October were observed. However, this effect on the HLW was positive for Tm, TA, and TM in November. Regarding TKW, both SW and WW were negatively affected by temperature during spring. In SW, TA and Tm were negatively correlated with TKW in May. Moreover, at WW, the Tm was negatively correlated with TKW in May. Finally, the NG for SW was positively correlated with Tm and TA in May and with Tm in June.

4 Discussion

4.1 Recent climate change observations in Catalonia

Temperature in the main SW and WW locations of Catalonia (since 1990) exhibited an overall increase. This finding agrees with previous reports, indicating an increase of 0.050°C per year in Southwest Europe during the last 30 years and 0.055°C per year for

the entire European continent (Twardosz et al., 2021). However, the timeframe (15 years) in which the genetic yield progress in Catalonia was evaluated showed higher rates of increase in mean annual TM (0.086°C per year) and TA (0.050°C per year), for the SW area. Moreover, the analysis of monthly weather data in the SW regions showed that May precipitation significantly decreased, and July and December temperatures increased. July TA and TM increased at rates of 0.102 and 0.170°C per year, which means a total increase in the past 15 years of 1.53°C and 2.55°C , respectively; similarly, TA and TM in December increased at rates of 0.104 and 0.114°C per year. In the WW regions, February TM increased at a substantial rate of 0.547°C per year and October TA and Tm decreased in the past 9 years. The frequency of exceptional warm months is increasing notably over the past 5 years (Skrzyńska and Twardosz, 2023), which is in accordance with the observation of this study for WW regions of Catalonia, Spain for February TM.

4.2 Is the wheat yield progress due to breeding sufficient to maintain the rate of yield increase in the Catalanian region?

The extensive body of literature on yield progress for SW and WW provides a comprehensive overview of the diverse range of annual growth rates, spanning from 0.5% to 1.6% , and encompassing various timeframes (Sayre et al., 1997; Zhou et al., 2007; Acreche et al., 2008; Sadras and Lawson, 2011; Green et al., 2012; Lopes et al., 2012; Sanchez-Garcia et al., 2013; Lo Valvo et al., 2018; Rife et al., 2019). These previous studies have assessed breeding advancements in crop yield by using historically cultivated varieties that have been widely grown in a specific region. These varieties are subjected to rigorous testing side by side, in replicated experimental trials, with the yields of each variety analyzed through regression analysis.

Another method to gauge yield progress involves post-registration trials, typically conducted by local agricultural services to aid farmers in selecting the most suitable varieties for their region. In these trials, all newly released wheat varieties (from

TABLE 6 Correlations of monthly weather variable means, including maximum temperature (TM), average temperature (TA), minimum temperature (Tm), solar radiation (SR), and rainfall (P) per month, from January to December with trait means of grain yield (GY), days to heading (DH), plant height (PH), hectoliter weight (HLW), thousand kernel weight (TKW), and number of grains (NG) shown.

Trait	Growth habit	N. of yr	Jan	Feb	Mar	Apr	May	Jun	Jul	Oct	Nov	Dec
GY	SW	15	Tm			Tm*		SR*			SR*	
	WW	9								TA		
										Tm		
DH	SW	15		TM								
				TA								
				Tm								
				SR*								
	WW	9		TM			TA*					TA
				TA			TM*					Tm
				Tm								P*
PH	SW	15		TM			TM*		TA*			
							Tm*		Tm			
							TA*		P*			
	WW	9								P*		
HLW	SW	15	P					P				
	WW	9	P			Tm*	Tm	P		TM*	TA	P*
						TA*					Tm	
											TM*	
TKW	SW	15					TA*		P			P*
							Tm*					SR*
	WW	9	TM*			TA*	Tm			TM		
						TM*				TA*		
NG	SW	15					Tm*	Tm*	P			
							TA*					
	WW	9		P*						P		

Only significant (p -value < 0.10) ($0.05 < p < 0.10$ indicated with “*”) correlations are indicated. “N. of yr” indicates the number of years included in the regressions. The colors reported in the figure indicate the type of correlation, if positive or negative, with shades of green and red, respectively. The reported results for spring wheat (SW) are data from 2007 and 2021, and those for winter wheat (WW) are data from 2013 to 2021.

the private and public sectors) are tested annually against a benchmark variety that is extensively cultivated in the area. Regression analysis is also applied in this context to measure yield progress accurately. However, it is essential to note that when evaluating genetic yield progress using historical post-registration trials, the yield calculations must be compared against the benchmark variety. This precaution ensures that changes in yield are attributed to genetic factors rather than fluctuations in agronomy or environmental conditions (e.g., [Graybosch and Peterson, 2010](#); [Crespo-Herrera et al., 2018](#) for further details on this methodology). In this study, the yield progress rates were computed by analyzing post-registration trials conducted locally in the Catalonia region every year (lead by the Institute of Agrifood Research and Technology, IRTA and the Ministry of Agriculture, Departament d’Acció Climàtica, Alimentació i Agenda Rural).

Notably, Artur Nick and Nogal (benchmark SW and WW varieties) have consistently ranked among the top 10 varieties with the highest production of certified seed in Spain over the past 15 years (Ministry of Agriculture, Departament d’Acció Climàtica, Alimentació i Agenda Rural). Regressions of normalized GY in SW from 2007 to 2021 did not reveal a significant improvement in the newly released varieties compared to the check variety “Artur Nick”. In the context of SW, a notable trend has emerged over the past 15 years, marked by a significant reduction in plant height. On average, SW varieties have shown a gradual decline at a rate of 0.3 cm per year (compared to the check variety) with an average plant height (all varieties over 15 years) of 90 cm, which is already 2 cm below the average plant height of the check variety (“Arthur Nick” with 92 cm). The continual reduction in plant height, historically undertaken to enhance

lodging tolerance, has now fallen below the critical threshold of 1 m as identified by Fischer (2007) for realizing the maximum yield potential. This decline in plant height raises concerns about potential constraints on grain formation, often referred to as “source limitations,” which may be impeding progress in yield enhancement in SW. Given these compelling findings, it is strongly recommended, particularly within the unique agricultural context of this region, to exercise caution when considering any further reductions in the height of SW new varieties. However, in WW, an increase of 1.31% per year was reported, compared to the check variety “Nogal” (Figure 1D). Therefore, the calculated genetic gain reported in this study for WW is still within the range of previous reports (from the 1950s onwards), though it also fitted a quadratic function suggesting recent stagnation. Moreover, in the WW regions of Catalonia, wheat yield progress was accompanied by increased HLW and NG over time (both expressed as percentages of the check variety), indicating that these two traits positively contributed to GY in the latest WW varieties released in the past 15 years. Grain HLW is a measure of grain density and size. Frequently, the number of grains per unit area increases simultaneously when selecting for grain yield in breeding programs. However, under certain conditions and germplasm, the genotypes with the highest yields are also those with the highest NG and grain size (Griffiths et al., 2015). Generally, increased GY has been achieved with stable or even reduced grain weight, evidencing higher levels of phenotypic plasticity in grain number in response to the environment (Sadras, 2007). The observations by Griffiths et al. (2015) are in accordance with the results presented here regarding yield, HLW, and NG progress over time in Catalonia, with more recent varieties showing the largest grains. Although historical progress in breeding has been clearly associated with grain number, other studies have highlighted the positive association between grain yield and grain size (Lopes et al., 2012; Sukumaran et al., 2018). These results together with other observations in the literature indicate that increased grain yield through boosting grain number and size is possible and the simultaneous improvement of these two traits has the potential to increase grain yields under rising temperatures.

Despite the positive linear yield progress due to breeding in WW, this genetic yield progress (Figure 1D) was not accompanied by an overall absolute yield increase in the region (Figure 1B). This result indicated that progress in WW yield due to breeding and variety improvement has not been sufficient to sustain the negative impacts of other factors, such as weather. Historical weather variables were analyzed to test this hypothesis.

4.3 Climate change and wheat breeding impact on productivity and associated traits

Absolute GY progress in Catalonia has been stagnant in both spring and WW between 2007 and 2021, which is in accordance with a previous analysis from 2001 and onwards in North and South Europe (Lopes, 2022), using FAO data (Supplementary Figure 2) and national data in the same timeframe analyzed in this study. The

SW area, including La Tallada and Lleida, is characterized by increased water availability resulting from high rainfall frequency (in La Tallada) or supplementary irrigation (in Lleida) and milder overall average temperatures. However, the WW areas are rainfed and generally cooler during winter. Under these conditions, even if there were no significant negative correlations between weather and annual GY averages, weather variables were correlated with HLW and DH in both SW and WW. In SW, both maximum (TM) and average temperatures (TA) were negatively correlated with HLW; for each °C increase in TM ($p < 0.0995$) and TA ($p < 0.0647$), a 1.932 and 3.129 kg hL⁻¹ decrease in HLW, were observed, respectively. In WW, Tm and P were correlated with HLW, and for each °C increase in Tm, a 6.977 kg hL⁻¹ ($p < 0.0229$) decrease in HLW was observed. A significant negative correlation was also observed between precipitation and HLW, and this may result from the erratic annual distribution of precipitation ($p < 0.0069$; Supplementary Figure 4). Furthermore, in SW, a decrease in the HLW was reported, corresponding to an average total loss of 5.73 kg hL⁻¹ from 2007–2021 (Table 5).

As mentioned above, DH has decreased over time, and this was correlated with weather variables. For each °C increase in Tm, a reduction of 8.2 days in DH was reported in SW, and in WW, for each °C increase in TA, a reduction of 12.5 days DH was observed. A temperature increase results in significant reduction on the time to flowering (Menzel et al., 2006) in 542 plant species (both wild and cultivate) in 21 European countries, showing that phenological phases advanced by up to 4.6 days per °C in spring and summer, for the period between 1971 and 2000. Here, the observed reductions in DH result frequently in smaller crops, lower biomass and photosynthesis, and decreased tillering capacity and yield (Asseng et al., 2015). Furthermore, the robust correlations observed between agronomic traits and temperatures from February to May substantiate the heightened influence of temperature during the “critical period” (Fischer, 1975) in wheat. This period denotes a growth stage (between stem elongation and the transition to reproductive growth) when the crop attains its greatest susceptibility to environmental stressors, especially those capable of affecting yield potential, and in the Catalonia region, the “critical period” occurs between February and May. Should the temperature continue to rise, it is expected that DH reductions will cause a decrease in yields. Currently, yields only stagnate; however, if temperatures continue to rise at the observed rates, it is expected that yields will eventually start to decrease. Increasing temperatures can act as a relevant limiting factor, forcing crops to close in advance of their cycle, and consequently reduce their yield potential (García et al., 2015; García et al., 2016; García et al., 2018). These results highlight the relevance of re-evaluating sowing dates and vernalization requirements to fit optimal weather conditions and growing two or more varieties on farms to buffer yields under an erratic distribution of precipitation and increasing temperature. There is a promising opportunity to investigate the advancement of the wheat planting schedule, the reduction of vernalization prerequisites, or the integration of earliness per se genes to expedite the wheat growth cycle, thereby mitigating the risk of encountering terminal heat stress. This avenue of research warrants thorough exploration in the future. The GY components

also showed negative correlations with the average April and May temperatures, significantly affecting grain size (negative correlation with TKW and HLW; see also [Supplementary Figure 5](#)). Previous studies (using controlled growth conditions) indicated the negative effect of nighttime temperatures ($>20^{\circ}\text{C}$) during the reproductive stage until maturity on grain size and yield ([Prasad et al., 2008](#)). The historical temperature increase observed under natural field conditions in the present study contributed to a decrease in grain size and has not yet resulted in grain yield reduction. However, if night and daytime temperatures continue to rise at the observed rates, a grain yield penalty will eventually be observed.

5 Concluding remarks

Recent historical data have brought to light a concerning trend in SW yields characterized by stagnation. This phenomenon is likely intertwined with the gradual decline in plant height over time, a factor that has pushed plant stature below the optimal threshold. This diminishing plant height has, in turn, led to reduced biomass and a compromised capacity for assimilation, potentially impacting grain formation. In the context of WW, recent historical records indicated significant positive yield progress, which was likely attributed to enhancements in both grain size and number. Moreover, the ongoing rise in temperature and unpredictable precipitation patterns have exerted a discernible and adverse influence on both SW and WW. These climatic variables have particularly affected two key traits: hectoliter weight and days to heading. Consequently, it is imperative that substantial breeding efforts are undertaken to adapt and optimize phenological traits to optimal sowing dates, maintain plant height, increase grain size and number in response to the unpredictability in temperature and precipitation distribution patterns. Simultaneously, within breeding programs, there should be a concerted focus on selecting for increased grain size and number, especially under conditions of high temperature and drought stress. This approach will be instrumental in safeguarding yield potential in emerging wheat varieties, ensuring they can thrive in the changing climate and meet the demand for sustainable crop production.

Data availability statement

The original contributions presented in the study are included in the article/[Supplementary Material](#). Further inquiries can be directed to the corresponding author.

Author contributions

DG analyzed the data and wrote the manuscript. RS collected and processed the data and reviewed the manuscript. JS collected data and reviewed the manuscript. JB collected data and reviewed

the manuscript. JD reviewed the manuscript. AG-R reviewed the manuscript. ML designed the study and prepared the manuscript. All authors contributed to the article and approved the submitted version.

Funding

This research was funded by the projects TED2021-131606B-C21 of the Spanish Ministry of Economy and Competitiveness and by the CROPDIVA (Climate Resilient Orphan CroPs for increased DIVERsity in Agriculture) project through the European Union's Horizon 2020 research and innovation program under grant agreement No. 101000847. The funders played no role in the study design, data collection and analysis, decision to publish, or manuscript preparation.

Acknowledgments

The authors acknowledge the contribution of the CERCA Program (Generalitat de Catalunya). The authors thank Andrea Lopez, Ezequiel Arqu , Jordi Companys, and Josep Millera for their technical contributions to the experimental setup of the field trials.

Conflict of interest

The authors declare that the research was conducted in the absence of any commercial or financial relationships that could be construed as a potential conflict of interest.

Publisher's note

All claims expressed in this article are solely those of the authors and do not necessarily represent those of their affiliated organizations, or those of the publisher, the editors and the reviewers. Any product that may be evaluated in this article, or claim that may be made by its manufacturer, is not guaranteed or endorsed by the publisher.

Supplementary material

The Supplementary Material for this article can be found online at: <https://www.frontiersin.org/articles/10.3389/fpls.2023.1245362/full#supplementary-material>

References

- Acreche, M. M., Briceño-Félix, G., Sánchez, J. A. M., and Slafer, G. A. (2008). Physiological bases of genetic gains in Mediterranean bread wheat yield in Spain. *Eur. J. Agron.* 28, 162–170. doi: 10.1016/j.eja.2007.07.001
- Asseng, S., Ewert, F., Martre, P., Rötter, R. P., Lobell, D. B., Cammarano, D., et al. (2015). Rising temperatures reduce global wheat production. *Nat. Clim. Chang.* 5, 143–147. doi: 10.1038/nclimate2470
- Crespo-Herrera, L. A., Crossa, J., Huerta-Espino, J., Vargas, M., Mondal, S., Velu, G., et al. (2018). Genetic gains for grain yield in CIMMYT's semi-arid wheat yield trials grown in suboptimal environments. *Crop Sci.* 58, 1890–1898. doi: 10.2135/cropsci2018.01.0017
- FAOSTAT (2021) *Area harvested*. Available at: <https://www.fao.org/faostat/en/#data/QCL>.
- Fischer, R. A. (1975). Yield potential in a dwarf spring wheat and the effect of shading. *Crop Sci.* 15, 607–613. doi: 10.2135/cropsci1975.0011183X001500050002x
- Fischer, R. A. (2007). Understanding the physiological basis of yield potential in wheat. *J. Agric. Sci.* 145, 99–113. doi: 10.1017/S0021859607006843
- García, G. A., Dreccer, M. F., Miralles, D. J., and Serrago, R. A. (2015). High night temperatures during grain number determination reduce wheat and barley grain yield: a field study. *Glob. Chang. Biol.* 21, 4153–4164. doi: 10.1111/gcb.13009
- García, G. A., Miralles, D. J., Serrago, R. A., Alzueta, I., Huth, N., and Dreccer, M. F. (2018). Warm nights in the Argentine Pampas: Modelling its impact on wheat and barley shows yield reductions. *Agric. Syst.* 162, 259–268. doi: 10.1016/j.agry.2017.12.009
- García, G. A., Serrago, R. A., Dreccer, M. F., and Miralles, D. J. (2016). Post-anthesis warm nights reduce grain weight in field-grown wheat and barley. *Field Crops Res.* 195, 50–59. doi: 10.1016/j.fcr.2016.06.002
- Graybosch, R. A., and Peterson, C. J. (2010). Genetic improvement in winter wheat yields in the Great Plains of North America 1959–2008. *Crop Sci.* 50, 1882–1890. doi: 10.2135/cropsci2009.11.0685
- Green, A. J., Berger, G., Griffey, C. A., Pitman, R., Thomason, W., Balota, M., et al. (2012). Genetic yield improvement in soft red winter wheat in the eastern United States from 1919 to 2009. *Crop Sci.* 52, 2097–2108. doi: 10.2135/cropsci2012.01.0026
- Griffiths, S., Wingen, L., Pietragalla, J., Garcia, G., Hasan, A., Miralles, D., et al. (2015). Genetic dissection of grain size and grain number trade-offs in CIMMYT wheat germplasm. *PLoS One* 10, e0118847. doi: 10.1371/journal.pone.0118847
- Heino, M., Kinnunen, P., Anderson, W., Ray, D. K., Puma, M. J., Varis, O., et al. (2023). Increased probability of hot and dry weather extremes during the growing season threatens global crop yields. *Sci. Rep.* 13, 3583. doi: 10.1038/s41598-023-29378-2
- Lopes, M. S. (2022). Will temperature and rainfall changes prevent yield progress in Europe? *Food Energy Secur.* 11, e372. doi: 10.1002/fes3.372
- Lopes, M. S., Reynolds, M. P., Manes, Y., Singh, R. P., Crossa, J., and Braun, H. J. (2012). Genetic yield gains and changes in associated traits of CIMMYT spring bread wheat in a “Historic” set representing 30 years of breeding. *Crop Sci.* 52, 1123–1131. doi: 10.2135/cropsci2011.09.0467
- Lo Valvo, P. J., Miralles, D. J., and Serrago, R. A. (2018). Genetic progress in Argentine bread wheat varieties released between 1918 and 2011: Changes in physiological and numerical yield components. *Field Crops Res.* 221, 314–321. doi: 10.1016/j.fcr.2017.08.014
- Menzel, A., Sparks, T., Estrella, N., Koch, E., Aasa, A., Ahas, R., et al. (2006). European phenological response to climate change matches the warming pattern. *Glob. Chang. Biol.* 12, 1969–1976. doi: 10.1111/j.1365-2486.2006.01193.x
- Pask, A., Pietragalla, J., Mullan, D., and Reynolds, M. (2012). *Physiological breeding II: A field guide to wheat phenotyping* (Mexico, D.F.: CIMMYT).
- Pequeno, D. N. L., Hernández-Ochoa, I. M., Reynolds, M., Sonder, K., Moleromilan, A., Robertson, R. D., et al. (2021). Climate impact and adaptation to heat and drought stress of regional and global wheat production. *Environ. Res. Lett.* 16, 54070. doi: 10.1088/1748-9326/abd970
- Prasad, P. V. V., Pisipati, S. R., Ristic, Z., Bukovnik, U., and Fritz, A. K. (2008). Impact of nighttime temperature on physiology and growth of spring wheat. *Crop Sci.* 48, 2372–2380. doi: 10.2135/cropsci2007.12.0717
- Rife, T. W., Graybosch, R. A., and Poland, J. A. (2019). A field-based analysis of genetic improvement for grain yield in winter wheat cultivars developed in the US central plains from 1992 to 2014. *Crop Sci.* 59, 905–910. doi: 10.2135/cropsci2018.01.0073
- Sadras, V. O. (2007). Evolutionary aspects of the trade-off between seed size and number in crops. *Field Crops Res.* 100, 125–138. doi: 10.1016/j.fcr.2006.07.004
- Sadras, V. O., and Lawson, C. (2011). Genetic gain in yield and associated changes in phenotype, trait plasticity and competitive ability of South Australian wheat varieties released between 1958 and 2007. *Crop Pasture Sci.* 62, 533–549. doi: 10.1071/CP11060
- Sanchez-Garcia, M., Royo, C., Aparicio, N., Martín-Sánchez, J. A., and Álvaro, F. (2013). Genetic improvement of bread wheat yield and associated traits in Spain during the 20th century. *J. Agric. Sci.* 151, 105–118. doi: 10.1017/S0021859612000330
- Sayre, K. D., Rajaram, S., and Fischer, R. A. (1997). Yield potential progress in short bread wheats in northwest Mexico. *Crop Sci.* 37, 36–42. doi: 10.2135/cropsci1997.0011183X003700010006x
- Skrzyńska, M., and Twardosz, R. (2023). Long-term changes in the frequency of exceptionally cold and warm months in Europe, (1831–2020). *Int. J. Climatol.* 43, 2339–2351. doi: 10.1002/joc.7978
- Statistical Institute of Catalonia (2021) *Superficie agrícola. Por productos. Provincias*. Available at: <https://www.idescat.cat/indicadors/?id=aec&n=15422&lang=es>.
- Sukumaran, S., Lopes, M. S., Dreisigacker, S., and Reynolds, M. (2018). Genetic analysis of multi-environmental spring wheat trials identifies genomic regions for locus-specific trade-offs for grain weight and grain number. *Theor. Appl. Genet.* 131, 985–998. doi: 10.1007/s00122-017-3037-7
- Twardosz, R., Walanus, A., and Guzik, I. (2021). Warming in Europe: recent trends in annual and seasonal temperatures. *Pure Appl. Geophys.* 178, 4021–4032. doi: 10.1007/s00024-021-02860-6
- Zhou, Y., Zhu, H. Z., Cai, S. B., He, Z. H., Zhang, X. K., Xia, X. C., et al. (2007). Genetic improvement of grain yield and associated traits in the southern China winter wheat region: 1949 to 2000. *Euphytica* 157, 465–473. doi: 10.1007/s10681-007-9376-8



OPEN ACCESS

EDITED BY

Ignacio Romagosa,
Agrotecnio Center, Spain

REVIEWED BY

Lingqiang Wang,
Guangxi University, China
Marian Moralejo,
Universitat de Lleida, Spain

*CORRESPONDENCE

Hongyu Yuan
✉ yhongyu92@163.com

RECEIVED 04 November 2023

ACCEPTED 02 February 2024

PUBLISHED 16 February 2024

CITATION

Wang Q, Gao H, Liu K, Wang H, Zhang F, Wei L, Lu K, Li M, Shi Y, Zhao J, Zhou W, Peng B and Yuan H (2024) CRISPR/Cas9-mediated enhancement of semi-dwarf glutinous traits in elite Xiangdaowan rice (*Oryza sativa* L.): targeting *SD1* and *Wx* genes for yield and quality improvement. *Front. Plant Sci.* 15:1333191. doi: 10.3389/fpls.2024.1333191

COPYRIGHT

© 2024 Wang, Gao, Liu, Wang, Zhang, Wei, Lu, Li, Shi, Zhao, Zhou, Peng and Yuan. This is an open-access article distributed under the terms of the [Creative Commons Attribution License \(CC BY\)](#). The use, distribution or reproduction in other forums is permitted, provided the original author(s) and the copyright owner(s) are credited and that the original publication in this journal is cited, in accordance with accepted academic practice. No use, distribution or reproduction is permitted which does not comply with these terms.

CRISPR/Cas9-mediated enhancement of semi-dwarf glutinous traits in elite Xiangdaowan rice (*Oryza sativa* L.): targeting *SD1* and *Wx* genes for yield and quality improvement

Quanxiu Wang, Haolin Gao, Ke Liu, Honglin Wang, Fan Zhang, Lanmeng Wei, Kaijing Lu, Mengmeng Li, Yiming Shi, Jinhui Zhao, Wei Zhou, Bo Peng and Hongyu Yuan*

College of Life Sciences, Institute for Conservation and Utilization of Agro-Bioresources in Dabie Mountains, Xinyang Normal University, Xinyang, China

In rice cultivation, the traits of semi-dwarfism and glutinous texture are pivotal for optimizing yield potential and grain quality, respectively. Xiangdaowan (XDW) rice, renowned for its exceptional aromatic properties, has faced challenges due to its tall stature and high amylose content, resulting in poor lodging resistance and suboptimal culinary attributes. To address these issues, we employed CRISPR/Cas9 technology to precisely edit the *SD1* and *Wx* genes in XDW rice, leading to the development of stable genetically homozygous lines with desired semi-dwarf and glutinous characteristics. The *sd1-wx* mutant lines exhibited reduced gibberellin content, plant height, and amylose content, while maintaining hardly changed germination rate and other key agronomic traits. Importantly, our study demonstrated that exogenous GA₃ application effectively promoted growth by compensating for the deficiency of endogenous gibberellin. Based on this, a semi-dwarf glutinous elite rice (*Oryza sativa* L.) Lines was developed without too much effect on most agronomic traits. Furthermore, a comparative transcriptome analysis unveiled that differentially expressed genes (DEGs) were primarily associated with the anchored component of the membrane, hydrogen peroxide catabolic process, peroxidase activity, terpene synthase activity, and apoplast. Additionally, terpene synthase genes involved in catalyzing the biosynthesis of diterpenoids to gibberellins were enriched and significantly down-regulated. This comprehensive study provides an efficient method for simultaneously enhancing rice plant height and quality, paving the way for the development of lodging-resistant and high-quality rice varieties.

KEYWORDS

rice, *Sd1*, *Wx*, gibberellin, amylose, transcriptome

Introduction

Rice (*Oryza sativa* L.) sustains over half of the world's population as a staple food, making the enhancement of grain quality and yield a global priority (Chandler and Wessler, 2001; Khush, 2005; Zhang, 2007; Demont and Stein, 2013; Qiao et al., 2021). Xiangdaowan (XDW) rice, esteemed for its robust aromatic qualities, confronts a challenge with its traditional varieties exhibiting excessive plant height and poor lodging resistance, adversely impacting rice yield (Singh et al., 2011). Conversely, excessively short plants produce smaller grains and exhibit diminished disease resistance, emphasizing the critical importance of maintaining an optimal plant height for maximizing rice yield (Liu et al., 2018). Gibberellin (GA), a pivotal plant hormone governing stem elongation, holds a key role in regulating plant height (Zhu et al., 2006; Zhang et al., 2014). Numerous genes contribute to GA biosynthesis and signaling, with *SD1* (semi dwarf1) standing out as the “Green Revolution” gene. *SD1* encodes the crucial enzyme gibberellin 20-oxidase 2 (GA20ox2), essential for gibberellin synthesis (Spielmeyer et al., 2002). Mutations in *SD1* result in reduced gibberellin production, leading to a shorter plant stature (Monna et al., 2002; Sasaki et al., 2002). Since the 1930s, the *sd1* allele has been used in rice breeding to produce rice varieties with short stature and excellent lodging resistance (Sakamoto and Matsuoka, 2004; Asano et al., 2007). The tall plant phenotype is governed by the *SD1* allele, while the recessive *sd1* allele induces the semi-dwarf phenotype (Monna et al., 2002; Berry et al., 2004; Magome et al., 2013). Gibberellins, such as GA₁ and GA₄, composed of diterpene carboxylic acids, play crucial roles in plant growth and development especially in regulating plant height (Thomas and Hedden, 2006; Hedden and Thomas, 2012; Marciniak et al., 2018).

Amylose content (AC) plays a pivotal role in the culinary and physical attributes of rice, exerting a profound influence on its eating and cooking quality (ECQ) (Li et al., 2016; Huang et al., 2021; Zhang et al., 2021a, b). The *Waxy* gene (*Wx*), a key player in this saga, encodes granule-bound starch synthase (GBSS) and stands as a major architect dictating amylose synthesis in rice grains. This synthesis, in turn, modulates the AC, gel consistency (GC), and viscosity (Wang et al., 1990; Su et al., 2011; Zhou et al., 2021; Zhang et al., 2021a). Rice varieties are classified into five types based on their AC: high (>25%), intermediate (20–25%), low (10–19%), very low (3–9%), and glutinous (0–2%) (Li and Gilbert, 2018). To date, at least nine allelic variations of *Wx*, *Wx^{da}*/*Wx^{mw}*, *Wx^{lv}*, *Wx^a*, *Wx^b*, *Wxⁱⁿ*, *Wx^{op}*/*Wx^{hp}*, *Wx^{mp}*, *Wx^{mq}*, and *wx*, have been related to the five AC types found in rice cultivars (Ayres et al., 1997; Cai et al., 1998; Sato et al., 2002; Larkin and Park, 2003; Wanchana et al., 2003; Mikami et al., 2008; Liu et al., 2009; Yang et al., 2013; Zhang et al., 2019; Zhou et al., 2021; Zhang et al., 2021a). In general, rice varieties with higher *Wx* gene expression exhibit higher GBSS enzyme activity, resulting in a higher AC content and, conversely, lower AC content (Kumar and Khush, 1986; Su et al., 2011). Researchers have explored manipulating the promoter or exon region of the *Wx* gene to regulated AC, resulting in the

development of soft or glutinous rice lines (Han et al., 2018; Yang et al., 2018; Zhang et al., 2018; Pérez et al., 2019; Yunyan et al., 2019; Zeng et al., 2020; Huang et al., 2021; Yang et al., 2022; Tian et al., 2023; Zhang et al., 2023).

Both *Wx* and *SD1* genes play crucial roles in determining rice grain quality and yield potential, respectively. Despite breeding efforts using diverse strategies such as marker-assisted selection, progress has been sluggish, especially in enhancing complex and multiple traits. In recent years, CRISPR/Cas9 genome editing technology has been successfully applied to improve crop traits in rice, maize, wheat, sorghum and soybean, which offers rapid and efficient trait modification (Jiang et al., 2013; Mao et al., 2013; Shan et al., 2013; Liang et al., 2014; Wang et al., 2014; Li et al., 2015). Although some researchers have employed gene editing technology to improve plant height or quality by targeting the *SD1* or *Wx* gene in elite rice landrace or hybrid rice (Zhang et al., 2018; Han et al., 2019; Hu et al., 2019; Yunyan et al., 2019; Nawaz et al., 2020; Zeng et al., 2020; Yang et al., 2022), the simultaneous editing of both genes in the same rice variety remains uncharted.

In this study, we examined Xiangdaowan (XDW) rice, a fragrant, high-quality rice variety characterized by poor lodging resistance and tough rice texture. Despite its robust aromatic qualities, it suffers from a tall stature and elevated AC, resulting in a low harvest index and suboptimal rice quality. Enhancing lodging resistance and refining the overall quality of rice are crucial objectives that can augment yield and the breeding and utilization value by altering plant height and AC. To address these challenges, we utilized CRISPR/Cas9 technology to develop *sd1-wx* double mutants in Xiangdaowan (XDW) rice. Across various generations, we successfully obtained genetically stable, homozygous mutants. Subsequently, we investigated the phenotype of *sd1-wx* double mutants, and constructed semi-dwarf glutinous rice varieties with low plant height and AC content without disrupting other essential agronomic characteristics. Further unraveling the intricacies of the *SD1* and *Wx* genes, we conducted comparative RNA-seq analysis on *sd1-wx* double mutants and the wild type (WT). In summary, our study not only promises increased yield and the provision of high-quality resources for the improvement of new rice varieties but also sheds light on the functional roles of *SD1* and *Wx* genes through advanced RNA-seq analysis.

Materials and methods

Plant material and measurement of agronomic traits

The genetic groundwork for the transgenic plants comprises the esteemed rice landraces Xiangdaowan (*Oryza sativa* L., ssp. Japonica). All rice cultivation occurred in the natural settings of paddy fields at Xinyang Normal University in Xinyang, China (32°8'30"N, 114°2'8"E). Following to rice harvest, a minimum of 10 randomly selected rice plants underwent analysis for agronomic traits, including plant height, tiller number, grain weight, and grain number per panicle.

Construction of CRISPR/Cas9 vectors and plant transformation

The CRISPR/Cas9 vector system tailored for simultaneous targeting of multiple gene sites in monocot plants was procured from Biogle Biotechnology Co., Ltd. The design of gRNA target sequences aligned with the exon sequence of *SD1* (LOC_Os01g66100) and *Wx* (LOC_Os06g04200), as outlined by the Rice Genomics Annotation website (<http://rice.plantbiology.msu.edu/>). In a nutshell, these target site sequences were incorporated into the sgRNA expression cassette, which included a rice promoter, and subsequently integrated into the *Bsa*I restriction sites of the pCRISPR/Cas9-BGK032 vector. Detailed primer information for constructing the sgRNA vectors for *Wx* and *SD1* can be found in [Supplementary Table S1](#). Following this, independent introductions of CRISPR/Cas9 constructs were made into *Agrobacterium tumefaciens* strain *EHA105*, followed by transformation into the elite rice landraces Xiangdaowan using a method described previously (Nishimura et al., 2006). Hygromycin phosphotransferase (*hpt*) served as the plant selectable agent during the screening process for positive rice transformants.

RNA-seq analysis

To assess the transcriptome profiling of edited lines resulting from the *Wx* and *SD1* gene modifications, we conducted transcriptomic analysis using both wild-type (WT) and mutant plants. Stem tissues at the heading stage were utilized for RNA extraction. The RNA samples underwent sequencing by APTBIO Co. in Shanghai, China, utilizing the Illumina HiSeqTM 2000 platform. For robustness, three biological replicates were included in the transcriptomic analysis. The analytical methods for transcriptomics were based on previous method (Wang et al., 2023). The resulting clean reads, stored in FASTQ format, were mapped to the reference genome using Bowtie2. Alignment to the Nipponbare reference genome (<http://rice.plantbiology.msu.edu/>) was achieved with an ideal match using HISAT2 software. The expression level of each gene was normalized to fragments per kilo base per million (FPKM) mapped reads. Differentially expressed genes (DEGs) between mutant and WT plants were identified based on a fold change ≥ 2 and a p -value < 0.05 . Mapping of DEGs to GO terms was performed, and the count of genes for each term was determined. Significance of GO term enrichment was assessed using the hypergeometric test, with p -values adjusted. GO terms were considered significantly enriched only when both the p -value and p -adjusted value were < 0.05 . Additionally, KEGG analysis was employed to identify significantly enriched signaling and metabolic pathways for each DEG compared with the reference genome. KEGG terms with both a p -value and p -adjusted value of < 0.05 were considered significantly enriched.

Real-time quantitative PCR assays

In order to verify the result of RNA-seq result, RT-qPCR was carried out on selected genes. Trizol reagent was used to isolate total RNA from rice stems tissue by following the manufacturer's protocol.

And then 3 μ g RNA samples were synthesized to cDNA using the reverse transcriptase. Quantitative RT-PCR assays were conducted analysis on the CFX96 thermocycler (Bio-rad, USA) PCR System using the SYBR green master. We used three biological and technical replicates. The rice ubiquitin gene was used as an internal control. The expression level of each gene was determined based on previous method (Livak and Schmittgen, 2001). Primers for real-time quantitative PCR are shown in [Supplementary Table S1](#).

Seed germination rate measurement and plant hormone treatments

Following harvest, rice was subjected to a drying process at 37°C for 5 days, after which it was immersed in water, and then placed in a growth chamber maintained at 30 °C in darkness. The assessment of seed dormancy involved visual scoring, specifically when the radicle exceeded 3 mm in length. For H₂O and 4 μ M GA₃ treatments, approximately 50 well-developed seeds were evenly distributed on wet filter paper in culture dishes with a diameter of 90 cm and were subsequently treated with the 8 mL specified reagents (H₂O or 4 μ M GA₃) in incubator at 30°C. It was ensured that the seeds remained moist during this experiment. Germination rates were monitored daily from day 3 to day 5. This process was replicated three times. The resulting germination percentages were averaged for subsequent genetic analysis.

Quantification of the endogenous plant hormone

Guangzhou Hellogene Biotechnology Company conducted the detection of GA compounds using the following procedure: The samples (~1 g) were finely powdered and combined with 4 mL of acetonitrile (v/v) containing 20 ng of each deuterium-labeled internal standard ([²H₂]GA₃ and [²H₆]ABA). This mixture was then placed on a shaker at 300 rpm in the dark at 4 °C for 24 hours. Afterward, the samples underwent centrifugation (12,000 g, 5 minutes), and the resulting supernatant was carefully transferred to a clean tube. To further purify the extract, it was passed through a poroshell 120 SB-C18 column, pre-equilibrated with methanol, followed by an extraction buffer. The column was subsequently rinsed with 500 μ L of methanol acidified with 0.1% methanoic acid. The purified extract was then dried using nitrogen gas and reconstituted with 400 μ L of 100% methanol at 4 °C in the dark for 24 hours. After centrifugation (12,000 g, 5 minutes), the supernatant was transferred into HPLC vials and subjected to liquid chromatography-mass spectrometry (LC-MS) analysis using a SCIEX6500QTRAP LC/MS/MS system, equipped with an ESI Turbo Ion-Spray interface.

Measurement of grain physicochemical properties

After plant maturation, the harvested rice grains underwent air-drying and were subsequently stored at room temperature for a

minimum of three months prior to testing. The flours and starches from brown rice were prepared as previously described (Bao et al., 2006). Measurement of the apparent amylose content (AC) and gel consistency (GC) of brown rice flours was conducted according to the method described by Bao et al. (Bao et al., 2006). For scanning and transmission electron microscopy analyses of starch granules, cross sections of brown white rice grains and rice powders were gold-coated under vacuum. Starch granule morphology was then examined using a scanning electron microscope (Regulus-8220, Japan) at an accelerating voltage of 3.0 kV and magnifications of 400×, 2,500×, and 3,000×. The SEM analysis was based on at least three biological replications of mounted specimens, and all procedures strictly adhered to the manufacturer's protocol.

The GT (gelatinization temperature) values were estimated indirectly by the alkali spreading score (ASS) method. Briefly, 6 grains of whole milled white rice from each strain were placed in a 90 mm petri dish along with 20 ml of 1.7% potassium hydroxide solution. The samples were separated from each other using forceps and incubated at 30°C for 23 h to allow the rice grains to spread. The spreading score of the grains was recorded visually follow previous method. The ASS score of 1–7 was recorded depending on the appearance and degree of dispersion of the endosperm. Unaffected or slightly swollen endosperm was recorded as 1, while completely disappeared was recorded as 7. The GT value was inversely proportional to the ASS score. There are three grades of GT: ASS grades 1 to 2 are high GT means gelatinization temperature >75°C, grades 3 are high-intermediate GT means gelatinization temperature between 70°C–74°C, grades 4 to 5 are intermediate GT means gelatinization temperature between 66°C–69°C, and grades 6 to 7 are low GT means gelatinization temperature between 55°C–65°C.

Statistical analysis

To characterize the samples, we conducted measurements in triplicate, unless stated otherwise. All data are expressed as mean ± standard deviation (SD). Statistical analyses, including one-way ANOVA and Student's t-test, were performed using the SPSS 16.0 software. $P < 0.05$ was deemed statistically significant.

Results

Editing of *OsSD1* and *OsWx* genes via CRISPR/Cas9 technology

To enhance the plant height and quality of elite rice landrace Xiangdaowan (XDW), we employed CRISPR/Cas9 technology to create single mutants for the *sd1* and *wx* genes, as well as double mutants (*sd1-wx*). Briefly, we designed and constructed the pCRISPR/Cas9-BGK032-*SD1* and pCRISPR/Cas9-BGK032-*Wx* single target vectors, along with the pCXUN-*Wx-SD1* dual target vector (Figure 1A). These vectors were introduced into XDW callus through *Agrobacterium*-mediated transformation. We obtained 21 XDW^{*sd1*} T₀ transgenic plants, 5 XDW^{*wx*} T₀ transgenic plants and 20 XDW^{*sd1-wx*} T₀ double mutants transgenic plants, respectively.

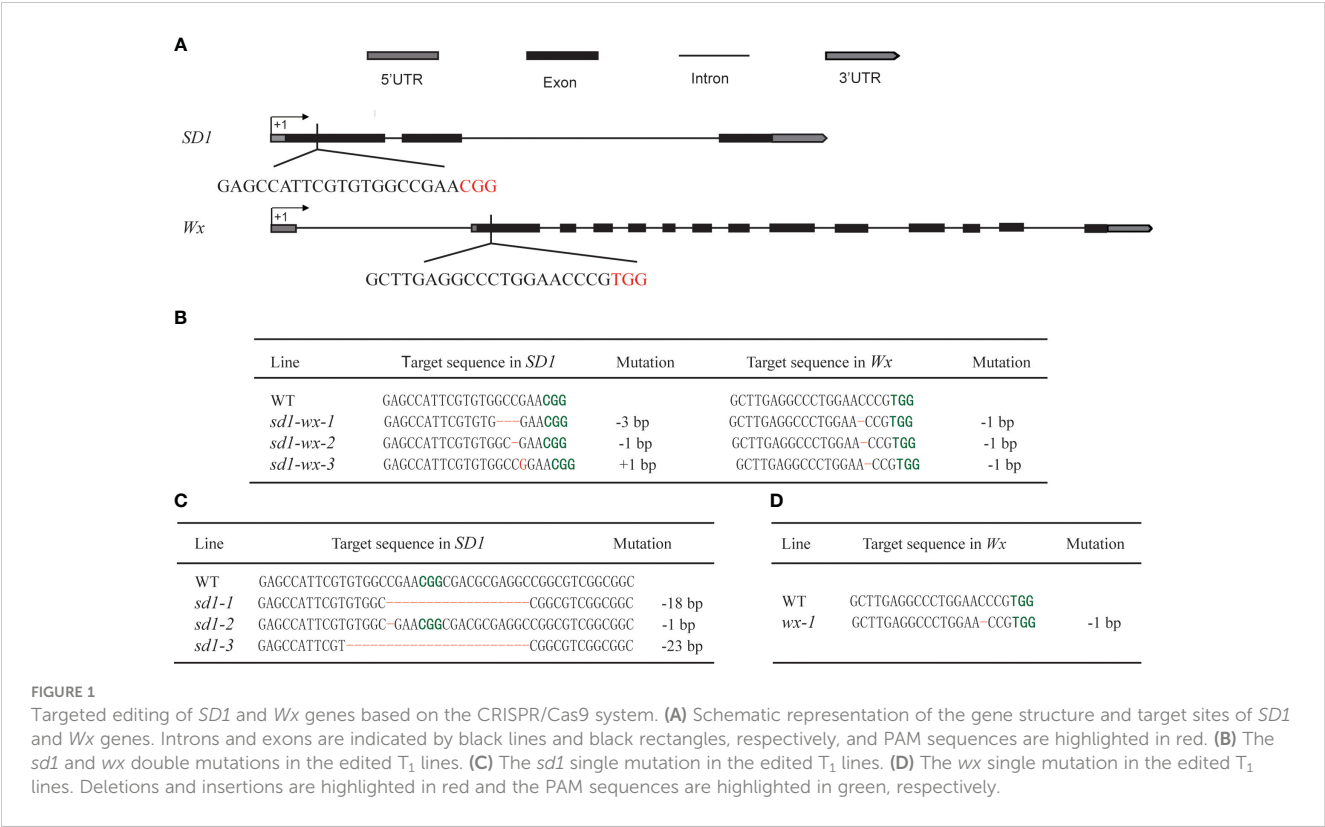
Subsequently, we utilized PCR to select plants that were free of *Cas9* and *HPT* plants from the transgenic (T₁–T₂) segregating families. Sanger sequencing of *SD1* and *Wx* target sites identified various insertion/deletion mutations. To produce desirable homozygous and non-transgenic plants, we closely monitored the genotypes of the target sites as well as the segregation of T-DNA from T₁ progeny plants to T₃ progeny plants. Ultimately, we successfully obtained three lines of homozygous and T-DNA-free editing in the single mutant XDW^{*sd1*}, one in the single mutant XDW^{*wx*}, and three in the double mutants XDW^{*sd1-wx*}. XDW^{*sd1-1*} contained eighteen nucleotide deletion in *SD1*, XDW^{*sd1-2*} consisted of one nucleotide deletion (ΔC) in *SD1*, and XDW^{*sd1-3*} contained twenty-three nucleotide deletion in *SD1* (Figure 1C). XDW^{*wx-1*} contained one nucleotide deletions (ΔC) in *Wx* (Figure 1D). XDW^{*sd1-wx-1*} comprised of three nucleotide deletion (ΔGCC) in *SD1* and one nucleotide deletions (ΔC) in *Wx* (Figure 1B). XDW^{*sd1-wx-2*} consisted of one nucleotide deletion (ΔC) in *SD1* and *Wx* (Figure 1B), respectively. XDW^{*sd1-wx-3*} contained one nucleotide insertion (ΔG) in *SD1* and one nucleotide deletion (ΔC) in *Wx* (Figure 1B). Most of the mutations were predicted to cause frameshifts, resulting in the translation of non-functional truncated proteins. In conclusion, we employed CRISPR/Cas9 technology to precisely edit the *SD1* and *Wx* genes in XDW rice, leading to the development of stable genetically homozygous lines.

Endogenous GA concentrations and plant heights in *sd1* mutants

To evaluate the effect of rice plant height in *sd1* mutants, we systematically measured the plant height and stem internode length of transgenic plants. The *sd1* mutant lines had shorter plant heights and lower GA concentrations compared to WT plants. Specifically, the mutant lines XDW^{*sd1-wx-1*}, XDW^{*sd1-1*}, XDW^{*sd1-2*}, and XDW^{*sd1-3*} showed plant heights of 136.9 cm, 117.6 cm, 114.9 cm and 105.7 cm in the T₂ generation, respectively, whereas WT had a maximum height of 158.8 cm (Table 1). Analysis of the length of each stem internode showed that the reduction in plant height was caused by a different degree of decline in the length of each stem internode (Figure 2). In order to confirm whether the reduction of mutant lines plant height was due to the reduction of endogenous gibberellin content, we measured the content of gibberellin (GA₁, GA₃, GA₄) through LC-MS analysis. The mutant line XDW^{*sd1-3*}, with the minimum plant height, had the lowest GA₃ content. The mutant lines XDW^{*sd1-1*} and XDW^{*sd1-2*} had the lowest GA₁ and GA₄ content (Table 1), respectively. In contrast, the WT with the maximum height had the highest gibberellin content. This suggests that editing the *SD1* gene significantly reduces plant height by decreasing endogenous gibberellin levels.

Seed germination and effect of exogenous GA₃ in *sd1* mutants

The concentration of endogenous gibberellin (GA) is crucial for the successful germination of seeds, ensuring the continuous life cycle of seed plants. Quality seed germination is indicative of robust seedling establishment and overall plant production. Herein, we



examined the germination rates of XDW, XDW^{*sd1-wx-1*} and XDW^{*sd1-3*} seeds between H₂O and GA₃ treatment groups. After imbibition for 5 days, we observed distinct germination responses among WT and mutant seeds. On the third day, the *sd1-wx-1* mutant exhibited remarkably lower germination rates compared to WT (Figure 3B), but this difference disappeared by the fifth day (Figures 3C, D). Compared with WT, *sd1-3* mutants displayed significantly lower germination rates (Figures 3C, D). Recognizing the pivotal role of GA in seed germination regulation, we explored the impact of exogenous 4 μM GA₃ treatment, revealing a significant increase in germination rates. We found that exogenous GA₃ treatment can partially compensate lower germination rates in *sd1* mutation compared with WT (Figures 3C, D). Further investigation indicated that the *sd1-3* mutation somewhat increased seed dormancy at the early stages of seed germination, aligning with previous findings (Ye et al.,

2015). Collectively, our results suggest that the *sd1* mutation may reduce endogenous GA₃ content, leading to decreased germination rates. However, this deficiency can be partially compensated by the application of exogenous GA.

To assess the potential of exogenous gibberellin application in addressing endogenous deficiency, we treated XDW plants and the height-reduced mutant line XDW^{*wx-sd1-1*} and XDW^{*sd1-3*} with 10 μM GA₃ at the seedling stage (30 days old) in the greenhouse. Under controlled conditions, XDW^{*wx-sd1-1*} and XDW^{*sd1-3*} plants initially displayed the lower height (14.11 cm, 12.55 cm) compared to WT XDW plants (19.99 cm) (Figures 3E, F). Following GA₃ treatment, the T₂ mutant line XDW^{*wx-sd1-1*} and XDW^{*sd1-3*} exhibited restored plant height (24.95 cm, 25.08 cm), nearly equivalent to that of WT plants (25.17 cm) (Figures 3E, F). These findings demonstrate that the application of exogenous GA₃ can enhance growth by supplementing the deficiency of endogenous gibberellin.

TABLE 1 GA content (μg/kg FW) and PH (cm) in WT and mutant lines.

Line	GA ₁	GA ₃	GA ₄	PH
WT	1.073 ± 0.058	0.655 ± 0.025	0.324 ± 0.005	158.8 ± 4.2
<i>sd1-wx-1</i>	0.841 ± 0.054**	0.501 ± 0.020**	0.265 ± 0.006**	136.9 ± 4.8**
<i>sd1-1</i>	0.611 ± 0.010**	0.426 ± 0.025**	0.202 ± 0.006**	117.6 ± 4.6**
<i>sd1-2</i>	0.729 ± 0.026**	0.319 ± 0.021**	0.158 ± 0.002**	114.9 ± 2.9**
<i>sd1-3</i>	0.657 ± 0.009**	0.281 ± 0.011**	0.177 ± 0.002**	105.7 ± 4.3**
<i>wx-1</i>	-	-	-	157.3 ± 4.0 ^{ns}

The data are the means of three replicates. ^{ns} and **represent non-significant differences and the significant (p<0.01), respectively.

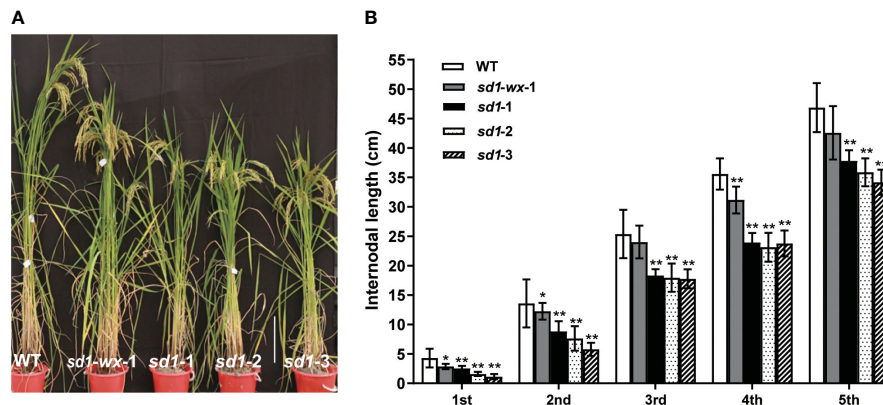


FIGURE 2 Phenotypes of *sd1* and WT lines. (A) The plant height between mutant lines and WT lines at heading stage. Bar = 25 cm. (B) Internode length of mutant and WT lines. **indicates the significant difference ($p < 0.01$).

Development of glutinous rice with decreased amylose content in grains

To determine the grain quality of mutant lines, amylose content (AC) was investigated. The amylose content of the mutant line $XDW^{sd1-wx-1}$ and XDW^{wx-1} were 5.4% and 5.2%, respectively, which showed a sharp decrease compared with the wild type (Figure 4N). All brown rice from the mutant line $XDW^{sd1-wx-1}$ and XDW^{wx-1} exhibited an opaque appearance (Figure 4E, I). In contrast, the WT grains had an AC of 22.5% (Figure 4N), and most of the grains displayed a transparent appearance (Figure 4A). Alongside the AC, the gel consistency (GC) in the $XDW^{sd1-wx-1}$ and XDW^{wx-1} mutant line showed a significant increase compared to that of WT (Figure 4O). To investigate the microstructural features of mature endosperm, we examined cross sections of the grains using a scanning electron microscope (SEM). The results revealed numerous small cavities in the core of starch granules within the glutinous endosperm of the $XDW^{sd1-wx-1}$ and XDW^{wx-1} mutant line (Figures 4F-H, J-L). Interestingly, similar structures were absent in starch granules from transparent WT grains (Figures 4B-D). These small cavities within the starch granules may account for the observed differences in physicochemical properties and transparency between WT and the $XDW^{sd1-wx-1}$ and XDW^{wx-1} mutant line. The gelatinization characteristics of starch in urea solution can reflect whether the physicochemical properties of rice have changed. Both WT and *wx* mutant line starch powder were dissolved in urea solution with different concentrations (0–9 mol/L). Intriguingly, we observed that at 0–3 mol/L urea concentrations, both starch varieties exhibited a certain resistance to dissolution. However, there were notable changes when the urea concentration elevated to the range of 4–9 mol/L. Starch powder of mutant line $XDW^{sd1-wx-1}$ and XDW^{wx-1} began to dissolve in a small amount in 4 mol/L urea solution, while the WT was difficult to dissolve (Figure 4M). These findings underscore a shift in the physicochemical attributes of starch subsequent to the editing of the *Wx* gene. In order to better evaluate the eating and cooking quality (ECQ), we examined the GT (gelatinization temperature) values by the alkali spreading score (ASS). According to the alkali

spreading value, the rice can be categorized into four types according to the GT value: high GT (75–79°C), high-intermediate GT (70–74°C), intermediate GT (66–69°C), and low GT (55–65) °C. In our study, the $XDW^{sd1-wx-1}$ and XDW^{wx-1} seeds were classified as having high-intermediate GT, while the WT was classified as having low GT (Figures 4P-S). Notable alterations include a marked reduction in AC, conspicuous increases in the GC of the gel and the GT, the emergence of small perforations in the endosperm microstructure, and discernible changes in starch gelatinization dynamics when exposed to urea solutions. These results indicate that the edited mutant line $XDW^{sd1-wx-1}$ and XDW^{wx-1} have the characteristics of glutinous rice with good rice quality.

Performance of agronomic and quality traits

To evaluate the impact of the *sd1-wx* double mutant lines on yield, we conducted a comprehensive analysis of major agronomic traits across multiple generations, ranging from T_1 to T_3 (Table 2). Consistently, the results demonstrated discernible effects of the mutations persisting through subsequent generations. Panicle numbers (PN) exhibited no significant difference between the WT plants and mutant lines, indicating a degree of stability in this trait. Significant variations emerged in certain semi-dwarf lines, with shorter panicle length (PL) and lower seed setting rates (SSR). Grain number per panicle (GNPP) displayed no marked distinctions in most mutants when compared to the WT, although specific *sd1-3* mutant lines exhibited diverse effects. Notably, the XDW^{sd1-3} mutant line, characterized by minimal plant height, exhibited substantial reductions in PL, GNPP, SSR, 1000-grain weight (GW), and yield per plant (YPP) compared to the WT. Intriguingly, it displayed longer grain length (GL) (Figure 3A). Of particular interest is the semi-dwarf $XDW^{sd1-wx-1}$ double mutant line, which demonstrated a comparable yield per plant to the WT. Across T_1 to T_3 generations, the YPP for WT and $XDW^{sd1-wx-1}$ double mutant line exhibited changes from 24.15 g to 25.26 g, 26.32 g to 26.78 g, and 31.97 g to 31.83 g, respectively. Besides, other

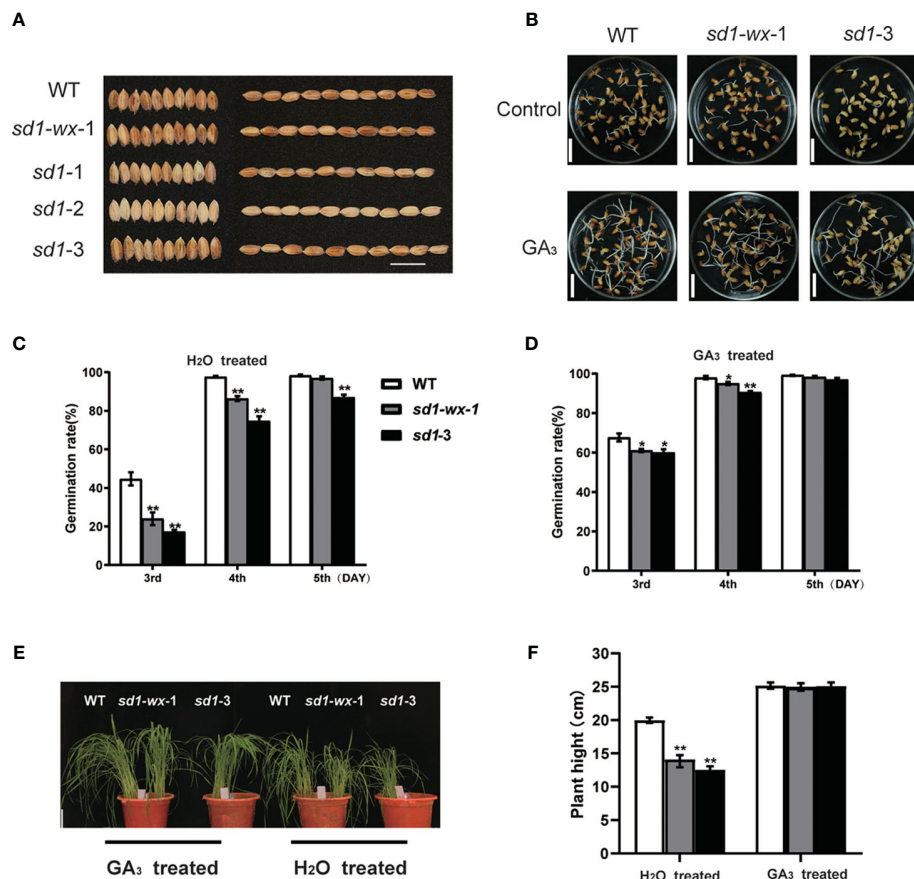


FIGURE 3

Seed germination and effect of exogenous GA₃ in mutant lines and WT. (A) The grain phenotype of mutant line and WT; Bar = 15 mm. (B) Germination phenotypes of WT, *sd1-wx-1*, and *sd1-3*. The germination phenotypes are shown at the 3th day after imbibition. Bar = 15 mm. The germination rates of WT, *sd1-wx-1*, and *sd1-3* under 4 μM GA₃ treated (C) and H₂O treated (D). Seed germination was measured after soaking for 2 days in treatment solution and then imbibing for 3 days. We recorded germination rates from day 3 to day 5. (E) Seedlings phenotype (30 day) of WT and *sd1-3* and *sd1-wx-1* under 10 μM GA₃ treated and H₂O treated, respectively. Bar = 4 cm. (F) The plant height of WT and *sd1-wx-1* and *sd1-3* under 10 μM GA₃ treated and H₂O treated, ^{ns} and ^{**} indicates the non-significant and significant difference at $p < 0.01$.

agronomic traits between WT and XDW^{*sd1-wx-1*} double mutant line showed no significant differences. This suggests that XDW^{*sd1-wx-1*} double mutant line holds promise as a potential breeding material. The application of CRISPR/Cas9-based mutagenesis targeting *Wx* and *SD1* in generating semi-dwarf glutinous elite rice lines could contribute to enhanced genetic diversity, ultimately benefiting rice yield and quality.

Transcriptomic analysis in *sd1-wx* double mutants

To evaluate the impact of the *sd1-wx* knockout double mutant line on the rice transcriptome, we employed RNA-seq analysis on both *sd1-wx* double mutant and WT plants at the heading stage. Comparison of the transcriptomes of WT and *sd1-wx* mutant stems during the heading stage revealed 1665 DEGs, with 787 downregulated and 878 upregulated genes (Figures 5A, B; Supplementary Table S3). Employing GOseq30 for functional categorization, the DEGs were classified into 76 subclasses (Supplementary Table S5). The enriched GO terms are

predominantly related to molecular functions and biological processes. Notably, the DEGs were significantly involved in biological processes and cellular components, with 54 secondary items exhibiting substantial enrichment (p value < 0.01 and p adjust value < 0.01). Among these, the top five items were apoplast (gene ratio 3.96%, GO:0048046), anchored component of membrane (gene ratio 3.14%, GO: 0031225), hydrogen peroxide catabolic process (gene ratio 2.72%, GO:0042744), peroxidase activity (gene ratio 2.72%, GO:0004601), and terpene synthase activity (gene ratio 1.90%, GO:0010333).

To further understand the biological function, we delving into biological pathways via KEGG pathways. 194 out of the 1665 DEGs were implicated in 12 pathways (Supplementary Table S4). The top two enriched pathways were phenylpropanoid biosynthesis (ko00940, gene ratio 10.50%) and diterpenoid biosynthesis (ko00904, gene ratio 4.11%), aligning with the results obtained from GO analysis. These pathways included annotations in peroxidase activity and terpene synthase activity. Additionally, other pathways such as photosynthesis-antenna proteins, pentose and glucuronate interconversions, flavonoid biosynthesis, tryptophan metabolism, MAPK signaling pathway-plant, amino

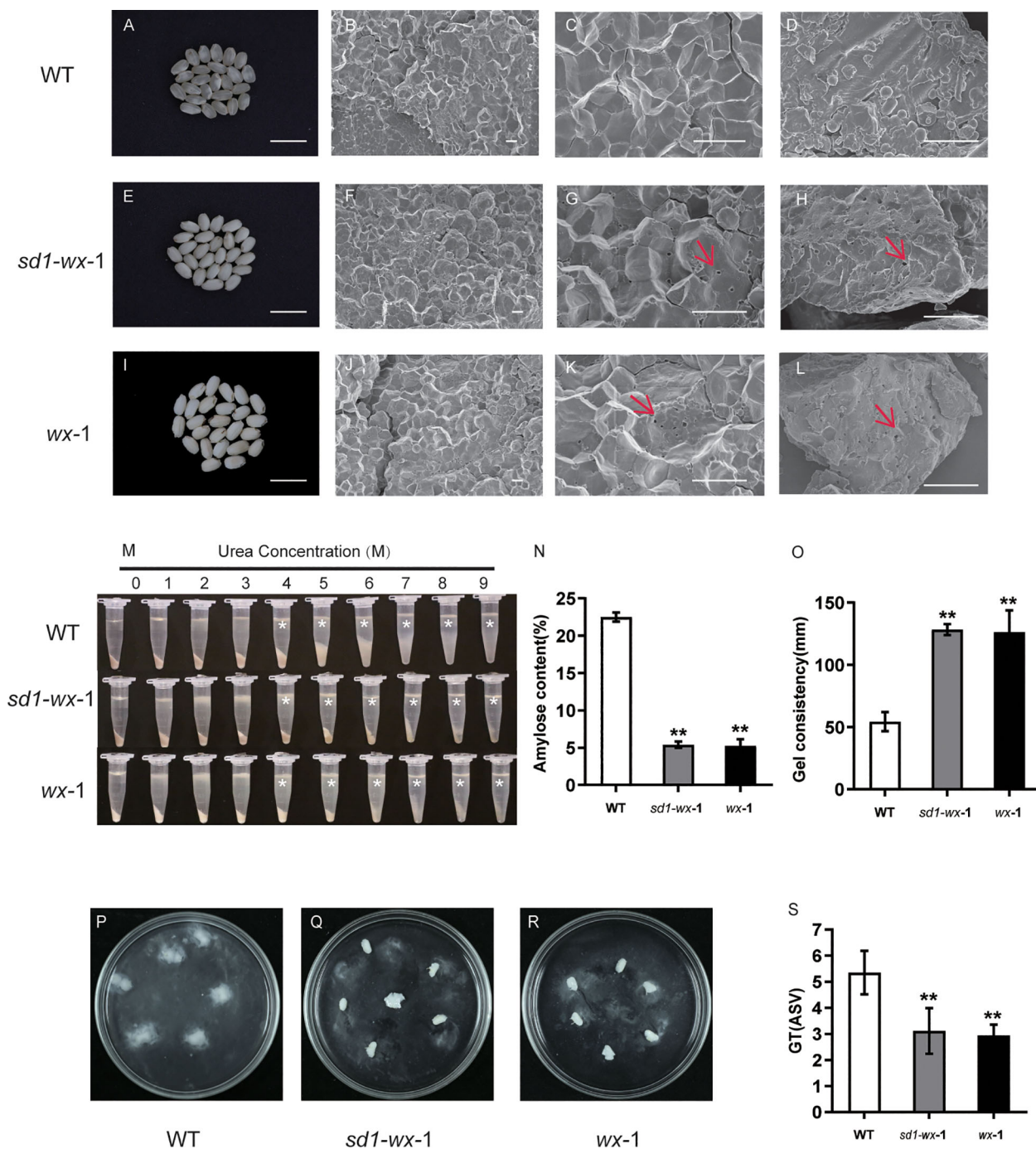


FIGURE 4

An analysis of starch phenotypic and physicochemical characteristics in WT and *wx* mutants. Comparative analysis of brown rice appearance between WT (A) and *sd1-wx-1* (E) and *wx-1* (I); Bar = 1 cm. Scanning electron microscopy images of cross sections of the WT (B, C) and *sd1-wx-1* mutant (F, G) grains and *wx-1* (J, K). Scale bars, 10 μ m and magnifications of 1,000 \times in (B, F, J); 10 μ m and magnifications of 3,000 \times in (C, G, K). Scanning electron microscope images of WT (D) and *sd1-wx-1* mutant (H) and *wx-1* (L) brown rice powders. Scale bars, 10 μ m and magnifications of 3,000 \times in (D, H, L). Small cavities are marked by red arrows. (M) Gelatinization properties of starch in urea solutions. Starch powder of WT and *sd1-wx-1* and *wx-1* was mixed with different concentrations of urea solution. * indicate the starch from the endosperm of *sd1-wx-1* and *wx-1* were more difficult to gelatinize than that from the endosperm of WT in urea solutions of 4–9 M. (N) The amylose content in endosperm of WT and *sd1-wx-1* and *wx-1*. (O) The gel consistency in endosperm of WT and *sd1-wx-1* and *wx-1*. The seed alkali spreading score (ASS) during WT (P) and *sd1-wx-1* (Q) and *wx-1* (R). The GT (gelatinization temperature) values were estimated indirectly by the alkali spreading score (ASS) during WT and *sd1-wx-1* and *wx-1* (S). ** indicate statistical significance between WT and *wx* mutant lines at $p < 0.01$.

TABLE 2 Major agronomic traits in WT and mutant lines from T₁ generation to T₃ generation.

Gener- ation	Line	PN	PL	GNPP	SSR(%)	1000- GW(g)	YPP(g)	GL (mm)	GW (mm)	GT(mm)
T ₁	WT	7.1 ± 1.5	27.38 ± 0.72	122.9 ± 10.3	83.7 ± 4.2	27.88 ± 0.43	24.15 ± 3.81	7.30 ± 0.09	3.60 ± 0.05	2.24 ± 0.07
	<i>sd1-wx-1</i>	7.3 ± 1.6 ^{ns}	26.04 ± 1.47*	126.5 ± 14.3 ^{ns}	76.3 ± 3.9**	27.29 ± 0.75 ^{ns}	25.26 ± 6.50 ^{ns}	7.27 ± 0.06 ^{ns}	3.59 ± 0.08 ^{ns}	2.22 ± 0.08 ^{ns}
	<i>sd1-1</i>	6.9 ± 0.9 ^{ns}	24.46 ± 0.78**	126.1 ± 21.1 ^{ns}	73.2 ± 4.4**	26.12 ± 1.77*	22.39 ± 3.96 ^{ns}	7.21 ± 0.08*	3.48 ± 0.07**	2.14 ± 0.08**
	<i>sd1-2</i>	6.8 ± 0.9 ^{ns}	25.15 ± 0.76**	123.9 ± 12.4 ^{ns}	72.2 ± 5.1**	27.06 ± 1.39 ^{ns}	22.45 ± 3.32 ^{ns}	7.34 ± 0.08 ^{ns}	3.64 ± 0.05 ^{ns}	2.20 ± 0.09**
	<i>sd1-3</i>	5.4 ± 1.1*	23.10 ± 0.99**	97.7 ± 16.2**	59.4 ± 3.6**	24.62 ± 1.12**	12.31 ± 2.10**	7.41 ± 0.07**	3.59 ± 0.09 ^{ns}	2.15 ± 0.08**
T ₂	WT	7.0 ± 1.4	24.02 ± 0.64	133.6 ± 9.2	85.0 ± 2.1	27.98 ± 0.88	26.32 ± 6.25	7.45 ± 0.11	3.70 ± 0.02	2.28 ± 0.07
	<i>sd1-wx-1</i>	7.4 ± 1.4 ^{ns}	23.59 ± 1.25 ^{ns}	133.2 ± 16.4 ^{ns}	80.8 ± 3.9 ^{ns}	27.35 ± 1.08 ^{ns}	26.78 ± 2.79 ^{ns}	7.48 ± 0.19 ^{ns}	3.69 ± 0.06 ^{ns}	2.23 ± 0.09**
	<i>sd1-1</i>	7.2 ± 1.9 ^{ns}	22.22 ± 0.84**	134.8 ± 18.5 ^{ns}	86.6 ± 4.7 ^{ns}	25.27 ± 0.92**	24.08 ± 3.11 ^{ns}	7.36 ± 0.08*	3.52 ± 0.08**	2.16 ± 0.07**
	<i>sd1-2</i>	6.7 ± 0.9 ^{ns}	23.31 ± 0.24**	133.2 ± 9.4 ^{ns}	74.8 ± 5.6**	25.84 ± 0.86**	22.95 ± 3.70 ^{ns}	7.55 ± 0.11*	3.66 ± 0.04*	2.22 ± 0.07**
	<i>sd1-3</i>	6.8 ± 1.0 ^{ns}	22.37 ± 0.83**	96.8 ± 10.6**	69.2 ± 3.4**	25.14 ± 0.95**	16.5 ± 2.47**	7.60 ± 0.09**	3.62 ± 0.05**	2.19 ± 0.08**
T ₃	WT	8.4 ± 0.5	28.50 ± 0.69	142.9 ± 13.5	78.9 ± 2.8	26.66 ± 0.74	31.97 ± 3.47	7.40 ± 0.09	3.77 ± 0.03	2.25 ± 0.07
	<i>sd1-wx-1</i>	9.0 ± 1.1 ^{ns}	25.18 ± 1.14**	136.1 ± 11.3 ^{ns}	75.6 ± 2.6 ^{ns}	26.12 ± 0.85 ^{ns}	31.83 ± 5.25 ^{ns}	7.40 ± 0.08 ^{ns}	3.78 ± 0.05 ^{ns}	2.23 ± 0.08 ^{ns}
	<i>sd1-1</i>	9.1 ± 1.6 ^{ns}	24.08 ± 1.09**	125.1 ± 10.7*	70.0 ± 2.6**	25.57 ± 0.32**	29.27 ± 5.72 ^{ns}	7.38 ± 0.07 ^{ns}	3.73 ± 0.05*	2.09 ± 0.07**
	<i>sd1-2</i>	9.3 ± 1.1 ^{ns}	24.36 ± 1.16**	123.7 ± 13.8*	64.1 ± 1.2**	25.78 ± 0.39**	29.50 ± 1.23 ^{ns}	7.55 ± 0.10**	3.79 ± 0.08 ^{ns}	2.20 ± 0.05**
	<i>sd1-3</i>	9.0 ± 0.7 ^{ns}	23.62 ± 0.82**	87.4 ± 11.8**	61.3 ± 4.9**	25.67 ± 0.33**	20.37 ± 4.34**	7.79 ± 0.10**	3.76 ± 0.05 ^{ns}	2.18 ± 0.09**

The data are the means of at least five duplicates. WT means wild-type, PN means panicle numbers, PL means panicle length, GNPP means grain number per panicle, SSR means seed setting rate, 1000-GW means 1000-grain weight, YPP means yield per plant, GL means grain length. GW means grain width and GT means grain thickness. * represent the significant difference $p < 0.05$, ^{ns} and ** represent the non-significant difference and significant difference at $p < 0.01$.

sugar and nucleotide sugar metabolism, plant-pathogen interaction, sesquiterpenoid and triterpenoid biosynthesis, cutin, suberine and wax biosynthesis, and biosynthesis of unsaturated fatty acids were identified (Figure 5C; Supplementary Table S4). Furthermore, we found that most of the DEGs related to diterpenoid biosynthesis were down-regulated in *sd1-wx* double mutants. There were 18 genes associated with diterpenoid biosynthesis, including two gene encoding ent-copalyl diphosphate synthase (*OsCPS2*, *OsCPS4*), which is the first key enzyme catalyzes gibberellin biosynthesis pathway, five genes encoding terpene synthase/ent-kaurene synthase (*OsKS3*, *OsKS4*, *OsKS5*, *OsKSL8*, *OsKSL10*), which is the second enzyme in the gibberellin synthesis step, one gene encoding ent-kaurene oxidase (*OsKO1*), six genes encoding cytochrome P450, two genes encoding short-chainalcohol dehydrogenase (*OsSDR110C-MS1*, *OsSDR110C-MS2*), two gene encoding

gibberellin biosynthesis gene (*OsGA20ox3*, *OsGA3ox2*) (Figure 6; Supplementary Table S2). This comprehensive RNA-seq analysis at the stem level unequivocally confirms the influence of *sd1* knockout on the expression of gibberellin biosynthesis-related genes.

To validate the DEGs identified from the RNA-seq analysis, we used RT-qPCR to determine the expression levels of the DEGs. We randomly selected 6 genes that were significantly up-regulated or down-regulated compared to WT. The results showed that the expression levels of three randomly selected up-regulated DEGs, *LOC_Os01g55200* (*KAT1*), *LOC_Os09g17740* (*LHCB1.3*), and *LOC_Os03g39610* (*LHCB2*) RT-qPCR results were greatly reduced, while three randomly selected down-regulated DEGs, *LOC_Os01g71340* (*PR2*), *LOC_Os07g48020* (*POX22.3*), and *LOC_Os11g37970* (*PR4a*) RT-qPCR results were greatly increased (Figures 5E-J). The RT-qPCR results were in good agreement with the RNA-seq analysis.

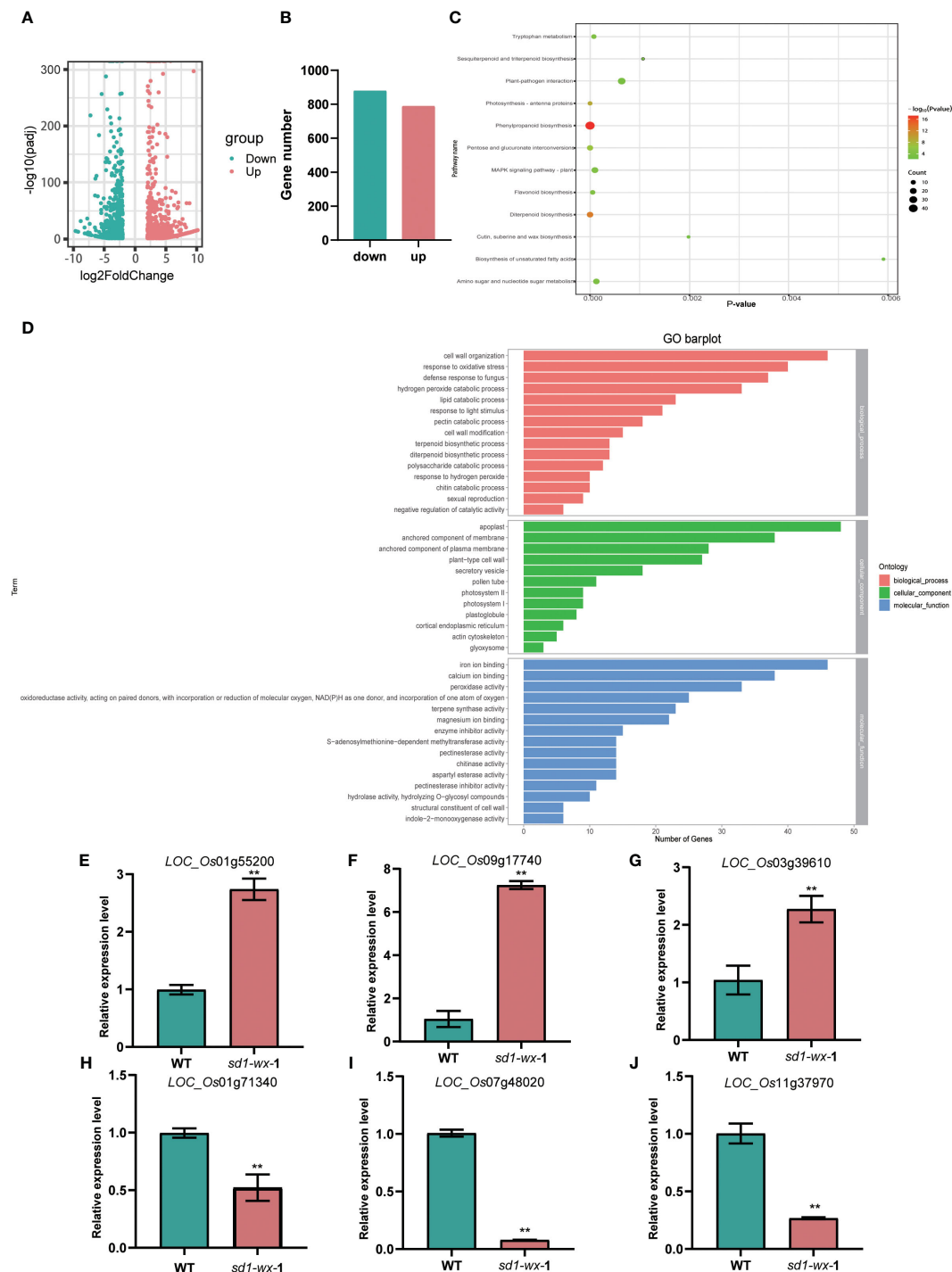


FIGURE 5

RNA-seq analysis between the *sd1-wx* and WT. (A) Volcano plot displaying DEGs between the *sd1-wx* and WT. (B) The number of DEGs in *sd1-wx* double mutant lines. (C) KEGG classifications of DEGs. Enrichment 12 significant pathways (both *p* value and *p* adjust value < 0.05). (D) GO analysis of the DEGs. Enriched significant different GO terms with both *p* value and *p* adjust value < 0.05. (E–J) RT-qPCR to confirm the transcript level of down-regulated genes *LOC_Os01g71340* (*PR2*), *LOC_Os07g48020* (*POX22.3*), and *LOC_Os11g37970* (*PR4a*) and up-regulated genes *LOC_Os01g55200* (*KAT1*), *LOC_Os09g17740* (*LHCB1.3*), and *LOC_Os03g39610* (*LHCB2*) at the stem.

Discussion

The quality of rice and its resistance to lodging are pivotal factors influencing both grain quality and yield potential. These traits are primarily governed by the major genes *Wx* and *SD1*,

respectively. Using CRISPR/Cas9 genome editing technology for crop improvement has demonstrated remarkable efficiency. In the present study, we not only employed this technology to generate *Wx* gene or *SD1* gene knockout single mutant, but also utilized it to produce *sd1-wx* double mutants. Ultimately, this approach led to

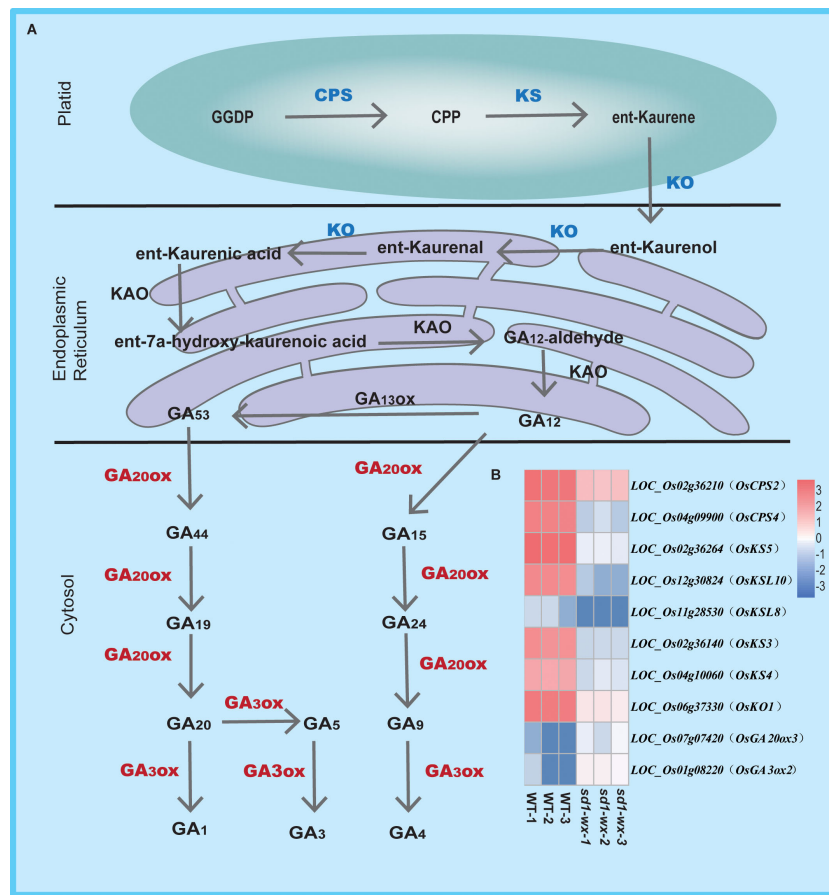


FIGURE 6

Pathway of gibberellin biosynthesis in WT and *sd1* knockout plants. (A) Pathway of gibberellin biosynthesis. (B) Heatmap analysis of the expression of 10 DEGs associated with gibberellin biosynthesis. Note: red indicates up-regulated genes, blue indicates down-regulated genes.

the development of elite rice lines with desirable traits, characterized by semi-dwarfism and glutinous properties. In addition, our investigation extended beyond genetic modifications to encompass a comprehensive analysis of various agronomic traits, quality attributes, physiological characteristics and physical properties of the modified plants. Furthermore, a comparative RNA-seq analysis was performed on both *sd1-wx* double mutants and WT plants. The integrative analysis of transcriptomic and physiological data of *sd1-wx* double mutants knockout lines could deepen our understanding of the development of plant height and amylose metabolism in rice.

In our current investigation, we have successfully generated an exceptional breeding line, denoted as XDW^{*sd1-wx-1*}, featuring double mutant plants. Notably, this edited line exhibited a reduction in endogenous gibberellin content, leading to a decrease in plant height, although it does not represent the absolute minimum height within the mutant lines, and a concomitant decline in amylose content. Interestingly, despite these alterations, agronomic traits, yield parameters, and seed germination rates demonstrated no statistically significant differences. Our findings align with previous reports highlighting the efficacy of CRISPR/Cas9 genome editing technology in manipulating the *SD1* gene to achieve lower plant height and enhanced yield potential (Han et al.,

2019; Hu et al., 2019; Nawaz et al., 2020). Some researchers have suggested that although plant height decreases, seed yield remains unaffected due to the selective expression of *GA20ox-2* in young tissues, while its homologous gene, *GA20ox-1*, is preferentially expressed in unopened flowers (Sasaki et al., 2002). Our exploration further uncovered intriguing characteristics in the XDW^{*sd1-3*} mutant line, characterized by the lowest endogenous gibberellin content and the most diminutive plant height among the mutants. Despite a lower seed setting rate, this mutant line exhibited an elongated grain length. The observed decrease in seed setting rate may be attributed to the absence of endogenous gibberellin content, potentially disrupting pollen development, as suggested by prior studies (Sakata et al., 2014).

Maintaining an optimal plant height is paramount for enhancing rice lodging resistance and overall yield. In our study, we engineered various alleles of the *SD1* gene, resulting in distinct plant height phenotypes. Specifically, the transgenic plants XDW^{*sd1-2*} and XDW^{*sd1-3*} harbored 1-bp and 23-bp nucleotide deletions in *SD1*, respectively. These deletions induced frame-shift mutations, predicting the translation of non-functional truncated proteins that disrupted gibberellin function. Consequently, these mutants exhibited the shortest plant height compared to the WT plants. Our observations extended to XDW^{*sd1-wx-1*} and XDW^{*sd1-1*} transgenic

plants, carrying 3-bp and 18-bp nucleotide deletions at the first exon of the *SD1* gene. These deletions caused either one or six amino acid deletions in the *SD1* protein, respectively. Intriguingly, we also found that *XDW^{sd1-wx-1}* and *XDW^{sd1-1}* transgenic plants displayed varying degrees of endogenous gibberellin content and plant height reduction compared to the WT plants. The *SD1* gene encodes gibberellin 20 oxidase 2, a pivotal enzyme in gibberellin biosynthesis. However, despite its crucial role, the *SD1* gene did not emerge as differentially expressed in the comparative transcriptome analysis between *sd1-wx-1* and WT plants. This anomaly suggests that the deletion of one or six amino acids might disrupt the catalytic activity of gibberellin 20 oxidase 2, thereby impairing the gibberellin metabolic pathway.

Gibberellins, a class of diterpenoids, are widely distributed in plants and are primarily synthesized in the young apical parts of plants (Hedden, 2020). The synthesis of gibberellins begins with the precursor geranylgeranyl diphosphate (GGPP), which undergoes sequential catalysis by ent-copalyl diphosphate synthase (CPS), ent-kaurenoic acid oxidase (KAO), ent-kaurene oxidase (KO), and ent-kaurene synthase (KS) to culminate in the formation of GA₁₂, an integral intermediate in the gibberellin biosynthetic pathway (Hedden and Thomas, 2012; Hedden and Sponsel, 2015; Salazar-Cerezo et al., 2018; Hedden, 2020). Our study, utilizing comparative transcriptome analysis, unveiled a significant enrichment and down-regulation of differentially expressed genes associated with diterpenoid biosynthesis. Particularly noteworthy were the findings that two genes encoding CPS, five genes encoding KS, and one gene encoding KO were substantially down-regulated in *sd1-wx* double mutants. This observation raises the possibility that the compromised catalytic activity of gibberellin 20 oxidase 2 restricts the efficient conversion of GGPP to GA₁₂ (Figure 6). Interestingly, we also found that two genes encoding gibberellin oxidase (*OsGA20ox3*, *OsGA3ox2*) exhibited remarkable up-regulated expression patterns in *sd1-wx* double mutants. This increased expression of gibberellin oxidase genes suggests a potential compensatory mechanism in response to the compromised function of gibberellin 20 oxidase 2. The up-regulation of these genes might serve to augment the production of downstream gibberellin compounds, offsetting the limitations imposed by the impairment in GA₁₂ biosynthesis.

In our transcriptome analysis, we unearthed compelling insights into the regulatory landscape of gene expression. Phenylpropanoid biosynthesis emerged as the most significantly enriched pathway in the KEGG analysis, leading to 46 DEGs. Furthermore, the hydrogen peroxide catabolic process (enriched with 33 genes) and peroxidase activity (also enriched with 33 genes) could act as the most prominently enriched terms in the GO analysis (Figure 5D; Supplementary Table S5). These findings underscore a pronounced modulation of the phenylpropanoid metabolism machinery in *sd1-wx* double mutants. Noteworthy is the absence of down-regulation of the *Wx* gene expression in *sd1-wx* double mutants compared to the WT plants, as revealed by our transcriptome analysis. Equally intriguing is the lack of enrichment

for genes related to the starch metabolism pathway. This discrepancy can be attributed to the specific high expression of *Wx* genes in the endosperm, contrasting with their low expression in the stem, a dynamic that underscores the intricacies of gene expression patterns in different plant tissues.

In conclusion, our study harnessed the precision of the CRISPR/Cas9 gene editing system to modify both the *SD1* and *Wx* genes in Xiangdaowan (XDW) rice, an elite landrace known for its robust aromatic properties. Across various generations, we successfully generated genetically stable, semi-dwarf glutinous rice lines, ensuring homozygosity. These edited lines exhibited a spectrum of alterations, including reduced gibberellin content, diminished plant height, lower AC, elevated GC, modified starch gelatinization characteristics in urea solutions, and the development of small holes in the endosperm microstructure. Notably, the germination rate and other key agronomic traits remained unaffected. To compensate for the growth defects associated with endogenous gibberellin deficiency, we applied exogenous GA₃, revealing its potential to mitigate the observed growth-related issues. Our comparative transcriptome analysis uncovered that the compromised catalytic activity of gibberellin 20 oxidase 2 played a pivotal role in limiting the metabolism of diterpenoid biosynthesis. Taken together, our results highlight the efficacy of CRISPR/Cas9 technology in enhancing both plant height and grain quality in rice. By strategically manipulating key genes, we achieved improvements that not only offer agronomic benefits but also hold the potential to increase overall yield and enhance the quality of the crop.

Data availability statement

The original contributions presented in the study are included in the article/Supplementary Material. Further inquiries can be directed to the corresponding author.

Author contributions

QW: Conceptualization, Data curation, Formal analysis, Funding acquisition, Project administration, Resources, Validation, Visualization, Writing – original draft, Writing – review & editing. HG: Data curation, Formal analysis, Investigation, Methodology, Software, Writing – review & editing. KLi: Data curation, Formal analysis, Investigation, Methodology, Software, Writing – review & editing. HW: Data curation, Formal analysis, Methodology, Software, Writing – review & editing. FZ: Data curation, Formal analysis, Investigation, Software, Writing – review & editing. LW: Formal analysis, Investigation, Methodology, Software, Writing – review & editing. KLu: Formal analysis, Investigation, Software, Writing – review & editing. ML: Formal analysis, Software, Writing – review & editing. YS: Formal analysis, Software, Writing – review & editing. JZ: Funding acquisition, Validation, Writing – review & editing. WZ:

Funding acquisition, Validation, Writing – review & editing. BP: Funding acquisition, Validation, Writing – review & editing. HY: Conceptualization, Project administration, Resources, Supervision, Validation, Writing – original draft, Writing – review & editing.

Funding

The author(s) declare financial support was received for the research, authorship, and/or publication of this article. The research work was supported by grant (31801332, 31901533, U2004141) of the National Natural Science Foundation of China, Scientific and Technological Frontiers in Project of Henan Province (222102110115, 212102110249), Key Scientific Research Projects of Universities in Henan Province (24B210016), and Nanhu Scholars Program for Young Scholars of XYNU.

Acknowledgments

We thank Xinyang Academy of Agricultural Sciences for providing rice varieties.

References

- Asano, K., Takashi, T., Miura, K., Qian, Q., Kitano, H., Matsuoka, M., et al. (2007). Genetic and molecular analysis of utility of *sdl* alleles in rice breeding. *Breed. Sci.* 57, 53–58. doi: 10.1270/jsbbs.57.53
- Ayres, N., Mcclung, A., Larkin, P., Bligh, H., Jones, C., and Park, W. (1997). Microsatellites and a single-nucleotide polymorphism differentiate apparent amylose classes in an extended pedigree of US rice germ plasm. *Theor. Appl. Genet.* 94, 773–781. doi: 10.1007/s001220050477
- Bao, J., Shen, S., Sun, M., and Corke, H. (2006). Analysis of genotypic diversity in the starch physicochemical properties of nonwaxy rice: apparent amylose content, pasting viscosity and gel texture. *Starch-Stärke* 58, 259–267. doi: 10.1002/star.200500469
- Berry, P., Sterling, M., Spink, J., Baker, C., Sylvester-Bradley, R., Mooney, S., et al. (2004). Understanding and reducing lodging in cereals. *Adv. Agron.* 84, 215–269. doi: 10.1016/S0065-2113(04)84005-7
- Cai, X. L., Wang, Z. Y., Xing, Y. Y., Zhang, J. L., and Hong, M. M. (1998). Aberrant splicing of intron 1 leads to the heterogeneous 5' UTR and decreased expression of waxy gene in rice cultivars of intermediate amylose content. *Plant J.* 14, 459–465. doi: 10.1046/j.1365-3113X.1998.00126.x
- Chandler, V. L., and Wessler, S. (2001). Grasses. A collective model genetic system. *Plant Physiol.* 125, 1540. doi: 10.2307/4279780
- Demont, M., and Stein, A. J. (2013). Global value of GM rice: a review of expected agronomic and consumer benefits. *New Biotechnol.* 30, 426–436. doi: 10.1016/j.nbt.2013.04.004
- Han, Y., Luo, D., Usman, B., Nawaz, G., Zhao, N., Liu, F., et al. (2018). Development of high yielding glutinous cytoplasmic male sterile rice (*Oryza sativa* L.) lines through CRISPR/Cas9 based mutagenesis of *Wx* and *TGW6* and proteomic analysis of anther. *Agronomy* 8, 290. doi: 10.3390/agronomy8120290
- Han, Y., Teng, K., and Nawaz, G. (2019). Generation of semi-dwarf rice (*Oryza sativa* L.) lines by CRISPR/Cas9-directed mutagenesis of *OsGA20ox2* and proteomic analysis of unveiled changes caused by mutations. *3 Biotech.* 9, 387. doi: 10.1007/s13205-019-1919-x
- Hedden, P. (2020). The current status of research on gibberellin biosynthesis. *Plant Cell Physiol.* 61, 1832–1849. doi: 10.1093/pcp/pcaa092
- Hedden, P., and Sponsel, V. (2015). A century of gibberellin research. *J. Plant Growth Regul.* 34, 740–760. doi: 10.1007/s00344-015-9546-1
- Hedden, P., and Thomas, S. G. (2012). Gibberellin biosynthesis and its regulation. *Biochem. J.* 444, 11–25. doi: 10.1042/BJ20120245
- Hu, X., Cui, Y., Dong, G., Feng, A., Wang, D., Zhao, C., et al. (2019). Using CRISPR-Cas9 to generate semi-dwarf rice lines in elite landraces. *Sci. Rep.* 9, 19096. doi: 10.1038/s41598-019-55757-9
- Huang, L., Gu, Z., Chen, Z., Yu, J., Chu, R., Tan, H., et al. (2021). Improving rice eating and cooking quality by coordinated expression of the major starch synthesis-related genes, *SSII* and *Wx*, in endosperm. *Plant Mol. Biol.* 106, 419–432. doi: 10.1007/s11103-021-01162-8
- Jiang, W., Zhou, H., Bi, H., Fromm, M., Yang, B., and Weeks, D. P. (2013). Demonstration of CRISPR/Cas9/sgrRNA-mediated targeted gene modification in Arabidopsis, tobacco, sorghum and rice. *Nucleic Acids Res.* 41, e188. doi: 10.1093/nar/gkt780
- Khush, G. S. (2005). What it will take to feed 5.0 billion rice consumers in 2030. *Plant Mol. Biol.* 59, 1–6. doi: 10.1007/S11103-005-2159-5
- Kumar, I., and Khush, G. (1986). Gene dosage effects of amylose content in rice endosperm. *Japan. J. Genet.* 61, 559–568. doi: 10.1266/jjg.61.559
- Larkin, P. D., and Park, W. D. (2003). Association of waxy gene single nucleotide polymorphisms with starch characteristics in rice (*Oryza sativa* L.). *Mol. Breed.* 12, 335–339. doi: 10.1023/B:MOLB.0000006797.51786.92
- Li, H., and Gilbert, R. G. (2018). Starch molecular structure: The basis for an improved understanding of cooked rice texture. *Carbohydr. Polymers* 195, 9–17. doi: 10.1016/j.carbpol.2018.04.065
- Li, Z., Liu, Z.-B., Xing, A., Moon, B. P., Koellhoffer, J. P., Huang, L., et al. (2015). Cas9-guide RNA directed genome editing in soybean. *Plant Physiol.* 169, 960–970. doi: 10.1104/pp.15.00783
- Li, H., Prakash, S., Nicholson, T. M., Fitzgerald, M. A., and Gilbert, R. G. (2016). The importance of amylose and amylopectin fine structure for textural properties of cooked rice grains. *Food Chem.* 196, 702–711. doi: 10.1016/j.foodchem.2015.09.112
- Liang, Z., Zhang, K., Chen, K., and Gao, C. (2014). Targeted mutagenesis in Zea mays using TALENs and the CRISPR/Cas system. *J. Genet. Genomics* 41, 63–68. doi: 10.1016/j.jgg.2013.12.001
- Liu, L., Ma, X., Liu, S., Zhu, C., Jiang, L., Wang, Y., et al. (2009). Identification and characterization of a novel Waxy allele from a Yunnan rice landrace. *Plant Mol. Biol.* 71, 609–626. doi: 10.1007/s11103-009-9544-4
- Liu, F., Wang, P., Zhang, X., Li, X., Yan, X., Fu, D., et al. (2018). The genetic and molecular basis of crop height based on a rice model. *Planta* 247, 1–26. doi: 10.1007/s00425-017-279
- Livak, K. J., and Schmittgen, T. D. (2001). Analysis of relative gene expression data using real-time quantitative PCR and the $2^{-\Delta\Delta CT}$ method. *Methods* 25, 402–408. doi: 10.1006/meth.2001.1262
- Magome, H., Nomura, T., Hanada, A., Takeda-Kamiya, N., Ohnishi, T., Shinma, Y., et al. (2013). *CYP714B1* and *CYP714B2* encode gibberellin 13-oxidases that reduce

Conflict of interest

The authors declare that the research was conducted in the absence of any commercial or financial relationships that could be construed as a potential conflict of interest.

Publisher's note

All claims expressed in this article are solely those of the authors and do not necessarily represent those of their affiliated organizations, or those of the publisher, the editors and the reviewers. Any product that may be evaluated in this article, or claim that may be made by its manufacturer, is not guaranteed or endorsed by the publisher.

Supplementary material

The Supplementary Material for this article can be found online at: <https://www.frontiersin.org/articles/10.3389/fpls.2024.1333191/full#supplementary-material>

- gibberellin activity in rice. *Proc. Natl. Acad. Sci.* 110, 1947–1952. doi: 10.1073/pnas.1215788110
- Mao, Y., Zhang, H., Xu, N., Zhang, B., Gou, F., and Zhu, J.-K. (2013). Application of the CRISPR–Cas system for efficient genome engineering in plants. *Mol. Plant* 6, 2008–2011. doi: 10.1093/mp/sst121
- Marciniak, K., Kućko, A., Wilmowicz, E., Świdziński, M., Kęsy, J., and Kopcewicz, J. (2018). Photoperiodic flower induction in *Ipomoea nil* is accompanied by decreasing content of gibberellins. *Plant Growth Regul.* 84, 395–400. doi: 10.1093/mp/sst121
- Mikami, I., Uwatoko, N., Ikeda, Y., Yamaguchi, J., Hirano, H.-Y., Suzuki, Y., et al. (2008). Allelic diversification at the *wx* locus in landraces of Asian rice. *Theor. Appl. Genet.* 116, 979–989. doi: 10.1007/s00122-008-0729-z
- Monna, L., Kitazawa, N., Yoshino, R., Suzuki, J., Masuda, H., Maehara, Y., et al. (2002). Positional cloning of rice semidwarfing gene, *sd-1*: rice “green revolution gene” encodes a mutant enzyme involved in gibberellin synthesis. *DNA Res.* 9, 11–17. doi: 10.1093/dnares/9.1.11
- Nawaz, G., Usman, B., Zhao, N., Han, Y., Li, Z., Wang, X., et al. (2020). CRISPR/Cas9 directed mutagenesis of *OsGA20ox2* in high yielding basmati rice (*Oryza sativa* L.) line and comparative proteome profiling of unveiled changes triggered by mutations. *Int. J. Mol. Sci.* 21, 6170. doi: 10.3390/ijms21176170
- Nishimura, A., Aichi, I., and Matsuoka, M. (2006). A protocol for Agrobacterium-mediated transformation in rice. *Nat. Protoc.* 1, 2796–2802. doi: 10.1038/nprot.2006.469
- Pérez, L., Soto, E., Farré, G., Juanos, J., Villorquina, G., Bassie, L., et al. (2019). CRISPR/Cas9 mutations in the rice *Waxy*/GBSSI gene induce allele-specific and zygosity-dependent feedback effects on endosperm starch biosynthesis. *Plant Cell Rep.* 38, 417–433. doi: 10.1007/s00299-019-02388-z
- Qiao, J., Jiang, H., Lin, Y., Shang, L., Wang, M., Li, D., et al. (2021). A novel miR167a-OsARF6-OsAUX3 module regulates grain length and weight in rice. *Mol. Plant* 14, 1683–1698. doi: 10.1016/j.molp.2021.06.023
- Sakamoto, T., and Matsuoka, M. (2004). Generating high-yielding varieties by genetic manipulation of plant architecture. *Curr. Opin. Biotechnol.* 15, 144–147. doi: 10.1016/j.copbio.2004.02.003
- Sakata, T., Oda, S., Tsunaga, Y., Shomura, H., Kawagishi-Kobayashi, M., Aya, K., et al. (2014). Reduction of gibberellin by low temperature disrupts pollen development in rice. *Plant Physiol.* 164, 2011–2019. doi: 10.1104/pp.113.234401
- Salazar-Cerezo, S., Martinez-Montiel, N., Garcia-Sánchez, J., Pérez-Y-Terrón, R., and Martinez-Contreras, R. D. (2018). Gibberellin biosynthesis and metabolism: A convergent route for plants, fungi and bacteria. *Microbiol. Res.* 208, 85–98. doi: 10.1016/j.micres.2018.01.010
- Sasaki, A., Ashikari, M., Ueguchi-Tanaka, M., Itoh, H., Nishimura, A., Swapan, D., et al. (2002). Green revolution: a mutant gibberellin-synthesis gene in rice. *Nature* 416, 701–702. doi: 10.1038/416701a
- Sato, H., Suzuki, Y., Sakai, M., and Imbe, T. (2002). Molecular characterization of *Wx-mq*, a novel mutant gene for low-amylose content in endosperm of rice (*Oryza sativa* L.). *Breed. Sci.* 52, 131–135. doi: 10.1270/jsbbs.52.131
- Shan, Q., Wang, Y., Li, J., Zhang, Y., Chen, K., Liang, Z., et al. (2013). Targeted genome modification of crop plants using a CRISPR–Cas system. *Nat. Biotechnol.* 31, 686–688. doi: 10.1038/nbt.2650
- Singh, A., Gopalakrishnan, S., Singh, V., Prabhu, K., Mohapatra, T., Singh, N., et al. (2011). Marker assisted selection: a paradigm shift in Basmati breeding. *Indian J. Genet. Plant Breed.* 71, 120. doi: 10.1002/pca.1274
- Spielmeier, W., Ellis, M. H., and Chandler, P. M. (2002). Semidwarf (*sd-1*), “green revolution” rice, contains a defective gibberellin 20-oxidase gene. *Proc. Natl. Acad. Sci.* 99, 9043–9048. doi: 10.1073/pnas.132266399
- Su, Y., Rao, Y., Hu, S., Yang, Y., Gao, Z., Zhang, G., et al. (2011). Map-based cloning proves *qGC-6*, a major QTL for gel consistency of japonica/indica cross, responds by *Waxy* in rice (*Oryza sativa* L.). *Theor. Appl. Genet.* 123, 859. doi: 10.1007/s00122-011-1632-6
- Thomas, S. G., and Hedden, P. (2006). Gibberellin metabolism and signal transduction. *Annu. Plant Rev. Vol. 24: Plant Hormone Signaling* 24, 147–184. doi: 10.1002/9780470988800.ch6
- Tian, Y., Zhou, Y., Gao, G., Zhang, Q., Li, Y., Lou, G., et al. (2023). Creation of two-line fragrant glutinous hybrid rice by editing the *Wx* and *OsBADH2* genes via the CRISPR/Cas9 system. *Int. J. Mol. Sci.* 24, 849. doi: 10.1007/s11032-023-01368-2
- Wanchana, S., Toojinda, T., Tragoonrungs, S., and Vanavichit, A. (2003). Duplicated coding sequence in the waxy allele of tropical glutinous rice (*Oryza sativa* L.). *Plant Sci.* 165, 1193–1199. doi: 10.1016/S0168-9452(03)00326-1
- Wang, Q., Chen, P., Wang, H., Chao, S., Guo, W., Zhang, Y., et al. (2023). Physiological and transcriptomic analysis of *OsLHCB3* knockdown lines in rice. *Mol. Breed.* 43, 38. doi: 10.1007/s11032-023-01387-z
- Wang, Y., Cheng, X., Shan, Q., Zhang, Y., Liu, J., Gao, C., et al. (2014). Simultaneous editing of three homoeoalleles in hexaploid bread wheat confers heritable resistance to powdery mildew. *Nat. Biotechnol.* 32, 947–951. doi: 10.1038/nbt.2969
- Wang, Z.-y., Wu, Z., Xing, Y., Zheng, F., Guo, X., Zhang, W., et al. (1990). Nucleotide sequence of rice *waxy* gene. *Nucleic Acids Res.* 18, 5898. doi: 10.1093/nar/18.19.5898
- Yang, J., Guo, X., Wang, X., Fang, Y., Liu, F., Qin, B., et al. (2022). Development of soft rice lines by regulating amylose content via editing the 5' UTR of the *wx* gene. *Int. J. Mol. Sci.* 23, 10517. doi: 10.3390/ijms231810517
- Yang, J., Wang, J., Fan, F. J., Zhu, J. Y., Chen, T., Wang, C. L., et al. (2013). Development of AS-PCR marker based on a key mutation confirmed by resequencing of *Wx-mp* in Milky P rincess and its application in japonica soft rice (*Oryza sativa* L.) breeding. *Plant Breed.* 132, 595–603. doi: 10.1111/pbr.12088
- Yang, B., Xu, S., Xu, L., You, H., and Xiang, X. (2018). Effects of *Wx* and its interaction with *SSIII-2* on rice eating and cooking qualities. *Front. Plant Sci.* 9. doi: 10.3389/fpls.2018.00456
- Ye, H., Feng, J., Zhang, L., Zhang, J., Mispan, M. S., Cao, Z., et al. (2015). Map-based cloning of seed dormancy1-2 identified a gibberellin synthesis gene regulating the development of endosperm-imposed dormancy in rice. *Plant Physiol.* 169, 2152–2165. doi: 10.1104/pp.15.01202
- Yunyan, F., Jie, Y., Fangquan, W., Fangjun, F., Wenqi, L., Jun, W., et al. (2019). Production of two elite glutinous rice varieties by editing *Wx* gene. *Rice Sci.* 26, 118–124. doi: 10.1016/j.rsci.2018.04.007
- Zeng, D., Liu, T., Ma, X., Wang, B., Zheng, Z., Zhang, Y., et al. (2020). Quantitative regulation of *Waxy* expression by CRISPR/Cas9-based promoter and 5'UTR-intron editing improves grain quality in rice. *Plant Biotechnol. J.* 18, 2385. doi: 10.1111/pbi.13427
- Zhang, Q. (2007). Strategies for developing green super rice. *Proc. Natl. Acad. Sci.* 104, 16402–16409. doi: 10.1073/pnas.0708013104
- Zhang, J., Liu, X., Li, S., Cheng, Z., and Li, C. (2014). The rice semi-dwarf mutant *sd37*, caused by a mutation in *CYP96B4*, plays an important role in the fine-tuning of plant growth. *PLoS One* 9, e88068. doi: 10.1371/journal.pone.0088068
- Zhang, C., Yang, Y., Chen, S., Liu, X., Zhu, J., Zhou, L., et al. (2021a). A rare *Waxy* allele coordinately improves rice eating and cooking quality and grain transparency. *J. Integr. Plant Biol.* 63, 889–901. doi: 10.1111/jipb.13010
- Zhang, C., Yun, P., Xia, J., Zhou, K., Wang, L., Zhang, J., et al. (2023). CRISPR/Cas9-mediated editing of *Wx* and *BADH2* genes created glutinous and aromatic two-line hybrid rice. *Mol. Breed.* 43, 24. doi: 10.1007/s11032-023-01368-2
- Zhang, J., Zhang, H., Botella, J. R., and Zhu, J. K. (2018). Generation of new glutinous rice by CRISPR/Cas9-targeted mutagenesis of the *Waxy* gene in elite rice varieties. *J. Integr. Plant Biol.* 60, 369–375. doi: 10.1111/jipb.12620
- Zhang, L., Zhang, C., Yan, Y., Hu, Z., Wang, K., Zhou, J., et al. (2021b). Influence of starch fine structure and storage proteins on the eating quality of rice varieties with similar amylose contents. *J. Sci. Food Agric.* 101, 3811–3818. doi: 10.1002/jsfa.11014
- Zhang, C., Zhu, J., Chen, S., Fan, X., Li, Q., Lu, Y., et al. (2019). *Wx^{la}*, the ancestral allele of rice *Waxy* gene. *Mol. Plant* 12, 1157–1166. doi: 10.1016/j.molp.2019.05.011
- Zhou, H., Xia, D., Zhao, D., Li, Y., Li, P., Wu, B., et al. (2021). The origin of *Wx^{la}* provides new insights into the improvement of grain quality in rice. *J. Integr. Plant Biol.* 63, 878–888. doi: 10.1111/jipb.13011
- Zhu, Y., Nomura, T., Xu, Y., Zhang, Y., Peng, Y., Mao, B., et al. (2006). ELONGATED UPPERMOST INTERNODE encodes a cytochrome P450 monooxygenase that epoxidizes gibberellins in a novel deactivation reaction in rice. *Plant Cell* 18, 442–456. doi: 10.1105/tpc.105.038455



OPEN ACCESS

EDITED BY

Gustavo A. Slafer,
Catalan Institution for Research and
Advanced Studies (ICREA), Spain

REVIEWED BY

Marta S. Lopes,
Institute of Agrifood Research and
Technology (IRTA), Spain
Nieves Aparicio,
Instituto Tecnológico Agrario de Castilla y
León, Spain

*CORRESPONDENCE

Jonas Anderegg
✉ jonas.anderegg@usys.ethz.ch

RECEIVED 08 November 2023

ACCEPTED 13 May 2024

PUBLISHED 04 June 2024

CITATION

Anderegg J, Kirchgessner N, Aasen H,
Zumsteg O, Keller B, Zenkl R, Walter A and
Hund A (2024) Thermal imaging can reveal
variation in stay-green functionality of wheat
canopies under temperate conditions.
Front. Plant Sci. 15:1335037.
doi: 10.3389/fpls.2024.1335037

COPYRIGHT

© 2024 Anderegg, Kirchgessner, Aasen,
Zumsteg, Keller, Zenkl, Walter and Hund. This is
an open-access article distributed under the
terms of the [Creative Commons Attribution
License \(CC BY\)](https://creativecommons.org/licenses/by/4.0/). The use, distribution or
reproduction in other forums is permitted,
provided the original author(s) and the
copyright owner(s) are credited and that the
original publication in this journal is cited, in
accordance with accepted academic
practice. No use, distribution or reproduction
is permitted which does not comply with
these terms.

Thermal imaging can reveal variation in stay-green functionality of wheat canopies under temperate conditions

Jonas Anderegg^{1*}, Norbert Kirchgessner², Helge Aasen³,
Olivia Zumsteg², Beat Keller², Radek Zenkl¹,
Achim Walter² and Andreas Hund²

¹Plant Pathology Group, Institute of Integrative Biology, ETH Zurich, Zurich, Switzerland, ²Crop Science Group, Institute of Agricultural Sciences, ETH Zurich, Zurich, Switzerland, ³Earth Observation of Agroecosystems Team, Research Division Agroecology and Environment, Agroscope, Zurich, Switzerland

Canopy temperature (CT) is often interpreted as representing leaf activity traits such as photosynthetic rates, gas exchange rates, or stomatal conductance. This interpretation is based on the observation that leaf activity traits correlate with transpiration which affects leaf temperature. Accordingly, CT measurements may provide a basis for high throughput assessments of the productivity of wheat canopies during early grain filling, which would allow distinguishing functional from dysfunctional stay-green. However, whereas the usefulness of CT as a fast surrogate measure of sustained vigor under soil drying is well established, its potential to quantify leaf activity traits under high-yielding conditions is less clear. To better understand sensitivity limits of CT measurements under high yielding conditions, we generated within-genotype variability in stay-green functionality by means of differential short-term pre-anthesis canopy shading that modified the sink:source balance. We quantified the effects of these modifications on stay-green properties through a combination of gold standard physiological measurements of leaf activity and newly developed methods for organ-level senescence monitoring based on timeseries of high-resolution imagery and deep-learning-based semantic image segmentation. In parallel, we monitored CT by means of a pole-mounted thermal camera that delivered continuous, ultra-high temporal resolution CT data. Our results show that differences in stay-green functionality translate into measurable differences in CT in the absence of major confounding factors. Differences amounted to approximately 0.8°C and 1.5°C for a very high-yielding source-limited genotype, and a medium-yielding sink-limited genotype, respectively. The gradual nature of the effects of shading on CT during the stay-green phase underscore the importance of a high measurement frequency and a time-integrated analysis of CT, whilst modest effect sizes confirm the importance of restricting screenings to a limited range of morphological and phenological diversity.

KEYWORDS

high throughput field phenotyping, physiological breeding, deep learning, semantic segmentation, remote sensing

1 Introduction

The onset of monocarpic senescence is a critical phenological event in annual crops, marking a basic transition of canopies from carbon assimilation to Nitrogen remobilization (Thomas and Ougham, 2014). Senescence-related remobilization processes are pivotal for yield and quality formation in wheat (Kichey et al., 2007), but an adequate post-anthesis green canopy duration preceding its onset is similarly important to avoid time- and resource-related constraints to grain filling. Indeed, maximizing carbon assimilation by a prolonged maintenance of green leaf area after anthesis (the “stay-green” trait) represents an important breeding aim in several crops (reviewed by Gregersen et al., 2013). In wheat, positive correlations between delayed senescence and grain yield are observed primarily under biotic and abiotic stress (Bogard et al., 2010; Christopher et al., 2014; Anderegg et al., 2020, 2008; Joshi et al., 2007; Lopes and Reynolds, 2012). Under such conditions, a longer preservation of green leaf area can be interpreted as a prevention of stress-induced premature senescence that could result in source-limitation of yields. The fine-tuning of senescence dynamics has therefore been proposed as a promising selection criterion in wheat breeding, especially under the scenario of an increasing frequency of weather extremes such as heat and drought.

Single genes with major effects on the timing and dynamics of senescence have been identified in wheat (Uauy et al., 2006), but senescence is generally considered to be under complex genetic and environmental control. Numerous studies highlighted the importance of the balance between Nitrogen uptake from the soil and Nitrogen demand by developing grains as a determinant of its timing and dynamics (Rajcan and Tollenaar, 1999; Triboi and Triboi-Blondel, 2002; Kichey et al., 2007; van Oosterom et al., 2010). From this perspective, a timely and rapid senescence indicates a high sink demand for assimilates and Nitrogen (Yang and Zhang, 2006; Xie et al., 2016), whereas an unfavorably delayed and slow senescence indicates sink-source imbalances, such as resulting from a low yield potential or overfertilization (Jiang et al., 2004; Yang and Zhang, 2006; Naruoka et al., 2012). When selecting for increased green canopy duration, it would therefore be imperative to distinguish between functional stay-green associated with enhanced photosynthetic activity required to meet a high sink demand, and dysfunctional stay-green resulting from slowed Nitrogen remobilization indicating low sink demand and, consequently, a low yield potential (Gregersen et al., 2008). A postulated senescence ideotype therefore consists in the maintenance of a highly productive green leaf area that supports complete grain filling, followed by rapid senescence involving efficient nutrient remobilization (Gregersen et al., 2008). Distinguishing functional from dysfunctional stay-green may be particularly important under high yielding conditions where strong external environmental triggers of senescence such as heat or drought events are absent in average years.

Key aspects of senescence and its dynamics, such as rates of chlorophyll degradation, are readily observable by the eye, both at the canopy level as well as at the level of visible parts of plant organs (e.g., leaves, peduncles, or ears). Numerous studies have used proximal sensing techniques based on average canopy light reflectance to track the dynamics of senescence (e.g., Anderegg

et al., 2020; reviewed by Chapman et al., 2021). High-resolution imaging combined with deep-learning-based semantic image segmentation additionally enabled tracking of senescence and overall healthiness of wheat stands at the organ-level (Anderegg et al., 2023). In comparison to visual assessments, these approaches offer the key advantages of objectivity and scalability. Unfortunately, however, much like visual assessments, they do not enable a distinction between functional and dysfunctional stay-green, nor a precise assessment of remobilization, grain filling rates or grain filling duration, since an increased green canopy duration as observed visually is not per se indicative of increased grain filling rates or duration. Therefore, measurements of canopy greenness must be complemented with measurements of “leaf activity” traits (Fischer et al., 1998), such as photosynthetic activity, gas exchange rates, or stomatal conductance.

Numerous retrospective studies on historical series of genetic lines have found remarkably strong correlations between increases in stomatal conductance and yield gains over time (i.e., with year of release; e.g., Fischer et al., 1998; reviewed by Roche, 2015). Increased sink-to-source ratios are hypothesized to contribute significantly to this relationship (Roche, 2015). With all else equal, higher transpiration rates (a greater stomatal conductance) decrease canopy temperature (CT) via evaporative cooling; therefore, CT measurements have been used as a fast surrogate measure for stomatal conductance (e.g., Rebetzke et al., 2013). Additionally, since photosynthetic gas exchange and stomatal conductance are intertwined, CT may provide an indirect measurement of photosynthetic rate (Amani et al., 1996; Fischer et al., 1998; Jones and Vaughan, 2011). Recently, CT measurements have been acquired using airborne imaging thermography, enabling the measurement of large experiments in short time, which greatly increased repeatability of measurements as compared to plot-by-plot measurements using hand-held thermometers (e.g., Deery et al., 2019, 2016; Perich et al., 2020).

While these studies represent significant methodological advances and provide convincing evidence for the potential usefulness of airborne CT measurements in breeding, some unexpected patterns also became apparent, including in our own data, which was collected using repeated drone-based thermal imaging of large germplasm collections throughout the grain filling phase (Perich et al., 2020; Anderegg et al., 2021). Most notably, a high heritability of plot-based CT was observed even at maturity, when no transpiring leaf tissue was left. Additionally, CT at maturity was moderately to highly correlated with CT shortly after flowering, as well as with CT measured throughout grain filling. These correlations were comparable in magnitude to correlations observed between CT values at earlier measurement dates during the stay-green phase (see for example Figures 8, 9 in Perich et al., 2020) and this cannot be well explained when interpreting CT primarily as a measure of leaf activity traits. Finally, but perhaps less surprisingly, moderate to strong correlations were observed between CT and structural, morphological, and phenological characteristics of genotypes (Anderegg et al., 2021), which is in line with results from numerous other studies (see reviews by Deery and Jones, 2021 and Prashar and Jones, 2014). Taken together, these observations

prompted some skepticism on our side regarding the existence of a direct and strong enough link between leaf activity traits and remotely sensed CT under the conditions of the study site (i.e., high-yielding zones of temperate Europe). This is mentioned here not to question the usefulness of CT as a valuable tool in breeding, for which ample evidence has been presented by others (e.g., Lopes and Reynolds, 2010; Rebetzke et al., 2013; Thapa et al., 2018; Li et al., 2019). However, we want to highlight the need for a better understanding of the extent to which CT measured at different growth stages and under different growing conditions can be interpreted as representing directly leaf activity traits. We anticipate that such an improved understanding will help quantify the value of CT measurements as a complement to precision assessments of phenology and measurement of canopy biophysical characteristics in the characterization of the status of stay-green canopies.

Therefore, the objective of this study was to isolate and quantify the direct effect of differences in leaf activity traits on remotely sensed CT. In other words, we aimed to establish whether differences in photosynthetic rates and stomatal conductance are detectable in canopies differing only with respect to these traits, but with all else as similar as possible and growing side-by-side. To this end, we aimed to introduce variation in terms of the functionality of stay-green in otherwise identical canopies. We modified sink-source relationships by applying short-term canopy shading during rapid spike growth with the aim of reducing potential yield, whereas directly neighboring control plots of the same genotype were left untreated. Plot CT was continuously monitored throughout grain filling by means of a pole-mounted thermal camera, and precision phenology assessments were made using frequent RGB imaging combined with segmentation of different organs based on deep learning models. Our results clearly indicate that differences between functional and dysfunctional stay-green translate into measurable differences in CT, and that they do so in the absence of co-variation in often correlated confounding traits.

2 Materials and methods

2.1 Plant materials, experimental design, and environmental data

A field experiment with two registered winter wheat cultivars ('Piznair', AGROSCOPE/DSP, Switzerland; and 'Campesino', SECOBRA Saatzucht GmbH, Germany) was carried out at the ETH Research Station for Plant Sciences Lindau-Eschikon, Switzerland (47.449°N, 8.682°E, 520 m above sea level; soil type: eutric cambisol) in the wheat growing season of 2022–2023. The two cultivars were selected for the experiment based on (i) their similarity in terms of canopy characteristics, particularly leaf and ear orientation and final height; (ii) their similar phenology: both cultivars are classified as mid-late in terms of ear emergence and maturation; and (iii) their strongly contrasting yield potential: 'Campesino' has a very high yield potential, whereas 'Piznair' has an intermediate yield potential but a high protein content (Strebel et al., 2022).

Each cultivar was grown in ten plots for a total of 20 experimental plots. Wheat was sown with a drill sowing machine in nine rows per plot with a row length of 1.7 m and a row spacing of 0.125 m at a density of 400 plants m⁻² on 18 October 2022. Plots were arranged in pairs sown with the same cultivar (Figure 1C). To avoid inhomogeneous neighboring effects on experimental plots, each pair of plots was bordered both in sowing direction as well as perpendicular to it by buffer plots sown with a late-maturing check with a very similar canopy height ('Montalbano', AGROSCOPE/DSP, Switzerland). Pairs of plots were arranged in a cultivar-alternating manner in two buffer-separated ranges (Figures 1A, C). At booting (growth stage [GS] 43; Lancashire et al., 1991; reached on 13 May 2023) one plot in each pair was shaded by suspending a polyethylene shading net that decreased light intensity by 73% (Agroflor, Wolfurt, Austria) approximately 25 cm above the top of the canopy (Figure 1B), whereas the adjacent plot was used as an unshaded control. The spatial arrangement of control and shaded plots was alternated across the pairs. Shading was applied after full flag leaf emergence in order to avoid undesired side-effects on canopy characteristics such as total above ground biomass, leaf area index, canopy cover, or leaf sizes. The shading nets were removed again at the late heading stage (approximately GS 59, reached on 29 May 2023). Crop husbandry was performed according to local agricultural practice. Temperature, rainfall, and wind speed data were retrieved from an on-site weather station.

2.2 Measurement of gas exchange and photosynthetic parameters

Gas exchange measurements were made plot-by-plot on eight dates between 8 June and 29 June 2023, using the portable photosynthesis system LI-6400XT (LI-COR, Inc., Lincoln, NE, USA). Measurements were made on fully sun-exposed, intact flag leaves with no visible disorders, at a position about halfway along its length. Measurements were made under clear sky conditions between 10 a.m. and 3 p.m. This ensured that leaves had been exposed to constant light prior to the measurement. One measurement lasted 3 min, with one value logged every 5 s. Air temperature in the chamber was regularly controlled and adjusted as needed to match the ambient temperature in the field. The air flow rate during the measurements was 300 $\mu\text{mol air s}^{-1}$. To ensure stable CO₂ concentration in the incoming airflow, a canister with an open cap was used as a buffer volume, as recommended by the manufacturer. Infrared gas analyzers were matched once before a measurement series. The light source intensity was set to 1500 $\mu\text{mol m}^{-2} \text{s}^{-1}$. All 20 plots of the experiment were routinely measured within 1.5 h. One or two measurement runs were made on each measurement date. For each measured sample, the first 6 logged values were removed. After that, one iteration of outlier removal was performed on logged values, defining an outlier as a value deviating from the median by more than 1.5 times the interquartile range. The remaining values were averaged to obtain one value for each measured leaf. The experiment was measured twice on 8 June and 12 June 2023, and once on all other measurement dates.

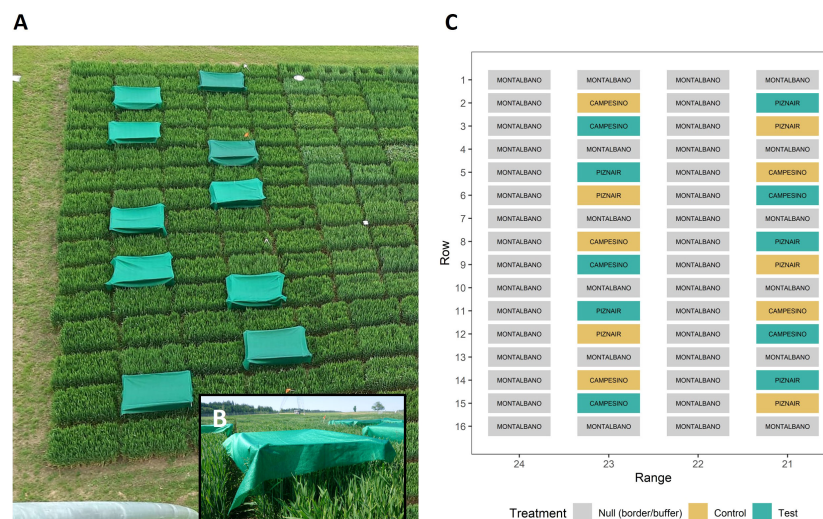


FIGURE 1

Design of the field experiment. (A) Image of the field experiment taken from the position where the thermal camera was mounted. The image was taken right after the shading tents were mounted on 13 May 2023 (GS 43); (B) close-up of a shading tent; (C) schematic of the experimental design. The scale of the axes was inverted to directly represent the view as seen in (A). Control plots were left untreated, whereas Test plots were shaded during rapid spike growth. Text labels within color boxes represent cultivar names. The experiment was bordered to the right side by an additional row of border plots, identical to range 24. The experiment was sown row-wise on 18 October 2022.

Whenever more than one measurement was performed, values across measurement runs were averaged on a plot basis.

Active fluorescence measurements were obtained on twelve dates between 1 June and 29 June 2023, using a MultispeQ device (PhotosynQ Inc, MI, USA). The 'Photosynthesis RIDES 2.0_short' protocol (photosynq.org) was used to measure the operating efficiency of photosystem II (F_q/F_m), photosynthetic photon flux rate (PPFR), and relative chlorophyll (SPAD) (Kuhlgert et al., 2016; Keller et al., 2023). Measurements were performed on leaves that were selected following the same principles as for gas exchange measurements. Between two and six measurement runs were performed on each date. Whenever more than one measurement was performed, values across measurement runs were averaged on a plot basis.

2.3 Crop phenology, morphology, and agronomic traits

The dynamics of senescence were monitored with nearly daily resolution at the level of individual organs by means of repeated imaging from a nadir as well as an off-nadir perspective (viewing angle of approximately 45°), using a measurement setup described in detail earlier (Grieder et al., 2015; Anderegg et al., 2023). The resulting image time series were first segmented into a vegetation and a soil fraction. Subsequently, ears were segmented in images captured from a nadir perspective, whereas ears and stems were segmented in off-nadir images. Nadir images were segmented using deep convolutional neural networks available from previous work, without modification (Anderegg et al., 2023). The stem and ear segmentation model for off-nadir images was developed in the context of this study, following the same procedure as described for

nadir images earlier (Anderegg et al., 2023). Briefly, 100 patches sized 600 × 600 pixels from carefully selected diverse images representing the entire grain filling phase, contrasting light conditions, and different genotypes, were manually annotated at pixel level, using polygons. This data set was complemented with 165 patches from images captured with a different setup and containing only stay-green canopies. Compared to the target domain, these images had a much higher resolution but a much shallower depth of field, resulting in a blurry background. These images were resized to match the target domain in terms of physical resolution. 24 randomly selected patches from the target domain were designated as the validation data set. Model hyper-parameters were optimized within a limited search space, in a stepwise procedure. First, the segmentation framework together with the input resolution were optimized, with resnet34 (He et al., 2016) as encoder. Next, the resnet encoder depth was optimized together with data augmentation (image resolution, rotation, horizontal and vertical flipping, down-scaling and up-scaling, color jittering, blurring), and the training strategy. Finally, parameters of the network training process were optimized. The resulting optimized segmentation model reached an overall validation F1-Score of 0.90 (see Figures 2G, H, and Supplementary Figure S1 for an illustration). The resulting segmentation masks enabled an estimation of the fraction of images representing different components of vegetation. The original images were further segmented pixel-wise based on color properties of pixels into a green, chlorotic, and necrotic fraction, using a previously trained classifier (Anderegg et al., 2023). The masks were combined through logical operations to obtain the fractions of green, chlorotic, and necrotic tissues for each vegetation component. For details, refer to (Anderegg et al., 2023). The annotated data sets representing the target domain will be made freely available via the

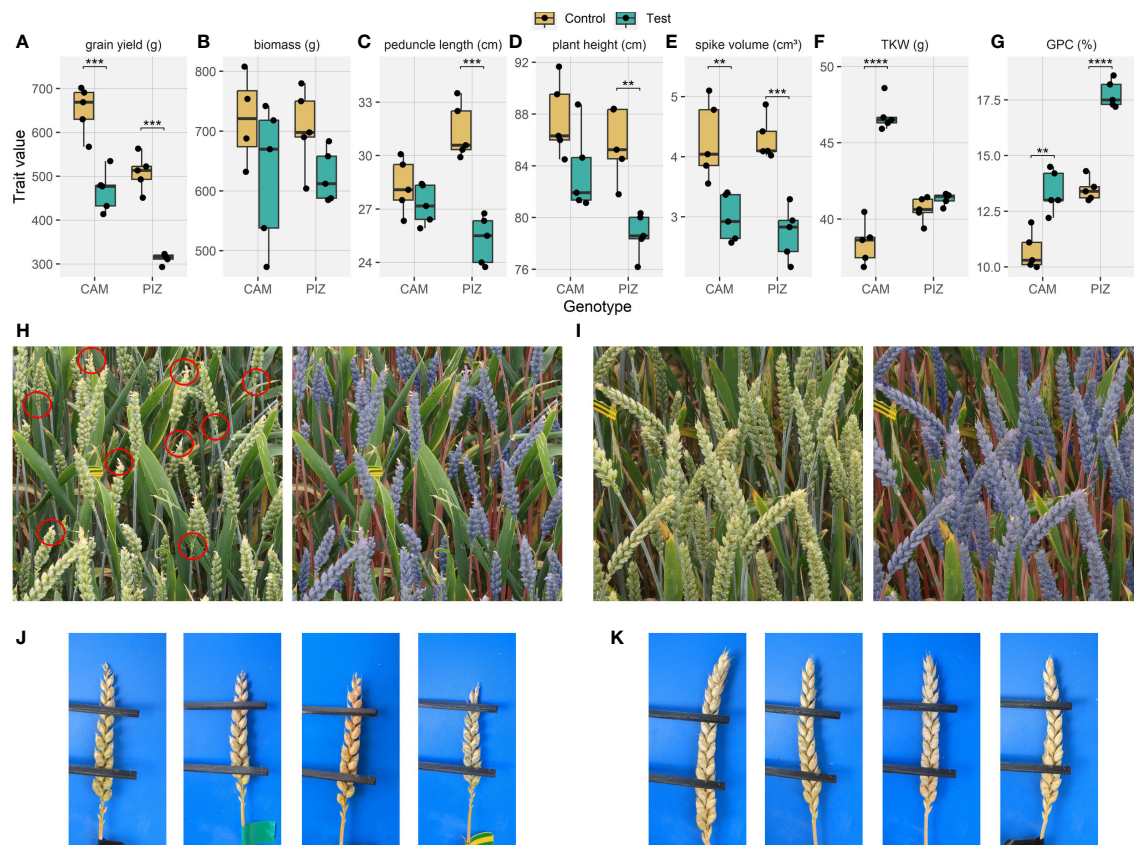


FIGURE 2

Effects of shading on agronomic traits and canopy characteristics. Effects of shading on (A) grain yield, (B) above ground vegetative dry biomass (total above ground biomass after threshing), (C) peduncle length, (D) plant height, (E) spike volume, (F) thousand kernel weight, (G) grain protein concentration. Where multiple measurements were made per plot, the mean value across repeat measurements is plotted. (H) Example of an image of a shaded plot with the corresponding segmentation model output overlaid (right side) for the cultivar 'Piznair'; red circles highlight some obvious instances of rudimentary basal and completely aborted apical spikelets; (I) image of the directly adjacent unshaded plot. See [Supplementary Figure S1](#) for quantitative results on organ contribution to images; (J) Close-up images of spikes from a shaded plot of 'Piznair'; (K) close-up images of spikes from the adjacent control plot of 'Piznair'. (*p < 0.05; **p < 0.01; ***p < 0.001; ****p < 0.0001).

Repository for Publications and Research data of ETH Zürich (<https://doi.org/10.3929/ethz-b-000668219>).

Peduncle length was measured shortly before harvest as the distance between the uppermost node on the stem and the spike collar for 12 randomly selected culms per plot with a precision of 1 cm, using a ruler. Peduncle senescence that can serve as a proxy for maturity (Chapman et al., 2021) was assessed by visually classifying them as either senescent or green. Three batches of 10 tillers were examined per plot, and the total fraction of senescent peduncles was recorded. All assessments were made as recommended by Chapman et al. (2021) and Pask et al. (2012). As peduncle senescence was used as a reference for the image-derived stem senescence score, plots in a separate experiment were additionally scored to broaden the validation basis, and off-nadir imagery was also collected in the context of that experiment.

Plant height was assessed as the median of six canopy height estimations carried out after heading. Individual estimations were based on RGB imagery from unmanned aerial vehicles and structure from motion (Roth et al., 2020).

Spikes were sampled for volume measurements on 10 June, 4 July, and 11 July 2023. On each date, two spikes were sampled for

each plot. Sampled spikes were stored under dry conditions and were later scanned using a 3D light scanner (Shining 3D Einscan-SE V2, SHINING3D, Hangzhou, China). Parts that were used to stabilize the spike in the scanner were removed from the resulting point cloud using a custom MatLab script (MatLab r2022b, Natick, MA, USA). The spike volume was extracted using pymeshlab (<https://github.com/cnr-isti-vclab/PyMeshLab>). Some strongly bent spikes had to be scanned in a special mounting. The points of these mountings were manually removed with 3dbuilder (<https://www.microsoft.com/en-us/3d-print/3d-builder-users-guide?rtc=1>) and the spike volume was determined using Meshlab 1.3.2_64 bit (<https://www.meshlab.net/>).

Grain yield and total above-ground biomass were assessed by manually harvesting the sowing rows 6, 7, and 8 (out of 9) on 12 July 2023. After the ears had been removed for determination of grain yield, the remaining biomass was cut approximately 1 cm above ground and dried to constant weight. Grain protein concentration (GPC) was determined using near-infrared transmission spectroscopy (IM-9500, Perten, Hagersten, Sweden). Thousand kernel weight (TKW) was measured using a MARViN ProLine II (MARViTECH GmbH, Wittenburg, Germany).

2.4 Thermal imaging and extraction of plot canopy temperature

A thermal camera (FLIR A655sc uncooled microbolometer camera with W/45° lens, 640 × 480 pixel; FLIR Systems AB, Sweden) was mounted on a pole of the ETH field phenotyping platform FIP (Kirchgessner et al., 2017) located right next to the experimental field (cf. Figure 1A) on May 24, 2023. The camera was mounted in a weatherproof housing (Tecnovideo, Villaverla, Italy) at a height of 23.5 m above ground and connected to a 12V power supply. It was controlled by a common PC at the bottom of the pole connected by LAN. Image acquisition was controlled through a Matlab script (r2022b, The Mathworks, Natick, USA), which wrote data directly to our NAS. Viewing angles for experimental plots were between 34° and 46.5° to nadir view. The used lens provides a field of view of 45° and 34°. An image was recorded every 20 s, resulting in approximately 140,000 images that covered the entire grain filling phase from flowering to shortly before harvest. From each image, median plot temperatures were extracted by generating a geojson file that contained the corner coordinates of polygons representing each experimental plot using the ‘ogr’ module of the python library ‘osgeo’. The shapes were generated by specifying the number of rows and ranges of the experiment as well as the size of a plot, with plot length set to 1.1 m, and plot width set to 0.8 m, thus leaving a buffer zone of approximately 0.3 m in sowing direction and 0.2 m perpendicular to it. Plot shape corner coordinates were then transformed by calculating their dot product with the homography matrix, which was determined by matching all four corners of the experiment to the pixel coordinates of the respective position in one example thermal image. These steps were accomplished using code associated with Treier et al. (2023). Before exporting summary statistics per plot, outliers were removed as pixel values that deviated from the median value of all pixels attributable to that plot by more than 1.5 times the interquartile range. This was deemed necessary to reduce the effect of obstructions in images, such as for example a person performing measurements in the experiment.

2.5 Statistical analysis

Canopy temperature time series were smoothed by fitting a smoothing spline using the function *smooth.spline()* of the R-package ‘stats’ (R Core Team, 2018), separately for each experimental plot. The number of spline knots was set to one tenth of the number of observations, and a prediction every 2 min from the resulting fits was retained for further analyses. To summarize the resulting smoothed time series of CT measurements, we extracted the area under the curves (AUC_{CT}) for the duration between 10 a.m. and 4 p.m. at each measurement date.

The experimental design resulted in a spatially perfectly homogeneous distribution of control and test plots for each of the two evaluated genotypes, and there were ten direct neighbor pairs of control and test plots (five for each cultivar), that were themselves

surrounded by invariable buffer plots. We therefore considered neighboring plots as representing paired samples. For canopy temperature measurements, this accounted for variation over time attributable to short-term fluctuations in environmental conditions, as well as for spatial effects related to field heterogeneity and measurement geometry. For plot-by-plot measurements, it additionally allowed for a correction of temporal effects since test and control plots were allocated to the members of a pair in a spatially alternating fashion (Figure 1). Plot-based values were therefore compared across the treatments by means of a paired samples t-test, carried out separately for each date.

The effects of genotype, treatment, and genotype-by-treatment interactions on phenological, morphological and agronomic trait values measured at the plot level were determined through a corresponding two-way analysis of variance, conducted independently for each trait, using the R-function *aov()*. Pairwise comparisons were made by means of a Tukey posthoc test, using the function *TukeyHSD()*. Where repeat measurements were made for each plot, a linear mixed effects model was fitted, with the experimental plot additionally considered as a random effect. These models were fitted using the function *lme()* of the R-package ‘nlme’ (Pinheiro et al., 2021) and all possible pair-wise contrasts were obtained from the function *emmeans()* of the R-package ‘emmeans’ (Lenth et al., 2020).

3 Results

3.1 Pre-anthesis canopy shading effectively modified the sink-source relationship with minor effects on other canopy characteristics

Canopy shading was applied during rapid spike growth and after full flag leaf emergence with the aim of generating variation in sink strength within each tested genotype. This, in turn, was expected to create variation in leaf activity traits in response to the modified sink-source balance, in canopies with otherwise very similar characteristics.

The shading treatment drastically reduced grain yield in both genotypes, with a larger relative reduction observed for the low-yielding cultivar ‘Piznair’ ($\Delta = -38.4\%$, $p < 0.001$; Figure 2A), than for the high-yielding cultivar ‘Campesino’ ($\Delta = -28.4\%$, $p < 0.001$). The reduction in yield potential for each genotype was clearly apparent already in the first measurement of ear volume on 10 June 2023 (i.e., 12 d after full heading [GS 59]) in terms of a reduced spike volume, which was also more prominent in the low-yielding cultivar ($\Delta = -36.5\%$, $p < 0.001$; Figure 2E) than in the high yielding cultivar ($\Delta = -30.1\%$, $p < 0.01$). The difference in spike volume was mostly attributable to an increased number of rudimentary basal and apical spikelets that did not develop grains (Figures 2H, J). This had notable canopy-level effects, with decreased ear coverage both in nadir and in oblique images for shaded than for control canopies (Figures 2H, I, Supplementary Figure S2). In contrast, ear volumes were not different between genotypes within each of the treatments despite the large differences

in end-of-season grain yield ($p > 0.8$ for both treatments; data not shown).

Thousand kernel weight was much increased under the shading treatment in ‘Campesino’ ($\Delta = +21.9\%$, $p < 0.001$; Figure 2F), indicating that grain yield in this genotype was source-limited under the control treatment; no increase in thousand kernel weight was observed for ‘Piznair’, indicating sink-limitation under the control treatment for this genotype. Grain protein concentration was increased in response to shading in both genotypes (Figure 2G). In ‘Piznair’, grain protein concentration reached a very high value of 17.8% under shading.

Despite the late application of the shading treatment, a trend towards a reduced above ground vegetative biomass was also observed, though these effects were not statistically significant ($\Delta = -12.8\%$, $p = 0.36$ and $\Delta = -11.2\%$, $p = 0.44$ for ‘Campesino’ and ‘Piznair’, respectively; Figure 2B). The observed trend towards a decreased vegetative biomass in shaded canopies can be partly explained by the effect of shading on peduncle length ($\Delta = -3.89\%$, $p = 0.64$ and $\Delta = -19.3\%$, $p < 0.001$ for ‘Campesino’ and ‘Piznair’, respectively; Figure 2C). In ‘Piznair’, the reduction in peduncle length was significantly correlated with the reduction in vegetative biomass (Pearson $r = 0.66$, $p < 0.001$; not shown). Plant height was also reduced by shading ($\Delta = -4.6\%$, $p = 0.12$ and $\Delta = -8.7\%$, $p = 0.004$ for ‘Campesino’ and ‘Piznair’, respectively; Figure 2D), which is accounted for mostly by the differences in peduncle length. In contrast, canopy cover was not affected by shading; it was nearly 100% in oblique-angle images and approximately 0.8 in nadir images, irrespective of the treatment (Supplementary Figure S2). We observed no differences in canopy

characteristics besides the mentioned differences in peduncle length and ear fraction. In particular, leaf sizes and orientation appeared to be unaffected by the treatment. No differences were expected, given the late application of the treatment.

3.2 Measurements of phenology, photosynthetic rates, and gas exchange indicated extensive dysfunctional stay-green in response to pre-anthesis canopy shading

Shading tended to delay senescence in both genotypes. In the absence of shading, the onset of senescence occurred at similar timepoints for both genotypes but progressed much faster in ‘Piznair’ than in ‘Campesino’ (Figure 3, left-most column). In both genotypes, the delay in senescence was most pronounced in leaves, but less in ears and stems (Figures 4A–C, G, H). As observed for agronomic traits, the delay in visible senescence in response to shading was greater for ‘Piznair’ than for ‘Campesino’ (Figures 3, 4A–C). On average, the mid-point of foliar senescence was delayed by 2.4 d ($p = 0.09$) and 4.4 d ($p < 0.001$) in ‘Campesino’ and ‘Piznair’, respectively (Figure 4C). In shaded plots of ‘Piznair’, senescence progressed much slower than in unshaded control plots, especially in leaves (Figures 4D–F). Strikingly, in shaded plots senescence progressed slower in ‘Piznair’ than ‘Campesino’, which is the opposite of what was observed in control plots (Figure 3). Thus, shading affected both the timing and the dynamics of senescence,

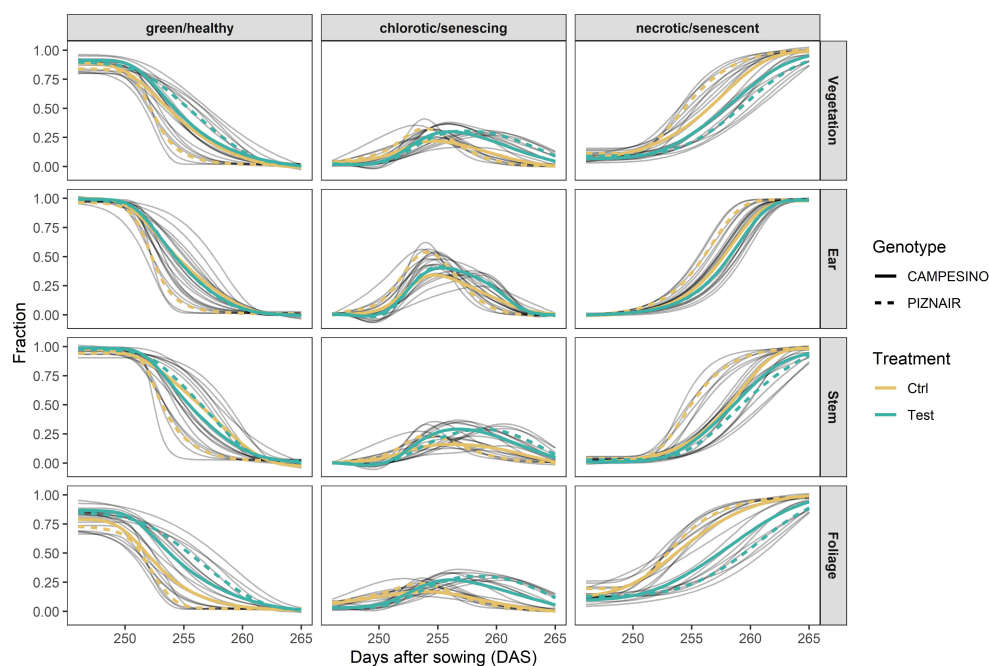


FIGURE 3

Relative contribution of green, chlorotic, and senescent tissue at organ level (total vegetation, ears, stems, and leaves) and their evolution over time between approximately 20 d after heading (21 June 2023) and physiological maturity (10 July 2023). Gray curves represent 4-parameter Gompertz model fits or P-spline fits to 16 data points for each experimental plot. Colored lines represent means for each treatment-by-genotype combination.

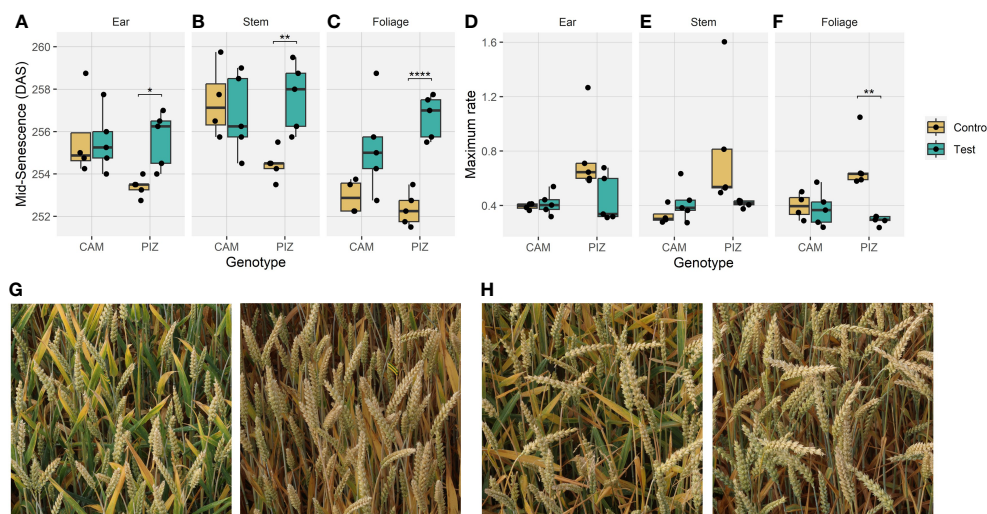


FIGURE 4
Effects of canopy shading on senescence dynamics. (A) Effects of shading on the midpoint of senescence observed for ears, (B) stems, (C) foliage; (D) Effects of shading on the maximum rate of senescence observed for ears, (E) stems, (F) foliage; (G) Example images of neighboring plots with shading (left) and without shading (right) for cultivar 'Piznair', (H) for cultivar 'Campesino'. Images in (G) and (H) were acquired on 1 July 2023, i.e., at around the midpoint of senescence (256 DAS). (*p < 0.05; **p < 0.01; ***p < 0.001; ****p < 0.0001)

and it affected both aspects of senescence more in 'Piznair', which was also more strongly affected by shading in its sink potential.

Overall, measurements of gas exchange and photosynthesis showed a high variation across measured leaves (raw data not shown), despite very stable weather conditions during the relevant period. Nonetheless, taken together the measurements indicated a trend towards reduced stomatal conductance and reduced photosynthetic activity in shaded plots compared to the controls (Figure 5), although these trends were not statistically significant for

either of the tested cultivars. Interestingly, the greater impact of shading on 'Piznair' was observable also in these measurements, except for stomatal conductance measured at 245 DAS (20 June 2023) corresponding to the last measurement before the onset of senescence (cf Figure 3). Across all measurement dates, the effects of shading were more pronounced in measurements of photosynthesis than in measurements of stomatal conductance for both tested cultivars (Figure 5). The F_q/F_m' showed the typical decrease with increasing PPFR which was more pronounced in 'Piznair' than in

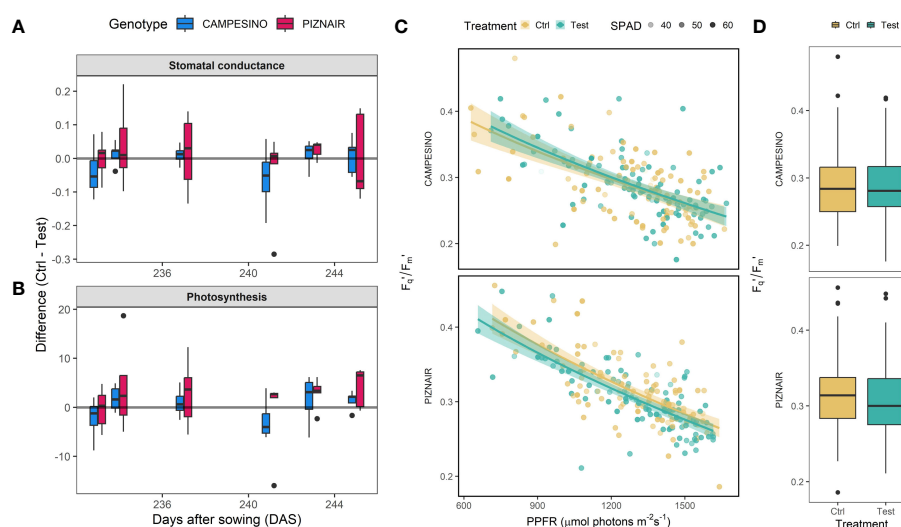


FIGURE 5
(A) Differences in stomatal conductance between members of pairs of directly adjacent plots, of which one each was exposed to pre-anthesis canopy shading ("Test") and one was left untreated ("Control"). Positive values indicate higher stomatal conductance and photosynthetic rates in untreated control plots than in shaded test plots; (B) Differences in photosynthesis as determined via gas exchange. (C) F_q/F_m' in response to increased photosynthetic photon flux rate (PPFR). Solid lines represent fitted values after square root transformation of PPFR. Relative chlorophyll (SPAD) is indicated by the transparency of the points. (D) Boxplot of F_q/F_m' for both genotypes and treatments. Data for six measurement days between June 1 and June 14 (DAS 226 to 239) was pooled.

‘Campesino’ (Figure 5C). In agreement with the photosynthesis measurements, shading slightly decreased F_q'/F_m' compared to the control, again more pronounced in ‘Piznair’ (Figure 5D).

3.3 Pre-anthesis canopy shading was associated with increasingly higher canopy temperature during early grain filling

CT values exhibited significant short-term variation, especially during early afternoons. Recurring rapid increases and decreases, typically in the range of 1–2 degrees, were observed within a timespan of a few minutes (cf. Supplementary Figure S3). Neighboring plots generally showed very similar temporal patterns in CT (Supplementary Figure S3), suggesting that this variation over time resulted from short-term changes in local meteorological conditions.

After a particularly wet spring season, early grain filling coincided with a period of very stable weather conditions, characterized by long periods of clear sky conditions during the day but moderate day-time temperatures (Figure 6). Significant rainfall was registered only on 19 June 2023, a few days before the onset of visually discernable senescence (Figure 6).

To isolate the effect of the treatment from effects related to genotype morphology, short-term changes in meteorological conditions, and spatial field heterogeneity, we calculated differences in CT between neighboring plots that had received either of the treatments, at the genotype level. When considering the entire measurement period (i.e., the period between flowering and harvest), contrasting effects of the treatment were observed (Figure 7). However, effects showed marked temporal continuity, allowing to distinguish three different phases (cf. Figure 6): In an

initial phase following the removal of the shading nets (Phase 1), shaded plots were consistently cooler during the day (approximately 0.5°C and 0.9°C on average across all pairs for ‘Campesino’ and ah‘Piznair’, respectively; Figure 7, top row). The difference between AUC_{CT} across the treatments were highly significant ($p < 0.01$; Figure 8, top row), but this difference progressively disappeared within the first 4–5 d. During the following days (Phase 2), the initially observed trend was gradually inverted, with shaded plots increasingly characterized by higher CT than control plots (between 9 June 2023 and 16 June 2023; Figure 7, panel rows 2 and 3). This observed difference in AUC_{CT} was statistically significant for ‘Piznair’, but not for ‘Campesino’. When data for both genotypes was pooled, differences were at the significance threshold on most measurement dates (Figure 8). The trend observed during Phase 1 was therefore continued during Phase 2. The gradual increase in CT during Phase 1 and Phase 2 in shaded relative to control plots becomes more obvious when comparing AUC_{CT} across the entire duration (Figure 9). This also reveals that the relative increase appeared to be stronger for ‘Piznair’ than for ‘Campesino’. Finally, a third phase (Phase 3) with stable patterns across multiple days was observed between 23 June and 29 June, when shaded test plots were again warmer than control plots (bottom rows of Figures 8, 9). This phase coincided with the onset of canopy senescence, which occurred earlier in control plots than in shaded test plots. Throughout the entire measurement period, differences between shaded and control plots did not exceed 1°C but were more often in the order of a few tens of degrees (Figure 7). Throughout the period, no sizable differences between differentially treated plots were observed during the night for either of the tested genotypes. Similarly, no differences in CT between shaded and control plots were apparent during the final days before maturity.

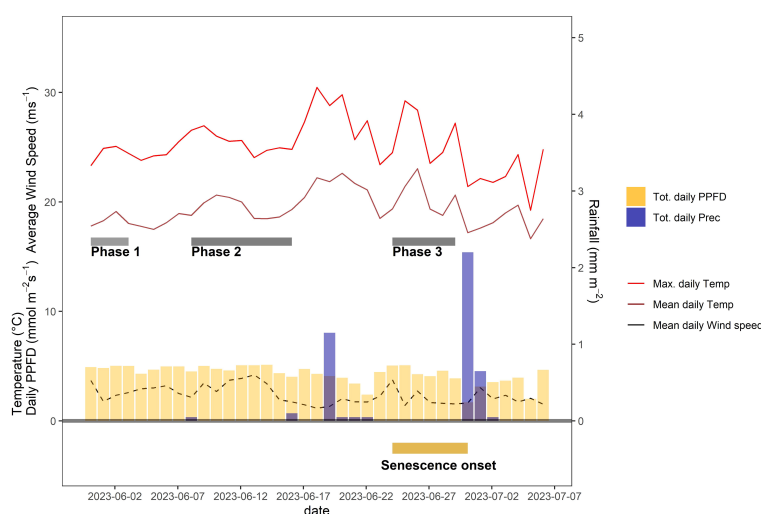


FIGURE 6

Daily average and maximum air temperature, daily rainfall, average daily wind speed, and daily incident light (photosynthetic photon flux density, PPFD) throughout the grain filling period of 2023. Except for rainfall, daily values were calculated based on data recorded between 10 a.m. and 4 p.m. each day. Dark grey bars indicate different phases during which distinct but temporally stable patterns in CT were observed. The dark yellow bar at the bottom of the plot indicates the time span during which plots started to senesce.

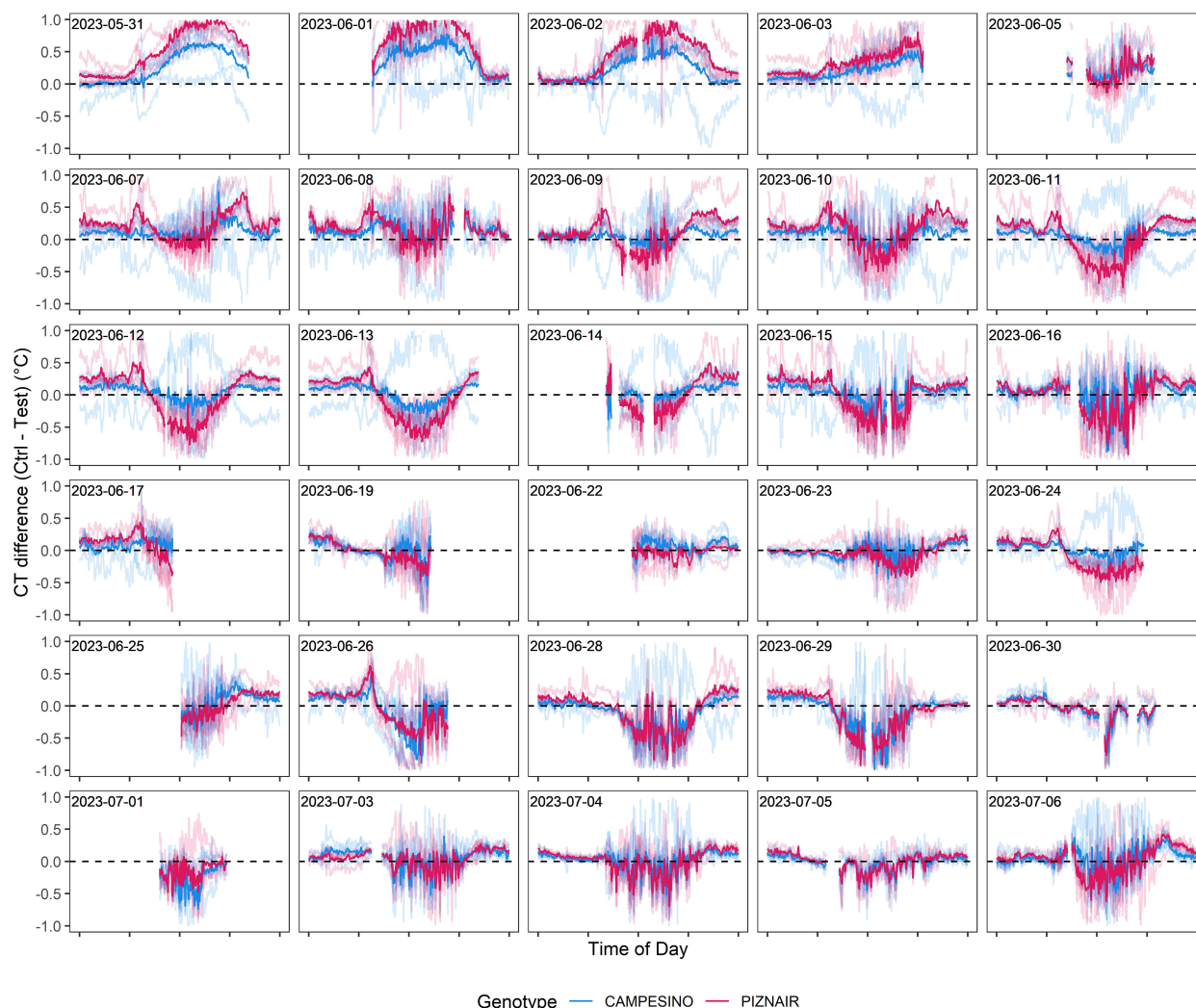


FIGURE 7

Differences in canopy temperature (CT) between pairs of plots with pre-anthesis shading ("Test") and without pre-anthesis shading ("Ctrl"). Negative values indicate higher CT in test plots than in adjacent control plots, and vice-versa. Solid lines represent genotype averages across five replicates, transparent lines represent differences between individual pairs of neighboring plots. Measurement dates with little or no data available for the period between 10 a.m. and 6 p.m. are not included.

4 Discussion

Canopy temperature is often interpreted as representing leaf activity traits, particularly stomatal conductance, and corresponding associations have been found by many researchers (e.g., Fischer et al., 1998; Rebetzke et al., 2013). However, it is well known that CT measurements are strongly affected by a multitude of other factors as well (Prashar and Jones, 2014; Anderegg et al., 2021; Deery and Jones, 2021). Depending on the objective of CT measurements, the influence of confounding variables may or may not be problematic. For example, if reasonably strong correlations between CT and yield are consistently observed under certain well-defined growing conditions at well-defined stages of crop development (e.g., because CT may provide a fast measure of overall vigor under stressful conditions at that time), then an exact understanding of the underlying functional relationship is not necessary to use it as a trait to select for higher-yielding

genotypes under these conditions (see Reynolds et al., 1994; Thapa et al., 2018; Li et al., 2019 for some examples). In contrast, if the objective of CT measurements is to complement other secondary traits (such as plant height and biomass) to enable a knowledge-based physiological selection, then a better understanding of the variables determining CT is indispensable. Only then will it be possible to estimate the feasibility of specific trait assessments, develop appropriate measurement protocols and define the scope of application. Here, our objective is of the latter sort: We aim to quantify a specific secondary trait (leaf activity traits during the stay-green phase of wheat), and we require this measurement to be *complementary* to (not indicative of) traits such as plant height, above-ground biomass, or phenology, for which more direct and precise high throughput assessment protocols are already available.

To better understand the potential and limitations of CT measurements in this context, we therefore performed an

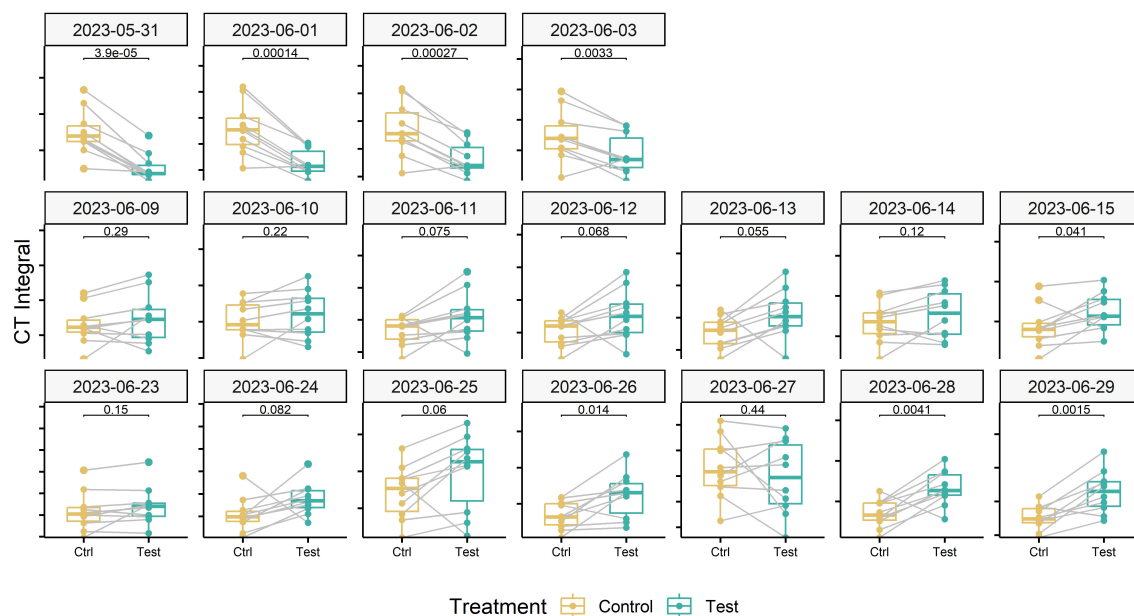


FIGURE 8

Effect of the pre-anthesis canopy shading treatment on the daily integral under the canopy temperature curves between 10 a.m. and 4 p.m. Data for measurement dates corresponding to three different phases of interest with stable environmental conditions are shown. Data for the two tested cultivars were pooled. Numbers above the black brackets indicate p-values of the paired sample t-test ($n = 10$), gray lines connect paired samples (i.e., neighboring plots of the same genotype having received the shading or control treatment).

experiment that isolated the effect of variation in the trait of interest on CT from variation in CT caused by such confounding and possibly co-varying traits. Below, we first discuss the experimental approach underlying this feasibility assessment. Then, we interpret and contextualize observed effects and effect sizes, and discuss implications for an optimized use of CT measurements to characterize stay-green canopies.

4.1 Pre-anthesis canopy shading to manipulate sink-source balances and create variation in stay-green functionality

We applied pre-anthesis canopy shading during rapid spike growth (but significantly after full flag leaf emergence) with the aim of creating variation in sink strength with minimum side-effects on the size and structure of the canopy. Given the importance of the sink-source balance in the regulation of senescence, shading was expected to result in dysfunctional stay-green *via* a reduced and delayed demand for remobilized assimilates and N.

Large effects of pre-anthesis shading on potential grain yield have been reported in several studies (e.g., Fischer, 1985, 1975; Savin and Slafer, 1991). Yield losses result primarily from a reduced number of kernels per spikelet (Slafer et al., 1994), and an increased number of rudimentary basal spikelets is often observed (Slafer et al., 1994; Backhaus et al., 2023), which appears to be the result of complete floret abortion in basal spikelets as a consequence of their delayed development (Backhaus et al., 2023). Though we did not perform detailed quantitative in-field assessments of spike fertility, it was obvious from ear volume measurements (Figure 2D) and

from examinations of organ contribution to vegetation sceneries (Supplementary Figure S2) that shading drastically affected spike fertility. Specifically, there was an obvious increase in the number of rudimentary basal spikelets and completely aborted apical spikelets (Figures 2E, 4D). Interestingly, eye-ball assessments in the field and re-examination of ears in images suggested that shading affected apical spikelets more than basal spikelets, especially in ‘Piznair’, which would be in contrast with common observation (Stockman et al., 1983; Slafer et al., 1994; Backhaus et al., 2023).

Because of the temporal overlap between rapid spike growth and elongation of the last internode (peduncle), canopy shading affected both traits (Figure 2). Peduncles are important as storage location for water-soluble carbohydrates, and canopy shading affects WSC accumulation within a few days of application (Stockman et al., 1983). Therefore, source strength must also have been affected by the shading treatment. However, this regarded primarily reserve and biomass accumulation of the peduncle and spike during the restricted period of shading, whereas photosynthetically active leaf area should not have been affected (Supplementary Figure S2). Given the size of the effects on sink potential, it seems highly likely that shading affected sink strength far more than source capacity, resulting in an increased source:sink ratio as compared to the untreated controls for both assimilates and Nitrogen. This is additionally supported by the increase in thousand kernel weight in ‘Campesino’ and the increase in grain protein concentration in response to shading in both tested genotypes. The lack of a sizable increase in TKW in ‘Piznair’ is likely a result of grain size limitations (i.e., the maximum capacity of grains to absorb assimilates, that is determined already at an early stage of grain filling (Brocklehurst, 1977; Borrás et al., 2004)) than the lack

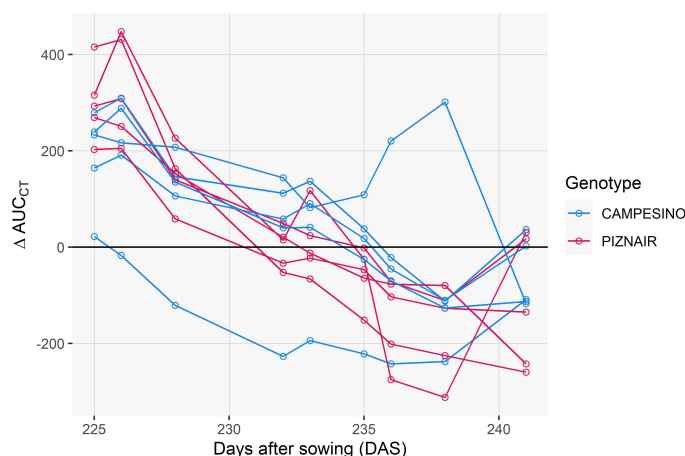


FIGURE 9

Differences between control plots and shaded plots in the area under the canopy temperature curve observed between 10 a.m. and 4 p.m. on each day (AUCCT). Data is shown for the early grain filling phase i.e., up until 20 June 2023, which corresponds to the phase preceding the onset of visually discernable senescence in the earliest maturing plots.

of assimilate supply, given that GPC is drastically increased despite its already high levels under control conditions.

The dynamics of senescence were strongly affected by shading, with magnitude and direction of the observed changes in good agreement with an interpretation of the shading treatment as a cause of dysfunctional stay-green mediated by source:sink imbalance. In apparently sink-limited ‘Campesino’, shading reduced grain number, but this was partly compensated for by a sizeable increase in TKW and in GPC (Figures 2E, F), which helped maintain a high sink demand for assimilates and remobilized Nitrogen. Consequently, only relatively small differences between treatments in the timing and dynamics of senescence were observed in this cultivar, and only for leaves (Figure 2). In contrast, ‘Piznair’ was unable to compensate *via* increases in TKW, and sink demand for assimilates and Nitrogen was therefore more strongly reduced. Accordingly, the delay in the onset and progression of senescence was accentuated in this cultivar, and the delay was also apparent in ears and stems. These patterns therefore confirm the importance of sink:source balances in the regulation of senescence under stress-free conditions and strongly suggest that pre-anthesis canopy shading caused dysfunctional stay-green.

In contrast to the obvious agronomic and phenological effects of shading, direct measurements of photosynthetic rate and stomatal conductance in the field were less conclusive, although direction and relative size of effects across the tested genotypes do seem to indicate that the expected decrease in photosynthetic rate and stomatal conductance did in fact occur (Figure 5). Reynolds et al. (2005) and Miralles and Slafer (1997) also suggested that sink strength should be a major factor determining post-anthesis growth, and a common observation has been that upon removal of source capacity during grain filling, stomatal conductance and photosynthetic rates are increased in compensation (Rawson et al., 1976; Richards, 1996); so the inverse should equally be true. In a similar experiment with zucchini, sink limitation did not significantly reduce photosynthetic rates, but nevertheless

increased leaf temperature and had other notable leaf- and canopy level effects that were readily detectable using reflectance-based approaches (Burnett et al., 2021). Thus, sink-limitation may not necessarily have immediate and strong effects on leaf photosynthesis. Here, an additional plausible explanation for the lack of a similarly clear difference between treatments in stomatal conductance and photosynthesis may be the difficulty in upscaling spot measurements performed on single and randomly selected leaves to entire field canopies.

4.2 Feasibility of stay-green functionality monitoring using high throughput canopy temperature measurements

CT differed significantly between the treatments in the initial phase immediately following the removal of the shading tents (Figures 8, 9, top rows), and this effect cannot be well explained by expected differences in leaf activity traits resulting from the shading treatment. It seems more likely that these initial differences represented side-effects of the shading treatment on canopy structure and on the contribution of different organs to plot-level CT signals (Supplementary Figure S2). Spikes and peduncles were found to be consistently warmer than flag leaves at different stages of grain filling by Ayeneh et al. (2002); Similarly, Vicente et al. (2018) found durum wheat ears to be consistently warmer than leaves, and Fernandez-Gallego et al. (2019) even exploited this fact to obtain automatic ear counts from thermal images. A higher contribution of warmer ears to plot-level CT signals is therefore a likely reason for the observed initial differences (cf. Supplementary Figure S2). When considering the entire stay-green phase, there was an obvious gradual increase in CT of shaded canopies relative to unshaded controls over a period of almost three weeks. This increase appeared to be nearly constant during the early grain filling phase (until approximately 18 June) and was then interrupted

by a period of less stable weather conditions (Figure 6); however, it quickly reestablished upon a return of more stable weather conditions shortly after. These basic observations are in full agreement with the indications based on all other measurements that shading introduced dysfunctional stay-green and it clearly suggests that this had a direct and measurable effect on CT. In particular, a gradually increasing contrast in CT between treatments is expected under the assumption of an increasingly downregulating effect of limited sink demand on grain filling rates and, consequently, leaf activity traits. Conversely, a more abrupt effect would be expected if the reduction in sink demand immediately triggered a proportional decrease in leaf activity. Unfortunately, to the best of our knowledge, sink-regulation of photosynthesis during grain filling in wheat (and thus the expected response of photosynthetic rates and stomatal conductance to reductions in sink strength) is poorly understood. Intuitively, it would seem more natural for this effect to build up gradually, since there should be no constraints to grain filling in an initial phase. In any case, this clear temporal pattern cannot be explained by the minor differences in canopy structure that were inadvertently introduced through the shading treatment (Figure 2), since only fully established, static canopies were monitored.

Despite the strong effects of the shading treatment on physiological and phenological traits of interest, observed differences in CT between the treatments were limited to less than 1°C. This is substantially less variation than we observed previously within a set of diverse genotypes measured during the same growth stages at the same site (Perich et al., 2020; Anderegg et al., 2021), where differences across measurement dates between coolest and hottest canopies ranged from 3.1°C to 11.8°C in raw data, and from 1.8°C to 6.8°C after spatial correction of the CT signals (reanalyzed from Perich et al., 2020; Anderegg et al., 2021). Limiting these analyses to Swiss elite breeding material resulted in a very similar picture. Similar ranges were observed across different years and time of day by (Deery et al., 2019, see e.g., Figure 9 in their paper). If our interpretation of the initial differences in CT is correct, then that should be considered the baseline for the quantification of the effect of differences in stay-green functionality on CT, i.e., the total effect would amount to approximately 1.5°C and 0.8°C for ‘Piznair’ and ‘Campesino’, respectively (cf. Figure 7). While this would be a sizeable effect, it clearly must be considered the maximum expected effect in experiments without treatments. In a set of historical lines from CIMMYT spanning 26 years of breeding, reported a decrease in CT of approximately 0.6°C that could be associated with higher stomatal conductance (Fischer et al., 1998). Yet, this number may have been influenced by traits other than leaf activity, although above ground biomass was ruled out as a relevant factor in that study.

The gradual nature of the observed effects of sink limitation on CT during grain filling confirms the hypothesized advantage of a time-integrated analysis of individual measurements (Anderegg et al., 2021). We already observed a moderate to high heritability of plot-based temporal trends in CT under the conditions of the study site, but it was unclear to what extent they represented genotype-specific reactions to progressive soil drying or again an

effect of confounding factors, such as heritable changes in canopy structure during the assessment period. Given the possibility of within-genotype comparisons in this study, these confounding effects could be excluded, underscoring the meaningfulness and advantage of time-integrated analysis of CT changes during periods of stable meteorological conditions.

5 Conclusions

This study integrated gold standard physiological measurements and traditional experimental approaches with recently developed RGB- and thermal-image-based high throughput phenotyping protocols, with the aim of developing a better understanding of the sensitivity limits of remote-sensing-based phenotyping approaches in stay-green wheat canopies. Our results clearly indicate differences in stay-green functionality translate into measurable differences in CT. Importantly, they appear to do so in the absence of co-variation in confounding traits (such as above ground biomass, green leaf area, or plant height), and in dense canopies with (near-)complete soil cover, as typically observed in high-yielding, stress-free environments. While it remains challenging to separate effects on CT related to stay-green properties from effects related to confounding factors in scenarios with more genotypic diversity, our findings provide a strong basis for future uses of CT for a better characterization of the physiological status of stay-green wheat canopies during early grain filling. Modest effect sizes highlight the importance of restricting screenings to a limited range of morphological and phenological diversity, as already recommended in a similar context by Lopes and Reynolds (2010). Finally, gradually increasing effects of sink limitation on CT underscore the importance of frequent measurements and a time-integrated analysis.

Data availability statement

The annotated data sets representing the target domain are available via the Repository for Publications and Research data of ETH Zürich (<https://doi.org/10.3929/ethz-b-000668219>). All other raw data supporting the conclusions of this article will be made available by the authors, without undue reservation.

Author contributions

JA: Validation, Writing – review & editing, Writing – original draft, Visualization, Software, Methodology, Investigation, Formal Analysis, Data curation, Conceptualization. NK: Writing – review & editing, Methodology, Investigation, Data curation. HA: Writing – review & editing, Methodology, Funding acquisition. OZ: Writing – review & editing, Investigation. BK: Writing – review & editing, Investigation, Formal Analysis. RZ: Writing – review & editing, Software, Methodology. AW: Writing – review & editing,

Resources, Conceptualization. AH: Writing – review & editing, Methodology, Investigation, Conceptualization.

Funding

The author(s) declare financial support was received for the research, authorship, and/or publication of this article. We acknowledge funding for the development and implementation of the multi-sensor pack within the Project CT-PhotoInd, funded under the SNF SPARK theme (Project Number CRSK-3_195591). The rest of the project was funded by ETH Zürich. Open access funding by ETH Zurich.

Acknowledgments

We thank Simon Corrado and Brigitta Herzog (both ETH Crop Science) for crop husbandry and assistance with seed preparation and management; Seraina Wagner, Sophie Vuillemin, Tenzin Khampo (all ETH Plant Pathology) and Michelle Kremers (ETH Crop Science) for assistance with field measurements and annotations; Mohammad Hosein Fakhrosae (ETH Crop Science) for help with harvest trait determination; Bruce McDonald (ETH Plant Pathology) for sharing resources and for assistance in project coordination and management; and Nicola Storni and Flavian Tschurr (ETH Crop Science) for preparing the plant height data.

References

- Amani, I., Fischer, R. A., and Reynolds, M. P. (1996). Canopy temperature depression association with yield of irrigated spring wheat cultivars in a hot climate. *J. Agron. Crop Sci.* 176, 119–129. doi: 10.1111/j.1439-037X.1996.tb00454.x
- Anderegg, J., Aasen, H., Perich, G., Roth, L., Walter, A., and Hund, A. (2021). Temporal trends in canopy temperature and greenness are potential indicators of late-season drought avoidance and functional stay-green in wheat. *Field Crops Res.* 274, 108311. doi: 10.1016/j.fcr.2021.108311
- Anderegg, J., Yu, K., Aasen, H., Walter, A., Liebisch, F., and Hund, A. (2020). Spectral vegetation indices to track senescence dynamics in diverse wheat germplasm. *Front. Plant Sci.* 10, 1749. doi: 10.3389/fpls.2019.01749
- Anderegg, J., Zenkl, R., Walter, A., Hund, A., and McDonald, B. A. (2023). Combining high-resolution imaging, deep learning, and dynamic modeling to separate disease and senescence in wheat canopies. *Plant Phenomics* 5, 53. doi: 10.34133/plantphenomics.0053
- Ayeneh, A., van Ginkel, M., Reynolds, M. P., and Ammar, K. (2002). Comparison of leaf, spike, peduncle and canopy temperature depression in wheat under heat stress. *Field Crops Res.* 79, 173–184. doi: 10.1016/S0378-4290(02)00138-7
- Backhaus, A. E., Griffiths, C., Vergara-Cruces, A., Simmonds, J., Lee, R., Morris, R. J., et al. (2023). Delayed development of basal spikelets in wheat explains their increased floret abortion and rudimentary nature. *J. Exp. Bot.* 74, 5088–5103. doi: 10.1093/jxb/erad233
- Bogard, M., Allard, V., Brancourt-Hulmel, M., Heumez, E., Machet, J.-M., Jeuffroy, M.-H., et al. (2010). Deviation from the grain protein concentration–grain yield negative relationship is highly correlated to post-anthesis N uptake in winter wheat. *J. Exp. Bot.* 61, 4303–4312. doi: 10.1093/jxb/erq238
- Borrás, L., Slafer, G. A., and Otegui, M. E. (2004). Seed dry weight response to source–sink manipulations in wheat, maize and soybean: a quantitative reappraisal. *Field Crops Res.* 86, 131–146. doi: 10.1016/j.fcr.2003.08.002
- Brocklehurst, P. A. (1977). Factors controlling grain weight in wheat. *Nature* 266, 348–349. doi: 10.1038/266348a0
- Burnett, A. C., Serbin, S. P., and Rogers, A. (2021). Source:sink imbalance detected with leaf- and canopy-level spectroscopy in a field-grown crop. *Plant Cell Environ.* 44, 2466–2479. doi: 10.1111/pce.14056
- Chapman, E. A., Orford, S., Lage, J., and Griffiths, S. (2021). Capturing and selecting senescence variation in wheat. *Front. Plant Sci.* 12. doi: 10.3389/fpls.2021.638738
- Christopher, J. T., MansChadi, A. M., Hammer, G. L., and Borrell, A. K. (2008). Developmental and physiological traits associated with high yield and stay-green phenotype in wheat. *Crop Pasture Sci.* 59, 354–364. doi: 10.1071/AR07193
- Christopher, J. T., Veyradier, M., Borrell, A. K., Harvey, G., Fletcher, S., and Chenu, K. (2014). Phenotyping novel stay-green traits to capture genetic variation in senescence dynamics. *Funct. Plant Biol.* 41, 1035–1048. doi: 10.1071/FP14052
- Deery, D. M., and Jones, H. G. (2021). Field phenomics: will it enable crop improvement? *Plant Phenomics* 2021. doi: 10.34133/2021/9871989
- Deery, D. M., Rebetzke, G. J., Jimenez-Berni, J. A., Bovill, W. D., James, R. A., Condon, A. G., et al. (2019). Evaluation of the phenotypic repeatability of canopy temperature in wheat using continuous-terrestrial and airborne measurements. *Front. Plant Sci.* 10. doi: 10.3389/fpls.2019.00875
- Deery, D. M., Rebetzke, G. J., Jimenez-Berni, J. A., James, R. A., Condon, A. G., Bovill, W. D., et al. (2016). Methodology for high-throughput field phenotyping of canopy temperature using airborne thermography. *Front. Plant Sci.* 7. doi: 10.3389/fpls.2016.01808
- Fernandez-Gallego, J. A., Kefauver, S. C., Vatter, T., Aparicio Gutiérrez, N., Nieto-Taladriz, M. T., and Araus, J. L. (2019). Low-cost assessment of grain yield in durum wheat using RGB images. *Eur. J. Agron.* 105, 146–156. doi: 10.1016/j.eja.2019.02.007
- Fischer, R. A. (1975). Yield potential in a dwarf spring wheat and the effect of shading1. *Crop Sci.* 15. doi: 10.2135/cropsci1975.0011183X001500050002x
- Fischer, R. A. (1985). Number of kernels in wheat crops and the influence of solar radiation and temperature. *J. Agric. Sci.* 105, 447–461. doi: 10.1017/S0021859600056495
- Fischer, R. A., Rees, D., Sayre, K. D., Lu, Z.-M., Condon, A. G., and Saavedra, A. L. (1998). Wheat yield progress associated with higher stomatal conductance and photosynthetic rate, and cooler canopies. *Crop Sci.* 38, 1467. doi: 10.2135/cropsci1998.0011183X003800060011x
- Gregersen, P. L., Culetic, A., Boschian, L., and Krupinska, K. (2013). Plant senescence and crop productivity. *Plant Mol. Biol.* 82, 603–622. doi: 10.1007/s11103-013-0013-8

Conflict of interest

The authors declare that the research was conducted in the absence of any commercial or financial relationships that could be construed as a potential conflict of interest.

The author(s) declared that they were an editorial board member of Frontiers, at the time of submission. This had no impact on the peer review process and the final decision.

Publisher's note

All claims expressed in this article are solely those of the authors and do not necessarily represent those of their affiliated organizations, or those of the publisher, the editors and the reviewers. Any product that may be evaluated in this article, or claim that may be made by its manufacturer, is not guaranteed or endorsed by the publisher.

Supplementary material

The Supplementary Material for this article can be found online at: <https://www.frontiersin.org/articles/10.3389/fpls.2024.1335037/full#supplementary-material>

- Gregersen, P. L., Holm, P. B., and Krupinska, K. (2008). Leaf senescence and nutrient remobilization in barley and wheat. *Plant Biol.* 10, 37–49. doi: 10.1111/j.1438-8677.2008.00114.x
- Grieder, C., Hund, A., and Walter, A. (2015). Image based phenotyping during winter: a powerful tool to assess wheat genetic variation in growth response to temperature. *Funct. Plant Biol.* 42, 387–396. doi: 10.1071/FP14226
- He, K., Zhang, X., Ren, S., and Sun, J. (2016). “Deep residual learning for image recognition, in: 2016 IEEE conference on computer vision and pattern recognition (CVPR),” in *Presented at the 2016 IEEE Conference on Computer Vision and Pattern Recognition (CVPR)*, Las Vegas, NV, USA. 770–778 (IEEE). doi: 10.1109/CVPR.2016.90
- Jiang, G. H., He, Y. Q., Xu, C. G., Li, X. H., and Zhang, Q. (2004). The genetic basis of stay-green in rice analyzed in a population of doubled haploid lines derived from an indica by japonica cross. *Theor. Appl. Genet.* 108, 688–698. doi: 10.1007/s00122-003-1465-z
- Jones, H. G., and Vaughan, R. A. (2011). Remote sensing of vegetation: principles, techniques and applications. By Hamlyn G. Jones Robin A Vaughan. *J. Vegetation Sci.* 22, 1151–1153. doi: 10.1111/jvs.2011.22.issue-6
- Joshi, A. K., Kumari, M., Singh, V. P., Reddy, C. M., Kumar, S., Rane, J., et al. (2007). Stay green trait: variation, inheritance and its association with spot blotch resistance in spring wheat (<Emphasis Type=“Italic”>Triticum</Emphasis><Emphasis Type=“Italic”> aestivum</Emphasis> L.). *Euphytica* 153, 59–71. doi: 10.1007/s10681-006-9235-z
- Keller, B., Soto, J., Steier, A., Portilla-Benavides, A. E., Raatz, B., Studer, B., et al. (2023). Linking photosynthesis and yield reveals a strategy to improve light use efficiency in a doubled bean breeding population. *J. Exp. Bot.* 5, 901–916. doi: 10.1093/jxb/erad416
- Kichey, T., Hirel, B., Heumez, E., Dubois, F., and Le Gouis, J. (2007). In winter wheat (*Triticum aestivum* L.), post-anthesis nitrogen uptake and remobilization to the grain correlates with agronomic traits and nitrogen physiological markers. *Field Crops Res.* 102, 22–32. doi: 10.1016/j.fcr.2007.01.002
- Kirchgessner, N., Liebisch, F., Yu, K., Pfeifer, J., Friedli, M., Hund, A., et al. (2017). The ETH field phenotyping platform FIP: a cable-suspended multi-sensor system. *Funct. Plant Biol.* 44, 154–168. doi: 10.1071/FP16165
- Kuhlert, S., Austic, G., Zegarac, R., Osei-Bonsu, I., Hoh, D., Chilvers, M. I., et al. (2016). MultispeQ Beta: a tool for large-scale plant phenotyping connected to the open PhotosynQ network. *R. Soc. Open Sci.* 3, 160592. doi: 10.1098/rsos.160592
- Lancashire, P. D., Bleiholder, H., Boom, T. V. D., Langelüddeke, P., Stauss, R., Weber, E., et al. (1991). A uniform decimal code for growth stages of crops and weeds. *Ann. Appl. Biol.* 119, 561–601. doi: 10.1111/j.1744-7348.1991.tb04895.x
- Lenth, R., Buerkner, P., Herve, M., Love, J., Riebl, H., and Singmann, H. (2020). *emmeans: estimated marginal means, aka least-squares means*.
- Li, X., Ingvordsen, C. H., Weiss, M., Rebetzke, G. J., Condon, A. G., James, R. A., et al. (2019). Deeper roots associated with cooler canopies, higher normalized difference vegetation index, and greater yield in three wheat populations grown on stored soil water. *J. Exp. Bot.* 70, 4963–4974. doi: 10.1093/jxb/erz232
- Lopes, M. S., and Reynolds, M. P. (2010). Partitioning of assimilates to deeper roots is associated with cooler canopies and increased yield under drought in wheat. *Funct. Plant Biol.* 37, 147–156. doi: 10.1071/FP09121
- Lopes, M. S., and Reynolds, M. P. (2012). Stay-green in spring wheat can be determined by spectral reflectance measurements (normalized difference vegetation index) independently from phenology. *J. Exp. Bot.* 63, 3789–3798. doi: 10.1093/jxb/ers071
- Miralles, D. J., and Slafer, G. A. (1997). Radiation interception and radiation use efficiency of near-isogenic wheat lines with different height. *Euphytica* 97, 201–208. doi: 10.1023/A:1003061706059
- Naruoka, Y., Sherman, J. D., Lanning, S. P., Blake, N. K., Martin, J. M., and Talbert, L. E. (2012). Genetic analysis of green leaf duration in spring wheat. *Crop Sci.* 52, 99. doi: 10.2135/cropsci2011.05.0269
- Pask, A., Pietragalla, J., Mullan, D., and Reynolds, M. P. (2012). *Physiological breeding II : a field guide to wheat phenotyping*, Vol. iv. 132 pages. Mexico, DF: CIMMYT.
- Perich, G., Hund, A., Anderegg, J., Roth, L., Boer, M. P., Walter, A., et al. (2020). Assessment of multi-image unmanned aerial vehicle based high-throughput field phenotyping of canopy temperature. *Front. Plant Sci.* 11. doi: 10.3389/fpls.2020.00150
- Pinheiro, J., Bates, D., DebRoy, S., and Sarkar, D. (2021). *nlme: linear and nonlinear mixed effects models*. R package version 3.1-155. Available at: <https://CRAN.R-project.org/package=nlme>.
- Prashar, A., and Jones, H. (2014). Infra-red thermography as a high-throughput tool for field phenotyping. *Agronomy* 4, 397–417. doi: 10.3390/agronomy4030397
- Rajcan, I., and Tollenaar, M. (1999). Source : sink ratio and leaf senescence in maize: II. Nitrogen metabolism during grain filling. *Field Crops Res.* 60, 255–265. doi: 10.1016/S0378-4290(98)00143-9
- Rawson, H. M., Gifford, R. M., and Bremner, P. M. (1976). Carbon dioxide exchange in relation to sink demand in wheat. *Planta* 132, 19–23. doi: 10.1007/BF00390326
- R Core Team (2018). R: A language and environment for statistical computing Vol. 2012 (Vienna, Austria: R Foundation for Statistical Computing). Available at: <http://www.R-project.org>.
- Rebetzke, G. J., Rattey, A. R., Farquhar, G. D., Richards, R. A., and Condon, A. (2013). enomic regions for canopy temperature and their genetic association with stomatal conductance and grain yield in wheat. *Funct. Plant Biol.* 40, 14–33. doi: 10.1071/FP12184
- Reynolds, M. P., Balota, M., Delgado, M. I. B., Amani, I., and Fischer, R. A. (1994). Physiological and morphological traits associated with spring wheat yield under hot, irrigated conditions. *Funct. Plant Biol.* 21, 717–730. doi: 10.1071/PP9940717
- Reynolds, M. P., Pellegrineschi, A., and Skovmand, B. (2005). Sink-limitation to yield and biomass: a summary of some investigations in spring wheat. *Ann. Appl. Biol.* 146, 39–49. doi: 10.1111/j.1744-7348.2005.03100.x
- Richards, R. A. (1996). “Increasing yield potential in wheat - source and sink limitations,” in *Increasing yield potential in wheat: breaking the barriers*. Mexico, DF: CIMMYT.
- Roche, D. (2015). Stomatal conductance is essential for higher yield potential of C3 crops. *Crit. Rev. Plant Sci.* 34, 429–453. doi: 10.1080/07352689.2015.1023677
- Roth, L., Camenzind, M., Aasen, H., Kronenberg, L., Barendregt, C., Camp, K.-H., et al. (2020). Repeated multiview imaging for estimating seedling tiller counts of wheat genotypes using drones [WWW document]. *Plant Phenomics*. doi: 10.34133/2020/3729715
- Savin, R., and Slafer, G. A. (1991). Shading effects on the yield of an Argentinian wheat cultivar. *J. Agric. Sci.* 116, 1–7. doi: 10.1017/S0021859600076085
- Slafer, G. A., Calderini, D. F., Miralles, D. J., and Dreccer, M. F. (1994). Preanthesis shading effects on the number of grains of three bread wheat cultivars of different potential number of grains. *Field Crops Res.* 36, 31–39. doi: 10.1016/0378-4290(94)90050-7
- Stockman, Y. M., Fischer, R. A., and Brittain, E. G. (1983). Assimilate supply and floret development within the spike of wheat (*Triticum aestivum* L.). *Funct. Plant Biol.* 10, 585–594. doi: 10.1071/PP9830585
- Strebel, S., Levy Häner, L., Mattin, M., Schaad, N., Morisoli, R., Watroba, M., et al. (2022). Liste der empfohlenen Getreidesorten für die Ernte 2023. *Agroscope Transfer* 443.
- Thapa, S., Jessup, K. E., Pradhan, G. P., Rudd, J. C., Liu, S., Mahan, J. R., et al. (2018). Canopy temperature depression at grain filling correlates to winter wheat yield in the U.S. South. *High Plains. Field Crops Res.* 217, 11–19. doi: 10.1016/j.fcr.2017.12.005
- Thomas, H., and Ougham, H. (2014). The stay-green trait. *J. Exp. Bot.* 65, 3889–3900. doi: 10.1093/jxb/eru037
- Treier, S., Roth, L., Hund, A., Kirchgessner, N., Aasen, H., Walter, A., et al. (2023). *Digital lean phenotyping methods in the context of wheat variety testing – the cases of canopy temperature and phenology (preprint)*. doi: 10.22541/essoar.169870265.59272601/v1
- Triboi, E., and Triboi-Blondel, A.-M. (2002). Productivity and grain or seed composition: a new approach to an old problem—invited paper. *Eur. J. Agron.* 16, 163–186. doi: 10.1016/S1161-0301(01)00146-0
- Uauy, C., Brevis, J. C., and Dubcovsky, J. (2006). The high grain protein content gene Gpc-B1 accelerates senescence and has pleiotropic effects on protein content in wheat. *J. Exp. Bot.* 57, 2785–2794. doi: 10.1093/jxb/erl047
- van Oosterom, E. J., Chapman, S. C., Borrell, A. K., Broad, I. J., and Hammer, G. L. (2010). Functional dynamics of the nitrogen balance of sorghum. II. Grain filling period. *Field Crops Res.* 115, 29–38. doi: 10.1016/j.fcr.2009.09.019
- Vicente, R., Vergara-Díaz, O., Medina, S., Chairi, F., Kefauver, S. C., Bort, J., et al. (2018). Durum wheat ears perform better than the flag leaves under water stress: Gene expression and physiological evidence. *Environ. Exp. Bot.* 153, 271–285. doi: 10.1016/j.envexpbot.2018.06.004
- Xie, Q., Mayes, S., and Sparkes, D. L. (2016). Early anthesis and delayed but fast leaf senescence contribute to individual grain dry matter and water accumulation in wheat. *Field Crops Res.* 187, 24–34. doi: 10.1016/j.fcr.2015.12.009
- Yang, J., and Zhang, J. (2006). Grain filling of cereals under soil drying. *New Phytol.* 169, 223–236. doi: 10.1111/j.1469-8137.2005.01597.x



OPEN ACCESS

EDITED BY

Ignacio Romagosa,
Agrotecnio Center, Spain

REVIEWED BY

Bernardo Ordas,
Spanish National Research Council (CSIC),
Spain
Zhenyu Gao,
Chinese Academy of Agricultural Sciences,
China

*CORRESPONDENCE

Gang Qin

✉ qingang@gxaas.net

Yuexiong Zhang

✉ zhangyx1518@126.com

[†]These authors have contributed equally to this work

RECEIVED 23 February 2024

ACCEPTED 20 May 2024

PUBLISHED 07 June 2024

CITATION

Wei M, Yan Q, Huang D, Ma Z, Chen S, Yin X, Liu C, Qin Y, Zhou X, Wu Z, Lu Y, Yan L, Qin G and Zhang Y (2024) Integration of molecular breeding and multi-resistance screening for developing a promising restorer line Guihui5501 with heavy grain, good grain quality, and endurance to biotic and abiotic stresses. *Front. Plant Sci.* 15:1390603. doi: 10.3389/fpls.2024.1390603

COPYRIGHT

© 2024 Wei, Yan, Huang, Ma, Chen, Yin, Liu, Qin, Zhou, Wu, Lu, Yan, Qin and Zhang. This is an open-access article distributed under the terms of the [Creative Commons Attribution License \(CC BY\)](#). The use, distribution or reproduction in other forums is permitted, provided the original author(s) and the copyright owner(s) are credited and that the original publication in this journal is cited, in accordance with accepted academic practice. No use, distribution or reproduction is permitted which does not comply with these terms.

Integration of molecular breeding and multi-resistance screening for developing a promising restorer line Guihui5501 with heavy grain, good grain quality, and endurance to biotic and abiotic stresses

Minyi Wei^{1†}, Qun Yan^{2†}, Dahui Huang¹, Zengfeng Ma¹, Shen Chen³, Xiaoting Yin⁴, Chi Liu¹, Yuanyuan Qin⁵, Xiaolong Zhou¹, Zishuai Wu¹, Yingping Lu⁶, Liuhui Yan⁶, Gang Qin^{1*} and Yuexiong Zhang^{1*}

¹Rice Research Institute, Guangxi Academy of Agricultural Sciences/Guangxi Key Laboratory of Rice Genetics and Breeding/State Key Laboratory for Conservation and Utilization of Subtropical Agro-bioresources, Nanning, China, ²Plant Protection Research Institute, Guangxi Academy of Agricultural Sciences, Nanning, China, ³Institute of Plant Protection, Guangdong Academy of Agricultural Sciences, Guangdong Provincial Key Laboratory of High Technology for Plant Protection, Guangzhou, China, ⁴Enping Plant Protection Station, Enping, China, ⁵Agricultural Science and Technology Information Research Institute, Guangxi Academy of Agricultural Sciences, Nanning, China, ⁶Liuzhou Branch, Guangxi Academy of Agricultural Sciences, Liuzhou Research Center of Agricultural Sciences, Liuzhou, China

Rice, a critical staple on a global scale, faces escalating challenges in yield preservation due to the rising prevalence of abiotic and biotic stressors, exacerbated by frequent climatic fluctuations in recent years. Moreover, the scorching climate prevalent in the rice-growing regions of South China poses obstacles to the cultivation of good-quality, heavy-grain varieties. Addressing this dilemma requires the development of resilient varieties capable of withstanding multiple stress factors. To achieve this objective, our study employed the broad-spectrum blast-resistant line Digu, the brown planthopper (BPH)-resistant line ASD7, and the heavy-grain backbone restorer lines Fuhui838 (FH838) and Shuhui527 (SH527) as parental materials for hybridization and multiple crossings. The incorporation of molecular markers facilitated the rapid pyramiding of six target genes (*Pi5*, *Pita*, *Pid2*, *Pid3*, *Bph2*, and *Wx^b*). Through a comprehensive evaluation encompassing blast resistance, BPH resistance, cold tolerance, grain appearance, and quality, alongside agronomic trait selection, a promising restorer line, Guihui5501 (GH5501), was successfully developed. It demonstrated broad-spectrum resistance to blast, exhibiting a resistance frequency of 77.33% against 75 artificially inoculated isolates, moderate resistance to BPH (3.78 grade), strong cold tolerance during the seedling stage (1.80 grade), and characteristics of heavy grains (1,000-grain weight reaching 35.64 g) with good grain quality. The primary rice quality parameters for GH5501, with the exception of alkali spreading value, either met or exceeded the second-grade national standard for premium edible rice

varieties, signifying a significant advancement in the production of good-quality heavy-grain varieties in the southern rice-growing regions. Utilizing GH5501, a hybrid combination named Nayou5501, characterized by high yield, good quality, and resistance to multiple stresses, was bred and received approval as a rice variety in Guangxi in 2021. Furthermore, genomic analysis with gene chips revealed that GH5501 possessed an additional 20 exceptional alleles, such as *NRT1.1B* for efficient nitrogen utilization, *SKC1* for salt tolerance, and *STV11* for resistance to rice stripe virus. Consequently, the restorer line GH5501 could serve as a valuable resource for the subsequent breeding of high-yielding, good-quality, and stress-tolerant hybrid rice varieties.

KEYWORDS

rice, restorer line, marker-assisted selection (MAS), blast, brown planthopper (BPH), cold tolerance, heavy-grain, quality

1 Introduction

Rice (*Oryza sativa* L.) stands as one of the world's most critical food crops, experiencing significant yield improvements after two Green Revolutions (dwarfing breeding and hybrid vigor utilization). However, breeding practices for rice quality and resistance have lagged behind (Lou et al., 2023). Hybrid rice exhibits a 10%–20% yield advantage over conventional varieties (Zeng et al., 2017), profoundly enhancing China's and the world's food self-sufficiency. Hybrid rice breeding, a complex procedure involving the development of male-sterile lines, restorer lines, and hybrid combinations, entails lengthy breeding cycles, technical intricacies, and tedious processes. The breeding of male-sterile lines, particularly cytoplasmic male-sterile (CMS) lines, necessitates multiple rounds of selection and sterility testing to ensure their stability, which consumes significant labor and time resources. In contrast, the breeding procedure for restorer lines is more straightforward and prone to breakthroughs. Hence, efficiently consolidating high yield, good quality, and stress tolerance traits into restorer lines to develop breakthrough hybrid rice varieties represents a crucial avenue for future rice breeding research.

Blast disease and brown planthopper (BPH) infestations are two of the most severe challenges in rice production, leading to significant reductions in yield and quality deterioration (Pennisi, 2010). The rice blast disease poses a significant threat to both northern and southern rice cultivation regions in China, with Guangxi emerging as a major hotspot for this pathogen. Varying degrees of annual damage are observed across these regions due to the prevalence of the disease. In recent years, the annual occurrence of blast disease in Guangxi has reached approximately 533,000 hectares, representing roughly a quarter of the total rice cultivation area in Guangxi. Previous studies have indicated that the most economically effective and environmentally friendly approach to controlling blast disease is through the breeding of broad-spectrum and durable resistant varieties, involving the utilization of broad-spectrum resistance genes

or combining multiple resistance genes (Tacconi et al., 2010; Devanna et al., 2022). To date, over 100 blast-resistant genes have been identified, with 38 R genes cloned (Ning et al., 2020). These findings provide crucial genetic resources for molecular breeding aimed at enhancing blast resistance.

The BPH is also a major pest affecting rice production (Du et al., 2009). Currently, 70 BPH resistance genes/quantitative trait loci (QTLs) have been identified in rice, with 17 resistance genes already cloned (Yan et al., 2023). Out of these, nine genes primarily utilized in BPH resistance breeding are *Bph1*, *Bph2*, *Bph3*, *Bph6*, *Bph9*, *Bph14*, *Bph15*, *Bph18*, and *Bph26*. Varieties bred with *Bph1*, *Bph2*, and *Bph3* have been widely promoted in Southeast Asian countries, showcasing the broad application of these resistance genes.

Rice, originating from tropical and subtropical regions, is a temperature-sensitive crop (Andaya and Mackill, 2003). Exposure to low temperatures during rice sowing and transplanting can lead to slow seedling growth, seedling decay, and seedling death, resulting in reduced yields. Seedling-stage cold damage is a significant concern affecting production in the double-season indica rice regions of southern China and the middle-lower reaches of the Yangtze River, where chill weather frequently returns in later spring (March–April), a phenomenon referred to as “cold spell in later spring”. In the past 15 years, Guangxi has experienced six such severe events in 2007, 2008, 2010, 2014, 2020, and 2023, causing extensive seedling decay and death, consequently resulting in significant yield losses for the early rice season. Therefore, breeding new rice varieties with strong cold tolerance during the seedling stage holds great significance for ensuring early rice production in southern China and the middle-lower reaches of the Yangtze River. It also helps prevent cold weather damage for early-seeded varieties in expanded planting regions with mid- and late-maturing varieties. Rice tolerance to low-temperature stress is a complex quantitative trait controlled by multiple genes. Currently, only a few genes related to seedling-stage cold tolerance have been identified, such as LTG1 (Lu et al., 2014), *Cold1* (Ma et al., 2015),

qCST-9 (Zhao et al., 2017), *HAN1* (Mao et al., 2019), and *OsSEH1* (Gu et al., 2023). Moreover, there are few reports on molecular breeding for improving rice seedling-stage cold tolerance.

As people's living standards rise rapidly, Chinese consumers are increasingly demanding high-quality rice. The breeding of inbred varieties with high-quality rice has been quite successful in the past decade, as the majority of current inbred varieties produce rice of high quality that meets the first or second standard of premium-quality rice in the Chinese market. However, there is still considerable room for improvement in the quality of hybrid rice (Yang et al., 2020; Seck et al., 2023). The *Wx* locus plays a pivotal role in influencing not only amylose content (AC) and appearance quality (AQ) but also the eating and cooking quality (ECQ) of rice, thus serving as a multifunctional locus (Lou et al., 2023). Many *Wx* alleles including *wx*, *Wx^a*, *Wx^b*, *Wxⁱⁿ* (*Wx^{g1}*), *Wx^{g2}*, and *Wx^{g3}* (*Wx^{lv}*) have been identified in rice (Teng et al., 2012; Huang et al., 2020). Of these *Wx* alleles, the *Wx^b* allele with low amylose has been demonstrated to have significantly higher appearance, palatability, and quality phenotypes compared to other *Wx* alleles (Teng et al., 2013; Lin et al., 2023; Zhu et al., 2024). Researchers have utilized a polymorphic (CT)_n microsatellite located in the 5'-untranslated region of the *Wx* gene, known as molecular marker RM190, for its extensive application in assisting breeding programs. This marker has been proven instrumental in enhancing the efficiency of rice quality improvement through selective breeding (Temnykh et al., 2000; Jantaboon et al., 2011).

Grain weight is a crucial component affecting rice yield, and increasing grain weight has been proven effective in enhancing rice production (Li et al., 2016; Hao et al., 2021). However, the hot weather prevalent in the South China rice region is not conducive to the development of desirable appearance quality in heavy-grain varieties. Shuhui527 (SH527) and Fuhui838 (FH838), two breakthrough heavy-grain restorer lines in China after Minghui 63, exhibit outstanding characteristics such as superior grain quality and robust resistance to both biotic and abiotic stresses. Many hybrid rice varieties derived from these two lines demonstrate broad adaptability, strong stress resistance, and high and stable yields (Ren et al., 2021) (<https://www.ricedata.cn/variety/varis/601150.htm>). Notably, SH527 is one of the most frequently used restorer lines in the breeding of hybrid rice combinations in China (<https://www.ricedata.cn/variety/index.htm>). Both FH838 and SH527 serve as backbone parents in hybrid rice breeding, giving rise to numerous excellent restorer lines that have found extensive application in production.

In this study, FH838 and SH527, two elite heavy-grain restorer lines, ASD7, a line with intermediate resistance to BPH, and Digu, an elite germplasm for broad-spectrum resistance to rice blast, were employed as parents for hybridization and multiple crossing. Through the utilization of molecular marker-assisted selection (MAS), six target genes (*Pi5*, *Pita*, *Pid2*, *Pid3*, *Bph2*, and *Wx^b*) were successfully pyramided. Additionally, phenotype-based selection was extensively employed to screen for blast resistance, BPH resistance, cold tolerance, grain appearance, and quality, as well as comprehensive agronomic traits. These efforts led to the successful breeding of GH5501, a superior restorer line with high-yielding potential, good grain quality, and resilience to both biotic

and abiotic stresses, characterized by long and heavy grains. The development of GH5501 not only provided a valuable and groundbreaking restorer line for hybrid rice breeding programs but also exemplified a practical strategy for pyramiding high yield, good grain quality, and multiple resistances to biotic and abiotic stressors in rice breeding.

2 Materials and methods

2.1 Plant materials and growth conditions

In this study, four different materials were employed as parents for hybridization, aiming to introduce disease resistance, pest resistance, and cold tolerance into high-yielding, superior-quality, and resistant heavy-grain new lines. Specifically, ASD7 was utilized as a *Bph2* gene-containing, BPH-resistant material, while Digu served as a blast-resistant material containing *Pid1*, *Pid2*, and *Pid3* genes, which were identified in February 2004 and August 2009, respectively (Chen et al., 2004; Shang et al., 2009). Additionally, the heavy-grain restorer lines FH838 and SH527 were employed as widely used and excellent three-line hybrid rice restorer lines in China, with a thousand-grain weight of 32.90 g and 29.83 g, respectively. SH527 contains *Pi5*, *Pita*, and *Wx^b* genes, showcasing outstanding characteristics such as excellent grain quality and resistance, while FH838 exhibits a high seed-setting rate, broad adaptability, and consistently high yields.

The control variety TY7118, part of the TY series of heavy-grain rice varieties that have dominated early rice cultivation in Guangxi for over a decade, serves as the reference variety for rice regional trials in the South of Guangxi. The three-line sterile lines used for evaluating heterosis are Nafeng A, Tianfeng A, and Longtepu A. Except for the materials employed in disease resistance identification, all other materials were cultivated in Nanning, Guangxi, situated in the southern rice region of China. Although rice was cultivated in two seasons, early and late, in this region, achieving good external grain quality posed a challenge for heavy-grain rice varieties, particularly those with early maturation.

2.2 Evaluation of blast disease resistance

Blast resistance evaluation of GH5501 and heavy-grain parents SH527 and FH838 was conducted collaboratively by the Plant Protection Research Institute of the Guangxi Academy of Agricultural Sciences and the Plant Protection Research Institute of the Guangdong Academy of Agricultural Sciences. This assessment involved an indoor artificial spraying test utilizing 75 *Magnaporthe oryzae* isolates collected over the past decade from various blast-prone areas in Guangxi and Guangdong. All of the materials identified underwent a spore suspension spray (1×10^5 spores/mL) at the three-leaf stage in a dark environment at 26°C for 24 hours. Subsequently, they were cultured in a greenhouse with a temperature range of 24°C–30°C and a relative humidity of 90%. Seven days after inoculation, blast symptoms were evaluated using a 0–9 scale standard based on the type and size of lesions described by

the International Rice Research Institute (IRRI, 2013). Rice plants showing disease rating scales of 0–3 are considered to be resistant, and those with disease rating scales of 4–9 are susceptible.

Evaluation of field blast resistance of GH5501 and NFA took place in Nansha Village, Limu Town, Cenxi City, Hezhou Base of Agricultural Science Institute of Hezhou City, and Xinrong Village, Xinja Township, Jingxi County. These areas represent regions with the most severe natural occurrence of blast disease in Guangxi and also serve as identification points for blast disease resistance in the regional trials of rice varieties in Guangxi. The data for field blast resistance evaluation of NY5501 and TY7118 were sourced from the joint comparative and regional trials for the late-maturing rice group of early seasons in the south of Guangxi from 2018 to 2020. The resistance identification, survey methods, and grading standards adhered to the technical regulations of the Ministry of Agriculture of China, as outlined in the “Technical Regulations for Identification and Evaluation of Rice Blast Resistance in Rice Variety Trials” (NY/T2426–2014).

2.3 BPH resistance identification

The BPH resistance identification was delegated to the Plant Protection Research Institute of the Guangxi Academy of Agricultural Sciences. The insect source was collected from rice fields in Nanning, Guangxi. The local biotype of BPH in Nanning is a mixed biotype with strong virulence. The Standard Seedbox Screening Technique (SSST) was employed with slight modifications. Seeds were sown in metal trays, with each material in a row of approximately 25 plants, repeated three times. When seedlings reached the three-leaf stage, weak seedlings were removed, and each plant was infested with five first-second instar nymphs of BPH. After 7–10 days from the wilting of the “TN1” plants, the phenotype of each plant was evaluated according to the “R” (resistant) and “S” (susceptible) grading system outlined in the “Standard Evaluation System for Rice” (IRRI, 2013). The weighted average damage level was then calculated for each variety, where the average damage level ranged from 1.0 to 1.9 [high resistance (HR)], 2.0 to 3.9 [moderate resistance (MR)], 4.0 to 5.9 [low resistance (LR)], 6.0 to 7.9 [moderate susceptibility (MS)], and 8.0 to 9.0 [high susceptibility (HS)].

2.4 Cold tolerance identification methods

2.4.1 Meteorological data

Natural low-temperature meteorological data were obtained from the nearby meteorological observation station of the experimental field, provided by the Nanning Meteorological Bureau. During the period from March 1 to March 30, 2014, the average temperature was only 17°C, with particularly low daily temperatures ranging from 12.5°C to 17.0°C for half a month from March 2 to March 17, representing typical low-temperature weather.

2.4.2 Seedling-stage cold tolerance identification

The identification of natural low-temperature tolerance was conducted by sowing seeds on February 28, 2014, during early spring's low-temperature weather, without covering plastic films. The assessment took place after 30 days. For artificial cold tolerance identification, seedlings were transferred to an artificial climate chamber for cold treatment upon reaching the three-leaf stage in the greenhouse. The conditions were set at a temperature of 9°C, with a relative humidity of 75% to 85%, a light intensity of 12,000 lx, with 12 hours of light and 12 hours of darkness each day, and continuous treatment for 5 days. Subsequently, the seedlings were moved to a 26°C climate chamber for recovery for 7 days, repeated three times. Following the “Standard Evaluation System for Rice” (IRRI, 2013), an assessment was conducted based on the degree of leaf redness after cold treatment. The phenotype of each seedling was observed, and the weighted average damage level was calculated for each variety. The average damage level ranged from 1.0 to 1.9 (HR), 2.0 to 3.9 (MR), 4.0 to 5.9 (LR), 6.0 to 7.9 (MS), and 8.0 to 9.0 (HS).

2.5 Genotyping and MAS

DNA extraction from rice fresh leaves of rice seedlings followed the simplified cetyltrimethylammonium bromide (CTAB) extraction method (Murray and Thompson, 1980). The molecular markers used in this study, as outlined in Table 1, were synthesized by AuGCT Biotech Co., Ltd. (Wuhan, China). PCR was primarily conducted on a PE Company 9700 PCR instrument. The reaction system (10 µL) comprised 5.0 µL of 2× Taq Plus Master Mix II, 0.5 µL each of forward and reverse primers (10 µmol/L), 1.0 µL of template DNA, and 3.0 µL of ddH₂O. The PCR program involved an initial denaturation at 95°C for 5 min, followed by 35 cycles of denaturation at 94°C for 30 sec, annealing at 55°C for 30 sec, extension at 72°C for 40 sec, and a final extension at 72°C for 5 min. The annealing temperature was adjusted based on the specific primers used. Amplified products were electrophoresed on an 8% non-denaturing polyacrylamide gel and stained using the rapid silver staining method (Shang et al., 2009). For the PCR product of *Pid3*, 10 µL was utilized as a template, digested with the restriction enzyme *Bam*HI (TaKaRa, Dalian, China) at 37°C for 1 hour, followed by agarose gel electrophoresis for detection.

2.6 Evaluation of key agronomic traits

Throughout the breeding process, observations and analyses of plant and leaf morphology, agronomic traits, and the growth period of rice were conducted to evaluate and select superior individual plants and lines. GH5501, a newly developed restorer line, along with its parents SH527 and FH838, were planted in plots with three replications, each comprising not less than 200 plants, arranged in a randomized block design for the evaluation of yield and agronomic

TABLE 1 Molecular markers used in this study.

Target genes	Chr.	Marker	Forward primer (F)	Reverse primer (R)	Type of marker	Enzyme	Reference
<i>Bph2</i>	12	RM463	TTCCCCTCCTTTTATGGTGC	TGTTCTCCTCAGTCACTGCG	SSR		(Sun et al., 2006)
<i>Pid1</i>	2	RM262	CATTCCGTCTCGGCTCAACT	CAGAGCAAGGTGGCTTGC	SSR		(Chen et al., 2004)
<i>Pid2</i>	6	RM527	GGCTCGATCTAGAAAATCCG	TTGCACAGGTTGCGATAGAG	SSR		(Chen et al., 2004)
		RM3	ACACTGTAGCGGCCACTG	CCTCCACTGCTCCACATCTT	SSR		
<i>Pid3</i>	6	Pid3-dCAPS	TACTACTCATGGAAGCTAGTTCTC	ACGTCACAAATCATTCGCTC	dCAPS	<i>Bam</i> HI	(Shang et al., 2009)
<i>Wx^b</i>	6	RM190	CTTTGTCTATCTCAAGACAC	TGCAGATTCTTCTCTGATA	SSR		(Bligh et al., 1995)
<i>Pi5</i>	9	M-Pi5	ATAGATCATGCGCCCTCTTG	TCATACCCCATTCGGTCATT	Indel		(Gao et al., 2010)
<i>Pita</i>	12	RM7102	TTGAGAGCGTTTTTAGGATG	TCGGTTTACTTGGTTACTCG	SSR		(Fjellstrom et al., 2004)

SSR, simple sequence repeat; InDel, insertion and deletion.

traits. Field water and fertilizer management followed the Guangxi rice regional trial management method.

For the evaluation of agronomic traits, including plant height, number of tillers per plant, total number of grains per spike, fruit set, 1,000-grain weight, and grain length and width, four plants in the middle of each plot were assessed. Statistical analysis was performed using LSD software. Data on the main agronomic traits of NY5501 and TY7118 were obtained from the 2018–2020 regional trials of the late-maturing rice group in the early season in the south of Guangxi.

2.7 Heterosis investigation

The selected restorer lines were crossbred with three male-sterile lines: Nafeng A, Tianfeng A, and Longtepu A. Each combination was planted in plots measuring 15 m², repeated three times, with plots arranged randomly. The plant spacing was set at 20 cm × 23 cm. Thirty days after rice heading, measurements of plant height, effective panicles, spikelet number per panicle, 1,000-grain weight, and grain-setting rate were conducted to assess yield traits. The collected data were entered into Excel (Microsoft Office 2003) for analysis, and yield comparisons were made for each combination in the plots. Comprehensive evaluations, considering factors such as plant and leaf morphology and growth period, were performed to preliminarily assess and select superior lines.

2.8 Rice quality analysis

The rice quality assessment for all test materials and restorer lines included sending samples to the Rice and Product Quality Supervision, Inspection, and Testing Center of the Ministry of Agriculture and Rural Affairs of China for rice quality analysis. Uniform samples of NY5501

and TY7118 were provided by the Guangxi Rice Variety Regional Trial Group and sent to the Agricultural Ministry Rice and Product Quality Supervision, Inspection, and Testing Center (Hangzhou) for analysis and evaluation. This process followed the NY/T593–2013 standards of the Ministry of Agriculture of China for edible rice variety quality.

2.9 Functional gene and resistance gene haplotype analysis of GH5501

During the rice tillering stage, fresh leaves were collected, and DNA extraction was carried out using the CTAB method. Subsequently, the high-density rice gene chip GSR40K was employed to analyze the single-nucleotide polymorphisms (SNPs) of 76 functional genes and resistance genes across the entire rice genome. This chip comprised 32,887 SNPs derived from resequencing results of 4,726 cultivated rice varieties worldwide. The samples were sent to Wuhan Greenfafa Institute of Novel Genechip Research and Development Co. Ltd. (Wuhan, China) for testing. The gene chip analysis detection method is detailed in the literature (Chen et al., 2014).

3 Results

3.1 Breeding of GH5501

The breeding process of GH5501 was meticulously detailed in Figure 1. In the late growing season of 2007, ASD7, a rice variety with intermediate resistance to BPH (containing *Bph2*), was outcrossed as the female parent to Digu, a broad-spectrum blast-resistant germplasm (containing *Pid1*, *Pid2*, and *Pid3*, identified in February 2004 and August 2009, respectively). The resulting F₁ generation plants were further crossed with the elite heavy-grain

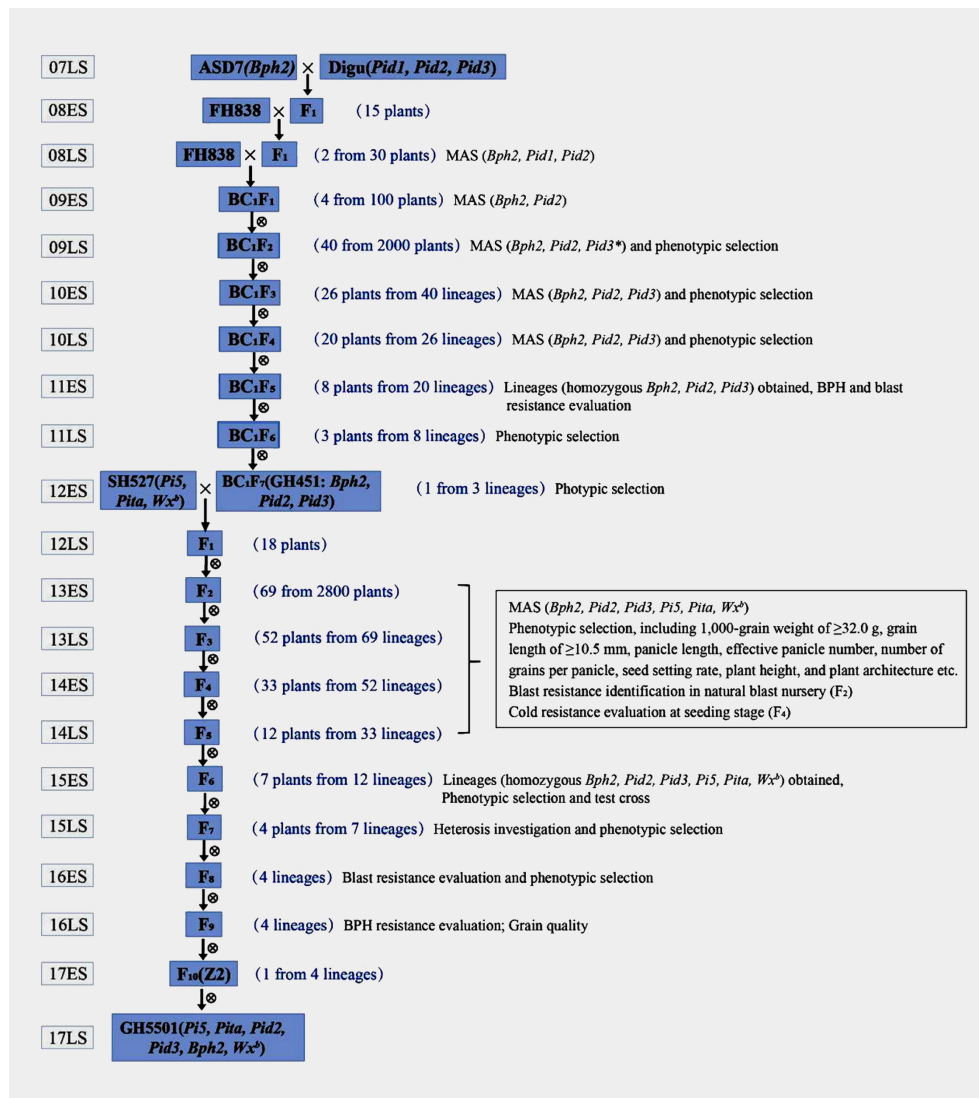


FIGURE 1

Breeding scheme for the development process of GH5501. "ES" and "LS" indicate the early season and the late season, respectively. In the late season of 2008, molecular markers of *Bph2*, *Pid1*, and *Pid2* were employed to detect three-way cross (FH838//ASD7/Digu) F₁ plants, two plants of which with both *Bph2* and *Pid2* in a heterozygous state were selected to backcrossed with FH838 (as female parent). BC₁F₁ plants were subject to molecular marker detection of *Bph2* and *Pid2* in early season in 2009, *Pid3* gene was published in August 2009, and molecular marker detection of the *Pid3* gene was not incorporated until late season in 2009.

restorer line FH838. Two plants from the intercross of FH838//ASD7/Digu, harboring both heterozygous *Bph2* and *Pid2* genes, were selected for backcrossing with FH838 (as the female parent) to produce BC₁F₁ plants. Forty plants containing heterozygous *Bph2*, *Pid2*, and *Pid3* genes were selected from BC₁F₂ for selfing to produce the BC₁F₃ generation in the late season of 2009. The *Pid3* gene was published in August 2009, and molecular marker detection of the *Pid3* gene was not incorporated until the late season of 2009. Subsequently, consecutive self-pollination, MAS, and phenotype-based screening of agronomic traits, particularly heavy grains, were carried out. In the BC₁F₇ generation, a line with all three target genes (*Bph2*, *Pid2*, and *Pid3*) in a homozygous state and a 1,000-grain weight of ≥32.0 g was selected and named Guihui451 (GH451) in the early season of 2012.

To further enhance the blast resistance and grain quality of GH451, another elite heavy-grain restorer, SH527 (containing *Pi5*, *Pita*, and *Wx*^b), was introduced as the male parent for hybridization in the early season of 2012. A total of 2,800 seedlings from the F₂ generation were grown in a natural blast nursery, and 69 individuals showing high resistance to blast were selected to propagate the F₃ generation. Starting from the F₃ to F₆ generations, MAS was employed in each generation for the six target genes (*Bph2*, *Pi5*, *Pita*, *Pid2*, *Pid3*, and *Wx*^b). In addition to MAS, phenotypic selection criteria including a 1,000-grain weight of ≥32.0 g, grain length of ≥10.5 mm, panicle length, effective panicle number, number of grains per panicle, seed setting rate, plant height, and plant architecture were applied in our breeding procedure to ensure that selected plants carried the targeted traits. Furthermore, in the

F₄ generation, under low-temperature conditions in the early season of 2014, field selection was conducted for natural cold tolerance. Only individuals showing robust growth, green leaves, and without seedling rot or leaf whitening were chosen for further selection (Figure 2). After multiple rounds of selection, seven individuals with homozygous *Bph2*, *Pi5*, *Pita*, *Pid2*, *Pid3*, and *Wx^b* genes, exhibiting excellent agronomic traits, were carefully selected in the F₆ generation and test-crossed with three elite CMS lines to evaluate heterosis (Supplementary Table S1). Three lines were eliminated, leaving four lines with strong heterosis for further blast, BPH resistance, and grain quality evaluation in the F₈ and F₉ generations. After a comprehensive evaluation of all the target traits, an individual line carrying high and broad-spectrum blast resistance, intermediate BPH resistance (rated \leq grade 5.0), strong cold tolerance, heavy grains, and good grain quality were obtained and referred to as Z2. Eventually, after further propagation and selection, the genetically stable Z2 line was produced. Later, the Z2 line was renamed GH5501.

3.2 Analysis of functional genes and resistance gene haplotypes in GH5501

A thorough analysis of GH5501 was undertaken using a high-density 40K rice gene chip to scrutinize 76 functional genes and resistance gene alleles. This analysis revealed that GH5501 not only possessed the six target genes identified through molecular markers but also accumulated 20 exceptional alleles (Table 2). The results underscored that GH5501 possessed a robust genetic foundation, contributing significantly to its outstanding field performance.

As shown in Table 2, eight genes associated with resistance to biotic stressors conferred protection against rice blast, rice yellow mottle virus, rice stripe virus, and BPH. Furthermore, six quality-related genes contributed to the development of heavier and longer grains, accompanied by characteristics such as high protein content, low amylose content, and a higher gelatinization temperature. Four genes related to abiotic stress provided GH5501 with salt tolerance, cold tolerance, and a strong nitrogen absorption capacity. Two

high-yield genes and three plant architecture genes contributed to higher yields and a semi-dwarf plant stature with inherent resistance to lodging. GH5501 also carried two heading date genes, one fertility gene, and one lodging-related gene, all closely associated with yield, quality, and resistance. The effective combination of these genes successfully achieved the breeding goal of high yield, quality, and robust stress resistance.

3.3 Major agronomic traits and yield performance of GH5501 and its derived hybrid

The main agronomic traits of GH5501 are detailed in Table 3; Figure 3. GH5501 featured a plant height of 116.40 cm, green leaf sheaths, and upright flag leaves. The grain length extended to 10.67 mm, with a grain width of 3.07 mm, resulting in a grain length-to-width ratio of 3.48. The grains were awnless, and the grain type was similar to SH527, but GH5501 had a higher 1,000-grain weight of 35.63 g. It demonstrated a higher effective panicle number, total grain number per panicle, and grain setting rate compared to SH527 and FH838. The differences between GH5501 and SH527 or FH838 in effective panicle number and total grain number per panicle were statistically significant. In addition to its excellent agronomic traits, GH5501 also exhibited prominent characteristics favorable for hybrid seed production. It featured densely packed panicles with abundant pollen. The anthers were well-developed, and the pollen shedding rate exceeded 80%. GH5501 showed great potential in hybrid rice production. In our previous heterosis testing, we observed that the GH5501-Nafeng A (NY5501) hybrid displayed robust hybrid vigor and higher grain quality compared to other testing hybrids we generated.

In 2018, the NY5501 hybrid entered the official variety approval trials process in the Guangxi region. That year, its average yield across five test locations was 8,696.22 kg/hm², marking an 8.74% increase over the control variety TY7118 (CK), an elite high-yield benchmark hybrid designated as the control variety for the late-maturing group of the early growing season by the Guangxi rice variety approval committee. Subsequently, in 2019 and 2020, the

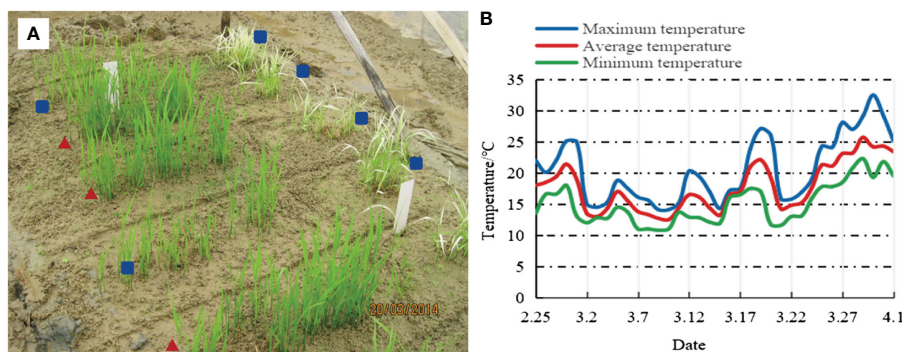


FIGURE 2
Natural cold tolerance identification in the F₄ generation. (A) Resistance performance, where \blacktriangle indicates selected lineages and \blacksquare indicates eliminated lineages. (B) Temperature fluctuations in Nanning City from February 25 to April 1, 2014.

TABLE 2 List of the identified functional genes in GH5501.

No.	Gene	Type	Chr.	Phenotype
1	<i>Gn1a</i>	Yield	1	Increased grains per spike
2	<i>OsSPL16</i>	Yield	8	High yield
3	<i>SKC1</i>	Anti-abiotic stress	1	Salt tolerance
4	<i>Cold1</i>	Anti-abiotic stress	4	Cold tolerance
5	<i>NRT1.1B</i>	Anti-abiotic stress	10	Increase nitrogen absorption
6	<i>Rymv1</i>	Anti-biotic stress	4	Resistance to yellow mottle virus disease
7	<i>STV11</i>	Anti-biotic stress	11	Resistance to rice stripe virus
8	<i>Bph2/Bph18</i>	Anti-biotic stress	12	Resistance to BPH
9	<i>Pi5</i>	Anti-biotic stress	9	Resistance to rice blast
10	<i>Pia</i>	Anti-biotic stress	11	Resistance to rice blast
11	<i>Pid2</i>	Anti-biotic stress	6	Resistance to rice blast
12	<i>Pid3</i>	Anti-biotic stress	6	Resistance to rice blast
13	<i>Pita</i>	Anti-biotic stress	12	Resistance to rice blast
14	<i>OsAAP6</i>	Quality	1	High protein
15	<i>GW2</i>	Quality	2	Large grain
16	<i>GS3</i>	Quality	3	Long grain, thermo-tolerance
17	<i>OsCYP704A3</i>	Quality	4	Long grain
18	<i>Wx^b</i>	Quality	6	In case of non-waxy, increase the content of amylopectin
19	<i>ALK</i>	Quality	6	Increase the content of medium-long amylopectin and gelatinization temperature
20	<i>Os01g62780</i>	Heading date	1	Delayed heading
21	<i>Hd3a</i>	Heading date	6	Photoperiod sensitivity
22	<i>S5</i>	Fertility	6	Wide-compatibility

(Continued)

TABLE 2 Continued

No.	Gene	Type	Chr.	Phenotype
23	<i>Sdt97</i>	Fertility	6	Semi-dwarf
24	<i>qNGR9</i>	Plant type	9	Erect panicle
25	<i>TAC1</i>	Plant type	9	Increased tillering angle
26	<i>sh4</i>	Other type	4	Non-seed shattering

BPH, brown planthopper.

average yields across six test locations were 8,574.03 kg/hm² and 8,476.35 kg/hm², respectively, representing increases of 5.33% and 6.38% over TY7118 (Table 4).

To summarize, over the 3-year regional trials conducted at 5–6 test locations each year, NY5501 consistently outperformed the control TY7118, with an average yield of 8,582.20 kg/hm², reflecting a 6.81% increase over the control. Most test locations exhibited significant improvements. Furthermore, in comparison with the control variety TY7118, the NY5501 hybrid demonstrated reduced plant height, increased grain length, grain width, and 1,000-grain weight, along with higher total grain number per panicle and grain setting rate (Figures 3A, B; Table 3).

As a result of its promising performance, the NY5501 hybrid successfully passed the regional approval trials in 2021 and received government authorization for commercial production.

3.4 Rice quality evaluation of GH5501 and its derived hybrid

The grain appearance and main rice quality parameters of GH5501 are presented in Figure 3C; Table 5. According to the Chinese Ministry of Agriculture and Rural Affairs standard NY/T 593–2013 “Quality Standards for Edible Rice Varieties”, among the seven main indicators influencing rice quality, GH5501 outperformed SH527 and FH838 in four indicators: brown rice rate, head rice rate, alkali spreading value, and gel consistency. GH5501 showed a similar excellent performance as SH527 in two indicators: transparency degree and amylose content. Only its chalkiness degree was slightly inferior to SH527. Compared to SH527 and FH838, GH5501 exhibited good rice quality, with the exception of chalkiness degree and alkali spreading value, meeting the top-grade rice (first grade) of the national standard for premium quality rice (NY/T 593–2013).

In comparison to the control TY7118, the hybrid combination NY5501 formed by GH5501 and NF A had longer grains, belonging to the long-grain rice type. Among the seven main indicators affecting rice quality, NY5501 outperformed TY7118 (CK) in five indicators: head rice rate, chalkiness degree, transparency degree, gel consistency, and amylose content. However, it slightly lagged behind TY7118 (CK) in brown rice rate and alkali spreading value. Overall, NY5501 exhibited superior rice quality compared to TY7118 (CK), with most main quality indicators (except for alkali spreading value) meeting the

TABLE 3 Yields and agronomic performances of GH5501 and its derived hybrid under field conditions.

Variety	PH (cm)	NTP	NGP	SSR (%)	GL (mm)	GW (mm)	GLWR	TWG (g)
GH5501	116.40 ± 1.35 a	9.67 ± 0.58 a	239.67 ± 7.51 a	87.91 ± 0.43 a	10.67 ± 0.15 a	3.07 ± 0.15 ab	3.48 ± 0.14 b	35.63 ± 0.47 a
SH527	118.33 ± 1.58 a	7.67 ± 0.58 b	181.33 ± 5.86 b	86.04 ± 0.40 ab	11.13 ± 0.12 a	2.87 ± 0.12 b	3.89 ± 0.14 a	32.90 ± 0.36 b
FH838	110.30 ± 1.74 b	7.33 ± 0.58 b	160.00 ± 6.56 c	84.62 ± 1.59 b	8.97 ± 0.42 b	3.27 ± 0.15 a	2.74 ± 0.01 c	29.83 ± 0.55 c
NY5501	120.07 ± 1.55 a	7.33 ± 0.58 a	169.00 ± 10.00 a	94.46 ± 0.46 a	10.63 ± 0.06 a	3.10 ± 0.10 a	3.43 ± 0.13 a	32.53 ± 0.55 a
TY7118 (CK)	122.53 ± 2.60 a	7.67 ± 0.58 a	158.40 ± 5.82 a	86.76 ± 0.61 b	8.77 ± 0.25 b	3.23 ± 0.15 a	2.71 ± 0.19 b	28.10 ± 1.11 b

Different lowercase letters in the same column indicate significant differences at the 0.05 level using the LSD method. GH5501, FH838, and SH527 were compared with each other, while NY5501 was compared with TY7118.
PH, plant height; NTP, number of tillers per plant; NGP, number of grains/panicle; SSR, seed setting rate; GL, grain length; GW, grain width; GLWR, ratio of length to width; TWG, 1,000-grain weight.

national standard (NY/T 593–2013) required for top-grade rice (second grade or above) (Figure 3C, Table 5).

3.5 Biotic and abiotic stress resistance evaluation of GH5501 and its derived hybrid

To assess the biotic resistance of GH5501, its seedlings were artificially inoculated indoors with 75 isolates of blast fungus collected from various ecological regions in Guangxi and Guangdong provinces for blast disease resistance identification (Figure 4, Supplementary Table S2). The results revealed that GH5501 exhibited strong resistance to 57 out of the 75 isolates tested, indicating a broad spectrum resistance of

77.32%. In contrast, SH527 and FH838 showed lower resistance to the blast fungus isolates, with resistance frequencies of 36.00% and 33.33%, respectively. Among the two varieties used as controls, Guangluai4 showed resistance to only 14.66% of the isolates, while LTH was susceptible to all 75 isolates tested.

Further investigation into blast resistance under field conditions involved cultivating GH5501 plants in a blast disease evaluation field nursery in Cenxi, Guangxi, where severe blast disease occurred frequently. GH5501 displayed robust high blast resistance, with a leaf blast level of 1.3 and a panicle blast loss rate of 6.1% (level 1.7), indicating overall high resistance (Figure 5A; Table 6).

NY5501, the hybrid combination of GH5501 and NF A, underwent blast resistance testing for 2 years and four times (twice a year) at three different blast resistance evaluation

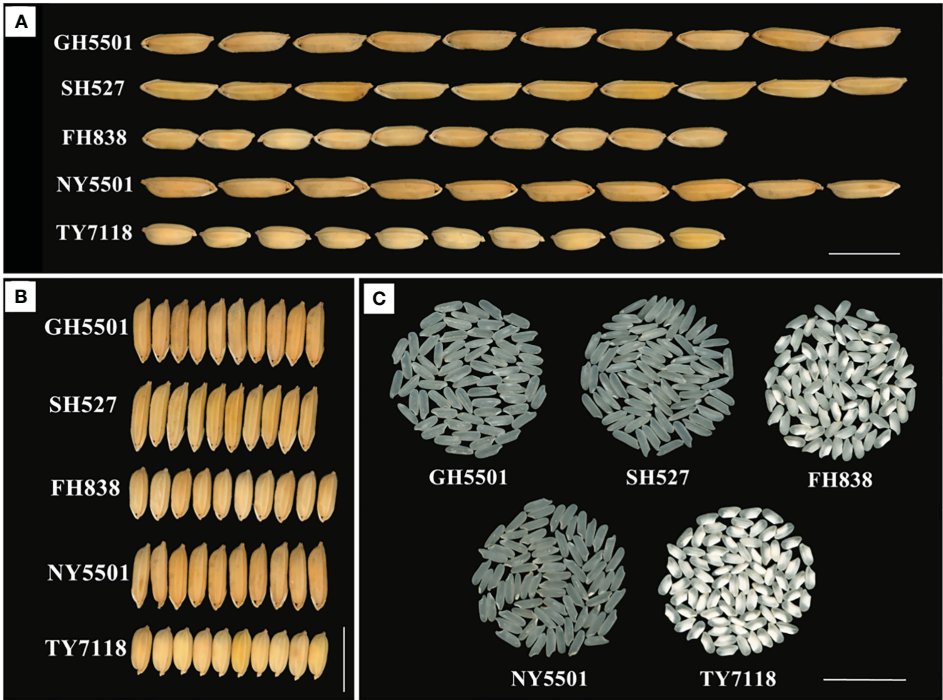


FIGURE 3 Grain type and rice quality of GH5501 and its derived hybrid NY5501. (A) Grain length of GH5501 and its derived hybrid NY5501. Bars = 1 cm. (B) Grain width of GH5501 and its derived hybrid NY5501. Bars = 1 cm. (C) Rice quality of GH5501 and its derived hybrid NY5501. Bars = 2 cm.

TABLE 4 Yield performances of hybrid combination NY5501 in seven regions of Guangxi.

Year	Variety	Yield in seven regions of Guangxi (kg/hm ²)							Average yield (kg/hm ²)	Compared with CK (%)
		Tengxian	Yuling	Wutang	Hepu	Tianyang	Guigang	Qinzhou		
2018	NY5501	8,265.00 ± 121.58 **	8,758.05 ± 200.43 *	9,703.50 ± 237.04**	8,202.00 ± 101.07 **	8,552.55 ± 104.93 **	–	–	8,696.22	8.74
	TY7118 (CK)	7,569.00 ± 102.72	8,265.00 ± 113.74	8,664.00 ± 116.71	7,689.00 ± 117.33	7,799.40 ± 132.29	–	–	7,997.28	
2019	NY5501	8,432.55 ± 126.92 **	8,297.55 ± 68.55 *	7,612.50 ± 161.21	–	9,469.05 ± 55.16 **	9,867.45 ± 332.80 *	7,765.05 ± 53.98 *	8,574.03	5.33
	TY7118 (CK)	7,927.50 ± 113.61	8,074.95 ± 50.28	7,415.70 ± 147.30	–	8,903.40 ± 128.99	9,184.95 ± 143.18	7,332.45 ± 198.68	8,139.83	
2020	NY5501	8,737.50 ± 138.27 **	7,833.45 ± 214.41	8,034.75 ± 135.69	–	9,522.45 ± 249.40 *	9,082.50 ± 251.05 *	7,647.45 ± 115.75 *	8,476.35	6.38
	TY7118 (CK)	8,067.45 ± 115.75	7,442.70 ± 217.14	7,833.75 ± 150.02	–	8,877.45 ± 163.34	8,410.05 ± 89.70	7,174.95 ± 160.16	7,967.73	

From 2018 to 2020, hybrid combinations NY5501 participated in the joint comparative and regional trials for late-maturing rice group of early growing season in south of Guangxi, which included seven different cities and counties.
* and ** represent significances at the 5% and 1% levels, respectively.

nurseries. The average leaf blast level of NY5501 was 4.0, and the average panicle blast loss rate was 12.0% (level 4.0), similar to TY7118. Both exhibited moderate resistance to blast disease (Table 6), despite NY5501’s maternal line NFA showing intermediate susceptibility to blast.

BPH resistance identification was conducted at the seedling stage on the two parental lines (GH5501 and NFA) and their hybrid NY5501, with RH and TN1 used as resistance and susceptible controls, respectively. The results revealed that GH5501 and NY5501 exhibited resistance levels of 3.78 and 3.93, respectively, indicating moderate resistance to BPH (Figure 5B; Table 7). Both showed resistance levels similar to the resistance control RH.

Cold tolerance tests were also conducted at the seedling stage on three restorer lines—GH5501, FH838, and SH527—the hybrid NY5501, and IR50 as the susceptible control. The results indicated that GH5501 exhibited a cold tolerance level of 1.80, comparable to that of SH527 (level 1.93), demonstrating strong cold tolerance during the seedling stage. In contrast, FH838 displayed a resistance level of 5.84, a much weaker cold tolerance than GH5501 and SH527, suggesting that the high level of cold resistance in GH5501 was mainly inherited from its parental line SH527. The hybrid combination NY5501 had a resistance level of 3.69, indicating an overall moderate cold tolerance at the seedling stage (Table 8).

TABLE 5 Rice quality of GH5501, its parents, and derived hybrid.

Rice quality detection index	Variety					Grade category of premium quality		
	GH5501	SH527	FH838	NY5501	TY7118 (CK)	1st grade	2nd grade	3rd grade
Brown rice rate (%) ^a	82.3 (1st grade)	80.8 (2nd grade)	81.0 (1st grade)	79.2 (2nd grade)	81.0 (1st grade)	≥81	≥79	≥77
Head rice rate (%) ^a	63.9 (1st grade)	52.4 (3rd grade)	60 (1st grade)	60.9 (1st grade)	49.1 (other)	≥58	≥55	≥52
Chalkiness degree ^a	2.9 (2nd grade)	2.0 (2nd grade)	3.4 (3rd grade)	0.2 (1st grade)	2.6 (2nd grade)	≤1.0	≤3.0	≤5.0
Transparency degree ^a	1.0 (1st grade)	1.0 (1st grade)	-	2.0 (2nd grade)	3 (other)	≤1	≤2	≤2
Alkali spreading value ^a	4.4 (other)	4 (other)	-	3.7 (other)	5.6 (3rd grade)	≥6.0	≥6.0	≥5.0
Gel consistency (mm) ^a	83 (1st grade)	76 (1st grade)	45 (other)	78 (1st grade)	74 (1st grade)	≥60	≥60	≥50
Amylose content (dry basis) (%) ^a	16.9 (1st grade)	16.9 (1st grade)	22 (3rd grade)	15.1 (1st grade)	26.8 (other)	13.0–18.0	13.0–20.0	13.0–22.0

^aEvaluation based on the criteria outlined in NY/T593–2013, the “Quality Standards for Edible Rice Varieties” by the Chinese Ministry of Agriculture and Rural Affairs. 1st grade indicates the highest rice quality, followed by 2nd grade and 3rd grade. Varieties reaching 3rd grade or above are considered premium high-quality edible rice, while others are classified as ordinary edible rice.

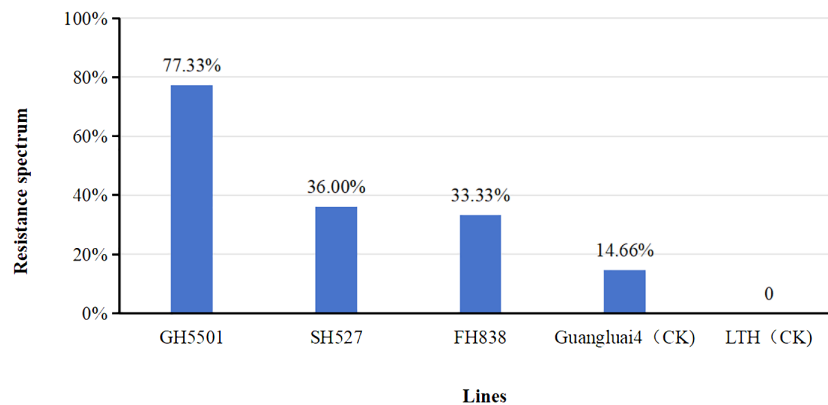


FIGURE 4

Artificial inoculation of 75 blast isolates for resistance evaluation in GH5501 and heavy-grain parents SH527 and FH838. Abbreviation: LTH, Lijiangxintuanheigu.

4 Discussion

China's southern rice region, located in a tropical and subtropical zone, often encounters prolonged high temperatures during the grain-filling and ripening stages of early rice. This leads to the phenomenon of "heat-induced maturity", where grains mature quickly before reaching their full size. Consequently, developing high-yielding varieties with heavy grain and good appearance quality becomes challenging. Addressing the trade-off, breeders in this region typically target a 1,000-grain weight of approximately 20.0 g to strike a balance between grain weight and quality, addressing the trade-off (Wang, 2022). While the positive correlation between 1,000-grain weight and yield is well-known, achieving equilibrium between grain weight and quality poses a technical challenge for breeders. In this study, we presented our concerted effort to tackle this challenge. Through a combination of MAS and phenotype-based selection, our team successfully developed GH5501, a high-yielding and good-quality restorer line with long and heavy grains. GH5501 boasted a remarkable 1,000-

grain weight of 35.63 g, categorized as an extra-heavy grain variety. Notably, its performance in terms of grain quality, with the exception of alkali spreading value, met or exceeded the standards for high-quality rice (second grade or above) defined by the Chinese Ministry of Agriculture. GH5501 served as a solid foundation for the future breeding of hybrid rice varieties with large and high-quality grains. Varieties with heavy grains are generally favored by farmers due to their characteristics of high and stable yields. The Teyou (TY) hybrid series of rice varieties, derived from CMS Longtepu A, with a 1,000-grain weight generally above 28.0 g, has dominated early rice cultivation in Guangxi, China, since the 1980s. Despite a three-decade-long promotion, these varieties still occupy a significant planting area in Guangxi's early rice-growing regions (Wang et al., 2015). However, the rice quality of the TY series is generally considered ordinary or poor. The development of the hybrid rice combination NY5501, resulting from the cross between GH5501 and the sterile line NF A, marked a significant achievement. With a 1,000-grain weight of 32.53 g, NY5501 consistently outperformed TY7118 (CK) in yield across 5–6 test

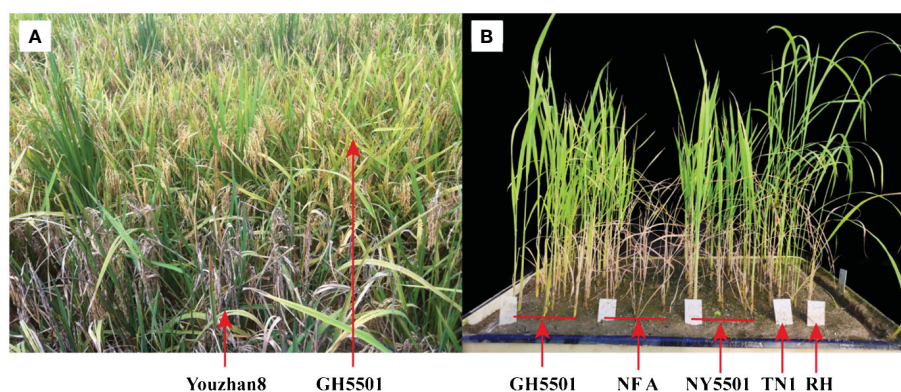


FIGURE 5

Resistance evaluation of GH5501 and its hybrid combination NY5501. (A) Resistance evaluation of GH5501 against blast disease in the natural identification plot, with Youzhan8 as the disease-susceptible control (CK). (B) Resistance evaluation of GH5501 and NY5501 against BPH. Rows 1–3 represent GH5501, Rows 4–6 represent NF A, Rows 7–9 represent NY5501, and Rows 10 and 11 represent the susceptible control TN1 and the resistant control RH, respectively. BPH, brown planthopper.

TABLE 6 Blast resistance evaluation in GH5501 and its hybrid combination NY5501 under field conditions.

Rice lines	Trait	Level						Resistance level
		Cenxi (2018)	Cenxi (2019)	Hezhou (2019)	Cenxi (2020)	Jinxi (2020)	Average	
GH5501	Leaf blast	1	2	–	1	–	1.3 ± 0.6	R
	Panicle blast loss rate (%)	3.2	11.1	–	4.0	–	6.1 ± 4.3	–
	Panicle blast loss rate (level)	1	3	–	1	–	1.7 ± 0.6	R
NF A	Leaf blast	5	5	–	4	–	4.7 ± 0.6	MS
	Panicle blast loss rate (%)	16.6	23.5	–	21.3	–	20.5 ± 3.5	–
	Panicle blast loss rate (level)	5	5	–	5	–	5.0 ± 0.0	MS
NY5501	Leaf blast	–	4	5	4	3	4.0 ± 0.8 a	MR
	Panicle blast loss rate (%)	–	15.7	5.6	11.6	15.2	12.0 ± 4.7 a	–
	Panicle blast loss rate (level)	–	5	3	3	5	4.0 ± 1.2 a	MR
TY7118 (CK)	Leaf blast	–	5	3	4	3	3.8 ± 1.0 a	MR
	Panicle blast loss rate (%)	–	16.6	3.5	6.6	19.9	11.7 ± 7.8 a	–
	Panicle blast loss rate (level)	–	5	1	3	5	3.5 ± 1.9 a	MR
Youzhan8 (CK)	Leaf blast	7	9	–	9	–	8.3 ± 1.2	S
	Panicle blast loss rate (%)	95.6	98.9	–	95.1	–	96.5 ± 2.1	–
	Panicle blast loss rate (level)	9	9	–	9	–	9.0 ± 0.0	S

The same lowercase letters indicate no significant difference using the LSD method. There are no significant differences between NY5501 and TY7118 at the 0.05 significance level. R, resistant; MS, moderate susceptibility; MR, moderate resistance; S, susceptible.

points in the late-maturing group in South Guangxi for three consecutive years. The primary grain quality indicators of NY5501 (excluding alkali spreading value) met or exceeded the standards for high-quality rice (level 2 or above), significantly surpassing the control variety (Table 5). Considering that the

average yield of approved hybrid rice varieties in Guangxi from 2004 to 2018 ranges from 6,910.4 to 8,080.6 kg/hm² (Luo et al., 2022), the yield of NY5501, reaching 8,582.25 kg/hm², indicated its high-yielding and good quality feature. Therefore, GH5501 was

TABLE 7 BPH resistance evaluation in GH5501 and its hybrid combination NY5501.

Lines	Average resistant grade	Resistance level
GH5501	3.78 ± 0.18 b	MR
NF A	8.65 ± 0.09 c	S
NY5501	3.93 ± 0.13 b	MR
RH (the resistant control)	3.46 ± 0.13 a	MR
TN1 (the susceptible control)	8.57 ± 0.09 c	S

Letters a to c indicate significantly different values according to statistical analysis using the LSD method (a = 0.05). MR, moderate resistance; S, susceptible.

TABLE 8 Seedling cold tolerance evaluation in GH5501 and its hybrid combination NY5501.

Lines	Average resistant grade	Resistance level
GH5501	1.80 ± 0.08 a	HR
NF A	6.47 ± 0.14 d	MS
NY5501	3.69 ± 0.17 b	MR
SH527	1.93 ± 0.08 a	HR
FH838	5.84 ± 0.12 c	LR
IR50 (CK)	8.73 ± 0.08 e	S

Letters a to e indicate significantly different values according to statistical analysis using the LSD method (a = 0.05). HR, high resistance; MS, moderate susceptibility; MR, moderate resistance; LR, low resistance; S, susceptible.

deemed an excellent long and heavy grain restorer line. Its utilization held the potential to lead to the development of more high-yielding, good-quality, and stress-tolerant hybrid rice combinations.

Given the escalating occurrence of biotic and abiotic stressors due to frequent climate fluctuations, the development of multi-stress-resistant rice varieties has become imperative to mitigate extensive yield losses (Dixit et al., 2020). Traditional conventional breeding has served as the primary approach for rice breeding since the 1930s. However, achieving the breeding goals of developing varieties resistant to multiple stresses, high-yielding, and good quality through conventional methods has become increasingly challenging (Dixit et al., 2020).

Advancements in rice genome sequencing and molecular biology have facilitated the identification of numerous beneficial genes, leading to significant progress in molecular marker-assisted breeding research (Xiao et al., 2018; Mohapatra et al., 2023). Several successful cases of developing multi-stress-resistant, high-quality, and high-yielding rice varieties have emerged by comprehensively utilizing molecular breeding in conjunction with other breeding methods. For instance, Dixit et al. (2020) successfully aggregated seven to 10 genes/QTLs targeting various biotic and abiotic stressors (e.g., *Pi9* gene for blast; *Xa4*, *xa5*, *xa13*, and *Xa21* genes for bacterial leaf blight; *Bph3* and *Bph17* genes for BPH; *Gm4* and *Gm8* genes for rice gall midge) into the Swarna genetic background using simple sequence repeat (SSR) and gene-based markers, which already has QTLs for drought tolerance (*qDTY1.1* and *qDTY3.1*). This effort resulted in the development of seven introgression lines (ILs) that exhibited higher yields under various stress conditions while maintaining excellent performance under non-stress conditions. Similarly, Mohapatra et al., (2023) successfully introgressed resistance genes (*Xa21*, *xa13*, and *xa5*) for bacterial leaf blight and the QTL *Sub1* for submergence tolerance into the popular Indian late-maturing variety Ranidhan through backcrossing and gene-based markers for MAS. This significantly enhanced its resistance to bacterial leaf blight and submergence tolerance. Liu et al. (2021) and Wang et al. (2022) utilized gene-based markers for MAS and stress screening to breed Huhan 74S (*Pi9*, *Pi5*, and *Pi54*), a two-line sterile line resistant to rice blast, and Huhan 106 (*Pita* and *Pib*), an early-maturing, blast-resistant, and drought-tolerant rice variety. Both varieties have been widely adopted in production. In the current study, a multi-stress-resistant and high-yielding restorer line, GH5501, has been developed through hybridization, multiple crossing, and marker-assisted selection for gene pyramiding (*Pi5*, *Pita*, *Pid2*, *Pid3*, *Bph2*, and *Wx^b*). We used the linked SSR markers for *Pita*, *Pid2*, *Pid3*, *Bph2*, *Wx^b*, and gene-based markers for *Pi5* and *Pid3*, but not functional markers for MAS, because our breeding program was started in 2007 when the application of functional markers in rice breeding was not the most efficient and practical method for most of the breeders compared to the SSR and gene-based marker. The prerequisite for the development of functional markers is that the difference in gene function is due to a difference in one or several functional base pairs, which was not successfully developed for every gene. As expected, the integration of MAS with screening for resistance to blast, BPH, and natural cold tolerance, as well as

assessments for appearance quality and grain quality, resulted in the successful breeding of GH5501. This restorer line exhibited broad-spectrum resistance to rice blast (with a resistance spectrum of 77.33%), intermediate resistance to BPH, and strong cold tolerance during the seedling stage. The development of GH5501 offered a promising solution for breeding varieties that were not only high-yielding and stress-resistant but also of good quality, contributing to the sustainable improvement of rice production in the face of changing climates.

GH5501 carries four rice blast resistance genes: *Pita*, *Pi5*, *Pid2*, and *Pid3*. *Pita*, located near the centromere on rice chromosome 12, encodes a cytoplasmic membrane receptor protein with a length of 928 amino acids (Bryan et al., 2000). The resistance mediated by *Pita* requires the involvement of *Ptr*, and the NLR protein *Pita* exhibits broad-spectrum resistance (Zhao et al., 2018; Wang et al., 2021). *Pi5* is situated on rice chromosome 9 and consists of two genes, *Pi5-1* and *Pi5-2*, both producing proteins with CC domains at the N-terminus. Gene expression analysis indicates that *Pi5-1* is pathogen-induced, while *Pi5-2* is consecutively expressed; simultaneous expression of both is necessary for *Pi5*-mediated rice blast resistance. *Pi5* demonstrates broad-spectrum resistance against 26 out of 29 isolates from six isolates in the Philippines and 29 isolates from Korea (Jeon et al., 2003). *Pid2* and *Pid3*, originating from broad-spectrum blast-resistant varieties, are located on rice chromosome 6. *Pid2*, positioned in the centromere-proximal region and linked with RM527 and RM3, encodes a receptor-like kinase, representing a novel type of resistance gene that shows gene-for-gene resistance against the Chinese rice blast strain ZB15 (Chen et al., 2004; Chen et al., 2006; Li et al., 2017). *Pid3*, sharing the same locus as *Pi25*, is on rice chromosome 6 and encodes a 923-amino-acid NBS-LRR domain protein (Shang et al., 2009). These four blast resistance genes have been extensively utilized in breeding for blast resistance, resulting in the development of a range of blast-resistant materials or varieties (Xiao et al., 2018; Xiao et al., 2019; Saichompoo et al., 2021). In this study, we utilized molecular markers to aggregate *Pita*, *Pi5*, *Pid2*, and *Pid3* resistance genes to breed the GH5501 restorer line. Through artificial inoculation with 75 isolates collected from Guangxi and Guangdong, GH5501 exhibited a resistance spectrum of 77.33%. Natural inoculation tests conducted over several years and locations also demonstrated high resistance. These results indicated that the GH5501 restorer line possessed broad-spectrum resistance against rice blast.

Initially, *Bph2* was described as a recessive gene (Athwal et al., 1971). However, Murai et al. challenged this notion, reporting *Bph2* as a dominant gene through genetic analysis of a segregating population of Norin-PL4 crossed with Tsukushibare, a susceptible japonica cultivar (Murai et al., 2001). In the 1970s and 1980s, the International Rice Research Institute developed blast-resistant rice varieties IR36 and IR42 using *Bph2* and extensively promoted them in Southeast Asia (Khush and Brar, 1991). In our breeding program 15 years ago, we utilized ASD7, carrying *Bph2*, as an insect-resistant parent to breed the restorer line GH5501. The hybrid combination NY5501, derived from GH5501, exhibited moderate resistance to the mixed biotype of BPH in the fields of Nanning, Guangxi, demonstrating strong tolerance to BPH. Reports have indicated that varieties developed using *Bph2*, such as the BPH-resistant varieties IR36 and IR42, lose their resistance gradually over 8 years of large-scale

promotion due to the emergence of new biotypes of BPH (Sogawa and Kilin, 1987). The Plant Protection Research Team of the Guangxi Academy of Agricultural Sciences, through long-term monitoring of ASD7 (*Bph2*) resistance, shows that its resistance to different biotypes of BPH is unstable, exhibiting moderate resistance to biotype II and moderate susceptibility to the Bangladesh biotype (Wu et al., 2009). In this study, GH5501 bred from the insect-resistant parent ASD7, along with its hybrid combination NY5501, displayed moderate resistance and strong tolerance to BPH, which might be associated with the biotype of BPH. Additionally, this resistance was correlated with the robust growth and stout stems of GH5501. Plant tolerance refers to a plant's ability to endure or compensate for damage when subjected to the same number of pests as susceptible varieties, relying on its robust growth and reproductive functions (Simms, 2000).

GH5501 exhibited extremely strong cold tolerance during the seedling stage. The F_4 progeny of this variety endured an average temperature of 17.4°C for 36 days from sowing, and the plants continued to grow robustly with green leaves. No symptoms of white seedlings, damping-off, or dead seedlings were observed (Figure 2). Furthermore, cold tolerance assessments confirmed that GH5501 possessed high cold resistance, with a resistance level of 1.80. Gene chip analysis of GH5501 revealed the presence of the cold-tolerance gene *Cold1*, validating its cold tolerance at the molecular level. The *Cold1* gene encodes a G-protein signaling regulator, COLD1, which interacts with the G-protein α -subunit RGA1 to sense low temperatures, activate Ca^{2+} channels, and enhance G-protein GTPase activity, thereby increasing rice cold tolerance (Ma et al., 2015).

Practically, our use of a backcross strategy was avoided in favor of a multiple-crossing method. This decision prevented improvement within the genetic background of a single parent, preserving the genetic diversity of the core parents SH527 and FH838. Simultaneously, we integrated broad-spectrum blast resistance genes and BPH resistance genes from the resistant varieties Digu and ASD7, respectively. Although this extended the breeding cycle, GH5501 selected through this approach showed significant improvements in stress resistance, yield, and quality compared to the parental lines SH527 and FH838 (Figures 3, 4, Tables 4, 5, 8). Notably, this represented a breakthrough in the breeding of heavy-grain varieties in the Southern rice region, particularly in terms of quality.

Gene chips play an increasingly important role in modern rice breeding, as they enable high-throughput detection of a large number of target genes (Li et al., 2023; Zhang et al., 2023). However, the current high cost of gene chip testing, ranging from USD 70 to 80 per rice sample in China, makes it impractical for large-scale screening of target genes in individual plants from segregating populations. Presently, gene chips are primarily utilized for backcross genetic background analysis and molecular characterization of specific genetic materials, such as parents or varieties (Ren et al., 2021). Gene chip analysis helps to gain a clear understanding of the genetic characteristics of hybrid rice parents, aiding in the rational selection of parent combinations to overcome their shortcomings and create the most hybrid combinations.

Our analysis of GH5501 using gene chips revealed that, in addition to the six target genes selected through molecular MAS, GH5501 also

harbored 20 excellent allelic genes, including genes such as *NRT1.1B* for efficient nitrogen utilization, *SKC1* for salt tolerance, and *STV11* for resistance to rice stripe virus. Notably, GH5501 lacked the major-effect gene *Chalk5*, which controls rice appearance quality, milling yield, and the total amount of storage proteins, with a significant impact on various rice quality traits (Li et al., 2014). Therefore, to further enhance the rice quality of future hybrid combinations involving GH5501, selecting hybrid parents with the *Chalk5* gene for compatibility testing with GH5501 is expected. This approach aims to breed hybrid rice varieties with lower chalkiness, thereby further improving rice quality.

The cost of producing hybrid rice seeds has emerged as a major impediment to the widespread adoption of hybrid rice cultivation. Mechanized seed production offers an effective solution to this issue. The diversity in grain types plays a crucial role in the mechanical production of hybrid rice seeds. Chinese breeders have actively explored approaches to tackle this challenge by cultivating small-grain male-sterile lines and heavy-grain restorer lines. They capitalize on substantial differences in grain types, particularly in grain thickness and 1,000-grain weight, as exemplified by varieties such as Zhuoliangyou 2115 and Zhuoliangyou 141 (with a female parent 1,000-grain weight of 14.10 g and male parents at 33.40 g and 28.20 g, respectively). This strategy facilitates the entire process of mechanical seed production, from mixed sowing of parental lines to mechanical separation after harvest, thereby reducing costs and enhancing efficiency in hybrid rice seed production (Lu et al., 2023; Ying et al., 2024). Consequently, the selection of parental lines with significant differences in grain characteristics is pivotal. The long and heavy-grain rice restorer line GH5501, developed in this study with a 1,000-grain weight as high as 35.63 g, exhibited strong heterosis in the resulting hybrid combinations. It could be effectively paired with common small-grain male-sterile lines, creating favorable conditions for mechanized rice seed production. GH5501 emerged as a promising and excellent rice restorer line with potential applications in the field.

5 Conclusion

This study successfully employed MAS and conducted multiple resistance screenings to develop GH5501, a novel restorer line characterized by long and heavy grains, low amylose content, broad-spectrum resistance to rice blast, resistance to BPH, and tolerance to low-temperature stress. Using GH5501 as a parent, a new hybrid rice variety named NY5501 was developed, demonstrating high yield, good quality, and resilience to both biotic and abiotic stresses. NY5501 was approved in Guangxi as a rice variety. GH5501 stood as a valuable resource for subsequent three-line hybrid rice breeding, providing a combination of high yield, good quality, and robust resistance to various stressors.

Data availability statement

The original contributions presented in the study are included in the article/Supplementary Material. Further inquiries can be directed to the corresponding authors.

Author contributions

MW: Writing – original draft, Data curation, Formal Analysis, Investigation, Methodology, Software. QY: Data curation, Formal Analysis, Investigation, Writing – review & editing. DH: Data curation, Formal Analysis, Writing – review & editing, Resources, Supervision. ZM: Data curation, Formal Analysis, Writing – review & editing, Methodology. SC: Data curation, Writing – review & editing, Investigation, Resources. XY: Data curation, Investigation, Writing – review & editing, Formal Analysis, Software. CL: Writing – review & editing, Data curation, Investigation, Methodology, Project administration. YQ: Writing – review & editing, Data curation, Project administration, Software. XZ: Writing – review & editing, Data curation, Investigation, Methodology. ZW: Writing – review & editing, Methodology, Software. YL: Writing – review & editing, Software, Data curation. LY: Writing – review & editing, Software, Formal Analysis. GQ: Writing – review & editing, Conceptualization, Data curation, Project administration, Supervision, Validation. YZ: Writing – review & editing, Conceptualization, Data curation, Supervision, Funding acquisition, Resources, Writing – original draft.

Funding

The author(s) declare financial support was received for the research, authorship, and/or publication of this article. This research was funded by the Key Project of Science and Technology of Guangxi Province of China (Grant No. GuikeAB21220016), the National Natural Science Foundation of China (Grant No. 32360490), the Key Project of Natural Science Foundation of Guangxi Province of China (Grant No. 2021GXNSFDA075013), Guangxi Academy of Agricultural

Sciences (Grant No. Guinongke2021YT027), and Foundation of Guangdong Provincial Key Laboratory of High Technology for Plant Protection (Zhizhong 2023-04).

Acknowledgments

We are grateful to Dr. Chonglie Ma and Dr. Bin Teng for offering valuable suggestions and helping to improve the manuscript.

Conflict of interest

The authors declare that the research was conducted in the absence of any commercial or financial relationships that could be construed as a potential conflict of interest.

Publisher's note

All claims expressed in this article are solely those of the authors and do not necessarily represent those of their affiliated organizations, or those of the publisher, the editors and the reviewers. Any product that may be evaluated in this article, or claim that may be made by its manufacturer, is not guaranteed or endorsed by the publisher.

Supplementary material

The Supplementary Material for this article can be found online at: <https://www.frontiersin.org/articles/10.3389/fpls.2024.1390603/full#supplementary-material>

References

- Andaya, V. C., and Mackill, D. J. (2003). Mapping of QTLs associated with cold tolerance during the vegetative stage in rice. *J. Exp. Bot.* 54, 2579–2585. doi: 10.1093/jxb/erg243
- Athwal, D. S., Pathak, M. D., Bacalango, E. H., and Pura, C. D. (1971). Genetics of resistance to brown planthopper and green leafhoppers in *Oryza sativa* L. *Crop Sci.* 11, 747–750. doi: 10.2135/cropsci1971.0011183X001100050043x
- Bligh, H., Till, R. I., and Jones, C. A. (1995). A microsatellite sequence closely linked to the *Waxy* gene of *Oryza sativa*. *Euphytica* 86, 83–85. doi: 10.1007/BF00022012
- Bryan, G. T., Wu, K. S., Farrall, L., Jia, Y., Hershey, H. P., McAdams, S. A., et al. (2000). A single amino acid difference distinguishes resistant and susceptible alleles of the rice blast resistance gene *Pi-ta*. *Plant Cell* 12, 2033–2046. doi: 10.2307/3871103
- Chen, X. W., Li, S. G., Xu, J. C., Zhai, W. X., Ling, Z. Z., Ma, B. T., et al. (2004). Identification of two blast resistance genes in a rice variety, digu. *J. Phytopathol.* 152, 77–85. doi: 10.1046/j.1439-0434.2003.00803.x
- Chen, X., Shang, J., Chen, D., Lei, C., Zou, Y., Zhai, W., et al. (2006). A B-lectin receptor kinase gene conferring rice blast resistance. *Plant J.* 46, 794–804. doi: 10.1111/j.1365-3113.2006.02739.x
- Chen, H., Xie, W., He, H., Yu, H. H., and Chen, W. (2014). A high-density SNP genotyping array for rice biology and molecular breeding. *Mol. Plant* 7, 541–553. doi: 10.1093/mp/sst135
- Devanna, B. N., Jain, P., Solanke, A. U., Das, A., Thakur, S., Singh, P. K., et al. (2022). Understanding the dynamics of blast resistance in rice-magnaporthe oryzae interactions. *J. Fungi* 8, 584. doi: 10.3390/jof8060584
- Dixit, S., Singh, U. M., Singh, A. K., Alam, S., Venkateshwarlu, C., Nachimuthu, V. V., et al. (2020). Marker assisted forward breeding to combine multiple biotic-abiotic stress resistance/tolerance in rice. *Rice* 13, 29. doi: 10.1186/s12284-020-00391-7
- Du, B., Zhang, W., Liu, B., Hu, J., Wei, Z., Shi, Z., et al. (2009). Identification and characterization of *Bph14*, a gene conferring resistance to brown planthopper in rice. *Proc. Natl. Acad. Sci. U.S.A.* 106, 22163–22168. doi: 10.1073/pnas.0912139106
- Fjellstrom, R., Conaway-Bormans, C. A., McClung, A. M., Marchetti, M. A., Shank, A. R., and Park, W. D. (2004). Development of DNA markers suitable for marker assisted selection of three *Pi* genes conferring resistance to multiple *Pyricularia grisea* pathotypes. *Crop Sci.* 44, 1790. doi: 10.2135/cropsci2004.1790
- Gao, L. J., Gao, H. L., Yan, Q., Zhou, M., Zhou, W. Y., Zhang, J., et al. (2010). Establishment of markers for four blast genes and marker distribution in rice parents (in Chinese with English abstract). *Hybrid Rice* 25, 294–298. doi: 10.16267/j.cnki.1005-3956.2010.s1.090
- Gu, S., Zhang, Z., Li, J., Sun, J., Cui, Z., Li, F., et al. (2023). Natural variation in OsSEC13 HOMOLOG 1 modulates redox homeostasis to confer cold tolerance in rice. *Plant Physiol.* 193, 2180–2196. doi: 10.1093/plphys/kiad420
- Hao, J., Wang, D., Wu, Y., Huang, K., Duan, P., Li, N., et al. (2021). The GW2-WG1-OsbZIP47 pathway controls grain size and weight in rice. *Mol. Plant* 14, 1266–1280. doi: 10.1016/j.molp.2021.04.011
- Huang, L., Sreenivasulu, N., and Liu, Q. (2020). *Waxy* editing: old meets new. *Trends Plant Sci.* 25, 963–966. doi: 10.1016/j.tplants.2020.07.009
- International Rice Research Institute (IRRI) (2013). *Standard evaluation system (SES) for Rice. 5th edn* (IRRI, Manila, the Philippines: IRRI), 46.

- Jantaboon, J., Siangliw, M., Im-Mark, S., Jamboonsri, W., Vanavichit, A., and Toojinda, T. (2011). Ideotype breeding for submergence tolerance and cooking quality by marker-assisted selection in rice. *Field Crop Res.* 123, 206–213. doi: 10.1016/j.fcr.2011.05.001
- Jeon, J. S., Chen, D., Yi, G. H., Wang, G. L., and Ronald, P. C. (2003). Genetic and physical mapping of *Pi5(t)* a locus associated with broad-spectrum resistance to rice blast. *Mol. Genet. Genomics* 269, 280–289. doi: 10.1007/s00438-003-0834-2
- Khush, G. S., and Brar, D. S. (1991). Genetics of resistance to insects in crop plants. *Adv. Agron.* 45, 223–274. doi: 10.1016/S0065-2113(08)60042-5
- Li, Y., Fan, C., Xing, Y., Yun, P., Luo, L., Yan, B., et al. (2014). *Chalk5* encodes a vacuolar H⁽⁺⁾-translocating pyrophosphatase influencing grain chalkiness in rice. *Nat. Genet.* 46, 398–404. doi: 10.1038/ng.2923
- Li, Q. L., Feng, Q., Wang, H. Q., Kang, Y. H., Zhang, C. H., Du, M., et al. (2023). Genome-wide dissection of quan 9311A breeding process and application advantages. *Rice Sci.* 30, 552–566. doi: 10.1016/j.rsci.2023.06.004
- Li, S., Gao, F., Xie, K., Zeng, X., Cao, Y., Zeng, J., et al. (2016). The OsMiR396c-OsGRF4-OsGIF1 regulatory module determines grain size and yield in rice. *Plant Biotechnol. J.* 14, 2134–2146. doi: 10.1111/pbi.12569
- Li, W., Zhu, Z., Chern, M., Yin, J., Yang, C., Ran, L., et al. (2017). A natural allele of a transcription factor in rice confers broad-spectrum blast resistance. *Cell* 170, 114–126.e15. doi: 10.1016/j.cell.2017.06.008
- Lin, L., Wang, Y., Xu, X., Teng, B., and Wei, C. (2023). Relationships between starch molecular components and eating and cooking qualities of rice using single-segment substitution lines with different *Wx* loci. *J. Cereal Sci.* 114, 103765. doi: 10.1016/j.jcs.2023.103765
- Liu, Y., Zhang, F., Luo, X., Kong, D., Zhang, A., Wang, F., et al. (2021). Mol breeding of a novel PTGMS line of WDR for broad-spectrum resistance to blast using *Pi9*, *Pi5*, and *Pi54* genes. *Rice* 14, 96. doi: 10.1186/s12284-021-00537-1
- Lou, G., Bhat, M. A., Tan, X., Wang, Y., and He, Y. (2023). Research progress on the relationship between rice protein content and cooking and eating quality and its influencing factors. *Seed Biol.* 2, 16. doi: 10.48130/SeedBio-2023-0016
- Lu, X. D., Li, F., Xiao, Y. H., Wang, F., Zhang, G. L., Deng, H. B., et al. (2023). Grain shape genes: shaping the future of rice breeding. *Rice Sci.* 30, 379–404. doi: 10.1016/j.rsci.2023.03.014
- Lu, G., Wu, F. Q., Wu, W., Wang, H. J., Zheng, X. M., Zhang, Y., et al. (2014). Rice *LTG1* is involved in adaptive growth and fitness under low ambient temperature. *Plant J.* 78, 468–480. doi: 10.1111/tpj.12487
- Luo, T. P., Chen, H. W., Qin, G., and M. H. L. (2022). Analysis of characteristics of rice varieties approved in guangxi, China, (2004–2018). *Mol. Plant Breed.* 1–17.
- Ma, Y., Dai, X., Xu, Y., Luo, W., Zheng, X., Zeng, D., et al. (2015). *COLD1* confers chilling tolerance in rice. *Cell* 160, 1209–1221. doi: 10.1016/j.cell.2015.01.046
- Mao, D., Xin, Y., Tan, Y., Hu, X., Bai, J., Liu, Z. Y., et al. (2019). Natural variation in the *HANI* gene confers chilling tolerance in rice and allowed adaptation to a temperate climate. *Proc. Natl. Acad. Sci. U.S.A.* 116, 3494–3501. doi: 10.1073/pnas.1819769116
- Mohapatra, S., Barik, S. R., Dash, P. K., Lenka, D., Pradhan, K. C., Raj, K. R. R., et al. (2023). Mol breeding for incorporation of submergence tolerance and durable bacterial blight resistance into the popular rice variety ‘Ranidhan’. *Biomolecules* 13, 198. doi: 10.3390/biom13020198
- Murai, H., Hashimoto, Z., Sharma, P. N., Shimizu, T., Muratam, K., Takumi, S., et al. (2001). Construction of a high-resolution linkage map of a rice brown planthopper (*Nilaparvata lugens* Stål) resistance gene *bph2*. *Theor. Appl. Genet.* 103, 526–532. doi: 10.1007/s001220100598
- Murray, M. G., and Thompson, W. F. (1980). Rapid isolation of high molecular weight plant DNA. *Nucleic Acids Res.* 8, 4321–4325. doi: 10.1093/nar/8.19.4321
- Ning, X., Yun, W., and Aihong, L. (2020). Strategy for use of rice blast resistance genes in rice molecular breeding. *Rice Sci.* 27, 263–277. doi: 10.1016/j.rsci.2020.05.003
- Pennisi, E. (2010). Armed and dangerous. *Science* 327, 804–805. doi: 10.1126/science.327.5967.804
- Ren, Y., Chen, D., Li, W., Tao, L., Yuan, G. Q., Cao, Y., et al. (2021). Genome-wide pedigree analysis of elite rice Shuhui 527 reveals key regions for breeding. *J. Integr. Agr.* 20, 35–45. doi: 10.1016/S2095-3119(20)63256-7
- Saichompoo, U., Narumol, P., Nakwilai, P., Thongyos, P., and Malumpong, C. (2021). Breeding novel short grain rice for tropical region to combine important agronomical traits, biotic stress resistance and cooking quality in koshihikari background. *Rice Sci.* 28, 479–492. doi: 10.1016/j.rsci.2021.07.008
- Seck, F., Covarrubias-Pazaran, G., Gueye, T., and Bartholome, J. (2023). Realized genetic gain in rice: achievements from breeding programs. *Rice* 16, 61. doi: 10.1186/s12284-023-00677-6
- Shang, J., Tao, Y., Chen, X., Zou, Y., Lei, C., Wang, J., et al. (2009). Identification of a new rice blast resistance gene, *Pid3*, by genomewide comparison of paired nucleotide-binding site-leucine-rich repeat genes and their pseudogene alleles between the two sequenced rice genomes. *Genetics* 182, 1303–1311. doi: 10.1534/genetics.109.102871
- Simms, E. L. (2000). Defining tolerance as a norm of reaction (in Chinese with English abstract). *Evol. Ecol.* 14, 563–570. doi: 10.1023/A:1010956716539
- Sogawa, K., and Kilin, D. (1987). Biotype shift in a brown planthopper(BPH) population on IR42. *Int. Rice Res. Newsl.* 12, 40.
- Sun, L. H., Wang, C. M., Changchao, S. U., Liu, Y. Q., Zhai, H. Q., and Wan, J. M. (2006). Mapping and marker-assisted selection of a brown planthopper resistance gene *bph2* in rice (*Oryza sativa* L.). *Acta Genetica Sin.* 33, 717–723. doi: 10.1016/S0379-4172(06)60104-2
- Tacconi, G., Baldassarre, V., Lanzanova, C., Faivre-Rampant, O., Cavigiolo, S., Urso, S., et al. (2010). Polymorphism analysis of genomic regions associated with broad-spectrum effective blast resistance genes for marker development in rice. *Mol. Breed.* 26, 595–617. doi: 10.1007/s11032-010-9394-4
- Temnykh, S., Park, W. D., Ayers, N., Cartinhour, S., and McCouch, S. R. (2000). Mapping and genome organization of microsatellite sequences in rice (*Oryza sativa* L.). *Theor. Appl. Genet.* 100, 697–712. doi: 10.1007/s001220051342
- Teng, B., Zeng, R., Wang, Y., Liu, Z., Zhang, Z., Zhu, H., et al. (2012). Detection of allelic variation at the *Wx* locus with single-segment substitution lines in rice (*Oryza sativa* L.). *Mol. Breed.* 30, 583–595. doi: 10.1007/s11032-011-9647-x
- Teng, B., Zhang, Y., Wu, J., Cong, X., Wang, R., Han, Y., et al. (2013). Association between allelic variation at the *Waxy* locus and starch physicochemical properties using single-segment substitution lines in rice (*Oryza sativa* L.). *Starch Strke* 65, 1069–1077. doi: 10.1002/star.v65.11-12
- Wang, F. (2022). Breeding and development of high-quality hybrid rice in south China (in Chinese with English abstract). *China Rice* 28, 107–116. doi: 10.3969/j.issn.1006-8082.2022.05.016
- Wang, F., Liu, Y., Zhang, A., Kong, D., Bi, J., Liu, G., et al. (2022). Breeding an early maturing, blast resistance water-saving and drought-resistance rice(WDR) cultivar using marker-assisted selection coupled with rapid generation advance. *Mol. Breed.* 42, 46. doi: 10.1007/s11032-022-01319-3
- Wang, J., Wang, R., Fang, H., Zhang, C., Zhang, F., Hao, Z., et al. (2021). Two VOZ transcription factors link an E3 ligase and an NLR immune receptor to modulate immunity in rice. *Mol. Plant* 14, 253–266. doi: 10.1016/j.molp.2020.11.005
- Wang, S. J., Wei, M. J., Feng, Z. G., Huang, J., Yan, Y. M., and Zeng, L. (2015). Breeding and application of good-quality *Indica* hybrid rice Teyou 7118 (in Chinese with English abstract). *Zhongzi (Seed)* 34, 108–110. doi: 10.16590/j.cnki.1001-4705.2015.04.054
- Wu, B. Q., Huang, F. K., Huang, S. S., Long, L. P., and Wei, S. M. (2009). Resistance stability of rice varieties to different biotypes of brown planthopper (in Chinese with English abstract). *J. App. Ecol.* 20, 1477–1482. Available at: <https://www.cjae.net/CN/abstract/abstract2304.shtml>.
- Xiao, W., Peng, X., Luo, L., Liang, K., Wang, J., Huang, M., et al. (2018). Development of elite restoring lines by integrating blast resistance and low amylose content using MAS. *J. Integr. Agr.* 17, 16–27. doi: 10.1016/S2095-3119(17)61684-8
- Xiao, W., Yang, Q., Huang, M., Guo, T., Liu, Y., Wang, J., et al. (2019). Improvement of rice blast resistance by developing monogenic lines, two-gene pyramids and three-gene pyramid through MAS. *Rice* 12, 78. doi: 10.1186/s12284-019-0336-4
- Yan, L., Luo, T., Huang, D., Wei, M., Ma, Z., Liu, C., et al. (2023). Recent advances in molecular mechanism and breeding utilization of brown planthopper resistance genes in rice: an integrated review. *Int. J. Mol. Sci.* 24, 12061. doi: 10.3390/ijms241512061
- Yang, Y. Z., Wang, K., Fu, C. J., Qin, P., Xie, Z. M., Hu, X. C., et al. (2020). hybrid rice Analysis on grain quality improvement of *Indica* hybrid rice in China (in Chinese with English abstract). *Hybrid Rice* 35, 1–7. doi: 10.16267/j.cnki.1005-3956.20190923.238
- Ying, J. Z., Qin, Y. B., Zhang, F. Y., Duan, L., Cheng, P., Yin, M., et al. (2024). A weak allele of *TGW5* confers higher seed propagations and efficient size-based seed sorting for hybrid rice production. *Plant Commun* 5, 100811. doi: 10.1016/j.xplc.2024.100811
- Zeng, D., Tian, Z., Rao, Y., Dong, G., Yang, Y., Huang, L., et al. (2017). Rational design of high-yield and superior-quality rice. *Nat. Plants* 3, 17031. doi: 10.1038/nplants.2017.31
- Zhang, C. P., Li, M., Liang, L. P., Xiang, J., Zhang, F., Zhang, C. Y., et al. (2023). Rice3K56 is a high-quality SNP array for genome-based genetic studies and breeding in rice (*Oryza sativa* L.). *Crop J.* 11, 800–807. doi: 10.1016/j.cj.2023.02.006
- Zhao, H., Wang, X., Jia, Y., Minkenberg, B., Wheatley, M., Fan, J., et al. (2018). The rice blast resistance gene *Ptr* encodes an atypical protein required for broad-spectrum disease resistance. *Nat. Commun.* 9, 2039. doi: 10.1038/s41467-018-04369-4
- Zhao, J., Zhang, S., Dong, J., Yang, T., Mao, X., Liu, Q., et al. (2017). A novel functional gene associated with cold tolerance at the seedling stage in rice. *Plant Biotechnol. J.* 15, 1141–1148. doi: 10.1111/pbi.12704
- Zhu, M., Liu, Y., Jiao, G., Yu, J., Zhao, R., Lu, A., et al. (2024). The elite eating quality alleles *Wx^b* and *ALK^b* are regulated by OsDOF18 and coordinately improve head rice yield. *Plant Biotechnol. J.* 22, 1582–1595. doi: 10.1111/pbi.14288



OPEN ACCESS

EDITED BY

Roxana Savin,
Universitat de Lleida, Spain

REVIEWED BY

C. Mariano Cossani,
South Australian Research and Development
Institute, Australia
Leonor Gabriela Abeledo,
University of Buenos Aires, Argentina

*CORRESPONDENCE

Karine Chenu

✉ karine.chenu@uq.edu.au

RECEIVED 06 December 2023

ACCEPTED 20 May 2024

PUBLISHED 07 June 2024

CITATION

Shazadi K, Christopher JT and Chenu K
(2024) Does late water deficit induce root
growth or senescence in wheat?
Front. Plant Sci. 15:1351436.
doi: 10.3389/fpls.2024.1351436

COPYRIGHT

© 2024 Shazadi, Christopher and Chenu. This
is an open-access article distributed under the
terms of the [Creative Commons Attribution
License \(CC BY\)](#). The use, distribution or
reproduction in other forums is permitted,
provided the original author(s) and the
copyright owner(s) are credited and that the
original publication in this journal is cited, in
accordance with accepted academic
practice. No use, distribution or reproduction
is permitted which does not comply with
these terms.

Does late water deficit induce root growth or senescence in wheat?

Kanwal Shazadi, John T. Christopher and Karine Chenu *

The University of Queensland, Queensland Alliance for Agriculture and Food Innovation (QAAFI),
Gatton, QLD, Australia

In crops like wheat, terminal drought is one of the principal stress factors limiting productivity in rain-fed systems. However, little is known about root development after heading, when water uptake can be critical to wheat crops. The impact of water-stress on root growth was investigated in two wheat cultivars, Scout and Mace, under well-watered and post-anthesis water stress in three experiments. Plants were grown outside in 1.5-m long pots at a density similar to local recommended farming practice. Differences in root development were observed between genotypes, especially for water stress conditions under which Scout developed and maintained a larger root system than Mace. While under well-watered conditions both genotypes had shallow roots that appeared to senesce after heading, a moderate water stress stimulated shallow-root growth in Scout but accelerated senescence in Mace. For deep roots, post-heading biomass growth was observed for both genotypes in well-watered conditions, while under moderate water stress, only Scout maintained net growth as Mace deep roots senesced. Water stress of severe intensity affected both genotypes similarly, with root senescence at all depths. Senescence was also observed above ground. Under well-watered conditions, Scout retained leaf greenness (i.e. stay-green phenotype) for slightly longer than Mace. The difference between genotypes accentuated under moderate water stress, with rapid post-anthesis leaf senescence in Mace while Scout leaf greenness was affected little if at all by the stress. As an overall result, grain biomass per plant ('yield') was similar in the two genotypes under well-watered conditions, but more affected by a moderate stress in Mace than Scout. The findings from this study will assist improvement in modelling root systems of crop models, development of relevant phenotyping methods and selection of cultivars with better adaptation to drought.

KEYWORDS

genotypic variation, root architecture, root development, root growth, root senescence, plant adaptation, drought, wheat

1 Introduction

Wheat cultivation in rain-fed agricultural systems is commonly challenged by water stress, especially during late crop development (Richter and Semenov, 2005; Farooq et al., 2009; Chenu et al., 2013; Collins and Chenu, 2021). Water stress affects many physiological traits both above and below ground with effects that depend on the timing, the intensity and the duration of the stress (Blum and Sullivan, 1997; Frensch, 1997; Munns, 2002; Collins et al., 2021; Mathew and Shimelis, 2022; Vadez et al., 2024).

One avenue to increase drought tolerance is to breed for varieties with increased capacity to extract soil water. While improving root architecture can assist crops access moist soil layers, the dynamic of root development can also be important to allow water uptake at critical stages (e.g. Veyradier et al., 2013). Beneficial root traits vary depending on the target population of environments. It has been suggested that in environments with shallow soils and frequent low-intensity rainfall, developing a dense root system in shallow soil layers may be advantageous to crops (Gregory et al., 1978; López-Castañeda and Richards, 1994). By contrast, in environments where crops rely heavily on water stored deep in the soil such as in north-eastern Australia (Chenu et al., 2011 and Chenu et al., 2013), a deep root system can benefit crops under late water stress.

Access to water late in the season is particularly important for grain filling. At that stage, a relatively small amount of subsoil water can translate to a major yield gain when crops are water stressed (Kirkegaard et al., 2007; Veyradier et al., 2013). In wheat, crop simulations have shown that an additional mm of water used after anthesis can lead to an extra 60 kg ha⁻¹ of grain yield (MansChadi et al., 2006 and MansChadi et al., 2010), and similar results have since been observed in field experiments (Kirkegaard et al., 2007). Candidate traits to increase water extraction at depth include higher root-length density at depth and more uniform root distribution at depth (MansChadi et al., 2006; Asseng and Turner, 2007; Lopes and Reynolds, 2010; Lilley and Kirkegaard, 2011; Ober et al., 2014). Maintaining water uptake under terminal drought typically helps to keep the canopy functional (Christopher et al., 2008) and increase yield (Dodd et al., 2011). Christopher et al. (2008) found that genotypes with contrasting root architecture at depth had different ability to retain green leaf area during the grain filling period (i.e. stay-green phenotype). Multiple studies have shown that post-anthesis water stress is associated with decreased photosynthetic capacity due to early leaf senescence (e.g. Yang et al., 2001), and that stay-green genotypes tend to yield more than others under terminal drought (Christopher et al., 2014 and Kumar et al., 2010; Christopher et al., 2016). Overall however, although higher root biomass and root distribution deeper in the profile has commonly been associated with better adaptation to water stress, little is known about the dynamics and genotypic variability of late root development both in well-watered and water-stress conditions (Palta et al., 2011).

The aims of this study were (i) to characterize wheat post-heading root growth over time in well-watered conditions, (ii) to

determine whether post-heading root growth or root senescence occur in response to drought, and (iii) to determine whether any such responses vary between genotypes. Three experiments were conducted with two Australian wheat cultivars with contrasting seedling root systems. The root systems of these cultivars were examined at key stages from heading to maturity in well-watered conditions and in a range of post-anthesis water-stress treatments. A system of 1.5-m polyvinyl chloride (PVC) pots was used to investigate phenotypic differences in both above- and below-ground responses to water stress up to physiological maturity.

2 Materials and methods

2.1 Growing conditions and experimental design

Three experiments were conducted with two wheat cultivars (Mace and Scout) grown in 1.5-m long polyvinyl chloride (PVC) pots of 90 mm diameter under different soil water conditions. Pots were placed in an outdoor open area in Toowoomba, Queensland, Australia (27.5598°S, 151.9507°E, 691 meters a.s.l.) and arranged to have a plant density similar to local grower's field (100 plant m⁻²). Furthermore, additional pots were positioned all around the experiment to avoid border effects (Rebetzke et al., 2014).

Mace and Scout are widely cultivated in western and southern cropping regions of Australia, respectively and differ in root architecture at the seedling stage, as Mace has wide root angle while Scout has narrow root angle (Richard et al., 2018). Three seeds of each genotype were placed in each pot at a depth of 2 cm. Sowing occurred on 4 August 2020 in the Experiment 1 (E1), 24 August 2021 in Experiment 2 (E2) and 4 July 2019 in Experiment 3 (E3). Following emergence, plants were thinned to one seedling per pot.

Seeds were sown in a packed soil consisting of a 50:50 mixture of a red alluvial soil from Redlands (-27.53°S, 153.25°E, ~20 m a.s.l.) and black vertosol soil from Kingsthorpe (27.51°S, 152.10°E, ~480 m a.s.l.). To ensure non-limiting nutrient supply, 2 gm L⁻¹ of Osmocote fertilizer containing trace elements (N 15.3% P 1.96%, K 12.6%) was added to the soil mix. The soil was watered to pot soil capacity at sowing.

Experimental treatments were denominated by the experiment number (E1, E2, E3) followed by "WW" for well-watered, "MDE" for moderate drought early in grain filling, "MDM" for moderate drought mid-grain filling or "SD" for severe drought with water being withheld from head emergence to maturity (Table 1). A cover was placed above the plants before any rainfall events and removed shortly after. Growth stages of individual replicate plants were monitored, and watering withheld between the required developmental periods (Table 1).

In the first experiment (E1), three irrigation treatments were applied; (i) well-watered conditions during the whole crop cycle (E1-WW); (ii) well-watered conditions followed by a water deficit applied by withholding irrigation between early anthesis (Zadoks decimal growth stage 61; Z61) (Zadoks et al., 1974) and early grain filling

TABLE 1 Characteristics for experiments (Exp.), treatments (Tmt) and sampling times, including the Zadoks developmental stages between which irrigation was withheld, number of days from sowing to anthesis (Anthesis), and from sowing to maturity (Maturity), green leaf area of the plant at heading (Z50) and grain yield per plant at maturity (Z92) for Mace and Scout.

Exp.	Sowing	Tmt*	Water withholding period**	Genotype	Sampling Time***	Anthesis (Z65) (days)	Maturity (Z92) (days)	Leaf area (Z50) (cm ² plt ⁻¹)	Yield (Z92) (g plt ⁻¹)
E1	4/08/2020	E1- WW	none	Mace	Z50, Z65, Z92	77 ± 0.9 ^{ns}	129 ± 0.8 ^{ns}	684 ± 55 ^b	16 ± 1.5 ^{ns}
				Scout		83 ± 0.8 ^{ns}	131 ± 0.9 ^{ns}	834 ± 78 ^a	14 ± 1.5 ^{ns}
	4/08/2020	E1-MDE	Z60–71	Mace	Z50, Z65, Z92	75 ± 0.9 ^b	117 ± 0.8 ^b	–	7 ± 1.6 ^b
				Scout		80 ± 0.8 ^a	133 ± 0.9 ^a		16 ± 1.8 ^a
	4/08/2020	E1-MDM	Z71–81	Mace	Z50, Z65, Z92	78 ± 0.9 ^b	117 ± 0.8 ^b	–	8 ± 1.8 ^b
				Scout		85 ± 0.8 ^a	131 ± 0.9 ^a		12 ± 1.5 ^a
E2	24/08/2021	E2-WW	none	Mace	Z75, Z92	68 ± 1.9 ^{ns}	106 ± 1.9 ^{ns}	–	12 ± 0.4 ^{ns}
				Scout		74 ± 2.2 ^{ns}	110 ± 2.2 ^{ns}		13 ± 0.5 ^{ns}
	24/08/2021	E2-MDE	Z60–71	Mace	Z75, Z92	65 ± 1.9 ^b	96 ± 1.9 ^b	–	8 ± 0.4 ^{ns}
				Scout		75 ± 2.2 ^a	119 ± 1.9 ^a		14 ± 0.4 ^{ns}
E3	4/07/2019	E3-SD	Z50–92	Mace	Z50, Z92	79 ± 0.8 ^{ns}	115 ± 0.78 ^{ns}	395 ± 48 ^{ns}	2.5 ± 0.19 ^{ns}
				Scout		86 ± 0.8 ^{ns}	120 ± 0.78 ^{ns}	573 ± 48 ^{ns}	3 ± 0.19 ^{ns}

Average and standard errors were presented for days to anthesis and maturity as well leaf area and yield (n=8). Means followed by different superscript letters are significantly different between genotypes within each treatment (P<0.05), “ns” indicates that the difference between genotypes is not significant (P>0.05). Each experiment was analyzed separately. *Experimental treatments (Tmt) were denominated by the experiment number followed by “WW” for well-watered, “MDE” for moderate drought early in grain filling, “MDM” for moderate drought mid-grain filling or “SD” for severe drought during grain filling. **Period of withholding watering are indicated by the number of the Zadoks growth stage from when watering was discontinued followed by the stage where watering was recommended. ***Harvest of plants occurred at heading (Z50), anthesis (Z65), mid grain filling (Z75) and/or physiological maturity (Z92).

(Z71) (E1-MDE), i.e. irrigation stopped 9.9 ± 0.3 days, and (iii) a water deficit imposed by withholding irrigation from early grain filling (Z71) to mid-grain filling (Z81) (E1-MDM), i.e. irrigation stopped for 10.0 ± 0.0 days. In this experiment, plants were harvested at heading (Z50), anthesis (Z65) and maturity (Z92). In a second experiment (E2), two irrigation treatments were applied; (i) well-watered conditions during the whole crop cycle (E2-WW); (ii) well-watered conditions followed by a water deficit applied by withholding irrigation between early anthesis (Z61) and early grain filling (Z71) (E2-MDE), i.e. irrigation stopped for 9.9 ± 0.3 days. In this experiment, plants were harvested at mid-grain filling (Z75) and maturity (Z92). In a third experiment (E3), water was withheld for the whole period from head emergence (Z50) to maturity (Z92) (E3-SD), i.e. irrigation stopped for 53.3 ± 2.1 days. In this experiment, plants were harvested at heading (Z50) and maturity (Z92). For all experiments, pots were watered weekly up to saturation, and let to drained. For each individual pot, watering was also performed up to saturation one day prior to the target growth stage, i.e. the stress was imposed at a date that varied between cultivar, treatments, and repetition). After the water-stress period, plants were rewatered up to saturation when they reached the target stage (Table 1). They were watered weekly up to saturation thereafter.

For each experiment, a randomized complete block design was used with eight replicates per cultivar for each treatment and each harvesting time (i.e. heading, anthesis, mid grain filling and/or physiological maturity), a replication being a single plant in a pot.

Environmental characterizations of the three experiments are presented in Table 2.

2.2 Plant measurements

Phenological development was monitored regularly by recording the growth stage using the Zadoks growth scale throughout the experiments (Zadoks et al., 1974). The greenness of the center of the flag leaf of the main stem was measured for each plant (i.e. eight replicates for each cultivar and treatment) at Z50, Z65, Z75 and Z81 using a Minolta SPAD 502 meter (Konica Minolta, Tokyo).

For each harvest, the shoots were excised at the crown. To maintain the root distribution, roots were washed and recovered on a nail board, with nails spaced every 20 mm. Only very few fine roots were lost in the process. Root sections were excised at 10-cm intervals for measurement of dry root biomass. The root biomass was measured following drying for 72h at 70°C. Total root biomass was calculated as the sum of dry weights for all 10 cm samples for each core. Average root diameter and root length were measured for a subset of soil layers (0–10 cm, 10–20 cm, and alternate 10-cm depth intervals there after (i.e., 30–40, 50–60, 70–80, 90–100, 110–120, and 130–140 cm) using WinRhizo Regular 2019. For each 10-cm depth, average root length density was calculated by dividing the total root length in a segment by the corresponding soil volume. To measure the differences in the partitioning of biomass between shallow, mid and deep roots, root fractions from 0–50 cm were summed to represent shallow roots, 50–100 cm to represent mid roots, and 100–150 cm to represent deep roots. Similarly, average root diameter and root length density were estimated for shallow,

TABLE 2 Environmental conditions in the three experiments (Exp.), including average temperature (Avg. Temp.), average daily maximum temperature (Tmax), average daily minimum temperature (Tmin), average daily evaporation (Avg. Evap.), average daily radiation (Avg. Radn) and cumulated radiation (Cum. Radn) from sowing to maturity of the last maturing plant.

Exp.	Avg. Temp. (°C)	Tmax (°C)	Tmin (°C)	Avg. Evap. (mm)	Avg. Radn (W m ⁻²)	Cum. Radn (W m ⁻²)
E1	19	25	13	5.1	19	20.1
E2	18.5	24	13.2	4.5	18.5	19.4
E3	17	22.5	10	4.6	17	18.4

mid and deep roots by averaging values from studied depths (0–10, 10–20 and 30–40 cm for shallow roots; 50–60, 70–80 cm for mid roots; and 90–100, 110–120 and 130–140 cm for deep roots). A small proportion of adventitious or nodal roots were present in the shallowest layer (0–10 cm) but not in other layers. Adventitious roots have a greater root diameter than the seminal roots (Christopher, 2024). However, the few adventitious roots were not separated and likely had only a small influence on the mean root diameter values calculated for the upper layers (0 to 50 cm).

The root: shoot ratio was computed by dividing total dry root biomass by the total dry shoot biomass. The total plant biomass was computed by combining the total dry shoot and dry root biomass.

For harvests at heading (Z50) and anthesis (Z65), leaf blades were separated for measurement of green leaf area using a leaf area meter (LI-3000, Li-COR Bioscience, Lincoln, NE, USA).

After threshing spikes by hand, yield was recorded at maturity as the total grain biomass (air dried) per plant.

2.3 Statistical analyses

Within each experiment, an analysis of variance (Figueroa-Bustos et al., 2020) was performed between genotypes, treatments and stages for total plant biomass, dry shoot biomass, total dry root biomass, average root length density, average root diameter, dry root biomass at depths, average root length density at depths and average root diameter at depths using the R platform (v3.2.5; Team, R.C., 2019). A Student–Newman–Keuls (SNK) test was used to compare means for genotypes and treatments, with a significance level of 0.05.

3 Results

3.1 Water stress reduced the duration of the plant growth cycle in Mace but not in Scout

Under well-watered conditions, the plant growth duration from sowing to anthesis and to maturity was slightly shorter for Mace than for Scout, but differences were not significant (Table 1).

Application of a post-anthesis moderate water stress shortened the duration from sowing to maturity in Mace but not Scout. While under well-watered conditions the difference in time to maturity between genotypes was relatively small at 2 or 4 days in Experiments 1 or 2, respectively, this difference ranged from 14 to 23 days under moderate stress (Table 1).

For the severe stress (E3-SD), the 5d difference between genotypes was not significant and relatively small compared to moderately water-stressed plants in the other two experiments.

Overall, both genotypes had similar phenology under well-watered condition and severe water stress, but only Mace has a post-anthesis period significantly reduced by a moderate water stress.

3.2 Under well-watered conditions, dry root biomass at depth increased post anthesis in Scout but not in Mace

Under well-watered conditions, whole-plant dry biomass significantly increased from anthesis to maturity for both Scout and Mace, but genotype x stage interactions were not significantly different (Figure 1A; Supplementary Table S1). Mace tended to have a smaller total plant biomass than Scout both at anthesis and maturity (Figure 1A) mainly due to a smaller shoot system. Root biomass only accounted for 2.5–10% of the shoot biomass (Figures 1B–D). Mace also tended to have lesser root biomass than Scout, especially at maturity (Z92; Figure 1C).

Significant post-anthesis root growth occurred for roots deeper than 50 cm in Scout under well-watered conditions (Figures 2A, D), with a net increase in root biomass between anthesis and maturity (Figures 2A, D). In contrast, for Mace, root biomass changed little from anthesis and maturity at all depths deeper than 50 cm, while some reduction in root biomass was observed for the shallow soil layers (Figures 2A, D).

Overall, the post-anthesis increase in shoot biomass with little or no increase in root biomass led to a decrease in the root: shoot ratio from anthesis to maturity for both genotypes (Figure 1D).

Post-anthesis root length density tended to decrease in both genotypes (Figure 1E). This decrease was observed for shallow roots (<50 cm) in both genotypes, while post-anthesis root length density tended to increase in deep roots (> 50 cm) in Scout (Figures 3A, C).

For both genotypes, average root diameter tended to decrease after anthesis at all depths under well-watered conditions (Figures 1F, 3B, D).

3.3 Moderate water stress reduced both shoot and root biomass in Mace, while Scout was more tolerant

Total plant biomass at maturity in well-watered conditions was not significantly different between Scout and Mace although Mace tended to have a lower mean value (Figure 4A). In contrast, significant differences were observed between genotypes in

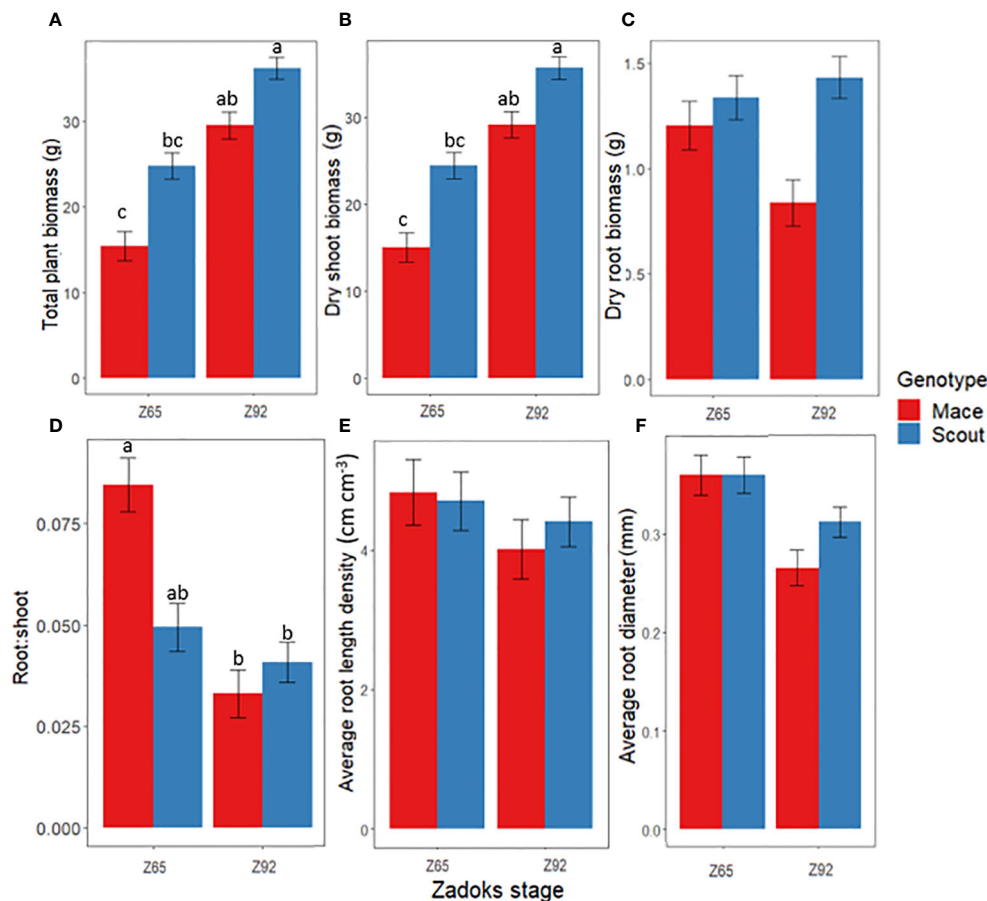


FIGURE 1

Changes between anthesis (Z65) and maturity (Z92) under well-watered conditions (E1-WW) in (A) whole-plant dry biomass, (B) shoot dry biomass, (C) root dry biomass, (D) root: shoot dry biomass ratio, (E) average root length density, and (F) average root diameter for Mace (red bars) and Scout (blue bars). Different letters indicate mean values that are significantly different at $P < 0.05$. Error bars represent the standard error of the mean ($n=8$). The results from the analysis of variance associated to those data are presented in [Supplementary Table S1](#).

moderately water-stressed treatments (Figure 4A). Moderate water-stress treatments during the early or mid-grain filling period significantly reduced whole-plant biomass at maturity in Mace, with a reduction by 48.8%, 37.6% and 32.78% for E1-MDE, E1-MDM, and E2-MDE, respectively, compared to their respective well-watered controls (E1-WW and E2-WW; Figure 4A). By contrast, whole-plant biomass of Scout was little affected by moderate water stress and remained similar to that observed in well-watered conditions. This distinction between genotypes was lost in the severe water stress treatment (E3-SD) in experiment E3, which substantially reduced the total plant biomass of both genotypes to similarly low values.

A similar trend was observed for dry shoot biomass with greater difference between the genotypes for moderate water stress treatments (E1-MDE, E1-MDM and E2-MDE) compared to either the well-watered or severe water stressed treatments (Figure 4B).

Root biomass and root length density also followed an overall similar trend (Figures 4C, E). Average root diameter was greater in Scout than in Mace in most treatments, including under well-watered conditions. By contrast, a moderate water stress had either no effect or increased the average root diameter in Mace, while it decreased average root diameter in Scout in experiment E1 (Figure 4F).

The root: shoot ratio at maturity did not vary significantly between treatments or between genotypes in experiment E1 (Figure 4D; [Supplementary Table S2](#)). However, in experiment E2, significant differences were observed between genotypes both in E2-WW and E2-MDE, with Scout having a greater root: shoot ratio than Mace (Figure 4D). For the severe water-stress treatment of experiment E3 (E3-SD), no significant difference was observed between Scout and Mace for root: shoot ratio. The mean values for root: shoot ratio, although they cannot be formally compared between experiments, were much lower in E3 than in any of the treatments in E1 and E2.

3.4 Moderate water stress induced root senescence at all depths in Mace, and in shallow roots in Scout

For the studied root traits, significant differences were found between genotypes, treatments, depths and their interactions ([Supplementary Table S3](#)).

For Mace, no significant difference was observed in root biomass between water treatments at shallow depths (0–50 cm),

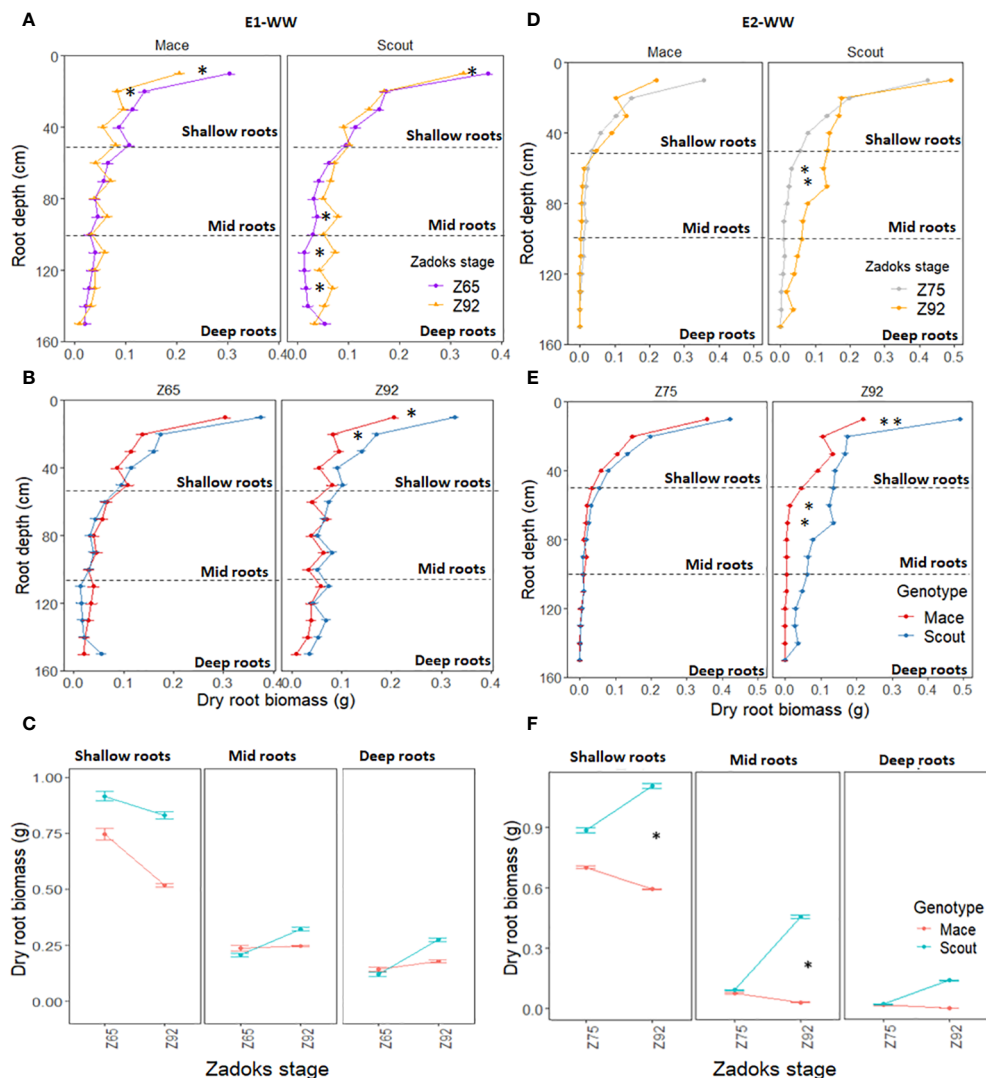


FIGURE 2

Dry root biomass at different depths (0 to 150 cm) for Mace and Scout plants grown under well-watered conditions in E1-WW (A–C) and E2-WW (D–F) and harvested at different stages, including anthesis (Z65), mid-grain filling (Z75) and maturity (Z92). In (A, B, D, E), the horizontal dashed lines represent partitions between shallow (0 to 50 cm), mid (50 to 100 cm), and deep (100 to 150 cm) root layers. Error bars represent the standard error of the mean ($n=8$). Significant differences between means for root layers are indicated by asterisks for $P<0.05^*$ and $P<0.01^{**}$.

but moderate water stress (E1-MDE, E1-MDM and E2-MDE) caused root senescence for lower depths (100–150 cm) compared to well water treatments (E1-WW and E2-WW; Figure 5; Supplementary Figure S1). By contrast in Scout, no substantial difference in root biomass was observed for deep roots between well-watered (E1-WW and E2-WW) and moderate water stress treatments. However, shallow roots of Scout after a moderate stress during mid-grain filling (E1-MDM) or a severe stress (E3-SD) had less biomass than well-watered plants at maturity, indicating root senescence after anthesis. By contrast, for an earlier moderate stress during early grain filling (E1-MDE and E2-MDE), Scout shallow roots tended to grow more than under the other treatments, including well-watered conditions (E1-WW and E2-WW). In the severely water stressed treatment (E3-SD), dry root biomass for shallow and deep roots was similarly severely reduced for both genotypes at maturity.

Root length density and average root diameter for shallow and deep layers had a similar trend to that of root biomass under all treatments for both Scout and Mace (Figure 6; Supplementary Figures S2, S3).

To investigate dynamic changes in root development, variations in dry root biomass distribution between heading (Z50) and maturity (Z92) were estimated by subtracting the root biomass at heading from the root biomass at maturity (Figure 7A; Supplementary Figure S4), complementing comparison previously done between anthesis and maturity (e.g., Figures 1, 2A–C, 3). For Mace, all water-stress treatments tended to cause net shallow and deep root senescence between heading and maturity, while in well-watered conditions, net senescence was only observed in shallow roots and to a lesser extent than for stressed conditions (Figure 7A). In contrast for Scout, deep root biomass increased between heading and maturity in all treatments, except for the severe water-stress

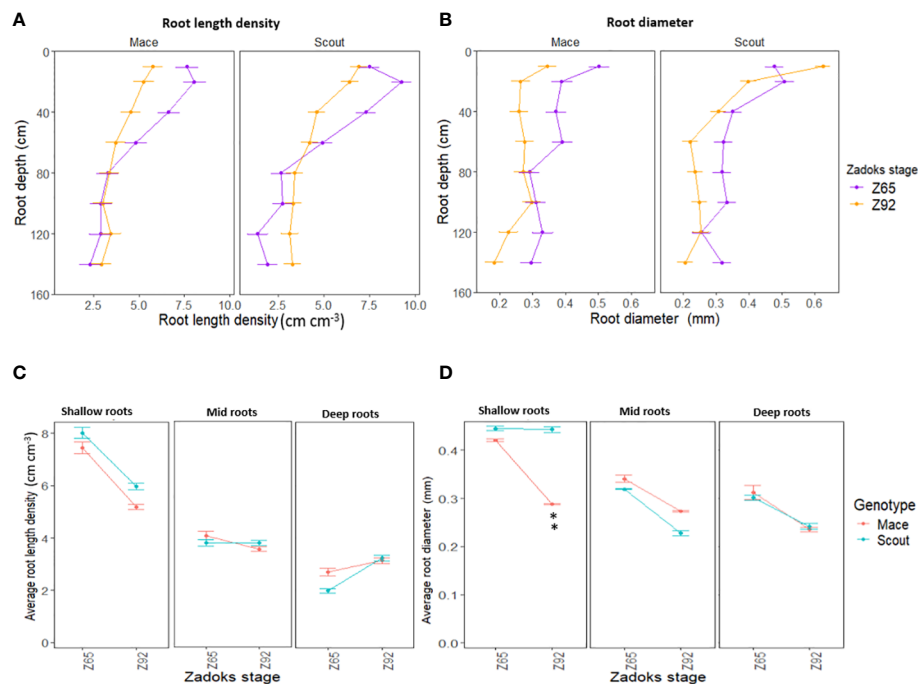


FIGURE 3

Average root length density (A, C) and root diameter (B, D) of Mace and Scout at anthesis (Z65) and maturity (Z92) under well-watered conditions (E1-WW) at different 10-cm depth intervals (0–10, 20–30, 50–60, ..., 130–140 cm) (A, B), and for corresponding shallow (0 to 50 cm), mid (50 to 100 cm) and deep (100 to 150 cm) roots (C, D). Error bars represent the standard error of the mean (n=8). Asterisks (**) indicate significant genotypic difference at $P < 0.01$.

treatment (E3-SD) where net senescence was observed. For Scout shallow roots, senescence was observed for all treatments except E1-MDE. In other words, deep roots for Scout grew between heading and maturity in all studied conditions, except the severe stress E3-SD which induced a net root senescence in all soil layers.

Root length density in Scout was greater at maturity than at heading for all depths in all treatments except E3-SD where a small net senescence occurred (Figure 7B). Roots of Scout also increased in diameter on average between heading and maturity for all treatments except E3-SD (Figure 7C). For Mace, shallow and deep layer root length density between heading and maturity was reduced by water stress. Mace average root diameter was also reduced by water stress, except for shallow roots under moderate water stress which had a similar root diameter as under well-watered conditions (Figure 7C; Supplementary Figure 3C). The differences in root diameter between Scout and Mace were accentuated by all water stress treatments.

3.5 Water stress induced more canopy senescence in Mace than Scout

To address the question of whether root senescence observed for some water-stress treatments was related to canopy senescence, the greenness of the flag leaf was followed post anthesis using SPAD measurements (Figures 8, 9). Significant differences were found for SPAD values between genotypes, stages, treatments, and their interactions (Supplementary Table S4).

Under well-watered conditions (E1-WW and E2-WW), both cultivars exhibited relatively high leaf SPAD values greater than 38 arbitrary SPAD units until late grain filling (Z81). In E1-WW, Scout had higher chlorophyll content than Mace at heading and anthesis and exhibited a small drop over the grain filling period, which was also observed in Mace (Figure 8). Leaf area was also significantly higher for Scout than Mace at heading (Z50) under well-watered conditions (Table 1).

Moderate water stress (E1-MDE, E1-MDM, E2-MDE) resulted in accelerated leaf senescence during the grain filling (e.g., Z75) in Mace, while there was little or no effect on Scout flag leaf greenness (Figure 8). Severe water stress (E3-SD) caused a rapid decrease in leaf greenness for both cultivars after anthesis (Z65) although Scout had significantly higher mean SPAD values than Mace up until mid-grain filling (Z75). Although not formally comparable, the mean leaf greenness (SPAD) for Scout at late grain filling (Z81) for E3-SD were reduced to a lower value than for any of the treatments in either experiment E1 or E2 for this genotype.

Mace showed leaf senescence from anthesis (Z65) to maturity (Figure 8) which was correlated with loss of deep root biomass between heading (Z50) and maturity (Figure 7) under moderate and severe stress. Similarly, leaf senescence in Scout correlated with root senescence in severe stress, while little or no senescence was observed in either deep roots or shoots of Scout under moderate stress (Figures 7, 8).

A strong correlation was found between root dry biomass at maturity (which results from root growth and senescence that occurring during the whole plant cycle) and leaf greenness (SPAD) at mid grain filling (Figure 9).

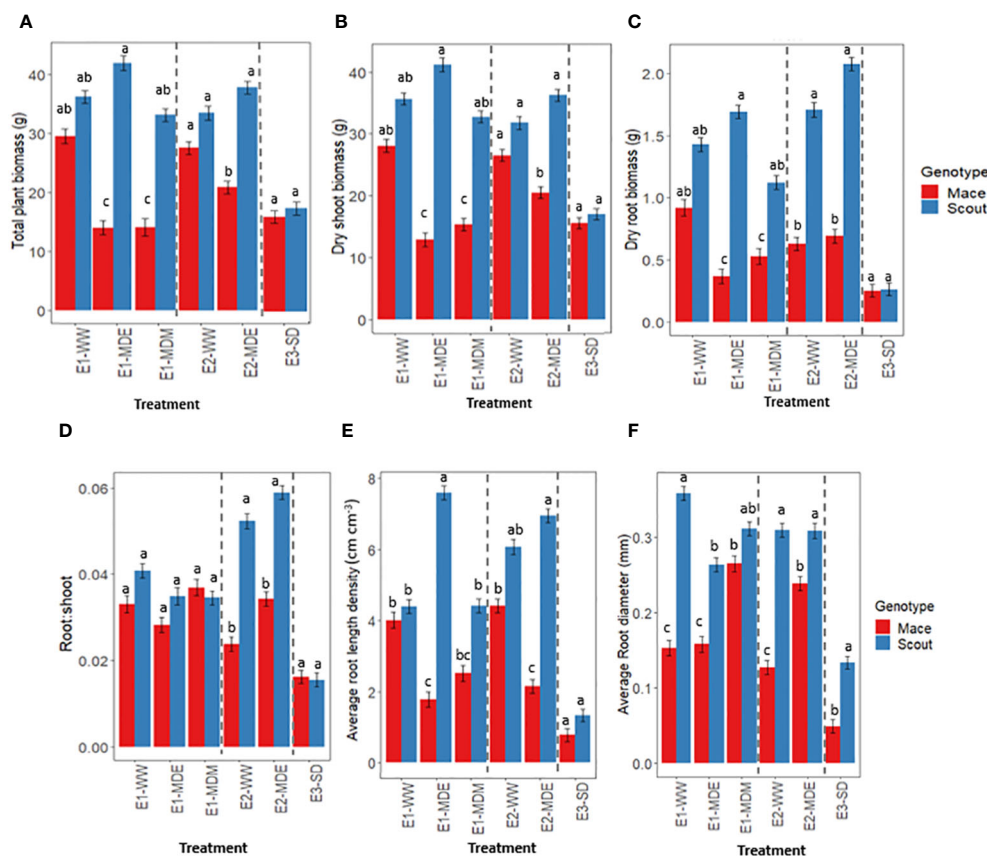


FIGURE 4

Response to different soil water status at maturity for (A) whole-plant dry biomass, (B) shoot dry biomass, (C) root dry biomass, (D) root: shoot dry biomass ratio, (E) average root length density, and (F) average root diameter in Mace (red bars) and Scout (blue bars). The names of the different treatments correspond to the experiment (E1, E2, E3) followed by “WW” for well-watered, “MDE” for moderate drought early in grain filling, “MDM” for moderate drought mid-grain filling or “SD” for severe drought with water being withheld from head emergence to maturity (Table 1). In each panel, dashed lines separate the data from the three experiments. Analysis of variance was performed separately for each experiment (Supplementary Table S2). Different letters indicate mean values that are significantly different at $P < 0.05$ within each experiment. Error bars represent the standard error of the mean ($n=8$).

3.6 Water stress induced more yield loss in Mace than Scout

In well-watered conditions, the grain yield per plant in Mace (16 ± 1.5 and 12 ± 0.4 g in E1-WW and E2-WW, respectively) was similar to that of Scout (14 ± 1.5 and 13 ± 0.5 g; Table 1).

For moderate water stress, the yield per plant in Scout in treatments E1-MDE (16 ± 1.8 g), E1-MDM (12 ± 1.5 g) and E2-MDE (14 ± 0.4 g) remained similar to that in well-watered plants. In contrast, for Mace, the yield per plant was significantly lower for E1-MDE (7 ± 1.6 g), E2-MDE (8 ± 0.4 g), and E1-MDM (8 ± 1.8 g) compared with E1-WW and E2-WW, respectively (Table 1).

In severe water stress (E3-SD), yield of both genotypes was severely reduced compared with E1-WW or E2-WW with similarly low values of 2.5 ± 0.19 g for Mace and 3 ± 0.19 g for Scout (Table 1).

Overall, while Mace and Scout had similar grain yield per plant when well watered, only Scout maintained it under moderate drought. Severe water stress severely affected yield of both genotypes.

4 Discussion

The polyvinyl chloride (PVC) pot system was successfully used to identify genotypic differences in the response of wheat roots to drought. Two wheat cultivars known to differ in seedling seminal root angle were used to demonstrate this (Richard, 2017; Richard et al., 2018).

4.1 Moderate water stress induced root senescence or root growth depending on the genotype

In this study, Scout had similar or significantly greater shallow and deep root biomass than Mace at maturity (Figures 2, 5; Supplementary Figure S1). Deep root biomass of Scout (i) significantly increased after anthesis under well-watered conditions (Figures 2A, C), (ii) tended to slightly increase between heading and maturity when under moderate water stress

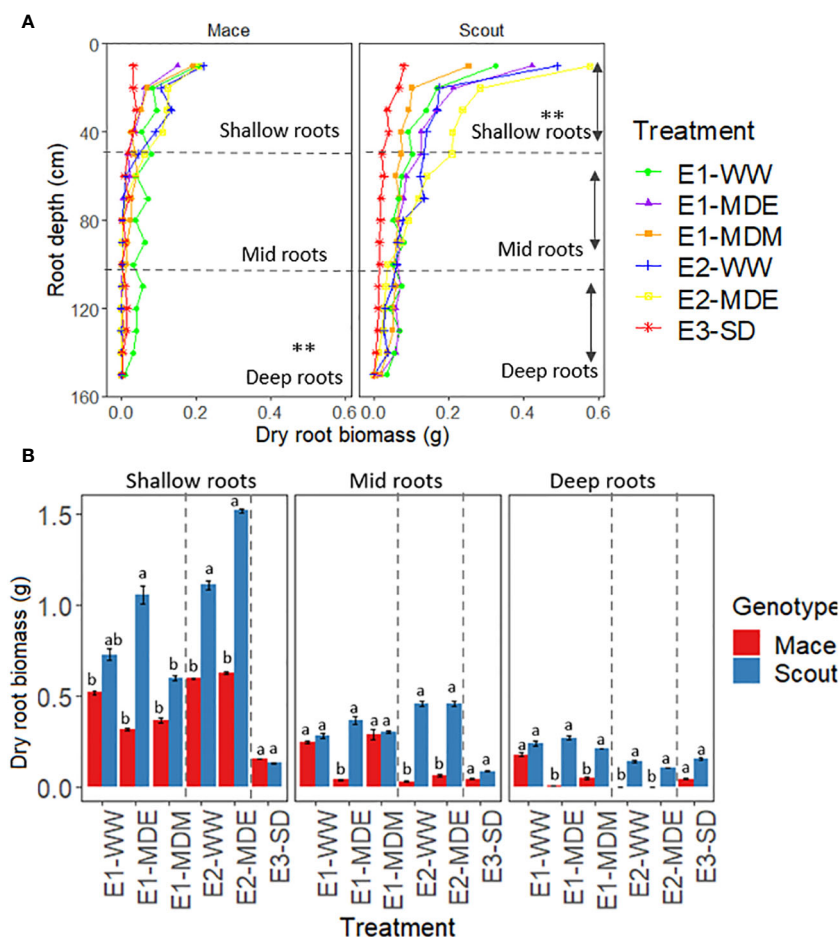


FIGURE 5

Distribution of dry root biomass per plant for different soil water treatments at maturity for (A) 10-cm increment depths (0 to 150 cm) and (B) shallow (0 to 50 cm), mid (50 to 100 cm), and deep (100 to 150 cm) roots in Mace and Scout. In (A), asterisks (**) indicate differences between treatments for dry biomass of shallow, mid or deep roots ($P < 0.01$). In (B), the dotted lines separate the three independently analyzed experiments; means that are significantly different ($P < 0.05$) within each experiment are indicated by different letters above the bars. Error bars represent the standard error of the mean ($n=8$). The results of analyses of variance from each experiment are presented in [Supplementary Table S3](#).

(Figure 5), but (iii) decreased post-heading in severe water-limited conditions (Figures 3, 7; [Supplementary Figure S4A](#)). By contrast, shallow root biomass of Scout (i) senesced post-heading under well-watered, mid-grain filling moderate water-stress and severe water-stress conditions and (ii) tended to have a similar biomass at heading and maturity under early-grain-filling water stress, thus indicating some stress-induced root growth in these conditions. Overall, under water deficit conditions, Scout maintained deep roots more than shallow roots (Figure 7).

Conversely, Mace did not have post-anthesis deep root growth under well-watered conditions (Figure 2), showed post-anthesis root senescence of shallow roots under well-watered conditions (Figure 2), and showed shallow and deep root senescence for moderate and severe post-anthesis water stress treatments (Figure 7). Notably, Mace had a slightly smaller green leaf area than Scout at anthesis (Table 1) and experienced earlier leaf senescence (Figure 8), indicating that Mace may be less prone to soil water loss by transpiration due to its slightly smaller green leaf area (Table 1). However, Mace may also have been

more prone to water loss, due to a higher hydraulic conductance suggested by observations of greater normalized transpiration rate at high evaporative demand (Chenu et al. unpublished) and lower transpiration efficiency (Fletcher et al., 2018) in Mace than Scout. Overall, in the present study, Mace appeared more susceptible to the imposed water stress conditions than Scout in terms of root development, which is likely to at least partly explain the greater yield reductions observed in Mace compared to Scout. The greater plasticity of Mace in response to late water stress was also observed in a field trial at Hermitage, Queensland, where Mace yield was reduced by 15% in the rainfed treatment, while Scout maintained its yield under these conditions (Christopher et al., unpublished).

Despite these results, Mace is reputed to be well-adapted for other drought-prone regions, such as the Southern and Western parts of the Australian wheatbelt. Mace has been widely grown in these regions (Ehdaie et al., 2012). Mace was also observed to produce a similar or greater yield than Scout in field trials in these regions (Christopher et al., unpublished). Large parts of those regions have a Mediterranean

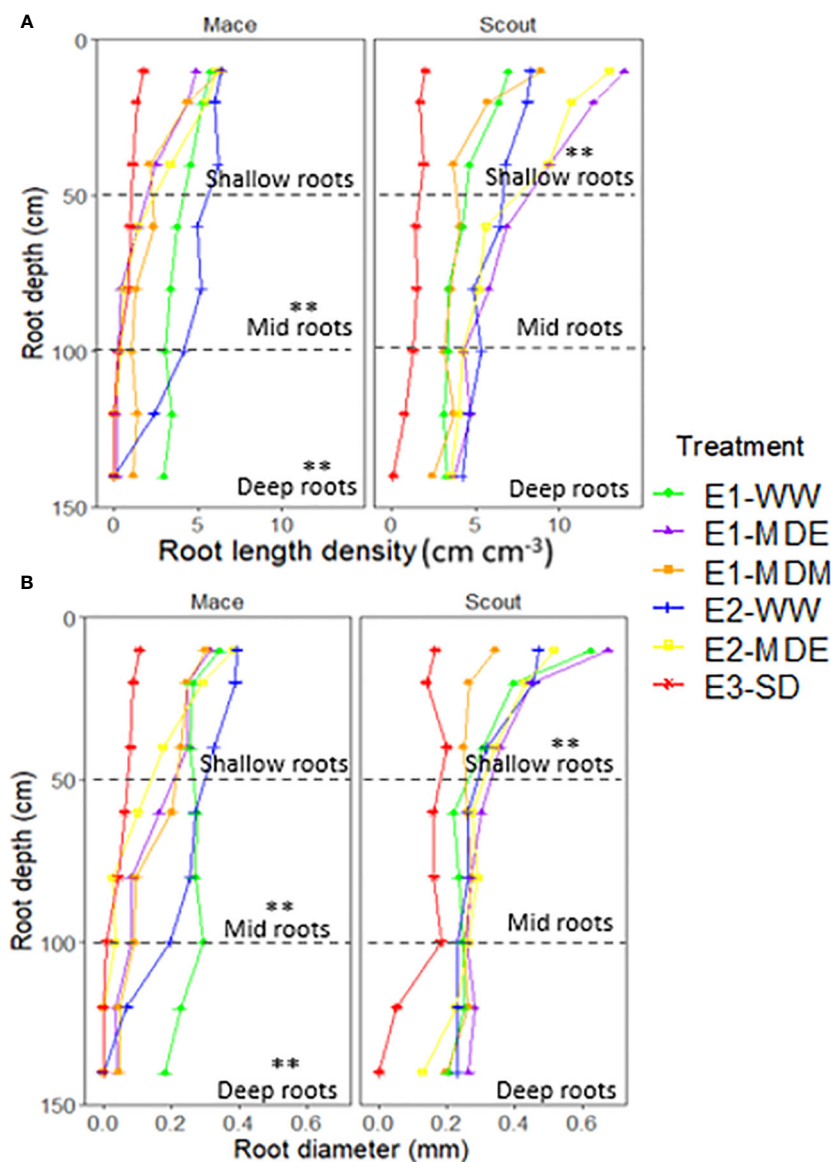


FIGURE 6

Root length density (A) and root diameter (B) of Mace and Scout for different depths (0 to 150 cm) at maturity for different water status treatments. The dashed lines represent partitions between shallow (0 to 50 cm), mid (50 to 100 cm), and deep (100 to 150 cm) roots. Asterisks (**) indicate differences between treatments for shallow, mid or deep roots ($P < 0.01$). The results of analyses of variance from each experiment are presented in [Supplementary Table S3](#).

climate characterized by winter-dominant rainfall (Singh et al., 2011) with medium to light soils, in which a quick finish to avoid terminal drought and heat may be more advantageous than developing post-anthesis root growth to extend the grain filling period (Shavrukov et al., 2017). Such traits were observed in Mace under stress in the current study (Table 1). The wide root angle observed at the seedling stage in Mace (Richard et al., 2018) may also confer some benefit for shallow root development in field conditions to better forage for water from small rainfall events leading to only shallow moisture infiltration. It is noteworthy that in the long PVC pot, roots were constrained laterally (90 mm diameter), which may have affected the development of shallow roots. In this system, roots could for example choose the

path of least resistance down the side of the soil column. For instance, it has been observed that roots have a propensity to develop in pores at depth in the field (White and Kirkegaard, 2010; Hodgkinson et al., 2017). However, in the current experiments, the soil was well watered up until heading, and later in most conditions, and any shrinkage of soil leading to gaps at the sides of the columns would likely have occurred too late in the crop cycle to have a major effect on root accumulation at the edges. Also, the root: shoot ratios observed in the current study were relatively low compared to some other studies, but they were in a similar order to post-anthesis root: shoot ratios estimated based on soil cores in irrigated wheat field trials (Lopes and Reynolds, 2011; Heinemann et al., 2023).

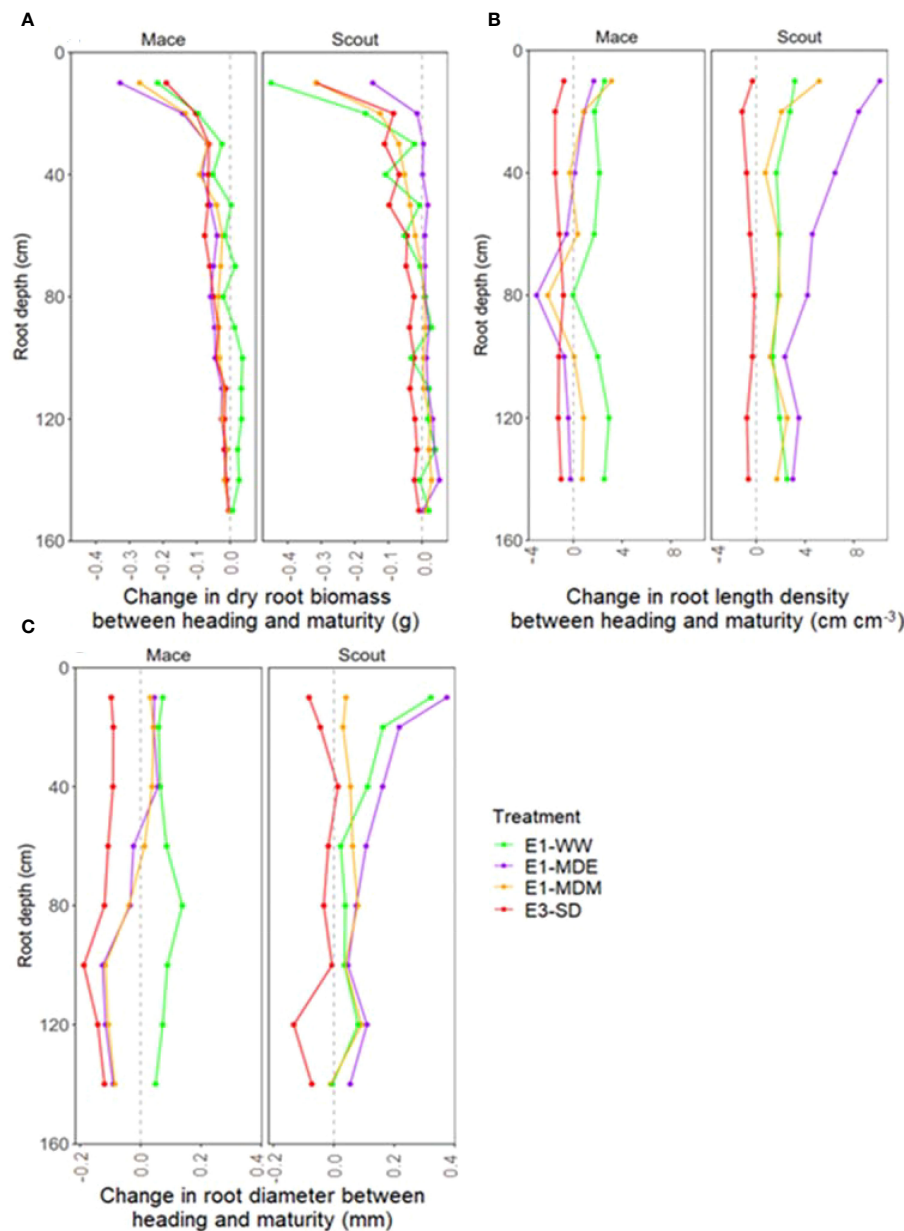


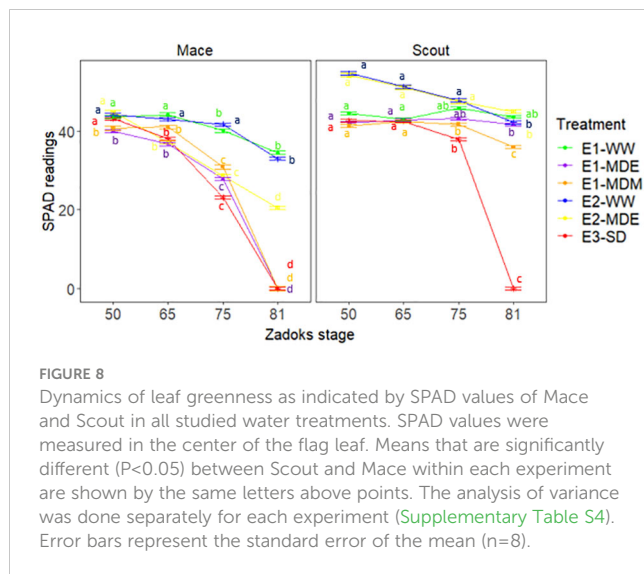
FIGURE 7

Change in whole-plant root biomass (A), root length density (B), and root diameter (C) between heading (Z50) and maturity (Z92) for Mace and Scout at different soil depths (0 to 150 cm) in all studied water treatments where measurements at such stages were performed (i.e. all treatments of experiments E1 and E3). In each panel, the vertical dashed grey line corresponds to a value of zero representing no change between stages. Values to the left of the line (A) represent a decrease in biomass (net root senescence) while values to the right represent increase in biomass (net root growth).

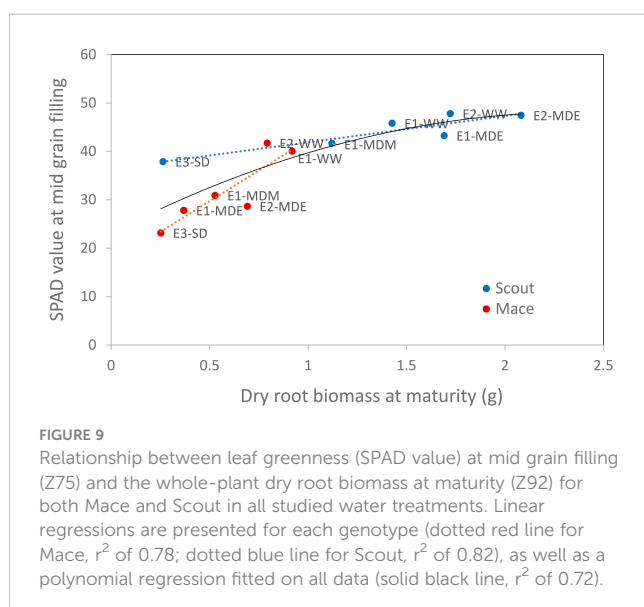
4.2 Deep rooting as a drought adaptative trait associated with stay-green, increased crop cycle duration and enhanced yield

The narrow seedling root angle previously reported for Scout has been associated for other wheat genotypes exhibiting development of deep roots and the ability to access water stored deep in the soil (Ludlow and Muchow, 1990). In agreement with this, in the current study, Scout also had a greater root biomass and root length density at depth than Mace late in the season, especially under moderate water stress (Figure 5; Supplementary Figure S1). However, the severe

prolonged water-stress treatment caused both root and leaf senescence for the two genotypes, as plants cannot survive without access to water (Vadez et al., 2024). The greater deep root biomass and root length density observed for Scout post-anthesis, especially following moderate late water stress (e.g., Supplementary Figures S1–S2), is likely to have allowed Scout to access more water at depth than Mace, although water uptake was not directly measured. However, the observed stay-green phenotype with plants retaining a higher green leaf area content until close to maturity tend to support the notion that Scout could access water for longer in the season (Figures 8, 9). Such a stay-green phenotype can allow plants to



accumulate biomass for longer and to mature later than plants lacking the stay-green phenotype, helping to explain the greater duration to maturity time observed in Scout versus Mace under water stress (Table 1). Concordantly, in field study, the stay-green phenotype with retention of both green leaf area and photosynthetic capacity for longer during grain filling, has been associated with higher yield for several plant species (Thomas and Smart, 1993; Nawaz et al., 2013; Christopher et al., 2014). This is in particular the case under post-anthesis drought stress for bread wheat (Christopher et al., 2008; Adu et al., 2011; Bogard et al., 2011; Lopes and Reynolds, 2012), durum wheat (Spano et al., 2003), and other cereals such as maize (Crafts-Brandner et al., 1984; Gentinetta et al., 1986; Zheng et al., 2009), rice (Mondal et al., 1985; Wada and Wada, 1991; Ba Hoang and Kobata, 2009), and sorghum (Borrell et al., 2014 and Borrell et al., 2023).



4.3 Implication for plant breeding

High levels of variation in root traits, and possible emergent traits such as stay-green and canopy temperature have been reported across large populations in different crops including wheat (Christopher et al., 2014; Richard et al., 2015 and Lopes and Reynolds, 2010; Christopher et al., 2016). However, the value of root traits for crop improvement in different target populations of environments (TPE) remains vaguely defined. Crop modelling studies have been conducted in an attempt to assess these values (e.g. MansChadi et al., 2006; Veyradier et al., 2013; Casadebaig et al., 2016; Lilley and Kirkegaard, 2016), but with models that are not well adapted to simulate root growth and development, especially not across genotypes. The present study is a step forwards to characterize the dynamics of root architecture in response to environments, as demonstrated by the contrast between the two genotypes studied here. This, and further such studies can help to improve our modelling capability for the effects of root traits in various environments (Chenu et al., 2017).

Genetics studies have also examined correlations between root traits with yield as well as the co-location of QTL for root traits and yield. In sorghum, QTL for nodal root angle at the seedling stage were found to co-locate with QTL for traits associated with drought adaptation (Mace et al., 2012), indicating the potential value of this trait. In barley, correlation between seedling root traits and yield were highly dependent on the environment considered (Robinson et al., 2018). The relationship between QTL for seminal root traits and yield was less clear in bread wheat (Christopher et al., 2021).

To advance in this field, phenotyping methods such as the one presented here should be adapted to be able to screen large populations for root characteristics at important stages such as during the grain filling. In the field, methods using minirhizotrons or soil cores associated for instance with fluorescence spectroscopy exist to look at deep rooting (Wasson et al., 2016; Christopher, 2024). Recently, a field-based method based on electro-magnetic induction (EMI) sensors (DualEM 21S) was proposed to screen for changes in soil water at different depths to indirectly characterize root systems at depth (Zhao et al., 2022). This non-destructive method was successfully applied to investigate differences between sorghum hybrids (Zhao et al., 2023; Zhao et al., 2024) and could potentially be extended to investigate root plasticity to water stress and to identify underlying genetic controls in different crops including wheat.

5 Conclusion

The results of this study suggest that Scout maintained post-anthesis deep root growth under moderate post-anthesis water-stress treatment whereas deep roots of Mace senesced. Deep root development potentially enabled access to water late in the season which likely aided Scout to maintain a stay-green phenotype and produce higher yield per plant under moderated water stress. The reported findings based on two contrasting genotypes could be extended to a greater range genotypes.

The results have implications for crop modelling which does not yet adequately consider root growth, development and water-and-nutrient uptake.

Identification of root traits that may enhance water uptake late in crop development, such as deep root length density for drought-prone locations with heavy deep soils, is anticipated to improve wheat adaptation in regions prone to late season water stress.

Data availability statement

The raw data supporting the conclusions of this article will be made available by the authors, without undue reservation.

Author contributions

KS: Conceptualization, Data curation, Formal analysis, Investigation, Methodology, Visualization, Writing – original draft. JC: Conceptualization, Investigation, Methodology, Resources, Supervision, Writing – review & editing. KC: Conceptualization, Data curation, Investigation, Methodology, Resources, Supervision, Writing – review & editing.

Funding

The author(s) declare financial support was received for the research, authorship, and/or publication of this article. KS received a Research Training Program PhD scholarship from The University of Queensland. The authors also acknowledge the support from the Grains Research and Development Corporation of Australia (Project UQ00068) and the Australian Research Council (ARC Linkage Project LP210200723).

References

- Adu, M. O., Sparkes, D. L., Parmar, A., and Yawson, D. O. (2011). 'Stay green' in wheat: comparative study of modern bread wheat and ancient wheat cultivars. *J. Agric. Biol. Sci.* 17, 24.
- Asseng, S., and Turner, N. (2007). *Modelling genotypex environment x management interactions to improve yield, water use efficiency and grain protein in wheat* (Dordrecht: Springer), 91–102. doi: 10.1007/1-4020-5906-X_8
- Ba Hoang, T., and Kobata, T. (2009). Stay-green in rice (*Oryza sativa* L.) of drought-prone areas in desiccated soils. *Plant Production. Sci.* 12, 397–408. doi: 10.1626/pps.12.397
- Blum, A., and Sullivan, C. (1997). The effect of plant size on wheat response to agents of drought stress. I. Root drying. *Funct. Plant Biol.* 24, 35–41. doi: 10.1071/PP96022
- Bogard, M., Jourdan, M., Allard, V., Martre, P., Perretant, M. R., Ravel, C., et al. (2011). Anthesis date mainly explained correlations between post-anthesis leaf senescence, grain yield, and grain protein concentration in a winter wheat population segregating for flowering time QTLs. *J. Exp. Bot.* 62, 3621–3636. doi: 10.1093/jxb/err061
- Borrell, A. K., Christopher, J. T., Kelly, A., Collins, B., and Chenu, K. (2023). Balancing pre- and post-anthesis growth to maximise water-limited yield in cereals. *Field Crops Res.* 296, 108919. doi: 10.1016/j.fcr.2023.108919
- Borrell, A. K., Mullet, J. E., George-Jaeggli, B., van Oosterom, E. J., Hammer, G., L., Klein, P. E., et al. (2014). Drought adaptation of stay-green sorghum is associated with canopy development, leaf anatomy, root growth, and water uptake. *J. Exp. Bot.* 65, 6251–6263. doi: 10.1093/jxb/eru232
- Casadebaig, P., Zheng, B. Y., Chapman, S., Huth, N., Faivre, R., and Chenu, K. (2016). Assessment of the potential impacts of wheat plant traits across environments by combining crop modeling and global sensitivity analysis. *PLoS One* 11, 1–27. doi: 10.1371/journal.pone.0146385
- Chenu, K., Cooper, M., Hammer, G., Mathews, K. L., Dreccer, M., and Chapman, S. C. (2011). Environment characterization as an aid to wheat improvement: interpreting genotype–environment interactions by modelling water-deficit patterns in North-Eastern Australia. *J. Exp. Bot.* 62, 1743–1755. doi: 10.1093/jxb/erq459
- Chenu, K., Dehilmfard, R., and Chapman, S. C. (2013). Large-scale characterization of drought pattern: a continent-wide modelling approach applied to the Australian wheatbelt—spatial and temporal trends. *New Phytol.* 198, 801–820. doi: 10.1111/nph.12192
- Chenu, K., Porter, J. R., Martre, P., Basso, B., Chapman, S. C., Ewert, F., et al. (2017). Contribution of crop models to adaptation in wheat. *Trends Plant Sci.* 22, 472–490. doi: 10.1016/j.tplants.2017.02.003
- Christopher, J. (2024). "Advances in phenotyping to identify drought-resistance traits in cereal roots, Ch 5," in *Developing drought resistant cereals*. Ed. R. Tuberosa (Burleigh Dodds, Cambridge, UK), 149–180.
- Christopher, J., MansChadi, A., Hammer, G., and Borrell, A. (2008). Developmental and physiological traits associated with high yield and stay-green phenotype in wheat. *Aust. J. Agric. Res.* 59, 354–364. doi: 10.1071/AR07193
- Christopher, J. T., Christopher, M. J., Borrell, A. K., Fletcher, S., and Chenu, K. (2016). Stay-green traits to improve wheat adaptation in well-watered and water-limited environments. *J. Exp. Bot.* 67, 5159–5172. doi: 10.1093/jxb/erw276
- Christopher, J. T., Veyradier, M., Borrell, A. K., Harvey, G., Fletcher, S., and Chenu, K. (2014). Phenotyping novel stay-green traits to capture genetic variation in senescence dynamics. *Funct. Plant Biol.* 41, 1035–1048. doi: 10.1071/FP14052
- Christopher, M., Paccapelo, V., Kelly, A., Macdonald, B., Hickey, L., Richard, C., et al. (2021). QTL identified for stay-green in a multi-reference nested association mapping population of wheat exhibit context dependent expression and parent-specific alleles. *Field Crops Res.* 270, 108181.
- Collins, B., Chapman, S., Hammer, G., and Chenu, K. (2021). Limiting transpiration rate in high evaporative demand conditions to improve Australian wheat productivity. *Silico. Plants* 3, diab006. doi: 10.1093/insilicoplants/diab006
- Collins, B., and Chenu, K. (2021). Improving productivity of Australian wheat by adapting sowing date and genotype phenology to future climate. *Climate Risk Manage.* 32, 100300. doi: 10.1016/j.crm.2021.100300

Acknowledgments

The authors are grateful for Renier Synman for technical help, and Bethany Rognoni and Michael Mumford for assistance in the statistical analysis.

Conflict of interest

The authors declare that the research was conducted in the absence of any commercial or financial relationships that could be construed as a potential conflict of interest.

Publisher's note

All claims expressed in this article are solely those of the authors and do not necessarily represent those of their affiliated organizations, or those of the publisher, the editors and the reviewers. Any product that may be evaluated in this article, or claim that may be made by its manufacturer, is not guaranteed or endorsed by the publisher.

Supplementary material

The Supplementary Material for this article can be found online at: <https://www.frontiersin.org/articles/10.3389/fpls.2024.1351436/full#supplementary-material>

- Crafts-Brandner, S. J., Below, F. E., Harper, J. E., and Hageman, R. H. (1984). Differential senescence of maize hybrids following ear removal: I. whole plant. *Plant Physiol.* 74, 360–367. doi: 10.1104/pp.74.2.360
- Dodd, I. C., Whalley, W. R., Ober, E. S., and Parry, M. A. J. (2011). Genetic and management approaches to boost UK wheat yields by ameliorating water deficits. *J. Exp. Bot.* 62, 5241–5248. doi: 10.1093/jxb/err242
- Ehdaie, B., Layne, A. P., and Waines, J. G. (2012). Root system plasticity to drought influences grain yield in bread wheat. *Euphytica* 186, 219–232. doi: 10.1007/s10681-011-0585-9
- Farooq, M., Wahid, A., Kobayashi, N., Fujita, D., and Basra, S. M. A. (2009). Plant drought stress: effects, mechanisms and management. *Sustain. Agric.* 29, 153–188. doi: 10.1051/agro:2008021
- Figuerola-Bustos, V., Palta, J. A., Chen, Y., Stefanova, K., and Siddique, K. H. M. (2020). Wheat cultivars with contrasting root system size responded differently to terminal drought. *Front. Plant Sci.* 11, 1285. doi: 10.3389/fpls.2020.01285
- Fletcher, A., Christopher, J., Hunter, M., Rebetzke, G., and Chenu, K. (2018). A low-cost method to rapidly and accurately screen for transpiration efficiency in wheat. *Plant Methods* 14, 77.
- Frensch, J. (1997). Primary responses of root and leaf elongation to water deficits in the atmosphere and soil solution. *J. Exp. Bot.* 48, 985–999. doi: 10.1093/jxb/48.5.985
- Gentinetta, E., Ceppl, D., Lepori, C., Perico, G., Motto, M., and Salamini, F. (1986). A major gene for delayed senescence in maize. Pattern of photosynthates accumulation and inheritance. *Plant Breed.* 97, 193–203. doi: 10.1111/j.1439-0523.1986.tb01053.x
- Gregory, P., McGowan, M., Biscoe, P., and Hunter, B. (1978). Water relations of winter wheat: I. Growth of the root system. *J. Agric. Sci.* 91, 91–102. doi: 10.1017/S0021859600056653
- Heinemann, H., Hirte, J., Seidel, F., and Don, A. (2023). Increasing root biomass derived carbon input to agricultural soils by genotype selection - a review. *Plant Soil* 490, 19–30. doi: 10.1007/s11104-023-06068-6
- Hodgkinson, L., Dodd, I. C., Binley, A., Ashton, R. W., White, R. P., Watts, C. W., et al. (2017). Root growth in field-grown winter wheat: Some effects of soil conditions, season and genotype. *Eur. J. Agronomy*. 91, 74–83. doi: 10.1016/j.eja.2017.09.014
- Kirkegaard, J. A., Lilley, J. M., Howe, G. N., and Graham, J. M. (2007). Impact of subsoil water use on wheat yield. *Aust. J. Agric. Res.* 58, 303–315. doi: 10.1071/AR06285
- Kumar, U., Joshi, A. K., Kumari, M., Paliwal, R., Kumar, S., and Röder, M. S. (2010). Identification of QTLs for stay green trait in wheat (*Triticum aestivum* L.) in the 'Chirya 3' × 'Sonalika' population. *Euphytica* 174, 437–445. doi: 10.1007/s10681-010-0155-6
- Lilley, J., and Kirkegaard, J. (2011). Benefits of increased soil exploration by wheat roots. *Field Crops Res.* 122, 118–130. doi: 10.1016/j.fcr.2011.03.010
- Lilley, J. M., and Kirkegaard, J. A. (2016). Farming system context drives the value of deep wheat roots in semi-arid environments. *J. Exp. Botany*. 67, 3665–3681. doi: 10.1093/jxb/erw093
- Lopes, M. S., and Reynolds, M. P. (2010). Partitioning of assimilates to deeper roots is associated with cooler canopies and increased yield under drought in wheat. *Funct. Plant Biol.* 37, 147–156. doi: 10.1071/FP09121
- Lopes, M. S., and Reynolds, M. P. (2011). Drought adaptive traits and wide adaptation in elite lines derived from resynthesized hexaploid wheat. *Crop Sci.* 51, 1617–1626. doi: 10.2135/cropsci2010.07.0445
- Lopes, M. S., and Reynolds, M. P. (2012). Stay-green in spring wheat can be determined by spectral reflectance measurements (normalized difference vegetation index) independently from phenology. *J. Exp. Bot.* 63, 3789–3798. doi: 10.1093/jxb/ers071
- López-Castañeda, C., and Richards, R. (1994). Variation in temperate cereals in rainfed environments I. Grain yield, biomass and agronomic characteristics. *Field Crops Res.* 37, 51–62. doi: 10.1016/0378-4290(94)90081-7
- Ludlow, M. M., and Muchow, R. C. (1990). A critical-evaluation of traits for improving crop yields in water-limited environments. *Adv. Agron.* 43, 107–153. doi: 10.1016/S0065-2113(08)60477-0
- Mace, E. S., Singh, V., Van Oosterom, E. J., Hammer, G. L., Hunt, C. H., and Jordan, D. R. (2012). QTL for nodal root angle in sorghum (*Sorghum bicolor* L. Moench) co-locate with QTL for traits associated with drought adaptation. *Theor. Appl. Genet.* 124, 97–109.
- Manschadi, A. M., Christopher, J., Devoil, P., and Hammer, G. L. (2006). The role of root architectural traits in adaptation of wheat to water-limited environments. *Funct. Plant Biol.* 33, 823–837. doi: 10.1071/FP06055
- Manschadi, A., Christopher, J., Hammer, G., and Devoil, P. (2010). Experimental and modelling studies of drought-adaptive root architectural traits in wheat (*Triticum aestivum* L.). *Plant Biosyst.* 144, 458–462. doi: 10.1080/11263501003731805
- Mathew, I., and Shimelis, H. (2022). Genetic analyses of root traits: Implications for environmental adaptation and new variety development: A review. *Plant Breed.* 141, 695–718. doi: 10.1111/pbr.13049
- Mondal, W., Dey, B., and Choudhuri, M. (1985). Proline accumulation as a reliable indicator of monocarpic senescence in rice cultivars. *Experientia* 41, 346–348. doi: 10.1007/BF02004497
- Munns, R. (2002). Comparative physiology of salt and water stress. *Plant. Cell Environ.* 25, 239–250. doi: 10.1046/j.0016-8025.2001.00808.x
- Nawaz, A., Farooq, M., Cheema, S. A., Yasmeen, A., and Wahid, A. (2013). Stay green character at grain filling ensures resistance against terminal drought in wheat. *Int. J. Agric. Biol.* 15, 1272–1276.
- Ober, E. S., Werner, P., Flatman, E., Angus, W. J., Jack, P., Smith-Reeve, L., et al. (2014). Genotypic differences in deep water extraction associated with drought tolerance in wheat. *Funct. Plant Biol.* 41, 1078–1086. doi: 10.1071/FP14094
- Palta, J. A., Chen, X., Milroy, S. P., Rebetzke, G. J., Dreccer, M. F., and Watt, M. (2011). Large root systems: are they useful in adapting wheat to dry environments? *Funct. Plant Biol.* 38, 347–354. doi: 10.1071/FP11031
- Rebetzke, G. J., Fischer, R. A., van Herwaarden, A. F., Bonnett, D. G., Chenu, K., Rattey, A. R., et al. (2014). Plot size matters: interference from intergenotypic competition in plant phenotyping studies. *Funct. Plant Biol.* 41, 107–118. doi: 10.1071/FP13177
- Richard, C. (2017). *Breeding wheat for drought adaptation: development of selection tools for root architectural traits* (Brisbane, Australia: University of Queensland), 136pp.
- Richard, C., Christopher, J., Chenu, K., Borrell, A., Christopher, M., and Hickey, L. (2018). Selection in early generations to shift allele frequency for seminal root angle in wheat. *Plant Genome* 11, 170071. doi: 10.3835/plantgenome2017.08.0071
- Richard, C. A. I., Hickey, L. T., Fletcher, S., Jennings, R., Chenu, K., and Christopher, J. T. (2015). High-throughput phenotyping of seminal root traits in wheat. *Plant Methods* 11, 1–11. doi: 10.1186/s13007-015-0055-9
- Richter, G., and Semenov, M. (2005). Modelling impacts of climate change on wheat yields in England and Wales: assessing drought risks. *Agric. Syst.* 84, 77–97. doi: 10.1016/j.agry.2004.06.011
- Robinson, H., Kelly, A., Fox, G., Franckowiak, J., Borrell, A., and Hickey, L. (2018). Root architectural traits and yield: exploring the relationship in barley breeding trials. *Euphytica* 214, 151. doi: 10.1007/s10681-018-2219-y
- Shavruk, Y., Kurishbayev, A., Jatayev, S., Shvidchenko, V., Zotova, L., Koekemoer, F., et al. (2017). Early flowering as a drought escape mechanism in plants: how can it aid wheat production? *Front. Plant Sci.* 8, 1950. doi: 10.3389/fpls.2017.01950
- Singh, V., van Oosterom, E. J., Jordan, D. R., Hunt, C. H., and Hammer, G. L. (2011). Genetic variability and control of nodal root angle in sorghum. *Crop Sci.* 51, 2011–2020. doi: 10.2135/cropsci2011.01.0038
- Spano, G., Di Fonzo, N., Perrotta, C., Platani, C., Ronga, G., Lawlor, D., et al. (2003). Physiological characterization of 'stay green' mutants in durum wheat. *J. Exp. Bot.* 54, 1415–1420. doi: 10.1093/jxb/erg150
- Team, R. C. (2019). *R: A language and environment for statistical computing* (Version 3.5 (Vienna, Austria: 2, R Foundation for Statistical Computing). 2018
- Thomas, H., and Smart, C. M. (1993). Crops that stay green 1. *Ann. Appl. Biol.* 123, 193–219. doi: 10.1111/j.1744-7348.1993.tb04086.x
- Vadez, V., Grondin, A., Chenu, K., Henry, A., Laplace, L., Millet, E. J., et al. (2024). Context-dependent water-related traits determine crop production under drought. *Nat. Rev. Earth Environ.* 5, 211–225.
- Veyradier, M., Christopher, J. T., and Chenu, K. (2013). *Quantifying the potential yield benefit of root traits in a target population of environments* (Helsinki, Finland: Finnish Society of Forest Science, Vantaa, Finland Finnish Forest Research Institute, Vantaa, Finland Department of Forest Sciences, University of Helsinki). 9–14.
- Wada, Y., and Wada, G. (1991). Varietal difference in leaf senescence during ripening period of advanced indica rice. *Japanese. J. Crop Sci.* 60, 529–536. doi: 10.1626/jcs.60.529
- Wasson, A., Bischof, L., Zwart, A., and Watt, M. (2016). A portable fluorescence spectroscopy imaging system for automated root phenotyping in soil cores in the field. *J. Exp. Botany*. 67, 1033–1043. doi: 10.1093/jxb/erv570
- White, R. G., and Kirkegaard, J. A. (2010). The distribution and abundance of wheat roots in a dense, structured subsoil - implications for water uptake. *Plant. Cell Environment*. 33, 133–148. doi: 10.1111/j.1365-3040.2009.02059.x
- Yang, J., C., Zhang, J. H., Wang, Z. Q., Zhu, Q. S., and Liu, L. J. (2001). Water deficit-induced senescence and its relationship to the remobilization of pre-stored carbon in wheat during grain filling. *Agron. J.* 93, 196–206. doi: 10.2134/agronj2001.931196x
- Zadoks, J. C., Chang, T. T., and Konzak, C. F. (1974). A decimal code for the growth stages of cereals. *Weed. Res.* 14, 415–421. doi: 10.1111/j.1365-3180.1974.tb01084.x
- Zhao, D., Eyre, J. X., Wilkus, E., de Voil, P., Broad, I., and Rodriguez, D. (2022). 3D characterization of crop water use and the rooting system in field agronomic research. *Comput. Electron. Agricult.* 202, 107409. doi: 10.1016/j.compag.2022.107409
- Zhao, D., deVoil, P., Rognoni, B. G., Wilkus, E., Eyre, J. X., and Broad I and Rodriguez, D. (2024). Sowing summer grain crops early in late winter or spring: effects on root growth, water use, and yield. *Plant Soil*. doi: 10.1007/s11104-024-06648-0
- Zhao, D., de Voil, P., Sadras, V., Palta, J., and Rodriguez, D. (2023). Root phenotypic plasticity: agronomic, breeding and modelling implications. *Res. Square*. doi: 10.21203/rs.3.rs-4120028/v1
- Zheng, X., Chen, B., Lu, G., and Han, B. (2009). Overexpression of a NAC transcription factor enhances rice drought and salt tolerance. *Biochem. Biophys. Res. Commun.* 379, 985–989. doi: 10.1016/j.bbrc.2008.12.163



OPEN ACCESS

EDITED BY

Iker Aranjuelo,
Spanish National Research Council
(CSIC), Spain

REVIEWED BY

Santiago Alvarez Prado,
National Scientific and Technical Research
Council (CONICET), Argentina
Raffaella Battaglia,
Council for Agricultural and Economics
Research (CREA), Italy
Luis Morales-Quintana,
Autonomous University of Chile, Chile
Jan Hejatkó,
Central European Institute of Technology
(CEITEC), Czechia

*CORRESPONDENCE

Daniel F. Calderini
✉ danielcalderini@uach.cl

RECEIVED 01 February 2024

ACCEPTED 20 May 2024

PUBLISHED 11 June 2024

CITATION

Vicentin L, Canales J and Calderini DF (2024)
The trade-off between grain weight and grain
number in wheat is explained by the
overlapping of the key phases determining
these major yield components.
Front. Plant Sci. 15:1380429.
doi: 10.3389/fpls.2024.1380429

COPYRIGHT

© 2024 Vicentin, Canales and Calderini. This is
an open-access article distributed under the
terms of the [Creative Commons Attribution
License \(CC BY\)](#). The use, distribution or
reproduction in other forums is permitted,
provided the original author(s) and the
copyright owner(s) are credited and that the
original publication in this journal is cited, in
accordance with accepted academic
practice. No use, distribution or reproduction
is permitted which does not comply with
these terms.

The trade-off between grain weight and grain number in wheat is explained by the overlapping of the key phases determining these major yield components

Lucas Vicentin^{1,2}, Javier Canales^{3,4} and Daniel F. Calderini^{2*}

¹Graduate School, Faculty of Agricultural Science, Universidad Austral de Chile, Valdivia, Chile,

²Institute of Plant Production and Protection, Universidad Austral de Chile, Valdivia, Chile, ³Institute of Biochemistry and Microbiology, Universidad Austral de Chile, Valdivia, Chile, ⁴National Agency for Research and Development of Chile-Millennium Science Initiative Program-Millennium Institute for Integrative Biology (iBio), Santiago, Chile

Enhancing grain yield is a primary goal in the cultivation of major staple crops, including wheat. Recent research has focused on identifying the physiological and molecular factors that influence grain weight, a critical determinant of crop yield. However, a bottleneck has arisen due to the trade-off between grain weight and grain number, whose underlying causes remain elusive. In a novel approach, a wheat expansin gene, *TaExpA6*, known for its expression in root tissues, was engineered to express in the grains of the spring wheat cultivar Fielder. This modification led to increases in both grain weight and yield without adversely affecting grain number. Conversely, a triple mutant line targeting the gene *TaGW2*, a known negative regulator of grain weight, resulted in increased grain weight but decreased grain number, potentially offsetting yield gains. This study aimed to evaluate the two aforementioned modified wheat genotypes (*TaExpA6* and *TaGW2*) alongside their respective wild-type counterparts. Conducted in southern Chile, the study employed a Complete Randomized Block Design with four replications, under well-managed field conditions. The primary metrics assessed were grain yield, grain number, and average grain weight per spike, along with detailed measurements of grain weight and dimensions across the spike, ovary weight at pollination (Waddington's scale 10), and post-anthesis expression levels of *TaExpA6* and *TaGW2*. Results indicated that both the *TaExpA6* and the triple mutant lines achieved significantly higher average grain weights compared to their respective wild types. Notably, the *TaExpA6* line did not exhibit a reduction in grain number, thereby enhancing grain yield per spike. By contrast, the triple mutant line showed a reduced grain number per spike, with no significant change in overall yield. *TaExpA6* expression peaked at 10 days after anthesis (DAA), and its effect on grain weight over the WT became apparent after 15 DAA. In contrast, *TaGW2* gene disruption in the triple mutant line increased ovary size at anthesis, leading to improved grain weight above the WT from the onset of grain filling. These findings suggest that the trade-off between grain weight and number could be attributed to the overlapping of the critical periods for the determination of these traits.

KEYWORDS

TaExpA6, *TaGW2*, source-sink, expansins, ovary weight, grain size regulation, grain yield, cereals

1 Introduction

Advancements in the understanding of physiological and molecular control of grain weight and size in wheat and other staple food crops have been significant over the past decade (Brinton and Uauy, 2019; Slafer et al., 2023). This progress has been driven by rapid molecular developments, leading to the identification of key genes, and Quantitative Trait Loci (QTL) linked to grain weight and size in various crops (barley: Yang et al., 2023; rapeseed: Canales et al., 2021; rice: Zuo and Li, 2014; sorghum: Tao et al., 2021; sunflower: Castillo et al., 2018; wheat: Simmonds et al., 2014; Kumar et al., 2016; Simmonds et al., 2016; Adamski et al., 2021; Khan et al., 2022; Tillett et al., 2022; Mira et al., 2023). These studies assume that grain weight, which is a key yield component, could lead to the yield increase required to meet the challenge of food security. However, the relationship between increased grain weight and overall yield improvement is complex due to the reported trade-off between grain weight and grain number in wheat and other crops. In wheat, grain weight improvement has been addressed through various strategies, from classical breeding focusing on increasing grain weight through recurrent selection (Wiersma et al., 2001), to molecular breeding techniques such as mutating the wheat orthologue of rice *Grain Weight 2* gene (*TaGW2*), a known negative regulator of grain size and weight (Song et al., 2007; Yang et al., 2012; Hong et al., 2014; Wang et al., 2018; Zhang et al., 2018). Additional methods include gene introgression, like *TaGSNE* (Khan et al., 2022), and overexpression of genes such as *TaBG1* and *TaCYP78A5* (Milner et al., 2021; Guo et al., 2022). Although most of these attempts successfully increased grain weight of wheat, they failed to improve grain yield due to the trade-off between grain weight and number (Wiersma et al., 2001; Okamoto and Takumi, 2013; Brinton et al., 2017; Milner et al., 2021; Mora-Ramirez et al., 2021).

The causes of the trade-off between grain weight and number are not fully understood, despite extensive research (Wiersma et al., 2001; Sadras, 2007; Dwivedi et al., 2021; Fischer, 2022; Slafer et al., 2023). Initial hypotheses and few subsequent studies suggested that growing grains of wheat are limited by the source of assimilates during grain filling (Sinclair and Jamieson, 2006; Golan et al., 2019; Rosati and Benincasa, 2023). However, most of the research has demonstrated that wheat grains are not, or scarcely, limited by assimilate supply during post-anthesis (Slafer and Savin, 1994; Borrás et al., 2004; Fischer, 2008; Serrago et al., 2013; Slafer et al., 2021; Murchie et al., 2023), except under extreme source restriction in high-yielding environments (Beed et al., 2007; Sandaña et al., 2009; Alonso et al., 2018). An alternative explanation involves the increased proportion of smaller distal grains when grain number is increased through breeding or crop management, since distal grains are intrinsically smaller than proximal ones (Acreche and Slafer, 2006; Ferrante et al., 2015, 2017). However, this does not account for situations where grain weight improvements lead to an actual trade-off with grain number (e.g., Wiersma et al., 2001; Brinton et al., 2017; Wang et al., 2018). Notably, interventions that successfully increased grain weight in both proximal and distal grain positions within the spike often resulted in a reduced grain number per spike and area (Wiersma et al., 2001; Okamoto and

Takumi, 2013; Brinton et al., 2017; Quintero et al., 2018; Wang et al., 2018; Zhai et al., 2018; Adamski et al., 2021; Milner et al., 2021), confirming a genuine trade-off between yield components. Furthermore, recent genomic studies indicate that many regions associated with grain number and grain weight coincide and have inverse phenotypic effects, suggesting a strong genetic basis for this trade-off (Xie and Sparkes, 2021).

Trade-offs between grain number subcomponents have been documented in wheat. For instance, a higher plant number correlates with a lower number of spikes per plant (Slafer et al., 2021). It is generally accepted these trade-offs are due to the feedback between grain number components, whose settings overlap during the crop cycle (Slafer et al., 2021). For a long time, this explanation left aside the trade-off between grain weight and grain number, as these yield components were thought to have minimal overlap. From this perspective, the critical period for grain number determination accounts for 20 days before and 10 days after anthesis (DAA) (Fischer, 1985; Savin and Slafer, 1991; Abbate et al., 1997), whereas grain weight determination occurs during the grain filling period. However, several evidence now suggest that potential grain weight is established between booting and early grain filling in wheat (Calderini et al., 1999; Calderini and Reynolds, 2000; Ugarte et al., 2007; Hasan et al., 2011; Simmonds et al., 2016; Parent et al., 2017). This process is strongly influenced by maternal tissues, which impose a physical upper limit on grain weight in wheat (Millet and Pinthus, 1980; Calderini and Reynolds, 2000; Xie et al., 2015; Yu et al., 2015; Brinton et al., 2017; Reale et al., 2017; Brinton and Uauy, 2019; Calderini et al., 2021), a phenomenon also observed under increased temperature conditions (Calderini et al., 1999; Ugarte et al., 2007; Kino et al., 2020). The relevance of maternal tissues in determining grain size is also evident in other grain crops, for instance barley (Scott et al., 1983; Ugarte et al., 2007; Radchuk et al., 2011), sorghum (Yang et al., 2009) and sunflower (Lindström et al., 2006, 2007; Rondanini et al., 2009; Castillo et al., 2017). Additionally, the relationship between fruit size and flower ovary size has been reported in berries and fruit trees (Kiwifruit: Lai et al., 1990; Cruz-Castillo, 1992; olive: Rosati et al., 2009; peach: Scorzal et al., 1991; strawberry: Handley and Dill, 2003).

In wheat, various molecular strategies have been explored to increase grain weight. However, only a few have been successful in improving this trait (e.g. Hong et al., 2014; Simmonds et al., 2016; Brinton et al., 2017; Wang et al., 2018; Adamski et al., 2021; Jablonski et al., 2021; Milner et al., 2021; Mora-Ramirez et al., 2021), and even fewer have managed to increase grain weight without a trade-off with grain number (Calderini et al., 2021; Guo et al., 2022). Remarkably, one such improvement was achieved under field conditions at farmer's plant density rate, where grain weight increased by 12.3% and grain yield by 11.3%, without affecting grain number (Calderini et al., 2021). Against this background, the present study aims to deepen the understanding of the trade-off between grain weight and grain number in wheat by evaluating lines with and without this trade-off. For this assessment, wheat lines previously tested under agronomic conditions were selected. We included the triple mutant line for the *TaGW2* gene (Wang et al., 2018), which releases grain growth by breaking the negative control of *TaGW2* over grain weight but demonstrates a

trade-off with grain number. This gene codes for a RING-type E3 ligase, which mediates proteolysis through the ubiquitin-proteasome pathway (Song et al., 2007). In contrast, the selected genotype without a trade-off is a line with ectopic expression of the α -expansin gene *TaExpA6*, which is naturally expressed in wheat roots but was cloned with a promoter for expression in growing grains (Calderini et al., 2021). Expansins are small proteins crucial for plant cell growth, facilitating cell wall stress relaxation induced by turgor pressure (McQueen-Mason et al., 1992; Cosgrove, 2021; 2023). The expression of different expansins during wheat grain growth has been documented in wheat (Lin et al., 2005; Lizana et al., 2010; Kino et al., 2020; Xie and Sparkes, 2021; Mira et al., 2023). Both the triple mutant and transgenic lines were evaluated alongside their respective wild types (WT).

The ectopic expression of *TaExpA6* and its protein in growing grains of wheat was evident from 10 DAA on (Calderini et al., 2021). This led the authors to propose that the trade-off between grain weight and grain number is potentially associated with the overlapping of the critical window for these two traits determinations. Our study aims to elucidate this trade-off by evaluating two genetically distinct wheat genotypes, known for increased grain weight but differing in the trade-off between both major yield components. These genotypes, along with their respective wild types, were examined under field conditions. By dissecting grain yield components, along with physiological and molecular characteristics at the spike level, the study seeks to minimize confounding variables and clarify the underlying mechanisms of the observed trade-off.

2 Materials and methods

2.1 Field conditions and experimental setup

Two field experiments were conducted on a Typic Hapludand soil at the Universidad Austral de Chile's Experimental Station (EEAA) in Valdivia (39°47'S, 73°14'W). The first experiment spanned the 2021–2022 growing season (referred to as Exp. 1), while the second was conducted in the 2022–2023 season (Exp. 2). To fulfil the proposed objective, four spring wheat cultivars were selected for both experiments: (i) *TaExpA6*, a transgenic line expressing the expansin gene *TaExpA6* ectopically in grains, as described by Calderini et al. (2021); (ii) its segregant wild type cv. Fielder; (iii) *TaGW2*, a triple knock-out mutant of *TaGW2* gene (referred to as “aabbdd” in Wang et al., 2018); and (iv) its segregant wild type cv. Paragon. These genotypes were chosen due to their contrasting effects on the trade-off between grain weight (GW) and grain number (GN). Specifically, while line *TaGW2* exhibits reduced GN, line *TaExpA6* improves GW without impacting GN.

The *TaExpA6* line features overexpression of *TaExpA6* (REFSEQ v.1.1: *TraesCS4A02G034200*) in the endosperm, aleurone, and pericarp tissues of developing grains. This overexpression is controlled by the wheat *puroindoline-b* (*PinB*) gene promoter (REFSEQ v.1.1: *TraesCS7B02G431200*), as detailed by Gautier et al. (1994) and Digeon et al. (1999). The *TaExpA6* line and its segregant WT were developed by Dr. Emma Wallington

from the National Institute of Agricultural Botany (NIAB), UK (Calderini et al., 2021). In contrast, the *TaGW2* gene in line *TaGW2* harbors mutations leading to a truncated, non-functional protein, as reported by Simmonds et al. (2016) and Wang et al. (2018). An in depth description of the mutated alleles can be found in Wang et al. (2018). These *GW2* lines were generously provided by Prof. Cristóbal Uauy from John Innes Center, UK.

Exp. 1 was sown on September 21, 2021. Due to phenological differences observed between both groups of lines in Exp. 1, sowing dates in Exp. 2 were modified. Thus, *GW2* lines, with longer crop cycles, were sown earlier on August 20, 2022, while the shorter-cycle *ExpA6* lines were sown later on September 2, 2022. Both experiments followed a randomized complete block design with four replications. Each plot measured 2 m in length and 1.2 m in width, consisting of 9 rows with 0.15 m spacing, and was sown at a density of 300 plants per square meter.

Optimal agronomic management was employed for all plots to prevent biotic and abiotic stress. Fertilization at sowing included 150 kg N ha⁻¹, 150 kg P₂O₅ ha⁻¹, and 100 kg K₂O ha⁻¹. An additional 150 kg N ha⁻¹ was applied at tillering. To address potential aluminum toxicity brought about by low soil pH, the experimental site was treated with 4 Tn ha⁻¹ of CaCO₃ one month prior to sowing. Pests and diseases were managed using chemical treatments as per manufacturer recommendations. Drip irrigation supplemented rainfall to avoid water stress throughout the crop cycle.

Meteorological data, including air temperature and incident photosynthetically active radiation (PAR), were recorded daily from sowing until harvest at the Austral Meteorological Station of EEAA (<http://agromet.inia.cl/>), located approximately 150 m from the experimental plots. Photothermal quotient was calculated as the ratio of mean daily incident radiation to mean temperature above 4.5°C, in line with Fischer (1985).

2.2 Crop sampling and measurements

Crop phenology was recorded twice weekly according to the decimal code scale (Zadoks et al., 1974). At harvest, 45 spikes of main stems were sampled along 1m from the central row of each plot in both experiments. Grain yield per spike, grain number per spike and average grain weight were measured or calculated as previously (Bustos et al., 2013; Quintero et al., 2018). In addition, 10 more main shoot spikes of similar development and size were sampled from each plot to quantify grain weight and dimensions (length and width) at each grain position from every spikelet of the spike. From each spike, half the spikelets (i.e. all the spikelets along one longitudinal side of the spike) were measured, considering the spike symmetry. Grains from positions G1 to G4 (G1 being the closest grain to the rachis and G4 the most distal, if present) within each spikelet were taken out, oven dried (48 h at 65°C) and weighted separately using an electronic balance (Mettler Toledo, XP205DR, Greifensee, Switzerland). The length and width of each grain was recorded using a Marvin Seed Analyzer (Marvitech GmbH, Wittenburg, Germany). Grain number per spike and per spikelet were also recorded.

In Exp. 2, the weight of ovaries from florets at positions G1 to G4 was measured at pollination (stage 10 in Waddington et al., 1983) by sampling 20 ovaries of each floret position from the four central spikelets of five spikes per plot. In this experiment the time-course of grain weight and dimensions were also measured. From anthesis onwards, four main shoot spikes were sampled from each experimental unit twice weekly until physiological maturity to record grain fresh and dry weight and dimensions (i.e. length and width) of six individual grains corresponding to a proximal (G2) and a distal (G3) grain position of two central spikelets. The fresh weight and the length and width of grains were recorded immediately after sampling as described above. Dry weight of grains was measured with the same electronic balance, after drying the samples at 65°C in an oven for 48 h.

In both experiments, grain quality was assessed by measuring grain protein concentration to determine the impact of GW changes on this quality trait. Accordingly, grains from positions G1 to G3 within the four central spikelets of the 10 main shoot spikes samples were bulked at each experimental unit and then milled using a Perten 120 laboratory mill (Huddinge, Sweden). The quantification of total nitrogen was executed using the Kjeldahl method. Protein content was then calculated by multiplying the total nitrogen value by a factor of 5.7, in accordance with the approach of Merrill and Watt (1973) as applied in Lizana and Calderini (2013).

2.3 Time-course expression analyses by reverse transcription quantitative PCR

To elucidate the relationship between grain growth dynamics and gene expression, we conducted time-course expression analyses of *PinB::TaExpA6* in the *ExpA6* lines and *TaGW2* in the *GW2* lines. These analyses were performed using reverse transcription quantitative PCR (RT-qPCR) on grains at positions G1 and G2. Specifically, G1 and G2 grains from central spikelets on the main stem spikes were collected from a minimum of eight spikes at 4, 7, 10, 14, and 21 days after anthesis (DAA) for each experimental plot.

Immediately following collection, samples were secured in cryotubes, snap-frozen in liquid nitrogen, and subsequently preserved at -80°C until further processing. Total RNA was isolated using NucleoSpinTM columns (Macherey-Nagel), employing a standardized protocol adapted from Sangha et al. (2010). RNA samples were then subjected to DNaseI (Invitrogen) treatment, and cDNA synthesis was performed using the ImProm-IITM Reverse Transcription System with an input of 500 ng RNA per reaction.

Quantitative PCR (qPCR) was carried out in a 25 µL reaction volume using the Brilliant II SYBR Green PCR Master Mix (Stratagene, Agilent technologies). Primer concentrations were set at 0.2 µM. For *TaExpA6*, the primers Transgene*TaExpA6_F1* (5'-ATCTCCACCACCACCAAAACA-3') and Transgene*TaExpA6_R1* (5'-GAAGCAGAACGCGAGAACGG-3') were used. In the case of *TaGW2*, genome-specific primers for its homoeologues, as described by Wang et al. (2018), were utilized. Controls without

template and transcriptase were included to check for genomic DNA contamination.

The relative mRNA abundance of the target genes in grain tissues was determined using the comparative CT ($\Delta\Delta CT$) method, as proposed by Pfaffl (2001). The ubiquitin conjugating enzyme (*Traes_4AL_8CEA69D2E.1*) served as the internal reference gene, amplified with primers *Traes_4AL_8CE_esF* (5'-CGGGCCCGAAGAGAGTCT-3') and *Traes_4AL_8CE_esR* (5'-ATTAACGAAACCAATCGACGGA-3'). Data analysis for gene expression quantification was conducted using LinRegPCR software (Ruijter et al., 2009).

2.4 Statistical analysis

Analysis of variance (ANOVA) was applied to evaluate the effect of genotype on main shoot grain yield and associated traits, by using Statgraphics Centurion 18 software. Fisher's least significant difference test *post hoc* and/or Student's t-test were employed to identify each significant difference within the evaluated group of lines. Additionally, a Two-way ANOVA analysis was performed to assess significant differences in *TaExpA6* gene expression between line *TaExpA6* and its respective WT, whereas one-way ANOVA analysis was performed to assess significant differences in *TaGW2* gene expression in the WT across sampling times using GraphPad Prism 8 software. Linear regression analysis was performed to assess the associations between measured grain traits. A tri-linear model was fitted to estimate the rate and duration of the lag and linear phases of grain filling, and final grain weight in the individual seed weight dynamics.

Extra sum of squares F test was used for the comparison of the slopes and timings between each modified line and its respective WT. To model the dynamics of individual grain water content during the grain filling period, a second order polynomial model was employed. All model fittings were performed using GraphPad Prism 8 software.

3 Results

3.1 Environmental conditions and crop phenology across seasons

Environmental conditions from seedling emergence to physiological maturity were consistent between experiments (Table 1). Temperature variations between Exps. 1 and 2 were minimal, with differences of less than 1°C observed during the emergence-anthesis and grain filling periods. Incident PAR differed between the experiments, being 2.3 MJ m⁻² d⁻¹ higher in Exp. 1 than in Exp. 2 during the Emergence-Bootling (Em-Bo) and grain filling phases (10.4 vs. 8.1 MJ m⁻² d⁻¹ and 12.8 vs. 10.5 MJ m⁻² d⁻¹, respectively). However, no significant difference in PAR was noted during the Bootling-Anthesis (Bo-An) period. Despite these variations, the photothermal quotient (Q) remained constant at 2.5 MJ m⁻² d⁻¹ °C⁻¹ across the entire crop cycle in both seasons. A

TABLE 1 Average mean temperature, incident photosynthetically active radiation (PAR), photothermal quotient (Q) and photoperiod during the Emergence-Booting (Em-Bo), Booting-Anthesis (Bo-An) and Anthesis-Physiological Maturity (An-PM) periods in experiments 1 and 2.

Experiment	Line*	Mean temperatures (°C)			Incident PAR (MJ m ⁻² d ⁻¹)			Q (MJ m ⁻² d ⁻¹ °C ⁻¹)**			Photoperiod (h)
		Em - Bo	Bo - An	An - PM	Em - Bo	Bo - An	An - PM	Em - Bo	Bo - An	An - PM	Em - An
Exp.1 (2021–2022)	<i>TaExpA6</i> / WT _{<i>TaExpA6</i>}	12.3	14.2	17.2	10.3	12.3	12.8	2.9	2.6	2.1	14.6
	<i>TaGW2</i> / WT _{<i>TaGW2</i>}	12.9	16.4	16.7	10.6	12.2	12.8	2.8	2.2	2.2	14.8
Exp. 2 (2022–2023)	<i>TaExpA6</i> / WT _{<i>TaExpA6</i>}	11.2	14.5	16.1	7.9	12.1	10.8	3.2	2.4	1.9	14.1
	<i>TaGW2</i> / WT _{<i>TaGW2</i>}	11.3	15.4	16.3	8.2	13.2	10.3	3.1	2.5	1.8	14.1

*Since no phenological difference was recorded between modified lines and their respective WT, values were calculated for the mean duration of each phenological period for the *ExpA6* and *GW2* line groups. **Photothermal quotient was calculated as the ratio of mean daily incident radiation to mean temperature above 4.5°C.

comparative analysis of the *ExpA6* and *GW2* genotype lines revealed similar weather exposure in both experiments, except for the Bo-An period in Exp. 1, where *GW2* lines experienced a mean temperature 2.2°C higher than *ExpA6* lines, leading to a 17% lower photothermal quotient for *GW2* lines during this phase.

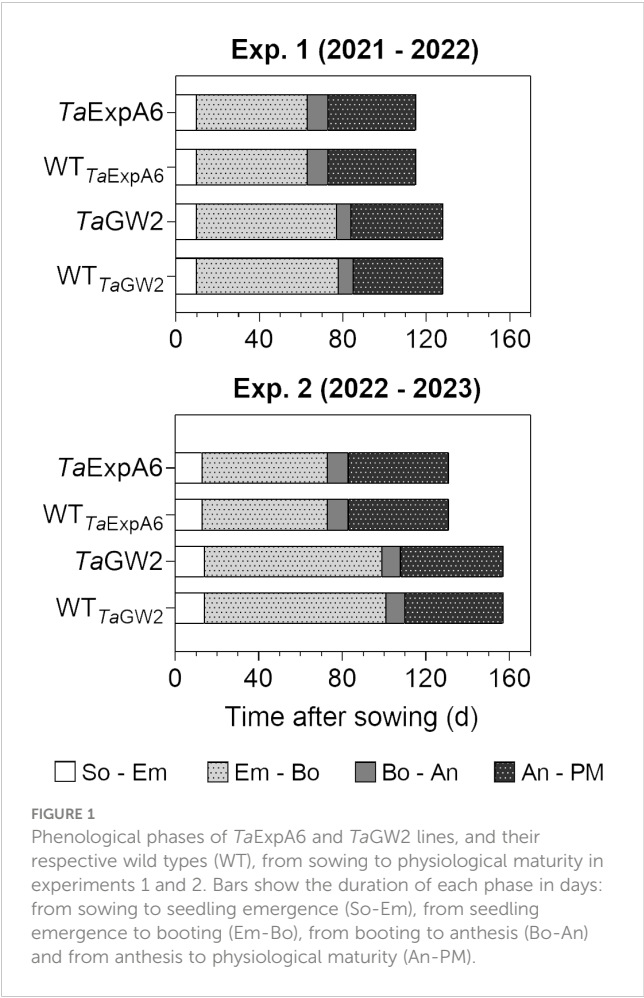
The length of the crop cycle averaged 123 days for *ExpA6* lines and 142 days for *GW2* lines across experiments (Figure 1). In experiments 1 and 2, *GW2* lines reached physiological maturity 13 and 26 days later, respectively, than *ExpA6* lines. This delay is primarily attributed to the longer Emergence-Booting (Em-Bo) period in *GW2* lines, as they exhibited a slower development rate. Post-booting, the differences in phenological stages, specifically Booting-Anthesis (Bo-An) and Anthesis-Physiological Maturity (An-PM), were negligible (i.e. less than 2 days) between the line groups. Despite minor climatic differences, the crop cycle in Exp. 2 extended by 16 and 27 days for *ExpA6* and *GW2* lines, respectively, compared to Exp. 1. This extension corresponds to an accumulated difference of 84 and 180°Cd for each line group (Supplementary Figure S1). The extended crop cycle in *GW2* lines, particularly in Exp. 2, is likely due to their heightened sensitivity to photoperiod compared to *ExpA6* lines (see photoperiods in Table 1).

3.2 Grain yield per spike, yield components per spike and quality trait

Differences in grain yield per spike were observed between line groups ($P < 0.05$), with *GW2* lines exhibiting higher yields compared to *ExpA6* lines in both experimental seasons, averaging 2.39 g and 1.94 g, respectively (Table 2). Notably, the ectopic expression of *TaExpA6* gene resulted in a significant increase in spike yield compared to the wild type (WT), showing increments of 14.0% and 8.2% in Exps. 1 and 2, respectively ($P < 0.05$). In contrast, the triple mutant of *TaGW2* and its WT displayed similar spike yields in both experiments ($P < 0.05$) (Table 2).

Regarding grain yield components, genotype significantly influenced these traits, contingent on the line group ($P < 0.05$). Average grain weight (TGW) was similar between both groups in Exp. 1 ($P > 0.05$) but was marginally higher in the *GW2* lines (6.6% increase, $P < 0.01$) in Exp. 2, with weights of 51.2 g and 48.1 g for *GW2* and *ExpA6* line groups, respectively (Table 2). Both *TaExpA6* and *TaGW2* lines surpassed the grain weight of their respective WTs in both experiments ($P < 0.001$). Averaging across Exps. 1 and 2, *TaExpA6* and *TaGW2* lines exhibited increases in TGW of 8.6% and 23.7% above their WTs, respectively (Table 2). Conversely, contrasting results were found for the grain number per spike; the *TaExpA6* line maintained a similar number to its WT ($P > 0.05$), whereas the *TaGW2* line exhibited a reduction in grain number compared to its WT in both experiments, with declines of 13.5% and 9.1% in Exps. 1 and 2, respectively (Table 2; Supplementary Figure S2). These findings align with previous reports indicating no trade-off in the *TaExpA6* overexpressed line and a detrimental effect of the *TaGW2* loss-of-function triple mutant on grain number.

In addition, we assessed a critical wheat quality trait, such as grain protein concentration. For this analysis, grains from G1 to G3 positions of the four central spikelets were pooled from each experimental unit. The results indicated no significant impact of transgenesis or tilling on grain protein concentration ($P > 0.05$), although an interaction ($P < 0.05$) between these factors was observed (Table 2). Grains from plants with the *TaExpA6* gene exhibited similar protein concentrations to the WT, highlighting the relevance of the *TaExpA6* construct. Conversely, the *TaGW2* triple mutant either increased (by 1.1 percentage points) or did not affect grain protein concentration in Experiments 1 and 2, respectively. Furthermore, no correlation ($R^2 = 0.05$; $P > 0.05$) was observed between grain protein concentration and grain yield per spike across genotypes and experiments, suggesting that the *TaGW2* triple mutation improved this quality trait independently from a dilution-concentration effect.



3.3 Individual grain weight and dimensions along the spike

To have a deeper understanding of the impact of *TaExpA6* overexpression and the *TaGW2* triple mutation, we dissected the spike evaluating grain weight, number and dimensions at each grain position along the spike (usually referred to as spike map) in both experiments. Our analysis revealed that across spikelets and grain positions, *TaExpA6* overexpression resulted in increases in grain weight compared to its wild type (WT) in both experiments. Specifically, grain weight enhancement in the *TaExpA6* line was observed as follows: in Exp.1, grains at positions G1, G2, G3, and G4 showed increases of 9%, 8%, 11%, and 25%, respectively, and in Exp. 2, increases of 9%, 6%, 10%, and 10% for G1, G2, G3, and G4, respectively (see [Figure 2](#)). In comparison, the *TaGW2* triple mutant exhibited a more pronounced increase in grain weight above the WT across all grain positions in both experiments: in Exp. 1, increases of 19%, 21%, 30%, and 37% for G1, G2, G3, and G4, respectively, and in Exp. 2, increases of 23%, 23%, 18%, and 19% for the same positions ([Figure 2](#)). On the other hand, when averaging across experiments, the ExpA6 lines showed similar grain number per spikelet across the spike (i.e. -1%), while the triple mutation of *TaGW2* gene caused a reduction of 11% in this trait in regard to its WT ([Supplementary Figure S2](#)).

Subsequent analysis focused on the relationship between grain dimensions and final grain weight. A strong association ($P < 0.001$) was observed between grain weight and both grain length and width, with determination coefficients ranging from 0.92 to 0.96 ([Figure 3](#)). This relationship was consistent within each genotype group ([Supplementary Figure S3](#)).

TABLE 2 Grain yield per spike (GY Spike⁻¹), grain number per spike (GN Spike⁻¹), average grain weight (TGW) and protein concentration (%) of grains recorded in *TaExpA6* and *TaGW2* lines and their WTs in the field experiments 1 and 2.

Experiment	Genotype (G)	Transgenesis or Tilling (T)	Main Stem Spike							
			GY Spike ⁻¹ (g)		GN Spike ⁻¹		TGW (g)		Protein (%)	
			Mean	s.e.m	Mean	s.e.m	Mean	s.e.m	Mean	s.e.m
Exp. 1	ExpA6 lines	<i>TaExpA6</i>	2.12 a	0.06	42.4 a	1.0	50.0 a	1.1	11.1 a	0.3
		WT _{<i>TaExpA6</i>}	1.86 b	0.03	40.4 a	0.3	46.0 b	1.0	10.9 a	0.5
	GW2 lines	<i>TaGW2</i>	2.33 a	0.10	43.6 b	1.6	53.4 a	1.0	11.5 a	0.3
		WT _{<i>TaGW2</i>}	2.18 a	0.10	50.4 a	1.5	43.3 b	0.8	10.4 b	0.2
	ANOVA p-value (G)		*		**		ns		ns	
	ANOVA p-value (T)		*		ns		**		ns	
	ANOVA p-value (G*T)		ns		*		**		ns	
	<i>t</i> -test p-value (<i>TaExpA6</i>)		**		ns		*		ns	
	<i>t</i> -test p-value (<i>TaGW2</i>)		ns		*		**		*	
Exp. 2	ExpA6 lines	<i>TaExpA6</i>	1.97 a	0.03	39.4 a	0.4	50.0 a	0.5	10.6 a	0.1
		WT _{<i>TaExpA6</i>}	1.82 b	0.04	39.6 a	0.7	46.1 b	0.4	11.2 a	0.3
	GW2 lines	<i>TaGW2</i>	2.68 a	0.09	47.1 b	1.0	56.7 a	0.9	11.4 a	0.2

(Continued)

TABLE 2 Continued

Experiment	Genotype (G)	Transgenesis or Tilling (T)	Main Stem Spike							
			GY Spike ⁻¹ (g)		GN Spike ⁻¹		TGW (g)		Protein (%)	
			Mean	s.e.m	Mean	s.e.m	Mean	s.e.m	Mean	s.e.m
		WT _{TaGW2}	2.38 a	0.11	51.8 a	1.2	45.7 b	1.1	10.4 a	0.6
	ANOVA p-value (G)		**		**		**		ns	
	ANOVA p-value (T)		*		*		**		ns	
	ANOVA p-value (G*T)		ns		*		**		*	
	<i>t</i> -test p-value (<i>TaExpA6</i>)		*		ns		**		ns	
	<i>t</i> -test p-value (<i>TaGW2</i>)		ns		*		**		ns	

ANOVA P-value is shown in the table. All data are shown as mean and SEM. The phenotype data of each transformed/mutant line was compared with the respective WT using Student's *t*-test; different letters indicate significant effects: *, *P* < 0.05; **, *P* < 0.01; ns, not significant.

3.4 Ovary weight, grain weight dynamics and gene expression

In Exp. 2, we assessed ovary weight at pollination (stage 10 according to Waddington et al., 1983) in florets at positions F1, F2, F3 and F4 from the central spikelets of spikes in each evaluated line. A linear association between final grain weight and ovary weight was found across lines and grain positions (Figure 4). In agreement with this association, GW2 lines exhibited increased ovary weight compared to ExpA6 genotypes (Figures 4, 5). However, contrasting results were found between both groups of lines, as the *TaGW2* triple mutant showed a significant increase (*P* < 0.05) in ovary weight compared to its WT in all but the G3 floret position, whereas the *TaExpA6* construct showed no significant (*P* > 0.05) alteration in ovary weight at pollination, mirroring its WT (Figure 5). This suggests that *TaGW2* gene mutation impacts ovary size prior to anthesis.

When the time-course of grain weight from positions G2 and G3 was monitored through the grain filling period, both modified lines (*TaExpA6* and *TaGW2*) surpassed their respective WTs in grain weight, though, the onset of these differences varied between groups. The GW2 triple mutant showed higher grain weight than the WT from the starting of measurements at 4 DAA (Figure 6D; Supplementary Figure S4), while the *TaExpA6* line exhibited higher grain weights at these grain positions from 20 DAA on (Figure 6A; Supplementary Figure S4). For both line groups, a tri-linear function accurately depicted individual grain weight dynamics (Supplementary Figure S5), with enhanced grain filling rates at the linear phase accounting for the increased final grain weights in both G2 and G3 grains (*R*² = 0.99; *P* < 0.05). No significant difference was observed in the duration of grain filling, which was approximately 40 days (Supplementary Table S1). Higher grain weights in modified lines were also coupled with an increased maximum grain water content (Figures 6A, D; Supplementary Figure S4).

Grain dimension dynamics also varied between the line groups. The *TaExpA6* line increased grain length by 3% and 4% in grain positions G2 and G3, respectively, over the WT (*P* < 0.05) without affecting grain width (Figure 6B; Supplementary Figure S4).

Conversely, the GW2 triple mutant improved both grain length and width along grain filling (*P* < 0.05) by 6.2 and 6.7%, respectively, when both grain positions were averaged (Figure 6E; Supplementary Figure S4). Notably, differences in grain width in the ExpA6 lines became evident only at the ending of dimension dynamics analysis, coinciding with reduced grain water content (< 30%) (Figure 6B; Supplementary Figure S4).

The observed divergence in grain length between the transgenic *TaExpA6* line and its WT counterpart became apparent at 20 DAA. This divergence appears to coincide with the expression profile of the *TaExpA6* gene. Remarkably, *TaExpA6* expression remains undetectable until 5 DAA, subsequently peaking between 10 and 15 DAA (see Figure 6C). Two-way ANOVA revealed highly significant genotype effects for *TaExpA6* (*p* < 0.0001), with Bonferroni's multiple comparisons test showing consistent and significant changes in mRNA levels at 10, 14, and 21 DAA (adjusted *p*-value < 0.05, Figure 6E). In contrast, the grain dimensions in the GW2 triple mutant consistently exceeded those of the WT throughout the observation period (Figure 6E), suggesting a constitutive effect of the *TaGW2* knockout on grain size. Furthermore, *TaGW2* expression was monitored from 4 to 21 DAA, as depicted in Figure 6F. One-way ANOVA revealed a significant effect of developmental stage on *TaGW2* expression in the wild-type (*p*-value: 0.0005). Bonferroni's test showed significantly lower *TaGW2* levels at 21 DAA compared to 4 DAA (adjusted *p*-value < 0.05, Figure 6F), suggesting a potential role in earlier stages of grain growth.

4 Discussion

This study aimed to elucidate the mechanisms underlying the trade-off between grain weight and grain number in wheat, when grain weight is improved by genetic manipulations. To realize this objective, field evaluations of two genetically distinct wheat line groups, ExpA6 and GW2, were conducted under optimal conditions. The GW2 lines had 20 days longer crop cycle than the ExpA6 lines, but the climatic conditions during critical phenophases between both groups were similar across the two

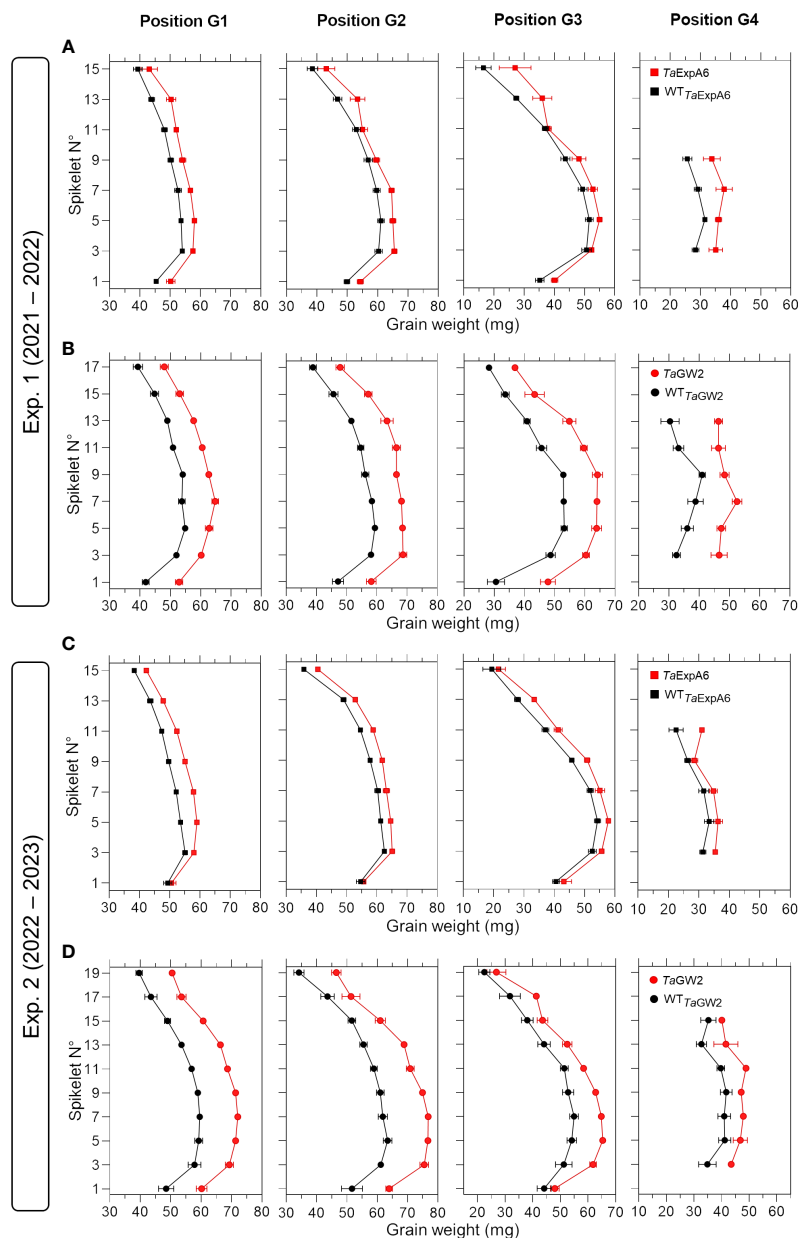


FIGURE 2

Grain weight in grain positions G1, G2, G3 and G4 from each spikelet along the spike of ExpA6 lines (A, C) and GW2 lines (B, D) in experiments 1 and 2. The transgenic *TaExpA6* line and the triple mutant of *TaGW2* gene, and their WT are depicted by red and black symbols, respectively.

experimental years. As hypothesized, the transgenic and triple mutant lines displayed analogous phenology with their respective wild types, as well as plant height and architecture (data not shown).

Significant increments in grain weight were observed in the manipulated lines over the WT, although differing in magnitude, i.e. by 8.6 and 23.7% in the *TaExpA6* and *TaGW2* lines, respectively, without and with trade-off with grain number. These results agree with previous evaluations of the *TaExpA6* and *TaGW2* lines (Wang et al., 2018; Zhai et al., 2018; Calderini et al., 2021), however, a direct comparison between both groups was feasible in our study as they were assessed in the same experiment sharing the same growing conditions and management. Notably, our study expands on previous work by demonstrating that both

manipulations improved individual grain weight and grain dimensions across all grain positions of the spike, a feature not fully addressed in earlier research.

Comparative analyses between genetic resources and elite wheat varieties by Philipp et al. (2018) revealed that breeding process in wheat uniformly increased grain number and yield across the spike without altering individual spikelets relative contribution to overall yield. The observed increase in individual grain weight in our study aligns with these breeding trends, suggesting a similar pattern when grain weight is genetically improved. However, manipulation of *TaExpA6* showed a higher impact on distal grains (G3 and G4) than on proximal ones (G1 and G2), while the *TaGW2* triple mutant line showed similar increase across these grain positions.

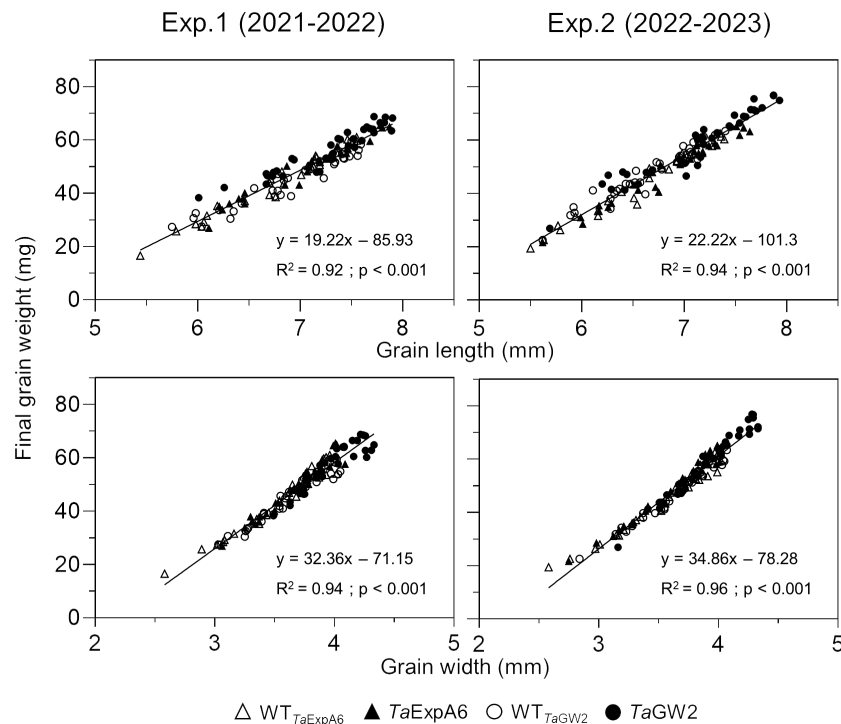


FIGURE 3

Relationship between grain weight and grain length (upper panel) or grain width (lower panel) of grain positions G1, G2, G3 and G4 from each spikelet along the spike, across genotype groups in experiments 1 (left panel) and 2 (right panel). TaExpA6 line and its WT are denoted by closed and open triangles respectively, while the TaGW2 triple mutant line and its WT are denoted by closed and open circles, respectively.

Both genetic manipulations in our study successfully increased individual grain weight through an enhanced grain filling rate, maintaining the same grain filling duration as their respective WT. Additionally, both modified lines reached higher maximum grain water content than their respective WT, which has been ascribed as a driver of grain weight potential (Saini and Westgate, 1999; Pepler et al., 2006; Hasan et al., 2011; Alvarez Prado et al., 2013), suggesting increased sink strength which sequentially resulted in a higher grain

filling rate and final grain weight. However, the impact of TaExpA6 and TaGW2 manipulations on grain dimensions varied, since the

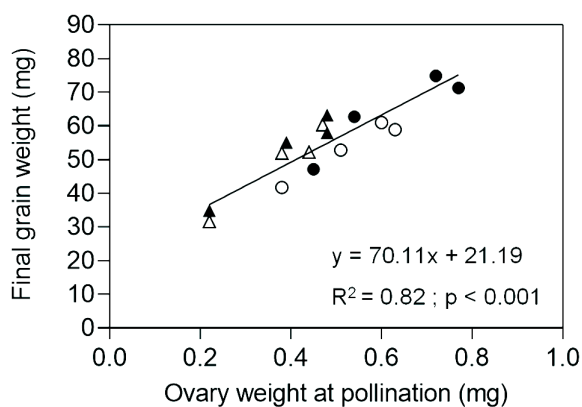


FIGURE 4

Relationship between final grain weight and ovary weight at pollination (W10, Waddington et al., 1983) of grain positions G1, G2, G3 and G4 from the central spikelets of the spike corresponding to the TaExpA6 line (closed triangles), TaGW2 line (closed circles) and their WT (open triangles and open circles, respectively).

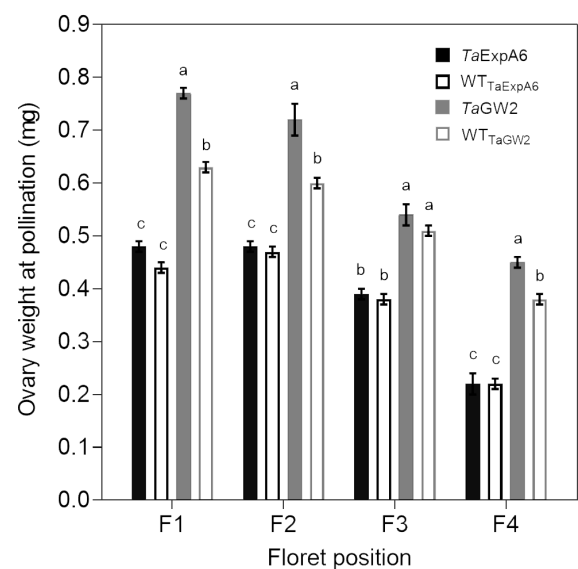


FIGURE 5

Ovary weight at pollination (W10, Waddington et al., 1983) of florets set at floret positions F1, F2, F3 and F4 from the central spikelets of the spike corresponding to the TaExpA6 line (solid black bars), TaGW2 triple mutant line (solid grey bars) and their WT (empty black and grey bars, respectively). Different letters indicate significant effects ($P < 0.05$).

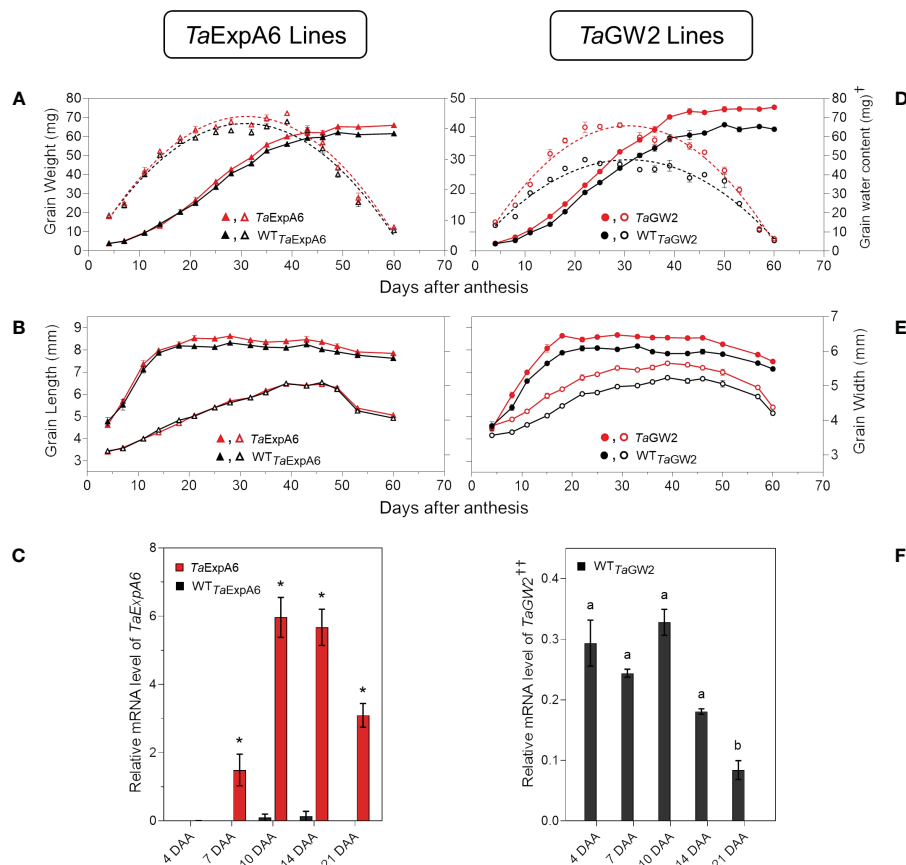


FIGURE 6

Grain weight dynamics and gene expression. (A) Grain weight and water content dynamics at grain position G2 from the central spikelets of the spike corresponding to the ExpA6 lines and (D) GW2 lines. (B) Grain length and grain width dynamics at the same grain position corresponding to the ExpA6 lines and (E) GW2 lines. (C) Relative *TaExpA6* gene expression level in developing grains in the ExpA6 lines; asterisks indicate significant differences (adjusted p-value < 0.05) between line *TaExpA6* and its WT according to two-way ANOVA Bonferroni's test *post hoc*. (F) Relative *TaGW2* gene expression level in developing grains of the GW2 WT line; different letters indicate significant effect (adjusted p-value < 0.05) between developmental times according to Bonferroni's test *post-hoc*. In all cases, bars show the standard error of the means. [†]Note that different scales were used to plot grain water content of ExpA6 and GW2 lines. ^{††}Data shows the average value of *TaGW2*-A, B and D homoeologue's expression..

transgenic approach primarily augmented grain length, while the triple mutation affected both length and width. This differential impact suggests distinct underlying mechanisms between manipulations. In the *TaExpA6* line, the cloned expansin possibly facilitates cell wall loosening along the grain longitudinal axis, consistent with expansins extensively reported mode of action (McQueen-Mason et al., 1992; Cosgrove, 2000; Wang et al., 2019; Cosgrove, 2023). Additionally, the influence of the *TaExpA6* gene would seem more related to cell size than number, considering the cessation of cell proliferation in grains outer layers and starchy endosperm by 6 and 14 DAA, respectively (Olsen et al., 1992; Drea et al., 2005; Radchuk et al., 2011), and the linear relationship found between the length of grains and epidermal cells length during grain filling across wheat ploidies (Muñoz and Calderini, 2015). However, the mechanisms of the overexpression of the gene *TaExpA6* remains to be assessed. Conversely, the higher GW obtained in previous studies by manipulation of the *TaGW2* gene has been ascribed to increases in both the cell number and size of maternal tissues around anthesis, leading to longer and wider grains

(Simmonds et al., 2016; Geng et al., 2017; Zhang et al., 2018). Increases in both grain dimensions in our study are in alignment with these findings. In either case, further histological analysis of grains from ExpA6 and GW2 lines is required to confirm these assumptions. The significance of cell number and size in the outer tissues for potential grain weight previously exposed in bread wheat and across wheat ploidies (Lizana et al., 2010; Muñoz and Calderini, 2015; Brinton et al., 2017; Brinton and Uauy, 2019; Liu et al., 2020; Guo et al., 2022; Tillett et al., 2022), together with the findings from this study, support the hypothesis that potential grain weight is constrained by physical limitations imposed by maternal outer layers.

The effect of the manipulated lines on grain number per spike was contrasting as expected. The *TaExpA6* gene did not affect this yield component, whereas the *TaGW2* triple mutation reduced it by 11.3% relative to the WT, across both seasons. This trade-off between grain weight and grain number when grain weight is increased has been widely reported (Wiersma et al., 2001; Brinton et al., 2017; Quintero et al., 2018; Wang et al., 2018; Golan et al.,

2019; Milner et al., 2021). In previous studies, modified lines with GW increases comparable to the one observed in line *TaExpA6*, (i.e. between 5.5% and 8%) have also been associated with concomitant reductions in GN (Brinton et al., 2017; Adamski et al., 2021; Mora-Ramirez et al., 2021). Therefore, the contrasting trade-off observed between both genotype groups in this study would not be attributed to the quantitative difference in the GW increase induced by the molecular manipulation in modified lines. Notably, the magnitude of average grain weight increase did not directly correlate with grain number reduction, refuting the notion of a strict negative compensation between these spike yield components. These results align with the consensus that wheat grain filling is not source-limited (Slafer and Savin, 1994; Borrás et al., 2004; Reynolds et al., 2009; Quintero et al., 2018; Murchie et al., 2023; Slafer et al., 2023). However, an up-regulation of the source as a consequence of improved sink strength displayed by manipulation of *TaExpA6* and *TaGW2* genes should not be disregarded. In fact, previous studies have demonstrated that a high sink to source ratio can lead to an increased post-anthesis radiation use efficiency (RUE) (Bustos et al., 2013) or extended green canopy duration during grain filling (Lichthardt et al., 2020). Interestingly, the lack of effect on grain number showed by the ectopic expression of the *TaExpA6* gene is consistent with two previous experiments at different plant rates (Calderini et al., 2021). The *TaExpA6* and *TaGW2* genes expression profile along with grain weight dynamics of the transgenic and mutant lines, allowed us to highlight a distinctive pattern in the effect of these manipulations on early grain development. The disruption of *TaGW2* gene in the triple mutant line improved grain weight above the WT from the onset of the grain filling period. In contrast, the higher grain weight reached by the *TaExpA6* transgenic line became apparent at 21 DAA. Furthermore, the triple mutant exhibited heavier ovaries at pollination than the WT across different positions in the spikelet, indicating that the *TaGW2* gene functions in floret tissues before the gynoecium becomes a grain. This finding is in agreement with field experiments carried out by Simmonds et al. (2016), who identified increased carpel size and weight around anthesis as drivers of grain weight increase in *TaGW2* knockout mutants. In contrast, ovary weight at pollination did not differ significantly between *TaExpA6* line and its WT in the present study, reinforcing the post-anthesis timing of the transgene effect as previously reported (Calderini et al., 2021).

It has been demonstrated that grain number and weight determinations overlap between booting and a week after anthesis (Calderini et al., 1999, 2001; Ugarte et al., 2007; Hasan et al., 2011; Simmonds et al., 2014; Parent et al., 2017; Calderini et al., 2021). This overlap was proposed as the cause of the trade-off between this key yield components in wheat (Calderini et al., 2021). The effectiveness of the *TaExpA6* gene in increasing grain weight without a trade-off with grain number supports this hypothesis, given that *TaExpA6* expression begins at post-anthesis, particularly from 10 DAA onwards, and its effect on grain length and weight over the WT becomes detectable after 15 DAA. Conversely, when the enhancement commences at pre-anthesis as in *TaGW2* triple mutant, showed by both increased ovary size and grain weight, a trade-off occurs. Thus, our results suggest that the trade-off between grain weight and number is attributable to the temporal overlap of

determinant periods for these grain components. Previous research found that the likelihood of grain setting in distal florets of wheat associates with ovary size (Calderini and Reynolds, 2000; Guo et al., 2016). However, contrary to our assumption, the higher ovary weight in floret position G4 observed in line *TaGW2* was accompanied by a reduction of the number of grains set at this distal position across the spike, which led to the reduced number of grains per spikelet reported in the triple mutant.

In addition to the effects of *TaExpA6* and *TaGW2* gene manipulations on grain weight and number, recent elucidation of the role of the *GN1* gene offers additional insights into the genetic regulation of these yield components. Research by Sakuma et al. (2019) highlighted that the *GN1* gene, coding for a homeodomain leucine zipper class I transcription factor, plays a pivotal role in floret fertility in wheat. Their findings revealed an evolutionary adaptation in the expression of *GN1*, leading to an increase in grain number per spikelet in domesticated wheat, suggesting a genetic basis for the observed trade-off between grain weight and grain number. Complementing this, Golan et al. (2019) proposed the *GN1-A1* gene, a variant of *GN1*, as a mediator of this trade-off. Remarkably, *GN1* is predominantly expressed in immature spikes before anthesis (Sakuma et al., 2019), further highlighting the relevance of the overlap between grain number and weight determinations as key to unravel the underlying causes for the trade-off. Additionally, Xie and Sparkes (2021) found an overlapping between major regions associated with grain number and grain weight in a mapping population of 226 RILs.

The integration of these insights with the results of our study suggests a multifaceted genetic network influencing wheat yield. While our study focuses on the phenotypic outcomes of *TaExpA6* and *TaGW2* gene manipulations, the role of the *GN1* gene underscores the importance of genetic control in floret fertility and assimilate allocation. This understanding complements our observations of the trade-off between grain weight and grain number, indicating that both targeted genetic modifications and natural genetic variations, such as those in *GN1*, are crucial in determining these key agronomic traits. Therefore, a comprehensive strategy that considers both natural gene variants like *GN1* and targeted modifications such as *TaExpA6* and *TaGW2* may be essential for the development of wheat varieties that optimally balance grain weight and number.

5 Concluding remarks

In conclusion, the results of this study emphasize the complexity of the genetic control of grain weight and number in wheat. The findings reveal that modification of the *TaExpA6* gene enhances grain weight without reducing grain number, indicating a deviation from the traditionally assumed trade-off between these yield components. In contrast, alterations in the *TaGW2* gene, while highly increasing grain weight, also result in a reduction in grain number, aligning with the conventional understanding of this trade-off. These outcomes highlight distinct genetic pathways influencing wheat yield traits. The differential impacts of *TaExpA6* and *TaGW2* on wheat grain development, and the overlapping of both yield

components determination between booting and a week after anthesis, offer valuable insights for future overcoming this common bottleneck and to improve grain yield in wheat breeding programs through targeted genetic modifications.

Data availability statement

The original contributions presented in the study are included in the article/**Supplementary material**, further inquiries can be directed to the corresponding author/s.

Author contributions

LV: Data curation, Formal analysis, Investigation, Supervision, Writing – original draft, Writing – review & editing. JC: Data curation, Methodology, Supervision, Writing – review & editing. DC: Conceptualization, Formal analysis, Funding acquisition, Project administration, Supervision, Writing – original draft.

Funding

The author(s) declare financial support was received for the research, authorship, and/or publication of this article. This research was supported by Project FONDECYT Regular 1211040 (Chilean National Research and Development Agency -ANID-). The authors acknowledge the contribution of PhD scholarship Folio 21220957 (ANID), Chile.

Acknowledgments

The authors wish to warmly thank Dr. Emma Wallington and the National Institute of Agricultural Botany (NIAB, UK) for kindly facilitating the ExpA6 lines, and Prof. Cristobal Uauy and John Innes Center (JIC, UK) for their generous provision of the GW2 lines. Japan Tobacco Inc. is recognized as a holder for the

technology included in PureWheat® licenced from Japan Tobacco Inc. We also thank the experimental field staff of the Austral Farming Experimental Station of Universidad Austral de Chile for the technical assistance provided. Technical contributions and management of field trials by Marcelo Castro Moraga and Cristóbal Castro Villalón is truly appreciated. We are also very grateful to María Beatriz Ugalde Jaramillo and Dr. Anita Arenas Miranda (Plant Nutrition and Genomics Lab – UACH) for performing the molecular analysis included in this study. The samples processing by Beatriz Shibar (UACH) and Magda Lobnik is recognized. JC was supported by ANID–Millennium Science Initiative Program–ICN17-022 and FONDECYT Regular 1230833. LV was supported by PhD scholarship 21220957-2022 from ANID, Chile.

Conflict of interest

The authors declare that the research was conducted in the absence of any commercial or financial relationships that could be construed as a potential conflict of interest.

Publisher's note

All claims expressed in this article are solely those of the authors and do not necessarily represent those of their affiliated organizations, or those of the publisher, the editors and the reviewers. Any product that may be evaluated in this article, or claim that may be made by its manufacturer, is not guaranteed or endorsed by the publisher.

Supplementary material

The Supplementary Material for this article can be found online at: <https://www.frontiersin.org/articles/10.3389/fpls.2024.1380429/full#supplementary-material>

References

- Abbate, P. E., Andrade, F. H., Culot, J. P., and Bindran, P. S. (1997). Grain yield in wheat: Effects of radiation during spike growth period. *Field Crops Res.* 54, 245–257. doi: 10.1016/S0378-4290(97)00059-2
- Acreche, M. M., and Slafer, G. A. (2006). Grain weight response to increases in number of grains in wheat in a Mediterranean area. *Field Crops Res.* 98, 52–59. doi: 10.1016/j.fcr.2005.12.005
- Adamski, N. M., Simmonds, J., Brinton, J. F., Backhaus, A. E., Chen, Y., Smedley, M., et al. (2021). Ectopic expression of *Triticum polonicum* VRT-A2 underlies elongated glumes and grains in hexaploid wheat in a dosage-dependent manner. *Plant Cell* 33, 2296–2319. doi: 10.1093/plcell/koab119
- Alonso, M. P., Abbate, P. E., Mirabella, N. E., Aramburu Merlos, F., Pano, J. S., and Pontaroli, A. C. (2018). Analysis of sink/source relations in bread wheat recombinant inbred lines and commercial cultivars under a high yield potential environment. *Eur. J. Agron.* 93, 82–87. doi: 10.1016/j.eja.2017.11.007
- Alvarez Prado, S., Gallardo, J. M., Serrago, R. A., Kruk, B. C., and Miralles, D. J. (2013). Comparative behavior of wheat and barley associated with field release and grain weight determination. *Field Crops Res.* 144, 28–33. doi: 10.1016/j.fcr.2012.12.018
- Beed, F. D., Paveley, N. D., and Sylvester-Bradley, R. (2007). Predictability of wheat growth and yield in light-limited conditions. *J. Agric. Sci.* 145, 63–79. doi: 10.1017/S0021859606006678
- Borrás, L., Slafer, G. A., and Otegui, M. E. (2004). Seed dry weight response to source–sink manipulations in wheat, maize and soybean: a quantitative reappraisal. *Field Crops Res.* 86, 131–146. doi: 10.1016/j.fcr.2003.08.002
- Brinton, J., Simmonds, J., Minter, F., Leverington-Waite, M., Snape, J., and Uauy, C. (2017). Increased pericarp cell length underlies a major quantitative trait locus for grain weight in hexaploid wheat. *New Phytol.* 215, 1026–1038. doi: 10.1111/nph.14624
- Brinton, J., and Uauy, C. (2019). A reductionist approach to dissecting grain weight and yield in wheat. *J. Integr. Plant Biol.* 61, 337–358. doi: 10.1111/jipb.12741
- Bustos, D. V., Hasan, A. K., Reynolds, M. P., and Calderini, D. F. (2013). Combining high grain number and weight through a DH-population to improve grain yield potential of wheat in high-yielding environments. *Field Crops Res.* 145, 106–115. doi: 10.1016/j.fcr.2013.01.015
- Calderini, D. F., Abeledo, L. G., Savin, R., and Slafer, G. A. (1999). Effect of temperature and carpel size during pre-anthesis on potential grain weight in wheat. *J. Agric. Sci.* 132, 453–459. doi: 10.1017/S0021859699006504

- Calderini, D. F., Castillo, F. M., Arenas, M. A., Molero, G., Reynolds, M. P., Craze, M., et al. (2021). Overcoming the trade-off between grain weight and number in wheat by the ectopic expression of expansin in developing seeds leads to increased yield potential. *New Phytol.* 230, 629–640. doi: 10.1111/nph.17048
- Calderini, D. F., and Reynolds, M. P. (2000). Changes in grain weight as a consequence of de-graining treatments at pre- and post-anthesis in synthetic hexaploid lines of wheat (*Triticum durum* x *T. tauschii*). *Funct. Plant Biol.* 27, 183–191. doi: 10.1071/PP99066
- Calderini, D. F., Savin, R., Abeledo, L. G., Reynolds, M. P., and Slafer, G. A. (2001). The importance of the period immediately preceding anthesis for grain weight determination in wheat. *Euphytica* 119, 199–204. doi: 10.1023/A:101759723568
- Canales, J., Verdejo, J., Carrasco-Puga, G., Castillo, F. M., Arenas-M, A., and Calderini, D. F. (2021). Transcriptome analysis of seed weight plasticity in brassica napus. *Int. J. Mol. Sci.* 22, 4449. doi: 10.3390/ijms22094449
- Castillo, F. M., Canales, J., Claude, A., and Calderini, D. F. (2018). Expansin genes expression in growing ovaries and grains of sunflower are tissue-specific and associate with final grain weight. *BMC Plant Biol.* 18, 327. doi: 10.1186/s12870-018-1535-7
- Castillo, F. M., Vázquez, S. C., and Calderini, D. F. (2017). Does the pre-flowering period determine the potential grain weight of sunflower? *Field Crops Res.* 212, 23–33. doi: 10.1016/j.fcr.2017.06.029
- Cosgrove, D. J. (2000). Loosening of plant cell walls by expansins. *Nature* 407, 321–326. doi: 10.1038/35030000
- Cosgrove, D. J. (2021). Expanding wheat yields with expansin. *New Phytol.* 230, 403–405. doi: 10.1111/nph.17245
- Cosgrove, D. J. (2024). Structure and growth of plant cell walls. *Nat. Rev. Mol. Cell Biol.* 25, 340–358. doi: 10.1038/s41580-023-00691-y
- Cruz-Castillo, J. G., Lawes, G. S., and Woolley, D. J. (1992). The influence of the time of anthesis, seed factor(s), and the application of a growth regulator mixture on the growth of kiwifruit. *Acta Hort.* 297, 475–480. doi: 10.17660/ActaHortic.1992.297.62
- Digeon, J.-F., Guiderdoni, E., Alary, R., Michaux-Ferrière, N., Joudrier, P., and Gautier, M.-F. (1999). Cloning of a wheat puroindoline gene promoter by IPCR and analysis of promoter regions required for tissue-specific expression in transgenic rice seeds. *Plant Mol. Biol.* 39, 1101–1112. doi: 10.1023/A:1006194326804
- Drea, S. A., Leader, D. J., Arnold, B. C., Shaw, P., Dolan, L., and Doonan, J. H. (2005). Systematic spatial analysis of gene expression during wheat caryopsis development. *Plant Cell* 17, 2172–2185. doi: 10.1105/tpc.105.034058
- Dwivedi, S. L., Reynolds, M. P., and Ortiz, R. (2021). Mitigating tradeoffs in plant breeding. *iScience* 24, 102965. doi: 10.1016/j.isci.2021.102965
- Ferrante, A., Cartelle, J., Savin, R., and Slafer, G. A. (2017). Yield determination, interplay between major components and yield stability in a traditional and a contemporary wheat across a wide range of environments. *Field Crops Res.* 203, 114–127. doi: 10.1016/j.fcr.2016.12.028
- Ferrante, A., Savin, R., and Slafer, G. A. (2015). Relationship between fruiting efficiency and grain weight in durum wheat. *Field Crops Res.* 177, 109–116. doi: 10.1016/j.fcr.2015.03.009
- Fischer, R. A. (1985). Number of kernels in wheat crops and the influence of solar radiation and temperature. *J. Agric. Sci.* 105, 447–461. doi: 10.1017/S0021859600056495
- Fischer, R. A. (2008). The importance of grain or kernel number in wheat: A reply to Sinclair and Jamieson. *Field Crops Res.* 105, 15–21. doi: 10.1016/j.fcr.2007.04.002
- Fischer, R. A. (2022). “History of Wheat Breeding: A Personal View,” in *Wheat Improvement*. Eds. M. P. Reynolds and H.-J. Braun (Springer, Switzerland), 17–30.
- Gautier, M.-F., Aleman, M.-E., Guirao, A., Marion, D., and Joudrier, P. (1994). *Triticum aestivum* puroindolines, two basic cysteine-rich seed proteins: cDNA sequence analysis and developmental gene expression. *Plant Mol. Biol.* 25, 43–57. doi: 10.1007/BF00024197
- Geng, J., Li, L., Lv, Q., Zhao, Y., Liu, Y., Zhang, L., et al. (2017). TaGW2-6A allelic variation contributes to grain size possibly by regulating the expression of cytokinins and starch-related genes in wheat. *Planta* 246, 1153–1163. doi: 10.1007/s00425-017-2759-8
- Golan, G., Ayalon, I., Perry, A., Zimran, G., Ade-Ajayi, T., Mosquana, A., et al. (2019). GNI-A1 mediates trade-off between grain number and grain weight in tetraploid wheat. *Theor. Appl. Genet.* 132, 2353–2365. doi: 10.1007/s00122-019-03358-5
- Guo, L., Ma, M., Wu, L., Zhou, M., Li, M., Wu, B., et al. (2022). Modified expression of TaCYP78A5 enhances grain weight with yield potential by accumulating auxin in wheat (*Triticum aestivum* L.). *Plant Biotechnol. J.* 20, 168–182. doi: 10.1111/pbi.13704
- Guo, Z., Slafer, G. A., and Schnurbusch, T. (2016). Genotypic variation in spike fertility traits and ovary size as determinants of floret and grain survival rate in wheat. *J. Exp. Bot.* 67, 4221–4230. doi: 10.1093/jxb/erw200
- Handley, D. T., and Dill, J. F. (2003). *Vegetative and floral characteristics of six strawberry cultivars associated with fruit size, yield and susceptibility to tarnished plant bug injury* (Leuven, Belgium: International Society for Horticultural Science (ISHS), 161–167. doi: 10.17660/ActaHortic.2003.626.21
- Hasan, A. K., Herrera, J., Lizana, C., and Calderini, D. F. (2011). Carpel weight, grain length and stabilized grain water content are physiological drivers of grain weight determination of wheat. *Field Crops Res.* 123, 241–247. doi: 10.1016/j.fcr.2011.05.019
- Hong, Y., Chen, L., Du, L. P., Su, Z., Wang, J., Ye, X., et al. (2014). Transcript suppression of TaGW2 increased grain width and weight in bread wheat. *Funct. Integr. Genomics* 14, 341–349. doi: 10.1007/s10142-014-0380-5
- Jablonski, B., Szala, K., Przyborowski, M., Bajguz, A., Chmur, M., Gasparis, S., et al. (2021). TaCKX2.2 genes coordinate expression of other taCKX family members, regulate phytohormone content and yield-related traits of wheat. *Int. J. Mol. Sci.* 22. doi: 10.3390/ijms22084142
- Khan, N., Zhang, Y., Wang, J., Li, Y., Chen, X., Yang, L., et al. (2022). TaGSNE, a WRKY transcription factor, overcomes the trade-off between grain size and grain number in common wheat and is associated with root development. *J. Exp. Bot.* 73, 6678–6696. doi: 10.1093/jxb/erac327
- Kino, R. I., Pellny, T. K., Mitchell, R. A. C., Gonzalez-Uriarte, A., and Tosi, P. (2020). High post-anthesis temperature effects on bread wheat (*Triticum aestivum* L.) grain transcriptome during early grain-filling. *BMC Plant Biol.* 20, 170. doi: 10.1186/s12870-020-02375-7
- Kumar, A., Mantovani, E. E., Seetan, R., Soltani, A., Echeverry-Solarte, M., Jain, S., et al. (2016). Dissection of Genetic Factors underlying Wheat Kernel Shape and Size in an Elite x Nonadapted Cross using a High Density SNP Linkage Map. *Plant Genome* 9, plantgenome2015.2009.0081. doi: 10.3835/plantgenome2015.09.0081
- Lai, R., Woolley, D. J., and Lawes, G. S. (1990). The effect of inter-fruit competition, type of fruiting lateral and time of anthesis on the fruit growth of kiwifruit (*Actinidia deliciosa*). *J. Hortic. Sci.* 65, 87–96. doi: 10.1080/00221589.1990.11516034
- Lichtardt, C., Chen, T. W., Stahl, A., and Stutzel, H. (2020). Co-evolution of sink and source in the recent breeding history of winter wheat in Germany. *Front. Plant Sci.* 10, 1771. doi: 10.3389/fpls.2019.01771
- Lin, Z., Ni, Z., Zhang, Y., Yao, Y., Wu, H., and Sun, Q. (2005). Isolation and characterization of 18 genes encoding α - and β -expansins in wheat (*Triticum aestivum* L.). *Mol. Genet. Genomics* 274, 548–556. doi: 10.1007/s00438-005-0029-0
- Lindström, L. I., Pellegrini, C. N., Aguirrezábal, L. A. N., and Hernández, L. F. (2006). Growth and development of sunflower fruits under shade during pre and early post-anthesis period. *Field Crops Res.* 96, 151–159. doi: 10.1016/j.fcr.2005.06.006
- Lindström, L. I., Pellegrini, C. N., and Hernández, L. F. (2007). Histological development of the sunflower fruit pericarp as affected by pre- and early post-anthesis canopy shading. *Field Crops Res.* 103, 229–238. doi: 10.1016/j.fcr.2007.06.005
- Liu, H., Li, H., Hao, C., Wang, K., Wang, Y., Qin, L., et al. (2020). TaDA1, a conserved negative regulator of kernel size, has an additive effect with TaGW2 in common wheat (*Triticum aestivum* L.). *Plant Biotechnol. J.* 18, 1330–1342. doi: 10.1111/pbi.13298
- Lizana, X. C., and Calderini, D. F. (2013). Yield and grain quality of wheat in response to increased temperatures at key periods for grain number and grain weight determination: considerations for the climatic change scenarios of Chile. *J. Agric. Sci.* 151, 209–221. doi: 10.1017/S0021859612000639
- Lizana, X. C., Riegel, R., Gomez, L. D., Herrera, J., Isla, A., McQueen-Mason, S. J., et al. (2010). Expansins expression is associated with grain size dynamics in wheat (*Triticum aestivum* L.). *J. Exp. Bot.* 61, 1147–1157. doi: 10.1093/jxb/erp380
- McQueen-Mason, S., Durachko, D. M., and Cosgrove, D. J. (1992). Two endogenous proteins that induce cell wall extension in plants. *Plant Cell* 4, 1425–1433.
- Merrill, A. L., and Watt, B. K. (1973). *Energy Value of Foods: Basis and Derivation* (Washington DC, United States: United States Department of Agriculture (USDA)).
- Millet, E., and Pinthus, M. J. (1980). Genotypic effects of the maternal tissues of wheat on its grain weight. *Theor. Appl. Genet.* 58, 247–252. doi: 10.1007/BF00265174
- Milner, M. J., Bowden, S., Craze, M., and Wallington, E. J. (2021). Ectopic expression of TaBG1 increases seed size and alters nutritional characteristics of the grain in wheat but does not lead to increased yields. *BMC Plant Biol.* 21, 524. doi: 10.1186/s12870-021-03294-x
- Mira, J. P., Arenas-M, A., Calderini, D. F., and Canales, J. (2023). Integrated transcriptome analysis identified key expansin genes associated with wheat cell wall, grain weight and yield. *Plants* 12, 2868. doi: 10.3390/plants12152868
- Mora-Ramirez, I., Weichert, H., Von Wiren, N., Froberg, C., De Bodt, S., Schmidt, R. C., et al. (2021). The da1 mutation in wheat increases grain size under ambient and elevated CO₂ but not grain yield due to trade-off between grain size and grain number. *Plant Environ. Interact.* 2, 61–73. doi: 10.1002/pei3.10041
- Muñoz, M., and Calderini, D. F. (2015). Volume, water content, epidermal cell area, and XTH5 expression in growing grains of wheat across ploidy levels. *Field Crops Res.* 173, 30–40. doi: 10.1016/j.fcr.2014.12.010
- Murchie, E. H., Reynolds, M., Slafer, G. A., Foulkes, M. J., Acevedo-Siaca, L., McAusland, L., et al. (2023). A ‘wiring diagram’ for source strength traits impacting wheat yield potential. *J. Exp. Bot.* 74, 72–90. doi: 10.1093/jxb/erac415
- Okamoto, Y., and Takumi, S. (2013). Pleiotropic effects of the elongated glume gene P1 on grain and spikelet shape-related traits in tetraploid wheat. *Euphytica* 194, 207–218. doi: 10.1007/s10681-013-0916-0
- Olsen, O. A., Kalla, R., and Potter, R. H. (1992). Histo-differentiation and molecular biology of developing cereal endosperm. *Seed Sci. Res.* 2, 117–131. doi: 10.1017/S0960258500001240
- Parent, B., Bonneau, J., Maphosa, L., Kovalchuk, A., Langridge, P., and Fleury, D. (2017). Quantifying wheat sensitivities to environmental constraints to dissect genotype x environment interactions in the field. *Plant Physiol.* 174, 1669–1682. doi: 10.1104/pp.17.00372
- Pepler, S., Gooding, M. J., and Ellis, R. H. (2006). Modelling simultaneously water content and dry matter dynamics of wheat grains. *Field Crops Res.* 95, 49–63. doi: 10.1016/j.fcr.2005.02.001

- Pfaffl, M. W. (2001). A new mathematical model for relative quantification in real-time RT-PCR. *Nucleic Acids Res.* 29, e45–e45. doi: 10.1093/nar/29.9.e45
- Philipp, N., Weichert, H., Bohra, U., Weschke, W., Schulthess, A. W., and Weber, H. (2018). Grain number and grain yield distribution along the spike remain stable despite breeding for high yield in winter wheat. *PLoS One* 13, e0205452. doi: 10.1371/journal.pone.0205452
- Quintero, A., Molero, G., Reynolds, M. P., and Calderini, D. F. (2018). Trade-off between grain weight and grain number in wheat depends on GxE interaction: A case study of an elite CIMMYT panel (CIMCOG). *Eur. J. Agron.* 92, 17–29. doi: 10.1016/j.eja.2017.09.007
- Radchuk, V., Weier, D., Radchuk, R., Weschke, W., and Weber, H. (2011). Development of maternal seed tissue in barley is mediated by regulated cell expansion and cell disintegration and coordinated with endosperm growth. *J. Exp. Bot.* 62, 1217–1227. doi: 10.1093/jxb/erq348
- Reale, L., Rosati, A., Tedeschini, E., Ferri, V., Cerri, M., Ghitarrini, S., et al. (2017). Ovary size in wheat (*Triticum aestivum* L.) is related to cell number. *Crop Sci.* 57, 914–925. doi: 10.2135/cropsci2016.06.0511
- Reynolds, M. P., Foulkes, M. J., Slafer, G. A., Berry, P., Parry, M. A. J., Snape, J. W., et al. (2009). Raising yield potential in wheat. *J. Exp. Bot.* 60, 1899–1918. doi: 10.1093/jxb/erp016
- Rondanini, D. P., Mantese, A. I., Savin, R., and Hall, A. J. (2009). Water content dynamics of achene, pericarp and embryo in sunflower: Associations with achene potential size and dry-down. *Eur. J. Agron.* 30, 53–62. doi: 10.1016/j.eja.2008.07.002
- Rosati, A., and Benincasa, P. (2023). Revisiting source versus sink limitations of wheat yield during grain filling. *Agron. J.* 115, 3197–3205. doi: 10.1002/aj2.21454
- Rosati, A., Zupančič, M., Caporali, S., and Padula, G. (2009). Fruit weight is related to ovary weight in olive (*Olea europaea* L.). *Scientia Hort.* 122, 399–403. doi: 10.1016/j.scienta.2009.05.034
- Ruijter, J. M., Ramakers, C., Hoogaars, W. M. H., Karlen, Y., Bakker, O., Van Den Hoff, M. J. B., et al. (2009). Amplification efficiency: linking baseline and bias in the analysis of quantitative PCR data. *Nucleic Acids Res.* 37, e45–e45. doi: 10.1093/nar/gkp045
- Sadras, V. O. (2007). Evolutionary aspects of the trade-off between seed size and number in crops. *Field Crops Res.* 100, 125–138. doi: 10.1016/j.fcr.2006.07.004
- Saini, H. S., and Westgate, M. E. (1999). “Reproductive Development in Grain Crops during Drought,” in *Advances in Agronomy*. Ed. D. L. Sparks (San Diego, USA: Academic Press), 59–96.
- Sakuma, S., Golan, G., Guo, Z., Ogawa, T., Tagiri, A., Sugimoto, K., et al. (2019). Unleashing floret fertility in wheat through the mutation of a homeobox gene. *Proc. Natl. Acad. Sci. U.S.A.* 116, 5182–5187. doi: 10.1073/pnas.1815465116
- Sandaña, P. A., Harcha, C. I., and Calderini, D. F. (2009). Sensitivity of yield and grain nitrogen concentration of wheat, lupin and pea to source reduction during grain filling. A comparative survey under high yielding conditions. *Field Crops Res.* 114, 233–243. doi: 10.1016/j.fcr.2009.08.003
- Sangha, J. S., Gu, K., Kaur, J., and Yin, Z. (2010). An improved method for RNA isolation and cDNA library construction from immature seeds of *Jatropha curcas* L. *BMC Res. Notes* 3, 126. doi: 10.1186/1756-0500-3-126
- Savin, R., and Slafer, G. A. (1991). Shading effects on the yield of an Argentinian wheat cultivar. *J. Agric. Sci.* 116, 1–7. doi: 10.1017/S0021859600076085
- Scorza, R., May, L. G., Purnell, B., and Upchurch, B. (1991). Differences in number and area of mesocarp cells between small- and large-fruited peach cultivars. *J. Am. Soc. Hortic. Sci. JASHS* 116, 861–864. doi: 10.21273/JASHS.116.5.861
- Scott, W. R., Appleyard, M., Fellowes, G., and Kirby, E. J. M. (1983). Effect of genotype and position in the ear on carpel and grain growth and mature grain weight of spring barley. *J. Agric. Sci.* 100, 383–391. doi: 10.1017/S0021859600033530
- Serrago, R. A., Alzueta, I., Savin, R., and Slafer, G. A. (2013). Understanding grain yield responses to source-sink ratios during grain filling in wheat and barley under contrasting environments. *Field Crops Res.* 150, 42–51. doi: 10.1016/j.fcr.2013.05.016
- Simmonds, J., Scott, P., Brinton, J., Mestre, T. C., Bush, M., Del Blanco, A., et al. (2016). A splice acceptor site mutation in TaGW2-A1 increases thousand grain weight in tetraploid and hexaploid wheat through wider and longer grains. *Theor. Appl. Genet.* 129, 1099–1112. doi: 10.1007/s00122-016-2686-2
- Simmonds, J., Scott, P., Leverington-Waite, M., Turner, A. S., Brinton, J., Korzun, V., et al. (2014). Identification and independent validation of a stable yield and thousand grain weight QTL on chromosome 6A of hexaploid wheat (*Triticum aestivum* L.). *BMC Plant Biol.* 14, 191. doi: 10.1186/s12870-014-0191-9
- Sinclair, T. R., and Jamieson, P. D. (2006). Grain number, wheat yield, and bottling beer: An analysis. *Field Crops Res.* 98, 60–67. doi: 10.1016/j.fcr.2005.12.006
- Slafer, G. A., Foulkes, M. J., Reynolds, M. P., Murchie, E. H., Carmo-Silva, E., Flavell, R., et al. (2023). A ‘wiring diagram’ for sink strength traits impacting wheat yield potential. *J. Exp. Bot.* 74, 40–71. doi: 10.1093/jxb/erac410
- Slafer, G. A., and Savin, R. (1994). Source-sink relationships and grain mass at different positions within the spike in wheat. *Field Crops Res.* 37, 39–49. doi: 10.1016/0378-4290(94)90080-9
- Slafer, G. A., Savin, R., Pinochet, D., and Calderini, D. F. (2021). “‘Wheat,’” in *Crop Physiology. Case Histories for Major Crops*. Eds. V. Sadras and D. F. Calderini (Academic Press, Elsevier, London), 99–145.
- Song, X. J., Huang, W., Shi, M., Zhu, M. Z., and Lin, H. X. (2007). A QTL for rice grain width and weight encodes a previously unknown RING-type E3 ubiquitin ligase. *Nat. Genet.* 39, 623–630. doi: 10.1038/ng2014
- Tao, Y., Trusov, Y., Zhao, X., Wang, X., Cruickshank, A. W., Hunt, C., et al. (2021). Manipulating assimilate availability provides insight into the genes controlling grain size in sorghum. *Plant J.* 108, 231–243. doi: 10.1111/tpj.15437
- Tillett, B. J., Hale, C. O., Martin, J. M., and Giroux, M. J. (2022). Genes Impacting Grain Weight and Number in Wheat (*Triticum aestivum* L. ssp. *aestivum*). *Plants (Basel)* 11. doi: 10.3390/plants11131772
- Ugarte, C., Calderini, D. F., and Slafer, G. A. (2007). Grain weight and grain number responsiveness to pre-anthesis temperature in wheat, barley and triticale. *Field Crops Res.* 100, 240–248. doi: 10.1016/j.fcr.2006.07.010
- Waddington, S. R., Cartwright, P. M., and Wall, P. C. (1983). A quantitative scale of spike initial and pistil development in barley and wheat. *Ann. Bot.* 51, 119–130. doi: 10.1093/oxfordjournals.aob.a086434
- Wang, W., Li, Q., Tian, F., Deng, Y., Wang, W., Wu, Y., et al. (2019). Wheat NILs contrasting in grain size show different expansin expression, carbohydrate and nitrogen metabolism that are correlated with grain yield. *Field Crops Res.* 241. doi: 10.1016/j.fcr.2019.107564
- Wang, W., Simmonds, J., Pan, Q., Davidson, D., He, F., Battal, A., et al. (2018). Gene editing and mutagenesis reveal inter-cultivar differences and additivity in the contribution of TaGW2 homoeologues to grain size and weight in wheat. *Theor. Appl. Genet.* 131, 2463–2475. doi: 10.1007/s00122-018-3166-7
- Wiersma, J. J., Busch, R. H., Fulcher, G. G., and Hareland, G. A. (2001). Recurrent selection for kernel weight in spring wheat. *Crop Sci.* 41, 999–1005. doi: 10.2135/cropsci2001.414999x
- Xie, Q., Mayes, S., and Sparkes, D. L. (2015). Carpel size, grain filling, and morphology determine individual grain weight in wheat. *J. Exp. Bot.* 66, 6715–6730. doi: 10.1093/jxb/erv378
- Xie, Q., and Sparkes, D. L. (2021). Dissecting the trade-off of grain number and size in wheat. *Planta* 254, 3. doi: 10.1007/s00425-021-03658-5
- Yang, Z., Bai, Z., Li, X., Wang, P., Wu, Q., Yang, L., et al. (2012). SNP identification and allelic-specific PCR markers development for TaGW2, a gene linked to wheat kernel weight. *Theor. Appl. Genet.* 125, 1057–1068. doi: 10.1007/s00122-012-1895-6
- Yang, Z., Van Oosterom, E. J., Jordan, D. R., and Hammer, G. L. (2009). Pre-anthesis ovary development determines genotypic differences in potential kernel weight in sorghum. *J. Exp. Bot.* 60, 1399–1408. doi: 10.1093/jxb/erp019
- Yang, X., Wilkinson, L. G., Aubert, M. K., Houston, K., Shirley, N. J., and Tucker, M. R. (2023). Ovule cell wall composition is a maternal determinant of grain size in barley. *New Phytol.* 237, 2136–2147. doi: 10.1111/nph.18714
- Yu, X., Li, B., Wang, L., Chen, X., Wang, W., Wang, Z., et al. (2015). Systematic analysis of pericarp starch accumulation and degradation during wheat caryopsis development. *PLoS One* 10, e0138228. doi: 10.1371/journal.pone.0138228
- Zadoks, J. C., Chang, T. T., and Konzak, C. F. (1974). A decimal code for the growth stages of cereals. *Weed Res.* 14, 415–421. doi: 10.1111/j.1365-3180.1974.tb01084.x
- Zhai, H., Feng, Z., Du, X., Song, Y., Liu, X., Qi, Z., et al. (2018). A novel allele of TaGW2-A1 is located in a finely mapped QTL that increases grain weight but decreases grain number in wheat (*Triticum aestivum* L.). *Theor. Appl. Genet.* 131, 539–553. doi: 10.1007/s00122-017-3017-y
- Zhang, Y., Li, D., Zhang, D., Zhao, X., Cao, X., Dong, L., et al. (2018). Analysis of the functions of TaGW2 homoeologs in wheat grain weight and protein content traits. *Plant J.* 94, 857–866. doi: 10.1111/tpj.13903
- Zuo, J., and Li, J. (2014). Molecular genetic dissection of quantitative trait loci regulating rice grain size. *Annu. Rev. Genet.* 48, 99–118. doi: 10.1146/annurev-genet-120213-092138



OPEN ACCESS

EDITED BY

Gustavo A. Slafer,
Catalan Institution for Research and
Advanced Studies (ICREA), Spain

REVIEWED BY

Sivakumar Sukumaran,
The University of Queensland, Australia
Francis Chuks Ogonnaya,
Grains Research and Development
Corporation, Australia

*CORRESPONDENCE

Elisabetta Frascaroli
✉ elisabetta.frascaroli@unibo.it

RECEIVED 28 February 2024

ACCEPTED 30 May 2024

PUBLISHED 28 June 2024

CITATION

Groli EL, Frascaroli E, Maccaferri M, Ammar K
and Tuberosa R (2024) Dissecting the
effect of heat stress on durum wheat
under field conditions.
Front. Plant Sci. 15:1393349.
doi: 10.3389/fpls.2024.1393349

COPYRIGHT

© 2024 Groli, Frascaroli, Maccaferri, Ammar
and Tuberosa. This is an open-access article
distributed under the terms of the [Creative
Commons Attribution License \(CC BY\)](#). The
use, distribution or reproduction in other
forums is permitted, provided the original
author(s) and the copyright owner(s) are
credited and that the original publication in
this journal is cited, in accordance with
accepted academic practice. No use,
distribution or reproduction is permitted
which does not comply with these terms.

Dissecting the effect of heat stress on durum wheat under field conditions

Eder Licieri Groli¹, Elisabetta Frascaroli^{1*}, Marco Maccaferri¹,
Karim Ammar² and Roberto Tuberosa¹

¹Department of Agricultural and Food Sciences, DISTAL, University of Bologna, Bologna, Italy,

²International Maize and Wheat Improvement Center, CIMMYT, El Batán, Mexico

Introduction: Heat stress negatively affects wheat production in several ways, mainly by reducing growth rate, photosynthetic capacity and reducing spike fertility. Modeling stress response means analyzing simultaneous relationships among traits affecting the whole plant response and determinants of grain yield. The aim of this study was to dissect the diverse impacts of heat stress on key yield traits and to identify the most promising sources of alleles for heat tolerance.

Methods: We evaluated a diverse durum wheat panel of 183 cultivars and breeding lines from worldwide, for their response to long-term heat stress under field conditions (HS) with respect to non stress conditions (NS), considering phenological traits, grain yield (GY) and its components as a function of the timing of heat stress and climatic covariates. We investigated the relationships among plant and environmental variables by means of a structural equation model (SEM) and Genetic SEM (GSEM).

Results: Over two years of experiments at CENEB, CIMMYT, the effects of HS were particularly pronounced for the normalized difference vegetation index, NDVI (-51.3%), kernel weight per spike, KWS (-40.5%), grain filling period, GFP (-38.7%), and GY (-56.6%). Average temperatures around anthesis were negatively correlated with GY, thousand kernel weight TKW and test weight TWT, but also with spike density, a trait determined before heading/anthesis. Under HS, the correlation between the three major determinants of GY, i.e., fertile spike density, spike fertility and kernel size, were of noticeable magnitude. NDVI measured at medium milk-soft dough stage under HS was correlated with both spike fertility and grain weight while under NS it was less predictive of grain weight but still highly correlated with spike fertility. GSEM modeling suggested that the causal model of performance under HS directly involves genetic effects on GY, NDVI, KWS and HD.

Discussion: We identified consistently suitable sources of genetic resistance to heat stress to be used in different durum wheat pre-breeding programs. Among those, Desert Durums and CIMMYT'80 germplasm showed the highest degree of adaptation and capacity to yield under high temperatures and can be considered as a valuable source of alleles for adaptation to breed new HS resilient cultivars.

KEYWORDS

durum wheat, field condition, heat-stress, modeling, yield components

1 Introduction

Wheat (*Triticum* spp.) is one of the most important staple foods for the human diet worldwide. In 2022, wheat has been cultivated in 219.2 million ha worldwide with a total production of over 808.4 million tons (FAO, 2024, <https://www.fao.org/faostat/en>). This makes it the third most important crop in terms of global production. Wheat is cultivated across a wide range of latitudes, from 67° North to 45° South including highly diverse environmental conditions (FAO, 2021). About 10% of wheat production is attributed to durum wheat (*Triticum durum* Desf.), a species of strategic importance in Mediterranean countries. The lower genome content of tetraploid wheat as compared to hexaploid wheat makes durum wheat a simplified proxy to better understand the complex, highly quantitative response of polyploid wheat to environmental factors at a physiological and molecular level (Adamski et al., 2020).

Wheat plays a crucial role in the human diet (Shewry and Hey, 2015), but different environmental conditions, including high temperatures, frequently cause significant yield losses in this crop (Pequeno et al., 2021). The current situation is predicted to become worse, especially due to climate change effects and the resulting increase in temperatures. The Intergovernmental Panel on Climate Change (IPCC) predicts that the increase in temperature will range from 2.7 to 4.8°C by 2100 (IPCC (IPCC, 2023). Semenov and Shewry (2011) predicted that heat stress (HS) will have a stronger negative impact on wheat production in Europe than drought stress. Indeed, it has been reported that, on average, each 1°C of further temperature increase will reduce grain yield in wheat by 6% (Graziani et al., 2014; Asseng et al., 2015; Martre et al., 2017; Zhao et al., 2017).

Heat stress (HS) negatively affects wheat in several ways. It imposes a reduction in photosynthetic capacity (Feng et al., 2014; Posch et al., 2019), an alteration in the plant water relations (Hasanuzzaman et al., 2013) and metabolic activities (Farooq et al., 2011), increases the production of reactive oxygen species (Sharma et al., 2019; Chen and Yang, 2020), and reduces spike fertility and grain filling when occurring at flowering or during the grain filling period (Akter and Islam, 2017; Balla et al., 2019; El Hassouni et al., 2019; Fabian et al., 2019; Balla et al., 2021). At the vegetative stage, the primary effect of HS on wheat is a reduction of seed germination, potentially leading to a poor stand establishment (Hossain et al., 2013; Akter and Islam, 2017). When occurring at tillering, HS negatively affects the survival/growth of fertile tillers, significantly compromising the yield potential of the crop (Poudel et al., 2021; Poudel et al., 2022). According to Porter and Gawith (1999), HS can reduce the number of fertile tillers by 15.38%. Additionally, HS impairs meristem development and reduces plant growth due to leaf senescence and abscission (Balla et al., 2019), and reduction of photosynthesis (Posch et al., 2019) leading to lower biomass production as well as reduced grain yield.

Although HS has a significant impact on plants during vegetative stages (seedling growth, tillering and stem elongation), it is during the reproductive stages (booting, flowering, and grain filling) that has a more pronounced effect on plant development, fertility, and crop performance (Akter and Islam, 2017; Hussain

et al., 2018; Telfer et al., 2018; Balla et al., 2019; Fabian et al., 2019; Sharma et al., 2019; Balla et al., 2021). According to Porter and Gawith (1999), the negative effect of HS depends on the timing, duration, and magnitude of the stress imposed on the plants. The optimal temperatures for plant growth and function vary depending on the developmental stage of the plant. The optimal temperature for wheat growth is around 21°C during anthesis and grain filling. In an extensive review, Porter and Gawith (1999) reported that wheat can withstand up to 31°C at anthesis and 35.4°C during grain filling, when even a short period of stress might seriously damage grain yield and yield components. Additionally, HS at anthesis reduces pollen fertility and/or its viability and growth leading to poor fertilization as well as abnormal ovary development, hence reducing seed setting and the number of kernels per spike (Djanaguiraman and Prasad, 2014; Fabian et al., 2019; Ullah et al., 2022) hence grain yield directly. After anthesis ('terminal stress'), HS reduces thousand kernel weight and volumetric weight (Rehman et al., 2021).

Depending on the timing and duration, HS can directly affect plant development, hence phenology and more specifically tillering, time of heading and flowering, particularly under conditions of early HS and relatively high night and day temperatures during early development (Mamrutha et al., 2020). On the opposite, variation for heading date caused by genetic determinants other than heat stress (e.g., photoperiod response, vernalization response), indirectly affects HS response and should be considered as a co-variate, rather than a directly causing the physiological response (Tuberosa, 2012). As pointed out by van Eeuwijk et al. (2019) traits related to phenology such as flowering time can make it difficult to evaluate and dissect the genetic control of other traits that are indirectly influenced by phenology itself. Moreover, breeders are interested in defining the causal relationship among the traits involved in stress tolerance, to define which traits to consider for predicting breeding values. This knowledge can be also be deployed to reduce the number of traits to consider for GY prediction (Abdalla et al., 2021; Powell et al., 2021).

Structural Equation Models (SEM) (Wright, 1921) can be applied to study relationships among phenotypes in multivariate systems and can produce an interpretation of relationships among traits different from that obtained with standard multiple trait models, where all relationships are represented by linear associations among random variables. Unlike in multiple trait models, in SEM a given trait can be treated as a predictor of another one, providing a functional (causal) link between both (Rosa et al., 2011). SEM has been described and used in quantitative genetics models (Gianola and Sorensen, 2004), pre-selecting the causal relationships based on prior knowledge. More recently, Valente et al. (2013) proposed searching for recursive causal structures in the context of mixed models for the genetic analysis of multiple traits, showing that it may be possible to infer phenotypic networks and causal effects even without QTL or marker information (Rosa et al., 2011). In SEM a primary trait can be modeled in terms of its component traits, as in factorial regression and crop growth models, but they are also suitable for modeling other biological components of traits (van Eeuwijk et al., 2019) which can be considered in designing an ideotype, helping

breeders to define a selection strategy. Network models can be extended to multiple environments since variation in genetic correlations between traits across environmental conditions is an important cause of G×E and SEM could make such changes visible in a biologically meaningful way (Topner et al., 2017; Momen et al., 2019; van Eeuwijk et al., 2019; Kruijer et al., 2020; He et al., 2021).

This study was designed to evaluate the response to crop cycle-long heat stress under field conditions with respect to non stressed optimal conditions in a diverse durum wheat panel from different countries. The aim of this study was to dissect the diverse impacts of heat stress on key yield traits and to identify the most promising sources of alleles for heat tolerance. We considered phenological traits, grain yield and its components as a function of the extent of heat stress and weather covariates. We investigated the use of different SEMs to identify a network of traits that could help in the identification of heat tolerant genotypes. We took into account the genetic population structure and origin of the analyzed germplasm, drawing on a collection representing genetic diversity from around the world, to identify those to be considered as suitable sources of genetic tolerance to heat stress for use in durum wheat breeding programs.

2 Materials and methods

2.1 Genetic materials

The plant material used in this study consisted of a durum wheat diversity panel (namely UNIBO-Durum Panel) of 183 accessions (cultivars and elite breeding lines) from Mexico (CIMMYT), USA and Mediterranean countries (Italy, Morocco, Spain, Syria, Tunisia), which were selected from a larger panel (336 accessions) based on their pedigree and heading date to minimize variation due to phenology while maximizing variation in origins. Accordingly, accessions with high identity-by-descent value based on pedigree and molecular markers data (Maccaferri et al., 2007b; Maccaferri et al., 2007a) and/or with differences higher than 7 days in heading date in Mediterranean countries (Maccaferri et al., 2011) were excluded to reduce possible bias caused by phenology. Additional information about UNIBO-Durum Panel is reported in (Maccaferri et al., 2005; Maccaferri et al., 2007a; Maccaferri et al., 2007b). Additionally, five elite cultivars used as parental lines in different Recombinant Inbred Lines (RILs) populations at CIMMYT and the University of Bologna were added to the experiment in order to evaluate their response to HS (Supplementary Table 1) (Condorelli et al., 2018).

2.2 Environment characterization

The field experiment was carried out at the Campo Experimental Norman E. Borlaug (CENEB), CIMMYT's experimental station, near Ciudad Obregon (Sonora) located in northwest Mexico (27° 33' N; 109° 09' W; 38 masl) (Honsdorf et al., 2020). The weather at the CENEB station is characterized by an arid climate with highly variable rainfall (Verhulst et al., 2011). The

annual mean temperature is approximately 23.5°C ranging from 16.0°C in January to 31.0°C in July (Honsdorf et al., 2020). Based on the World Reference Base (Verhulst et al., 2009), classified the soil at CENEB location as a Hyposolic Vertisol (Calcic, Chromic), with low soil organic matter (SOM < 12 g kg⁻¹ of soil) as well as slight alkalinity (pH 8) which is well within the non-toxic range for wheat. According to the world Mega-Environments (MEs) classification system developed by CIMMYT, the CENEB location includes ME1 (temperate, completely irrigated optimal conditions) when wheat is sown at optimal time (November 15–December 15) and ME5 (high heat exposure with non-water limiting conditions) when wheat is planted late (February 15–March 1) for heat tolerance evaluation (Mondal et al., 2013). Meteorological data from the 2017/18 and 2018/19 were collected at a meteorological station approximately 2 km from the experimental area.

2.3 Experimental design and field evaluation

The UNIBO durum panel was evaluated in two crop seasons (2017/18, 2018/19 – referred to as 2018 and 2019 hereafter, respectively) as well as two different environmental conditions, namely (i) control (non-stressed NS) with optimal sowing date, last week of November/first week of December, and (ii) heat-stressed (HS) with late sowing date, last week of February/first week of March to expose plants to higher than the normal temperature during their entire cycle.

The experiment was carried out in a complete randomized block design with two replicates, arranged in a rectangular grid with 10 rows by 56 columns. Each experimental unit (plots) consisted of two rows of 2.1 meters accounting for a plot area of 1.68 m². Plot management, including fertilizer regimes, weed, pest, and disease control followed CIMMYT agronomic practices to optimize growing conditions regardless of testing environment and maintain plots free of weeds and diseases or pests. To avoid any confounding effects due to drought stress, plants received at least four auxiliary irrigations per season using a furrow irrigation system.

The following traits were measured and are described in details in Supplementary Table 2: days to heading (HD), days to maturity (DTM), grain filling period (GFP), plant height (PH), number of spikes per linear meter (SPM), kernel number per spike (KNS), kernel weight per spike (KWS), number of spikelets per spike (SKT), grain yield (GY), thousand kernel weight (TKW), test weight (TWT), kernel length (KLE) and kernel width (KWI). Additionally, as a proxy for total biomass, normalized difference vegetation index (NDVI) was estimated on different dates during the whole cycle for both experiments (NS, HS) and for both crop seasons. NDVI was estimated with individual measurements during the vegetative and grain filling growth stages as reported in Supplementary Table 3. NDVI was measured by canopy reflectance using the GreenSeeker RT100 equipment (Optical Sensor Unit, NTECH Industries, Inc.). After performing all individual measurements, for each experiment we chose the single most significant NDVI measurement identified by ANOVA to

represent the trait, which corresponded to the reading taken at Zadoks stage 75–83, corresponding to medium milk-soft dough stage (Supplementary Table 3) (Zadoks et al., 1974). Furthermore, the four most significant NDVI measurements were used to derive an index (IT_NDVI), calculating the area under NDVI progress curve by adapting equation (Equation 1) reported in (Simko and Piepho, 2012).

$$IT_NDVI = \sum_{i=1}^{n-1} \left(\left(\frac{NDVI_i + NDVI_{i+1}}{2} \right) * (GDD_{i+1} - GDD_i) \right) \quad (1)$$

Where: $NDVI_i$ is NDVI at i^{th} measurement; GDD_i is accumulated growing degree days at the i^{th} measurement and n is the total number of measurements. GDD refers to the number of heat units, degree days in °C, required for a crop to progress from stage 1 to stage X. In this study we used the method proposed by Davidson and Campbell (1983) (Equation 2).

$$GDD = \sum \left(\left(\frac{T_{max} + T_{min}}{2} \right) - T_b \right) \quad (2)$$

Where: GDD is growing degree days in °C; T_{max} is maximum daily temperature; T_{min} is the minimum daily temperature in °C; T_b is base temperature, for wheat is 0°C). The chosen NDVI measurements, either for the NDVI or for the IT_NDVI, were almost at the same GDD accumulation level (Supplementary Table 3).

2.4 Weather parameters

To monitor the environmental conditions specific of each genotype based on its specific phenological stage, four additional temperature parameters were calculated independently for each single plot within each experimental condition as described by (Telfer et al., 2018). According to Dreccer et al. (2008), the anthesis period is defined as the period from 300 GDD before to 100 GDD post-anthesis time. Similarly, the grain filling period is defined as the period from 100 GDD to 600 GDD post-anthesis time. We did not collect data for anthesis time, and for the purpose of this study we considered HD as a rough indicator of the beginning of anthesis period. The following temperature-derived variables were calculated for anthesis (A) as well the as for grain filling (GF) growth stage as described above. The temperature-derived variables used to quantify the duration and intensity of heat stress were: average maximum temperature (AMT), number of days with temperature > 30°C (NDTH30), number of days with temperature > 35°C (NDTH35) and heat degree days (HDD) (Table 1). HDD was estimated by adapting the equation of (Liu et al., 2016) (Equation 3).

$$HDD = \sum (T_{max} - T_h) \quad (3)$$

Where: HDD is the accumulated heat degree days in °C; T_{max} is the maximum daily temperature in °C; T_h is the temperature threshold for heat stress. Considering the results obtained from the literature (Farooq et al., 2011; Liu et al., 2016; Liu et al., 2016; Telfer et al., 2018) we defined 30°C as the temperature threshold for heat stress.

TABLE 1 Weather variables calculated independently for each single plot to determine the heat stress experienced by plants from yield trials conducted under in Non-Stressed control and late planted Heat Stressed conditions involving the UNIBO-Durum Diversity Panel evaluated at CENEB-Cd. Obregon, Mexico, in 2018 and 2019.

Growth stage	Range of degree days
Anthesis (A)	300°C days before to 100°C post anthesis
Grain filling (GF)	100°C days to 600°C post anthesis
Weather variables ¹	Description
AMT_A and AMT_GF	Average maximum temperature (°C);
NDTH30_A and NDTH30_GF	Number of days with temperature > 30°C
NDTH35_A and NDTH35_GF HDD_A and HDD_GF	Number of days with temperature > 35°C Heat stress Degree Days °C

¹ _A and _GF: indicate Anthesis and Grain Filling, respectively.

2.5 Statistical analyses

2.5.1 Data analyses

Analyses were performed separately for the different treatments, control (non-stress, NS) and heat-stress (HS), in two crop seasons (2018 and 2019) as well as jointly. The best linear unbiased estimates (BLUEs) for each trait in each treatment and year were calculated using the following mixed model (Equation 4):

$$y_{ijkl} = \mu + g_i + t_j + s_{k(j)} + r_{l(jk)} + (g \times t)_{ij} + (g \times s)_{ik(j)} + (g \times t \times s)_{ijk(j)} + \epsilon_{ijkl} \quad (4)$$

where y_{ijkl} is the observed trait, μ is the overall mean, g_i is the fixed effect of the genotype, t_j is the fixed effect of the treatment, $s_{k(j)}$ is the random effect of the season (year) within the treatment, $r_{l(jk)}$ is the random effect of the replicate within the treatment, and the year and ϵ_{ijkl} is the residual assumed to be normally and independently distributed (0, σ^2). BLUEs were calculated using the *lmer4* package (Bates et al., 2015).

The statistical analysis was also performed within treatments with the following linear model (Equation 5):

$$y_{ikl} = \mu + g_i + s_k + r_{l(k)} + (g \times s)_{ik} + \epsilon_{ikl} \quad (5)$$

Broad-sense heritability for each treatment as well as crop season was calculated with the equation (Equation 6) using the function repeatability of the package repeatability (Wolak et al., 2012) in R software.

$$h^2 = \frac{\sigma_g^2}{\sigma_g^2 + \frac{\sigma_e^2}{r}} \quad (6)$$

Where: h^2 is the broad-sense heritability, σ_g^2 and σ_e^2 are the genotype and error variance, respectively, and r is the number of replicates.

For the combined analysis, broad-sense heritability was calculated as (Equation 7) using the same function and software previously described.

$$h^2 = \frac{\sigma_g^2}{\sigma_g^2 + \frac{\sigma_{gs}^2}{s} + \frac{\sigma_{sr}^2}{sr}} \quad (7)$$

Where the new term σ_{gs}^2 is the genotype \times season interaction and s is the number of seasons (years) in the experiment.

2.5.2 Relationships among traits and structural equation models

Relationships among phenotypic traits were studied within each environmental condition (treatment), *i.e.*, control (non-stress, NS) and heat-stress (HS) treatments. The BLUEs were then used in all the subsequent analyses as adjusted phenotypic means. The relationships among all variables, *i.e.*, both plant traits and environmental covariates, were first evaluated by using Pearson phenotypic correlation calculated within treatment. To investigate the role of correlated traits in determining the final yield in the NS and in the HS environment, *i.e.*, to choose the most important traits to be included in a multi-trait model, the stepwise regression and LASSO (least absolute shrinkage and selection operator) (Tibshirani, 1996, Tibshirani, 2011) allowed us to select a subset of variables according to the results obtained and to previous knowledge. In addition, structural equation modeling (Gleason et al., 2019) was used to represent the relative importance of the yield component under NS and HS conditions. The final set of variables was combined into a SEM, where traits were treated as predictors (exogenous) or responses (endogenous) in a system of simultaneous equations, hence allowing us to establish functional (causal) links between phenotypes. The initial phenotypic SEM model was tested and then subjected to optimization by removing non-significant paths, one path at a time, in model testing and selection (He et al., 2021). For individual traits in the SEM the R^2 statistic was calculated. Analyses were performed using the R package *lavaan* (Rosseel, 2012). Finally, based on SEM path coefficients, the net effects for each trait were estimated for both NS and HS environments.

In addition, the causal genotypic effects of traits on yield were investigated using Genetic-SEM (GSEM), as proposed by Kruijer et al. (2020) and implemented in the R package *pcgen*. The GSEM model was investigated by using the BLUEs from the two years for each stress treatment and assuming a threshold alpha at $P = 0.01$, obtained by bootstrapping. Only traits with direct or indirect genotypic effect on yield were retained in the final model and proposed as informative for prediction.

2.5.3 Identification of sources of genetic tolerance to heat stress

Genotypes considered to be possible sources of genetic tolerance to heat stress were identified as those better performing under high temperature and/or those that registered the smallest decline from the NS to the HS treatment. Moreover, in the attempt to take into account the different phenology observed in the present study, performances were estimated as marginal means after adjusting for HD as covariate. We then fitted the BLUE data of

HS and NS in the two seasons to a linear model including genotypes and HD as GDD as covariate, and calculating the marginal means with the package *emmeans* in R (Lenth, 2024).

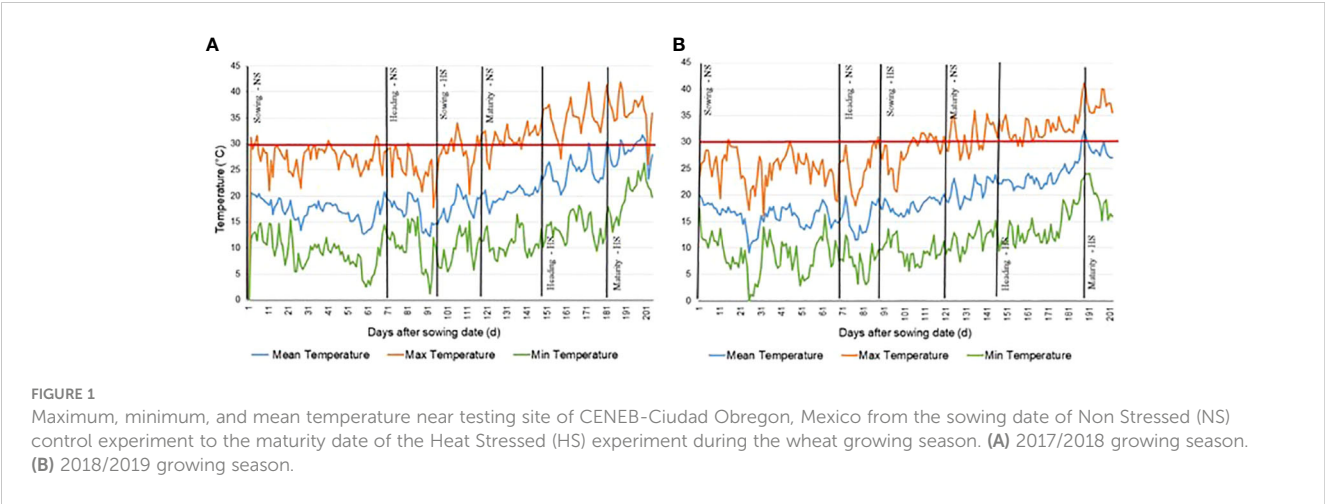
3 Results

3.1 Effect of the growing conditions

The first aim of this study was to evaluate the effect of increased temperatures on morpho-physiological traits relevant to grain yield and yield components, and their relationship with environmental parameters, using a panel of durum wheat of diverse origins. The elite durum panel previously assembled at the University of Bologna (Maccaferri et al., 2005, Maccaferri et al., 2011) was evaluated in Obregon, Mexico, under field conditions in two contrasting environments, namely, timely-sown, optimal growth and management conditions (control or not stressed, NS) and late-sown with otherwise optimal management conditions, simulating a scenario of long exposure to supra-optimal temperatures and heat stress (HS) during all growing stages.

The difference in GDD and HDD accumulation across two consecutive crop seasons were considered. Figure 1 reports the minimum, maximum and mean temperature during both crop seasons and shows that in 2018 the maximum temperature frequently, and right around heading, reached levels above 35°C during the grain filling period (GFP) in the HS experiment where values > 40°C were recorded in several days. This was the most important factor influencing the higher accumulation of HDD in 2018. On the other hand, the maximum temperature did not reach 35°C until the end of the plant growth cycle in 2019. The difference in HDD is thus one of the most important environmental parameters, accounting for the differences in phenotypic values for all traits in crop season 2018 when compared with the 2019 crop season. Plants evaluated over 2018 and 2019 accumulated different amounts of GDD and HDD to reach HD and DTM phenological growth stage (Table 2).

Slightly higher levels of GDD were observed in the NS treatment than in the HS, for both time to heading and time to maturity. However, the late sowing-generated heat stress did not have a very pronounced effect on GDD, with about 15.0% of difference in GDD between the timely and late planting treatments. The HDD was lower in NS than in HS for both HD and DTM, with late sowing dramatically increasing HDD, especially when considering DTM. This result is obviously consistent with a higher level of temperature stress in the late sowing trials. The level of heat stress was slightly different in the two years, more pronounced in 2018 than in 2019. HDD accumulation was more pronounced in 2018 with 32.8% more HDD from sowing to HD and 42.8% from sowing to DTM (Table 2). However, since the mean square for the year \times treatment interaction was consistently lower than those for year and treatment for all traits (Table 3), we hereafter report the analyses combined over years.



3.2 Phenotypic field response to heat stress

The analysis of variance (ANOVA) showed significant effects for all single factors (year, treatment, and genotype) as well as for all interactions (genotype x treatment, year x genotype, year x treatment, year x genotype x treatment) for almost all traits Table 3. Summary statistics combined over years are reported in Table 4, while the results for a single year and a single treatment are reported in Supplementary Tables 4, 5. The heat stress experienced by plants during both crop seasons significantly reduced the phenotypic value for all traits. The effect of heat stress was particularly pronounced for GY (-56.6%), NDVI as a proxy measurement for total biomass (-51.3%) and KWS (-40.5%). All yield components were affected, from SPM (-23.9%) through KNS (-29.2%) to TKW (-14.7%). It also substantially affected phenological traits with reductions of 25.8% for HD, 30.6% for DTM and 38.7% for GFP. TWT (-2.8%) and other kernel shape measurements (KLE, -2.7% and KWI, -7.6%) were the least affected.

3.3 Relationship among traits and modeling of the stress response

Phenotypic correlations among plant traits in NS and HS treatments are presented numerically in Table 5 and graphically

in Supplementary Figure 1. The analysis of relationships among traits revealed that the phenological parameters (HD, DTM) were negatively, but weakly, correlated with GY in both testing conditions, suggesting a very weak trend that earlier genotypes were, to some extent, higher yielding than later ones under optimal conditions, a trend that maintained its small magnitude under HS. On the other hand, the association between phenological parameters and the most important kernel characteristics (TKW and TWT) indicated a different dynamic. Correlations of intermediate magnitude indicated that genotypes heading or maturing earlier generally had larger kernels with greater test weights under non-stressed conditions. These relationships changed under heat stress, with no significant association observed between HD and TKW and a reversed positive, albeit very weak, association between DTM and TKW. The intermediate strong associations between phenological parameters and TWT observed under NS conditions were maintained under HS but with an observable or substantial decrease in magnitude. There was no association detected between phenological parameters and spike number (SPM) under NS conditions, while a weak negative association was detected between HD and SPM under HS suggesting, to a small extent, that earlier genotypes tended to produce more spikes than later ones. Both phenological parameters were strongly and positively associated with spike size, as determined by SKT, under NS and, to a somewhat smaller extent, under HS conditions, indicating a strong and across-environment

TABLE 2 Growing degree days (GDD) and heat degree days (HDD) accumulated up to heading (HD) and maturity (DTM) by plants from yield trials conducted under in Non-Stressed (NS) control and late planted Heat Stressed (HD) conditions involving the UNIBO-Durum Diversity Panel evaluated at CENEB-Cd. Obregon, Mexico, in 2018 and 2019.

Evaluation condition (Treatment)	Trait	GDD (d)			HDD (d)			Difference in GDD between years		Difference in HDD between years	
		2018	2019	Mean	2018	2019	Mean	%		%	
NS	HD	1481.7	1360.2	1421.0	6.6	0.8	3.7	8.2		87.9	
	DTM	2280.0	2296.6	2288.3	26.1	25.9	26.0	0.7		0.8	
HS	HD	1251.0	1202.5	1226.8	93.0	62.5	77.8	3.9		32.8	
	DTM	1912.5	1896.9	1904.7	230.5	131.8	181.2	0.8		42.8	

TABLE 3 Summary, two-years combined, ANOVA for days to heading (HD), days to maturity (DTM), grain filling period (GFP), plant height (PH), grain yield (GY), thousand kernel weight (TKW), test weight (TWT), spikes per linear meter (SPM), spikelets per spike (SKT), kernel number per spike (KNS), kernel weight per spike (KWS), kernel length (KLE), kernel width (KWI), normalized difference vegetation index (NDVI), and area under heat stress progress curve for NDVI (IT_NDVI) collected on plants from yield trials conducted under in Non-Stressed control and late planted Heat Stressed conditions involving the UNIBO-Durum Diversity Panel evaluated at CENEB-Cd. Obregon, Mexico, in 2018 and 2019.

Mean squares							
Trait	Year	Treatment	Genotype	GenxTreat ¹	YearxGen	YearxTreat	YearxGenx-Treat
HD	24.0***	165203***	176.0***	31.0***	7.0***	467.0***	5.0***
DTM	11657***	580606***	119.0***	24.0***	6.0***	1771***	4.0***
GFP	10367***	124619***	23.0***	17.0***	7.0***	480.0***	8.0***
PH	12087***	263490***	481.0***	103.0***	29.0***	6.0ns	19.0***
GY	456.0***	4780***	3.1***	0.8***	0.7**	49.0***	0.5***
TKW	12724***	26371***	156.0***	35.0***	8.0***	1356***	5.0***
TWT	32.0***	1968***	19.0***	3.0***	1.0***	96.6***	0.67***
SPM	13848***	329166***	755.0***	298.0***	228.0***	1664***	166.0**
SKT	336.0***	2503***	11.0***	4.0***	2.0***	216.0***	1.0***
KNS	14005***	94141***	279.0***	54.0***	32.0***	2539***	23.0***
KWS	164.0***	594.0***	0.7***	0.2.0***	0.1***	3.0***	0.1*
KLE	0.3***	17.0***	0.5***	0.03***	0.01***	8.3***	0.01***
KWI	3.0***	27.0***	0.1***	0.02***	0.005***	0.003ns	0.004**
NDVI	0.57***	57240***	0.017***	0.009***	0.004***	0.022***	0.003***
IT_NDVI	6639333***	12181038***	4596***	2137***	865.0***	3178566***	905.0***

¹ Genxtreat, genotype per treatment interaction; YearxTreat, year per treatment interaction, and YearxGenxTreat, year per genotype per treatment interaction.
***P-v alue< 0.001, **P-value< 0.01, *P-value< 0.05, ns, not significant at P< 0.05.

TABLE 4 Two-years combined summary statistics for days to heading (HD), days to maturity (DTM), grain filling period (GFP), plant height (PH), grain yield (GY), thousand kernel weight (TKW), test weight (TWT), spikes per linear meter (SPM), spikelets per spike (SKT), kernel number per spike (KNS), kernel weight per spike (KWS), kernel length (KLE), kernel width (KWI), normalized difference vegetation index (NDVI), and area under heat stress progress curve for NDVI (IT_NDVI), observed in a yield trials conducted under in Non-Stressed control and late planted Heat Stressed conditions involving the UNIBO-Durum Diversity Panel evaluated at CENEB-Cd.

Trait	Non Stressed					Heat Stressed					% of change ⁴
	Mean	Range	Std ¹	CV (%) ²	h ² ³	Mean	Range	Std	CV (%)	h ²	
HD (d)	80.3	67.0–108.0	6.60	2.71	0.97	59.6	52.0–84.0	3.84	2.54	0.95	25.8
DTM (d)	126.9	116.0–147.0	6.51	1.80	0.74	88.1	80.0–104.0	4.19	2.13	0.86	30.6
GFP (d)	46.8	32.0–59.0	4.62	9.64	0.21	28.7	18.0–40.0	3.26	10.44	0.43	38.7
PH (cm)	83.6	60.0–150.0	11.17	5.23	0.93	57.5	30.0–105.0	8.38	7.68	0.82	31.2
GY (t/ha)	6.2	2.9–10.3	1.26	13.13	0.34	2.7	0.2–5.4	0.94	21.90	0.72	56.6
TKW (g)	56.1	37.1–71.6	5.92	3.74	0.92	47.8	30.7–65.7	6.21	4.56	0.70	14.7
TWT (kg/hL)	80.4	70.2–83.9	1.76	0.84	0.96	78.1	70.7–82.3	1.81	1.13	0.91	2.8
SPM (n)	122.0	82.0–190.0	18.57	11.66	0.65	92.8	48.0–138.0	15.48	13.44	0.53	23.9

(Continued)

TABLE 4 Continued

Trait	Non Stressed					Heat Stressed					% of change ⁴
	Mean	Range	Std ¹	CV (%) ²	<i>h</i> ² ³	Mean	Range	Std	CV (%)	<i>h</i> ²	
SKT (n)	18.4	14.2–28.0	2.15	7.08	0.74	15.9	12.2–20.0	1.29	5.55	0.82	13.8
KNS (n)	53.7	31.2–84.5	9.49	9.16	0.77	38.0	14.7–65.2	6.75	10.88	0.83	29.2
KWS (g)	3.1	1.6–4.8	0.59	9.40	0.55	1.8	0.5–3.3	0.42	11.76	0.50	40.5
NDVI	7.6	6.6–8.5	0.28	1.14	0.95	7.4	6.4–8.2	0.29	1.51	0.91	2.7
IT_NDVI	3.5	3.1–3.9	0.15	1.59	0.91	3.2	2.7–3.8	0.15	2.02	0.89	7.6
KLE (mm)	0.8	0.546–0.870	0.04	4.92	0.64	0.4	0.163–0.727	0.10	20.44	0.73	51.3
KWI (mm)	435.9	208.2–598.6	114.12	29.81	0.20	257.3	122.6–418.0	52.49	16.58	0.64	41.0

1 std, standard deviation. 2 CV (%), coefficient of variation. 3 *h*², broad-sense heritability. 4% of change, percentage of variation in heat stress treatment relative to value under optimal conditions.

trend that later heading and/or maturing genotypes tended to produce more spikelets per spikes and therefore larger spikes, regardless of heat stress. The relationships between phenological traits and biomass indicators (NDVI and IT-NDVI) were among the strongest observed under NS and, while somewhat decreased in magnitude under HS for HD, they were maintained, indicating that later and/or later-maturing genotypes tended to produce more biomass in normal conditions as well as under heat.

To adjust for differences in phenology among the diverse genotypes included in the panel, we performed again the analysis for all traits using HD as covariate. To get HD-unbiased indications of trends, the adjusted data (marginal means) were again inspected for correlation patterns (Supplementary Figure 2). The adjusted correlation data clearly pointed out that under non-stressed conditions GY was primarily and positively associated with spike size and fertility (GY-SKT, *r* = 0.79; GY-KNS, *r* = 0.77), with kernel size (GY-TKW, *r* = 0.25; GY-KWS, *r* = 0.85) and moderately but negatively associated with spike number (GY-SPM, *r* = -0.29). This indicated that with bigger and more fertile spikes, producing larger grains and generally having less spikes per area, tended to be those which yielded the most under optimal conditions. Under the heat stress condition of this experiment, the association between GY spike size/fertility (SKT, KNS) or kernel size (KWS, TKW), was either lower or similar in magnitude (GY-SKT, *r* = 0.37; GY-KNS, *r* = 0.59; GY-KWS, *r* = 0.77; and GY-TKW, *r* = 0.59). The association with spike number was significantly modified under heat becoming moderately positive (GY-SPM, *r* = 0.36). The adjustment for HD covariate made a considerable difference in detecting the association between GY and biomass indicators (NDVI and IT_NDVI) under NS conditions. Although no significant correlation was initially found between GY and biomass indicators under optimal conditions using the non-adjusted data, the adjustment revealed a very strong positive association between these traits. This indicates that, with similar phenology, genotypes with higher biomass production tend to have higher yields (GY-NDVI, *r* = 0.88; IT_NDVI, *r* = 0.87). Under heat stress, the adjustment transformed weak positive correlations into very strong ones (GY-NDVI, *r* = 0.77; IT_NDVI, *r* = 0.78), confirming that the

relationship between GY and biomass indicators persists even under thermal stress. NDVI measured at medium milk-soft dough stage under non-stressed conditions was only weakly associated with grain weight (TKW-NDVI, *r* = 0.25) but highly correlated with spike fertility (KNS-NDVI, *r* = 0.78). Under HS however, the biomass indicator became strongly associated with grain weight (TKW-NDVI, *r* = 0.74), maintaining a relatively robust association with spike fertility parameters (SKT-NDVI, *r* = 0.49; KNS-NDVI, *r* = 0.44).

Table 6 reports the correlations between original non-adjusted phenotypic traits and weather variables. Under both NS and HS conditions, GY and temperature-related variables showed always negative correlations, but very weak, if at all significant. The associations involving PH or TKW were moderate under NS conditions and non-significant under HS. SPM, weakly correlated with temperature variables in grain fill under NS, became slightly negatively correlated under heat. All other yield components showed generally low correlations with weather variables, especially under HS. TWT was variably correlated with temperature variables under NS, especially to those indicative of high temperatures during grain fill, but showed correlation generally non-significant in HS condition. In terms of the biomass indicators, NDVI and IT_NDVI showed the highest magnitude associations with temperature derived variables, more so with those related to temperatures during grain fill under non-stressed conditions and these associations remained significant under heat stress, albeit with a reduced strength.

After considering direct or simple correlations between variables and to better understand the complex picture of the factors involved and their interactions, multiple models were considered. Stepwise regression and LASSO were used to evaluate which traits were the best predictors for GY under the two testing conditions and the best set of variables for the comparison between NS and HS environments (Table 7). Results from the stepwise regression showed that in non-stress conditions, 11 out of 22 traits were retained, with the Adj. *R*². *i.e.*, the *R*² adjusted for the number of traits, increasing from 0.441 to 0.453 while under heat stress conditions, 12 of the 23 traits resulted in an increased Adj. *R*² from

TABLE 5 Pearson correlation coefficient between traits observed under in Non-Stressed Control (below diagonal) and under late planted Heat Stress (above diagonal) conditions in a durum diversity panel (N=187) evaluated at CENEB-Cd Obregon, Mexico in 2018 and 2019 (values are 2-years average BLUEs). Traits: days to heading date (HD), days to maturity (DTM), grain filling period (GFP), plant height (PH), grain yield (GY), thousand kernel weight (TKW), test weight (TWT), spikes per linear meter (SPM), spikelets per spike (SKT), kernel number per spike (KNS), kernel weight per spike (KWS), kernel length (KLE), kernel width (KWI), normalized difference vegetation index (NDVI), and area under heat stress progress curve for NDVI (IT_NDVI).

		Heat Stressed														
		HD	DTM	GFP	PH	GY	TKW	TWT	SPM	SKT	KNS	KWS	KLE	KWI	NDVI	IT_NDVI
Non Stressed	HD		0.82**	-0.03ns	-0.03ns	-0.29**	-0.04ns	-0.35**	-0.23**	0.54**	-0.01ns	-0.10ns	-0.04ns	-0.01ns	0.56**	0.50**
	DTM	0.93**		0.54**	0.27**	-0.06ns	0.21**	-0.22**	-0.10ns	0.57**	0.08ns	0.13ns	0.02ns	0.22**	0.77**	0.71**
	GFP	-0.69**	-0.37**		0.51**	0.32**	0.43**	0.14ns	0.15 *	0.22**	0.17 *	0.36**	0.09ns	0.42**	0.53**	0.52**
	PH	0.45**	0.44**	-0.27**		0.51**	0.24**	0.36**	0.40**	0.13ns	0.26**	0.37**	-0.03ns	0.18 *	0.47**	0.47**
	GY	-0.20**	-0.25**	0.02ns	-0.05ns		0.29**	0.49**	0.58**	-0.05ns	0.49**	0.64**	0.19 *	0.09ns	0.36**	0.44**
	TKW	-0.42**	-0.44**	0.21**	-0.25**	0.18**		0.07ns	0.02ns	-0.02ns	-0.23 *	0.31**	0.65**	0.82**	0.32**	0.33**
	TWT	-0.49**	-0.51**	0.24**	-0.09ns	0.43**	0.26**		0.47**	-0.12ns	0.30**	0.36**	-0.14ns	-0.11ns	0.11ns	0.12ns
	SPM	0.12ns	0.10ns	-0.10ns	0.49**	0.11ns	-0.28**	0.01ns		-0.10ns	0.16 *	0.18 *	0.02ns	-0.12ns	0.19 *	0.28**
	SKT	0.75**	0.77**	-0.37**	0.37**	-0.16**	-0.45**	-0.45**	-0.01ns		0.31**	0.27**	-0.07ns	-0.02ns	0.45**	0.42**
	KNS	0.19**	0.17 *	-0.15 *	0.02ns	0.19**	-0.46**	0.06ns	-0.31**	0.35**		0.82**	-0.23 *	-0.24 *	0.25**	0.25**
	KWS	-0.13ns	-0.17 *	0.01ns	-0.16 *	0.36**	0.28**	0.28**	-0.55**	0.02ns	0.69**		0.16 *	0.18 *	0.36**	0.38**
	KLE	-0.09ns	-0.17 *	-0.10ns	-0.17 *	0.06ns	0.61**	-0.21**	-0.13ns	-0.19 *	-0.32 *	0.14 *		0.32**	0.11ns	0.17 *
	KWI	-0.38**	-0.36**	0.24**	-0.18 *	0.08ns	0.87**	0.24**	-0.29**	-0.37**	-0.41**	0.22**	0.29**		0.18 *	0.20**
	NDVI	0.75**	0.73**	-0.45**	0.15 *	0.06ns	-0.26**	-0.29**	0.02ns	0.53**	0.16 *	-0.06ns	-0.02ns	-0.28 *		0.95**
	IT_NDVI	0.79**	0.78**	-0.45**	0.21**	0.04ns	-0.28**	-0.28**	0.01ns	0.56**	0.20**	-0.02ns	-0.07ns	-0.28**	0.92**	

*p<0.1; **p<0.05; ***p<0.01; ns, non significant.

TABLE 6 Pearson correlation coefficient between plant traits (see text for description) measured in yield trials conducted under in Non-Stressed control and late planted Heat Stressed conditions involving the UNIBO-Durum Diversity Panel evaluated at CENEB-Cd. Obregon, Mexico, in 2018 and 2019 and weather variables: average maximum temperature at anthesis (AMT_A) and grain filling period (AMT_GF), number of days with temperature higher than 30°C at anthesis (NDTH30_A) and grain filling period (NDTH30GF), number of days with temperature higher than 35°C at anthesis (NDTH35_A) and grain filling period (NDTH35_GF), and heat degree days at anthesis (HDD_A) and grain filling period (HDD_GF).

	AMT_ A	AMT_ GF	NDTH 30_A	NDTH 35_A	NDTH 30_GF	NDTH 35_GF	HDD_ A	HDD_ GF
Non Stressed								
HD	0.39**	0.73**	0.55**		0.97**	0.73**	0.24**	0.97**
DTM	0.33**	0.65**	0.51**		0.90**	0.69**	0.21**	0.90**
GFP	-0.33**	-0.54**	-0.39**		-0.67**	-0.48**	-0.18 *	-0.65**
PH	0.20**	0.29**	0.35**		0.48**	0.24**	0.21**	0.42**
GY	-0.08ns	-0.18 *	-0.16 *		-0.22**	-0.18 *	-0.22**	-0.20**
TKW	-0.24**	-0.32**	-0.28**		-0.43**	-0.35**	-0.10ns	-0.43**
TWT	-0.25**	-0.37**	-0.29**		-0.49**	-0.49**	-0.25**	-0.51**
SPM	0.11ns	0.10ns	0.11ns		0.17 *	0.22**	0.10ns	0.17 *
SKT	0.33**	0.53**	0.51**		0.75**	0.59**	0.27**	0.75**
KNS	0.16 *	0.13ns	0.18 *		0.14ns	-0.02ns	-0.05ns	0.13ns
KWS	-0.05ns	-0.11ns	-0.04ns		-0.18 *	-0.30**	-0.15 *	-0.21**
KLE	0.03ns	-0.12ns	0.01ns		-0.10ns	-0.09ns	0.11ns	-0.12ns
KWI	-0.25**	-0.28**	-0.28**		-0.38**	-0.30**	-0.12ns	-0.38**
NDVI	0.27**	0.54**	0.35**		0.71**	0.54**	0.07ns	0.71**
IT_NDVI	0.27**	0.60**	0.36**		0.75**	0.54**	0.05ns	0.74**
Heat Stressed								
HD	0.72**	0.94**	0.32**	0.79**	0.61**	0.25**	0.60**	0.95**
DTM	0.59**	0.80**	0.25**	0.65**	0.51**	0.22**	0.50**	0.81**
GFP	-0.04ns	0.01ns	-0.03ns	-0.02ns	0.01ns	0.02ns	-0.01ns	0.02ns
PH	0.01ns	0.02ns	0.04ns	-0.06ns	0.07ns	0.12ns	0.05ns	-0.01ns
GY	-0.22**	-0.24**	-0.10ns	-0.28**	-0.06ns	0.03ns	-0.15 *	-0.24**
TKW	-0.03ns	0.01ns	-0.04ns	-0.05ns	0.05ns	0.11ns	0.02ns	-0.02ns
TWT	-0.23**	-0.32**	-0.01ns	-0.35**	-0.10ns	-0.09ns	-0.19 *	-0.35**
SPM	-0.12ns	-0.21**	0.02ns	-0.23**	-0.09ns	0.02ns	-0.09ns	-0.21**
SKT	0.32**	0.53**	0.20**	0.35**	0.34**	0.14ns	0.24**	0.51**
KNS	-0.05ns	-0.02ns	0.12ns	-0.12ns	0.05ns	-0.05ns	-0.10ns	-0.02ns
KWS	-0.11ns	-0.07ns	0.04ns	-0.16**	0.05ns	-0.01ns	-0.11ns	-0.09ns
KLE	-0.02ns	-0.02ns	-0.01ns	-0.08ns	0.10ns	0.06ns	0.01ns	-0.03ns
KWI	0.01ns	0.01ns	-0.02ns	0.01ns	0.01ns	0.06ns	0.05ns	-0.01ns
NDVI	0.41**	0.55**	0.25**	0.38**	0.43**	0.16 *	0.35**	0.55**
IT_NDVI	0.37**	0.49**	0.22**	0.33**	0.37**	0.18 *	0.33**	0.50**

*p<0.1; **p<0.05; ***p<0.01.

0.761 to 0.771. With LASSO lambda min, 12 traits were retained under normal conditions, with Adj. R² 0.430 while 18 traits were left in the set selected for the HS treatment, with an Adj. R² of 0.766. Stepwise regression and LASSO revealed that three plant variables

most affecting GY under both testing conditions were DTM (negatively), SPM (positively) and biomass (NDVI or IT_NDVI, both positively) and the temperature-related variables with most impact on GY were AMTGF (negatively) and HDD_GF

TABLE 7 Multiple regression models fitted in Non Stressed or Heat Stressed treatments from yield trials involving the UNIBO-Durum Diversity Panel evaluated at CENEB-Cd. Obregon, Mexico, in 2018 and 2019, with the dependent variable grain yield (GY).

Independable variable	Dependent variable GY (t ha ⁻¹)					
	Non Stressed			Heat Stressed		
	No selection	Stepwise selection	LASSO selection	No selection	Stepwise selection	LASSO selection
HD	1.554	1.531	-0.017	-0.018		-0.014
	(0.962)	(0.928)	(0.021)	(0.494)		(0.062)
DTM	-1.683*	-1.639*	-0.046*	-0.059	-0.079***	-0.069***
	(0.964)	(0.929)	(0.025)	(0.479)	(0.018)	(0.02)
GFP	1.630*	1.599*		-0.01		
	(0.966)	(0.931)		(0.478)		
PH	0.001			0.016***	0.017***	0.016***
	(0.006)			(0.006)	(0.005)	(0.005)
TKW	0.026		0.004	0.042*	0.061***	0.043*
	(0.034)		(0.012)	(0.024)	(0.011)	(0.023)
TWT	0.079**	0.083***	0.073**	0.020		0.021
	(0.039)	(0.03)	(0.036)	(0.025)		(0.025)
SPM	0.025***	0.024***	0.025***	0.018***	0.019***	0.018***
	(0.005)	(0.004)	(0.004)	(0.004)	(0.003)	(0.003)
SKT	0.056			-0.055	-0.056*	-0.054
	(0.046)			(0.034)	(0.032)	(0.033)
KNS	-0.007			0.053***	0.056***	0.053***
	(0.023)			(0.019)	(0.005)	(0.018)
KWS	1.027**	1.024***	0.913***	0.074		0.054
	(0.402)	(0.144)	(0.153)	(0.396)		(0.381)
KLE	-0.084		0.064	0.17		0.17
	(0.323)		(0.244)	(0.204)		(0.194)
KWI	-0.77			-0.279	-0.582*	-0.282
	(0.864)			(0.491)	(0.351)	(0.463)
NDVI	7.242**	11.004***	7.472**	0.102		
	(3.545)	(2.024)	(3.456)	(1.441)		
IT_NDVI	0.009		0.008	0.008***	0.008***	0.008***
	(0.006)		(0.006)	(0.003)	(0.001)	(0.001)
AMTA	0.424*	0.319*		-0.292		-0.288
	(0.227)	(0.186)		(0.795)		(0.781)
AMTGF	-0.101*	-0.089*	-0.05	-1.157**	-1.122**	-1.183**
	(0.059)	(0.052)	(0.048)	(0.579)	(0.461)	(0.564)
NDTH30A	-0.062		0.082	-0.344**	-0.340***	-0.310***
	(0.228)		(0.2)	(0.154)	(0.078)	(0.111)

(Continued)

TABLE 7 Continued

Independable variable	Dependent variable GY (t ha ⁻¹)					
	Non Stressed			Heat Stressed		
	No selection	Stepwise selection	LASSO selection	No selection	Stepwise selection	LASSO selection
NDTH35A				-0.063		
				(0.194)		
NDTH30GF	-0.128			-0.054		-0.025
	(0.171)			(0.154)		(0.119)
NDTH35GF	-0.776			0.068		0.088
	(0.74)			(0.142)		(0.12)
HDD_A	-0.099	-0.148**	-0.112	0.058	0.026**	0.049
	(0.148)	(0.07)	(0.121)	(0.054)	(0.012)	(0.046)
HDD_GF	0.174*	0.084**		0.074**	0.066**	0.074**
	(0.092)	(0.04)		(0.037)	(0.031)	(0.036)
Constant	-10.143	-10.822**	-6.548	45.143*	38.963***	45.168*
	(8.197)	(5.175)	(4.953)	(25.03)	(13.396)	(24.556)
Observations	183	183	183	181	181	181
R ²	0.505	0.486	0.467	0.790	0.787	0.790
Adjusted R ²	0.441	0.453	0.430	0.761	0.771	0.766
Residual Std. Error	0.544	0.538	0.549	0.348	0.340	0.345
F Statistic	7.826***	14.690***	12.429***	27.098***	51.645***	31.945***
	(df = 21; 161)	(df = 11; 171)	(df = 12; 170)	(df = 22; 158)	(df = 12; 168)	(df = 19; 161)

*p<0.1; **p<0.05; ***p<0.01.
Models were defined as No selection, with all plant and environmental independent variables; Stepwise selection, with independent variables selected with stepwise procedure; LASSO selection, with dependent variable were selected by the least absolute shrinkage and selection operator method (Tibshirani, 1996, Tibshirani, 2011). (SE in parentheses).

(positively). These models also revealed several variables which contributed to GY in only one or the other testing environment: TWT and KWS only under NS conditions while PH, TKW and KNS exclusively under HS conditions. In terms of the temperature-related variables affecting GY only in one testing environment, NDTH30A was detected by both stepwise regression and LASSO as negatively affecting performance under heat stress.

The final network was translated into a SEM, where phenotypes can be treated both as predictor (exogenous) and response (endogenous) in a system of simultaneous equations, hence allowing to postulate functional (causal) links between traits (Supplementary Figure 3). SEM coefficients were estimated and standardized path coefficients are represented by arrows, with the green indicating a positive relationship while the red ones indicate a negative relationship, the thickness being proportional to the relative coefficient size. The results of the analysis are reported in Supplementary Table 6. The final set of variables reached an R² 0.423 in NS and 0.712 under HS conditions. These values are not much lower than those obtained with the whole model. In the best-fitted model, in NS conditions, GY appeared to be directly related to TKW, TWT, SPM, KNS, and HDD did not show significant adverse effects regardless of when, up to anthesis or during grain filling, it

was accumulated. Under HS conditions, the plant variables PH, TKW, SPM, KNS and IT_NDVI were directly related to GY while HDD during grain fill showed a negative effect on GY.

The PCgen reconstruction of networks is presented in Figure 2. PCgen was applied to the BLUES of the single year for each treatment rather than to single plot values, and for this reason the genetic relationship among traits is not affected by the residual genotype by year interaction. With this method, the genetic effects are incorporated in the network reconstruction and thus direct genetic effects can be detected. In timely-sown control conditions, only PH, TKW, KNS showed a direct genetic effect, while GY showed an indirect effect through TKW. Under HS conditions, a direct significant genetic effect was detected for HD, PH, NDVI, KNS, and GY. The other traits showed edges not significant at P 0.01 (Supplementary Table 7). The reconstruction of networks, reported in Figure 2, also includes the effects of HDD. In control conditions, the HDD_GF showed no connection with other traits, while HDD_A was connected with NDVI and KWS, even though not through genetic effects. Under stress conditions HDD_A was connected with HD, PH, TKW, and KWS. On the other hand, HDD_GF was in turn connected in a cluster with GFP-DTM and KWS, in accordance with what was already seen in SEM analysis.

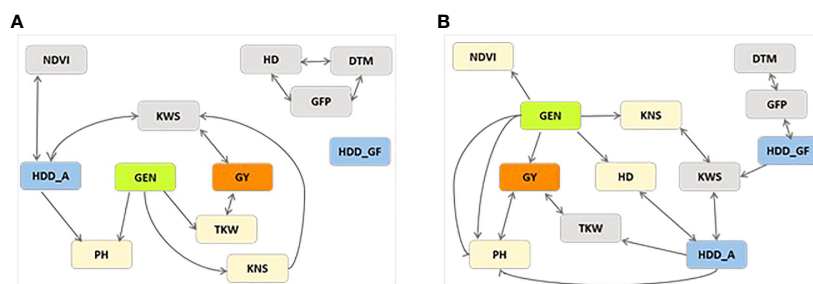


FIGURE 2

GSEM estimated networks with $P < 0.01$ for traits days to heading (HD), days to maturity (DTM), grain filling period (GFP), plant height (PH), grain yield (GY), thousand kernel weight (TKW), kernel number per spike (KNS), kernel weight per spike (KWS), normalized difference vegetation index (NDVI) and heat degree days at anthesis (HDD_A) and at grain filling period (HDD_GF), collected on plants from yield trials involving the UNIBO-Durum Diversity Panel evaluated at CENEB-Cd. Obregon, Mexico, in 2018 and 2019. Besides GEN representing the genetic effect in green, GY is highlighted in orange and the other traits directly connected with GEN were highlighted in pale-orange. Weather variables were highlighted in blue. (A) Non Stressed control. (B) Heat Stressed.

3.4 Identification of sources of genetic tolerance to heat stress

The performances of varieties in NS and HS conditions, and the GY loss due to heat stress were considered in order to identify potential sources of tolerance to heat stress. Based on a significant confounding effect of phenology on yield performance in the different testing conditions, the performances of genotypes were also estimated as marginal means from the average response to HD (see the [Supplementary Tables 8 and S9](#) for the detailed non adjusted or adjusted values based on HD covariate genotype values).

In reaction to heat stress, all varieties showed a reduction in HD, ranging from -3% to -23%. Groups of varieties already adapted to warm growing environments with relatively short growing cycle like the Desert Durums (Kofa, Kronos, WestBred881, Bravadur) and CIMMYT'80s cultivars (Altar 84, Iride, several CIMMYT lines and Spanish varieties) showed a reduction in HD generally below 10%. Conversely, Italian and, in part, ICARDA varieties and lines bred for longer growing cycles showed a more marked reduction in HD.

Based on the marginal means after adjustment for HD ([Supplementary Table 9](#)), the three variables that were most reduced by heat stress were GY, then biomass (NDVI) and then the variables related to spike fertility (KWS/KNS). Losses in GY ranged from -22.8% to -85.8%, with an average loss of -56.0%. In terms of biomass (NDVI), losses ranging from 28% to 77%, with an average of 52% were recorded. Losses in spike fertility were indicated by a loss in KWS ranging from 3% to 70%, averaging 39%. The varieties that showed lower-than-average yield losses were frequently found again among the Desert Durums, CIMMYT'80s and with some ICARDA temperate groups. When dissecting the overall grain yield loss at the level of the less complex grain yield components, we could identify varieties/variety groups which responded to HS differently. Considering the major subpopulations/groups, Subpop 1 - ITALY-MEDITERRANEAN and Subpop 2 - ICARDA-DRYLAND were mainly affected for biomass production (IT_NDVI or NDVI) and therefore canopy development, growth, biomass accumulation, and photosynthetic capacity. The Italian varieties were less affected at the level of grain

weight TKW and test weight TWT but with marked reductions observed in spike fertility. Subpop 3 - ICARDA-TEMPERATE, also including some Desert Durums, showed a wide range of responses with varieties more resilient in terms of their biomass production and spike fertility (SKT and KNS). These included the Desert Durums Bravadur, WB881, Produra, Kofa, and ICARDA (Cham1, Stojocri). Notably, Subpop 4 - CIMMYT'70 - ICARDA also showed also a wide range of responses with the absence of a clear trend. Subpop 5 - CIMMYT'80 included the best materials in terms of biomass production and fertile culms/spike density, as well as for maintenance of spike fertility.

4 Discussion

The frequency and severity of high-temperature stress have increased consistently in the past decade and are expected to reach worrisome levels soon ([Asseng et al., 2017](#); [Zhao et al., 2017](#); [IPCC, 2023](#)), which underlines the urgency for a better dissection of the genetic control of HS resilience in order to identify native haplotypes which may allow to mitigate the effects of heat stress in crops like durum wheat which is prevalently grown in relatively heat-prone regions such as the Mediterranean Basin ([Kutiel, 2019](#)), and areas already characterized by high heat stress such as Central and Peninsular India and Iran or west Africa such as Senegal valley ([Sall et al., 2018](#)). The heat stress intensity to which plants were exposed in this study proved to be very effective, as expected based on the average temperatures typical of the location and sowing times. The experimental location was chosen because it is highly productive when wheat is sown at optimum time, and with a major constraint due to high temperature associated to late sowing is applied. The present study was conducted over two years, with higher GY in 2019, due to less extreme temperatures during grain filling, both under control and late sowing treatment. Even with this difference between testing years, the heat stress to which the panel was subjected reduced GY by 57% on average, with a very wide range of yield losses observed overall, both within and among the different germplasm groups represented in this panel. Other authors

(Sukumaran et al., 2018), working at the same location on durum wheat, have reported a higher reduction of GY (71.7%) due to HS. As an effect of the HS, the time to maturity was markedly shortened as well, in agreement with previous observations (Djanaguiraman et al., 2020). Temperature-related variables that affected yield under HS were generally those calculated based on temperatures at grain fill (post anthesis), confirming what has been observed in several small-grains species, that some of the most important yield-limiting effects of heat on the present durum panel were related to high temperatures from flowering through grain filling stages, which affects several reproductive and/or physiological processes (Cossani and Reynolds, 2012; Fabian et al., 2019), or grain metabolic pathways (Wahid et al., 2007; Farooq et al., 2011; Gautam et al., 2014; Sharma et al., 2017). However, HS prior to anthesis and grain fill is also critically detrimental, affecting final yield consequent to a reduced source capacity and/or biomass available to support grain filling, particularly in its final stages (Xu et al., 2022; Barratt et al., 2024; Sall et al., 2024). In the current study, a substantial reduction was observed in biomass accumulated up to shortly after anthesis (NDVI), averaging 52%, second only to the effect on final GY. For this trait as well, a wide range of losses due to heat were observed both between and within germplasm groups included in the panel.

Environmental variables were used as covariates when they were proven to affect genotypes' performance. Inevitably, different lines were subjected to different conditions due to their specific phenology that, notably, was purposely kept within a 1-week interval among the tested genotypes. Moreover, the effect of the stress treatment imposed by delayed sowing likely induced differential responses depending on the timing of the most limiting conditions, particularly whether they occurred before or after heading. For these reasons, to get a comprehensive picture of the inter-relations among several environmental parameters and with yield and the other traits, we undertook further analyses following three steps. First we applied stepwise regression and LASSO for reducing the confounding factors in the predictive model to keep only those which mostly affected GY. Based on this analysis, NDTH30_A and AMT_GF impacted significantly and negatively final yield to a higher extent as compared to the other environmental variables that showed some significant effects such as AMT_A, HDD_A, HDD_GF. Other environmental variables such as NDTH35_A, NDTH30_GF, and NDTH35_GF did not affect significantly GY. This means that the negative effects on GY are already, and mostly, determined by the cumulative number of days with temperatures passing the relatively mild sensitivity threshold of 30°C, rather than 35°C which corresponds to the typical heat stress wave, and are already determined between anthesis and grain filling, reviewed by Ullah et al. (2022) and Akter and Islam (2017).

Structural Equation Models (SEMs) have been used to study recursive and simultaneous relationships among phenotypes in multivariate systems such as multiple-trait models in quantitative genetics (Valente et al., 2010) to identify a network of correlated traits (He et al., 2021), together with genome-wide SNP profiles. As a second step toward the understanding of the response to HS, we employed SEM based on phenotypic and environmental variables. The possible use of SEMs to understand physiological causes of

genotype by environment or management interaction was explored by Vargas et al. (2007), who concluded that the approach can facilitate the understanding of the effects of environmental covariates on yield performances or can be used to generate hypotheses (Valente et al., 2013). Under heat stress, SEM confirmed the role of HDD_A and HDD_GF in controlling NDVI (as NDVI and IT_NDVI), hence plant growth and biomass development, which in turn plays a key pivotal role in influencing of PH, KNS, TKW and finally GY, as recently pointed out by Kumar et al. (2023).

Finally, as the third step to improve the understanding of the multiple trait models, we considered one of the methods suggested to identify which variable most affects genotypes' performance (Maathuis et al., 2009; Maathuis et al., 2010; Buhlmann et al., 2014; Buhlmann, 2020). Recently, GSEM has been proposed (Kruijer et al., 2020), i.e., the linear genetic structural equation models, which allows for the reconstruction of a causal model compatible with observed results. The PCgen algorithm used to obtain GSEM in this study belongs to the recursive causal structure as represented by a directed acyclic graph, DAG, which is a set of variables (nodes) connected by directed edges (arrows) representing direct causal relationships. More precisely, the GSEM can include genetic effects, and it allows for the reconstruction of a causal model attempting to explain the observed data. Notably, these methods do not permit to infer the actual size of causal effects (Buhlmann et al., 2014), while allowing one to rank the importance of variables, and their prioritization with respect to their causal strength (Maathuis et al., 2010). We did not consider population structure in the analysis since statistical inference can become biased under possible model misspecification, such as epistasis (Kruijer, 2016) which has proven to play a role for TKW and GY in durum wheat (Maccaferri et al., 2011). On the other hand, with PCgen, direct genetic effects and structural relations among traits can be inferred, regardless of the population structure and genetic architecture (Kruijer et al., 2020). With GSEM, we revealed that, in our study, the genetic effect on GY was mainly mediated by TKW in non-stress condition, while in case of heat stress GY, NDVI, KWS and HD all showed to be under direct genetic control, then all are expected to be involved in the response to stress and should be taken into account during selection for heat prone environments.

The methods herein employed aimed at identify the variables to be considered in breeding for heat tolerance and therefore reduce the number of secondary traits to be managed either when modeling physiological components of a trait or when selecting those to be considered for genomic prediction (Momen et al., 2018; Arouisse et al., 2021) and breeding. The screening could be based on the target trait or on those genetically correlated with it, as for the indirect selection or for the application of selection indices (Falconer and MacKay, 1996). Recently, the use of selection index in breeding and in genomic selection has been explored in combination with SEM by Hidalgo-Contreras et al. (2021) who concluded that taking into account the causal effects from the structural model notably improved the relative effectiveness of the index with respect to models with no causal information.

The role of environmental covariates is discussed in Arouisse et al. (2021) while Millet et al. (2019) commented on their role in

predicting genotypes' performances in new environments. For this reason, environmental variables are of great interest, besides their use as covariates to correct for spurious associations. In fact, the accurate parametrization of environmental effects is of great importance in "enviromics" (Costa-Neto et al., 2021; Costa-Neto and Fritsche-Neto, 2021; Crossa et al., 2021; Fritsche-Neto et al., 2021) where multi-trait models are integrated with the environmental information into a powerful prediction model (Crossa et al., 2021). The relationship between environmental covariates and the target trait is the first step to pursue the so-called "enviromic" assembly approach (Costa-Neto et al., 2021), which may include different parameters so that genome predictions can be tailored for specific environments. The definition of "envirotyping" by means of a SEM combining both phenotypic and environmental variables provides a powerful framework for synergizing multidisciplinary efforts (Smith et al., 2014) together with other approaches (Porker et al., 2020; Cooper and Messina, 2021), facilitating the discovery of causal pathways as empirical data are tested statistically against the model. Recently, applications of these methods were explored by applying Bayesian estimation for eco-physiological modeling of wheat yield as a function of its component and of weather conditions during key stages of development (Poudel et al., 2022).

This study showed that the response to HS under field conditions of the durum wheat cultivated germplasm worldwide is not homogeneous. Overall, the screening pointed out the presence of a number of genotypes showing relatively tolerant heat stress responses at different developmental and reproductive stages, and more specifically for each of the three main and critical yield-determinants: (i) biomass development/spike number per meter, (ii) spike fertility/kernel number per spike, (iii) grain filling/kernel weight. This finding indicates that breeding strategies aimed at cumulating independent beneficial alleles for different HS tolerance determinants are feasible and could be pursued within the elite germplasm, either by classical breeding or marker-assisted aided breeding. Among the main breeding groups/lineages tested, the best materials in terms of biomass production and fertile culms/spike density, as well as for maintenance of spike fertility were found among the Desert Durum[®], CIMMYT'80 and ICARDA breeding pools. This observation confirms recent finding by Emebiri et al. (2023) who identified several heat-stress tolerant CIMMYT'80 genotypes in a controlled environment screening of durum germplasm specifically targeted for heat-induced floret sterility due to controlled heat exposure at heading/flowering. This finding is overall relevant for future breeding, in view of the expected impact of increased average temperatures due to Global Climate Change on durum wheat production areas such as the Mediterranean Basin. In this respect, it is appropriate to point out that in practical breeding improving a single specific component of heat stress tolerance is not resolute and could even lead to detrimental side effects. In this

case, maintenance of fertility under stress should necessarily be associated to maintenance of physiological senescence and translocation processes and hormonal balance associated to a regular, not accelerated grain filling (Ashfaq et al., 2022; Xu et al., 2022).

This study allowed us to analyze the response to heat stress of a panel of durum wheat genotypes representing a relevant portion of the genetic diversity available worldwide. We identified in the panel a large variability for the performance under heat stress, which will provide a valuable source of alleles/haplotypes for adaptation to heat-prone environments. We also considered the relations among plant variables and environmental covariates identified by means of a SEM, confirming that heat stress affects yield mostly after anthesis. The study of structural models, and in particular of GSEM, lays a foundation for the next steps in elucidating the physiological response to heat by mapping QTLs controlling the trait (Igolkina et al., 2020) and to implement either marker-assisted selection, if large effects QTLs are identified, or genomic prediction tailored to heat tolerance improvement of durum wheat (Costa-Neto et al., 2021). Most importantly, we believe that meaningful tools to link genetic knowledge and environmental specificity, such as those employed in the present study, can be part of the most needed translational research aimed at actually improving crop cultivars (Kole et al., 2015; Millet et al., 2019; Reynolds et al., 2021; Welcker et al., 2022; Della Coletta et al., 2023; Sall et al., 2024).

In conclusion, the dissection of traits involved in response to heat showed that the effects of HS were particularly pronounced for NDVI, KWS, GFP, and GY. Combination of plant and weather related variables in GSEM modeling suggested that the causal model of performance under HS directly involves genetic effects on GY, NDVI, KNS and HD. Among factors determining response to heat stress, environmental variables have a role and could be integrated in multi-trait prediction models. We identified consistently suitable sources of genetic resistance to heat stress to be used in different durum wheat pre-breeding programs. Among those, Desert Durums and CIMMYT'80 germplasm showed the highest degree of adaptation and capacity to yield under high temperatures and can be considered as a valuable source of alleles for adaptation to breed new HS resilient cultivars.

Finally, the next steps should include mapping genomic regions and characterizing QTLs controlling the traits involved in performance under high heat stress and/or developing multi-trait selection criteria to predict genotypes that could be best adapted to heat-prone environments. From a breeding standpoint, and given the wide genetic diversity of the present panel, and the fact that genotypes with low reduction in GY and related traits were identified in all of the germplasm groups herein tested, the identification and possibly cloning of heat tolerance QTLs from the most representative collections of durum germplasm publicly available (Maccaferri et al., 2019; Mazzucotelli et al., 2020) will

eventually allow breeders to systematically accumulate the favorable alleles/hapotypes with outstanding performance under heat conditions.

Data availability statement

The original contributions presented in the study are included in the article/[Supplementary Material](#), further inquiries can be directed to the corresponding author.

Author contributions

EG: Conceptualization, Writing – review & editing. EF: Conceptualization, Writing – review & editing. MM: Conceptualization, Writing – review & editing. KA: Conceptualization, Writing – review & editing. RT: Conceptualization, Writing – review & editing.

Funding

The author(s) declare financial support was received for the research, authorship, and/or publication of this article. EG was supported by Monsanto's Beachell-Borlaug International Scholars Program (MBBISP).

References

- Abdalla, E. A., Wood, B. J., and Baes, C. F. (2021). Accuracy of breeding values for production traits in Turkeys (*Meleagris gallopavo*) using recursive models with or without genomics. *Genet. Selection Evol.* 53. doi: 10.1186/s12711-021-00611-8
- Adamski, N. M., Borrill, P., Brinton, J., Harrington, S. A., Marchal, C., Bentley, A. R., et al. (2020). A roadmap for gene functional characterisation in crops with large genomes: Lessons from polyploid wheat. *Elife* 9. doi: 10.7554/eLife.55646
- Akter, N., and Islam, M. R. (2017). Heat stress effects and management in wheat. A review. *Agron. Sustain. Dev.* 37. doi: 10.1007/s13593-017-0443-9
- Arousse, B., Tpjim Theeuwien, F. A., Eeuwijk, v., and Kruijer, W. (2021). "Improving genomic prediction using high-dimensional secondary phenotypes. *Front. Genet.* 12. doi: 10.3389/fgene.2021.667358
- Ashfaq, W., Brodie, G., Fuentes, S., and Gupta, D. (2022). Infrared thermal imaging and morpho-physiological indices used for wheat genotypes screening under drought and heat stress. *Plants-Basel* 11. doi: 10.3390/plants11233269
- Asseng, S., Cammarano, D., Basso, B., Chung, U., Alderman, P. D., Sonder, K., et al. (2017). Hot spots of wheat yield decline with rising temperatures. *Global Change Biol.* 23, 2464–2472. doi: 10.1111/gcb.13530
- Asseng, S., Ewert, F., Martre, P., Rotter, R. P., Lobell, D. B., Cammarano, D., et al. (2015). Rising temperatures reduce global wheat production. *Nat. Climate Change* 5, 143–147. doi: 10.1038/nclimate2470
- Balla, K., Karsai, I., Bonis, P., Kiss, T., Berki, Z., Horvath, A., et al. (2019). Heat stress responses in a large set of winter wheat cultivars (*Triticum aestivum* L.) depend on the timing and duration of stress. *PLoS One* 14. doi: 10.1371/journal.pone.0222639
- Balla, K., Karsai, I., Kiss, T., Horvath, A., Berki, Z., Cseh, A., et al. (2021). Single versus repeated heat stress in wheat: What are the consequences in different developmental phases? *PLoS One* 16. doi: 10.1371/journal.pone.0252070
- Barratt, L. J., Ortega, S. F., and Harper, A. L. (2024). Identification of candidate regulators of the response to early heat stress in climate-adapted wheat landraces via transcriptomic and co-expression network analyses. *Front. Plant Sci.* 14. doi: 10.3389/fpls.2023.1252885
- Bates, D., Mächler, M., Bolker, B. M., and Walker, S. C. (2015). Fitting linear mixed-effects models using lme4. *J. Stat. Software* 67, 1–48. doi: 10.18637/jss.v067.i01
- Buhlmann, P. (2020). Invariance, causality and robustness. *Stat. Sci.* 35, 404–426. doi: 10.1214/19-STS721
- Buhlmann, P., Kalisch, M., Meier, L., and Fienberg, S. E. (2014). "High-dimensional statistics with a view toward applications in biology," in *Annual review of statistics and its application*, vol. 1, 255–U809. Durham, NC, USA: Duke University Press.
- Chen, Q. H., and Yang, G. W. (2020). Signal function studies of ROS, especially RBOH-dependent ROS, in plant growth, development and environmental stress. *J. Plant Growth Regul.* 39, 157–171. doi: 10.1007/s00344-019-09971-4
- Condorelli, G. E., Maccaferri, M., Newcomb, M., Andrade-Sanchez, P., White, J. W., French, A. N., et al. (2018). Comparative aerial and ground based high throughput phenotyping for the genetic dissection of NDVI as a proxy for drought adaptive traits in durum wheat. *Front. Plant Sci.* 9. doi: 10.3389/fpls.2018.00893
- Cooper, M., and Messina, C. D. (2021). Can we harness "Enviromics" to accelerate crop improvement by integrating breeding and agronomy? *Front. Plant Sci.* 12, 2. doi: 10.3389/fpls.2021.735143
- Cossani, C. M., and Reynolds, M. P. (2012). Physiological traits for improving heat tolerance in wheat. *Plant Physiol.* 160, 1710–1718. doi: 10.1104/pp.112.207753
- Costa-Neto, G., Crossa, J., and Fritsche-Neto, R. (2021). Enviromic Assembly Increases Accuracy and Reduces Costs of the Genomic Prediction for Yield Plasticity in Maize. *Front. Plant Sci.* 12. doi: 10.3389/fpls.2021.717552
- Costa-Neto, G., and Fritsche-Neto, R. (2021). "Enviromics: bridging different sources of data, building one framework" in *Crop breeding and applied biotechnology* 21. Vicosa-MG-Brazil. doi: 10.1590/1984-70332021v21Sa25
- Costa-Neto, G., Galli, G., Carvalho, H. F., Crossa, J., and Fritsche-Neto, R. (2021). EnvRtype: a software to interplay enviromics and quantitative genomics in agriculture. *G3-Genes Genomes Genet.* 11. doi: 10.1093/g3journal/jkab040
- Crossa, J., Fritsche-Neto, R., Osval, A., Montesinos-Lopez, Costa-Neto, G., Dreisigacker, S., et al. (2021). The modern plant breeding triangle: optimizing the use of genomics, phenomics, and enviromics data. *Front. Plant Sci.* 12. doi: 10.3389/fpls.2021.651480
- Davidson, H. R., and Campbell, C. A. (1983). The effect of temperature, moisture and nitrogen on the rate of development of spring wheat as measured by degree days. *Can. J. Plant Sci.* 63, 833–846. doi: 10.4141/cjps83-106

Conflict of interest

The authors declare that the research was conducted in the absence of any commercial or financial relationships that could be construed as a potential conflict of interest.

The author(s) declared that they were an editorial board member of Frontiers, at the time of submission. This had no impact on the peer review process and the final decision.

Publisher's note

All claims expressed in this article are solely those of the authors and do not necessarily represent those of their affiliated organizations, or those of the publisher, the editors and the reviewers. Any product that may be evaluated in this article, or claim that may be made by its manufacturer, is not guaranteed or endorsed by the publisher.

Supplementary material

The Supplementary Material for this article can be found online at: <https://www.frontiersin.org/articles/10.3389/fpls.2024.1393349/full#supplementary-material>

- Della Coletta, R., Liese, S. E., Fernandes, S. B., Mikel, M. A., Bohn, M. O., Lipka, A. E., et al. (2023). Linking genetic and environmental factors through marker effect networks to understand trait plasticity. *Genetics* 224. doi: 10.1101/2023.01.19.524532
- Djanaguiraman, M., Narayanan, S., Erdyani, E., and Prasad, P. V. V. (2020). Effects of high temperature stress during anthesis and grain filling periods on photosynthesis, lipids and grain yield in wheat. *BMC Plant Biol.* 20. doi: 10.1186/s12870-020-02479-0
- Djanaguiraman, M., and Prasad, P. V. V. (2014). High temperature stress. *Plant Genet. Resour. Climate Change* 4, 201–220.
- El Hassouni, K., Belkadi, B., Filali-Maltouf, A., Tidiane-Sall, A., Al-Abdallat, A., Nachit, M., et al. (2019). Loci controlling adaptation to heat stress occurring at the reproductive stage in durum wheat. *Agronomy-Basel* 9. doi: 10.3390/agronomy9080414
- Emebiri, L., Erena, M. F., Taylor, K., Hildebrand, S., Maccaferri, M., and Collins, N. C. (2023). Field screening for heat-stress tolerance of floret fertility in wheat (*Triticum aestivum* and *Triticum durum*). *Crop Pasture Sci.* 75. doi: 10.1071/CP23214
- Fabian, A., Safran, E., Szabo-Eitel, G., Barnabas, B., and Jager, K. (2019). Stigma functionality and fertility are reduced by heat and drought co-stress in wheat. *Front. Plant Sci.* 10. doi: 10.3389/fpls.2019.00244
- Falconer, D. S., and MacKay, T. F. C. (1996). *Introduction to quantitative genetics*, 4th Edn. Addison Wesley Longman, Harlow.
- Farooq, M., Bramley, H., Palta, J. A., and Siddique, K. H. M. (2011). Heat stress in wheat during reproductive and grain-filling phases. *Crit. Rev. Plant Sci.* 30, 491–507. doi: 10.1080/07352689.2011.615687
- Feng, B., Liu, P., Li, G., Dong, S. T., Wang, F. H., Kong, L. A., et al. (2014). Effect of heat stress on the photosynthetic characteristics in flag leaves at the grain-filling stage of different heat-resistant winter wheat varieties. *J. Agron. Crop Sci.* 200, 143–155. doi: 10.1111/jac.12045
- Fritsche-Neto, R., Galli, G., Borges, K. L. R., Costa-Neto, G., Alves, F. C., Sabadin, F., et al. (2021). Optimizing genomic-enabled prediction in small-scale maize hybrid breeding programs: A roadmap review. *Front. Plant Sci.* 12. doi: 10.3389/fpls.2021.658267
- Gautam, A., Agrawal, D., SaiPrasad, S. V., and Jajoo, A. (2014). A quick method to screen high and low yielding wheat cultivars exposed to high temperature. *Physiol. Mol. Biol. Plants* 20, 533–537. doi: 10.1007/s12298-014-0252-4
- Gianola, D., and Sorensen, D. (2004). Quantitative genetic models for describing simultaneous and recursive relationships between phenotypes. *Genetics* 167, 1407–1424. doi: 10.1534/genetics.103.025734
- Gleason, S. M., Cooper, M., Wiggins, D. R., Bliss, C. A., Romay, M. C., Gore, M. A., et al. (2019). Stomatal conductance, xylem water transport, and root traits underpin improved performance under drought and well-watered conditions across a diverse panel of maize inbred lines. *Field Crops Res.* 234, 119–128. doi: 10.1016/j.fcr.2019.02.001
- Graziani, M., Maccaferri, M., Royo, C., Salvatorelli, F., and Tuberosa, R. (2014). QTL dissection of yield components and morpho-physiological traits in a durum wheat elite population tested in contrasting thermo-pluviometric conditions. *Crop Pasture Sci.* 65, 80–95. doi: 10.1071/CP13349
- Hasanuzzaman, M., Nahar, K., Alam, M. M., Roychowdhury, R., and Fujita, M. (2013). Physiological, biochemical, and molecular mechanisms of heat stress tolerance in plants. *Int. J. Mol. Sci.* 14, 9643–9684. doi: 10.3390/ijms14059643
- He, T. H., Angessa, T. T., Hill, C. B., Zhang, X. Q., Chen, K. F., Luo, H., et al. (2021). Genomic structural equation modelling provides a whole-system approach for the future crop breeding. *Theor. Appl. Genet.* 134, 2875–2889. doi: 10.1007/s00122-021-03865-4
- Hidalgo-Contreras, J. V., Salinas-Ruiz, J., Kent, M. E., and Baenziger, S. P. (2021). Incorporating molecular markers and causal structure among traits using a smith-hazel index and structural equation models. *Agronomy* 11, 1953. doi: 10.3390/agronomy11101953
- Honsdorf, N., Verhulst, N., Crossa, J., Vargas, M., Govaerts, B., and Ammar, K. (2020). Durum wheat selection under zero tillage increases early vigor and is neutral to yield. *Field Crops Res.* 248. doi: 10.1016/j.fcr.2019.107675
- Hossain, A., Sarker, M. A. Z., Saifuzzaman, M., da Silva, J. A. T., Lozovskaya, M. V., and Akhter, M. M. (2013). Evaluation of growth, yield, relative performance and heat susceptibility of eight wheat (*Triticum aestivum* L.) genotypes grown under heat stress. *Int. J. Plant Production* 7, 615–636.
- Hussain, H. A., Hussain, S., Khaliq, A., Ashraf, U., Anjum, S. A., Men, S. N., et al. (2018). Chilling and drought stresses in crop plants: implications, cross talk, and potential management opportunities. *Front. Plant Sci.* 9. doi: 10.3389/fpls.2018.00393
- Igolkina, A. A., Meshcheryakov, G., Gretsova, V., Nuzhdin, S. V., and Samsonova, M. G. (2020). Multi-trait multi-locus SEM model discriminates SNPs of different effects. *BMC Genomics* 21. doi: 10.1186/s12864-020-06833-2
- IPCC (2023). “Climate change 2023: synthesis report,” in *Contribution of working groups I, II and III to the sixth assessment report of the intergovernmental panel on climate change*. Geneva, Switzerland: World Meteorological Organization.
- Kole, C., Muthamilarasan, M., Henry, R., Edwards, D., Sharma, R., Abberton, M., et al. (2015). Application of genomics-assisted breeding for generation of climate resilient crops: progress and prospects. *Front. Plant Sci.* 6. doi: 10.3389/fpls.2015.00563
- Kruijer, W. (2016). Misspecification in mixed-model-based association analysis. *Genetics* 202, 363–364. doi: 10.1534/genetics.115.177212
- Kruijer, W., Behrouzi, P., Bustos-Korts, D., Rodriguez-Alvarez, M. X., Mahmoudi, S. M., Yandell, B., et al. (2020). Reconstruction of networks with direct and indirect genetic effects. *Genetics* 214, 781–807. doi: 10.1534/genetics.119.302949
- Kumar, M., Mishra, V. K., Chand, R., Sharma, S., Kumar, J. P., et al. (2023). NDVI and grain fill duration are important to be considered in breeding for terminal heat stress tolerance in wheat. *J. Agron. Crop Sci.* 209, 489–501. doi: 10.1111/jac.12637
- Kutiel, H. (2019). Climatic uncertainty in the mediterranean basin and its possible relevance to important economic sectors. *Atmosphere* 10. doi: 10.3390/atmos10010010
- Lenth, R. (2024). *emmeans: Estimated Marginal Means, aka Least-Squares Means. R package version 1.10.0*. Available at: <https://CRAN.R-project.org/package=emmeans>.
- Liu, B., Asseng, S., Liu, L., Tang, L., Cao, W., and Zhu, Y. (2016). Testing the responses of four wheat crop models to heat stress at anthesis and grain filling. *Global Change Biol.* 22, 1890–1903. doi: 10.1111/gcb.13212
- Maathuis, M. H., Colombo, D., Kalisch, M., and Buhlmann, P. (2010). Predicting causal effects in large-scale systems from observational data. *Nat. Methods* 7, 247–248. doi: 10.1038/nmeth0410-247
- Maathuis, M. H., Kalisch, M., and Buhlmann, P. (2009). Estimating high-dimensional intervention effects from observational data. *Ann. Stat.* 37, 3133–3164. doi: 10.1214/09-AOS685
- Maccaferri, M., Harris, N. S., Twardziok, S. O., Pasam, R. K., Gundlach, H., Spannagl, M., et al. (2019). Durum wheat genome highlights past domestication signatures and future improvement targets. *Nat. Genet.* 51, 885–88+. doi: 10.1038/s41588-019-0381-3
- Maccaferri, M., Sanguineti, M. C., Demontis, A., El-Ahmed, A., Moral, L. G. d., Maalouf, F., et al. (2011). Association mapping in durum wheat grown across a broad range of water regimes. *J. Exp. Bot.* 62, 409–438. doi: 10.1093/jxb/erq287
- Maccaferri, M., Sanguineti, M. C., Noli, E., and Tuberosa, R. (2005). Population structure and long-range linkage disequilibrium in a durum wheat elite collection. *Mol. Breed.* 15, 271–289. doi: 10.1007/s11032-004-7012-z
- Maccaferri, M., Sanguineti, M. C., Xie, C., Smith, J. S. C., and Tuberosa, R. (2007a). Relationships among durum wheat accessions. II. A comparison of molecular and pedigree information. *Genome* 50, 385–399. doi: 10.1139/G07-017
- Maccaferri, M., Stefanelli, S., Rotondo, F., Tuberosa, R., and Sanguineti, M. C. (2007b). Relationships among durum wheat accessions. I. Comparative analysis of SSR, AFLP, and phenotypic data. *Genome* 50, 373–384. doi: 10.1139/G06-151
- Mamrutha, H. M., Rinki, K., Venkatesh, K., Gopalareddy, K., Khan, H., Mishra, C. N., et al. (2020). Impact of high night temperature stress on different growth stages of wheat. *Plant Physiol. Rep.* 25, 707–715. doi: 10.1007/s40502-020-00558-w
- Martre, P., Yin, X., and Frank, E. (2017). Modeling crops from genotype to phenotype in a changing climate. *Field Crops Res.* 202, 1–4. doi: 10.1016/j.fcr.2017.01.002
- Mazzucotelli, E., Sciarra, G., Mastrangelo, A. M., Desiderio, F., Xu, S. S., Faris, J., et al. (2020). The global durum wheat panel (GDP): an international platform to identify and exchange beneficial alleles. *Front. Plant Sci.* 11. doi: 10.3389/fpls.2020.569905
- Millet, E. J., Kruijer, W., Coupel-Ledru, A., Prado, S. A., Cabrera-Bosquet, L., Lacube, S., et al. (2019). Genomic prediction of maize yield across European environmental conditions. *Nat. Genet.* 51, 952–95+. doi: 10.1038/s41588-019-0414-y
- Momen, M., Campbell, M. T., Walia, H., and Morota, G. (2019). Utilizing trait networks and structural equation models as tools to interpret multi-trait genome-wide association studies. *Plant Methods* 15. doi: 10.1186/s13007-019-0493-x
- Momen, M., Mehrgardi, A. A., Roudbar, M. A., Kranis, A., Pinto, R. M., Valente, B. D., et al. (2018). Including phenotypic causal networks in genome-wide association studies using mixed effects structural equation models. *Front. Genet.* 9. doi: 10.3389/fgene.2018.00455
- Mondal, S., Singh, R. P., Crossa, J., Huerta-Espino, J., Sharma, I., Chatrath, R., et al. (2013). Earliness in wheat: A key to adaptation under terminal and continual high temperature stress in South Asia. *Field Crops Res.* 151, 19–26. doi: 10.1016/j.fcr.2013.06.015
- Pequeno, D. N. L., Hernández-Ochoa, I. M., Reynolds, M., Sonder, K., MoleroMilan, A., Robertson, R. D., et al. (2021). Climate impact and adaptation to heat and drought stress of regional and global wheat production. *Environ. Res. Lett.* 16. doi: 10.1088/1748-9326/abd970
- Porker, K., Coventry, S., Fittell, N. A., Cozzolino, D., and Eglinton, J. (2020). Using a novel PLS approach for envirotyping of barley phenology and adaptation. *Field Crops Res.* 246. doi: 10.1016/j.fcr.2019.107697
- Porter, J. R., and Gawith, M. (1999). Temperatures and the growth and development of wheat: a review. *Eur. J. Agron.* 10, 23–36. doi: 10.1016/S1161-0301(98)00047-1
- Posch, B. C., Kariyawasam, B. C., Bramley, H., Coast, O., Richards, R. A., Reynolds, M. P., et al. (2019). Exploring high temperature responses of photosynthesis and respiration to improve heat tolerance in wheat. *J. Exp. Bot.* 70, 5051–5069. doi: 10.1093/jxb/erz257
- Poudel, P., Bello, N. M., Marburger, D. A., Carver, B. F., Liang, Y., and Alderman, P. D. (2022). Ecophysiological modeling of yield and yield components in winter wheat using hierarchical Bayesian analysis. *Crop Sci.* 62, 358–373. doi: 10.1002/csc2.20652
- Poudel, P. B., Poudel, M. R., and Puri, R. R. (2021). Evaluation of heat stress tolerance in spring wheat (*Triticum aestivum* L.) genotypes using stress tolerance indices in western region of Nepal. *J. Agric. Food Res.* 5. doi: 10.1016/j.jafr.2021.100179

- Powell, O. M., Voss-Fels, K. P., Jordan, D. R., Hammer, G., and Cooper, M. (2021). Perspectives on applications of hierarchical gene-to-phenotype (G2P) maps to capture non-stationary effects of alleles in genomic prediction. *Front. Plant Sci.* 12. doi: 10.3389/fpls.2021.663565
- Rehman, H. U., Tariq, A., Ashraf, I., Ahmed, M., Muscolo, A., Basra, S. M. A., et al. (2021). Evaluation of physiological and morphological traits for improving spring wheat adaptation to terminal heat stress. *Plants-Basel* 10. doi: 10.3390/plants10030455
- Reynolds, M. P., Lewis, J. M., Ammar, K., Basnet, B. R., Crespo-Herrera, L., Crossa, J., et al. (2021). Harnessing translational research in wheat for climate resilience. *J. Exp. Bot.* 72, 5134–5157. doi: 10.1093/jxb/erab256
- Rosa, G. J. M., Valente, B. D., Campos, G. I., Wu, X. L., Gianola, D., and Silva, M. A. (2011). Inferring causal phenotype networks using structural equation models. *Genet. Selection Evol.* 43. doi: 10.1186/1297-9686-43-6
- Rosseel, Y. (2012). lavaan: an R package for structural equation modeling. *J. Stat. Software* 48, 1–36. doi: 10.18637/jss.v048.i02
- Sall, A. T., Cisse, M., Gueye, H., Kabbaj, H., Ndoeye, I., Filali-Maltouf, A., et al. (2018). Heat tolerance of durum wheat (*Triticum durum* Desf) elite germplasm tested along the Senegal River. *J. Agric. Sci.* 10, 217. doi: 10.5539/jas.v10n2p217
- Sall, A. T., Kabbaj, H., Menoum, S. E., Cisse, M., Geleta, M., Ortiz, R., et al. (2024). Durum wheat heat tolerance loci defined via a north-south gradient. *Plant Genome* 17, e20414. doi: 10.1002/tpg2.20414
- Semenov, M. A., and Shewry, P. R. (2011). Modelling predicts that heat stress, not drought, will increase vulnerability of wheat in Europe. *Sci. Rep.* 1. doi: 10.1038/srep00066
- Sharma, D., Pandey, G. C., Mamrutha, H. M., Singh, R., Singh, N. K., Singh, G. P., et al. (2019). Genotype-phenotype relationships for high-temperature tolerance: an integrated method for minimizing phenotyping constraints in wheat. *Crop Sci.* 59, 1973–1982. doi: 10.2135/cropsci2019.01.0055
- Sharma, P., Sareen, S., Saini, M., and Shefali, (2017). Assessing genetic variation for heat stress tolerance in Indian bread wheat genotypes using morpho-physiological traits and molecular markers. *Plant Genet. Resources-Characterization Utilization* 15, 539–547. doi: 10.1017/S1479262116000241
- Shewry, P. R., and Hey, S. J. (2015). The contribution of wheat to human diet and health. *Food Energy Secur.* 4, 178–202. doi: 10.1002/fes3.64
- Simko, I., and Piepho, H. P. (2012). The area under the disease progress stairs: calculation, advantage, and application. *Phytopathology* 102, 381–389. doi: 10.1094/PHYTO-07-11-0216
- Smith, R. G., Davis, A. S., Jordan, N. R., Atwood, L. W., Daly, A. B., Grandy, A. S., et al. (2014). Structural equation modeling facilitates transdisciplinary research on agriculture and climate change. *Crop Sci.* 54, 475–483. doi: 10.2135/cropsci2013.07.0474
- Sukumaran, S., Reynolds, M. P., and Sansaloni, C. (2018). Genome-wide association analyses identify QTL hotspots for yield and component traits in durum wheat grown under yield potential, drought, and heat stress environments. *Front. Plant Sci.* 9. doi: 10.3389/fpls.2018.00081
- Telfer, P., Edwards, J., Bennett, D., Ganesalingam, D., Able, J., and Kuchel, H. (2018). “A field and controlled environment evaluation of wheat (*Triticum aestivum*) adaptation to heat stress. *Field Crops Res.* 229, 55–65. doi: 10.1016/j.fcr.2018.09.013
- Tibshirani, R. (1996). Regression shrinkage and selection via the Lasso. *J. R. Stat. Soc. Ser. B-Methodological* 58, 267–288. doi: 10.1111/j.2517-6161.1996.tb02080.x
- Tibshirani, R. (2011). Regression shrinkage and selection via the lasso: a retrospective. *J. R. Stat. Soc. Ser. B-Statistical Method.* 73, 273–282. doi: 10.1111/j.1467-9868.2011.00771.x
- Topner, K., Rosa, G. J. M., Gianola, D., and Schon, C. C. (2017). Bayesian networks illustrate genomic and residual trait connections in maize (*Zea mays* L.). *G3-Genes Genomes Genet.* 7, 2779–2789. doi: 10.1534/g3.117.044263
- Tuberosa, R. (2012). Phenotyping for drought tolerance of crops in the genomics era. *Front. Physiol.* 3. doi: 10.3389/fphys.2012.00347
- Ullah, A., Nadeem, F., Nawaz, A., Siddique, K. H. M., and Farooq, M. (2022). Heat stress effects on the reproductive physiology and yield of wheat. *J. Agron. Crop Sci.* 208, 1–17. doi: 10.1111/jac.12572
- Valente, B. D., Rosa, G. J. M., Campos, G. I., Gianola, D., and Silva, M. A. (2010). Searching for recursive causal structures in multivariate quantitative genetics mixed models. *Genetics* 185, 633–U361. doi: 10.1534/genetics.109.112979
- Valente, B. D., Rosa, G. J. M., Gianola, D., Wu, X.-L., and Weigel, K. (2013). Is structural equation modeling advantageous for the genetic improvement of multiple traits? *Genetics* 194, 561–572. doi: 10.1534/genetics.113.151209
- van Eeuwijk, F. A., Bustos-Korts, D., Millet, E. J., Boer, M. P., Kruijer, W., Thompson, A., et al. (2019). Modelling strategies for assessing and increasing the effectiveness of new phenotyping techniques in plant breeding. *Plant Sci.* 282, 23–39. doi: 10.1016/j.plantsci.2018.06.018
- Vargas, M., Crossa, J., Reynolds, M. P., Dhungana, P., and Eskridge, K. M. (2007). Structural equation modelling for studying genotype x environment interactions of physiological traits affecting yield in wheat. *J. Agric. Sci.* 145, 151–161. doi: 10.1017/S0021859607006806
- Verhulst, N., Carrillo-Garcia, A., Moeller, C., Trethowan, R., Sayre, K. D., and Govaerts, B. (2011). Conservation agriculture for wheat-based cropping systems under gravity irrigation: increasing resilience through improved soil quality. *Plant Soil* 340, 467–479. doi: 10.1007/s11104-010-0620-y
- Verhulst, N., Govaerts, B., Sayre, K. D., Deckers, J., Francois, I. M., and Dendooven, L. (2009). Using NDVI and soil quality analysis to assess influence of agronomic management on within-plot spatial variability and factors limiting production. *Plant Soil* 317, 41–59. doi: 10.1007/s11104-008-9787-x
- Wahid, A., Gelani, S., Ashraf, M., and Foolad, M. R. (2007). Heat tolerance in plants: An overview. *Environ. Exp. Bot.* 61, 199–223. doi: 10.1016/j.envexpbot.2007.05.011
- Welcker, C., Spencer, N. A., Turc, O., Granato, I., Chapuis, R., Madur, D., et al. (2022). Physiological adaptive traits are a potential allele reservoir for maize genetic progress under challenging conditions. *Nat. Commun.* 13. doi: 10.1038/s41467-022-30872-w
- Wolak, M. E., Fairbairn, D. J., and Paulsen, Y. R. (2012). Guidelines for estimating repeatability. *Methods Ecol. Evol.* 3, 129–137. doi: 10.1111/j.2041-210X.2011.00125.x
- Wright, S. (1921). Correlation and causation. *J. Agric. Res.* 201, 28.
- Xu, J., Lowe, C., Sergio, G., Hernandez-Leon, S., Dreisigacker, S., Reynolds, M. P., et al. (2022). The effects of brief heat during early booting on reproductive, developmental, and chlorophyll physiological performance in common wheat (*Triticum aestivum* L.). *Front. Plant Sci.* 13. doi: 10.3389/fpls.2022.886541
- Zadoks, J. C., Chang, T. T., and Konzak, C. F. (1974). A decimal code for the growth stages of cereals. *Weed Res.* 14, 415–421. doi: 10.1111/j.1365-3180.1974.tb01084.x
- Zhao, C., Liu, B., Piao, S. L., Wang, X. H., Lobell, D. B., Huang, Y., et al. (2017). Temperature increase reduces global yields of major crops in four independent estimates. *Proc. Natl. Acad. Sci. U.S.A.* 114, 9326–9331. doi: 10.1073/pnas.1701762114

Glossary

CENEB	Campo Experimental Normal E Borlaug
CIMMYT	Centro Internacional de Mejoramiento de Maize Y Trigo
DTM	Date To Maturity
GFP	Grain Filling Period
HD	Heading Date
HS	heat-stress trial, delayed sowing
LASSO	last absolute Shrinkage and selection operator
ME	Mega Environment
MTM	Multiple Trait Model
NS	non-stress trial
QTL	Quantitative Trait Locus
RIL	Recombinant Inbred Line
SEM	Structural Equation Model
GSEM	Genetic-SEM
SOM	Soil Organic Matter
UNIBO	University of Bologna
<i>Environmental parameters</i>	
AMT	Average Maximum Temperature
GDD	Growing Degree Days
HDD	Heat Degree Days
HDD_A	HDD during Anthesis
HDD_GF	HDD during Grain Filling
NDTH30	Number of Days with Temperature > 30°
NDTH35	Number of Days with Temperature > 35°
<i>Phenotypic traits</i>	
GY	Grain Yield
IT_INDEX	NDVI area under heat stress progress curve
KLE	Kernel Length
KNS	Kernel Number per Spike
KWI	Kernel Width
KWS	Kernel Weight per Spike
NDVI	Normalized Difference Vegetation Index
PH	Plant Height
SKT	number of spikelets per spike
SPM	number of Spikes per linear meter
TKW	Thousand Kernel Weight
TWT	Test Weight



OPEN ACCESS

EDITED BY

Ignacio Romagosa,
Agrotecnio Center, Spain

REVIEWED BY

Paula Martins-Lopes,
University of Trás-os-Montes and Alto Douro,
Portugal
Jose Miguel Soriano,
Universitat de Lleida, Spain

*CORRESPONDENCE

Pilar Prieto

✉ pilar.prieto@ias.csic.es

[†]These authors share first authorship

RECEIVED 29 February 2024

ACCEPTED 29 June 2024

PUBLISHED 23 July 2024




CITATION

Cifuentes Z, Calderón M-C, Miguel-Rojas C,
Sillero JC and Prieto P (2024) Development
and characterisation of novel durum wheat–
H. chilense 4H^{ch} chromosome lines as a
source for resistance to Septoria tritici blotch.
Front. Plant Sci. 15:1393796.
doi: 10.3389/fpls.2024.1393796

COPYRIGHT

© 2024 Cifuentes, Calderón, Miguel-Rojas,
Sillero and Prieto. This is an open-access article
distributed under the terms of the [Creative
Commons Attribution License \(CC BY\)](#). The
use, distribution or reproduction in other
forums is permitted, provided the original
author(s) and the copyright owner(s) are
credited and that the original publication in
this journal is cited, in accordance with
accepted academic practice. No use,
distribution or reproduction is permitted
which does not comply with these terms.

Development and characterisation of novel durum wheat–*H. chilense* 4H^{ch} chromosome lines as a source for resistance to Septoria tritici blotch

Zuny Cifuentes^{1†}, Maria-Carmen Calderón^{1†},
Cristina Miguel-Rojas ², Josefina C. Sillero ²
and Pilar Prieto ^{1*}

¹Plant Breeding Department, Institute for Sustainable Agriculture, Agencia Estatal Consejo Superior de Investigaciones Científicas (CSIC), Córdoba, Spain, ²Area of Plant Breeding and Biotechnology, IFAPA Alameda del Obispo, Córdoba, Spain

The use of wild species as a source of genetic variability is a valued tool in the framework of crop breeding. *Hordeum chilense* Roem. et Schult is a wild barley species that can be a useful genetic donor for sustainable wheat breeding which carries genes conferring resistance to some diseases or increasing grain quality, among others. Septoria tritici blotch (STB), caused by the *Zymoseptoria tritici* fungus, is one of the most important wheat diseases worldwide, affecting both bread and durum wheat and having a high economic impact. Resistance to STB has been previously described in *H. chilense* chromosome 4H^{ch}. In this study, we have developed introgression lines for *H. chilense* chromosome 4H^{ch} in durum wheat using interspecific crosses, advanced backcrosses, and consecutive selfing strategies. Alien *H. chilense* chromosome segments have been reduced in size by genetic crosses between *H. chilense* disomic substitution lines in durum wheat and durum wheat lines carrying the *Ph1* deletion. *Hordeum chilense* genetic introgressions were identified in the wheat background through several plant generations by fluorescence *in situ* hybridisation (FISH) and simple sequence repeat (SSR) markers. An STB infection analysis has also been developed to assess STB resistance to a specific *H. chilense* chromosome region. The development of these *H. chilense* introgression lines with moderate to high resistance to STB represents an important advance in the framework of durum breeding and can be a valuable tool for plant breeders.

KEYWORDS

Septoria leaf blotch, plant breeding, *Ph1* locus, foliar disease, chromosome manipulation

Introduction

Increasing human population and climate change demand greater agricultural productivity. Wheat is a strategic crop, essential for Western countries. It is the most important source of protein, providing 20% of the calories consumed daily by humans, and its consumption is increasing, mainly in developing countries. Although the yield of primary crops, including wheat, in 2022 was double that of 2000, it is estimated that the global demand for wheat production will increase by 60% in 2050 to meet the requirements of a growing population (<http://www.fao.org>). Europe is the first-world producer of bread wheat and within the European Union; Spain ranks in the fifth position considering cereal production, mainly wheat, only behind France, Germany, Romania, and Poland (<http://www.fao.org>). Thus, the economic relevance of wheat as a strategic crop in agriculture is clear, but several biotic (diseases) and abiotic (higher temperatures, soil erosion, salinity, water availability, etc.) stresses can compromise the future of this crop. A solid strategy, based on the development of new approaches that allow the adaptation of wheat to climate change and are respectful of the principles of sustainable agriculture, is needed to face the challenge of feeding the expected human population (Hamblin, 1995). Plant breeders are playing a major role in worldwide efforts to understand gene functions and interactions, so the introduction of tolerant genes to both biotic and abiotic stresses can increase the quality and productivity of a key crop such as wheat (Mamrutha et al., 2019; Mondal et al., 2021; Pérez-Méndez et al., 2022).

Durum wheat (*Triticum turgidum*, $2n = 4x = 28$) is a globally relevant species for agriculture and also has an enormous impact in Spain since it is one of the most cultivated cereals together with bread wheat and barley. Despite its high productivity, annual fluctuations can be associated with biotic and abiotic stresses. One of the most important diseases affecting durum wheat is Septoria tritici blotch (STB) caused by the fungus *Zymoseptoria tritici* (Desm.) (Quaedvlieg et al., 2011), previously known as *Septoria tritici* (teleomorph *Mycosphaerella graminicola* (Fuckel) J. Schröt.), which triggers severe losses in yield that can reach 50% in susceptible cultivars (Fones and Gurr, 2015). Severe epidemics occur both in areas with frequent rains and in others where rainfall does not exceed 250 mm during the crop cycle. The wide range of temperatures in which the fungus can develop, the use of susceptible varieties, and the rapid evolution and adaptation of *Z. tritici* to diverse agricultural conditions have allowed a wide geographical distribution of the disease (Fones and Gurr, 2015).

The introgression of resistance genes in the framework of breeding programs is considered the main protection against this disease, and several sources of resistance have yielded adequate protection (Rubiales et al., 2001). Wheat resistance to STB can be qualitative (isolate-specific), depending on major genes with a strong effect according to a gene-for-gene interaction, or quantitative (isolate-non-specific) displaying a partial phenotype controlled by various genes with moderate to small effects (Kema et al., 2000; Brading et al., 2002; Brown et al., 2015). Quantitative resistance is quite significant for its effectiveness against all genotypes of the pathogen and its durability (Brown et al., 2015; Porras et al., 2021). When no sufficient genetic variability or resistant varieties are available, the incorporation of new

alleles into the wheat germplasm is considered essential. Thus, genetic crosses between donor species and the crop itself can be a powerful tool to transfer chromosome segments carrying desirable genes from the alien species into wheat.

Breeders have been using related species as genetic donors with the target of widening the genetic basis of this crop obtaining, for example, wheat cultivars better adapted to specific agro-climatic conditions, carrying resistance to pests (Lukaszewski, 2000; Shubing and Honggang, 2005). Indeed, wide-crossing in plant breeding programmes is such an important tool that, sometimes the results are the starting point for new crops (O'mara, 1953; Martin and Sanchez-Mongelaguna, 1982) and marked a milestone in a breeding framework.

Diploid wild barley *Hordeum chilense* Roem. et Schultz ($2n = 2x = 14 H^{ch}H^{ch}$) exhibits valuable agronomic and quality traits for wheat improvement, and it has already been crossed with some species of the tribe Triticeae (grasses), particularly with both durum and bread wheat (Martin et al., 1996; Calderón et al., 2012). This wild species also has enormous potential as a donor of other genetic features such as drought and salt tolerance as well as resistance to pests and diseases (Gallardo and Fereres, 1989; Bothmer et al., 1995; Martin et al., 1996). Particularly, *H. chilense* contains interesting genes for biotic and abiotic stress resistance, such as resistance to STB, conferred mainly by the $4H^{ch}$ chromosome (Rubiales et al., 2000). The transfer of *H. chilense* chromosome 4 in durum wheat has been already developed (Calderón et al., 2012), but, in a plant breeding framework, the size of full introgressed chromosomes from relatives must be reduced to diminish the drag linkage of undesirable genes.

Much of the work aimed to promote interspecific chromosome associations to transfer genetic variability from wild relatives into wheat has relied on the use of the *ph1b* mutant (Sears and Okamoto, 1958). Homoeologous recombination between chromosomes from related but different genomes can occur in the absence of the *Ph1* locus, resulting in the generation of interspecific recombinant chromosomes (Sears and Okamoto, 1958; Othmeni et al., 2019). In the absence of the *Ph1* locus, chromosome rearrangements in bread wheat involving wheat and relative *H. chilense* and *H. vulgare* chromosomes have already been obtained (Rey et al., 2015a, 2015). In this work, we used the *ph1* mutant and the previously developed *H. chilense* chromosome $4H^{ch}$ substitution line (Calderón et al., 2012), both in durum wheat background, to carry out genetic crosses to facilitate durum wheat-wild barley interspecific recombination. A set of durum wheat-*H. chilense* chromosome $4H^{ch}$ translocation lines were obtained and characterised using molecular markers and fluorescence *in situ* hybridisation. We also analysed these lines for the incidence of STB under controlled conditions in growth chambers to assess resistance to STB to an *H. chilense* chromosome $4H^{ch}$ segment.

Materials and methods

Plant materials

Genetic crosses between the $4H^{ch}$ ($4B$) substitution line in durum wheat cv. Langdon (*T. turgidum*, $2n=4x = 28$; (Calderón et al., 2012) and durum wheat cv. Capelli carrying the *Ph1* deletion

(Ceoloni et al., 1992) have been carried out. F1 plants were backcrossed with durum wheat cv. Capelli in the *ph1* mutant background. Plants were selected using molecular markers and by *in situ* hybridisation and then selfed. The procedure is described in Figure 1, and the chromosomal composition of *Hordeum chilense* chromosome 4H^{ch} introgression lines in durum wheat is summarized in Table 1. Plants carrying *H. chilense* introgressions were selected for analysis.

Seeds were incubated in Petri dishes on wet filter paper in the dark for 5 days at 4°C, followed by 24 h of incubation at 24°C to allow germination. Then, roots were cut and incubated for 4 h in 0.05% colchicine solutions at 24°C to accumulate somatic cells in metaphase and finally fixed in ethanol/glacial acetic acid 3:1 (v/v) for 1 month at 4°C.

Cytogenetic analysis

For identification and characterisation of the *H. chilense* chromosome 4H^{ch} introgressions and wheat chromosomes involved in translocations, fluorescence *in situ* hybridisation (FISH) using *H. chilense* DNA, the GAA-satellite sequence, and the pAs1 probe (Cabrera et al., 1995; Pedersen et al., 1997) was performed. DNA probes were labelled by nick translation with biotin-11 dUTP (Roche Corporate, Basel, Switzerland) and digoxigenin 11-dUTP (Roche Corporate, Basel, Switzerland) and detected with streptavidin-Cy3

(Sigma, St Louis, MO, USA) and anti-digoxigenin-FITC (Roche Corporate Basel, Switzerland), respectively.

Metaphase mitotic chromosomes were hybridised with total genomic *H. chilense* DNA as a probe to identify the chromosome segment introgressed from *H. chilense* chromosome 4H^{ch}. Afterwards, the preparations were hybridised using the repetitive sequence GAA and the pAs1 probe to characterise both the *H. chilense* chromosome segment and the wheat chromosome involved in interspecific chromosome translocations. The *in situ* protocol was performed according to Prieto et al. (2004).

Hybridisation signals were visualised using a Nikon eclipse inflorescence microscopy, and the images were captured with a Nikon CCD camera using the appropriate Nikon 3.0 software (Nikon Instrument Europe BV, Amstelveen, The Netherlands) and processed with Photoshop 4.0 software for brightness and contrast (Adobe Systems Inc., San Jose, CA, USA).

Molecular marker characterisation

Molecular markers were selected and tested for the specific identification of the short and long arms of *H. chilense* chromosome 4H^{ch} according to available information (Said and Cabrera, 2009; Sakata et al., 2010).

Genomic DNA was extracted from frozen young leaves using the CTAB method described by Murray and Thompson (1980). We

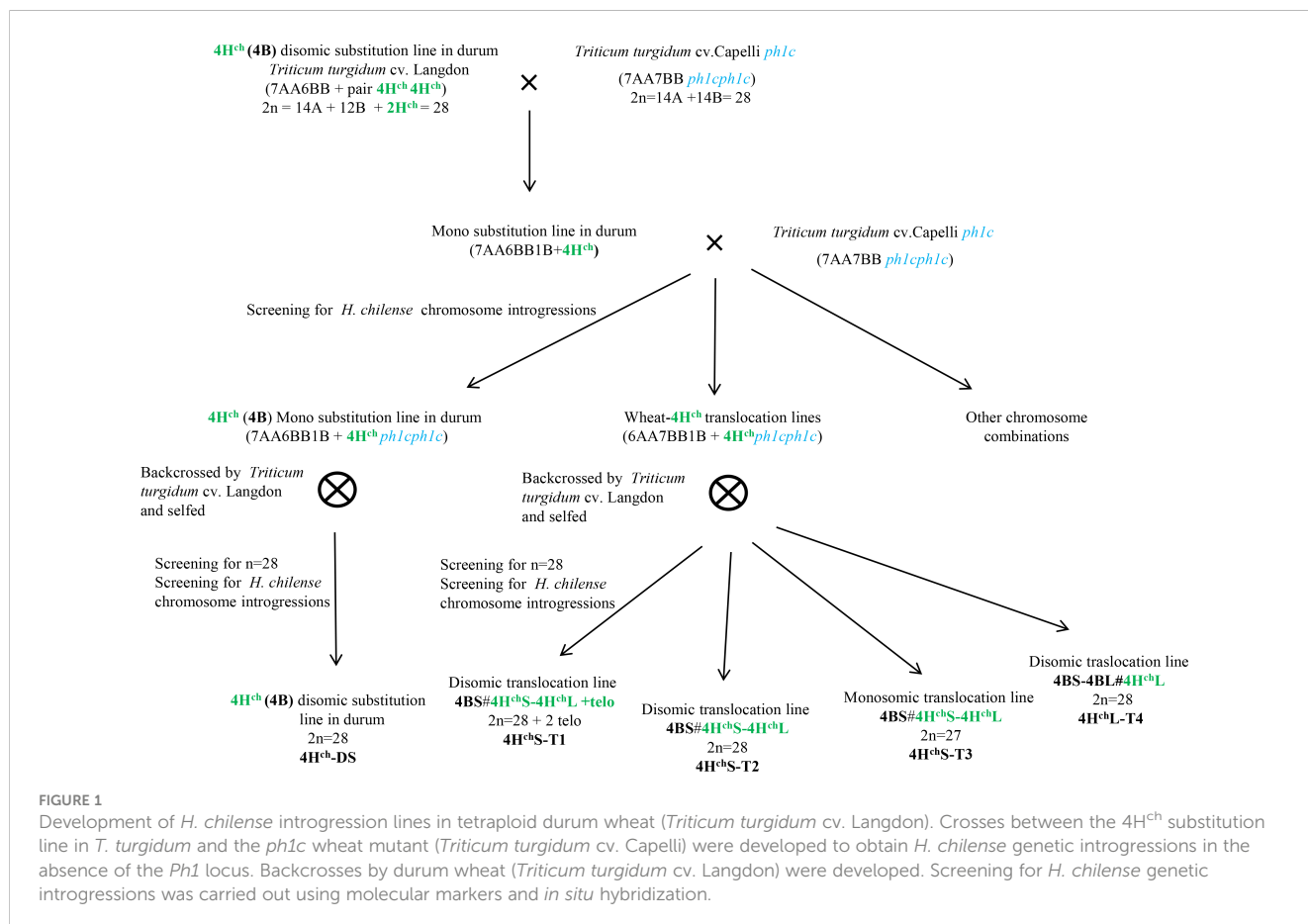


TABLE 1 Progeny of the crosses between the 4H^{ch}(4B) substitution line in durum wheat (*Triticum turgidum*) and the durum wheat carrying the *Ph1* deletion.

Plant line	Chromosome number	Chromosomal composition	Number of plants obtained (% fertility)
4H ^{ch} -DS	28	4H ^{ch} disomic substitution line	103 (100%)
4H ^{ch} S-T1	28 + 2 telo	Disomic translocation 4BS#4H ^{ch} S-4H ^{ch} L+telo	45 (50%)
4H ^{ch} S-T2	28	Disomic translocation 4BS#4H ^{ch} S-4H ^{ch} L	29 (50%)
4H ^{ch} S-T3	27	Monosomic translocation 4BS#4H ^{ch} S-4H ^{ch} L	59 (50%)
4H ^{ch} L-T4	28	Disomic translocation 4BS-4BL#4H ^{ch} L	52 (40%)

Chromosomal composition of *Hordeum chilense* chromosome 4H^{ch} introgression lines in durum wheat after backcrossed and selfed generations.

tested 25 and 9 markers to specifically identify both the short arm and the long arm of chromosome 4H^{ch}, respectively. The polymerase chain reaction (PCR) experiments were performed in 20 µL of a mixture containing 4 µL of reaction buffer containing MgCl₂ and dNTPs, 5 pmol of selected primers, and 0.4 µL of MyTaq DNA polymerase. Specific primers and PCR conditions to amplify these markers were according to Masaya [Sakata et al. \(2010\)](#) and [Said and Cabrera \(2009\)](#). The PCR products were visualized using SafeView (NBS Biologicals, Cambridgeshire, UK) in an agarose (1%) electrophoresis gel (120 V, 45 min).

We have also used the NCBI's BLAST (Basic Local Alignment Search Tool) to perform retro-transcription-PCR (RT-PCR) *in silico* on *H. chilense* genome and to locate the position of the primers on the *H. chilense* physical map using the reference genome (txid15565) from the NCBI database (National Center for Biotechnology Information).

Infection assay

The inoculation process was developed as reported by [Stewart and McDonald \(2014\)](#), following minor modifications described by [Porrás et al. \(2021\)](#). Briefly, seeds of the 10 durum wheat genotypes, including the positive control, were sown in 8 × 7 × 7 cm pots containing a mix (1:1, v/v) of commercial compost (Suliflor SF1 substrate; Suliflor Lithuania) and sand. Pots were incubated in a growth chamber at 21°C and 70% relative humidity (RH), with 16 h of light. After 16 days, seedlings were fungal inoculated when the second and third leaves emerged [growth stage Z13; [Zadoks et al., 1974](#)]. *Zymoseptoria tritici* (isolated from infected durum wheat of Santaella (Cordoba, Spain) and deposited at the NCBI database under the SUB9540116 accession number) inoculum was adjusted to 10⁷ spores mL⁻¹ in distilled water and 0.1% Tween 20. Seedlings were inoculated using a hand sprayer. Once leaves were totally dry, plants were sealed in clear plastic bags to provide 100% RH and maintained for 48 h in a growth chamber at 22/18°C day/night with a 16-h

photoperiod. After 48 h, plastic bags were removed, and plants were kept at 75%–80% RH. The amount of infected plants per family was variable, ranging from 6 to 18, based on seed availability. The positive control check, the commercial cultivar 'SY Leonardo', was inoculated following the same treatment. Three independent experiments with three replicates each were performed.

Disease assessment

At 21 days post-inoculation, the third leaf of each plant was evaluated. The infection process was qualitatively scored using the disease severity (DS) rating scale from 0 to 5 ([McCartney et al., 2002](#)), as follows: 0 = immune with no visible symptoms, 1 = highly resistant with hypersensitive flecking, 2 = resistant with small chlorotic or necrotic lesions and no pycnidial development, 3 = moderately resistant, characterised by coalescence of chlorotic and necrotic lesions with slight pycnidial development, 4 = susceptible with moderate pycnidial development and coalesced necrotic lesions, and 5 = very susceptible with large, abundant pycnidia and extensively coalesced necrotic lesions. [Porrás et al. \(2021\)](#) showed a digitally infected leaves scale with STB that was used as a reference to evaluate the families of the present study. Reaction types 0–3 were considered resistant, whereas reaction types 4 and 5 were considered susceptible. Although reaction type 3 includes pycnidium development, it is considered resistant because the growth and sporulation of the fungus are quite restricted, and the chlorotic reaction is similar to the chlorotic blotches of reaction type 2.

Results

Cytogenetic and molecular marker analysis

Crosses between the 4H^{ch}(4B) substitution line in durum wheat cv. Langdon and the durum wheat cv. Capelli carrying the *Ph1* deletion were carried out to promote interspecific recombination between chromosome 4H^{ch} and the homoeologous wheat chromosomes in the absence of the *Ph1* locus. To obtain the *Ph1* deletion in homozygosis, one backcross to durum wheat cv. Capelli carrying the *Ph1* deletion was carried out. Wheat plants carrying monosomic and disomic *H. chilense* introgressions were selected and analysed by multicolour *in situ* hybridisation and molecular markers. The procedure is summarised in [Figure 1](#). We obtained more than 200 plants having either monosomic or disomic genetic introgressions involving *H. chilense* chromosome 4H^{ch} in durum wheat ([Table 1](#)).

A total of 24 EST-SSR (Expressed Sequence Tags-Simple Single Repeat) specific markers for the short arm of *H. chilense* chromosome 4H^{ch} and nine barley markers for the long arm of the same chromosome were tested to identify those markers displaying polymorphism between durum wheat and the wild barley ([Table 2](#)). Most of them did not show polymorphism between the 4H^{ch} *H. chilense* and the 4A wheat homoeologous chromosome and were not used for the genetic screening. Only 10

markers revealed polymorphism between 4H^{ch} *H. chilense* and wheat and were used to identify and characterise the size of the 4H^{ch} *H. chilense* introgressions (Table 3).

The chromosomal location of polymorphic molecular markers on the 4H^{ch} chromosome was performed by *in silico* RT-PCR on the *H. chilense* genome, using NCBI's BLAST for lining up the preexisting primers. Five markers were located on the short arm of chromosome 4H^{ch} (K00607, BAWU505, GBM1028, BAWU303, and K02539) and another five on the 4H^{ch}L (BAWU217, BAWU152, BAWU497, BAWU312, and K04754). The molecular analysis of the four translocation lines obtained showed that marker K02539, located near the centromere of 4H^{ch}S, amplified in 4H^{ch}S-T1, 4H^{ch}S-T2, and 4H^{ch}S-T3 and was absent in 4H^{ch}L-T4, revealing that wheat-*H. chilense* recombination in 4H^{ch}S-T1, 4H^{ch}S-T2, and 4H^{ch}S-T3 did occur between 4H^{ch}S and wheat chromosomes. Only 4H^{ch}S-T1 and 4H^{ch}S-T2 were positive for the BAWU303 marker. K00607, BAWU505, and GBM1028 markers, located in a distal position on 4H^{ch}S, were absent in all translocation lines (Table 3). Thus, three wheat-*H. chilense* translocation lines involving the short arm of chromosome 4H^{ch} were obtained. Recombination events did occur at least in two different positions on the 4H^{ch} chromosome as 4H^{ch}S-T1 and 4H^{ch}S-T2 displayed a similar molecular pattern and were different from the 4H^{ch}S-T3 translocation line. Related to the molecular analysis of those markers located on the long arm of 4H^{ch} *H. chilense* chromosome, all translocation lines were positive for distal BAWU312 and K04754 markers. BAWU217, BAWU152, and BAWU497 were positive in all translocation lines except in 4H^{ch}L-T4. In fact, the 4H^{ch}L-T4 translocation line was only positive for the distal K04754 and BAWU312 markers. Our results displayed that this 4H^{ch}L-T4 translocation line only retained a distal 4H^{ch}L chromosome segment in the durum wheat background.

Depending on the recombination event between *H. chilense* and wheat chromosomes, four different types of genetic introgressions for *H. chilense* chromosome 4H^{ch} were obtained in durum wheat in the *ph1* mutant background (Table 1; Figures 2, 3). Most of the interspecific recombination events that we were able to recover occurred between the short 4H^{ch} and 4A chromosome arms. Thus, we obtained three different translocation lines involving the short 4H^{ch} and 4A chromosome arms, named 4H^{ch}S-T1, 4H^{ch}S-T2, and 4H^{ch}S-T3 and one involving the long 4H^{ch} and 4A chromosome arms, named 4H^{ch}L-T4.

Genomic *in situ* hybridisation contributed to elucidate the exact chromosomal composition of all translocation lines obtained (Figure 2). All the *H. chilense*-wheat translocation lines obtained were disomic except 4H^{ch}S-T3, which was monosomic. The cytogenetic analysis using the psA1 and GAA repeat sequences contributed to characterise the chromosome segment of the *H. chilense* chromosome 4H^{ch} introgressed in durum wheat by their specific pattern on this chromosome 4H^{ch} (Figure 3B). Thus, 4H^{ch}S-T1, 4H^{ch}S-T2, and 4H^{ch}S-T3 translocation lines contained the full 4H^{ch}L chromosome arm and a fragment of the 4H^{ch}S chromosome arm, which vary among these translocation lines

TABLE 2 Molecular markers used for the screening of *Hordeum chilense* chromosome introgressions in the durum wheat (DW) background.

Markers for 4H ^{ch}	DW	<i>H. chilense</i> (line H1)	4H ^{ch} -DS
4H ^{ch} S			
K07854	×	×	×
K03491	–	–	–
K00607	–	x	x
K00967	×	×	×
K03028	×	×	–
K00266	×	×	×
K00201	–	–	–
K02131	×	×	×
K00230	×	×	×
K02013	×	×	×
K01265	×	×	×
K04643	×	×	×
BAWU505	–	x	x
K02029	×	×	×
GBM1028	–	x	x
K00783	×	×	×
BAWU303	–	x	x
K02529	–	x	x
MWG542	–	×	–
K07933	×	×	×
K05013	×	×	×
K06310	×	×	×
K00552	×	×	×
BAWU852	–	×	–
4H ^{ch} L			
K05042	×	×	×
K04115	×	×	×
K00136	×	×	–
K03089	–	–	–
BAWU217	–	x	x
BAWU152	–	x	x
BAWU312	–	x	x
BAWU497	–	x	x
K04754	–	x	x

Polymorphic markers between durum wheat and *H. chilense* line H1 (in bold) were used for the assessment of the introgression lines. Although BAWU852 and MWG542 markers showed polymorphism between durum wheat and the H1 *H. chilense* line, signals were not strong enough to be used for a reliable screening and were discarded.

TABLE 3 Barley SSR markers used for the identification of *Hordeum chilense* chromosome 4H^{ch} introgressions in the durum wheat (DW) background.

Marker	Genetic position	Genotype						
		DW	H1	4H ^{ch} -DS	4H ^{ch} S-T1	4H ^{ch} S-T2	4H ^{ch} S-T3	4H ^{ch} L-T4
4H ^{ch} S								
K00607	27.6 cM (Sakata et al., 2010)	–	×	×	–	–	–	–
BAWU505	70% distal (Said and Cabrera, 2009)	–	×	×	–	–	–	–
GBM1028	52.3 cM (Said and Cabrera, 2009)	–	×	×	–	–	–	–
BAWU303	70% distal (Said and Cabrera, 2009)	–	×	×	×	×	–	–
K02539	106.0cM (Sakata et al., 2010)	–	×	×	×	×	×	–
4H ^{ch} L								
BAWU217	70% distal (Said and Cabrera, 2009)	–	×	×	×	×	×	–
BAWU152	70% distal (Said and Cabrera, 2009)	–	×	×	×	×	×	–
BAWU497	70% distal (Said and Cabrera, 2009)	–	×	×	×	×	×	–
BAWU312	70% distal (Said and Cabrera, 2009)	–	×	×	×	×	×	×
K04754	249.0 cM (Sakata et al., 2010)	–	×	×	×	×	×	×

All the durum wheat–*H. chilense* translocation lines obtained in this work were identified and characterised using this set of 10 markers.

depending on the position of the recombination event (Figure 3B). The cytogenetic analysis using the psA1 and GAA repeat sequences revealed a similar cytogenetic pattern between 4H^{ch}S-T1 and 4H^{ch}S-T2 translocation lines (Figure 3B), which agrees with the equivalent result obtained using molecular markers (Table 3). These results suggest that the recombination events occurring between wheat and barley chromosomes in these two 4H^{ch}S-T1 and 4H^{ch}S-T2 translocation lines were extremely close to each other along the 4H^{ch}S chromosome. In addition, a recombination event on the distal region of chromosome 4H^{ch}L did occur in the 4H^{ch}L-T4 translocation line, retaining only a small 4H^{ch}L chromosome segment (Figures 2, 3).

STB infection analysis

The development of STB in the *H. chilense* translocation lines obtained in the durum wheat background is shown in Table 4 and Figure 4. Two different experiments were carried out, and differences in Disease Severity (DS) rating scale scores were recorded. DS scores showed differences among the plants studied, ranging from 2 to 4. Most of the studied durum wheat lines exhibited a resistant to moderately resistant reaction, displaying DS ≤ 3, which indicated a restricted growth and sporulation of the fungus. The 4H^{ch} *H. chilense* disomic substitution line (4H^{ch}-DS) could be considered the most resistant one, showing a heterogeneous behaviour against the disease but with the

lowest DS scores (1-2). This means that some leaves presented reaction types highly resistant with hypersensitive flecking (DS 1), and others showed small necrotic lesions with no pycnidia development (DS 2). No remarkable differences were found between durum wheat–*H. chilense* translocation lines 4H^{ch}S-T1, 4H^{ch}S-T2, and 4H^{ch}L-T4, showing an average DS score of 3 (moderately resistant), with limited production of pycnidia (DS 3) and small necrosis lesions. In lines 4H^{ch}S-T2 and 4H^{ch}L-T4, most leaves displayed a mainly moderately resistant response with limited production of pycnidia with chlorotic/necrotic lesions (DS 3), although some leaves allowed higher pycnidia development. Only the family 4H^{ch}S-T3 displayed an average DS score higher than 3, showing leaves with two different reaction types, moderately resistant (DS 3) and susceptible (DS 4). This result could be because this translocation line has only one copy of the *H. chilense* chromosome segment (monosomic translocation line). Lastly, durum wheat cv. Langdon, which is the genetic background of the translocation lines developed in this work, presented an average DS score of 4 (susceptible), which indicates significant fungus-reproduction capability in the form of pycnidia in the necrotic lesions. Strikingly, none of the analysed durum wheat including the Langdon cultivar showed a DS score of 5 (very susceptible with abundant pycnidia and extensively coalesced necrotic lesions). As it was expected, the other control used in this work, cultivar SY Leonardo, was very susceptible, showing most of the screened plants high reproduction of the fungus and extensively coalesced lesions (DS 5).

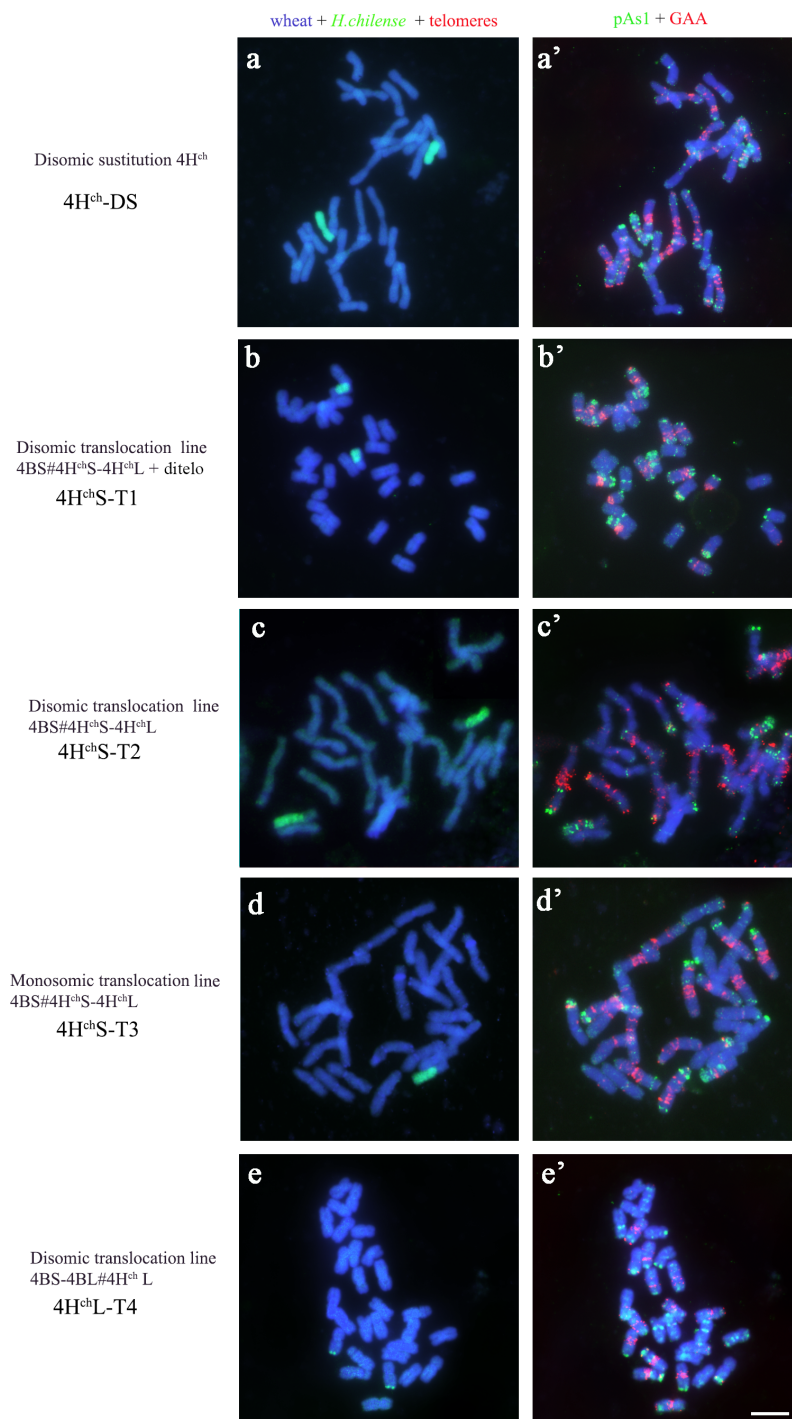


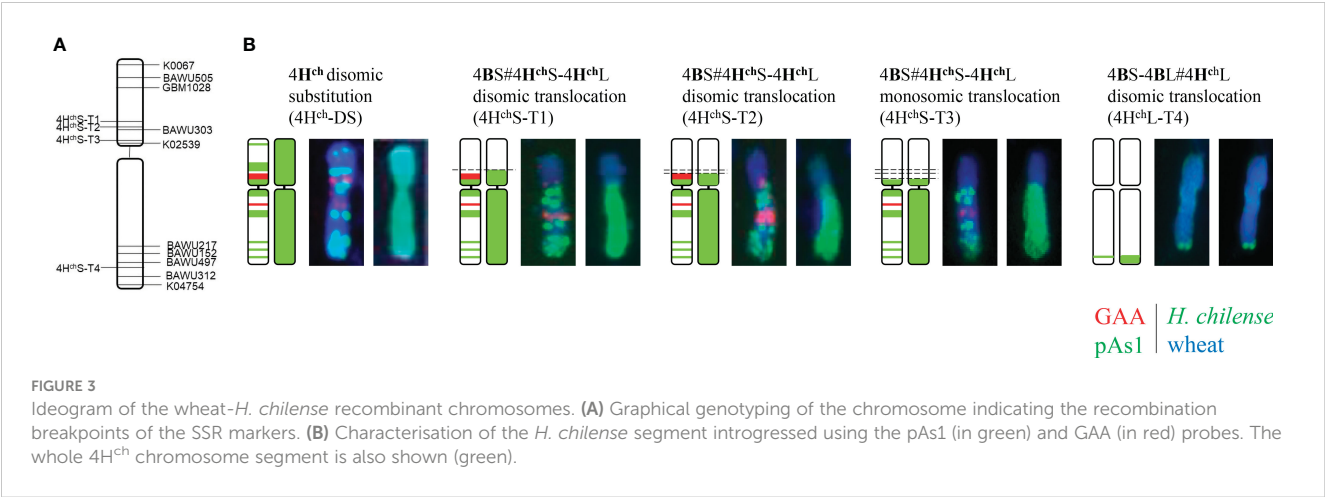
FIGURE 2

Cytogenetic visualisation of the introgression lines obtained for chromosome 4H^{ch} in *Triticum turgidum* using fluorescence *in situ* hybridisation. *Hordeum chilense* genomic introgressions are shown in green (A–E). Chromosome identification and orientation were confirmed by reprobing with the pAs1 (green) and GAA (red) probes in (A'–E'). DNA was counterstained with DAPI (blue). (A–A') 4H^{ch} disomic substitution line; (B–B') 4H^{ch}S-T1 translocation line; (C–C') 4H^{ch}S-T2 translocation line, (D–D') 4H^{ch}S-T3 translocation line; (E–E') 4H^{ch}L-T4 translocation line. Scale bar for all panels = 10 μ m.

Discussion

The effective introgression of genes from alien species like *H. chilense* into cultivated species such as durum wheat entails that target genes or the chromosome segment carrying them must be incorporated into wheat chromosomes as recombinant segments or

translocations. Examples of an important source of chromosome introgressions are centric-break fusion events found several decades ago in bread wheat–rye translocations (e.g., 1BL-IRS and 1AL-IRS), which have importantly contributed to global wheat production (Pena et al., 1990). Genetic introgressions from *H. chilense* chromosome 4H^{ch}, which contains resistance to STB (Rubiales



et al., 2000), have been previously developed in the durum wheat background (Calderón et al., 2012). In this work, genetic crosses between the durum wheat line carrying a disomic 4H^{ch}(4B) chromosome substitution and durum wheat carrying the *Ph1* deletion were developed to promote interspecific recombination between wheat and *H. chilense*. Recombination events between bread wheat and *H. chilense* lines in the absence of the *Ph1* locus have been previously promoted for both fundamental and applied purposes, which is to shed light into the mechanism of this *Ph1* locus or in a plant breeding framework to specifically introgress *H. chilense* chromosome 7H^{ch} to increase the carotenoid content in bread wheat (Rey et al., 2015a). To the best of our knowledge, it is the first time that the *ph1* mutant has been used in genetic crosses between *H. chilense* and wheat in the tetraploid durum background. The use of the *ph1* mutants in this work has enabled the possibility of promoting recombination events between 4A wheat and 4H^{ch} *H. chilense* homoeologous chromosomes, providing the opportunity to introgress part of 4H^{ch} chromosome in durum wheat and the development of a series of genetic introgressions for this *H. chilense* chromosome for durum breeding purposes. The durum wheat-*H. chilense* introgression lines for chromosome 4H^{ch}

developed in this work might facilitate the possibility of transferring resistance to STB in durum wheat as the 4H^{ch} chromosome was previously targeted as a potential source to introduce this type of resistance in wheat (Rubiales et al., 2000). The interaction between *Z. tritici* and durum wheat has been poorly studied, and no *Stb* genes have been identified in durum wheat so far (Somai-Jemmali et al., 2017). This lack of identified and characterised *Stb* resistance genes is a challenge for plant breeders to find durable sources of resistance to STB in durum wheat. Resistance to STB is generally expressed through the reduction of the foliar area covered with pycnidia and necrosis (Porrás et al., 2021). In this work, we have obtained several durum wheat-*H. chilense* translocation lines including chromosome 4H^{ch} that present a moderate resistance to STB. The reduction of the diseased in the 4H^{ch} *H. chilense* introgression lines in durum wheat is attributed to the contribution of chromosome 4H^{ch} compared with both control lines, the cultivar Langdon, which is the genetic background of the *H. chilense* introgressions developed, and the cultivar SY Leonardo, which is routinely used as a susceptible control to STB. Both durum cultivars displayed elevated susceptibility with abundant development of the fungus

TABLE 4 Classification of studied families according to their Disease Severity (DS) rating scale (McCartney et al., 2002).

Line	Number of plants	Percentage of plants with DS score					Average	Reaction types
		DS 1	DS 2	DS 3	DS 4	DS 5		
4H ^{ch} -DS	27	36	59	5	0	0	1-2	R
4H ^{ch} S-T1	18	0	22	67	17	5	3	MR
4H ^{ch} S-T2	6	0	0	67	33	0	3	MR
4H ^{ch} S-T3	24	0	4	57	39	0	3-4	MS
4H ^{ch} L-T4	9	0	0	78	22	0	3	MR
Langdon	14	0	0	21	79	0	4	S
SY Leonardo	10	0	0	0	20	80	5	S

The commercial cultivar 'SY Leonardo' and durum wheat cv. Langdon were used as positive control of STB infection. R, resistant; MR, moderately resistant; MS, moderately susceptible; S, susceptible. DS rating scale: 1 = highly resistant with hypersensitive flecking, 2 = resistant with small chlorotic or necrotic lesions and no pycnidial development, 3 = moderately resistant, characterised by coalescence of chlorotic and necrotic lesions with slight pycnidial development, 4 = susceptible with moderate pycnidial development and coalesced necrotic lesions, and 5 = very susceptible with large, abundant pycnidia and extensively coalesced necrotic lesions.

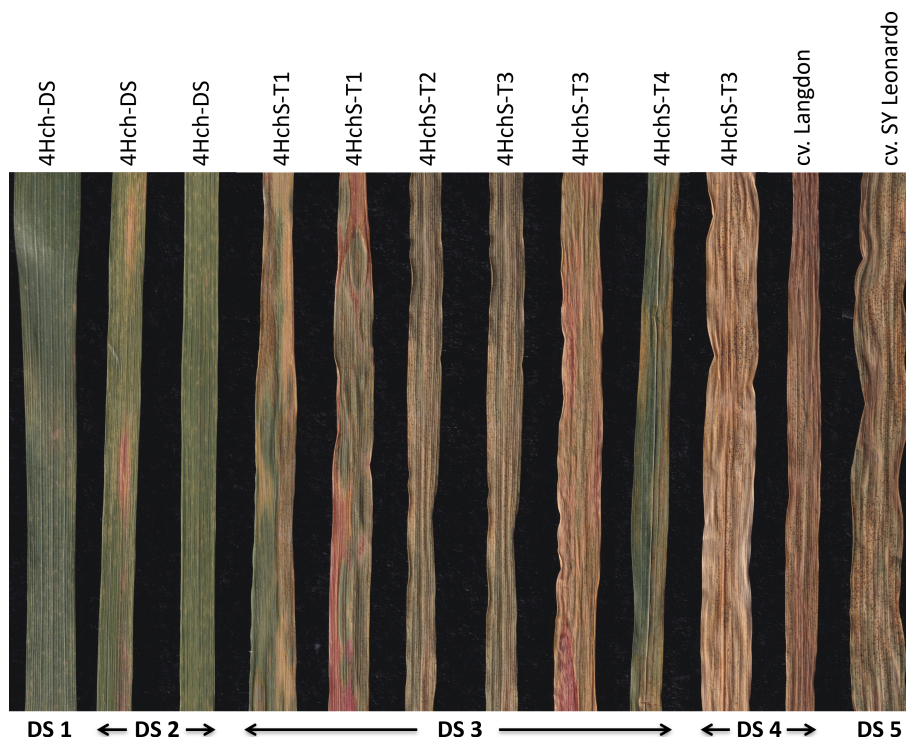


FIGURE 4

Examples of infected leaves with *Septoria tritici* blotch (STB) showing diverse disease severity rating scale (DS) scores. Leaves from the studied genotypes with different average DS scores. The 4H^{ch} disomic substitution, 4H^{ch}-DS, line displayed DS1-2. All the translocation lines 4H^{ch}S-T1, 4H^{ch}S-T2, 4H^{ch}S-T3, and 4H^{ch}L-T4 displayed DS 3, although some leaves from 4H^{ch}S-T3 also showed DS4 as the durum wheat cultivar Langdon. The most sensitive line (DS5) was the control cultivar SY Leonardo.

and extensively coalesced lesions (DS 4 and 5, respectively) in contrast to the DS scores 1 and 2 expressed by the 4H^{ch} disomic substitution line, 4H^{ch}-DS, or the average DS score of 3 displayed by the translocation lines 4H^{ch}S-T1, 4H^{ch}S-T2, and 4H^{ch}L-T4. Thus, our results demonstrate the contribution of chromosome 4H^{ch} for introgressing resistance to STB in durum wheat.

The combination of cytogenetic tools with a molecular analysis offers a reliable method of selection of *H. chilense* introgressions in the durum wheat background during a plant breeding programme. These combined approaches provide the possibility to detect and analyse a high number of plant lines carrying chromosome modifications in a suitable frame of time, and for this, they have been extensively used for the identification and characterisation of plant material for decades (Nalam et al., 2006; Faris et al., 2008; Wang et al., 2009; Calderón et al., 2012). In this work, genomic *in situ* hybridisation contributed to elucidate the exact chromosomal composition of all translocation lines obtained. All the *H. chilense*-wheat translocations obtained were disomic except 4H^{ch}S-T3, which was monosomic. Disomic 4H^{ch}S-T1, 4H^{ch}S-T2, and 4H^{ch}L-T4 translocation lines showed moderate resistance to STB, with limited production of pycnidia and small necrosis lesions, although the monosomic 4H^{ch}S-T3 line displayed moderately susceptible reaction with limited pycnidia development (DS 3-4). In contrast, the disomic line 4H^{ch}-DS showed a resistant behaviour to STB displaying hypersensitive flecking (DS1) and necrotic lesions with no presence of pycnidia (DS 2). These results confirmed an

apparent dosage effect on STB resistance as it was previously described in *Agropyron*-wheat derivatives (Rillo et al., 1970) and agree with the presence of different *Stb* genes along the *H. chilense* chromosome 4H^{ch}.

The similar pattern obtained by the cytogenetic analysis and molecular markers in 4H^{ch}S-T1 and 4H^{ch}S-T2 translocation lines suggested that the recombination events occurring in each of these translocation lines were extremely close to each other along the 4H^{ch}S chromosome. The fact of being the same recombination event is discarded as both 4H^{ch}S-T1 and 4H^{ch}S-T2 translocation lines were obtained from different genetic crosses between the original 4H^{ch}disomic line and the *ph1* mutants.

All the durum wheat-*H. chilense* translocation lines obtained in this work retained the distal region of *H. chilense* chromosome 4H^{ch}L, which might contain some homology to bread wheat chromosome 4AL, where QTL7 and *Stb7* and *Stb12* resistance genes are located (Brown et al., 2015). All the durum wheat-*H. chilense* translocation lines developed in this work (4H^{ch}S-T1, 4H^{ch}S-T2, 4H^{ch}S-T3, and 4H^{ch}L-T4) displayed moderate resistance to STB compared with the control lines. However, some other gene(s) might also be located on the distal region of chromosome 4H^{ch}S, as the 4H^{ch} *H. chilense* disomic substitution (4H^{ch}DS) line could be considered the most resistant one, showing a heterogeneous behaviour against the disease but with the lowest DS scores (1-2). In addition, no remarkable differences in the STB resistance were found between 4H^{ch}S-T1 and 4H^{ch}S-T2 translocation lines, indicating that putative resistance genes

might not be located in the small segment of chromosome 4H^{chS} in which these two durum wheat–*H. chilense* translocation lines might be different. Thus, that putative additional gene(s) should be included in the most distal 4H^{chS} chromosome region. Consequently, our results suggest that *H. chilense* chromosome 4H^{chL} might contain genes conferring resistance to STB on the distal 4H^{chL} chromosome arm. These genes could be homoeologous to those *Stb7* and *Stb12* resistance genes or STB7 QTL described previously in the 4A bread wheat chromosome (Brown et al., 2015), but, interestingly enough, additional gene(s) conferring stronger resistance to STB might also be included in the distal region of the *H. chilense* chromosome 4H^{chS}. To sum up, this present study sheds light on the interaction of *Z. tritici* and durum wheat, giving some clues to identify possible *Stb* genes in durum wheat. Therefore, the plant material obtained in this work constitutes a valuable germplasm to introduce resistance to STB in durum wheat.

Data availability statement

The original contributions presented in the study are included in the article/supplementary material, further inquiries can be directed to the corresponding authors. *Zymoseptoria tritici* isolated is deposited in the public NCBI database under the MZ026796 accession number.

Author contributions

ZC: Writing – original draft, Investigation. M-CC: Investigation, Writing – review & editing. CM-R: Investigation, Writing – review & editing. JS: Investigation, Writing – review & editing. PP: Conceptualization, Funding acquisition, Investigation,

Project administration, Resources, Supervision, Writing – original draft, Writing – review & editing.

Funding

The author(s) declare financial support was received for the research, authorship, and/or publication of this article. This work has been supported by P20_00971 grant and the Qualifica Project QUAL21_023 IAS both from Consejería de Transformación Económica, Industria, Conocimiento y Universidades/ Cofinanciación FEDER 80%—Programa Operativo FEDER de Andalucía 2014-2020.

Conflict of interest

The authors declare that the research was conducted in the absence of any commercial or financial relationships that could be construed as a potential conflict of interest.

The author(s) declared that they were an editorial board member of Frontiers, at the time of submission. This had no impact on the peer review process and the final decision.

Publisher's note

All claims expressed in this article are solely those of the authors and do not necessarily represent those of their affiliated organizations, or those of the publisher, the editors and the reviewers. Any product that may be evaluated in this article, or claim that may be made by its manufacturer, is not guaranteed or endorsed by the publisher.

References

- Bothmer, R., Jacobsen, N., Baden, C., Jørgensen, R., and Linde-Laursen, I. (1995). *An ecological study of the genus Hordeum*. 2nd edition (Rome: IPGRI). pp. 129.
- Brading, P. A., Verstappen, E. C. P., Kema, G. H. J., and Brown, J. K. M. (2002). A gene-for-gene relationship between wheat and mycosphaerella graminicola, the septoria tritici blotch pathogen. *Phytopathology* 92, 439–445. doi: 10.1094/PHYTO.2002.92.4.439
- Brown, J. K. M., Chartrain, L., Lasserre-Zuber, P., and Saintenac, C. (2015). Genetics of resistance to *Zymoseptoria tritici* and applications to wheat breeding. *Fungal Genet. Biol.* 79, 33–41. doi: 10.1016/j.fgb.2015.04.017
- Cabrera, A., Friebe, B., Jiang, J., and Gill, B. S. (1995). Characterization of *Hordeum Chilense* chromosomes by C-banding and *in situ* hybridization using highly repeated DNA probes. *Genome* 38, 435–442. doi: 10.1139/g95-057
- Calderón, M. C., Ramírez, M. C., Martín, A., and Prieto, P. (2012). Development of *Hordeum Chilense* 4Hch introgression lines in durum wheat: A tool for breeders and complex trait analysis. *Plant Breed.* 131, 733–738. doi: 10.1111/j.1439-0523.2012.02010.x
- Ceoloni, C., Signore, G., Ercoli, L., and Donini, P. (1992). Locating the alien chromatin segment in common wheat- *Aegilops longissima* mildew resistant transfers. *Hereditas* 116, 239–245. doi: 10.1111/j.1601-5223.1992.tb00148.x
- Faris, J. D., Xu, S. S., Cai, X., Friesen, T. L., and Jin, Y. (2008). Molecular and cytogenetic characterization of a durum wheat- *Aegilops speltoides* chromosome translocation conferring resistance to stem rust. *Chromosom. Res.* 16, 1097–1105. doi: 10.1007/s10577-008-1261-3
- Fones, H., and Gurr, S. (2015). The impact of *Septoria tritici* Blotch disease on wheat: An EU perspective. *Fungal Genet. Biol.* 79, 3–7. doi: 10.1016/j.fgb.2015.04.004
- Gallardo, M., and Fereres, E. (1989). Drought resistance in tritordeum (*Hordeum Chilense* x *Triticum turgidum*) in relation to wheat, barley and triticale. *Invest. Agrar. Prod. Prot. Veg.* 4, 361–375.
- Hamblin, A. (1995). *The concept of agricultural sustainability*. Ed. J. H. Andrews (Tommurup: Academic Press). I. C. B. T.-A. @ in P. P. doi: 10.1016/S0736-4539(06)80003-6
- Kema, G. H. J., Verstappen, E. C. P., and Waalwijk, C. (2000). Avirulence in the wheat *Septoria tritici* leaf blotch fungus *Mycosphaerella graminicola* is controlled by a single locus. *Mol. Plant-Microbe Interact.* 13, 1375–1379. doi: 10.1094/MPMI.2000.13.12.1375
- Lukaszewski, A. J. (2000). Manipulation of the 1RS.1BL translocation in wheat by induced homoeologous recombination. *Crop Sci.* 40, 216–225. doi: 10.2135/cropsci2000.401216x
- Mamrutha, H. M., Singh, R., Sharma, D., Venkatesh, K., Pandey, G. C., Kumar, R., et al. (2019). *Physiological and Molecular Basis of Abiotic Stress Tolerance in Wheat BT - Genetic Enhancement of Crops for Tolerance to Abiotic Stress: Mechanisms and Approaches, Vol. I*. Eds. V. R. Rajpal, D. Sehgal, A. Kumar and S. N. Raina (Cham: Springer International Publishing), 99–124. doi: 10.1007/978-3-319-91956-0_5
- Martin, A., Martínez-Araque, C., Rubiales, D., and Ballesteros, J. (1996). "Tritordeum: Triticale's New Brother Cereal," in *Triticale: Today and Tomorrow. Developments in Plant Breeding*, vol. 5. Eds. H. Guedes-Pinto, N. Darvey and V. P. Carnide (Springer, Dordrecht), 57–72.
- Martin, A., and Sanchez-Mongelaguna, E. (1982). Cytology and morphology of the amphiploid *Hordeum Chilense* x *Triticum turgidum* conv. Durum. *Euphytica* 31, 261–267. doi: 10.1007/BF00028329

- McCartney, C. A., Brûlé-Babel, A. L., and Lamari, L. (2002). Inheritance of race-specific resistance to *Mycosphaerella graminicola* in wheat. *Phytopathology* 92, 138–144. doi: 10.1094/PHYTO.2002.92.2.138
- Mondal, S., Sallam, A., Sehgal, D., Sukumaran, S., Farhad, M., Navaneetha Krishnan, J., et al. (2021). “Advances in Breeding for Abiotic Stress Tolerance in Wheat BT,” in *Genomic Designing for Abiotic Stress Resistant Cereal Crops*. Ed. C. Kole (Springer International Publishing, Cham), 71–103. doi: 10.1007/978-3-030-75875-2_2
- Murray, M. G., and Thompson, W. F. (1980). Rapid isolation of high molecular weight plant DNA. *Nucleic Acids Res.* 8, 4321–4326. doi: 10.1093/nar/8.19.4321
- Nalam, V. J., Vales, M. L., Watson, C. J. W., Kianian, S. F., and Riera-Lizarazu, O. (2006). Map-based analysis of genes affecting the brittle rachis character in tetraploid wheat (*Triticum turgidum* L.). *Theor. Appl. Genet.* 112, 373–381. doi: 10.1007/s00122-005-0140-y
- O'mara, J. G. (1953). The cytogenetics of triticales. *Bot. Rev.* 19, 587–605. doi: 10.1007/BF02861827
- Othmeni, M., Grewal, S., Hubbart-Edwards, S., Yang, C., Scholefield, D., Ashling, S., et al. (2019). The use of pentaploid crosses for the introgression of *amblyopyrum muticum* and D-genome chromosome segments into durum wheat. *Front. Plant Sci.* 10. doi: 10.3389/fpls.2019.01110
- Pedersen, C., Zimny, J., Becker, D., Jähne-Gärtner, A., and Lörz, H. (1997). Localization of introduced genes on the chromosomes of transgenic barley, wheat and triticales by fluorescence *in situ* hybridization. *Theor. Appl. Genet.* 94, 749–757. doi: 10.1007/s001220050474
- Pena, R. J., Amaya, A., Rajaram, S., and Mujeeb-Kazi, A. (1990). Variation in quality characteristics associated with some spring 1B/1R translocation wheats. *J. Cereal Sci.* 12, 105–112. doi: 10.1016/S0733-5210(09)80092-1
- Pérez-Méndez, N., Miguel-Rojas, C., Jimenez-Berni, J. A., Gomez-Candon, D., Pérez-De-luque, A., Fereres, E., et al. (2022). Plant breeding and management strategies to minimize the impact of water scarcity and biotic stress in cereal crops under mediterranean conditions. *Agronomy* 12 (1), 75. doi: 10.3390/agronomy12010075
- Porras, R., Pérez-De-luque, A., Sillero, J. C., and Miguel-Rojas, C. (2021). Behavior of spanish durum wheat genotypes against *Zymoseptoria tritici*: Resistance and susceptibility. *Spanish J. Agric. Res.* 19 (3), e1002. doi: 10.5424/sjar/2021193-17953
- Prieto, P., Martín, A., and Cabrera, A. (2004). Chromosomal distribution of telomeric and telomeric-associated sequences in *Hordeum chilense* by *in situ* hybridization. *Hereditas* 141, 122–127. doi: 10.1111/j.1601-5223.2004.01825.x
- Quaedvlieg, W., Kema, G. H. J., Groenewald, J. Z., Verkley, G. J. M., Seifbarghi, S., Razavi, M., et al. (2011). *Zymoseptoria* gen. nov.: A new genus to accommodate *Septoria*-like species occurring on graminicolous hosts. *Persoonia Mol. Phyl. Evol. Fungi* 26, 57–69. doi: 10.3767/003158511X571841
- Rey, M.-D., Calderón, M. C., and Prieto, P. (2015b). The use of the *ph1b* mutant to induce recombination between the chromosomes of wheat and barley. *Front. Plant Sci.* 6. doi: 10.3389/fpls.2015.00160
- Rey, M.-D., Calderón, M.-C., Rodrigo, M. J., Zacarias, L., Alós, E., and Prieto, P. (2015a). Novel bread wheat lines enriched in carotenoids carrying *Hordeum chilense* chromosome arms in the *ph1b* background. *PLoS One* 10 (8), e0134598. doi: 10.1371/journal.pone.0134598
- Rillo, A. O., Caldwell, R. M., and Glover, D. V. (1970). Cytogenetics of resistance to wheat leaf blotch (*Septoria tritici*) in backcross derivatives of an agrotic line. *Crop Sci.* 10, 223–227. doi: 10.2135/cropsci1970.0011183X001000030004x
- Rubiales, D., Moral, A., and Martín, A. (2001). Chromosome location of resistance to septoria leaf blotch and common bunt in wheat-barley addition lines. *Euphytica* 122, 369–372. doi: 10.1023/A:1012952819255
- Rubiales, D., Reader, S. M., and Martín, A. (2000). Chromosomal location of resistance to *Septoria tritici* in *Hordeum chilense* determined by the study of chromosomal addition and substitution lines in “Chinese Spring” wheat. *Euphytica* 115, 221–224. doi: 10.1023/A:1004097830103
- Said, M., and Cabrera, A. (2009). A physical map of chromosome 4Hch from *Hordeum chilense* containing SSR, STS and EST-SSR molecular markers. *Euphytica* 167, 253–259. doi: 10.1007/s10681-009-9895-6
- Sakata, M., Nasuda, S., and Endo, T. R. (2010). Dissection of barley chromosome 4H in common wheat by the gametocidal system and cytological mapping of chromosome 4H with EST markers. *Genes Genet. Syst.* 85, 19–29. doi: 10.1266/ggs.85.19
- Sears, E. R., and Okamoto, M. (1958). “Intergenomic chromosome relationships in hexaploid wheat,” in *Paper Presented at the Proceedings of the 10th International Congress of Genetics*. (Montreal) 258–259.
- Shubing, L., and Honggang, W. (2005). Characterization of a wheat- *Thinopyron intermedium* substitution line with resistance to powdery mildew. *Euphytica* 143, 229–233. doi: 10.1007/s10681-005-3862-7
- Somai-Jemmal, L., Siah, A., Harbaoui, K., Fergaoui, S., Randoux, B., Magnin-Robert, M., et al. (2017). Correlation of fungal penetration, CWDE activities and defense-related genes with resistance of durum wheat cultivars to *Zymoseptoria tritici*. *Physiol. Mol. Plant Pathol.* 100, 117–125. doi: 10.1016/j.pmpp.2017.08.003
- Stewart, E. L., and McDonald, B. A. (2014). Measuring quantitative virulence in the wheat pathogen *zymoseptoria tritici* using high-throughput automated image analysis. *Phytopathology* 104, 985–992. doi: 10.1094/PHYTO-11-13-0328-R
- Wang, B., Ding, Z., Liu, W., Pan, J., Li, C., Ge, S., et al. (2009). Polyploid evolution in *Oryza officinalis* complex of the genus *Oryza*. *BMC Evol. Biol.* 9, 1–13. doi: 10.1186/1471-2148-9-250
- Zadoks, J. C., Chang, T. T., and Konzak, C. F. (1974). A decimal code for the growth stages of cereals. *Weed Res.* 14, 415–421. doi: 10.1111/j.1365-3180.1974.tb01084.x



OPEN ACCESS

EDITED BY

Gustavo A. Slafer,
Catalan Institution for Research and
Advanced Studies (ICREA), Spain

REVIEWED BY

John Foulkes,
University of Nottingham, United Kingdom
Christine Girousse,
INRAE, France

*CORRESPONDENCE

Roi Ben-David

✉ roib@volcani.agri.gov.il

RECEIVED 20 February 2024

ACCEPTED 02 July 2024

PUBLISHED 25 July 2024

CITATION

Ntawuguranayo S, Zilberberg M, Nashef K,
Bonfil DJ, Bainsla NK, Piñera-Chavez FJ,
Reynolds MP, Peleg Z and Ben-David R
(2024) Stem traits promote wheat
climate-resilience.
Front. Plant Sci. 15:1388881.
doi: 10.3389/fpls.2024.1388881

COPYRIGHT

© 2024 Ntawuguranayo, Zilberberg, Nashef,
Bonfil, Bainsla, Piñera-Chavez, Reynolds, Peleg
and Ben-David. This is an open-access article
distributed under the terms of the [Creative
Commons Attribution License \(CC BY\)](#). The
use, distribution or reproduction in other
forums is permitted, provided the original
author(s) and the copyright owner(s) are
credited and that the original publication in
this journal is cited, in accordance with
accepted academic practice. No use,
distribution or reproduction is permitted
which does not comply with these terms.

Stem traits promote wheat climate-resilience

Simeon Ntawuguranayo^{1,2}, Michael Zilberberg^{1,2},
Kamal Nashef², David J. Bonfil³, Naresh Kumar Bainsla⁴,
Francisco J. Piñera-Chavez⁵, Matthew Paul Reynolds⁵,
Zvi Peleg¹ and Roi Ben-David^{2*}

¹The Robert H. Smith Faculty of Agriculture, Food and Environment, The Hebrew University of Jerusalem, Rehovot, Israel, ²The Institute of Plant Sciences, Agriculture Research Organization (ARO) - Volcani Institute, Rishon LeZion, Israel, ³The institute of plant sciences, Agricultural Research Organization, Gilat Research Center, Gilat, Israel, ⁴Division of Genetics, Indian Agricultural Research Institute (IARI), New Delhi, India, ⁵International Maize and Wheat Improvement Center (CIMMYT), Texcoco, Mexico

Introduction: Wheat grain filling processes under post-anthesis stress scenarios depend mainly on stem traits and remobilization of stem water-soluble carbohydrates (WSC).

Methods: A diverse panel of advanced semi-dwarf spring wheat lines, representing a natural variation in stem traits (WSC content, stem diameter, peduncle length, and stem wall width), was used to identify specific traits that reliably reflect the relationship between WSC and grain yield. The panel was phenotyped under various environmental conditions: well-watered, water-limited, and heat stress in Mexico, and terminal-drought in Israel.

Results: Environmental stresses reduced grain yield (from 626 g m⁻² under well-watered to 213 g m⁻² under heat), lower internode diameter, and peduncle length. However, stem-WSC generally peaked 3–4 weeks after heading under all environmental conditions except heat (where it peaked earlier) and expressed the highest values under water-limited and terminal-drought environments. Increased investment in internode diameter and peduncle length was associated with a higher accumulation of stem WSC, which showed a positive association with yield and kernel weight. Across all environments, there were no apparent trade-offs between increased crop investment in internode diameter, peduncle length, and grain yield.

Discussion: Our results showed that selecting for genotypes with higher resource investment in stem structural biomass, WSC accumulation, and remobilization could be a valuable strategy to ameliorate grain size reduction under stress without compromising grain yield potential. Furthermore, easy-to-measure proxies for WSC (stem diameter at specific internodes and length of the last internode, i.e., the peduncle) could significantly increase throughput, potentially at the breeding scale.

KEYWORDS

grain filling, peduncle length, stem diameter, stem solidness, water-soluble carbohydrates, wheat breeding

1 Introduction

Wheat (*Triticum* sp.) is a major staple food crop in both the Global North and South and the most widely grown crop at 700m ha worldwide (Braun et al., 2010). Water scarcity and heat stress are the primary environmental constraints affecting wheat growth and production and are increasingly exacerbated due to climatic fluctuations, which jeopardize future food security. Thus, to meet the global demand of the rising population, there is an urgent need to develop wheat cultivars that are better adapted to the changing environment. Thus, identifying novel adaptive traits and their underlying mechanisms will serve as promising genetic resources for breeding.

In cereals, the grain-filling rate depends on the photo-assimilates supply and the remobilization of pre-anthesis water-soluble carbohydrate (WSC) reserve content from the stem. Under optimal conditions, pre-anthesis assimilate reserves in the stem contribute up to 10–40% of the final grain weight (Dreccer et al., 2009), whereas, under stressful conditions, it can reach up to 40–70% (Gaur et al., 2022). Stem reserves from pre-anthesis assimilation, mainly in the form of fructan (additional forms are sucrose, glucose, and starch), have been recognized as an essential source of carbon for grain filling when current photosynthesis is inhibited by abiotic stress (Fischer, 2011). Moreover, the efficiency of reserve mobilization, especially under terminal-drought, might also impact the grain yield (Morgun et al., 2022).

Stem reserve mobilization is a dynamic process, and while it serves as a strong sink at pre-anthesis, during the grain-filling phase, it turns into a source for the later remobilization process (Blum, 1998). Under water stress conditions, the mobilization of the reserves is controlled by stem fructan exohydrolase activity (FEH), which hydrolyses the stored fructans into mobile fructose (Wardlaw and Willenbrink, 2000; Zhang et al., 2008). Wheat genotypes with higher stem WSC reserves and mobilization rate were more adapted to grain filling under heat stress (Talukder et al., 2013) and water stress (Yáñez et al., 2017). A wide genotypic variation at the onset of grain growth was found for WSC, and a complex genetic control with a moderate to high narrow-sense heritability suggests that phenotypic selection will be the preferred approach to improve this trait (Fischer, 2011). Studies on water stress during grain filling indicate that higher WSC storage capacity does not always indicate higher grain-filling, as the remobilization rate differs among genotypes of the same stem reserve storage capacity (Zhang et al., 2009). Therefore, Blum (2011) suggests an independent genotype selection for WSC storage capacity (selecting for high WSC content) and WSC mobilization (selecting for grain size under desiccation treatment).

In the last decade, spring wheat breeders have optimized biomass partitioning close to its upper limit with values between ~0.50 and ~0.62 for actual and hypothetical harvest index (HI) (Bainsla et al., 2020). The current urgent challenge is to maximize biomass production while maintaining optimal biomass partitioning. Canopy traits could include sink-source dynamics during stem elongation and spike development. It is unclear how stem morphology (stem width, stem wall width, peduncle length,

etc.) might be associated with stem source strength and its role in defining sink (i.e., ear) development. The solid stem was associated with enhanced source capacity via higher WSC, which provides better resilience to abiotic stress during grain filling (Saint Pierre et al., 2010). Moreover, Ahmed et al. (2014) found a strong association between stem diameter with thousand kernel weight, single grain weight, and grain yield per spike under drought stress, indicating the importance of this trait in sustaining grain filling through the provision of greater stem capacity for storing assimilates before mobilizing it to grains.

The stem internode length and weight also affect stem reserve accumulation and remobilization, suggesting that larger stem diameter and stem density would be advantageous for grain filling under stress conditions (Ehdaie et al., 2006b). The peduncle (i.e., the uppermost internode) is an important organ for WSC storage, as the largest pool of carbon and nitrogen during grain filling (Martínez-Peña et al., 2023). The peduncle length is closely associated with inflorescence development and reserve transportation into the spike and grains (Reynolds et al., 2009). The peduncle dry weight is positively associated with peduncle WSC content (Talukder et al., 2013), and higher peduncle WSC content can contribute to better adaptability to heat stress.

Our working hypothesis was that genotypes with high levels of stem WSC around anthesis and high WSC mobilization to the developing grains are associated with heat and water stress adaptability during the critical grain-filling stage. To identify stem traits that reliably reflect the relationship between WSC and grain yield, we evaluated a diverse set of spring wheat, developed for natural variations in stem morphology and stem WSC accumulation at anthesis and post-anthesis, under various environmental conditions. The current study aimed to: (i) Test the association between stem characteristics and WSC reserves. (ii) Characterize the dynamic of WSC in the stem during grain filling from anthesis to maturity. (iii) Test the association between stem traits and yield components under different environmental conditions.

2 Materials and methods

2.1 Plant material

The panel used in this study includes 25 breeding lines of spring wheat selected from the International Maize and Wheat Improvement Centre (CIMMYT) collection based on differences in stem solidness, width, and water-soluble carbohydrates (WSC) (Supplementary Table S1). To prevent any confounding effects, emphasis was given to lines with minimum variability for phenology and plant height traits.

2.2 Experimental design and environmental conditions

Four field experiments were conducted. Three environments at Campo Experimental Norman E. Borlaug (CENEB) in the Valle del Yaqui, Obregon, Mexico (27°24'N; 109°56'W; 38 m above sea

level) during the 2018–2019 growing season: Well-watered (WW, with a total of 526.4 mm where 100 mm was applied before sowing, 26.4 mm of seasonal rainfall, and 400 mm applied as supplemental flood irrigation for entire growing season), water-limited (WL, with a total of 166.3 mm, where 100 mm applied before sowing, 26.3 mm seasonal rainfall, and 40 mm applied as supplemental flood irrigation), and heat where the crops were sown at the beginning of March so that they can grow under high temperature throughout (with total irrigation of 506.7 mm including pre-sowing irrigation of 100 mm, 6.7 mm rainfall and 400 mm supplemental flood irrigation applied during the growing season). The site is temperate, and the soil is a montmorillonitic typic Calciorthid (coarse sandy clay), low in organic matter and slightly alkaline (pH 7.7). The fourth environment was a rain-fed Mediterranean, referred to as terminal-drought (TD). This environment is characterized by low soil moisture and heat waves during the grain-filling stage, with a total precipitation of 564 mm during the winter of 2020–21 season (Net house, Rishon LeZion, Israel). The seasonal temperatures, precipitation, and supplemental irrigations are presented in [Supplementary Figure S1](#). The experiments were sown on 28 November-2018 (WW) and 03-December- 2018 (WL), 05-March-2019 (Heat), and on 11- November-2020 (TD).

α -lattice design ([Falconer, 1989](#)) with three replicates was used for WW, WL, and heat environments ($n=3$). For the TD environment, a randomized block design was employed ($n=3$). Plants were sown in 2-row beds plot of 2 m, the distance between rows within a plot was 0.25 m, and the distance between adjacent plots was 0.5 m across all experiments. A seeding rate of 220 plants m^{-2} was employed. All plots received single fertilization of 50 kg N ha^{-1} (Urea) and 40 kg P ha^{-1} (triple superphosphate) before sowing in all environments.

The fields were treated with fungicides and pesticides periodically to prevent the development of fungal pathogens or insect pests and were manually weeded monthly. The growing season from sowing to harvesting lasted 160 days for WW, 145 days for WL, 127 days for Heat, and 210 days for TD.

2.3 Phenotyping stem traits

2.3.1 Measuring stem WSC

At 15 and 25 days after heading (DAH) and at maturity, five primary main stems were selected randomly from each plot, avoiding plot edges. Stem samples were separated from spikes and oven-dried at 65°C for 48 hours. After weighing the total plant dry matter (DM), leaf sheaths were carefully removed from the stems and weighed again to record stem DM. Stem-dried samples were ground using a sieve mesh of 0.5 mm. Samples were then scanned for WSC content using Near-Infrared Spectroscopy (NIRSystems 6500 FOSS), and the spectral signature was calculated. The software WINISI FOSS was used to estimate the concentration of soluble sugars. Stem WSC was calibrated separately as a ratio per growing degree days (GDD) in each environment. From the data of the WSC on each of the measurement dates, it was possible to calculate the change in concentration over time in each line and to examine the effect on

the weight of the final grains. WSC accumulation = WSC at the peak, and WSC remobilization was obtained by WSC at the peak minus WSC at maturity.

2.3.2 Measuring stem characteristics

When sampling for stem DM and WSC at 25 DAH, five main stems with leaf sheath removed were used for recording internode diameter (ID), internode wall width (IWW), stem solidness score (0 for complete hollow and 1 for complete solid stem) and peduncle length (PL-the uppermost internode). Following the methodology outlined by [Piñera-Chavez et al. \(2016\)](#) on measuring stem characters, ID and IWW were measured in the middle of the second internode using digital calipers ([Figure 1](#)). From the measurement data, stem solidness was found by the following formula:

$$\text{Stem solidness} = \text{Stem area} - \text{Hollow area}$$

$$\text{Stem area} = 3.14 \times \left(\frac{\text{Stem diameter}}{2} \right)^2$$

$$\text{Hollow area} = 3.14 \times \left(\frac{\text{Hollow diameter}}{2} \right)^2$$

$$\text{Hollow diameter} = \text{Stem diameter} - (\text{Stem wall thickness} \times 2)$$

2.3.3 Additional crop trait characterization and yield components assessment

Plants were characterized for phenology traits: Days to heading (DTH) were calculated from emergence to heading and were converted to Growing Degree Days (GDD) for each environment separately. The heading date was recorded when 80% of the spikes in the plot were fully exposed above the flag leaf, Zadoks stage 59 ([Zadoks et al., 1974](#)). Plant height (PH) was measured before harvest using a ruler from the base of the plant to the terminal spikelet.

Yield components: Grain yield (GY), grain number (GN), and thousand-grain weight (TGW) were counted manually and weighted using a digital scale. Dry biomass (BM) at physiological maturity calculated with yield components was recorded based on random samples of 0.25 m^2 in each plot ($n=3$) and was calculated as gram per m^2 . The harvest index (HI) was calculated from a manual harvest of 0.25 m^2 (weight ratio of the grains to total above-ground biomass). Each plot was manually harvested for grain yield.

2.4 Data analysis

The JMP® ver. 17.0 pro statistical package (SAS Institute, Cary, NC, USA) was used for all statistical analyses. Descriptive statistics were performed on the full dataset to illustrate the variable distribution and to calculate the coefficient of variance (CV). Analysis of Variance (ANOVA) was used to assess the possible effect of genotype (G), environment (E), and G×E interactions on the performance of the genotype. Principle Component Analysis (PCA) was performed based on a correlation matrix. Initially,

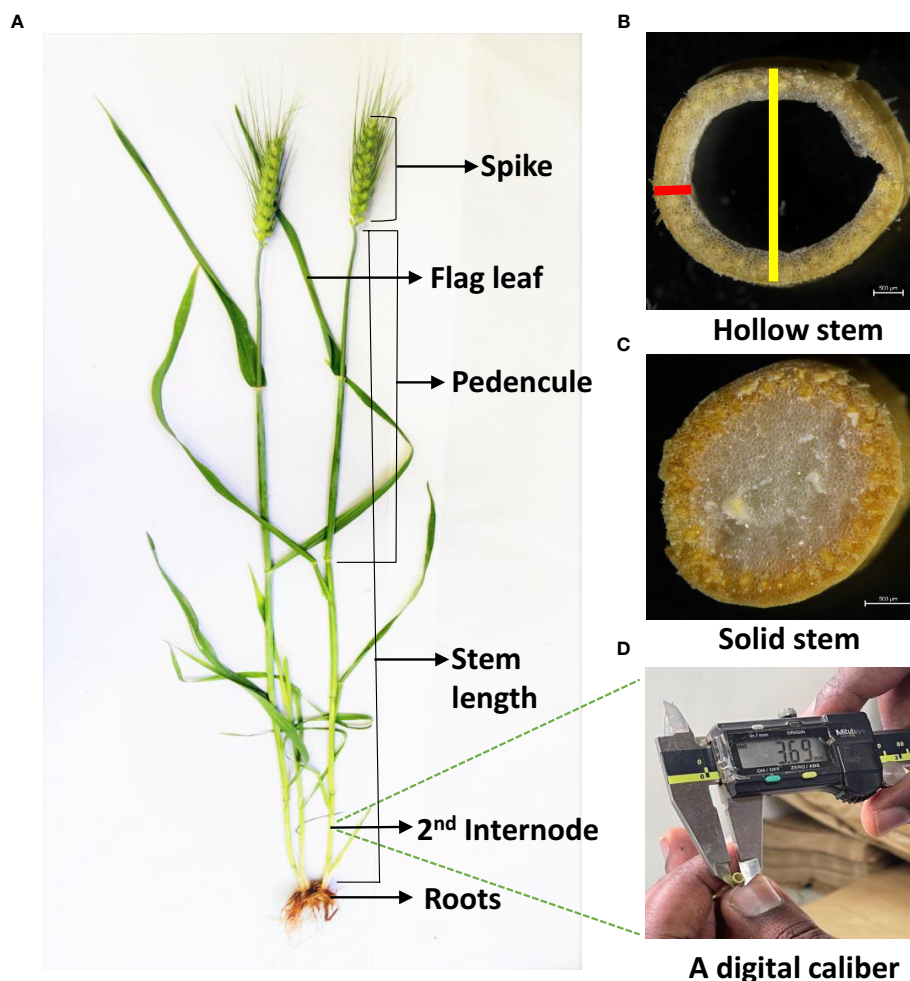


FIGURE 1

Display of measured wheat stem traits. (A) Wheat main parts, (B) Hollow stem at second internode; (C) Solid stem at second internode; (D) Digital caliper used to measure diameter and wall width. The yellow line shows the measured stem diameter, and the red line shows the measured wall width.

highly auto-correlated variables (when the vector was overlapping) were removed from the analysis. Broad-sense heritability (h^2) was estimated using ANOVA-based variance components $h^2 = V_G / (V_G + V_{GE} + V_e)$, where V_G = Genotypic variance, V_{GE} = genotype by environment variance, and V_e is the residual.

3 Results

3.1 Stem traits are affected by complex genotype × environment interactions

PCA of agronomic, stem, and yield-related traits extracted two principal components (Eigenvalues >1), accounting collectively for 73.3% of phenotypic variance across all environments (Figure 2). PC1 (X-axis) explained 49.1% of the variation and was positively loaded with GY, BM, GN, stem DW, ID, PL, TGW, GDDTH, the quantity of WSC/GDD, WSC remobilization and accumulation/GDD and was negatively loaded with stem solidness. PC2 (Y-axis) explained 24.2% of the

variation and was positively loaded with WSC remobilization and accumulation/GDD, quantity of WSC/GDD, GDDTH, TGW and negatively loaded with GY, BM, stem DW, ID, GN, and IWW. The amount of available water mainly drove the environments separation. The well-watered environment is clustered on the fourth quadrant of the PCA toward GY and BM. The water-limited (assembled in the second quadrant close to the third quadrant) and terminal-drought (clustered in the first quadrant) positively affected the accumulation and remobilization of water-soluble carbohydrates with a positive loading of both WSC accumulation, remobilization, and the quantity of water-soluble carbohydrates per growing degree days.

The heat (clustered close to the third quadrant) and water-limited environments negatively affected the stem traits (internode diameter and peduncle), yield traits (grain yield and thousand kernel weight), and biomass. Stem solidness and internode wall width negatively loaded in the third quadrant were positively affected by water-limited and heat stress.

The panel showed wide variability for stem characters under all four environments; IWW mean was 0.86, 0.75, and 0.61 mm for

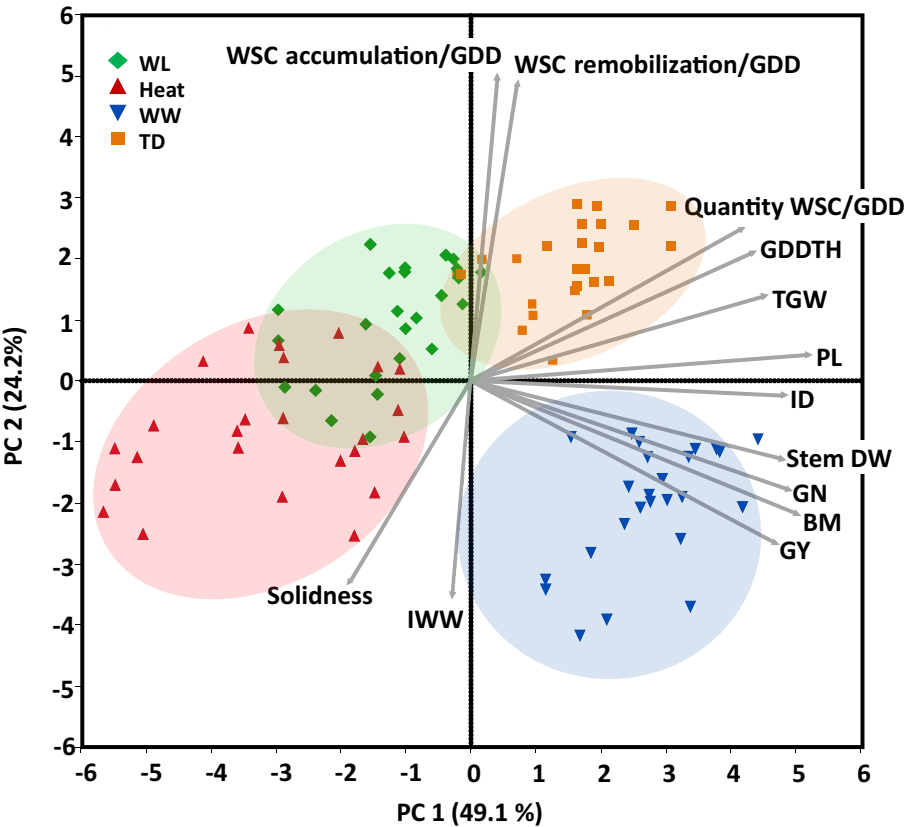


FIGURE 2
Principal components analysis (based on correlation matrix) of continuous phenotypic and yield components recorded for 25 genotypes under four environments: water-limited (WL, green); Heat stress (Heat, red), well-watered (WW, blue), and terminal-drought (TD, orange). Biplot vectors are trait factor loadings for principal component (PC) 1 and PC2. Growing degree days to heading (GDDTH), thousand-grain weight (TGW), grain number (GN), quantity of water-soluble carbohydrates per growing degree days (Quantity WSC per shoot/GDD), water-soluble carbohydrate accumulation and remobilization per shoot/GDD, peduncle length (PL), individual stem dry weight at the peak of water-soluble carbohydrates (Stem DW, g), internode diameter (ID), biomass (BM), grain yield (GY) and internode wall width (IWW).

TABLE 1 Summary of the mean performance, standard error (SE), and coefficient of variance (CV) for the phenotypic traits of 25 genotypes under four environmental conditions: Well-watered, water-limited, heat stress, and terminal-drought.

Trait ^a	Well-watered		Water-limited		Heat stress		Terminal-drought	
	Mean ± SE	CV	Mean ± SE	CV	Mean ± SE	CV	Mean ± SE	CV
GDDTH (°C)	1262 ± 5.69	3.90	1133 ± 6.79	5.18	1022 ± 6.67	5.64	1400 ± 13.52	8.36
Plant height (cm)	101 ± 0.78	6.73	71.00 ± 0.73	8.99	62.00 ± 1.27	17.88	98.00 ± 0.84	7.46
GDDTM (°C)	2175 ± 5.47	2.17	1936 ± 6.97	3.11	1668 ± 8.17	4.24	2242 ± 10.96	4.23
Peduncle length (cm)	39.04 ± 0.37	8.29	27.44 ± 0.30	9.60	20.96 ± 0.47	19.72	39.56 ± 0.45	9.85
Internode diameter (mm)	4.22 ± 0.03	7.99	3.31 ± 0.03	10.15	3.18 ± 0.03	9.45	3.98 ± 0.07	15.55
Internode wall width (mm)	0.86 ± 0.04	43.10	0.75 ± 0.04	47.04	0.61 ± 0.02	40.81	0.48 ± 0.01	20.39
Stem solidness (%)	62.29 ± 1.9	26.54	65.60 ± 2.14	28.31	59.69 ± 0.02	29.48	43.31 ± 1.22	23.25
Stem DW (g)	2.89 ± 0.05	16.63	1.82 ± 0.03	15.35	1.35 ± 0.03	25.13	2.04 ± 0.06	27.48
WSC accumulation per shoot/GDD (mg/°C)	0.014 ± 0.01	15.05	0.02 ± 0.01	11.18	0.01 ± 0.01	21.72	0.03 ± 0.01	12.04

(Continued)

TABLE 1 Continued

Trait ^a	Well-watered		Water-limited		Heat stress		Terminal-drought	
	Mean ± SE	CV	Mean ± SE	CV	Mean ± SE	CV	Mean ± SE	CV
WSC remobilization per shoot/GDD (mg/°C)	0.011 ± 0.01	18.87	0.02 ± 0.01	10.91	0.01 ± 0.01	27.43	0.02 ± 0.01	13.45
Harvest index	0.44 ± 0.01	9.10	0.49 ± 0.01	9.06	0.39 ± 0.01	14.33	0.34 ± 0.35	11.85
Biomass(g/m ²)	1413.4 ± 24.30	14.94	591.36 ± 17.02	24.92	522.40 ± 31.37	52.00	885.44 ± 4.49	35.16
Grain yield ((g/m ²)	626.55 ± 8.01	11.07	287.02 ± 7.67	23.01	213.50 ± 13.85	56.19	311.60 ± 14.82	41.20
Thousand-grain weight (g)	46.6 ± 8.01	11.06	40.72 ± 0.49	10.59	35.72 ± 0.56	13.71	49.08 ± 0.68	12.14

^aThe phenotypic traits: Growing degree days to heading (GDDTH), growing degree days to maturity (GDDTM), individual stem dry weight at the peak of water-soluble carbohydrates (stem DW), water-soluble carbohydrates accumulation per growing degree days (WSC accumulation per shoot/GDD), and water-soluble carbohydrates remobilization per growing degree days (WSC remobilization per shoot/GDD).

TABLE 2 Analysis of variance for the effects of genotype (G), environments (E), and their interactions (G × E) on 25 genotypes under four environmental conditions: well-watered, water-limited, heat stress, and terminal-drought.

Trait ^a	Source	d.f. ^b	MS ^c	F Ratio	Prob > F	R square	<i>bs</i> h ² ^d
GDDTH (°C)	Genotype	24	30121	74.1731	<.0001	0.99	0.25
	Environment	3	1990881	4902.488	<.0001		
	Genotype*Environment	72	12417	30.5758	<.0001		
Plant height (cm)	Genotype	24	330.98	15.4791	<.0001	0.96	0.29
	Environment	3	28929.31	1352.959	<.0001		
	Genotype*Environment	72	99.05	4.6321	<.0001		
GDDTM (°C)	Genotype	24	23052	8.8184	<.0001	0.97	0.29
	Environment	3	5094375	1948.824	<.0001		
	Genotype*Environment	72	5516	2.1101	<.0001		
Peduncle length (cm)	Genotype	24	67.099	14.251	<.0001	0.96	0.34
	Environment	3	6228.241	1322.793	<.0001		
	Genotype*Environment	72	15.688	3.3319	<.0001		
Internode diameter (mm)	Genotype	24	0.53399	6.3353	<.0001	0.85	0.13
	Environment	3	18.69812	221.8394	<.0001		
	Genotype*Environment	72	0.27454	3.2572	<.0001		
Stem Solidness (%)	Genotype	24	1541.144	17.1393	<.0001	0.82	0.4
	Environment	3	6674.832	74.2318	<.0001		
	Genotype*Environment	72	287.468	3.197	<.0001		
Internode wall width (mm)	Genotype	24	0.489888	17.4374	<.0001	0.82	0.38
	Environment	3	1.944447	69.2118	<.0001		
	Genotype*Environment	72	0.103703	3.6913	<.0001		
Stem DW (g)	Genotype	24	0.59258	7.3241	<.0001	0.89	0.13
	Environment	3	30.72106	379.7003	<.0001		
	Genotype*Environment	72	0.32165	3.9755	<.0001		

(Continued)

TABLE 2 Continued

Trait ^a	Source	d.f. ^b	MS ^c	F Ratio	Prob > F	R square	<i>b_sh²</i> ^d
WSC Accumulation per shoot/GDD (mg/°C)	Genotype	24	0.0000224	6.1742	<.0001	0.88	0.13
	Environment	3	0.0012874	355.6418	<.0001		
	Genotype*Environment	72	0.0000109	3.02	<.0001		
WSC Remobilization per shoot/GDD (mg/°C)	Genotype	24	0.0000195	4.4631	<.0001	0.87	0.09
	Environment	3	0.0014755	338.3954	<.0001		
	Genotype*Environment	72	0.0000116	2.6566	<.0001		
Harvest index	Genotype	24	0.005532	5.5918	<.0001	0.87	0.05
	Environment	3	0.3078202	311.1493	<.0001		
	Genotype*Environment	72	0.0041157	4.1602	<.0001		
Biomass (g/m ²)	Genotype	24	201174	5.7098	<.0001	0.87	0.17
	Environment	3	12322160	349.7319	<.0001		
	Genotype*Environment	72	78795	2.2364	<.0001		
Grain yield (g/m ²)	Genotype	24	37899	6.6865	<.0001	0.89	0.21
	Environment	3	2504437	441.8561	<.0001		
	Genotype*Environment	72	12800	2.2583	<.0001		
Thousand-grain weight (g)	Genotype	24	228.303	58.6595	<.0001	0.95	0.64
	Environment	3	2701.209	694.0414	<.0001		
	Genotype*Environment	72	20.796	5.3434	<.0001		

^aThe phenotypic traits: Growing degree days to heading (GDDTH), growing degree days to maturity (GDDTM), individual stem dry weight at the peak of water-soluble carbohydrates (stem DW), water-soluble carbohydrates accumulation per growing degree days (WSC accumulation per shoot/GDD), and water-soluble carbohydrates remobilization per growing degree days an (WSC remobilization per shoot/GDD).

^bd.f., Degree of freedom.

^cMS, Mean of square.

^dbsh², Broad sense heritability.

WW, WL, and heat environments, respectively, while in the TD environment, IWW was 0.48mm. Internode diameter showed a similar pattern with mean values of 4.22, 3.31, 3.19, and 3.98 mm for WW, WL, heat, and TD environments, respectively (Table 1). In addition, environments and genotypes significantly interact [$P(F) < 0.0001$] in both traits (Table 2). In the IWW trait, some genotypes showed stable performance across three environments except the TDS (e.g., lines C-SS-8, C-SS-16, and C-SS-23) (Supplementary Table S2). The environment highly affected the peduncle length, from the mean value of 39.5, and 39 cm under TD, WW to 27.4, 20.9, - cm under WL, and heat- respectively.

Across all environments, stem characteristics were highly affected by genotype, environment, and their interaction. $G \times E$ interactions were significant for all the phenotypic traits at $P < 0.0001$ (Table 2). The broad sense heritability ($b_s h^2$) for all the phenotypic traits was less than 0.5 except TGW with ($b_s h^2 = 0.64$), indicating the effect of environmental factors on the phenotypic traits measured. The heritability of the stem traits (IWW, ID, PL was 0.38, 0.13, and 0.34, respectively). IWW had higher heritability compared with other stem traits. The environment highly affected the accumulation and remobilization of WSC/GDD, with $b_s h^2 = 0.13$ and $b_s h^2 = 0.09$, respectively (Table 2).

3.2 Water soluble carbohydrate dynamics are affected by changing environmental conditions

To better understand the dynamics of WSC, we selected two genotypes with high stem WSC (C-SS-1 and C-SS-13) and two with low stem WSC (C-SS-3 and C-SS-7). These genotypes exhibited stability in WSC accumulation across all four environments (Figure 3). Across all environments except heat, the concentration of WSC in the stem reaches the peak 25 days after heading, and translocation to the developing grains occurs from this stage until physiological maturation. Under heat stress, the concentration of stem WSC reached a peak earlier. Under WL, heat, and WW, C-SS-1, and C-SS-13 exhibited significantly higher stem WSC at ($P = 0.05$) than C-SS-3 and C-SS-7 at 15 and 25 DAH. However, there were no significant differences between the 2 groups of genotypes under TD at 15 and 25 DAH, which appeared only at maturity.

After analyzing the dynamics of WSC in the stem, WSC was estimated per growing degree days (GGD) in each environment separately. A highly significant variation ($P < 0.0001$) among the genotypes for both WSC accumulation and remobilization per GDD

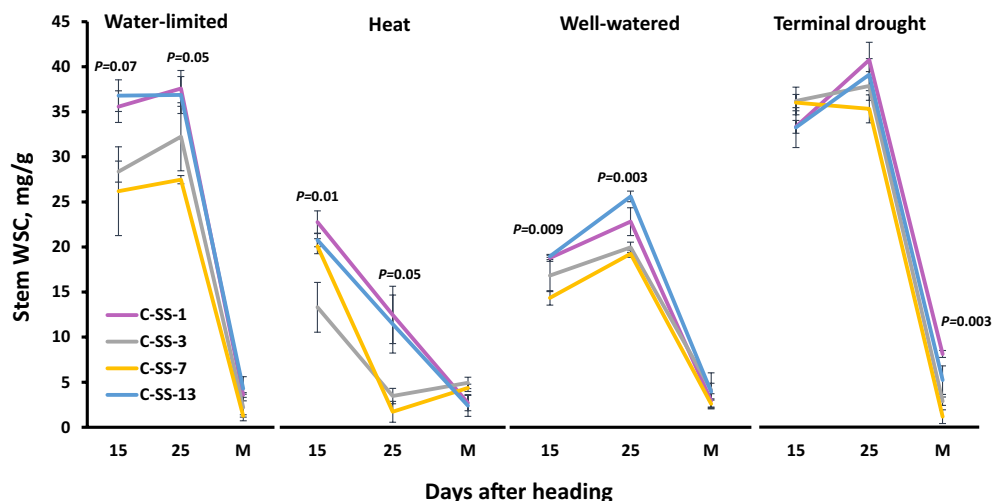


FIGURE 3

Stem water-soluble carbohydrates (WSC) dynamic during grain filling for two genotypes with high stem WSC (C-SS-1 and C-SS-13) and two with low stem WSC (C-SS-3 and C-SS-7) across four environmental conditions: well-watered (WW), water-limited (WL), heat stress (heat) and terminal-drought (TD). The values are the mean ($n=4$) and standard error of WSC at three time points after heading: 15 and 25 days after heading and at maturity (M).

was found in all environments. The accumulation of WSC/GDD under water-limited stress and the terminal-drought was significantly higher ($P < 0.0001$) compared to the heat and well-watered. The remobilization of WSC/GDD was significantly higher ($P < 0.0001$) under water-limited stress and terminal-drought stress compared to heat and well-watered conditions (Figure 4A). The result of ANOVA shows that genotype, environment, and their interaction were significant for WSC accumulation and remobilization/GDD ($P < 0.0001$, $P < 0.0001$, respectively). We compared the concentration of WSC accumulated in the stem per GDD up to the peak point (WSC accumulation/GDD), and the amount of sugars transferred to the spike until maturity (WSC remobilization/GDD). A significant

positive correlation was found ($R^2 = 0.94$, $P < 0.0001$) across all environmental conditions (Figure 4B).

3.3 Water-soluble carbohydrates contribute to grain filling under stress conditions

In general, high SWSC lines attained high grain size. When we examined the contribution of the quantity of stem WSC to TGW and GY; a significant positive relationship ($r = 0.6$, $P = 0.002$; $r = 0.67$, $P = 0.001$; $r = 0.46$, $P = 0.019$) was found between the quantity

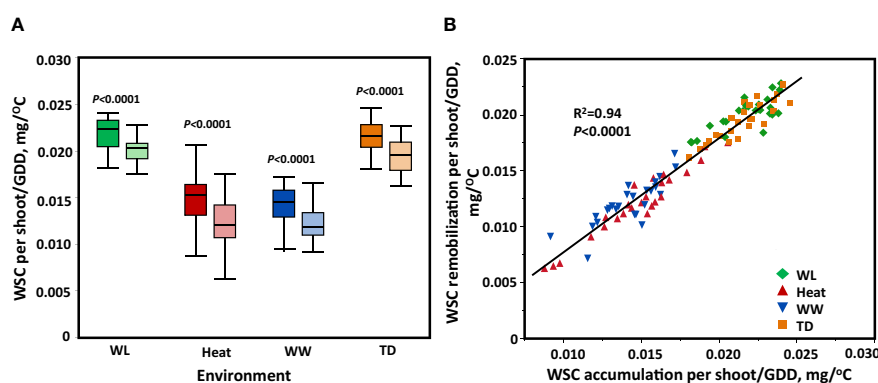


FIGURE 4

The process of accumulating the WSC and remobilizing it to the grains from heading to maturity between environments. (A) Comparison of WSC per shoot/GDD accumulated in the stem up to the peak point (dark color) and WSC/GDD transferred to the spike until maturity (light color) between environments using a t-test. (B) Relationship between WSC per shoot/GDD accumulated in the stem up to the peak point, and WSC per shoot/GDD transferred to the spike until maturity. These data represent the rate of accumulation and transfer of WSC per shoot/GDD. Shape and color represent different environments. Well-watered (WW, Blue), water-limited (WL, Green), heat stress (heat, Red), and terminal-drought (TD, Orange).

of WSC accumulation/GDD and TGW (Figure 5A) under water-limited, heat, and well-watered, respectively. We assessed the association between WSC remobilization/GDD and TGW, and a significant positive association was found between the quantity of WSC remobilization/GDD and TGW for heat, water-limited, and well-watered ($r = 0.65$, $P = 0.0004$; $r = 0.57$, $P = 0.0034$; and $r = 0.43$, $P = 0.0332$, respectively; Figure 5B). We assessed the effect of the quantity of WSC accumulation and remobilization/GDD on grain yield. A significant positive association between the quantity of WSC accumulation/GDD and GY was found for water-limited and heat ($r = 0.57$, $P = 0.003$ and $r = 0.54$, $P = 0.0054$, respectively; Figure 5C). Additionally, the quantity of WSC remobilization/GDD also had a significant positive effect on the grain yield under WL and heat environments ($r = 0.57$, $P = 0.0033$ and $r = 0.53$, $P = 0.0057$, respectively; Figure 5D).

We checked the associations between WSC accumulation per unit area with GN and GY. We found a significant positive relationship ($r = 0.88$, $P < 0.0001$; $r = 0.80$, $P < 0.0001$) between WSC accumulated per unit area (g/m^2) and GN per m^2 under heat and WL respectively (Supplementary Figure S4C). WSC accumulated per unit area was positively associated with GY under heat ($r = 0.89$, $P < 0.0001$), and WL ($r = 0.88$, $P < 0.0001$) (Figure 5E). WSC remobilization per unit area correlated positively with GN ($r = 0.85$, $P < 0.0001$; $r = 0.79$, $P < 0.0001$) under heat and WL respectively (Supplementary Figure S4D). This contributed to GY ($r = 0.87$, $P < 0.0001$) under heat, and ($r = 0.86$, $P < 0.0001$) under WL (Figure 5F). The correlation was not significant in the WW environment for both WSC accumulated and remobilized per unit area with GY and GN. In the terminal-drought environment, we had missing data on stem dry weight at maturity; therefore, we could not check the association between TGW, GY, GN, and the quantity of

WSC remobilized and WSC remobilized per unit area from the stem to the spike under the terminal-drought environment.

3.4 Internode diameter and peduncle length contribute to water-soluble carbohydrates under stress conditions with no trade-off in grain yield

Assessment of the stem traits' contribution to crop growth under four environments showed a significant positive correlation between stem internode diameter with the quantity of WSC accumulation/GDD in the stem ($r = 0.67$, $P = 0.0003$ and $r = 0.38$, $P = 0.060$ under heat and WL, respectively; Figure 6A), under WW and TD the correlation was not significant. In addition, stem diameter was also positively correlated with WSC accumulation per unit area under heat stress ($r = 0.64$, $P = 0.0005$, Supplementary Figure S4A). A positive correlation was found between peduncle length and the quantity of WSC accumulation/GDD ($r = 0.41$, $P = 0.047$, and $r = 0.56$, $P = 0.0038$, for WL and heat, respectively; Figure 6B). Peduncle length was positively associated with WSC accumulated per unit area ($r = 0.74$, $P < 0.0001$) under heat, and WL ($r = 0.49$, $P = 0.013$, Supplementary Figure S4B).

For stem solidness, a negative correlation was found between the quantity of WSC accumulation/GDD and stem solidness ($r = -0.4$, $P = 0.043$ and $r = -0.39$, $P = 0.05$ for WL and heat, respectively) (Supplementary Figure S2A).

The correlation was not significant under WW and TD environments. However, at 15DAH, the internode diameter correlated positively with WSC under TD environments, heat, and water-limited (Supplementary Figure S2B).

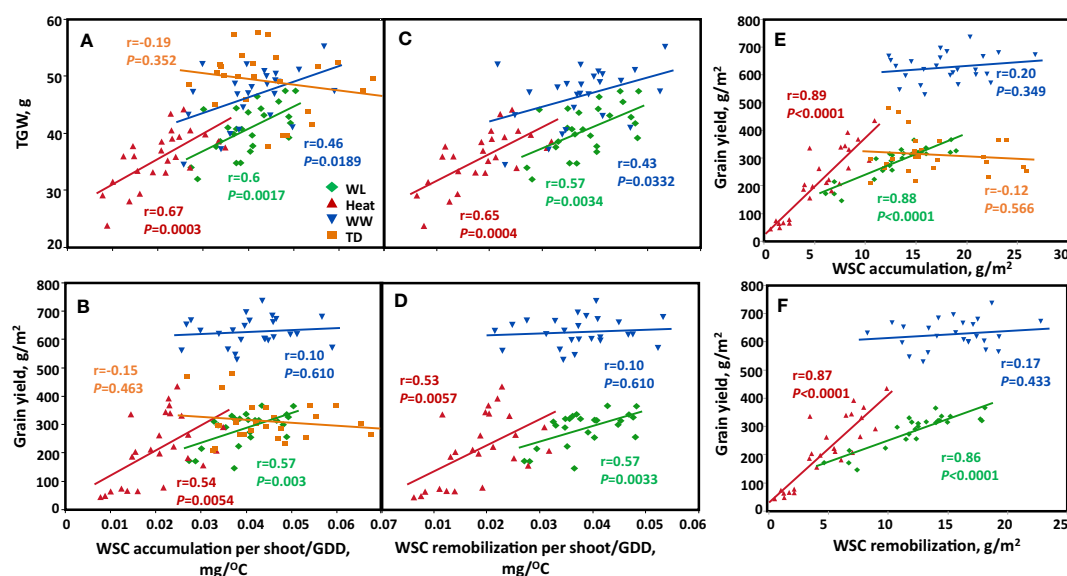


FIGURE 5

Correlation between stem-WSC accumulation and remobilization ratio (WSC per shoot/GDD) with TGW and GY. (A, B) WSC accumulation per shoot/GDD, (C, D) WSC remobilization ratio (WSC per shoot/GDD). (E, F) WSC accumulation and remobilization per unit area and GY. Correlations are calculated based on genotype mean ($n=25$) across four environmental conditions: Well-watered (WW, Blue), water-limited (WL, Green), heat stress (heat, Red), and terminal-drought (TD, Orange).

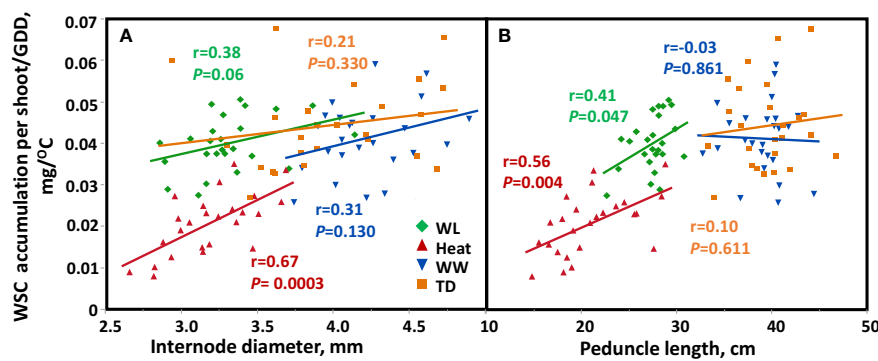


FIGURE 6

Correlation between (A) internode diameter or (B) peduncle length and stem water soluble (WSC) accumulation ratio (WSC per shoot/GDD) based on genotype mean ($n=25$) across four environmental conditions: Well-watered (WW, Blue), water-limited (WL, Green), heat stress (heat, red), and terminal-drought (TD, Orange).

The stem characteristics (internode diameter and peduncle length) contributed to the grain filling under water-limited and heat stress. A highly significant positive relationship between peduncle length and TGW under heat ($r = 0.7$, $P = 0.0001$), WL ($r = 0.38$, $P = 0.06$), and TD ($r = 0.5$, $P = 0.01$) environments (Supplementary Figure S3B). In addition, peduncle length was positively associated with GY under heat and WL environments ($r = 0.76$, $P < 0.0001$ and $r = 0.45$, $P = 0.002$, respectively; - Figure 7B). On the other hand, internode diameter showed a strong correlation with TGW under heat stress ($r = 0.8$, $P < 0.0001$) and WW ($r = 0.48$, $P = 0.015$) (Supplementary Figure S3A), which contributed to increased GY ($r = 0.67$, $P = 0.0003$ and $r = 0.35$, $P = 0.08$, respectively) (Figure 7A). WL and heat environments negatively affected crop productivity and structural stem biomass, as

expressed in lower ID and short PL (Figures 7A, B). The PL was significantly different between environments ($P < 0.0001$), with the lowest value recorded under heat (20.0 cm) compared to TD (39.6 cm). Peduncle, SWSC content, and remobilization were positively associated with significantly enhanced grain filling (TGW and GY) under WL and heat conditions.

In WW and TD environments, there was no trade-off between increased crop investment in internode diameter and peduncle length and GY Figures 7A, B).

We checked the association between ID, PL, and grain number per m^2 . Across environments, there was no trade-off between ID, PL, and grains per m^2 . Under heat stress internode diameter correlated positively ($r = 0.60$, $P = 0.013$) with grains per m^2 .

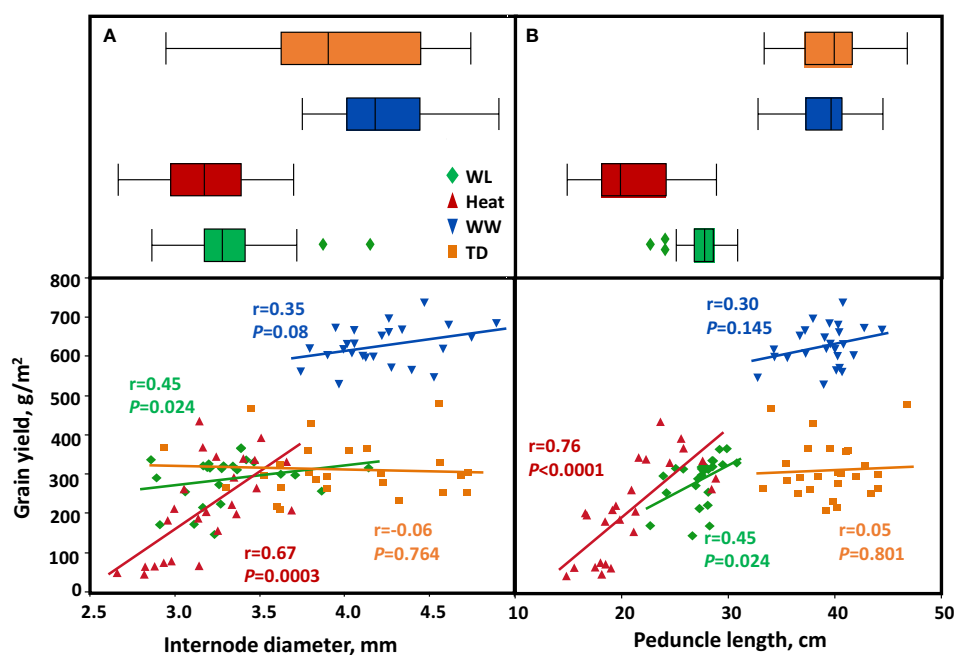


FIGURE 7

Correlation between stem characters and grain yield. (A) internode diameter, (B) peduncle length. Correlations are calculated based on genotype mean ($n=25$) across four environmental conditions: Well-watered (WW, Blue), water-limited (WL, Green), heat stress (heat, Red), and terminal-drought (TD, Orange).

On the other hand, peduncle length was positively associated with grain number per m^2 ($r = 0.71$, $P < 0.0001$ and $r = 0.34$, $P = 0.09$) under heat and WL environments respectively (Supplementary Figures S3C, D).

4 Discussion

To face the challenges of increasing wheat production under the current and projected climate change, wheat research, and breeding requires a comprehensive exploration of potential genetic resources and an in-depth understanding of their underlying environmental adaptations. Blum (1998) suggested that improving stem reserve storage and remobilization can contribute to grain filling under terminal-drought conditions. Moreover, crop investment in stem solidness is associated with high stem WSC and can facilitate improved grain filling under water-limited conditions (Saint Pierre et al., 2010). Here, we want to re-evaluate these findings in light of the contribution of other stem characteristics (including water-soluble carbohydrate, solidness, diameter, and peduncle length) to yield components under various environmental conditions (water-limited, heat stress, and terminal-drought).

4.1 Changing environmental conditions cause stem traits' phenotypic instability

Adaptation to drought and heat stress involves a suite of traits, including stem traits. Understanding how stem traits interact with different environmental conditions is crucial in developing an ideal wheat stem ideotype that can adapt to changing climate conditions. In the current study stem characteristics were highly affected by the genotype, environment, and their interaction (Figure 2).

The broad sense heritability (h^2) for stem traits (IWW, ID, and PL) was less than 0.5 (Table 1), indicating an effect of environmental cues. Stem solidness exhibited the highest values under WL (65%) and the lowest under TD (43%) (Table 2). Similarly, Hayat et al. (1995) showed that the expression level of stem solidness is affected by the environment, and stems tend to be more solid when plants get exposed to drought or high temperatures during stem elongation. However, unlike Saint Pierre et al. (2010), our multi-environment trials showed that an increase in stem solidness was negatively correlated with the amount of stem WSC (Supplementary Figure S2A). The stem solidness may combine with yield-attributing traits differently in different genetic backgrounds. Bainsla et al. (2020) found that in a segregating population (HD2967 \times RAJ 4422), the frequency of favorable segregants with optimum plant height, increased spikelet number, and more stem solidness were relatively high compared to other parental combinations. WL and heat stress conditions had a detrimental impact on structural stem biomass, which was evident in reduced ID and PL under WL and heat (Figures 7A, B).

Our results are in agreement with the finding reported by Sallam et al. (2015), who observed a substantial decrease in stem diameter as a result of heat stress, which was positively and significantly associated with a reduction in TGW and grain yield

per spike. In addition (Ehdaie et al., 2006a) reported that internode length and weight were reduced under drought. These results are similar to the findings of Ahmed et al. (2014), who stated that drought stress reduced stem diameter (25%) and heat stress by 6%. The combined drought and heat stress amounted to a 31% reduction in stem diameter. WL and heat stress reduced stem diameter by 21.5 and 24.5% and PL by 29 and 46%, respectively. This reduction in crop stem structural biomass could probably be explained by the lower availability of resources under stress conditions (WL and heat). Still, these results highlight the necessity and significance of improving stem diameter and peduncle length, particularly under stressful conditions.

4.2 The peak of water-soluble carbohydrate accumulation in the stem is environmentally dependent

The maximum WSC mg g^{-1} accumulated occurred approximately 25 days after heading across all environments except heat (Figure 3), with the highest value recorded in WL and TD environments (Figure 4A). These results are in accordance with Liu et al. (2020) and Ruuska et al. (2006), who found that stem WSC accumulation increased under drought conditions, and the remobilization to the spike occurs from this stage until physiological maturation. Our results also indicate that WSC accumulation increases under WL and TD compared to WW and heat stress.

Depending on the level of stress, the peak can be reached much earlier, as it was found from the WSC dynamic under heat (Figure 3). Three out of four genotypes, the peak can also be reached earlier (before 15 days after heading) with the WL environment. WL would reduce the period of WSC accumulation after anthesis, allowing for earlier remobilization. Wardlaw and Willenbrink (1994) found in a pot experiment that under non-stress conditions, plants showed a maximum accumulation of WSC between 20 to 25 days after anthesis, and the mobilization varied between cultivars. In our field-based study, WSC results revealed a similar trend, including significant ($P < 0.0001$) differences between genotypes in both accumulation and remobilization, which were highly correlated (Figure 4B). In contrast, Yáñez et al. (2017) found that maximum accumulation of WSC occurred 10–20 days after anthesis under water stress and full irrigation (50% and 100% field capacity, respectively).

WSC accumulation (peak) correlated positively with WSC remobilization ($R^2 = 0.94$, $P < 0.0001$) across all environments (Figure 4B). Zamani and Nabipour (2014) found similar results under non-stress conditions ($R^2 = 0.69$, $P < 0.001$) and heat stress conditions ($R^2 = 0.72$, $P < 0.001$). These findings support Blum's et al. (1994) findings that a cultivar with more stem reserves remobilized two to three times more stem reserves than a cultivar with less stem reserves. These results indicate that regardless of environmental conditions, the accumulation of WSC is correlated with WSC remobilization.

Therefore, the WSC accumulation ratio could be considered a suitable trait for breeders when selecting genotypes with maximum

storage capacity and remobilization of stem reserves. The remobilization rate suggests that stem WSC had been mobilized toward the developing grain, highlighting WSC as a potential trait for selection in pre-breeding programs that focus on grain-filling resilience in wheat under stress conditions.

4.3 Water limitation accelerates the remobilization of water-soluble carbohydrates enhancing grain filling

During grain-filling, WSC remobilization into the grain is one of the physiological adjustments that wheat plants use to adapt to stressful environmental conditions. In this study, we checked the contribution of stem WSC to grain filling under WW, WL, heat, and TD. We found that WSC stem reserve utilization by the developing grains depends on the environment and remobilization ability during grain filling. The remobilization rate of WSC was high under WL and TD compared to the heat and WW environments (Figure 4A).

This finding is consistent with the other reports, which found that water deficit during grain filling of wheat facilitates the mobilization efficiency of WSC in the stem through the regulation of enzymes involved in fructan and sucrose metabolism (Yang et al., 2004; Hou et al., 2018; Islam et al., 2021; Morgun et al., 2022). Liu et al. (2020) also stated that drought stress curtailed the peak of WSC levels and depressed WSC accumulation but significantly accelerated the remobilization of pre-anthesis WSC during the grain filling. These results indicate that the highest remobilization of WSC under WL and TD is due to the decline in assimilating sources from photosynthesis, which leads the plants to depend on stem storage.

Previous studies have found that WSC contributes to grain filling (grain weight per spike) under water deficit ($r = 0.5$, $P < 0.001$); heat ($r = 0.72$, $P < 0.001$), and combined water deficit and heat stress ($r = 0.67$, $P < 0.001$) (Gurumurthy et al., 2023). In the present study, we found similar results where both WSC accumulation ratio positively correlated with TGW and GY under heat and WL conditions (Figures 5A, B), and the remobilization ratio with TGW and GY under heat and WL (Figures 5C, D). A similar observation was reported by (Fu et al., 2020), who found a positive correlation between WSC and TGW in the WL environment. Other studies also found that WSC correlated positively with grain weight and grain yield under rain-fed conditions (McIntyre et al., 2012); and grain yield in droughted field conditions (Ehdaie et al., 2008).

In the present study, WSC accumulated and remobilized per unit area were positively associated with grain number per m^2 under heat and WL (Supplementary Figures S4C, D) which contributed to GY under heat and WL environments (Figures 5E, F). These findings indicate the importance of this trait to the grain-filling process under water-limited, drought, and heat stress conditions. Furthermore, these relationships illustrate that genotypes with higher stem WSC are likely to be less affected by WL and heat stress compared to genotypes that accumulate lower stem WSC.

Our results show that the lines that accumulate more WSC (e.g., C-SS-1; C-SS-13, C-SS-17) also remobilize more WSC ($P < 0.0001$),

benefitting in higher grain size and yield compared to low WSC lines (e.g., C-SS3; C-SS-7). In addition, these lines exhibit a low reduction in grain number per m^2 , and GY under WL, heat, WW, and TD environments, respectively (Supplementary Table S2). These results are consistent with the findings reported by Hou et al. (2018) and Liu et al. (2020), who found that high WSC lines had a greater amount of WSC and higher remobilization efficiency in addition to high grain yield compared to the lines with low WSC under drought stress. In addition, similar to our results, Rebetzke et al. (2008) reported that lines with high WSC had more grain number, yield, and kernel weight or size compared with genotypes with low WSC. This is also consistent with the finding of Islam et al. (2021), who observed that BARI Gom 24 (a line with high stem reserves) showed high remobilization and higher grain yield under drought stress compared to Kanchan and BARI Gom 25 (lines with low stem reserves).

In our study, the correlation between WSC remobilization and TGW, GN, GY under WL, and heat stress shows that the genotypes that exhibit higher WSC remobilization also maintain a high sink strength under stress conditions. Therefore, selecting genotypes with a higher stem WSC accumulation and remobilization ratio could be utilized as a strategy to buffer grain growth and development under WL and heat stress conditions.

4.4 Increased internode diameter and peduncle length are associated with water-soluble carbohydrates and grain size with no yield penalty across environments

Although stem WSC plays a role in grain filling, it is a complex trait to measure and requires a substantial investment of time and money. Consequently, there is a need to identify easily measurable traits correlated with WSC which can be used as an effective selection tool for this trait. In our study, we aimed to determine which stem traits positively correlate with WSC, thereby serving as suitable proxies for selecting high-stem WSC. Our results show that a positive correlation between structural stem diameter (measured at the 2nd internode) did result in a higher amount of WSC in the stem under heat and WL conditions (Figure 6A), similar to the results found by (Ehdaie et al., 2006b). In addition, stem diameter was correlated with WSC accumulation per unit area under heat stress (Supplementary Figure S4A). Stem diameter was also positively correlated with TGW (Supplementary Figure S3), and GY (Figure 7A) under heat and WL environments. These results are in agreement with the finding of Ahmed et al. (2014), who found a significant positive correlation between stem diameter with TGW ($r = 0.56$, 0.53 and 0.56 $P < 0.01$) and grain yield per spike ($r = 0.4$, $r = 0.4$ and 0.5 , $P < 0.05$) under favorable, drought and drought + heat stress environments respectively. In the current study, we found that internode diameter (measured at the second internode) was correlated positively with grain number per m^2 , under heat stress, while under WL, TD, and WW environments there is no trade-off, between internode diameter and GN (Supplementary Figure S3C), unlike the results reported by Sierra-Gonzalez et al. (2021) who found

that internode 3 (below the penultimate internode) and internode 2 (below the peduncle, Rivera-Amado et al., 2019) dry matter partitioning were negatively associated with GN.

Sallam et al. (2015) also observed a highly significant correlation ($r = 0.56$, under drought and 0.66 under drought + heat) between stem diameter and TGW. The correlation between stem diameter and WSC, TGW, and GY under WL and heat confirms the strong relationship between this trait and yield attributes under stressful environmental conditions. Therefore, stem diameter is important in sustaining grain filling under stressful conditions due to the ability to store stem reserves. In addition, we found that increased investment in peduncle length ($b_s h^2 = 0.34$) results in higher WSC accumulation under stress (Figure 6B). Moreover, it was also positively associated with WSC accumulated per unit area (Supplementary Figure S4B), TGW under heat, WL, and TD environments (Supplementary Figure S3B); and GY under heat and WL conditions (Figure 7B), while under WW, the correlation was not significant. These results are in accordance with previous findings, which showed that the highest levels of WSC are located between the peduncle and penultimate internode (Zhang et al., 2015); and upper internodes during the early period of grain filling (Morgun et al., 2022).

Peduncle length and penultimate internode length were also positively correlated with a high number of spikelets, which is an important contributor to grain yield in different genetic combinations (Bainsla et al., 2020). In our study peduncle length was positively associated with grain number per m^2 under heat and WL conditions (Supplementary Figure S4D). A positive correlation ($r = 0.49$) between the total amount of WSC in the upper internode and grain yield under water deficiency was found in the study done by Saint Pierre et al. (2010) evaluating 36 wheat genotypes differing in stem solidness, this indicates a positive contribution of WSC to the grain yield. The contribution of peduncle length to WSC and its correlation between TGW, GN, and GY shows how important this trait is in sustaining grain filling under stressful conditions mainly due to its ability to store more stem reserves. Therefore, ID and PL play an important role in grain filling under stressful conditions, and selecting genotypes with wider diameters and long peduncles can result in high WSC in addition to GY under water-limited and heat stress. However, more research is needed to validate these trends.

Internode diameter and peduncle length were correlated positively with stem dry weight at the peak of WSC under heat, WL, and WW environments, furthermore, stem dry weight was positively correlated with WSC across all environments (results not shown). Both stem dry and water-soluble carbohydrates contributed significantly to the accumulation of WSC across environments. Internode diameter was positively correlated with the concentration of WSC (%) in the stem under heat, but the correlation was not significant under WL, TD, and WW. On other hand, PL correlated negatively with WSC concentration under WW environments (results not shown).

In the current study, under WL and TD, there was no trade-off between grain yield and increased investment in ID and PL (Figures 7A, B). However, under WL and heat stress conditions, there was a significant increase in grain (Figures 7A, B). Therefore, stem diameter and peduncle length could be combined in a single plant ideotype to maximize WSC reserves targeting TGW and yield

improvement under water-limited and heat-stress conditions. For example, C-SS-1 and C-SS-13 with significant wide diameter ($P < 0.0001$) and long peduncle ($P < 0.0001$) (Supplementary Table S2) had higher WSC accumulation, WSC remobilization, TGW and GY compared to C-SS-3 and C-SS-6 across all environments. The reduction in stem characters (ID and PL) and its relationship with the decrease in GY, GN, and TGW due to drought and heat stress demonstrate the importance of the stem characters in sustaining grain size and GY under stress due to their ability to store WSC supporting post-anthesis photosynthesis.

5 Conclusions and application for breeding

The results of our study show that water-limited and heat stress conditions negatively affected both biomass and grain yield, but also structural stem biomass as expressed in lower internode diameter and peduncle length. Nevertheless, internode diameter, peduncle length, stem WSC accumulation, and remobilization were positively associated and significantly enhanced grain filling under water-limited and heat stress conditions. It is worth noting that there was no trade-off between grain yield and increased crop investment in both internode diameter and peduncle length under optimal conditions and terminal-drought. However, under water-limited and heat stress conditions increased crop investment in stem diameter and peduncle length promotes higher grain yield.

WSC content has not been widely used as a direct breeding objective (Ruuska et al., 2006), possibly due to the combined limitations of WSC phenotyping and environmental variability. Our results show that genotypes with high SWSC content also have high WSC remobilization. However, the maximum accumulation (the peak) depends on environmental conditions, as also observed in other reports (Foulkes et al., 2002; Shearman et al., 2005; Ruuska et al., 2006) where under severe heat stress the peak of WSC accumulation can be reached early. In the pre-breeding context, we showed that stem characters (stem diameter and peduncle length) play a key role in sustaining grain filling under stressful conditions and can be good indicators (proxies) of high WSC under water-limited and heat stress. We suggest that crop investment in structural biomass traits might be a worthwhile strategy to offset TGW reduction under water-limited and high-temperature conditions in semi-dwarf spring wheat.

Data availability statement

The raw data supporting the conclusions of this article will be made available by the authors, without undue reservation.

Author contributions

SN: Conceptualization, Data curation, Formal analysis, Methodology, Writing – original draft, Writing – review & editing, Validation, Visualization, Investigation. MZ: Investigation, Data

curation, Writing – original draft, Writing – review & editing. KN: Writing – original draft, Writing – review & editing, Data curation, Investigation. DB: Data curation, Writing – original draft, Writing – review & editing, Conceptualization, Methodology, Visualization, Resources. NB: Writing – original draft, Writing – review & editing, Data curation, Methodology, Conceptualization, Investigation. FP-C: Data curation, Methodology, Writing – original draft, Writing – review & editing, Conceptualization, Validation, Investigation. MR: Conceptualization, Data curation, Methodology, Writing – original draft, Writing – review & editing, Visualization, Investigation. ZP: Conceptualization, Investigation, Visualization, Writing – original draft, Writing – review & editing, Supervision. RB-D: Conceptualization, Investigation, Project administration, Resources, Supervision, Validation, Visualization, Writing – original draft, Writing – review & editing, Methodology, Data curation.

Funding

The author(s) declare financial support was received for the research, authorship, and/or publication of this article. This research was funded by the Israel Ministry of Agriculture grant 20-01-02030. This research was partially supported by the Dutch Ministry of Foreign Affairs under Dutch development/foreign policy (Project BreedME) and BARD Research Project IS-5608-23.

Acknowledgments

The authors thank Dr. Francisco Pinto Espinosa for providing climate data and Dr. Carolina Rivera for helping with genotype

selection. The research was conducted as part of Roi Ben-David sabbatical at International Maize and Wheat Improvement Center (CIMMYT).

Conflict of interest

The authors declare that the research was conducted in the absence of any commercial or financial relationships that could be construed as a potential conflict of interest.

The handling editor GS declared a past co-authorship with the authors MR, DB, and RB-D.

Publisher's note

All claims expressed in this article are solely those of the authors and do not necessarily represent those of their affiliated organizations, or those of the publisher, the editors and the reviewers. Any product that may be evaluated in this article, or claim that may be made by its manufacturer, is not guaranteed or endorsed by the publisher.

Supplementary material

The Supplementary Material for this article can be found online at: <https://www.frontiersin.org/articles/10.3389/fpls.2024.1388881/full#supplementary-material>

References

- Ahmed, S., El-Sayed, H., Mervat, H., Mohamed, O., Ahmed, S., El-Sayed, H., et al. (2014). Inheritance of stem diameter and its relationship to heat and drought tolerance in wheat (*Triticum aestivum* L.). *J. Plant Breed. Crop Sci.* 6, 11–23. doi: 10.5897/JPCS11.017
- Bainsla, N. K., Yadav, R., Singh, G. P., and Sharma, R. K. (20207336). Additive genetic behavior of stem solidness in wheat (*Triticum aestivum* L.). *Sci. Rep.* 10, 1–9. doi: 10.1038/s41598-020-64470-x
- Blum, A. (1998). Improving wheat grain filling under stress by stem reserve mobilization. *Euphytica* 100, 77–83. doi: 10.1023/A:1018303922482
- Blum, A. (2011). *Plant breeding for water-limited environments* (New York: Springer). doi: 10.1007/978-1-4419-7491-4
- Blum, A., Sinmena, B., Mayer, J., Golan, G., and Shpiler, L. (1994). Stem reserve mobilization supports wheat-grain filling under heat stress. *Funct. Plant Biol.* 21, 771–781. doi: 10.1071/PP99040771
- Braun, H. J., Atlin, G., and Payne, T. (2010). “Multi-location testing as a tool to identify plant response to global climate change,” in *Climate change and crop production*. Ed. M. P. Reynolds (CABI, Wallingford), 115–138. doi: 10.1079/9781845936334.0115
- Dreccer, M. F., van Herwaarden, A. F., and Chapman, S. C. (2009). Grain number and grain weight in wheat lines contrasting for stem water soluble carbohydrate concentration. *Field Crops Res.* 112, 43–54. doi: 10.1016/j.fcr.2009.02.006
- Ehdaie, B., Alloush, G. A., Madore, M. A., and Waines, J. G. (2006a). Genotypic variation for stem reserves and mobilization in wheat: I. postanthesis changes in internode dry matter. *Crop Sci.* 46, 735–746. doi: 10.2135/cropsci2005.04-0033
- Ehdaie, B., Alloush, G. A., Madore, M. A., and Waines, J. G. (2006b). Genotypic variation for stem reserves and mobilization in wheat: II. postanthesis changes in internode water-soluble carbohydrates. *Crop Sci.* 46, 2093–2103. doi: 10.2135/cropsci2006.01.0013
- Ehdaie, B., Alloush, G. A., and Waines, J. G. (2008). Genotypic variation in linear rate of grain growth and contribution of stem reserves to grain yield in wheat. *Field Crops Res.* 106, 34–43. doi: 10.1016/j.fcr.2007.10.012
- Falconer, D. S. (1989). *Introduction to quantitative genetics*. 3rd (NY: John Wiley and Sons).
- Fischer, R. A. (2011). Wheat physiology: A review of recent developments. *Crop Pasture Sci.* 62, 95. doi: 10.1071/CP10344
- Foulkes, M. J., Scott, R. K., and Sylvester-Bradley, R. (2002). The ability of wheat cultivars to withstand drought in UK conditions: formation of grain yield. *J. Agric. Sci.* 138, 153–169. doi: 10.1017/S0021859601001836
- Fu, L., Wu, J., Yang, S., Jin, Y., Liu, J., Yang, M., et al. (2020). Genome-wide association analysis of stem water-soluble carbohydrate content in bread wheat. *Theor. Appl. Genet.* 133, 2897–2914. doi: 10.1007/s00122-020-03640-x
- Gaur, A., Sharma, D., Sheoran, S., Chahal, S., Chaudhary, K., Singh, G., et al. (2022). Role of water-soluble carbohydrates in improving drought stress tolerance in wheat: An Overview | Semantic Scholar. *Wheat Barley Res.* 14, 1–16. doi: 10.25174/2582-2675/2022
- Gurumurthy, S., Arora, A., Krishna, H., Chinnusamy, V., and Hazra, K. K. (2023). Genotypic capacity of post-anthesis stem reserve mobilization in wheat for yield sustainability under drought and heat stress in the subtropical region. *Front. Genet.* 14. doi: 10.3389/fgene.2023.1180941
- Hayat, M. A., Martin, J. M., Lanning, S. P., McGuire, C. F., and Talbert, L. E. (1995). Variation for stem solidness and its association with agronomic traits in spring wheat. *Can. J. Plant Sci.* 75, 775–780. doi: 10.4141/cjps95-131
- Hou, J., Huang, X., Sun, W., Du, C., Wang, C., Xie, Y., et al. (2018). Accumulation of water-soluble carbohydrates and gene expression in wheat stems correlates with drought resistance. *J. Plant Physiol.* 231, 182–191. doi: 10.1016/j.jplph.2018.09.017

- Islam, M., De, R. K., Hossain, M., Haque, M., Uddin, M., et al. (2021). Evaluation of the tolerance ability of wheat genotypes to drought stress: dissection through culm-reserves contribution and grain filling physiology. *Agronomy* 11, 1–17. doi: 10.3390/agronomy11061252
- Liu, Y., Zhang, P., Li, M., Chang, L., Cheng, H., Chai, S., et al. (2020). Dynamic responses of accumulation and remobilization of water-soluble carbohydrates in wheat stem to drought stress. *Plant Physiol. Biochem.* 155, 262–270. doi: 10.1016/j.plaphy.2020.07.024
- Martínez-Peña, R., Vergara-Díaz, O., Schlereth, A., Höhne, M., Morcuende, R., Nieto-Taladriz, M. T., et al. (2023). Analysis of durum wheat photosynthetic organs during grain filling reveals the ear as a water stress-tolerant organ and the peduncle as the largest pool of primary metabolites. *Planta* 257, 81. doi: 10.1007/s00425-023-04115-1
- McIntyre, C. L., Seung, D., Casu, R. E., Rebetzke, G. J., Shorter, R., and Xue, G. P. (2012). Genotypic variation in the accumulation of water-soluble carbohydrates in wheat. *Funct. Plant Biol.* 39, 560–568. doi: 10.1071/FP12077
- Morgun, V. V., Tarasiuk, M. V., Priadkina, G. O., and Stasik, O. O. (2022). Depositing capacity of winter wheat stem segments under natural drought during grain filling in Ukrainian forest steppe conditions. *Biosys. Divers.* 30, 163–172. doi: 10.15421/012217
- Piñera-Chavez, F. J., Berry, P. M., Foulkes, M. J., Jesson, M. A., and Reynolds, M. P. (2016). Avoiding lodging in irrigated spring wheat. I. Stem and root structural requirements. *Field Crops Res.* 196, 325–336. doi: 10.1016/j.fcr.2016.06.009
- Rebetzke, G. J., van Herwaarden, A. F., Jenkins, C., Weiss, M., Lewis, D., Ruuska, S., et al. (2008). Quantitative trait loci for water-soluble carbohydrates and associations with agronomic traits in wheat. *Aust. J. Agric. Res.* 59, 891–905. doi: 10.1071/AR08067
- Reynolds, M., Foulkes, M. J., Slafer, G. A., Berry, P., Parry, M. A. J., Snape, J. W., et al. (2009). Raising yield potential in wheat. *J. Exp. Bot.* 60, 1899–1918. doi: 10.1093/jxb/erp016
- Rivera-Amado, C., Trujillo-Negrellos, E., Molero, G., Reynolds, M. P., Sylvester-Bradley, R., and Foulkes, M. J. (2019). Optimizing dry-matter partitioning for increased spike growth, grain number, and harvest index in spring wheat. *Field Crops Res.* 240, 154–167. doi: 10.1016/j.fcr.2019.04.016
- Ruuska, S. A., Rebetzke, G. J., van Herwaarden, A. F., Richards, R. A., Fettell, N. A., Tabe, L., et al. (2006). Genotypic variation in water-soluble carbohydrate accumulation in wheat. *Funct. Plant Biol.* 33, 799–809. doi: 10.1071/FP06062
- Saint Pierre, C., Trethowan, R., and Reynolds, M. (2010). Stem solidness and its relationship to water-soluble carbohydrates: association with wheat yield under water deficit. *Funct. Plant Biol.* 37, 166–174. doi: 10.1071/FP09174
- Sallam, A., Hashad, M., Hamed, E.-S., and Omara, M. (2015). Genetic variation of stem characters in wheat and their relation to kernel weight under drought and heat stresses. *J. Crop Sci. Biotechnol.* 18, 137–146. doi: 10.1007/s12892-015-0014-z
- Shearman, V. J., Sylvester-Bradley, R., Scott, R. K., and Foulkes, M. J. (2005). Physiological processes associated with wheat yield progress in the UK. *Crop Sci.* 45, 175–185. doi: 10.2135/cropsci2005.0175a
- Sierra-Gonzalez, A., Molero, G., Rivera-Amado, C., Babar, M. A., Reynolds, M. P., and Foulkes, M. J. (2021). Exploring genetic diversity for grain partitioning traits to enhance yield in a high biomass spring wheat panel. *Field Crops Res.* 260, 107979. doi: 10.1016/j.fcr.2020.107979
- Talukder, A. S. M. H. M., McDonald, G. K., and Gill, G. S. (2013). Effect of short-term heat stress prior to flowering and at early grain set on the utilization of water-soluble carbohydrates by wheat genotypes. *Field Crops Res.* 147, 1–11. doi: 10.1016/j.fcr.2013.03.013
- Wardlaw, I. F., and Willenbrink, J. (1994). Carbohydrate storage and mobilization by the culm of wheat between heading and grain maturity: the relation to sucrose synthase and sucrose-phosphate synthase. *Funct. Plant Biol.* 21, 255–271. doi: 10.1071/PP9940255
- Wardlaw, I. F., and Willenbrink, J. (2000). Mobilization of fructan reserves and changes in enzyme activities in wheat stems correlate with water stress during kernel filling. *New Phytol.* 148, 413–422. doi: 10.1046/j.1469-8137.2000.00777
- Yáñez, A., Tapia, G., Guerra, F., and Del Pozo, A. (2017). Stem carbohydrate dynamics and expression of genes involved in fructan accumulation and remobilization during grain growth in wheat (*Triticum aestivum* L.) genotypes with contrasting tolerance to water stress. *PloS One* 12, e0177667. doi: 10.1371/journal.pone.0177667
- Yang, J., Zhang, J., Wang, Z., Xu, G., and Zhu, Q. (2004). Activities of key enzymes in sucrose-to-starch conversion in wheat grains subjected to water deficit during grain filling. *Plant Physiol.* 135, 1621–1629. doi: 10.1104/pp.104.041038
- Zadoks, J. C., Chang, T. T., and Konzak, C. (1974). A decimal code for the growth stages of cereals. *Weed Res.* 14, 415–421. doi: 10.1111/j.1365-3180.1974.tb01084.x
- Zamani, M. M., and Nabipour, M. (2014). Stem water soluble carbohydrate remobilization in wheat under heat stress during the grain filling. *Int. J. Agric. Biol.* 16, 401–405.
- Zhang, J., Huang, S., Fosu-Nyarko, J., Dell, B., McNeil, M., Waters, I. (2008), et al. The genome structure of the 1-FEH genes in wheat (*Triticum aestivum* L.): new markers to track stem carbohydrates and grain filling QTLs in breeding. *Mol. Breed.* 22, 339–351. doi: 10.1007/s11032-008-9179-1
- Zhang, J., Chen, W., Dell, B., Vergauwen, R., Zhang, X., Mayer, J. E., et al. (2015). Wheat genotypic variation in dynamic fluxes of WSC components in different stem segments under drought during grain filling. *Front. Plant Sci.* 6. doi: 10.3389/fpls.2015.00624
- Zhang, J., Dell, B., Conocono, E., Waters, I., Setter, T., and Appels, R. (2009). Water deficits in wheat: fructan exohydrolase (1-FEH) mRNA expression and relationship to soluble carbohydrate concentrations in two varieties. *New Phytol.* 181, 843–850. doi: 10.1111/j.1469-8137.2008.02713.x



OPEN ACCESS

EDITED BY

Roxana Savin,
Universitat de Lleida, Spain

REVIEWED BY

Ernesto Igartua,
Spanish National Research Council (CSIC),
Spain
Salar Shaaf,
Leibniz Institute of Plant Genetics and Crop
Plant Research (IPK), Germany

*CORRESPONDENCE

Fred A. Van Eeuwijk
✉ fred.vaneeuwijk@wur.nl

RECEIVED 01 April 2024

ACCEPTED 27 June 2024

PUBLISHED 31 July 2024

CITATION

Li W, Boer MP, Joosen RVL, Zheng C,
Percival-Alwyn L, Cockram J and
Van Eeuwijk FA (2024) Modeling
QTL-by-environment interactions for
multi-parent populations.
Front. Plant Sci. 15:1410851.
doi: 10.3389/fpls.2024.1410851

COPYRIGHT

© 2024 Li, Boer, Joosen, Zheng,
Percival-Alwyn, Cockram and Van Eeuwijk. This
is an open-access article distributed under the
terms of the [Creative Commons Attribution
License \(CC BY\)](#). The use, distribution or
reproduction in other forums is permitted,
provided the original author(s) and the
copyright owner(s) are credited and that the
original publication in this journal is cited, in
accordance with accepted academic
practice. No use, distribution or reproduction
is permitted which does not comply with
these terms.

Modeling QTL-by-environment interactions for multi-parent populations

Wenhao Li¹, Martin P. Boer¹, Ronny V. L. Joosen²,
Chaozhi Zheng¹, Lawrence Percival-Alwyn³, James Cockram³
and Fred A. Van Eeuwijk^{1*}

¹Biometris, Wageningen University and Research Center, Wageningen, Netherlands, ²Rijk Zwaan Breeding B.V., De Lier, Netherlands, ³Plant Genetics, NIAB, Cambridge, United Kingdom

Multi-parent populations (MPPs) are attractive for genetic and breeding studies because they combine genetic diversity with an easy-to-control population structure. Most methods for mapping QTLs in MPPs focus on the detection of QTLs in single environments. Little attention has been given to mapping QTLs in multi-environment trials (METs) and to detecting and modeling QTL-by-environment interactions (QEIs). We present mixed model approaches for the detection and modeling of consistent versus environment-dependent QTLs, i.e., QTL-by-environment interaction (QEI). QTL effects are assumed to be normally distributed with variances expressing consistency or dependence on environments and families. The entries of the corresponding design matrices are functions of identity-by-descent (IBD) probabilities between parents and offspring and follow from the parental origin of offspring DNA. A polygenic effect is added to the models to account for background genetic variation. We illustrate the wide applicability of our method by analyzing several public MPP datasets with observations from METs. The examples include diallel, nested association mapping (NAM), and multi-parent advanced inter-cross (MAGIC) populations. The results of our approach compare favorably with those of previous studies that used tailored methods.

KEYWORDS

multi-parent population, diallel, NAM, MAGIC, QTL-by-environment interaction, multi-environment trial, maize, wheat

1 Introduction

Genotype-by-environment interaction (GEI) implies the differential behavior of genotypes across a range of environmental conditions. Broadly adapted genotypes show stable performance across environmental conditions, whereas narrowly adapted genotypes do well under specific conditions. Adequate description and understanding of GEI patterns is fundamental to the creation of better adapted varieties that comply with environmental and

societal challenges. Obviously, adaptation to conditions imposed by climate change will be a major target for many breeding programs.

GEI is a common phenomenon in many crops, and cereals are no exception to that. Typically, a diversity panel is evaluated in a multi-environment trial (MET) or a number of managed stress trials and the GEI is explained in terms of marker or QTL effects that are environment dependent. Some recent examples of this approach using a QTL analysis in the form of a genome-wide association analysis are Bustos-Korts et al. (2019) and Bretani et al. (2022) in barley and Millet et al. (2016) and Shu et al. (2023) in maize. Examples of the same approach with an emphasis on genomic prediction are Burgueño et al. (2012); Lopez-Cruz et al. (2015), and Jarquín et al. (2017) in wheat and Millet et al. (2019) and Barreto et al. (2024) in maize, whereas Cuevas et al. (2017) give examples in wheat and maize. It is less common to use biparental populations for the investigation of the genetic bases of GEI in the form of QTL by environment interactions (QEI). Two somewhat older examples are Boer et al. (2007) for maize and Mathews et al. (2008) for wheat. All the above papers use a linear mixed model approach or a Bayesian equivalent to model the data. For a description of such models in relation to the modeling of GEI and QEI, see van Eeuwijk et al. (2010); Malosetti et al. (2013), and Van Eeuwijk et al. (2016).

The utilization of multi-parent populations (MPPs) in the investigation of QEI offers several advantages. Compared with the use of biparental populations in METs, the higher genetic diversity of MPPs will increase the chance of displaying polymorphisms at QTLs that interact with environments. In comparison with diversity panels, the known pedigree of MPPs alleviates the problems of population structure and minor allele frequencies. A few papers have attempted to analyze multi-environment trials for multi-parent populations (MET&MPP) with often QTL analyses per environment and subsequent comparison of QTL test statistics or

$-\log_{10}(p\text{-value})$ profiles. An attractive variation on this single-environment single-response QTL analysis was given by Coles et al. (2010) for a maize diallel design where QTLs for the photoperiod sensitivity were mapped using an integrated response variable, i.e., the difference between observations under long-day and short-day conditions was analyzed (Coles et al., 2010). In a maize NAM design, QTL effects for yield were assessed between two weakly correlated trial locations with consideration of the genetic covariance between environments (Garin et al., 2020). Other examples of maize NAM and diallel MET&MPPs (Buckler et al., 2009; Giraud et al., 2014) demonstrated QTL detection for the average response across environments, ignoring QEI. For MAGIC populations, Verbyla et al. (2014) present mixed model technology to study QEI. Puglisi et al. (2021) analyzed a barley MAGIC population in a MET for genomic prediction.

A generic statistical approach for studying QEI for any type of MPP seems to be missing. We propose such an approach in the form of an IBD-based mixed model framework with random QTL effects whose stability depends on both the environment and the family. A background polygenic effect is added that itself can be structured again by family and environment. We illustrate our approach in several MET&MPP cereal datasets: a maize diallel (Coles et al., 2010), two maize NAM designs (Bauer et al., 2013; Giraud et al., 2014; Garin et al., 2020), and a wheat MAGIC population (Scott et al., 2021).

2 Materials and methods

2.1 General framework

Figure 1 illustrates the framework of MET&MPP analysis for investigating QEI. The process begins with the computation of IBD

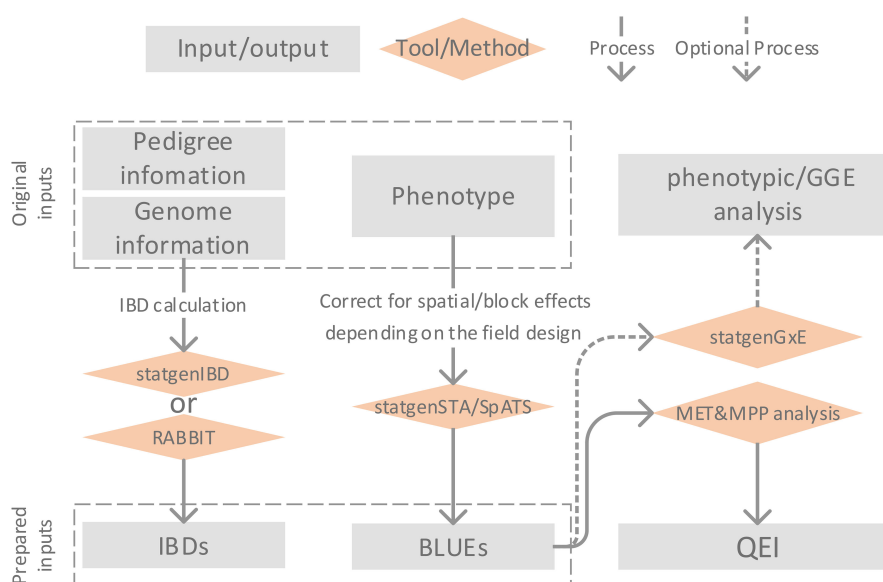


FIGURE 1

Description of framework for Identity By Descent (IBD)-based QTL analysis of Multi-Environment Trial (MET) data collected for a Multi-Parent Population (MPP) allowing the study of QTL by environment interactions (QEI).

probabilities using pedigree and genome information of parents and progenies. Next, the best linear unbiased estimates (BLUEs) for genotypic means are obtained through single-trial analysis, which includes corrections for block and spatial effects. Subsequently, a MET&MPP analysis is conducted using mixed model approaches to study QEI. An important issue in the building of mixed models for GEI and QEI in METs is the formulation of the variance–covariance (VCOV) structure between trials (Smith et al., 2005; Boer et al., 2007). An informal exploration of this structure is possible via the fitting of a genotype-plus-genotype-by-environment interaction (GGE) model and the corresponding visualization by a GGE biplot (Yan et al., 2000; Yan and Kang, 2002). Details of each step in Figure 1 are described below, and descriptions of the proposed IBD-based MET&MPP analysis using mixed models for QEI are elaborated in section 2.2 “Mixed models for IBD-based QTL analysis of METs for MPPs”.

The entries of design matrices, representing genetic predictors for testing QTL main effects and QEI, are derived from marker information and have the form of expected numbers of alleles originating from individual parents. These expected allele numbers are simple functions of IBD probabilities between parents and offspring. IBD probabilities can be calculated using the R package *statgenIBD* (Boer and van Rossum, 2021) for a wide range of MPP designs, whereas a Mathematica tool called RABBIT can be used for more complex designs (Zheng, 2019). Both RABBIT and *statgenIBD* employ hidden Markov models (HMM) and inheritance vectors to calculate IBD probabilities based on the pedigree and genome information of parents and offspring (Zheng et al., 2014, 2015; Boer and van Rossum, 2021). In the current paper, we chose to compute IBD probabilities at a grid of 5 cM along the genome for the empirical MET&MPP datasets as a compromise between mapping resolution and computation time. The exception was the analysis of a MAGIC wheat data set for which we defined a grid at 0.5 cM.

The multi-environment phenotypes used as inputs to our MET&MPP models are typically genotypic means for offspring belonging to segregating families evaluated in multiple field trials. Trial-specific genotypic means, which have been corrected for block, row, column, and spatial effects, are calculated as best linear unbiased estimators (BLUEs). The R package *SpATS* (Rodriguez-Alvarez et al., 2018) offers a convenient and efficient way to convert the trial data at plot level into vectors of adjusted genotypic means. Similarly, the R package *statgenSTA* (Rossum et al., 2021b) can be employed to compute genotypic BLUEs per trial together with corresponding standard errors.

To explore the heterogeneity of genotypic variances and correlations across trials, we performed a GGE biplot analysis (Yan et al., 2000). The GGE biplot is a rank 2 principal component fit to the genotype-by-trial table of BLUEs in which the first axis is closely related to the genotypic main effects whereas the second axis shows GEI effects. The R package *statgenGxE* (Rossum et al., 2021a) was used to create the GGE biplots. These

plots can be helpful to investigate whether the contributions of individual QTLs to the genetic correlations between trials align with the overall correlations.

2.2 Mixed models for IBD-based QTL analysis of METs for MPPs

2.2.1 Models for QTL effects

Four QTL models are proposed differing in the effect types at a putative QTL in terms of stability across families and environments: consistent across both environments and families (environment-consistent and family-consistent, EC&FC QTL), environment-specific and family-consistent (ES&FC QTL), environment-consistent and family-specific (EC&FS QTL), or environment-specific and family-specific (ES&FS QTL). For MAGIC populations, we consider the consistency and specificity of QTL effects only in relation to the environments.

We elaborate these four QTL models for a MET&MPP with C crosses (or families) derived from P parents across J environments or trials; n_{cj} denotes the number of observations (genotypic BLUEs) for the c -th family in the j -th environment; the total number of observations from the c -th family across all J environments is $\sum_j n_{cj} = n_c$; the total number of observations in the j -th environment across all C families is $\sum_c n_{cj} = n_j$; so the total number of observations in the MET&MPP is $\sum_j \sum_c n_{cj} = \sum_c n_c = \sum_j n_j = N$. In all model descriptions, we present later, matrices (and vectors) are presented in bold font and random terms are underlined. The general mixed model for a single-locus QTL model at the q -th genomic position can be expressed as:

$$\underline{Y} = \mathbf{X}\boldsymbol{\beta} + \mathbf{Z}_q \underline{\mathbf{u}}_q + \underline{\mathbf{g}} + \underline{\boldsymbol{\varepsilon}}$$

\underline{Y} is the $N \times 1$ column vector for all N observations in a MET&MPP. The fixed part, $\mathbf{X}\boldsymbol{\beta}$, models effects for families and environments and their interactions. The structure of the design matrix for the random QTL effects, \mathbf{Z}_q , and the vector of QTL effects, $\underline{\mathbf{u}}_q$, is determined by the effect type at the QTL. The four QTL models have different design matrices \mathbf{Z}_q and QTL effect vectors $\underline{\mathbf{u}}_q$ and will be described with superscripts to indicate the matrix dimensions to help distinguish the model structures.

In the EC&FC QTL model, the QTL effect at the q -th genomic position is assumed to be stable across environments and families, which is comparable with the generic IBD-based mixed model approach to map additive QTLs in previous studies (Li et al., 2021, 2022):

$$\mathbf{Z}_q^{(N \times P)} = [\boldsymbol{\pi}_{q,1}^{(N \times 1)} \dots \boldsymbol{\pi}_{q,k}^{(N \times 1)} \dots \boldsymbol{\pi}_{q,P}^{(N \times 1)}],$$

$$\underline{\mathbf{u}}_q^{(P \times 1)} = [\underline{a}_{q,1} \dots \underline{a}_{q,k} \dots \underline{a}_{q,P}]^T \sim MVN(\mathbf{0}, \mathbf{I}_P \Sigma_q^2)$$

(EC&FC QTL model)

$\mathbf{Z}_q^{(N \times P)}$ is a $N \times P$ design matrix that can be partitioned into P column vectors. Each of the P column vectors is a $N \times 1$ column vector, $\boldsymbol{\pi}_{q,k}^{(N \times 1)}$, containing expected numbers of allelic copies associated with the k -th ($k = 1, 2, \dots, P$) parent for all N observations. The $P \times 1$ column vector $\mathbf{u}_q^{(P \times 1)}$ contains element $a_{q,k}$ representing the QTL effect associated with the k -th parent. The variance of $\mathbf{u}_q^{(P \times 1)}$ is $\mathbf{I}_P \Sigma_q^2$, where \mathbf{I}_P is the P -dimensional identity matrix and Σ_q^2 is the genetic variance for the putative QTL, implying a homogeneous VCOV structure for the QTL effect across all environments and families.

In the ES&FC QTL model, the QTL effect is defined as being unstable across J environments due to QEI but consistent across C families. The design matrix and the QTL effects become:

$$\mathbf{Z}_q^{(N \times PJ)} = \bigoplus_{j=1}^J \mathbf{Z}_{qj}^{(n_j \times P)}$$

$$\mathbf{u}_q^{(PJ \times 1)} = \left[\left(\mathbf{u}_{q,1}^{(P \times 1)} \right)^T \dots \left(\mathbf{u}_{q,j}^{(P \times 1)} \right)^T \dots \left(\mathbf{u}_{q,J}^{(P \times 1)} \right)^T \right]^T \sim MVN(\mathbf{0}, \bigoplus_{j=1}^J \mathbf{I}_P \Sigma_{qj}^2)$$

(ES&FC QTL model)

$\mathbf{Z}_q^{(N \times PJ)}$ is a $N \times PJ$ design matrix that can be split into J diagonal components. Each of these J components is a $n_j \times P$ design matrix, $\mathbf{Z}_{qj}^{(n_j \times P)}$, whose entries correspond to an $n_j \times P$ sub matrix of $\mathbf{Z}_q^{(N \times P)}$, i.e., the entries corresponding to the j -th environment in $\mathbf{Z}_q^{(N \times P)}$ are copied to $\mathbf{Z}_{qj}^{(n_j \times P)}$, with n_j being the number of observations in the j -th environment. The vector of effects $\mathbf{u}_q^{(PJ \times 1)}$ is a $PJ \times 1$ column vector that can be partitioned into J sub vectors. Each of the J sub vectors is a $P \times 1$ column vector $\mathbf{u}_{qj}^{(P \times 1)}$ that contains the QTL effects of the P parents in the j -th environment with $\mathbf{I}_P \Sigma_{qj}^2$ being the environment-specific QTL variance. The \bigoplus symbol stands for a direct sum (Schott, 2016).

In the EC&FS QTL model, parental QTL effects are specified within each of C biparental families and therefore vary between families, while being stable across all J environments. The design matrix for the QTL effects and the vector of QTL effects are defined as follows:

$$\mathbf{Z}_q^{(N \times 2C)} = \bigoplus_{c=1}^C [\boldsymbol{\pi}_{q,P1_c}^{(n_c \times 1)} \quad \boldsymbol{\pi}_{q,P2_c}^{(n_c \times 1)}]$$

$$\mathbf{u}_q^{(2C \times 1)} = [a_{q,P1_1} \quad a_{q,P2_1} \quad \dots \quad a_{q,P1_c} \quad a_{q,P2_c} \quad \dots \quad a_{q,P1_C} \quad a_{q,P2_C}]^T \sim MVN(\mathbf{0}, \bigoplus_{c=1}^C \mathbf{I}_2 \Sigma_{q,c}^2)$$

(EC&FS QTL model)

$\mathbf{Z}_q^{(N \times 2C)}$ is a $N \times 2C$ design matrix that can be partitioned into C diagonal components. Each of these components contains two $n_c \times 1$ column vectors, $\boldsymbol{\pi}_{q,P1_c}^{(n_c \times 1)}$ and $\boldsymbol{\pi}_{q,P2_c}^{(n_c \times 1)}$, whose elements indicate the expected numbers of allele copies associated with the two parents of that family, $P1_c$ and $P2_c$. The random QTL effects $\mathbf{u}_q^{(2C \times 1)}$ form a $2C \times 1$ column vector associated with the pairs of parents across the families, and for the c -th family, the variance of the QTL effects is $\mathbf{I}_2 \Sigma_{q,c}^2$.

In the ES&FS QTL model, the QTL effects are stable across neither environments nor families, but both are environment and

family specific. The ES&FS QTL model is established by merging the ES&FC and EC&FS QTL models. The design matrix for the QTL effects and the corresponding vector of QTL effects is:

$$\mathbf{Z}_q^{(N \times 2CJ)} = \bigoplus_{j=1}^J \bigoplus_{c=1}^C [\boldsymbol{\pi}_{q,P1_c}^{(n_j \times 1)} \quad \boldsymbol{\pi}_{q,P2_c}^{(n_j \times 1)}]$$

$$\mathbf{u}_q^{(2JC \times 1)} = \left[\left(\mathbf{u}_{q,1}^{(2C \times 1)} \right)^T \dots \left(\mathbf{u}_{q,j}^{(2C \times 1)} \right)^T \dots \left(\mathbf{u}_{q,J}^{(2C \times 1)} \right)^T \right]^T \sim MVN(\mathbf{0}, \bigoplus_{j=1}^J \bigoplus_{c=1}^C \mathbf{I}_2 \Sigma_{qj,c}^2)$$

(ES&FS QTL model)

$\mathbf{Z}_q^{(N \times 2CJ)}$ is a $N \times 2CJ$ design matrix with JC diagonal components. Each of these components possesses a pair of $n_{cj} \times 1$ column vectors, $\boldsymbol{\pi}_{q,P1_c}^{(n_{cj} \times 1)}$ and $\boldsymbol{\pi}_{q,P2_c}^{(n_{cj} \times 1)}$, whose structure resembles that in the EC&FS QTL model, but now the vectors are designated for the j -th environment, where n_{cj} is the number of observations in the c -th family and j -th environment. Remember that $\sum_{j=1}^J \sum_{c=1}^C n_{cj} = N$. The $2JC \times 1$ column vector $\mathbf{u}_q^{(2JC \times 1)}$ can be partitioned into J column vectors with each column vector having the form $\mathbf{u}_{qj}^{(2C \times 1)}$, comparable with that in the EC&FS QTL model. For the j -th environment, the variance of the QTL effects across the C families can be written as $\bigoplus_{c=1}^C \mathbf{I}_2 \Sigma_{qj,c}^2$. QTL variances are heterogeneous and depend on environment and family simultaneously.

2.2.2 Models for polygenic effect

The QTL models above can be combined in single- or multi-QTL models with a structured polygenic effect, \mathbf{g} . We write for the VCOV of \mathbf{g} , $\Sigma_g = \Sigma_{MET} \otimes \Sigma_{MPP}$, with Σ_{MPP} defined by the relations between the families and Σ_{MET} by the relations between the environments. For Σ_{MPP} , we allowed for identity, i.e., homogeneity across families ($\Sigma_{MPP_{id}}$), heterogeneity across families ($\Sigma_{MPP_{idh}}$), or a population structure as a marker-based kinship matrix ($\Sigma_{MPP_{kin}}$). For Σ_{MET} , we assumed identity or homogeneity of genetic variance across environments and no genetic correlation between environments ($\Sigma_{MET_{id}}$), heterogeneity of genetic variance across environments and no genetic correlation ($\Sigma_{MET_{idh}}$), and an unstructured model with environment-specific genetic variances and correlations ($\Sigma_{MET_{us}}$). The combination of three structure models for Σ_{MPP} and three structure models for Σ_{MET} generates nine VCOV structures for the polygenic background effect. However, in practice for our data, the polygenic model that worked best in all cases was $\Sigma_g = \Sigma_{MET_{us}} \otimes \Sigma_{MPP_{idh}}$.

2.2.3 Model selection and genome-wide QTL scans

To conduct genome-wide QTL scans, several strategies can be employed. We adopted the following protocol. Based on preliminary analyses, we first chose the VCOV model for the polygenic effects in all genome-wide scans $\Sigma_g = \Sigma_{MET_{us}} \otimes \Sigma_{MPP_{idh}}$. We then conducted four series of full genome scans, one for each type of QTL (EC&FC, ES&FC, EC&FS, and ES&FS). Within each series of scans, we performed significance tests for QTLs using likelihood ratio tests (LRT) for single-variance components. The corresponding p -value followed from an approximation of the test statistic by a mixture of χ^2

distributions with 0 and 1 degrees of freedom (Self and Liang, 1987). A conservative Bonferroni-corrected significance threshold was used at a genome-wide level of 0.05. Within a series of scans for a particular QTL type, in the first round, we selected the most significant QTL with the highest $-\log_{10}(p\text{-value})$ as a cofactor for a second round. In this second round, an exclusion window of 20 cM around the cofactor was defined in which no tests for QTLs were performed. This is to avoid collinearity problems. The process of identifying cofactors was repeated in subsequent rounds of scans until no further QTLs were found and the $-\log_{10}(p\text{-value})$ profile stabilized. This procedure can be thought of as a forward regression variable selection procedure. For each particular type of QTL (EC&FC, ES&FC, EC&FS, and ES&FS), a multi-QTL model was produced that comprised all of the QTLs identified in the series of scans. The QTLs as appearing in the four final multi-QTL models corresponding to the four specific QTL types were then combined within one model. When in this combined model QTLs of different types (EC&FC, ES&FC, EC&FS, and ES&FS) coincided with respect to their position, we assessed for that position the nature of the QTL by comparing AIC values (Akaike, 1974) for models with different formulations for the QTL effect. The model with the smallest AIC value then determined the nature of the QTL effect.

2.3 Data

To test our approach, we collected several empirical MET&MPP datasets (Table 1) including a wheat MAGIC

population, a maize diallel, and two maize NAM designs. The wheat MAGIC population was phenotyped in two field trials in the UK in 2017 and 2018. The maize diallel designs were screened in managed stress trials, whereas the two maize NAM designs were screened across several geographic locations in the EU. In this paper, we did not distinguish the two types of trials and use the term “environments” to describe the trial conditions.


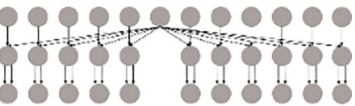
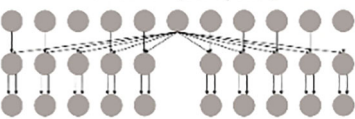
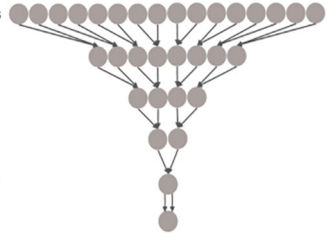
2.3.1 Maize diallel

In the maize diallel design, four biparental families were created by crossing each of two temperate inbred parents to each of two photoperiod-sensitive tropical parents (Coles et al., 2010). Recombinant inbred lines (RILs) were screened under long-day (summer seasons) and short-day (winter seasons) conditions for photoperiod-related traits, e.g., days to silking (DTS) and anthesis (DTA), whose measurements were converted to growing degree days (GDDTS and GDDTA) to account for the influence of temperature. In the previous study (Coles et al., 2010), QTL mapping for photoperiodic responses was performed by calculating the difference in responses between summer and winter conditions. In addition, QTL mapping for the separate conditions was performed by the tool MCQTL 4.0 (Jourjon et al., 2005).

2.3.2 Maize NAM, dent and flint panels

Two maize NAM designs, a flint panel and a dent panel, were taken from the maize EU-NAM project (Bauer et al., 2013; Giraud et al., 2014; Lehermeier et al., 2014). In the flint panel, 11 doubled haploid (DH) families were derived from the central parent UH007

TABLE 1 Overview of MET&MPP data sets. Structure, size, traits, nature of phenotypic data, and reference to earlier data presentations and analyses.

MPPs	Size	Traits	METs	Reference
<div>Parents</div> <div>F1</div> <div>...</div> <div>RIL</div> <div>Maize diallel</div> 	569	Growing degree days to silking (GDDTS) and anthesis (GDDTA)	Summer and winter seasons	Coles et al., 2010
<div>Parents</div> <div>F1</div> <div>DH</div> <div>Maize NAM (flint panel)</div> 	811	Dry matter yield (DMY), plant height (PH), days to silking (DtSILK)	Six geographic locations across EU	Giraud et al., 2014; Garin et al., 2020
<div>Parents</div> <div>F1</div> <div>DH</div> <div>Maize NAM (dent panel)</div> 	841	Dry matter yield (DMY), plant height (PH), days to silking (DtSILK)	Four geographic locations across EU	Giraud et al., 2014
<div>Parents</div> <div>2-way</div> <div>4-way</div> <div>8-way</div> <div>16-way</div> <div>RILs</div> <div>Wheat MAGIC (example of one funnel)</div> 	504	Grain yield (GY), grain protein content (GPC), height to flag leaf base (HFLB), flag leaf to ear distance (FLED)	Two year at same UK location. Environment 1 = 2016-2017 season. Environment 2 = 2017-2018 season	Scott et al., 2021

crossed with 11 peripheral parents. Multiple traits such as dry matter yield (DMY), days to silking (DtSILK), and plant height (PH) were measured across six locations in the EU, namely, Wadersloh (Germany), Ploudaniel (France), La Coruña (Spain), Einbeck (Germany), Roggenstein (Germany), and Eckartseier (Germany). In the dent panel, 10 families were derived from the central parent F353 which was crossed with 10 peripheral parents. The same traits as measured in the flint panel were measured again but across four locations only, namely, Wadersloh (Germany), Mons (Germany), Einbeck (Germany), and Roggenstein (Germany).

In previous work by Giraud et al. (2014), combined linkage and linkage disequilibrium mapping was performed for both NAM panels, whereas Garin et al. (2020) used the NAM flint panel as an example for a QEI study using only the Roggenstein and La Coruña locations.

2.3.3 Wheat MAGIC

Construction, genotyping, and phenotyping of the bread wheat (*Triticum aestivum* L.) cultivars in the NIAB Diverse MAGIC population was previously described (Scott et al., 2021). Briefly, 16 northwestern wheat cultivars were selected based on genetic diversity as founders. These were inter-crossed using a funnel design scheme across four generations, with the outputs of the crossing funnel selfed over six generations to produce 504 recombinant inbred lines (RILs). The founders were genotyped via exome capture and the RILs via whole-genome low-coverage sequencing, allowing 1.1 M high-quality single-nucleotide polymorphisms (SNPs) to be called in the RILs via imputation (Scott et al., 2021). The populations were phenotyped for agronomic traits in two field trials conducted in the United Kingdom in 2017 and 2018, as described by Scott et al. (2021). Although genome wide scans for QEI were performed for all traits recorded in both years, in this paper we will focus on QTLs close to the long-day photoperiod response locus *Photoperiod-B1* (*Ppd-B1*) on chromosome 2B for the traits grain yield (GY), grain protein content (GPC), flag leaf to ear distance (FLED), and height to flag leaf base (HFLB). Earlier QTL analyses on the same data were performed by Scott et al. (2021) for all trait-by-year combinations, where neither QEI issues nor allelic differences between parents were addressed.

3 Results

3.1 Detecting QEI from QTL models

We present the results of QEI analysis for the maize diallel, two maize NAM MET&MPPs, and for the NIAB Diverse wheat MAGIC population. For the maize diallel and NAM populations, we emphasize genome-wide QTL analyses. We also examined the GGE biplot to explore the genotypic correlations between the environments. Environments with weak correlations and therefore high GEI will reveal underlying QEI effects. We inspected environment-specific QTLs to see whether their effect

profiles corresponded to the genotypic correlations observed between the environments. For the wheat MAGIC, we concentrated on the interpretation of allele effect profiles for a pleiotropic QTL on chromosome 2B, more specifically the region around the *Ppd-B1* locus. We compared our findings with previous studies that employed different methods to investigate QEI.

3.2 Maize diallel design for days to silking and anthesis

Two flowering-related traits, growing degree days to silking (GDDTS) and growing degree days to anthesis (GDDTA), were measured in the summer and winter seasons to evaluate the photoperiod sensitivity under long-day and short-day conditions. For both traits, the correlations between summer and winter conditions were weak (Figures 2A, B).

In the QEI analysis, we found that nearly half of the identified QTLs were environment-specific QTLs for both GDDTS and GDDTA. For the trait GDDTA (Figure 2A), in total 10 QTLs were detected, among which six QTLs were environment specific. Five of the six environment-specific QTLs were comparable with QTLs for photoperiodic responses (calculated as differences of responses between the two seasons) from a previous study (Coles et al., 2010). Particularly strong environment-specific QTLs on chromosomes 8, 9, and 10 were identified with contrasting parental effects in especially the summer season. The same summer season, QTLs were identified by Coles et al. (2010) using single-environment analysis. As for the trait GDDTS (Figure 2B), we identified six environment-specific QTLs out of a total of 13 QTLs, which were in accordance with the QTLs for photoperiodic responses identified by Coles et al. (2010) with strong effects under summer conditions.

For both traits GDDTA and GDDTS, a few environment-consistent QTLs were estimated with specific effects within families (EC&FS QTLs), which implied QTL-by-family background interactions. We did not identify ES&FS QTLs for GDDTA and GDDTS, but analysis of other traits, such as plant height (PH), ear height (EH), and total leaf number (TLN) in this maize diallel MET&MPP, revealed some ES&FS QTLs (results not shown here).

3.3 Maize NAM design (dent panel) for dry matter yield, days to silking, and plant height

The NAM dent panel of maize was screened for important traits including dry matter yield (DMY), plant height (PH), and days to silking (DtSILK) across four locations in the EU. The GGE plots (Figure 3) depict varying levels of genetic correlations between the environments. For DMY, the environments Roggenstein and Mons exhibited a weak correlation, whereas the environments Einbeck and Wadersloh displayed a highly positive correlation. For PH, the

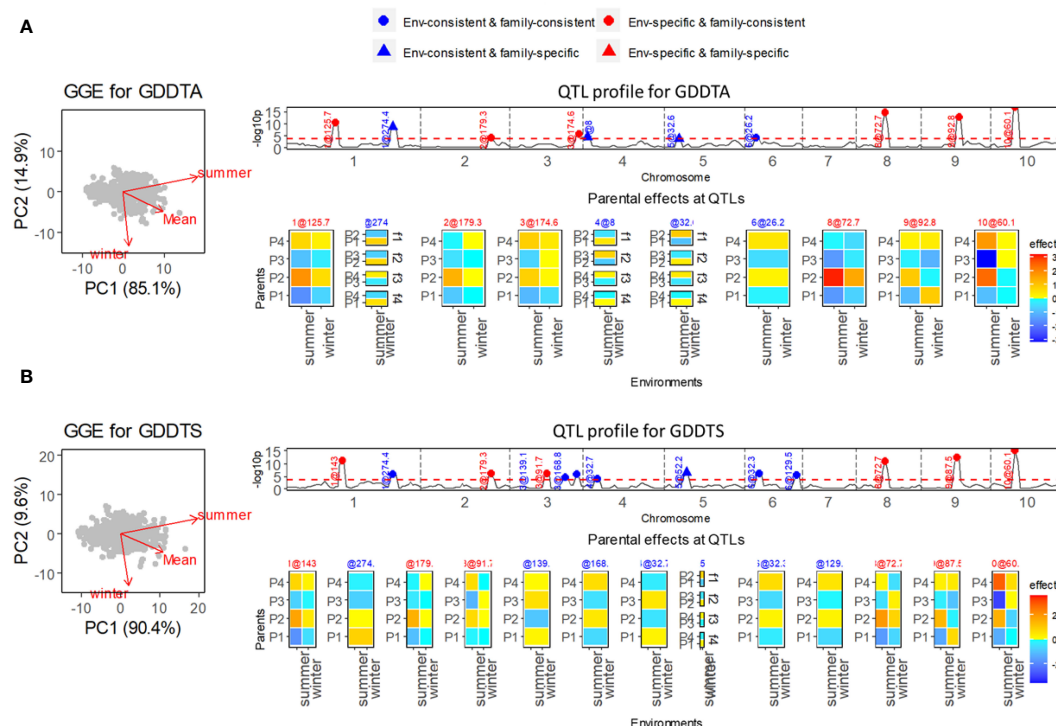


FIGURE 2

Results of QEI analysis of maize diallel. (A) Analysis for growing degree days to anthesis (GDDTA). (B) Analysis for growing degree days to silk (GDDTS). On the left, GGE biplot for exploring genetic correlations between environments. Top right shows the $-\log_{10}(p)$ profile for QTL detection with superimposition of QTL allele effect types indicating consistency of allele effects across environments and families. Bottom right shows allele effect profiles with alleles being either consistent or inconsistent across environments and/or families. Environment-consistent QTLs show the same color and intensity across environments. Environment-specific QTLs show environment specific colors and/or intensities. Family consistent QTLs show a parent specific color and intensity that does not depend on the family and that is either consistent across environments or particular to each environment. Family-specific QTLs show colors and/or intensities for parents that change across families.

Roggenstein environment stood apart with a weak correlation to the remaining environments. Regarding DtSILK, the environments Wadersloh, Mons, and Einbeck formed a cluster with a weak correlation to Roggenstein.

In our QEI analysis, we successfully identified several environment-specific QTLs for each trait. For instance, our methodology detected five environment-specific QTLs out of a total of 13 QTLs for the DMY trait (Figure 3A). The effect profiles of these five environment-specific QTLs exhibited strong variations between the two weakly correlated environments, Mons and Roggenstein. In a separate study, Giraud et al. (2014) conducted combined linkage disequilibrium linkage analysis (LDLA) using adjusted means across all environments. The environment-consistent QTLs identified through our QEI analysis were comparable with those QTLs on chromosome 1, 3, 6, and 7 reported by Giraud et al. (2014). However, it is worth noting that our study revealed environment-specific QTLs on chromosomes 1, 2, and 4 that were not previously reported by Giraud et al. (2014). For the PH trait, we found two environment-specific QTLs out of a total of 13 QTLs (Figure 3B), and these QTLs displayed differential effect profiles between the two weakly correlated environments, Roggenstein and Wadersloh. Regarding the DtSILK trait, our analysis identified five environment-specific QTLs out of a total

of 16 QTLs (Figure 3C), which exhibited distinct effect profiles between Roggenstein and the other environments.

For all traits, we detected QTLs with consistent effects across environments that could be either consistent across families as well as specific to families (EC&FC and EC&FS QTLs), but no environment-specific and family-specific (ES&FS) QTLs were found for any of the traits.

3.4 Maize NAM design (flint panel) for dry matter yield, days to silking and plant height

The flint panel of the maize NAM design was screened for DMY, PH, and DtSILK across six locations in the EU. For the DMY trait (Figure 4A), the GGE biplot reveals three clusters: La Coruña, Roggenstein, and the remaining environments. Among the detected nine QTLs, two QTLs on chromosomes 2 and 6 were found to be specific to certain environments. These environment-specific QTLs were previously studied by Garin et al. (2020), who assessed QEI between the weakly correlated environments La Coruña and Roggenstein. Our results corroborate Garin's work by confirming an environment-specific QTL on chromosome 6 with significant

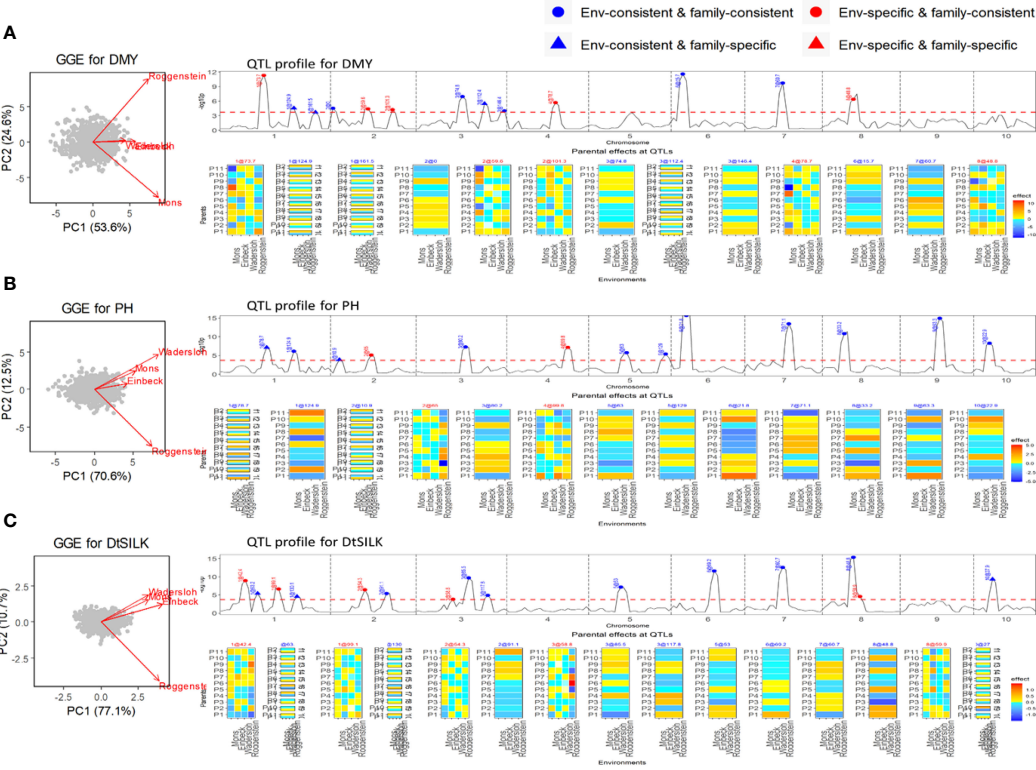


FIGURE 3 Results of QEI analysis of maize NAM dent design. (A) Dry matter yield (DMY), (B) Plant height (PH). (C) Days to silk (DtSILK). Interpretation of plots as in Figure 2.

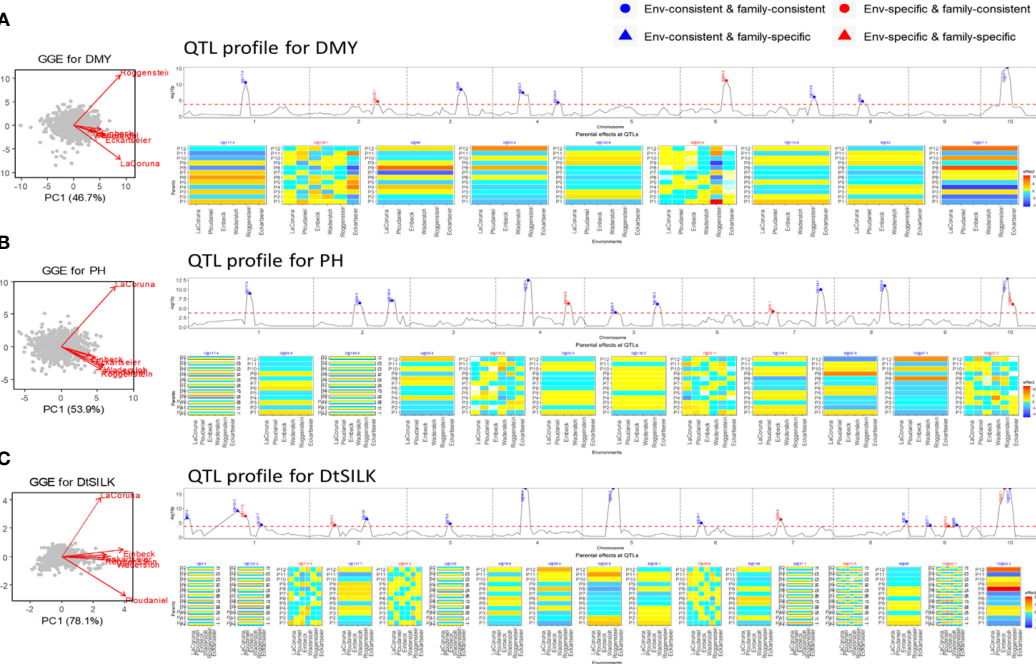


FIGURE 4 Results of QEI analysis of maize NAM flint design. (A) dry matter yield (DMY), (B) plant height (PH), and (C) days to silk (DtSILK). Interpretation of plots as in Figure 2.

effects in the Roggenstein environment. The QEI signal identified by Garin et al. (2020) on chromosome 5, displaying a relatively weak signal, was not detected in our analysis across the six environments. We discovered an additional environment-specific QTL on chromosome 2, which exhibited different effect profiles between Eckartseier and the other environments. This particular QTL was not reported in the study by Garin et al. (2020), which only considered the locations of Roggenstein and La Coruña.

For PH (Figure 4B), two QTLs were family-specific while being environment-consistent (EC&FS). For DtSILK (Figure 4C), we even found four such EC&FS QTLs. Furthermore, for this trait, we also identified two QTLs that were both environment- and family-specific (ES&FS).

3.5 NIAB diverse wheat MAGIC

Outcomes of genome wide QTL scans for two grain traits (GY, GPC) and two plant height related traits (HFLB, FLED) are presented in Figure 5. The most remarkable result of these scans is that on chromosome 2B, around 62 Mb, QEI was detected for all four traits with the direction of the allelic effect tending to reverse for the majority of founder alleles between the two seasons (Table 2). Notably, founder Kloka showed the most extreme QEI at this locus for all four traits. With respect to the two grain-related traits, the Kloka allele showed a strong negative effect for GY in 2016–2017, and a light negative effect in 2017–2018, whereas for GPC, the Kloka allele effect was strongly positive in 2016–2017 and

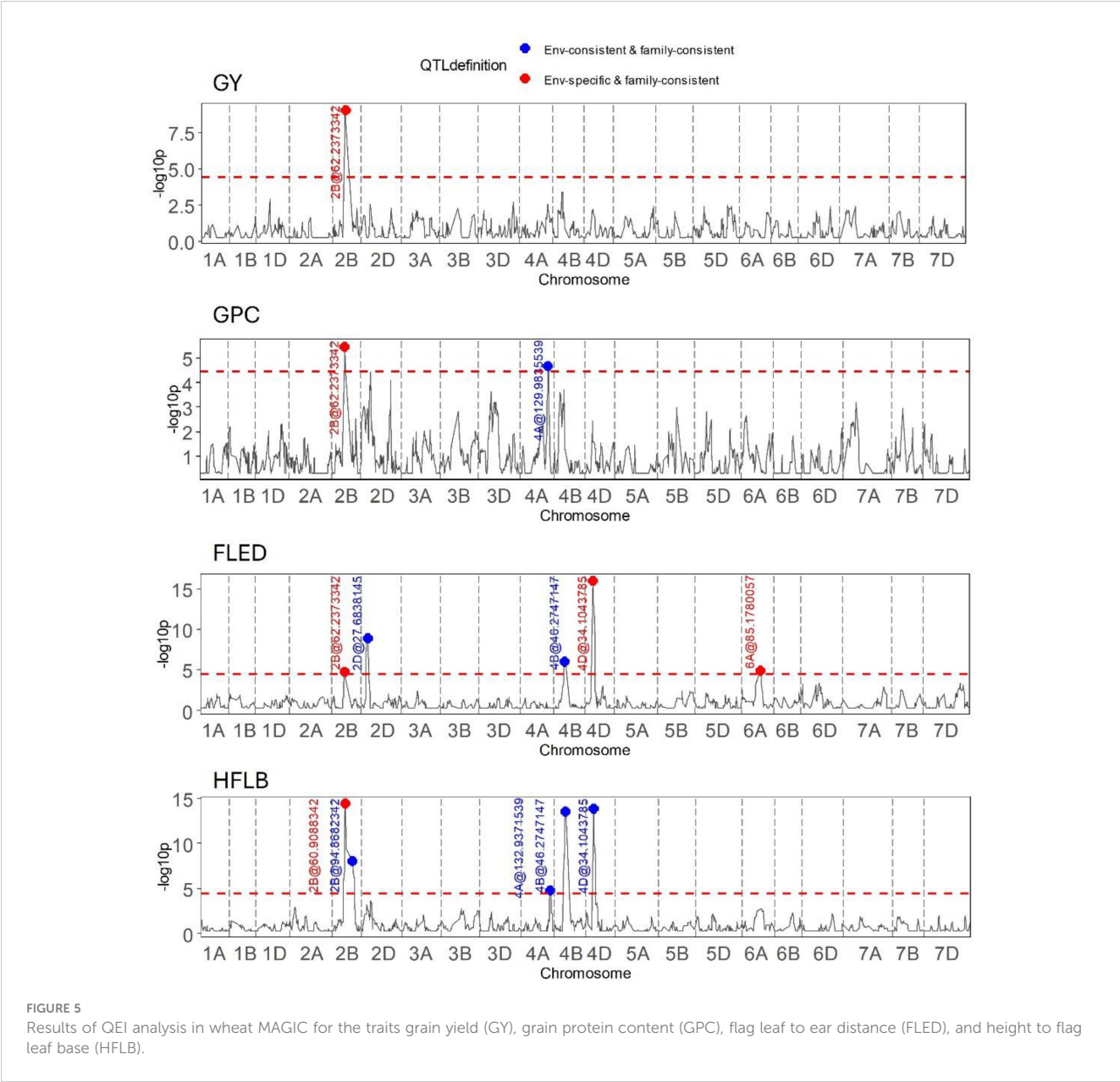


TABLE 2 Heat plot for parental allele effects estimated for four traits in wheat MAGIC in two environments (2016–2017, 2017–2018) at chromosome 2B close to *PpdB1* locus.

Season	Trait							
	GY		GPC		HFLB		FLED	
	2016–2017	2017–2018	2016–2017	2017–2018	2016–2017	2017–2018	2016–2017	2017–2018
Parent								
Banco	−0.03	0.06	0.01	−0.07	−0.18	−0.46	0.08	−0.10
Bersee	−0.18	0.01	−0.02	0.00	0.48	−0.03	−0.08	0.19
Brigadier	0.14	−0.06	0.00	0.10	0.75	1.29	0.23	0.02
Copain	0.10	0.01	−0.02	−0.05	1.54	0.57	−0.33	0.20
Cordiale	0.12	0.00	−0.15	0.02	−0.47	−0.48	0.17	−0.25
Flamingo	−0.03	−0.03	0.19	0.00	0.54	−0.47	−0.08	0.05
Gladiator	0.00	0.02	0.04	−0.04	−0.06	0.53	−0.16	0.00
Holdfast	0.02	−0.01	0.24	−0.02	−0.90	0.85	0.20	−0.12
Kloka	−0.44	−0.02	0.35	0.09	−4.11	−1.51	0.64	−0.22
Maris Fundin	−0.01	0.00	0.01	−0.02	−0.47	−1.30	−0.27	0.01
Robigus	0.01	0.03	−0.01	−0.04	0.32	−0.12	−0.40	0.10
Slejpner	−0.01	−0.02	−0.12	0.06	−0.03	0.55	0.21	0.05
Soissons	0.10	0.00	−0.23	−0.01	0.63	0.58	−0.12	0.12
Spark	0.12	−0.06	−0.11	0.13	0.30	−0.27	0.38	−0.28
Steadfast	0.04	0.03	−0.09	−0.09	0.93	−0.08	−0.31	−0.02
Stetson	0.03	0.04	−0.09	−0.06	0.74	0.35	−0.16	0.27

The color scales are defined per trait to run from strongly negative (deep blue), to moderately negative (light blue), neutral (white), moderately positive (light red), to strongly positive (deep red).

lightly positive in 2017–2018. Therefore, a strong negative correlation could be observed between the Kloka allele effects for GY and GPC at this locus, as would be expected from well-established trade-offs between yield and protein content in wheat (e.g., Scott et al., 2021; White et al., 2022). For the plant height traits, the QTL effect from Kloka at this locus on chromosome 2B reduced HFLB across both seasons, but very strongly in 2016–2017 and somewhat in 2017–2018. For FLED, the Kloka allele effect was moderately positive in 2016–2017 and somewhat negative in 2017–2018. Previous studies show that the long-day photoperiod response locus *Photoperiod-B1* (*Ppd-B1*) is located at this approximate genome position and that it affects flowering time in the NIAB Diverse MAGIC population (Scott et al., 2021). Allelic effects at *Ppd-B1* are known to be controlled by copy number variation (CNV) in the underlying gene, whereby wild-type photoperiod-sensitive *Ppd-B1b* alleles are associated with a haploid CNV of 1, whereas photoperiod-sensitive *Ppd-B1a* alleles that result in earlier flowering are associated with elevated copy number variation (e.g., CNV = 2 in the cultivar *Récital*, CNV = 3 in *Sonora64*, and CNV = 4 in *Chinese Spring*) (Díaz et al., 2012). To further determine whether allelic variation at *Ppd-B1* may underpin the environment-specific interactions at this genomic region for GY, GPD, HFLB, and FLED, we assessed *Ppd-B1* CNV in the 16 NIAB Diverse

MAGIC founders. Using quantitative TaqMan[®] assay, we found that whereas 14 founders carried one copy (indicative of wild-type *Ppd-B1b* alleles), two founders had increased CNV indicative of photoperiod insensitive *Ppd-B1a* alleles associated with early flowering: Kloka (CNV = 3) and Maris Fundin (CNV = 4).

4 Discussion

4.1 QEI analysis by assessing the stability of QTL effects across families and environments

The MET&MPP analysis employs IBD-based mixed model approaches to detect QEI by testing various types of QTL effects across diverse environments and families. Previous studies have discussed the advantages of utilizing multiallelic IBD markers compared with biallelic identity-by-state (IBS) markers (Jurcic et al., 2021; Li et al., 2021), as well as the distinction between modeling QTL terms as random or fixed effects (Boer et al., 2007; Wang et al., 2022). In our current study, we propose fitting functions of IBD probabilities as genetic predictors within the MET&MPP analysis. This approach enables the estimation of

multiallelic QTL effects with respect to parent origins, considering the expected numbers of allele copies from each parent (Wei and Xu, 2016; Li et al., 2021). In contrast to modeling fixed QTL effects in the MET&MPP analysis, treating QTL effects as random terms addresses the issue of overfitting the number of genetic parameters, particularly in complex MET&MPPs involving a large number of parents, families, and environments. Our QTL modeling approach allows for defining the nature of random QTL effects, such as EC&FC, ES&FC, EC&FS, and ES&FS, by modeling combinations of homogeneity or heterogeneity of genetic structures corresponding to both environments and families.

EC&FC QTLs can be regarded as the most stable QTLs in the MET&MPP analysis. EC&FC QTLs are comparable with those QTLs identified by an analysis on genotypic means across environments (Giraud et al., 2014; Garin et al., 2020). EC&FC QTLs identified in MET&MPP analyses at particular genomic positions will in general agree with QTLs for the same trait identified in single-environment analyses, like those in Coles et al. (2010), but there is no guarantee that all the QTLs identified in simpler types of analyses will be reproduced by a more complex MET&MPP analysis. EC&FC QTLs tend to be detected with higher power and resolution in MET&MPP analysis than when analyzing separate environments or a genotypic main effect across environments, as the joint analysis of all environments increases the sample size for mapping stable QTLs.

QTLs detected in separate environments with differential mapping profiles are likely to be detected as ES&FC QTLs by MET&MPP analysis. Parental effect profiles of ES&FC QTLs across environments tend to show differences between weakly correlated environments, whereas highly and positively correlated environments rarely convey QEI signals. Positions for ES&FC QTLs in our MET&MPP analyses coincided with QTLs found by a simpler single trait/environment QTL procedure in which the response variable was the difference between two environments, such as in the maize diallel MPP (Coles et al., 2010). However, we remark that with small population sizes, weak QEI signals that occur in a limited number of environments may not be detected as these signals are diluted by the noise in all those environments in which the QTL did not show an effect. For example, in the maize NAM flint panel (811 genotypes across 6 environments), the QEI signal on chromosome 5 specific to the environments La Coruña and Roggenstein (Garin et al., 2020) disappeared in our MET&MPP analysis on the full set of six environments, but this QTL was indeed identified when the MET&MPP analysis was restricted to La Coruña and Roggenstein.

Defining QTL effects to vary across families allows the evaluation of QTL-by-family interactions (QFI) (Jannink and Jansen, 2001; Blanc et al., 2006; Han et al., 2016). For family-specific QTLs that are stable across environments (EC&FS), simple digenic interaction can be investigated for pairs of markers by two-dimensional genome scans in families. Such two-dimensional QTL scans for epistatic interactions require large family sizes for sufficient detection power. For the detection of ES&FS QTLs with family-specific effects that are unstable across environments, even larger families are required. As an illustration of this point, we detected very few ES&FS QTLs in the maize diallel design, with

around 140 genotypes per family over two environments, and hardly any ES&FS QTL in the maize NAM design, with around 80 genotypes per family.

4.2 Pleiotropic effects of QTL at *Ppd-B1* in the NIAB Diverse MAGIC population

In a previous paper (Scott et al., 2021), it was shown that the photoperiod response locus *Ppd-B1* affects the time taken to reach key developmental stages in the NIAB Diverse MAGIC population, including flag leaf emergence (growth stage 39, GS39), ear emergence (GS55), and flowering time (GS65). Under field conditions, the increasing day length across spring and summer help trigger transition from vegetative to reproductive plant growth and rate of progress across all subsequent developmental stages. Thus, allelic variation at *Ppd-B1* helps define the timepoints that key development stages are exposed to the prevailing environmental conditions. Here, we identified QEI at a pleiotropic QTL controlling multiple plant height and grain traits at the *Ppd-B1* locus, finding QTL effects from the founder Klokka to be both notably strong, and affected by environment. Klokka was unique among the NIAB Diverse MAGIC founders in that it carried three copies of the *Ppd-B1* gene, predictive of an early flowering photoperiod insensitive *Ppd-B1a* allele. Interestingly, no QTL for total plant height was identified in the population at *Ppd-B1* (Scott et al., 2021). Together, these results indicate that *Ppd-B1a* alleles promote flowering and that whereas overall height is not affected, under some growth environments, the Klokka photoperiod-insensitive *Ppd-B1a* allele results in a shift in plant height ratios between the upper and lower stems and is associated with effects on final grain yield and protein content. In environment 1, height to flag leaf base (HFLB) showed a strong decrease whereas height from flag leaf to ear base (FLEB) exhibited a marked increase, whereas in environment 2 the effects of the Klokka *Ppd-B1a* allele were much reduced. While the two field trials investigated here were located on the same farm in the UK, analysis of weather data has shown that both years were unusual compared with historical data across the preceding 56 years: environment 1 was characterized by extreme high temperatures and drought in the developmental stages before anthesis (March and April), and extreme precipitation during grain filling, whereas environment 2 was characterized by extreme terminal heat and drought during the grain filling stage (June and July) (Fradgley et al., 2023). Thus, the combined effects of the early flowering Klokka *Ppd-B1a* allele in environment 1 would have led to earlier development of the reproductive meristem, stem extension, and mid-canopy emergence during extreme temperatures and low precipitation. As temperature was unusually high throughout anthesis and start of grain filling (May–June) in both test environments, and subsequent grain filling stages in environment 1 took place under average temperatures, it is not likely that the known negative impact of high temperatures around anthesis and grain filling on wheat yield (e.g., Djanaguiraman et al., 2020) are the cause of reduced yield and high grain protein content in environment 1. Interestingly, analysis of CNV at *Ppd-B1* genes in tetraploid wheat show that the photoperiod-insensitive *Ppd-B1b*

allele results in increased spikelet number per ear (Arjona et al., 2018). This suggests that the pronounced negative effect of allelic variation at *Ppd-B1* on yield in environment 1 may have been due to earlier exposure of each developmental stage to the extreme heat and drought conditions across the stem extension phases across which final spikelet number is determined in the shoot apical meristem as it reaches the terminal spikelet phase (as well as possible impacts of changed stem length ratios on later development during grain filling).

In addition to Klok, the only other founder to have increased *Ppd-B1* CNV was Maris Fundin, predicted to carry four copies via TaqMan[®]. While increased CNV is associated with early flowering photoperiod-insensitive *Ppd-B1a* alleles in wheat (Díaz et al., 2012; Würschum et al., 2015), other factors may influence the allelic effect. For instance, previous characterization of the photoperiod-insensitive *Ppd-B1a* allele in Chinese Spring found that it carries four tandemly duplicated copies of the gene: three intact and one truncated (Díaz et al., 2012). Indeed, analysis of three sets of near isogenic lines (NILs) in which photosensitive *Ppd-B1a* alleles from either Chinese Spring (CNV = 4), Sonora64 (CNV = 3), or Récital (CNV = 2) had been introgressed into a Paragon genetic background found the insensitive allele from Sonora64 to be significantly earlier flowering than that from Chinese Spring (Díaz et al., 2012). This highlights that whereas increased copy number results in an early flowering allele, the allelic effect is not wholly dependent on the number of copies of the genes present and that functionality of the copies present also plays a role. Indeed, whereas we found the NIAB Diverse MAGIC founder Maris Fundin to have four copies of *Ppd-B1*, analysis of allelic effects found that it did not have as strong an effect on the four target grain and plant height traits compared with the Klok allele (CNV = 3). Surveys of >1,100 global wheat varieties (Díaz et al., 2012; Kane et al., 2013; Würschum et al., 2015) finds that the occurrence of cultivars with four copies of *Ppd-B1* is very rare, having previously been identified in only a limited number of Australian cultivars with pedigree links to Chinese Spring (Kane et al., 2013). Comparison of the pedigree of Maris Fundin (Capelle Desprez × [Vilmorin-29 × Vogel-8058]) × TJB-16 (Fradgley et al., 2019), with cultivars previously assayed for *Ppd-B1* CNV, did not enable insight into the parental donor of the Maris Fundin CNV. However, collectively our results indicate that while the Maris Fundin allele characterized by the presence of four *Ppd-B1* copies likely confers a photoperiod-insensitive *Ppd-B1a* allele, its effect is not as strong as the CNV = 3 Klok allele identified here.

4.3 Conclusion

We introduced a general framework for studying QEI in METs for MPPs. The framework creates design matrices for QTL effects starting from IBD probabilities between parents and offspring for any kind of MPP. The IBD probabilities are combined with a standard procedure for creating factorial interactions between quantitative (IBD for genomic position) and qualitative (environment, family) covariates. In this way, four types of design matrices are produced that correspond to four types of QTL effects: EC&FC, ES&FC, EC&FS, and ES&FS. The effects are assumed to come from normal

distributions. Following up on the definition of the QTL models, a relatively simple stepwise protocol is followed to arrive at multi-QTL models with mixtures of QTL effect types at the different loci. We illustrated with various examples the power of our approach to dissect the genetic basis of GEI in any kind of MPP.

Data availability statement

Publicly available datasets were analyzed in this study. This data can be found here: https://git.wur.nl/li178/QxE_MPP.

Author contributions

WL: Conceptualization, Data curation, Formal analysis, Investigation, Methodology, Software, Validation, Visualization, Writing – original draft. MB: Conceptualization, Formal analysis, Investigation, Methodology, Software, Supervision, Validation, Visualization, Writing – original draft, Writing – review & editing. RJ: Conceptualization, Funding acquisition, Resources, Supervision, Writing – review & editing. CZ: Conceptualization, Formal analysis, Investigation, Methodology, Software, Supervision, Writing – review & editing. LPA: Data curation, Investigation, Validation, Writing – original draft. JC: Data curation, Investigation, Validation, Writing – original draft. FV: Conceptualization, Formal analysis, Funding acquisition, Investigation, Methodology, Project administration, Resources, Supervision, Validation, Writing – original draft, Writing – review & editing.

Funding

The author(s) declare financial support was received for the research, authorship, and/or publication of this article. Rijk Zwaan B.V. provided the funding for WL to work on this topic. JC and LPA were supported by Biotechnology and Biological Sciences Research Council (BBSRC) grant BB/Y514081/1.

Conflict of interest

Author RJ was employed by Rijk Zwaan Breeding B.V.

The remaining authors declare that the research was conducted in the absence of any commercial or financial relationships that could be construed as a potential conflict of interest.

Publisher's note

All claims expressed in this article are solely those of the authors and do not necessarily represent those of their affiliated organizations, or those of the publisher, the editors and the reviewers. Any product that may be evaluated in this article, or claim that may be made by its manufacturer, is not guaranteed or endorsed by the publisher.

References

- Akaike, H. (1974). A new look at the statistical model identification. *IEEE Trans. automatic control* 19, 716–723. doi: 10.1109/TAC.1974.1100705
- Arjona, J. M., Royo, C., Dreisigacker, S., Ammar, K., and Villegas, D. (2018). Effect of Ppd-A1 and Ppd-B1 allelic variants on grain number and thousand kernel weight of Durum wheat and their impact on final grain yield. *Front. Plant Sci.* 9, 888. doi: 10.3389/fpls.2018.00888
- Barreto, C. A. V., das Graças Dias, K. O., de Sousa, I. C., Azevedo, C. F., Nascimento, A. C. C., Guimarães, L. J. M., et al. (2024). Genomic prediction in multi-environment trials in maize using statistical and machine learning methods. *Sci. Rep.* 14, 1062. doi: 10.1038/s41598-024-51792-3
- Bauer, E., Falque, M., Walter, H., Bauland, C., Camisan, C., Campo, L., et al. (2013). Intraspecific variation of recombination rate in maize. *Genome Biol.* 14, R103. doi: 10.1186/gb-2013-14-9-r103
- Blanc, G., Charcosset, A., Mangin, B., Gallais, A., and Moreau, L. (2006). Connected populations for detecting quantitative trait loci and testing for epistasis: An application in maize. *Theor. Appl. Genet.* 113, 206–224. doi: 10.1007/s00122-006-0287-1
- Boer, M. P., and van Rossum, B. (2021). *statgenIBD: Calculation of IBD Probabilities*. doi: 10.32614/CRAN.packages
- Boer, M. P., Wright, D., Feng, L., Podlich, D. W., Luo, L., Cooper, M., et al. (2007). A mixed-model quantitative trait loci (QTL) analysis for multiple-environment trial data using environmental covariates for QTL-by-environment interactions, with an example in maize. *Genetics* 177, 1801–1813. doi: 10.1534/genetics.107.071068
- Bretani, G., Shaaf, S., Tondelli, A., Cattivelli, L., Delbono, S., Waugh, R., et al. (2022). Multi-environment genome-wide association mapping of culm morphology traits in barley. *Front. Plant Sci.* 13, 926277. doi: 10.3389/fpls.2022.926277
- Buckler, E. S., Holland, J. B., Bradbury, P. J., Acharya, C. B., Brown, P. J., Browne, C., et al. (2009). The genetic architecture of maize flowering time. *Science* 325, 714–718. doi: 10.1126/science.1174276
- Burgueño, J., de los Campos, G., Weigel, K., and Crossa, J. (2012). Genomic prediction of breeding values when modeling genotype × environment interaction using pedigree and dense molecular markers. *Crop Sci.* 52, 707–719. doi: 10.2135/cropsci2011.06.0299
- Bustos-Korts, D., Dawson, I. K., Russell, J., Tondelli, A., Guerra, D., Ferrandi, C., et al. (2019). Exome sequences and multi-environment field trials elucidate the genetic basis of adaptation in barley. *Plant J.* 99, 1172–1191. doi: 10.1111/tpj.14414
- Coles, N. D., McMullen, M. D., Balint-Kurti, P. J., Pratt, R. C., and Holland, J. B. (2010). Genetic control of photoperiod sensitivity in maize revealed by joint multiple population analysis. *Genetics* 184, 799–812. doi: 10.1534/genetics.109.110304
- Cuevas, J., Crossa, J., Montesinos-López, O. A., Burgueño, J., Pérez-Rodríguez, P., and de Los Campos, G. (2017). Bayesian genomic prediction with genotype × environment interaction kernel models. *G3: Genes Genomes Genet.* 7, 41–53. doi: 10.1534/g3.116.035584
- Díaz, A., Zikhali, M., Turner, A. S., Isaac, P., and Laurie, D. A. (2012). Copy number variation affecting the Photoperiod-B1 and Vernalization-A1 genes is associated with altered flowering time in wheat (*Triticum aestivum*). *PLoS One* 7, e33234. doi: 10.1371/journal.pone.0033234
- Djanaguiraman, M., Narayanan, S., Erdayani, E., and Prasad, P. V. V. (2020). Effects of high temperature stress during anthesis and grain filling periods on photosynthesis, lipids and grain yield in wheat. *BMC Plant Biol.* 20, 268. doi: 10.1186/s12870-020-02479-0
- Fradgley, N., Gardner, K. A., Bentley, A. R., Howell, P., Mackay, I. J., Scott, M. F., et al. (2023). Multi-trait ensemble genomic prediction and simulations of recurrent selection highlight importance of complex trait genetic architecture for long-term genetic gains in wheat. *silico Plants* 5, diad002. doi: 10.1093/insilicoplants/diad002
- Fradgley, N., Gardner, K. A., Cockram, J., Elderfield, J., Hickey, J. M., Howell, P., et al. (2019). A large-scale pedigree resource of wheat reveals evidence for adaptation and selection by breeders. *PLoS Biol.* 17, e3000071. doi: 10.1371/journal.pbio.3000071
- Garin, V., Malosetti, M., and van Eeuwijk, F. (2020). Multi-parent multi-environment QTL analysis: an illustration with the EU-NAM Flint population. *Theor. Appl. Genet.* 133, 2627–2638. doi: 10.1007/s00122-020-03621-0
- Giraud, H., Lehermeier, C., Bauer, E., Falque, M., Segura, V., Bauland, C., et al. (2014). Linkage disequilibrium with linkage analysis of multiline crosses reveals different multiallelic QTL for hybrid performance in the flint and dent heterotic groups of maize. *Genetics* 198, 1717–1734. doi: 10.1534/genetics.114.169367
- Han, S., Utz, H. F., Liu, W., Schrag, T. A., Stange, M., Würschum, T., et al. (2016). Choice of models for QTL mapping with multiple families and design of the training set for prediction of Fusarium resistance traits in maize. *Theor. Appl. Genet.* 129, 431–444. doi: 10.1007/s00122-015-2637-3
- Jannink, J. L., and Jansen, R. (2001). Mapping epistatic quantitative trait loci with one-dimensional genome searches. *Genetics* 157, 445–454. doi: 10.1093/genetics/157.1.445
- Jarquín, D., Lemes da Silva, C., Gaynor, R. C., Poland, J., Fritz, A., Howard, R., et al. (2017). Increasing genomic-enabled prediction accuracy by modeling genotype × environment interactions in Kansas wheat. *Plant Genome* 10, pp.plantgenome2016-12. doi: 10.3835/plantgenome2016.12.013
- Jourjon, M. F., Jasson, S., Marcel, J., Ngom, B., and Mangin, B. (2005). MCQTL: Multi-allelic QTL mapping in multi-cross design. *Bioinformatics* 21, 128–130. doi: 10.1093/bioinformatics/bth481
- Jurcic, E. J., Villalba, P. V., Pathauer, P. S., Palazzini, D. A., Oberschelp, G. P. J., Harrand, L., et al. (2021). Single-step genomic prediction of *Eucalyptus dunnii* using different identity-by-descent and identity-by-state relationship matrices. *Heredity* 127, 176–189. doi: 10.1038/s41437-021-00450-9
- Kane, H., Eagles, H. A., Laurie, D. A., Trevaskis, B., Vallance, N., Eastwood, R. F., et al. (2013). Ppd-B1 and Ppd-D1 and their effects in southern Australian wheat. *Crop Pasture Sci.* 64, 100–114. doi: 10.1071/CP13086
- Lehermeier, C., Krämer, N., Bauer, E., Bauland, C., Camisan, C., Campo, L., et al. (2014). Usefulness of multiparental populations of maize (*Zea mays* L.) for genome-based prediction. *Genetics* 198, 3–16. doi: 10.1534/genetics.114.161943
- Li, W., Boer, M. P., van Rossum, B.-J., Zheng, C., Joosen, R. V. L., and Van Eeuwijk, F. A. (2022). statgenMPP: an R package implementing an IBD-based mixed model approach for QTL mapping in a wide range of multi-parent populations. *Bioinformatics* 38(22):5134–5136. doi: 10.1093/bioinformatics/btac662
- Li, W., Boer, M. P., Zheng, C., Joosen, R. V. L., and van Eeuwijk, F. A. (2021). An IBD-based mixed model approach for QTL mapping in multiparental populations. *Theor. Appl. Genet.* 1, 1–18. doi: 10.1007/s00122-021-03919-7
- Lopez-Cruz, M., Crossa, J., Bonnett, D., Dreisigacker, S., Poland, J., Jannink, J. L., et al. (2015). Increased prediction accuracy in wheat breeding trials using a marker × environment interaction genomic selection model. *G3: Genes Genomes Genet.* 5, 569–582. doi: 10.1534/g3.114.016097
- Malosetti, M., Ribaut, J. M., and van Eeuwijk, F. A. (2013). The statistical analysis of multi-environment data: Modeling genotype-by-environment interaction and its genetic basis. *Front. Physiol.* 44. doi: 10.3389/fphys.2013.00044
- Mathews, K. L., Malosetti, M., Chapman, S., McIntyre, L., Reynolds, M., Shorter, R., et al. (2008). Multi-environment QTL mixed models for drought stress adaptation in wheat. *Theor. Appl. Genet.* 117, 1077–1091. doi: 10.1007/s00122-008-0846-8
- Millet, E. J., Kruijer, W., Coupel-Ledru, A., Alvarez Prado, S., Cabrera-Bosquet, L., Lacube, S., et al. (2019). Genomic prediction of maize yield across European environmental conditions. *Nat. Genet.* 51, 952–956. doi: 10.1038/s41588-019-0414-y
- Millet, E. J., Welcker, C., Kruijer, W., Negro, S., Coupel-Ledru, A., Nicolas, S. D., et al. (2016). Genome-wide analysis of yield in Europe: allelic effects vary with drought and heat scenarios. *Plant Physiol.* 172, 749–764. doi: 10.1104/pp.16.00621
- Puglisi, D., Visioni, A., Ozkan, H., Casas, A. M., Igarua, E., Valè, G., et al. (2021). Genomic prediction of grain yield in a barley MAGIC population modeling genotype per environment interaction. *Front. Plant Sci.* 12, 664148. doi: 10.3389/fpls.2021.664148
- Rodríguez-Alvarez, M. X., Boer, M. P., van Eeuwijk, F. A., and Eilers, P. H. (2018). Correcting for spatial heterogeneity in plant breeding experiments with P-splines. *Spatial Stat* 23, 52–71. doi: 10.1016/j.spsata.2017.10.003
- Rossum, B.-J., van, Eeuwijk, F., van, Boer, M., Malosetti, M., Bustos-Korts, D., Millet, E. J., et al. (2021a). *statgenGxE: Genotype by Environment (GxE) Analysis*. <https://CRAN.R-project.org/package=statgenGxE>.
- Rossum, B.-J., van, Eeuwijk, F., van, Boer, M. P., Malosetti, M., Bustos-Korts, D., Millet, E. J., et al. (2021b). *statgenSTA: Single Trial Analysis (STA) of Field Trials*. <https://CRAN.R-project.org/package=statgenSTA>.
- Schott, J. R. (2016). *Matrix analysis for statistics* (John Wiley & Sons).
- Scott, M. F., Fradgley, N., Bentley, A. R., Brabbs, T., Corke, F., Gardner, K. A., et al. (2021). Limited haplotype diversity underlies polygenic trait architecture across 70 years of wheat breeding. *Genome Biol.* 22, 137. doi: 10.1186/s13059-021-02354-7
- Self, S. G., and Liang, K. Y. (1987). Asymptotic properties of maximum likelihood estimators and likelihood ratio tests under nonstandard conditions. *J. Am. Stat. Assoc.* 82, 605–610. doi: 10.1080/01621459.1987.10478472
- Shu, G., Wang, A., Wang, X., Chen, R., Gao, F., Wang, A., et al. (2023). Identification of QTNs, QTN-by-environment interactions for plant height and ear height in maize multi-environment GWAS. *Front. Plant Sci.* 14, 1284403. doi: 10.3389/fpls.2023.1284403
- Smith, A. B., Cullis, B. R., and Thompson, R. (2005). The analysis of crop cultivar breeding and evaluation trials: An overview of current mixed model approaches. *J. Agric. Sci.* 143, 449–462. doi: 10.1017/S0021859605005587
- van Eeuwijk, F. A., Bink, M. C., Chenu, K., and Chapman, S. C. (2010). Detection and use of QTL for complex traits in multiple environments. *Curr. Opin. Plant Biol.* 13, 193–205. doi: 10.1016/j.pbi.2010.01.001
- Van Eeuwijk, F. A., Bustos-Korts, D. V., and Malosetti, M. (2016). What should students in plant breeding know about the statistical aspects of genotype × Environment interactions? *Crop Sci.* 56, 2119–2140. doi: 10.2135/cropsci2015.06.0375
- Verbyla, A. P., Cavanagh, C. R., and Verbyla, K. L. (2014). Whole-genome analysis of multi-environment or multitrait QTL in MAGIC. *G3: Genes Genomes Genet.* 4, 1569–1584. doi: 10.1534/g3.114.012971

- Wang, S., Xie, F., and Xu, S. (2022). Estimating genetic variance contributed by a quantitative trait locus: A random model approach. *PLoS Comput. Biol.* 18, e1009923. doi: 10.1371/journal.pcbi.1009923
- Wei, J., and Xu, S. (2016). A random-model approach to QTL mapping in multiparent advanced generation intercross (MAGIC) populations. *Genetics* 202 (2), 471–486.
- White, J., Sharma, R., Balding, D., Cockram, J., and Mackay, I. J. (2022). Genome-wide association mapping of Hagberg falling number, protein content, test weight, and grain yield in U.K. wheat. *Crop Sci.* 62, 965–981. doi: 10.1002/csc2.20692
- Würschum, T., Boeven, P. H., Langer, S. M., Longin, C. F., and Leiser, W. L. (2015). Multiply to conquer: Copy number variations at *Ppd-B1* and *Vrn-A1* facilitate global adaptation in wheat. *BMC Genet.* 16, 96. doi: 10.1186/s12863-015-0258-0
- Yan, W., Hunt, L. A., Sheng, Q., and Szlavics, Z. (2000). Cultivar evaluation and mega-environment investigation based on the GGE biplot. *Crop Sci.* 40, 597–605. doi: 10.2135/cropsci2000.403597x
- Yan, W., and Kang, M. S. (2002). *GGE biplot analysis: A graphical tool for breeders, geneticists, and agronomists* (CRC press). doi: 10.1201/9781420040371
- Zheng, C. (2019). *RABBIT (v3.2) Manual*.
- Zheng, C., Boer, M. P., and Van Eeuwijk, F. A. (2014). A general modeling framework for genome ancestral origins in multiparental populations. *Genetics* 198, 87–101. doi: 10.1534/genetics.114.163006
- Zheng, C., Boer, M. P., and van Eeuwijk, F. A. (2015). Reconstruction of genome ancestry blocks in multiparental populations. *Genetics* 200, 1073–1087. doi: 10.1534/genetics.115.177873



OPEN ACCESS

EDITED BY

Paul Christiaan Struik,
Wageningen University and Research,
Netherlands

REVIEWED BY

Andrea Visioni,
International Center for Agricultural Research
in the Dry Areas (ICARDA), Morocco
Elisabetta Mazzucotelli,
Council for Agricultural Research and
Economics- Research Centre for Genomics
and Bioinformatics, Italy

*CORRESPONDENCE

Gustavo A. Slafer
✉ gustavo.slafer@udl.cat

RECEIVED 10 March 2024

ACCEPTED 29 July 2024

PUBLISHED 03 September 2024

CITATION

Parrado JD, Savin R and Slafer GA (2024)
Dynamics of apex and leaf development in
barley as affected by *PPD-H1* alleles in two
contrasting *PHYC* backgrounds under short
or long photoperiod.
Front. Plant Sci. 15:1398698.
doi: 10.3389/fpls.2024.1398698

COPYRIGHT

© 2024 Parrado, Savin and Slafer. This is an
open-access article distributed under the terms
of the [Creative Commons Attribution License](#)
(CC BY). The use, distribution or reproduction
in other forums is permitted, provided the
original author(s) and the copyright owner(s)
are credited and that the original publication
in this journal is cited, in accordance with
accepted academic practice. No use,
distribution or reproduction is permitted
which does not comply with these terms.

Dynamics of apex and leaf development in barley as affected by *PPD-H1* alleles in two contrasting *PHYC* backgrounds under short or long photoperiod

Jorge D. Parrado¹, Roxana Savin¹ and Gustavo A. Slafer^{1,2*}

¹Department of Agricultural and Forest Sciences and Engineering, University of Lleida-AGROTECNIO-CERCA Center, Lleida, Spain, ²Catalonian Institution for Research and Advanced Studies (ICREA), Barcelona, Spain

Barley development from seedling to flowering involves both external and internal changes, the latter requiring microscopic observation. Internal changes allow for the classification of preflowering development into three phases: vegetative, early reproductive, and late reproductive. Genetic and environmental factors influence the duration of these phases, impacting grain yield. Photoperiod-sensitivity genes *PPD-H1* play a major role in flowering time, affecting adaptation; however, the effect might also be direct (beyond affecting phenology). In this paper, we aimed to assess how *PPD-H1* alleles affect barley development, including the progression of growth phases, leaf emergence, tillering dynamics, and spikelet development. Two experiments (field and controlled conditions) were conducted with a factorial combination of (i) four near-isogenic lines (NILs) for *PPD-H1* alleles (*ppd-H1* or *Ppd-H1*) under two contrasting *PHYC* genetic backgrounds (*PhyC-l* and *PhyC-e*) and (ii) two photoperiod conditions (short and long days). As expected, longer photoperiods led to a shorter growth cycle. All subphases of time to flowering, final leaf number, and phyllochron were affected by photoperiod. The effects of *PPD-H1* on flowering time depended on the *PHYC* genetic backgrounds and photoperiod conditions. *PPD-H1* effects on flowering time were associated with leaf number and phyllochron; the interplay between leaf number and phyllochron affected mainly the late reproductive phase. We also found that although *PPD-H1* did not affect the phyllochron of the first six leaves, the phyllochron of leaves appearing later, when grown under a short photoperiod, was consistently increased in lines carrying the *ppd-H1* allele. Tillering dynamics exhibited variability, but *PPD-H1* did not affect the final spike number under a 24-h photoperiod.

KEYWORDS

Hordeum vulgare, flowering, developmental phases, Phyllochron, heading

1 Introduction

Barley development from seedling emergence to flowering encompasses changes that are both external, visible to the naked eye, and internal, requiring dissection of the meristematic apex and observation under the microscope. Internal changes are the basis for the partitioning of time to flowering into a sequence of three consecutive phases: (i) vegetative (from seedling emergence to the first double ridge¹, mostly a leaf primordia initiation phase), (ii) early reproductive (from first double ridge to awn initiation, basically the spikelet initiation phase), and (iii) late reproductive (from awn initiation to flowering, when the survival of initiated spikelets takes place, resulting in the number of fertile florets) (Appleyard et al., 1982; Kirby and Appleyard, 1984; Sreenivasulu and Schnurbusch, 2012). The periodic determination of the number of spikelets initiated and the stage of floret development in each of them allows the determination of the dynamics of floret initiation and mortality, determining spike fertility, a major driver of yield in small grain cereals (Slafer et al., 2022; Serrago et al., 2023). External changes include the number of structures (number of leaves on the main shoot, number of tillers) that, when measured periodically along the season, allow determining the dynamics of both leaf appearance and tillering (Zadoks et al., 1974; Slafer and Rawson, 1994; González et al., 2002; Slafer et al., 2015). Both dynamics are relevant, the former because the time to flowering is strongly related to both the number of initiated leaves in the apex during the vegetative phase and their rate of appearance, and the dynamics of tillering and tiller mortality is relevant as they define the number of spikes, which is also a relevant component of barley yield (Miralles et al., 2021; Serrago et al., 2023).

The duration of preflowering phases, when major yield components are being formed in cereals (Slafer et al., 2023b), is controlled by genetic and environmental factors (Andrés and Coupland, 2012; Casal and Qüesta, 2018). Indeed, specific yield components are formed during distinct phases of plant development (Slafer and Rawson, 1994). Several studies reported phenotypic variability in the duration of preflowering phases among genotypes with similar flowering time (Appleyard et al., 1982; Kitchen and Rasmusson, 1983; Kernich et al., 1997; Whitechurch et al., 2007a, 2007b). Therefore, not only time to flowering is relevant but also the distribution of that time across its different subphases when affected by genetic or environmental factors.

Photoperiod sensitivity genes are critical for determining the time to flowering and adaptation in barley. Although there are two major photoperiod-sensitivity genes, *PPD-H1* is by far the most relevant and, therefore, the primary target for improving barley adaptation (Turner et al., 2005; Jones et al., 2008; Wang et al., 2010;

He et al., 2019; Fernández-Calleja et al., 2021). Barley is a quantitative long-day plant that accelerates its development under long photoperiods (Boyd et al., 2003; Karsai et al., 2004). The allelic version of *PPD-H1* modifies the photoperiod sensitivity (i.e., the dominant allele, *Ppd-H1*, confers photoperiod sensitivity, while the recessive allele, *ppd-H1*, is known as the photoperiod-insensitive² allele, even though it does also confer sensitivity, but noticeably less than *Ppd-H1*) (Laurie et al., 1994; Turner et al., 2005; Von Korff et al., 2010; Parrado et al., 2023; Slafer et al., 2023a). In fact, the effect of *PPD-H1* alleles on time to flowering in spring barley tends to be maximised at intermediate-long photoperiods (e.g., 12–16 h; Fernández-Calleja et al., 2021, and references therein), but minimised at extremely long photoperiods 21–24 h (Parrado et al., 2023).

Previous studies suggested a pleiotropic effect of the *PPD-H1* gene on yield components within the classical photoperiod range of 12 to 16 h (Von Korff et al., 2006; Wang et al., 2010; Borràs-Geloch et al., 2012; Ponce-Molina et al., 2012; Pankin et al., 2014; Bustos-Korts et al., 2019; Wiegmann et al., 2019). Determining whether *Ppd-H1* has true pleiotropic effects (beyond those on time to flowering) is required to grow the plants with contrasting photoperiod sensitivity at a photoperiod in which they flower simultaneously. In a previous paper (Parrado et al., 2023), we showed that under extremely long days, *PPD-H1*-sensitive and *PPD-H1*-insensitive lines tend to flower simultaneously. Consequently, under these conditions, genetic effects not associated with the crop cycle could be studied. In this scenario, we attempted to synchronise the flowering time of all lines, regardless of their photoperiod sensitivity, by saturating the photoperiod response with 24-h daylength and then studying whether these genes affect developmental components independently of flowering time. To gain consistency of conclusions regarding the possible true pleiotropic effects of *PPD-H1* on yield components or to show relevant interactions conditioning such effect, it would be beneficial to test the effects of *PPD-H1* alleles under contrasting genetic and environmental backgrounds.

Another gene affecting flowering time in barley related to the perception of light is the red/far-red light photoreceptor phytochrome C (*PHYC*), which is closely linked to *VRN-H1* (Szucs et al., 2006; Nishida et al., 2013; Pankin et al., 2014). Under vernalised conditions, *VRN-H1* would not have an effect on time to flowering; when both linked genes are modified together, any effect on time to flowering would be driven by the *PHYC* late- and early-flowering alleles (*PhyC-l* and *PhyC-e*, respectively; Ochagavía et al., 2022).

The aim of this study was to assess the effects of *PPD-H1* alleles on the phasic, leaf, tiller and spikelet development of barley. To strengthen the robustness of conclusions reached, we compared near-isogenic lines with *Ppd-H1* and *ppd-H1* alleles combined with contrasting *PHYC* backgrounds and under contrasting photoperiod conditions (i.e., we quantified the effects of *PPD-H1* alleles against

¹ Although floral initiation does normally occur earlier, with the first spikelets initiated as single ridges (Delécolle et al., 1989; Kirby, 1990; Ochagavía et al., 2018), it has been traditionally assumed that the stage of double ridge shows the transition from vegetative to reproductive apex (Slafer et al., 2021) because it is the first microscopic evidence that the apex is indubitably reproductive.

² Also referred to in the literature as the mutant *ppd-H1* allele, inducing reduced photoperiod sensitivity (Turner et al., 2005; Ejaz and von Korff, 2017).

contrasting overall times to flowering given by genetic and environmental factors) in experiments under field and controlled conditions.

2 Materials and methods

2.1 Experimental conditions and treatments

Two experiments (field and controlled conditions) were conducted during the 2019–2020 growing season. Treatments in each of the experiments consisted of a factorial combination of (i) four near-isogenic lines (NILs) for *PPD-H1* alleles (*ppd-H1* or *Ppd-H1*) under two contrasting *PHYC* genetic backgrounds (*PhyC-l* and *PhyC-e*) and (ii) two photoperiod conditions (short and long days). NILs were produced at CSIRO (Canberra, Australia) after five cycles of backcrossing, using different donors of *VRN-H1/PHYC* and *PPD-H1* alleles into the facultative recurrent barley cultivar “WI4441” (Oliver et al., 2013).

The four genotypes were actually aimed to be isogenic for allelic constitution of *PPD-H1* and *VRN-H1*, but as the latter is closely linked to *PHYC* (Szucs et al., 2006; Nishida et al., 2013; Pankin et al., 2014), the NILs were actually *vrn-H1+PhyC-e* and *Vrn-H1+PhyC-l* (Table 1), as demonstrated by Ochagavía et al. (2022) who genotyped these NILs, finding that winter (*vrn-H1*) lines carried the *PhyC-e* allele and spring (*Vrn-H1*) lines the late allele (*PhyC-l*). Although this linkage prevents a clear separation of the effects *VRN-H1* and *PHYC* genes, in the experiments reported here, plants were vernalised (see below), and therefore there were no effects of *VRN-H1* on any developmental attribute. Thus, for simplicity, we considered herein these NILs as the combinations of the two allelic constitutions of *PPD-H1* and *PHYC* (Table 1). All lines had the dominant *Vrn-H2* and *Ppd-H2* alleles and haplotype II of *HvCEN* (Oliver et al., 2013; Ochagavía et al., 2022); i.e., all effects on developmental characteristics will be due to the action of *PPD-H1* alleles under the particular backgrounds of contrasting alleles of *PHYC* and contrasting photoperiods.

The field experiment (Exp1) was sown on 03 December 2019 in a facility with photoperiod control available at the campus of the University of Lleida, Spain (41°37'50"N, 0°35'27"E; altitude 180 m) in a fine loamy, mixed (calcareous), thermic soil classified as Typic Xerofluent, according to the USDA taxonomy (Soil Survey Staff, 1999). Seeds of each material were distributed in strips of biodegradable paper, ensuring a uniform distance between plants within rows as well as a uniform seedling depth.

Plots were maintained throughout the whole cycle under either (i) natural conditions, with an average photoperiod from seedling emergence (SE) to flowering (Fw) of ca. 12 h (11.7 h ± 0.02 h), or (ii) a 24-h daylength, artificially extending the natural photoperiod with low-intensity (60 W) incandescent bulbs positioned on top of the designated plots. The radiation intensity was more than enough to produce the daylength signal, but increased radiation only negligibly (ca. ~ 3.6 μmol m⁻² s⁻¹ PAR at canopy level), below the light compensation point for barley (i.e., irradiance at which photosynthesis equals respiration and net photosynthesis is zero) normally around 10–15 μmol m⁻² s⁻¹ (Arenas-Corraliza et al., 2019; Chen et al., 2021), allowing plants to alter their developmental patterns but not affecting daily growth directly.

Exp1 was drip-irrigated when needed in order to avoid water stress. Weeds, diseases, and insects were controlled or prevented by spraying herbicides, fungicides, and insecticides at doses recommended by their manufacturers.

In the growth chamber experiment (Exp2), NILs were grown at the relatively low and constant temperature of 12°C (to expose plants to a temperature approaching the average temperature from SE to Fw more realistically than most controlled conditions growing temperate cereals that set growing temperatures at 18°C–25°C, accelerating development to minimise experimental duration). Indeed, the mean temperature from seedling emergence to flowering in the field experiment was 9.2°C. The two different temperature regimes in our experiments—lower average temperatures with natural daily and monthly variations in the field and slightly higher and constant temperatures in the growth chambers—along with other differences in the experimental setups could affect the strength of our conclusions. The conclusions will be more solid if the results are consistent across both experiments and weaker if the results are conflicting. The photoperiod treatments were 12 and 24 h; in the latter, only half of the lights were switched on during the duration of the day to compensate for the difference in daylength, so that in both conditions the daily radiation was the same (5.2 MJ m⁻² day⁻¹). In Exp2, seeds were germinated in 235 cm³ black plastic pots filled with 110 g of a soil mixture (70% w/w peat and 30% w/w organic amendment) freshly prepared before sowing. There was only one seedling per pot, and after being vernalised (see below), we transferred a set of 26 pots per NIL with seedlings at exactly the same stage (see below) to each of the two cabinets, previously configured for temperature and photoperiod conditions. Many of these plants were sampled for periodic dissections and intermediate determinations during the duration of the experiment, but at least three out of the 26 were left

TABLE 1 Allelic constitution of barley NILs analysed in this study for *PPD-H1* and *VRN-H1 + PHYC* genes.

Photoperiod sensitivity	<i>PPD-H1</i> allele	Earliness due to <i>PHYC</i>	<i>VRN-H1 + PHYC</i>	Denomination in this study
Sensitive (Ps)	<i>Ppd-H1</i>	Early (Ea)	<i>vrn-H1 + PhyC-e</i>	PsEa
Insensitive (Pi)	<i>ppd-H1</i>			PiEa
Sensitive (Ps)	<i>Ppd-H1</i>	Late (La)	<i>Vrn-H1 + PhyC-l</i>	PsLa
Insensitive (Pi)	<i>ppd-H1</i>			PiLa

intact until flowering. Within each chamber, the pots were distributed randomly on trays and rotated at least twice weekly to avoid any possible positional effect within the chamber. Plants were irrigated daily, and each pot was fertilised with both macro- and micronutrients to avoid nutritional deficiencies.

In both experiments, all plants were vernalised; in Exp1, plants were naturally vernalised when exposed to winter (as they were sown in late fall). From sowing to the end of winter, seedlings were exposed to 41 fully vernalising days (days with mean temperatures with maximum effect on vernalisation, between 0°C and 8°C; Flood and Halloran, 1986; Brooking and Jamieson, 2002; Figure 1) plus 26 days with mean temperatures between 8°C and 10°C [that are also strongly vernalising temperatures, considering that vernalisation is produced when temperatures are up to 15°C; Brooking and Jamieson (2002)]. In Exp2, pots were exposed to vernalising temperature (4°C constant during the whole day) for 29 days in a cold room. Firstly, the pots were filled and sown at exactly the same depth with one seed per pot, but with 35% more pots than needed for the experiment (i.e., we sowed and included 70 pots of each individual NIL in the vernalisation pretreatment; in each of the two growth chambers prepared for the experiment, we transferred only 26 pots per NIL). This allowed us to discard not only the few pots in which seedlings did not emerge but also the tails of early- and late-emerging seedlings. As a result, when the experiment started and we transferred the pots from the vernalisation room to the growth chambers at 12 or 24 h photoperiod, all plants were extremely uniform (averaging 1.06 ± 0.02 emerged leaves).

After sowing the pots, before transferring them to the cool room for vernalisation, they were watered and left for 1 day at room temperature to trigger the germination process. Subsequently, all pots were transferred to a cool room. Finally, the 52 pots per NIL selected for having homogeneous seedlings were transferred to the growth chambers, and the experiment started (and for simplicity and using the same terms in both experiments, the date of starting the experiment was identified as “seedling emergence”, which, strictly talking, was slightly later in Exp2).

Treatments in Exp1 were arranged in a split-plot design, where the main plots, allocated to three complete blocks, were assigned to the photoperiod treatments, and the subplots, allocated randomly within the main plots, were assigned to the NILs. Subplots were 3.5 m in length and 1.2 m wide, with six rows (0.2 m apart) and a seedling rate of 200 plants m^{-2} . In Exp2 within each cabinet, a set of 26 barley plants of each of the four NILs (i.e., 104 plants in each photoperiod condition) were arranged in a complete randomised design.

2.2 Measurements and analyses

The duration of both time from seedling emergence to flowering and of the phases composing it (i.e., from seedling emergence to awn initiation [SE-AI], from then to flag leaf [AI-FL], and from then to flowering [FL-Fw]) was expressed in thermal time, using the average temperature recorded at the site in Exp1

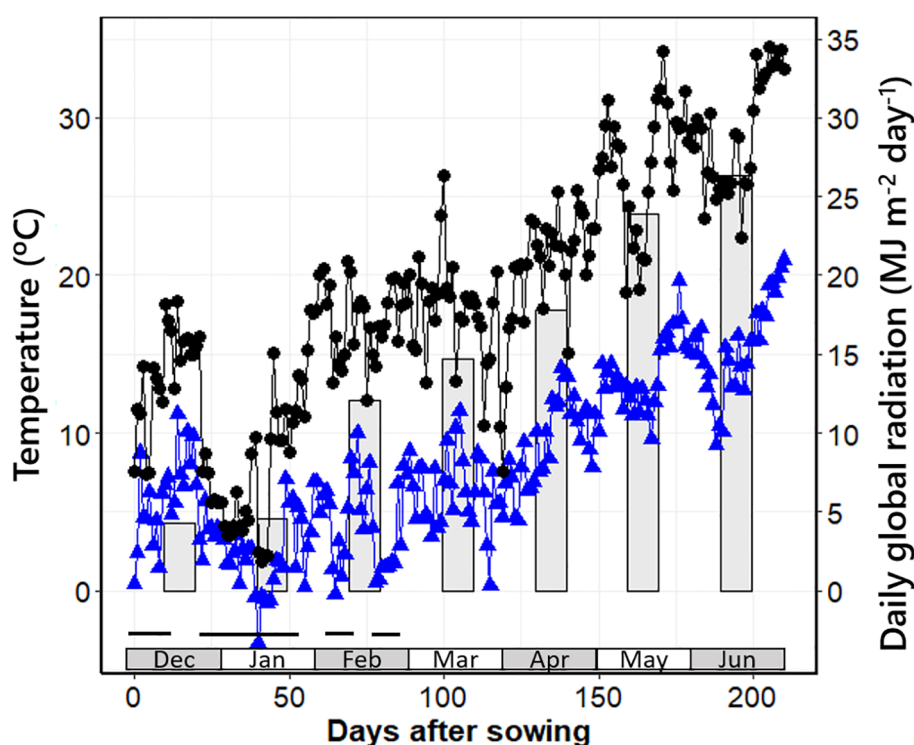


FIGURE 1

Minimum and maximum daily temperatures (triangles and circles, respectively) and daily global radiation averaged per month (bars) from sowing date to harvest of the latest plots in Exp1. The black horizontal bars at the bottom of the graph indicate periods with mean daily temperatures below 10°C.

(Meteorological station from the Meteorological Service of the Government of Catalonia [Meteocat]) and the temperature of the chamber in Exp2, assuming a base temperature of 0°C, as standardly done (Kirby, 1988). The developmental stages determined (SE, AI, FL, and Fw) were in accordance with the Zadoks' scale (Z09-10; Z31-33; Z39; Z55; Zadoks et al., 1974). However, for a more accurate determination, AI and Fw were determined, taking into account internal structures not normally visible to the naked eye. Awn initiation was determined microscopically when the tip of the lemma primordium started to grow and curve over the stamen primordia (~ W4.5). Flowering was determined as the time of pollination by regular microscopic dissection of the main spike and determining when it reached stage 10 on the Waddington et al. (1983) scale (i.e., when styles are curved outward with stigmatic branches widely spread and pollen grains visible on stigmatic hairs).

From SE to Fw, main stems were monitored once a week to determine the duration of different phenological phases [as delimited by stages determined externally by the scale of Zadoks et al. (1974) and internally by the scale of Waddington et al. (1983)]. In addition, three plants per experimental unit were randomly selected³ and tagged soon after SE, and the number of leaves that emerged on the main shoot was recorded twice a week following the scale developed by Haun (1973), while simultaneously the number of emerged and living tillers were determined.

From SE onward, representative plants of each NIL (three in each experimental unit of Exp1 and two in each chamber of Exp2) were sampled twice a week, and apical development was observed under the microscope after dissecting the main shoot apex. In addition, a detailed morphological analysis of spikelet and floret development of the main shoot spikes was carried out following the scale described by Waddington et al. (1983). The apices were dissected under a stereomicroscope Leica MZ 80 (Leica Microscopy System Ltd., Heerbrugg, Switzerland) equipped with a digital camera (model DFC420, Leica).

Phyllochron (i.e., the thermal time interval between the appearance of two successive leaves) was calculated as the reciprocal of the rate of leaf appearance (i.e., the slope of the relationship between the cumulative number of leaves on the main shoot and the thermal time). Whenever a linear model did not produce a random distribution of residuals, a bilinear model was fitted (with one phyllochron for the first leaves and another one for the last leaves) and, in these cases, considering the average phyllochron of all leaves as well as those for early- and late-appearing leaves.

Analysis of variance (ANOVA) was used to partition variation into effects of treatments and their interactions using the statistical software JMP[®] Pro version 16.0 (SAS Institute Inc., Cary, NC, USA). Differences among means were compared using the least significant difference test (LSD, considered to be statistically significant if $p < 0.05$). To assess the degree of relationships between variables, linear regression analyses were performed.

Polynomial regressions (Loess smooth line) were performed for the numbers of leaves, tillers, and floret dynamics, using an alpha of 0.75 and 95% confidence interval. Graphs were created in R using the package “ggplot2” (Wickham, 2016; R Core Team, 2020).

3 Results

3.1 Phenology

As expected for a quantitative long-day plant, the overall duration of the cycle from SE to Fw was reduced when plants were grown under long days (cf. right and left panels in Figure 2). More relevantly, in the context of the aims of this study, the effect of *PPD-H1* gene on time to flowering in each of the contrasting *PHYC* genetic backgrounds depended on the photoperiod condition. There was an interaction between NILs and photoperiod on time to flowering: at 12 h photoperiod, Fw was delayed by the action of the *ppd-H1*-insensitive allele (although the effect was a nonsignificant trend when the *PhyC-l* allele was in the background in Exp1, the direct effect of *ppd-H1* was still significant when considered across the two *PHYC* backgrounds; see boxplots in Figure 2A), while under 24 h photoperiod, the *ppd-H1* allele did not significantly delay Fw (Figures 2B, D). The responses of time to Fw caused by *PPD-H1* across the two *PHYC* backgrounds were clearer under controlled conditions, but importantly, we observed the same effects in the field (cf. see boxplots in Figures 2A, C).

Across all sources of variation, time to Fw was very strongly related ($R^2 > 0.95$; $p < 0.001$) to the duration of both component phases, from SE to AI (Figures 3A, B) and from AI to Fw (Figures 3C, D) consistently across the two different experiments (i.e., the effect of all treatments together on time to Fw was due to effects on both phases). However, a major part of the similarly strong relationships of time to Fw with its two component phases was driven by the photoperiod growing condition: the phases of leaf and spikelet initiation and of floret development within spikelets (and then of spikelet survival) were both similarly affected by the photoperiodic condition in both experiments (Figure 3). Focusing on the effects produced by the *PPD-H1* alleles, the delay in Fw produced by the insensitivity allele was only significant under short photoperiod conditions in both experiments (see boxplots in Figure 2), and this effect was clearer in the duration of the period from SE to AI than in that from AI to Fw (although the latter also showed a consistent, though non-significant, trend to be delayed due to the action of the *ppd-H1* allele; open boxplots in Figure 3). Thus, under these relatively short photoperiods, there seemed to have been a sort of knock-on effect caused by the *ppd-H1* allele, clearly lengthening the duration of the SE-AI phase but also tending to lengthen that of the AI-Fw phase.

3.2 Dynamics of leaf appearance and tillering

The leaf appearance rate was constant for the initial ca. six leaves across NILs, as indicated by the linear relationships when

³ Due to the dedicated system used to install the plots in Exp1 and the selection of uniform plants after vernalising them in Exp2, each of the plants was very representative.

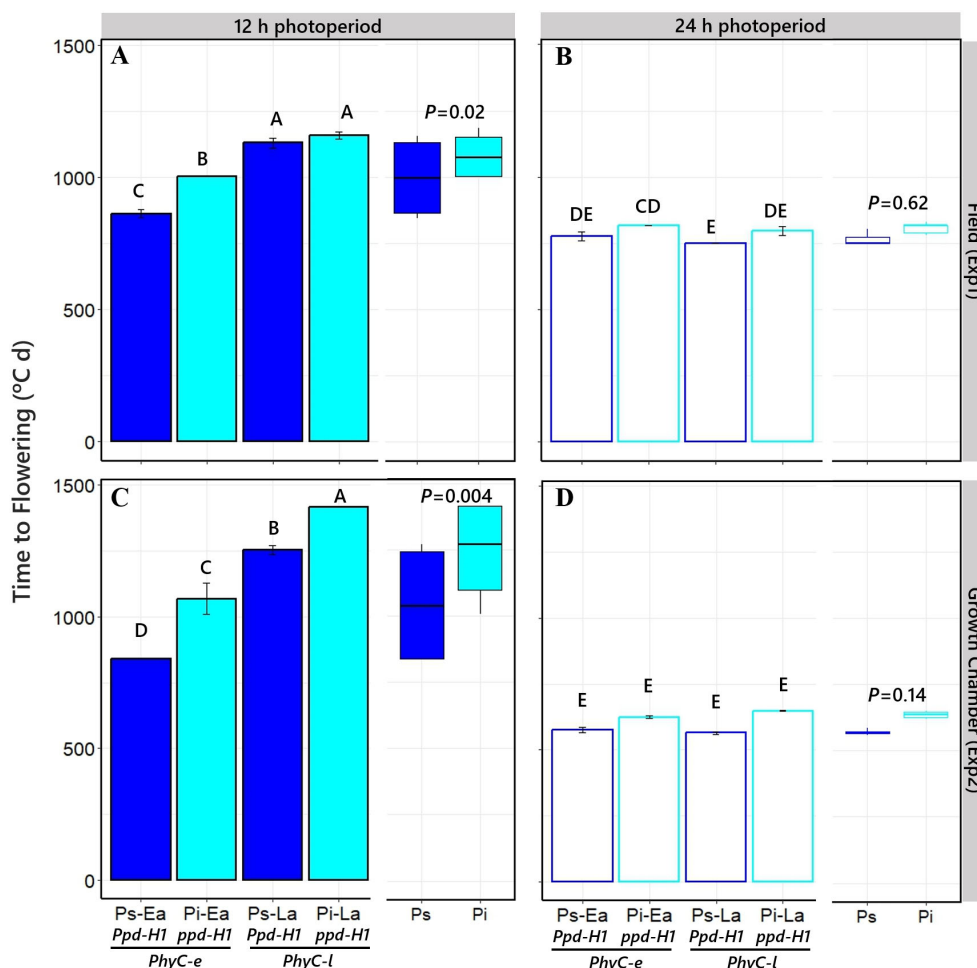


FIGURE 2

Time to flowering of the four different NILs grown under short [12 h; (A, C)] and long [24 h; (B, D)] photoperiods in field and growth chamber conditions (top and bottom, respectively). Different capital letters indicate significant differences ($p < 0.05$) between NILs with *Ppd-H1*-sensitive (Ps, dark blue bars) and *ppd-H1*-insensitive (Pi, light blue bars) alleles, combined with each of the two *PHYC* backgrounds within the left and right half of each panel, *PhyC*-e: early (Ea); *PhyC*-l: late (La). In the field experiment, a 12-h photoperiod corresponds to the average of the period from seedling emergence to flowering. Boxplots in each panel represent time to flowering for *Ppd-H1*-sensitive (dark blue) and *ppd-H1*-insensitive (light blue) alleles grouped across *PHYC* backgrounds, including the level of significance (p -value) of the difference between NILs with contrasting *PPD-H1* alleles within each photoperiod treatment.

plotting leaf number vs. thermal time. However, when the final leaf number (FLN) was clearly higher than this threshold (particularly under short photoperiod), the rate of leaf appearance for the later leaves decreased, exhibiting a bilinear relationship between leaf number and thermal time across NILs (and the higher the FLN, the stronger the increase in phyllochron; Figures 4A, C).

Time to the appearance of the flag leaf was clearly affected by photoperiod across NILs in both experiments (cf. the pairs of boxplots under short and long photoperiods in Figures 5A, B), driven by the effects of the photoperiod condition on both FLN and average phyllochron (Figures 5C, E [Exp1], Figures 5D, F [Exp2]).

The allelic form of the *PPD-H1* gene affected phyllochron slightly but consistently across photoperiods and experiments, although the effect was significant only under controlled conditions (Figures 5E, F). Under long photoperiods, NILs having *Ppd-H1*-sensitive and *ppd-H1*-insensitive alleles had phyllochrons of, on average, 77°C and 82°C day⁻¹ leaf in Exp1 and 68°C and 76°C

day⁻¹ leaf in Exp2, respectively (Figures 5E, F). Under a short photoperiod, NILs having the *Ppd-H1*-sensitive allele had on average a consistently shorter phyllochron (95°C and 112°C day⁻¹ leaf) than those carrying the *ppd-H1*-insensitive allele (98°C and 125°C day⁻¹ leaf, in Exp1 and Exp2, respectively). *PPD-H1* alleles did not affect FLN in Exp1 under either of the two photoperiod conditions (Figure 5C). However, in Exp2, NILs having *ppd-H1*-insensitive alleles increased FLN, though rather slightly by less than one leaf, in both photoperiod conditions (Figure 5D).

Thermal time to flag leaf was better explained by phyllochron ($R^2 = 0.94$ and $R^2 = 0.99$ for Exp1 and Exp2, respectively; Figures 6A, B) than by FLN ($R^2 = 0.87$ and $R^2 = 0.86$ for Exp1 and Exp2, respectively) (Figures 6C, D).

Tillering dynamics was similar across experiments and NILs with relatively limited tillering and consequently having very little tiller mortality (Figures 7A, C–E, G, H). The effects of *PPD-H1* alleles were not large nor consistent for all cases, but when the

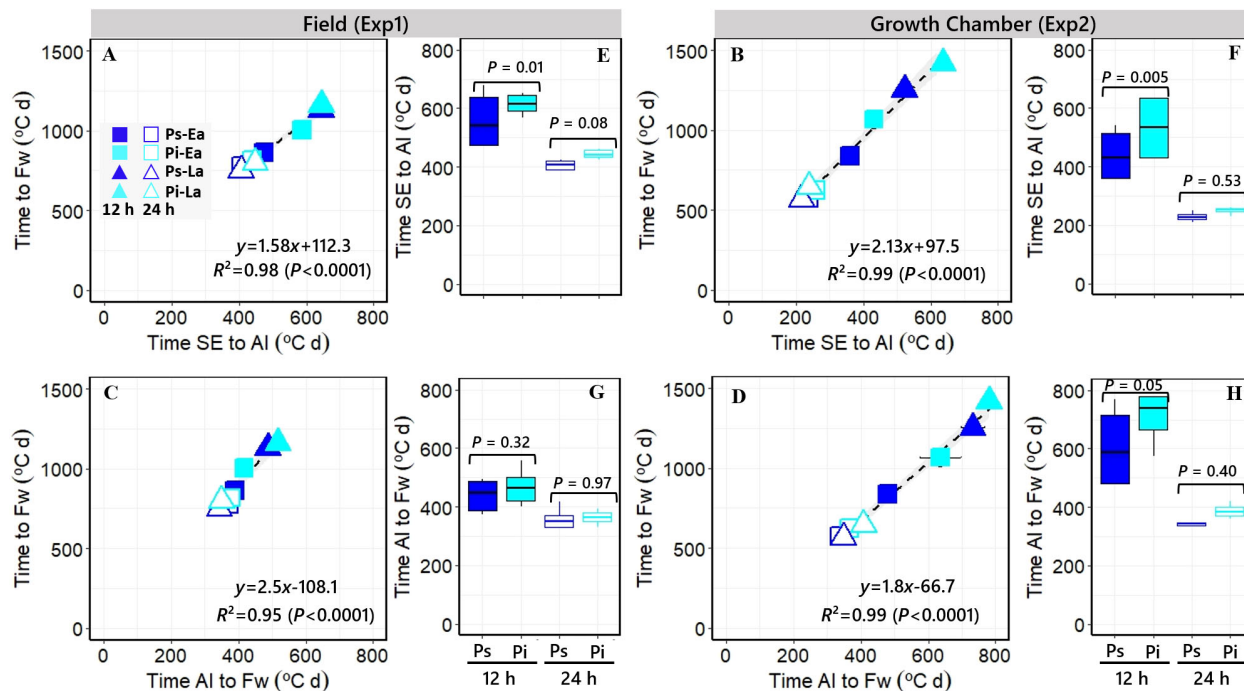


FIGURE 3

(A–D) Relationships between the durations of the whole phase from seedling emergence (SE) to flowering (Fw) and that of its component phases either from SE to awn initiation [AI; (A, B) in Exp1 and Exp2, respectively] or from AI to Fw [(C, D) in Exp1 and Exp2, respectively]. The segments on the symbols represent the standard errors of the means (not seen when smaller than the size of the symbol). Open and closed symbols correspond to long and short photoperiods, respectively. Squares: *PhyC-e*; triangles: *PhyC-l*; dark blue symbols: *Ppd-H1*; and light blue symbols: *ppd-H1*. (E–H) Boxplots grouping the NILs with *Ppd-H1*-sensitive (dark blue boxplots) and *ppd-H1*-insensitive (light blue boxplots) alleles across *PHYC* backgrounds for the duration of the phases from SE to AI [(E, F) in Exp1 and Exp2, respectively] and from AI to Fw [(G, H) in Exp1 and Exp2, respectively] under short (closed) and long (open) photoperiods, including the level of significance (p -value) of the difference between NILs with contrasting *PPD-H1* alleles within each photoperiod treatment. In the field experiment, a 12-h photoperiod corresponds to the average of the period from seedling emergence to flowering.

environmental background was the short photoperiod and the genetic background included the *PhyC-l* allele, in general, the NIL with the insensitive *ppd-H1* allele produced more spikes per plant due to reduced tiller mortality in Exp1 (Figure 7B) and maintained tillering a bit longer in Exp2 (Figure 7F).

3.3 Apex development

In general, in the central spikelets of the main shoot spike, awn initiation and flag leaf stages coincided with floret developmental stages of W4.75 and W8, respectively, of the scale of Waddington et al. (1983), varying only very slightly across NILs, experiments, and photoperiod conditions (Supplementary Figure S1).

NILs having sensitive *Ppd-H1* alleles slightly accelerated flowering by promoting early shoot apex development, whose magnitude depended on the photoperiod condition and *PHYC* genetic background (Figure 8; Supplementary Figures S2, S3). This effect of *PPD-H1* was only slight on long days (Figures 8C, D, G, H), when the time to flowering was not significantly delayed (see above). Under short photoperiod conditions, florets in the insensitive *ppd-H1* lines showed a much clearer development deceleration (Figures 8A, E, F), except for the *PhyC-l* background under natural photoperiod in Exp1, where the difference was not significant (Figure 8B).

This effect of *PPD-H1* is reflected in the developmental rates of a particular organ (florets), which has been observed for the phenological effects on flowering time.

4 Discussion

The effects of *PPD-H1* alleles on the components of time to flowering could be assessed both in terms of subphase durations (Slafer and Rawson, 1994; Kirby et al., 1999) and in terms of the number of leaves initiated and phyllochron (Slafer and Rawson, 1997; Jamieson et al., 1998). Many studies showed that under long days of 16–18 h, the time to flowering was significantly delayed by the action of the insensitivity allele *ppd-H1* (Laurie et al., 1994; Turner et al., 2005; Digel et al., 2015; Parrado et al., 2023; Slafer et al., 2023a). Indeed, introgressing this allele was critical for spring barley production at high latitudes to avoid the extremely short cycle of the sensitive cultivars possessing the *Ppd-H1* allele (Fernández-Calleja et al., 2021 and references quoted therein). However, lengthening the cycle under long days by introgressing insensitivity to photoperiod would be counterintuitive for a long-day plant (Slafer et al., 2009), and therefore, at photoperiods even longer than 21 h, lines should flower similarly (Parrado et al., 2023). We found here that when plants were grown at a 24-h photoperiod,

the effect of *ppd-H1* allele on phenology was negligible, which is consistent with a recent study where we uncovered responses of barley lines with contrasting photoperiod sensitivity to extreme photoperiods (Parrado et al., 2023).

In our set of NILs, time to flowering was related to the duration of both the vegetative plus the early reproductive phase (i.e., from SE to AI) and the late reproductive phase, mainly driven by variability in the short photoperiod treatment generated by the *PHYC* alleles, which is consistent with the findings of Pankin et al. (2014). Even though there was a relationship between the duration of the two phases, as reported in other studies (Appleyard et al., 1982; González et al., 2005; Whitechurch et al., 2007b; Borràs-Gelonch et al., 2012), the idea that the duration of these phases may be independent is still valid. This is evident when screening a large number of genotypes (e.g., Kitchen and Rasmusson, 1983; Kernich et al., 1997; Whitechurch et al., 2007a; Borràs et al., 2009), but the independent duration of these phases would be controlled by other minor genes (Borràs-Gelonch et al., 2010; Alqudah et al., 2014), as the major developmental genes like *PPD-H1* seem to affect all preflowering phases, in line with what previously reported in barley (Borràs-Gelonch et al., 2012; Digel et al., 2015; Fernández-Calleja et al., 2021), as well as in wheat (González et al., 2005).

Although there were slight phenological variations within contrasting photoperiods, the SE-AI period was more affected by the *ppd-H1* allele than the AI-Fw period. However, studies conducted under long photoperiods of 16 h showed that *ppd-H1* delayed both early and late reproductive development (Digel et al., 2015; Ejaz and von Korff, 2017). This would suggest that preflowering phases may vary in their sensitivity to *PPD-H1* depending on the duration of the day. Furthermore, it is well known that the impact of *PPD-H1* on time to flowering may be influenced by genetic background (Laurie et al., 1995; Szucs et al., 2006; Hemming et al., 2008; Nishida et al., 2013; Turner et al., 2013; Pankin et al., 2014). Therefore, since AI-Fw was significantly influenced by the photoperiodic environment (12 h vs. 24 h) and *PPD-H1* had a negligible effect on this period within the photoperiod treatments, the duration of AI-Fw must be regulated by another photoperiod response gene (or potentially interacting with *PPD-H1*) that has not yet been identified.

An overall view (including photoperiod treatment and *PHYC* background) of relationships between the number of leaves initiated, rate of leaf appearance, and time to flowering would suggest that most of the effects of *PPD-H1* alleles on time to flowering can be seen as a consequence of the effects on both

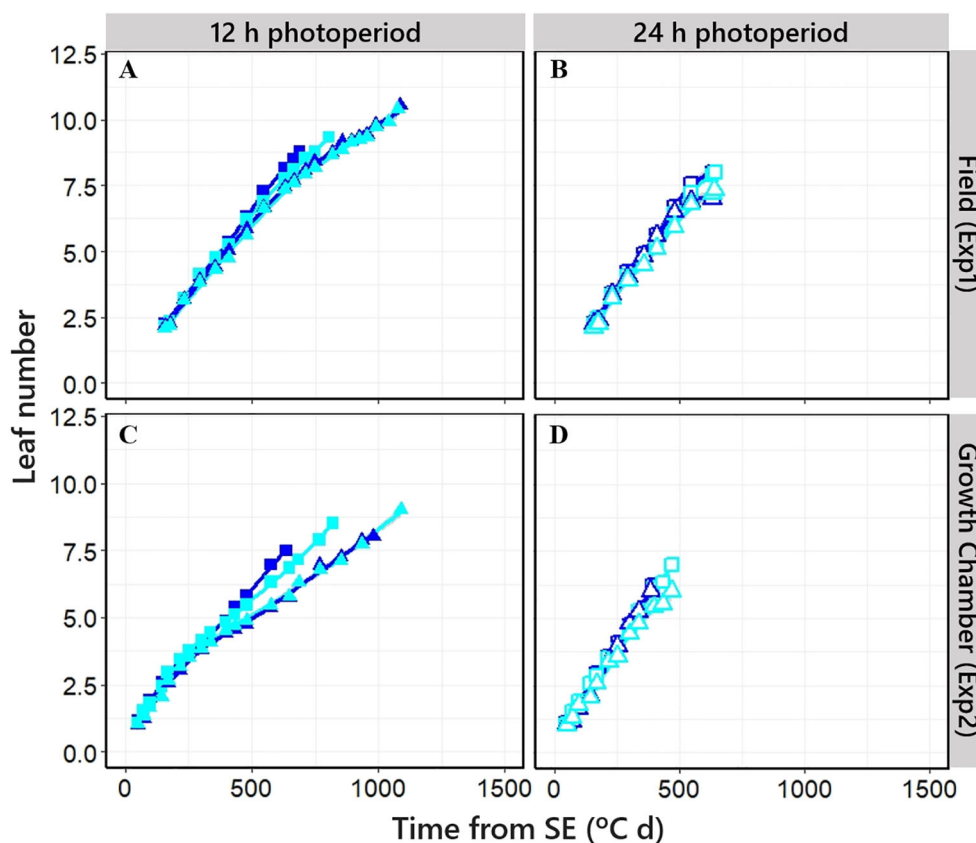


FIGURE 4

Relationship between cumulative leaf number on main shoot and time from seedling emergence in four different NILs grown at short [(A, C); closed symbols] and long photoperiod [(B, D); open symbols] in Exp1 (top) and Exp2 (bottom). Square: *PhyC-e*; triangle: *PhyC-l*. Dark blue symbols: *ppd-H1*; light blue symbols: *ppd-H1*. In the field experiment, a 12-h photoperiod corresponds to the average of the period from seedling emergence to flowering.

FLN and phyllochron, as reported when the treatments were not particular photoperiod-sensitivity genes by Kirby (1990) and Miralles et al. (2021) or specifically *PPD-H1* alleles exposed to different photoperiods (12 h vs. 16 h) during the early phase of development (Dígel et al., 2015). The increase in phyllochron observed under short days can be attributed to a significant decrease in the rate of leaf appearance after the first six leaves had appeared, as previously documented for wheat by Slafer and Rawson (1997), leading to the lengthening of the AI-Fw stage, complementing the most relevant effect of this gene on the duration of the phases of leaf and spikelet development. The interplay between FLN and phyllochron ends up making *PPD-H1* affect both phases of time to Fw (i.e., through reducing the rate of development in the vegetative phase, the insensitive allele increases FLN, and then as the last leaves appear more slowly

than the first leaves, this generates a carry-over effect on the duration of the late reproductive phase). This finding is consistent with that showing that the phyllochron of the initial leaves was unaffected by the *PPD-1* alleles in wheat, while that of the later leaves was sensitive (González et al., 2005). However, evaluating the effect of *PPD-H1* within photoperiodic environments and *PHYC* backgrounds, the elongation of the SE-AI period induced by the *ppd-H1* allele could be due to an elongation of the early reproductive phase and not of the vegetative stage, as suggested by a negligible change in the final number of leaves between NILs. This is consistent with previous work where *PPD-H1* did not induce changes in the vegetative stage (Pankin et al., 2014; Dígel et al., 2015; Ejaz and von Korff, 2017).

Although it has a slight effect on the duration of the AI-Fw period within photoperiod treatment, *PPD-H1* seems to have

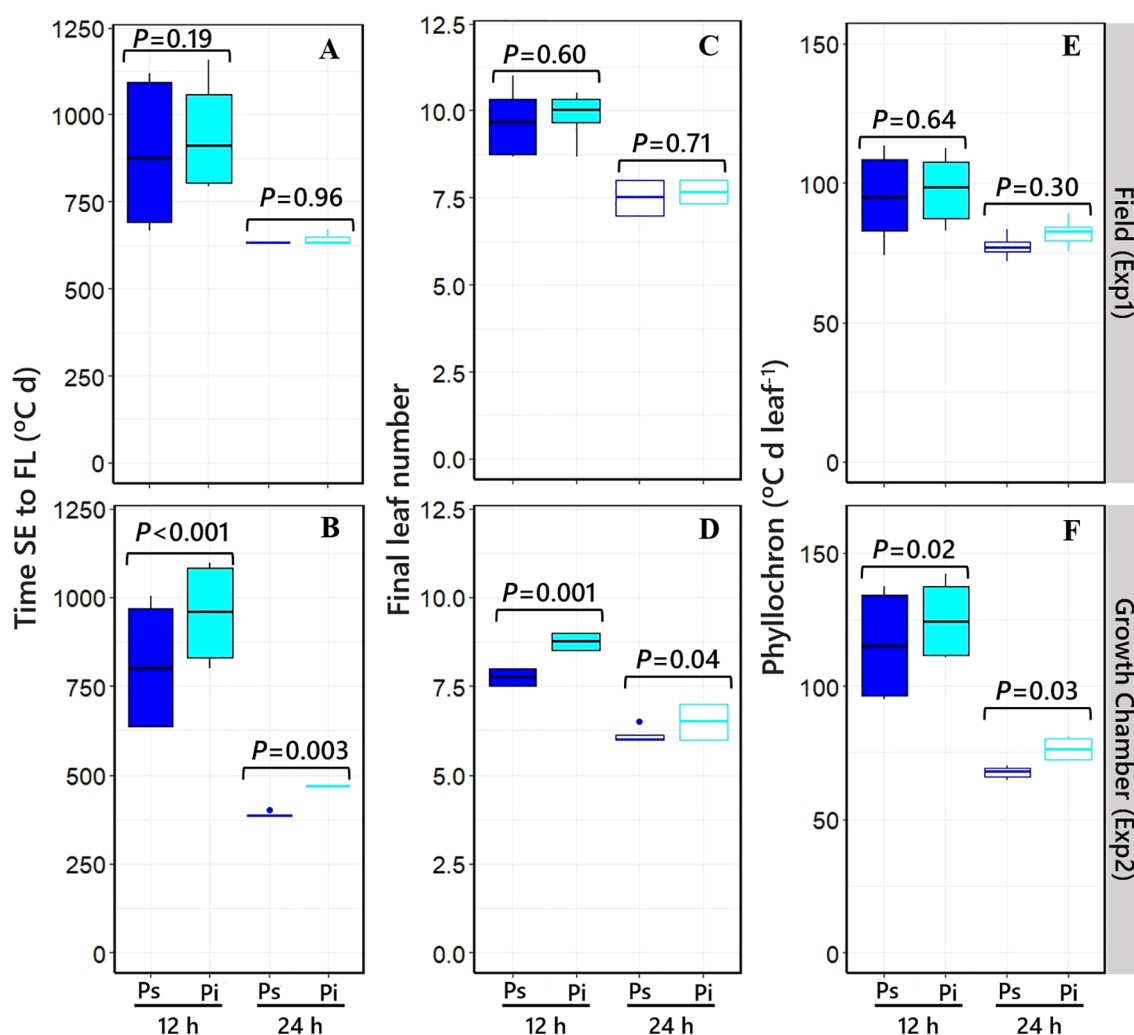


FIGURE 5

Boxplot grouping the NILs with *Ppd-H1*-sensitive (dark blue boxplots) and *ppd-H1*-insensitive (light blue boxplots) alleles across *PHYC* backgrounds for the duration of the phase from seedling emergence to flag leaf [(A, B) in Exp1 and Exp2, respectively], final leaf number [(C, D) in Exp1 and Exp2, respectively], and average phyllochron [(E, F) in Exp1 and Exp2, respectively] under short (closed) and long (open) photoperiods, including the level of significance (p-value) of the difference between NILs with contrasting *PPD-H1* alleles within each photoperiod treatment. In the field experiment, a 12-h photoperiod corresponds to the average of the period from seedling emergence to flowering.

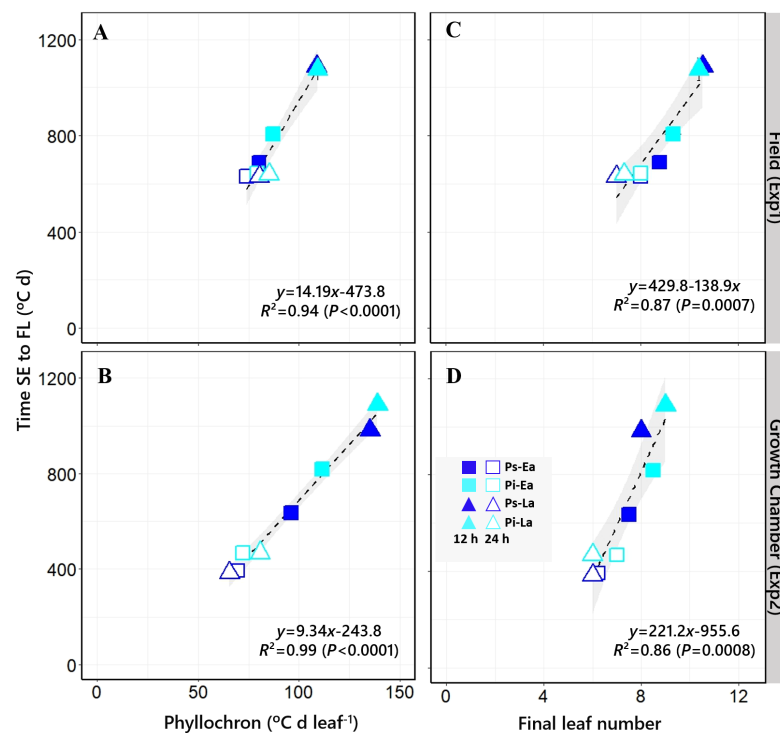


FIGURE 6

Relationship between the duration of the phase from seedling emergence to flag leaf and phylochron [(A, B) in Exp1 and Exp2, respectively] or final leaf number [(C, D) in Exp1 and Exp2, respectively]. Bars on the symbols represent the standard errors of the means (not seen when smaller than the size of the symbol). The equation, coefficient of determination (R^2), and level of significance (p -value) of the linear regression are shown. Open and closed symbols correspond to long and short photoperiods, respectively. Square: *PhyC-e*; triangle: *PhyC-l*. Dark blue symbols: *Ppd-H1*; light blue symbols: *ppd-H1*. In the field experiment, a 12-h photoperiod corresponds to the average of the period from seedling emergence to flowering.

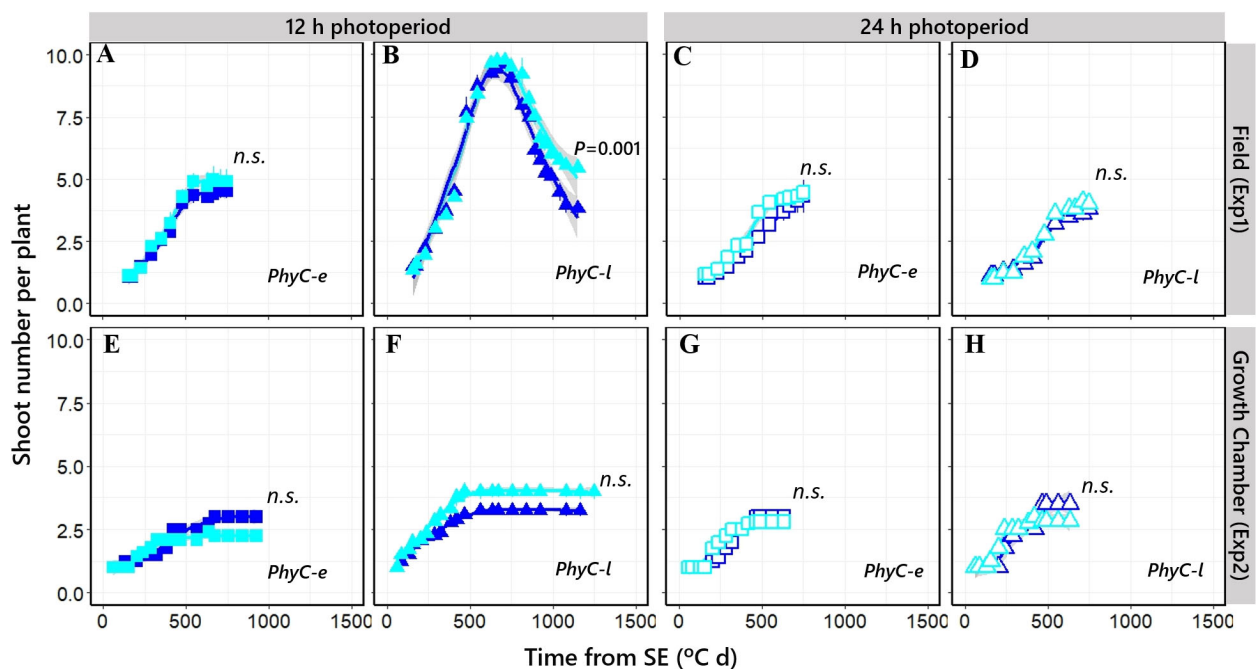


FIGURE 7

Relationship between shoot number per plant and time from seedling emergence in four different NILs grown at short photoperiod [closed symbols; (A, B, E, F)] and long photoperiod [open symbols; (C, D, G, H)] in Exp1 (top) and Exp2 (bottom). Square: *PhyC-e*; triangle: *PhyC-l*. Dark blue symbols: *Ppd-H1*; light blue symbols: *ppd-H1*. Bars on the symbols represent the standard errors of the means (not seen when smaller than the size of the symbol). In the field experiment, a 12-h photoperiod corresponds to the average of the period from seedling emergence to flowering. n.s., not significant.

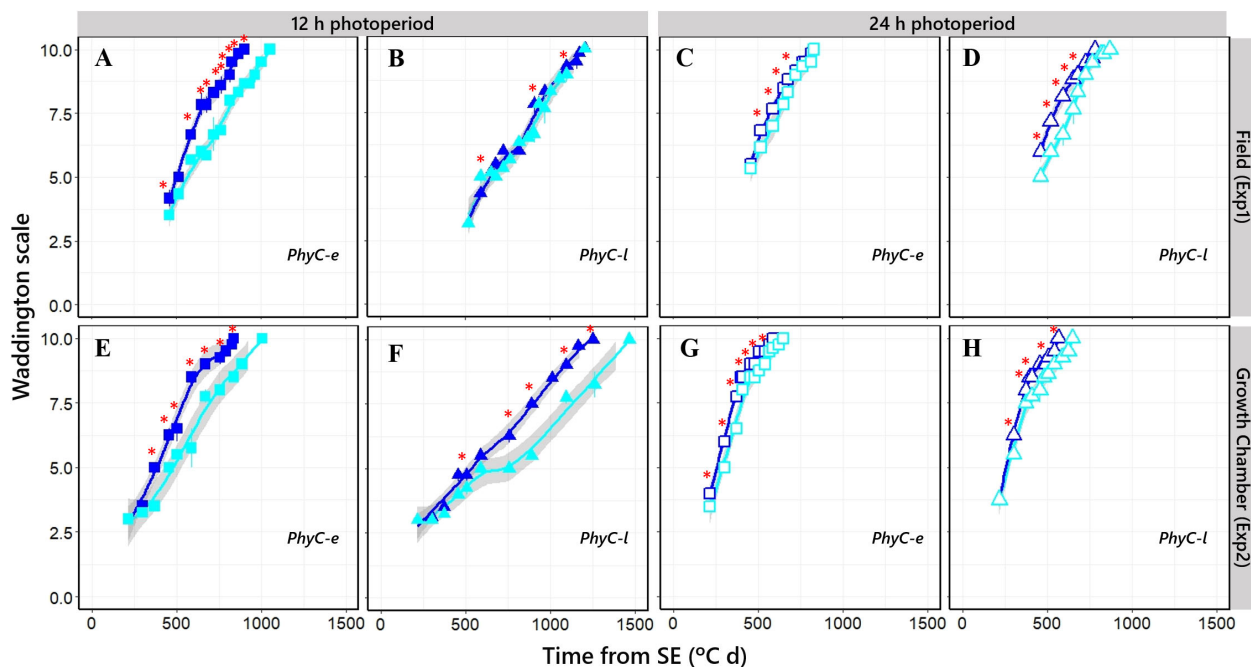


FIGURE 8

Floret development stages, assessed by the Waddington scale, along time from seedling emergence under short [closed symbols; (A, B, E, F)] and long [open symbols; (C, D, G, H)] photoperiod conditions in *Ppd-H1*-sensitive (dark blue symbols) and *ppd-H1*-insensitive (light blue symbols) alleles. Top, Exp1; bottom, Exp2. Values at each timing are means of three (Exp1) or two (Exp2) plants. Significant differences in floret development stage at each particular timing of sampling are indicated by asterisks (* $p < 0.05$).

affected floret development. This is, in turn, commensurate with the deceleration of floret primordia development under shorter photoperiods found in the present study, in line with what had been suggested by Digel et al. (2015).

As *PPD-H1* alleles did not affect the number of tillers and their dynamics (there was just a trend with *PHYC-l* under a short photoperiod), any effect of this gene on yield components will be mainly driven by an effect on spike fertility rather than by the number of spikes per unit land area, at least at the agronomically sound sowing densities used here.

Data availability statement

The raw data supporting the conclusions of this article will be made available by the authors, without undue reservation.

Author contributions

JP: Data curation, Methodology, Formal Analysis, Investigation, Writing – original draft. RS: Data curation, Formal Analysis, Conceptualization, Supervision, Writing – review & editing. GS: Conceptualization, Data curation, Supervision, Writing – review & editing, Funding acquisition, Methodology, Visualization.

Funding

The author(s) declare financial support was received for the research, authorship, and/or publication of this article. Funding was provided by the State Research Agency of Spain (AEI), grant PCI2019-103536.

Acknowledgments

Isogenic lines were developed at Ben Trevaskis' group, Black Mountain Laboratory, CSIRO Canberra, Australia. We thank Ernesto Igartua and Ana Casas for providing the seeds within the framework of the EU-PRIMA project GENDIBAR, in which we were involved. We are grateful to the team in the Crop Physiology Lab of the UdL for assisting during sample processing. JP held a predoctoral contract from the Agency for Management of University and Research Grants of Catalonia (AGAUR) and is a member of the National Institute of Agriculture Technology of Argentina (INTA).

Conflict of interest

The authors declare that the research was conducted in the absence of any commercial or financial relationships that could be construed as a potential conflict of interest.

The authors declared that they were an editorial board member of Frontiers, at the time of submission. This had no impact on the peer review process and the final decision.

Publisher's note

All claims expressed in this article are solely those of the authors and do not necessarily represent those of their affiliated organizations, or those of the publisher, the editors and the

reviewers. Any product that may be evaluated in this article, or claim that may be made by its manufacturer, is not guaranteed or endorsed by the publisher.

Supplementary material

The Supplementary Material for this article can be found online at: <https://www.frontiersin.org/articles/10.3389/fpls.2024.1398698/full#supplementary-material>

References

- Alqudah, A. M., Sharma, R., Pasam, R. K., Graner, A., Kilian, B., and Schnurbusch, T. (2014). Genetic dissection of photoperiod response based on gwas of pre-anthesis phase duration in spring barley. *PLoS One* 9, e1131120. doi: 10.1371/journal.pone.0113120
- Andrés, F., and Coupland, G. (2012). The genetic basis of flowering responses to seasonal cues. *Nat. Rev. Genet.* 13, 627–639. doi: 10.1038/nrg3291
- Appleyard, M., Kirby, E. J. M., and Fellowes, G. (1982). Relationships between the duration of phases in the pre-anthesis life cycle of spring barley. *Aust. J. Agric. Res.* 33, 917–925. doi: 10.1071/AR9820917
- Arenas-Corraliza, M. G., Rolo, V., López-Díaz, M. L., and Moreno, G. (2019). Wheat and barley can increase grain yield in shade through acclimation of physiological and morphological traits in Mediterranean conditions. *Sci. Rep.* 9, 9547. doi: 10.1038/s41598-019-46027-9
- Borràs, G., Romagosa, I., van Eeuwijk, F., and Slafer, G. A. (2009). Genetic variability in duration of pre-heading phases and relationships with leaf appearance and tillering dynamics in a barley population. *Field Crops Res.* 113, 95–104. doi: 10.1016/j.fcr.2009.03.012
- Borràs-Gelónch, G., Denti, M., Thomas, W. T. B., and Romagosa, I. (2012). Genetic control of pre-heading phases in the Steptoe × Morex barley population under different conditions of photoperiod and temperature. *Euphytica* 183, 303–321. doi: 10.1007/s10681-011-0526-7
- Borràs-Gelónch, G., Slafer, G. A., Casas, A. M., van Eeuwijk, F., and Romagosa, I. (2010). Conventional and molecular genetic analysis of factors contributing to variation in a double-haploid barley (*Hordeum vulgare* L.) population. *Field Crops Res.* 119, 36–47. doi: 10.1016/j.fcr.2010.06.013
- Boyd, W. J. R., Li, C. D., Grime, C. R., Cakir, M., Potipibool, S., Kaveeta, L., et al. (2003). Conventional and molecular genetic analysis of factors contributing to variation in the timing of heading among spring barley (*Hordeum vulgare* L.) genotypes grown over a mild winter growing season. *Aust. J. Agric. Res.* 54, 1277–1301. doi: 10.1071/ar03014
- Brooking, I. R., and Jamieson, P. D. (2002). Temperature and photoperiod response of vernalization in near-isogenic lines of wheat. *Field Crops Res.* 79, 21–38. doi: 10.1016/S0378-4290(02)00106-5
- Bustos-Korts, D., Dawson, I. K., Russell, J., Tondelli, A., Guerra, D., Ferrandi, C., et al. (2019). Exome sequences and multi-environment field trials elucidate the genetic basis of adaptation in barley. *Plant J.* 99, 1172–1191. doi: 10.1111/tpj.14414
- Casal, J. J., and Qüesta, J. I. (2018). Light and temperature cues: multitasking receptors and transcriptional integrators. *New Phytol.* 217, 1029–1034. doi: 10.1111/nph.14890
- Chen, Y., Xu, H., He, T., Gao, R., Guo, G., Lu, R., et al. (2021). Comparative analysis of morphology, photosynthetic physiology, and transcriptome between diploid and tetraploid barley derived from microspore culture. *Front. Plant Sci.* 12. doi: 10.3389/fpls.2021.626916
- Delécolle, R., Hay, R. K. M., Guérif, M., Pluchard, P., and Varlet-Grancher, C. (1989). A method of describing the progress of apical development in wheat, based on the time-course of organogenesis. *Field Crops Res.* 21, 147–160. doi: 10.1016/0378-4290(89)90050-6
- Digel, B., Pankin, A., and von Korff, M. (2015). Global transcriptome profiling of developing leaf and shoot apices reveals distinct genetic and environmental control of floral transition and inflorescence development in barley. *Plant Cell* 27, 2318–2334. doi: 10.1105/tpc.15.00203
- Ejaz, M., and von Korff, M. (2017). The genetic control of reproductive development under high ambient temperature. *Plant Physiol.* 173, 294–306. doi: 10.1104/pp.16.01275
- Fernández-Calleja, M., Casas, A. M., and Igartua, E. (2021). Major flowering time genes of barley: allelic diversity, effects, and comparison with wheat. *Theor. Appl. Genet.* 134, 1867–1897. doi: 10.1007/s00122-021-03824-z
- Flood, R. G., and Halloran, G. M. (1986). Genetics and physiology of vernalization response in wheat. *Adv. Agron.* 39, 87–125. doi: 10.1016/S0065-2113(08)60466-6
- González, F. G., Slafer, G. A., and Miralles, D. J. (2002). Vernalization and photoperiod responses in wheat pre-flowering reproductive phases. *Field Crops Res.* 74, 183–195. doi: 10.1016/S0378-4290(01)00210-6
- González, F. G., Slafer, G. A., and Miralles, D. J. (2005). Pre-anthesis development and number of fertile florets in wheat as affected by photoperiod sensitivity genes Ppd-D1 and Ppd-B1. *Euphytica* 146, 253–269. doi: 10.1007/s10681-005-9021-3
- Haun, J. R. (1973). Visual quantification of wheat development. *Agron. J.* 65, 116–119. doi: 10.2134/agronj1973.00021962006500010035x
- He, T., Hill, C. B., Angessa, T. T., Zhang, X. Q., Chen, K., Moody, D., et al. (2019). Gene-set association and epistatic analyses reveal complex gene interaction networks affecting flowering time in a worldwide barley collection. *J. Exp. Bot.* 70, 5603–5616. doi: 10.1093/jxb/erz332
- Hemming, M. N., Peacock, W. J., Dennis, E. S., and Trevaskis, B. (2008). Low-temperature and daylength cues are integrated to regulate FLOWERING LOCUS T in barley. *Plant Physiol.* 147, 355–366. doi: 10.1104/PP.108.116418
- Jamieson, P. D., Brooking, I. R., Semenov, M. A., and Porter, J. R. (1998). Making sense of wheat development: a critique of methodology. *Field Crops Res.* 55, 117–127. doi: 10.1016/S0378-4290(97)00072-5
- Jones, H., Leigh, F. J., Mackay, I., Bower, M. A., Smith, L. M. J., Charles, M. P., et al. (2008). Population-based resequencing reveals that the flowering time adaptation of cultivated barley originated east of the fertile crescent. *Mol. Biol. Evol.* 25, 2211–2219. doi: 10.1093/MOLBEV/MSN167
- Karsai, I., Hayes, P. M., Kling, J., Matus, I. A., Mészáros, K., Láng, L., et al. (2004). Genetic variation in component traits of heading date in *Hordeum vulgare* subsp. *spontaneum* accessions characterized in controlled environments. *Crop Sci.* 44, 1622–1632. doi: 10.2135/CROPSCI2004.1622
- Kernich, G. C., Halloran, G. M., and Flood, R. G. (1997). Variation in duration of pre-anthesis phases of development in barley (*Hordeum vulgare*). *Aust. J. Agric. Res.* 48, 59–66. doi: 10.17700/jai.2015.6.1
- Kirby, E. J. M. (1988). Analysis of leaf, stem and ear growth in wheat from terminal spikelet stage to anthesis. *Field Crops Res.* 18, 127–140. doi: 10.1016/0378-4290(88)90004-4
- Kirby, E. J. M. (1990). Co-ordination of leaf emergence and leaf and spikelet primordium initiation in wheat. *Field Crops Res.* 25, 253–264. doi: 10.1016/0378-4290(90)90008-Y
- Kirby, E., and Appleyard, M. (1984). *Cereal development guide* (Stoneleigh, England: Arable Unit, National Agricultural Centre). Available online at: <http://www.cabdirect.org/abstracts/19840768857.html> (Accessed September 13, 2022).
- Kirby, E. J. M., Spink, J. H., Frost, D. L., Sylvester-Bradley, R., Scott, R. K., Foulkes, M. J., et al. (1999). A study of wheat development in the field: Analysis by phases. *Eur. J. Agron.* 11, 63–82. doi: 10.1016/S1161-0301(99)00022-2
- Kitchen, B. M., and Rasmusson, D. C. (1983). Duration and inheritance of leaf initiation, spike initiation, and spike growth in barley. *Crop Sci.* 23, 939–943. doi: 10.2135/cropsci1983.0011183x002300050030x
- Laurie, D. A., Pratchett, N., Bezant, J. H., and Snape, J. W. (1994). Genetic analysis of a photoperiod response gene on the short arm of chromosome 2(2H) of *Hordeum vulgare* (barley). *Hered.* 1994 726 72, 619–627. doi: 10.1038/hdy.1994.85
- Laurie, D. A., Pratchett, N., Bezant, J. H., and Snape, J. W. (1995). RFLP mapping of five major genes and eight quantitative trait loci controlling flowering time in a winter x spring barley (*Hordeum vulgare* L.) cross. *Genome* 38, 575–585. doi: 10.1139/G95-074
- Miralles, D. J., Abeledo, L. G., Prado, S. A., Chenu, K., Serrago, R. A., and Savin, R. (2021). “Barley,” in *Crop Physiology Case Histories for Major Crops*. Eds. V. O. Sadras and D. F. Calderini (London: Academic Press Elsevier Inc), 164–195. doi: 10.1016/B978-0-12-819194-1.00004-9

- Nishida, H., Ishihara, D., Ishii, M., Kaneko, T., Kawahigashi, H., Akashi, Y., et al. (2013). Phytochrome C is a key factor controlling long-day flowering in barley. *Plant Physiol.* 163, 804–814. doi: 10.1104/pp.113.222570
- Ochagavia, H., Kiss, T., Karsai, I., Casas, A. M., and Igartua, E. (2022). Responses of barley to high ambient temperature are modulated by vernalization. *Front. Plant Sci.* 12. doi: 10.3389/fpls.2021.776982
- Ochagavia, H., Prieto, P., Savin, R., Griffiths, S., and Slafer, G. A. (2018). Earliness per se effects on developmental traits in hexaploid wheat grown under field conditions. *Eur. J. Agron.* 99, 214–223. doi: 10.1016/j.eja.2018.07.007
- Oliver, S. N., Deng, W., Casao, M. C., and Trevaskis, B. (2013). Low temperatures induce rapid changes in chromatin state and transcript levels of the cereal VERNALIZATION1 gene. *J. Exp. Bot.* 64, 2413–2422. doi: 10.1093/jxb/ert095
- Pankin, A., Campoli, C., Dong, X., Kilian, B., Sharma, R., Himmelbach, A., et al. (2014). Mapping-by-sequencing identifies HvPHYTOCHROME C as a candidate gene for the early maturity 5 locus modulating the circadian clock and photoperiodic flowering in barley. *Genetics* 198, 383–396. doi: 10.1534/GENETICS.114.165613
- Parrado, J. D., Savin, R., and Slafer, G. A. (2023). Photoperiod sensitivity of Ppd-H1 and ppd-H1 isogenic lines of a spring barley cultivar: exploring extreme photoperiods. *J. Exp. Bot.* 74, 6608–6618. doi: 10.1093/jxb/erac342
- Ponce-Molina, L. J., Casas, A. M., Gracia, M. P., Silvar, C., Mansour, E., Thomas, W. B. T., et al. (2012). Quantitative trait loci and candidate loci for heading date in a large population of a wide barley cross. *Crop Sci.* 52, 2469–2480. doi: 10.2135/cropsci2012.01.0029
- R Core Team (2020). *R: a language and environment for statistical computing* (Vienna, Austria: R Foundation for Statistical Computing).
- Serrago, R. A., García, G. A., Savin, R., Miralles, D. J., and Slafer, G. A. (2023). Determinants of grain number responding to environmental and genetic factors in two- and six-rowed barley types. *Field Crops Res.* 302, 109073. doi: 10.1016/j.fcr.2023.109073
- Slafer, G. A., Casas, A. M., and Igartua, E. (2023a). Sense in sensitivity: difference in the meaning of photoperiod insensitivity between wheat and barley. *J. Exp. Bot.* 74, 3923–3932. doi: 10.1093/jxb/erac128
- Slafer, G. A., Foulkes, M. J., Reynolds, M., Murchie, E. H., Carmo-Silva, E., Flavell, R. B., et al. (2023b). A 'wiring diagram' for sink strength traits impacting wheat yield potential. *J. Exp. Bot.* 74, 72–90. doi: 10.1093/jxb/erac415
- Slafer, G. A., García, G. A., Serrago, R. A., and Miralles, D. J. (2022). Physiological drivers of responses of grains per m² to environmental and genetic factors in wheat. *Field Crops Res.* 285, 108593. doi: 10.1016/j.fcr.2022.108593
- Slafer, G. A., Kantolic, A. G., Appendino, M. L., Miralles, D. J., and Savin, R. (2009). "Crop development: genetic control, environmental modulation and relevance for genetic improvement of crop yield," in *Crop Physiology: Applications for Genetic Improvement and Agronomy*. Eds. V. O. Sadras and D. F. Calderini (San Diego: Elsevier Inc), 277–308. doi: 10.1016/B978-0-12-374431-9.00012-8
- Slafer, G. A., Kantolic, A. G., Appendino, M. L., Tranquilli, G., Miralles, D. J., and Savin, R. (2015). "Genetic and environmental effects on crop development determining adaptation and yield," in *Crop Physiology: Applications for Genetic Improvement and Agronomy*. Eds. V. O. Sadras and D. F. Calderini (Academic Press), 285–319. doi: 10.1016/B978-0-12-417104-6.00012-1
- Slafer, G. A., and Rawson, H. M. (1994). Sensitivity of wheat phasic development to major environmental factors: A re-examination of some assumptions made by physiologists and modellers. *Aust. J. Plant Physiol.* 21, 393–426. doi: 10.1071/PP9940393
- Slafer, G. A., and Rawson, H. M. (1997). Phyllochron in wheat as affected by photoperiod under two temperature regimes. *Aust. J. Plant Physiol.* 24, 151–158. doi: 10.1071/PP96021
- Slafer, G. A., Savin, R., Pinochet, D., and Calderini, D. F. (2021). "Wheat," in *Crop Physiology Case Histories for Major Crops*. Eds. V. O. Sadras and D. F. Calderini (Academic Press Elsevier), 99–163. doi: 10.1016/B978-0-12-819194-1.00003-7
- Soil Survey Staff (1999). *Soil taxonomy: A basic system of soil classification for making and interpreting soil surveys. 2nd edition* Vol. 436 (Natural Resources Conservation Service. U.S. Department of Agriculture Handbook).
- Sreenivasulu, N., and Schnurbusch, T. (2012). A genetic playground for enhancing grain number in cereals. *Trends Plant Sci.* 17, 91–101. doi: 10.1016/j.tplants.2011.11.003
- Szucs, P., Karsai, I., Von Zitzewitz, J., Mészáros, K., Cooper, L. L. D., Gu, Y. Q., et al. (2006). Positional relationships between photoperiod response QTL and photoreceptor and vernalization genes in barley. *Theor. Appl. Genet.* 112, 1277–1285. doi: 10.1007/s00122-006-0229-y
- Turner, A., Beales, J., Faure, S., Dunford, R. P., and Laurie, D. A. (2005). The pseudo-response regulator Ppd-H1 provides adaptation to photoperiod in barley. *Science*. 310, 1031–1034. doi: 10.1126/science.1117619
- Turner, A. S., Faure, S., Zhang, Y., and Laurie, D. A. (2013). The effect of day-neutral mutations in barley and wheat on the interaction between photoperiod and vernalization. *Theor. Appl. Genet.* 126, 2267–2277. doi: 10.1007/S00122-013-2133-6
- Von Korff, M., Léon, J., and Pillen, K. (2010). Detection of epistatic interactions between exotic alleles introgressed from wild barley (*H. vulgare* ssp. *spontaneum*). *Theor. Appl. Genet.* 121, 1455–1464. doi: 10.1093/OXFORDJOURNALS.AOB.A086434
- Von Korff, M., Wang, H., Léon, J., and Pillen, K. (2006). AB-QTL analysis in spring barley: II. Detection of favourable exotic alleles for agronomic traits introgressed from wild barley (*H. vulgare* ssp. *spontaneum*). *Theor. Appl. Genet.* 112, 1221–1231. doi: 10.1007/s00122-006-0223-4
- Waddington, S. R., Cartwright, P. M., and Wall, P. C. (1983). A quantitative scale of spike initial and pistil development in barley and wheat. *Ann. Bot.* 59, 119–130. doi: 10.1093/oxfordjournals.aob.a086434
- Wang, G., Schmalenbach, L., von Korff, M., Léon, J., Kilian, B., Rode, J., et al. (2010). Association of barley photoperiod and vernalization genes with QTLs for flowering time and agronomic traits in a BC₂DH population and a set of wild barley introgression lines. *Theor. Appl. Genet.* 120, 1559–1574. doi: 10.1007/s00122-010-1276-y
- Whitechurch, E. M., Slafer, G. A., and Miralles, D. J. (2007a). Variability in the duration of stem elongation in wheat and barley genotypes. *J. Agron. Crop Sci.* 193, 138–145. doi: 10.1111/j.1439-037X.2007.00260.x
- Whitechurch, E. M., Slafer, G. A., and Miralles, D. J. (2007b). Variability in the duration of stem elongation in wheat genotypes and sensitivity to photoperiod and vernalization. *J. Agron. Crop Sci.* 193, 131–137. doi: 10.1111/j.1439-037X.2007.00259.x
- Wickham, H. (2016). *ggplot2: elegant graphics for data analysis* (New York, NY, USA: Springer-Verlag).
- Wiegmann, M., Maurer, A., Pham, A., March, T. J., Al-Abdallat, A., Thomas, W. T. B., et al. (2019). Barley yield formation under abiotic stress depends on the interplay between flowering time genes and environmental cues. *Sci. Rep.* 9, 1–16. doi: 10.1038/s41598-019-42673-1
- Zadoks, J. C., Chang, T. T., and Konzak, C. F. (1974). A decimal code for the growth stages of cereals. *Weed Res.* 14, 415–421. doi: 10.1111/J.1365-3180.1974.TB01084.X



OPEN ACCESS

EDITED BY

Yongfeng Guo,
Chinese Academy of Agricultural
Sciences, China

REVIEWED BY

Jiban Shrestha,
Nepal Agricultural Research Council, Nepal
Fabien Chardon,
Université Paris-Saclay, France
Peitao Lü,
Fujian Agriculture and Forestry
University, China

*CORRESPONDENCE

Venkata Rami Reddy Yannam
✉ rami.yannam@irta.cat

RECEIVED 11 March 2024

ACCEPTED 05 August 2024

PUBLISHED 06 September 2024

CITATION

Chibane N, Revilla P, Yannam VRR, Marcet P,
Covelo EF and Ordás B (2024) Impact of
irrigation, nitrogen fertilization, and plant
density on stay-green and its effects on
agronomic traits in maize.
Front. Plant Sci. 15:1399072.
doi: 10.3389/fpls.2024.1399072

COPYRIGHT

© 2024 Chibane, Revilla, Yannam, Marcet,
Covelo and Ordás. This is an open-access
article distributed under the terms of the
[Creative Commons Attribution License \(CC BY\)](#).
The use, distribution or reproduction in other
forums is permitted, provided the original
author(s) and the copyright owner(s) are
credited and that the original publication in
this journal is cited, in accordance with
accepted academic practice. No use,
distribution or reproduction is permitted
which does not comply with these terms.

Impact of irrigation, nitrogen fertilization, and plant density on stay-green and its effects on agronomic traits in maize

Nadia Chibane¹, Pedro Revilla¹, Venkata Rami Reddy Yannam^{2*},
Purificación Marcet³, Emma Fernández Covelo³
and Bernardo Ordás⁴

¹Maize Genetics and Breeding Group, Misión Biológica de Galicia [The Spanish National Research Council (CSIC)], Pontevedra, Spain, ²Sustainable Field Crops Program, Institute for Food and Agricultural Research and Technology (IRTA), Lleida, Spain, ³Area de Edafología y Química Agrícola, Facultad de Ciencias, Universidad de Vigo, Vigo, Spain, ⁴Crop Adaptation and Sustainability Group, Misión Biológica de Galicia [The Spanish National Research Council (CSIC)], Pontevedra, Spain

Introduction: The stay-green (SG) or delayed leaf senescence enables crop plants to maintain their green leaves and photosynthetic capacity for a longer time after flowering. It is considered an important trait in maize breeding, which has contributed to gain in grain yield of modern varieties. It has been also used to improve the tolerance to drought and deficiencies in nitrogen fertilization (NF). However, the objective of this study is to evaluate the influence of water irrigation (WI), NF, and plant density (PD) on SG and the effect of SG on agronomic traits in maize.

Methods: Four SG lines and four non-stay-green (NSG) lines were evaluated in four contrasting environments under two WI, three NF, and two PD levels.

Results and discussion: As expected, the chlorophyll content of leaves at 45 days after flowering (Chl₄₅) was, on average, higher in the SG group of lines. The difference in Chl₄₅ between the SG and NSG genotypes was consistent across WI, NF, and PD and the environments. This is indicative that internal or developmental factors were more important than external signals in controlling the senescence. The effect of SG increasing thousand-kernel weight, stover yield at harvest, or moisture was not influenced by WI, NF, or PD but was altered by the background environment. Our results have implications for the application of SG as a secondary trait for enhancing abiotic stress tolerance. Future studies could consider a wider range of environmental conditions to assess the performance of SG traits under different climatic and soil conditions.

KEYWORDS

maize (*Zea mays* L.), leaf senescence, stay-green, abiotic stress, plant density, nitrogen fertilization, water irrigation

1 Introduction

With global climate change and population growth, there is an increasing need for crop yield improvements to ensure food availability and to meet future agricultural production demands. In response to this critical demand, plant breeding must be accelerated to uncover traits that can increase the yield potential and better adapt to abiotic stress. One such strategy is the selection of stay-green (SG) genotypes, which can help meet anticipated population growth demands, particularly under adverse conditions (Harris, 2007; Luche et al., 2015; Kamal et al., 2019). SG genotypes are characterized by delayed senescence and reduced chlorophyll loss compared to non-stay-green (NSG) genotypes (Kamal et al., 2019; Jiao et al., 2020; Wang et al., 2021). This trait is considered important in agriculture as it allows plants to maintain photosynthetic activity, thereby improving the grain-filling process (Clay et al., 2009; Zhang et al., 2019). Maize is one of the three primary cereal crops, ranking third in cultivation, after rice and wheat. It is a versatile plant that can grow in various soils and climates and serves not only as a staple food but also as a raw material for animal feed and bioenergy production. It exhibits a highly efficient C4 photosynthetic mechanism, which results in substantial biomass production (Chen et al., 2015). Studies indicate that delayed senescence in SG maize hybrids can result in increased dry matter accumulation compared to that in NSG hybrids (Pommel et al., 2006). The usefulness of SG extends beyond its positive influence on post-flowering dry matter accumulation and post-flowering nitrogen (N) uptake (PostN) as it also has the capacity to enhance grain yield (Borrell and Hammer, 2000; Ning et al., 2013; Chibane et al., 2021).

Recent maize hybrids exhibit increased dry matter and nitrogen accumulation during grain filling, whereas nitrogen use efficiency (NUE) is inversely correlated with grain nitrogen concentration (GNC) in high-yielding modern hybrids (Rajcan and Tollenaar, 1999; Zhiipao et al., 2023). Studies have revealed that the accumulation of dry matter in maize kernels depends on nitrogen levels. Nitrogen availability is also crucial for determining the allocation, distribution, and reallocation of dry matter and nitrogen in maize (Liu et al., 2023). It has been found that modern maize hybrids with increased nitrogen uptake and partitioning can achieve equilibrium between nitrogen levels prior to silking (Subedi and Ma, 2005). During the post-silking phase, efficient nitrogen uptake is essential to minimize the requirement for nitrogen remobilization from vegetative to reproductive organs. Strategic nitrogen management contributes to the preservation of green leaf area and extension of dry matter (Rajcan and Tollenaar, 1999; Worku et al., 2007). The duration of canopy photosynthesis can be extended by steady nitrogen uptake during grain filling, leading to an increased final grain yield. Modern hybrids exhibit parallel grain yield and nitrogen efficiency due to increased total dry matter at maturity, particularly greater grain dry weight (Mueller et al., 2019). Nitrogen deficiency in maize typically presents visually as reduced leaf area, diminished chlorophyll in mature leaves, and a decrease in the overall vegetation index. These effects lead to a decrease in the capacity of the plant to absorb light and produce

photoassimilates, ultimately resulting in lower grain yields (Echarte et al., 2008). Evaluation of maize genotype performance under low-nitrogen conditions has demonstrated substantial differences compared to optimal conditions, with only a small percentage of genotypes showing resilience to low-nitrogen levels (Buchaillot et al., 2019). Recent studies have explored how genotypic variation in maize hybrids affects root anatomy under varying levels of nitrogen stress (Yang et al., 2019). The dynamics of post-silking nitrogen fluxes in maize are essential for grain yield because they affect NUE and the number of kernels. In maize, excessive vegetative nitrogen uptake can help maintain grain yield when there is post-silking nitrogen stress by increasing the number of kernels and remobilizing nitrogen to meet grain nitrogen demand. Post-silking nitrogen deficiency affects carbon partitioning, leading to reduced plant growth and lower grain yield compared to nitrogen-sufficient plants (Ning et al., 2017, 2018; Nasielski et al., 2019). An increase in maize yield over time has been associated with breeding for tolerance to higher plant densities (Antonietta et al., 2014). This suggests that modern maize hybrids have been developed to cope with the challenges posed by higher plant densities, potentially influencing the senescence patterns. The relationship between senescence and maize plant density (PD) is important for understanding crop physiology and optimizing yield (Jia et al., 2018). The greater the density of plants, the fewer the resources available per plant. Higher plant densities can accelerate the rate of leaf senescence, leading to reduced post-silking net photosynthesis and assimilation availability (Borrás et al., 2003; Tong et al., 2019). The reason for this is the elevated level of competition between plants, which leads to increased variability. For instance, dominant plants indulge in excessive nutrient consumption and disadvantaged subordinate plants. This suggests that PD influences the timing, rate, and intensity of senescence, affecting the ability of plants to photosynthesize and allocate resources effectively (Shafi et al., 2012; Burken et al., 2013). The interaction between PD and senescence underscores the complex relationship between resource availability, physiological processes, and crop productivity, a connection that has not been extensively described in the existing literature. In addition to the availability of nitrogen and PD, various levels of water stress can influence senescence and end products of maize in different ways. Mild water deficit conditions have been found to accelerate leaf senescence, which is considered an adaptive response in plants experiencing water shortage (Ye et al., 2020). This acceleration of senescence helps to reduce the overall water demand of the plant during periods of limited water availability (Pic et al., 2002). Under severe water stress conditions, such as post-silking drought, the consequences of leaf photosynthesis and senescence can be substantial and have an impact on grain yield (Trachsel et al., 2016a; Ye et al., 2020). A delay in leaf senescence has a positive influence on yield under water stress and nitrogen conditions, thereby emphasizing the complex interplay between environmental stressors and plant physiological responses (Riache et al., 2023). Furthermore, studies have linked plant senescence characteristics, such as green leaf area, with water availability, suggesting a close relationship between water stress and maize senescence. Overall, water deficit stress

during critical growth stages, such as pre-flowering and grain filling, can have a significant impact on maize performance, affecting phenology and yield components owing to altered physiological traits induced by water scarcity (Sah et al., 2020; Wu et al., 2023).

The relationship between SG traits and various physiological and agronomic traits under different stressors has been a topic of interest. SG refers to the ability of crop plants to maintain green leaves and photosynthetic capacity for an extended period, contributing to enhanced drought resistance and performance under low-nitrogen conditions (Thomas and Ougham, 2014; Kamal et al., 2019; Riache et al., 2023). This trait plays a crucial role in delaying foliar senescence, which is essential for sustaining photosynthesis and overall plant productivity (Ramkumar et al., 2019; Munaiz et al., 2020). Studies have demonstrated that the SG phenotype is associated with improved drought tolerance, delayed leaf senescence, and better performance under challenging conditions, such as low nitrogen availability and high PD (Kamal et al., 2019; Munaiz et al., 2020; Riache et al., 2023). In the SG genotypes, there was reduced remobilization of nitrogen from stover to grain, which led to a higher nitrogen content in stover at harvest and a lower content in grain (Zhang et al., 2019). The difference in nitrogen remobilization between the SG and NSG genotypes was less striking than the differences in biomass remobilization. Similarly, other studies have reported higher nitrogen uptake and lower remobilization in SG genotypes after flowering (Thomas et al., 2002; Havé et al., 2017; Zhang et al., 2019). The dynamics of post-silking nitrogen fluxes play a significant role in the NUE and grain yield in maize. It is crucial to understand the balance between nitrogen remobilization from vegetative tissues and post-silking nitrogen uptake to optimize the grain yield under various nitrogen conditions (Ning et al., 2017). Senescence is a complex process involving many biological and genetic influences, in addition to abiotic factors, such as water, nitrogen, and PD, which have been shown to affect various agronomic traits (Sade et al., 2018; Asad et al., 2019). This highlights that the understanding of these interactions between abiotic, nitrogen, and PD stresses for the development of crop improvement strategies remains unclear. The objective of this research is to assess the influence of WI, NF, and PD and environmental background on the progress of senescence and on the effect of SG on agronomic traits of economic interest.

2 Materials and methods

2.1 Plant materials

Eight inbred maize lines were used in this study, including four SG lines (PHW79, PHW52, PHP38, and PHBW8) and four NSG lines (PHBB3, B73, PHT11, and PHM10) (Table 1). These lines were selected from 197 inbred lines evaluated in Misión Biológica de Galicia for senescence-related traits under high water and nitrogen levels (Caicedo, 2018; Chibane et al., 2021). Except for B73, all these lines belong to two heterotic groups that are frequently used as parental breeds (Mikel and Dudley, 2006;

TABLE 1 Stay-green phenotype, heterotic groups, and origin of the eight inbred lines of maize.

Genotypes	Stay-green	Heterotic groups	Origin
PHBW8	SG	Amargo (PHG39)	Pioneer ExPVP
PHW52	SG	Amargo (PHG39)	Pioneer ExPVP
B73	NSG	Stiff stalk	Iowa State University
PHW79	SG	Oh07-Midland (PH595)	Pioneer ExPVP
PHP38	SG	Amargo (PHG39)	Pioneer ExPVP
PHT11	NSG	Amargo (PHG39)	Pioneer ExPVP
PHM10	NSG	Amargo (PHG39)	Pioneer ExPVP
PHBB3	NSG	Amargo (PHG39)	Pioneer ExPVP

White et al., 2020). B73, which belongs to the Stiff Stalk Synthetic (BSSS) heterotic group, a pivotal variety in temperate maize breeding history, has been utilized since the 1970s in developing Stiff Stalk inbreds and initiating its heterotic components across all hybrids maize breeding programs.

2.2 Experimental trial and management practices

The study was conducted in two locations in the Galicia region, Tomeza “TM” (latitude: 42.40°N and longitude: 8.63°W) in Pontevedra province and Xinzo “XZ” (latitude: 42.07°N and longitude: 7.73°W) in Ourense province. The experiments were repeated for two years: 2018 and 2019. The experimental design at each location was a split-plot design with four factors: water irrigation (WI), nitrogen fertilization (NF), planting density (PD), and genotypes (G). WI was assigned to main plots that were organized as a completed block design with two replications. NF was nested to WI, PD to NF, and G to PD. WI had two levels: high water level (HW) and low water level (LW). It was irrigated weekly in HW at 25 L/m and with half the amount of water every 15 days in LW at 12.5 L/m. NF had three levels (N1: without NF; N2: NF at 30 kg/ha; and N3: NF at 90 kg/ha). NF was applied two times, prior to sowing with half amount and at V6 stage the last part. N was applied as ammonium nitrate (27%). PD had two levels (a high density of 80,000 plants per ha and a low density of 50,000 plants per ha). Each experimental plot consisted of two rows, each row with 13 double-kernel hills planted manually, each block being 26.6 m × 3.25 m, spacing between rows was 0.8 m and between consecutive hills 0.16 m or 0.25 m for final density of 80,000 and 50,000 plants per ha, respectively. The trials were carried out using standard practices to control weeds and pests at the site [herbicides (pendimethalin 33% and sulcotrione 30%) and insecticides (lambda-cihalotrin 10%)]. Standard fertilization with phosphorus (P₂O₅ of 18%, 333 kg/ha) and potassium (potassium sulfate (K₂O) of 50%, 240 kg/ha) was applied prior to sowing.

2.3 Environmental and soil variables

A previous analysis of the nitrogen content in the soil for the first-year trial was performed before sowing. Soil samples from the 0-cm to 30-cm soil layer for each location were collected before planting and analyzed in the laboratory of the University of Vigo. The contents of various nutrients, such as the nitrogen fractions NO_3^- , NH_4^+ , and N, were measured following the method of (Houbá et al., 2000) (Supplementary Table 1). During the growing seasons of 2018 and 2019 in two locations, meteorological data were downloaded from a regional meteorological service (<http://meteogalicia.es>), to determine the following variables: average monthly minimum, maximum, and average temperature (T_{\min} , T_{\max} , and T_{avg} , in $^{\circ}\text{C}$) and precipitation (in L/m) (Supplementary Figure 1).

2.4 Physiological and phenological data

Chlorophyll content and quantum efficiency of PSII (FvFm) were measured with a portable SPAD recorder (CCM-200, Opti-Sciences, Tyngsboro, MA, USA) and a portable fluorometer (OS-30p, Opti-Sciences, Tyngsboro, MA, USA). Chlorophyll content and FvFm were measured 45 days after flowering (DAF) in the leaves of the principal ear of five plants per plot. Leaves of the principal ear were dark-adapted for 20 min with tweezers collocated in the leaf before measurements of FvFm. Days to silking (SD) and days to anthesis (AD) were recorded as the number of days from planting to the date when 50% of the plants had emerged silks and shed pollen, respectively. Then, we estimated the anthesis silking interval (ASI) as the difference between SD and AD. We considered that a plot had reached physiological maturity when at least five ears had a black layer on the seed basis and calculated the number of days from flowering to the physiological maturity of each plot (DPM).

2.5 Agronomic variables

The harvest was done after physiological maturity and dry down of the grain at the end of the cultivation season. Stover (leaves and stems) moisture was calculated as the difference between the fresh and dry weights of five random plants in each plot at flowering (SMF) and harvest (SMH). Similarly, kernel moisture [KM (%)] and cob moisture [CM (%)] were calculated as the difference between fresh and dried grains using five random ears of each plot at harvest. Ten plants were collected randomly from each plot at harvest to estimated thousand kernel weight [TKW (g)], cob yield [CY (kg/ha)], and stover yield at harvest SYH (kg/ha). Similarly, stover yield was taken at flowering SYF (kg/ha) sampling 10 plants per plot. All weights and yields were corrected by their respective moistures and were given at 0% of moisture.

2.6 Nitrogen content

Total nitrogen content [TN_HSoil (g/kg)] and nitrogen assimilable by plants [NO_3^- -HSoil (mg/kg) and NH_4^+ -HSoil (mg/

kg)] were calculated in soil samples taken from plots of six genotypes (three SG and three NSG) in the first year of the experiment at both locations at harvest. Total nitrogen and nitrogen assimilable by plants in soil were analyzed using elemental analysis (Flash EAI112 series) (Krotz and Giazzi, 2000). In the plots in which soil samples were taken, five random plants were collected at flowering and harvest, and the total nitrogen concentration was measured in the plant stover at flowering SNF (g/kg) and harvest SNH (g/kg) and in the kernels KN (g/kg) using elemental analysis (Flash EAI112 series).

2.7 Statistical analyses

Individual and combined analyses of variance (ANOVA) was performed for both years and locations using the mixed-model procedure (MIXED procedure) of the SAS statistical package (<https://odamid-euw1.oda.sas.com/SASStudio>). WI, NF, PD, and SG were considered fixed effects, and environment and blocks (environment) were considered random effects. Each environment was represented by one location in a year. Interaction terms only involving fixed effects were considered fixed, and interactions terms with at least one factor random were considered random. After doing the analyses, we found that the interactions were mostly not significant, and we repeated the analyses without including the interactions in the model. The Wald test was used to test if the variances were significantly different from zero (Covtest option of mixed procedure of SAS). Comparisons between means were made using Fisher's protected least significant difference (MDS) test at 5% probability. Combined and individual correlation analyses were performed using R Studio (R Core Team, 2013) with the sjPlot package (Lüdtke, 2021). The correlations between variables were assessed using Pearson's correlation coefficients with their significance.

3 Results

3.1 Correlation between SG phenotype and agronomic traits

The main objective of this research was to analyze the relationship of senescence or SG with agronomic traits and abiotic factors, specifically, WI, N fertilization, and PD. In our environmental conditions, the differences between SG and NSG genotypes are usually highest at 45 DAF (Chibane et al., 2021). For that reason, we used Chlor45 and FvFm45 to analyze the relationship of senescence with agronomic traits and genetic and abiotic factors. In addition to those variables related to leaf senescence, we measured variables related to phenology (flowering and grain filling) and variables related to yield and moisture of grain, stover, and cob. Regarding grain yield, we measured the yield component (TKW) that is more directly related to senescence (Chibane et al., 2021). The simple correlation between traits estimated from all plots of the experiment has shown that Chlor45 has moderate positive relationship ($0.4 < r < 0.5$, significant) with the weight of the kernels and the yield of stover (at harvest) and cobs (Figure 1).

The correlation between Chlor45 and SMH was slightly lower ($r = 0.26$) and significant. However, there was not relationship between Chlor45 and the moisture of kernels and cobs (0.07 and -0.02 , respectively, not significant). The correlations of FvFm45 with agronomic traits were similar to Chlor45, although the magnitude of the correlations was mostly lower. The relationships of other phenological traits with agronomic traits were different from those found with Chlor45 (Figure 1). Thus, SD had high or very high positive relationships with moisture related traits (0.87 for KM and 0.85 for CM, significant) but moderate negative with yield related traits. DPM had also positive relationship with moisture related traits but not of high magnitude and did not have correlations with yield related traits (Figure 1). The only physiological traits that had positive correlations with TKW and CY were Chlor45 and FvFm45. The correlation between Chlor45 and TKW within each level of water, N, and PD was similar to the combined value ($0.4 < r < 0.5$, significant), that is, the correlation between the two traits was not affected by those factors (Figure 2). If we considered the correlations between the two traits within environments, then we found similar values to the combined value in three of the environments, but, in Tomeza 2019, the correlation was slightly lower (Figure 2).

3.2 Comparison of SG vs. NG lines: main effects

The analysis of correlations suggests two main results: the phenological trait with highest effect on kernel weight is

senescence or SG, and this effect is independent of WI, N fertilization, and density. However, the specific conditions of the environments across the season could have an impact on the relationship of SG and kernel weight. To further investigate the effect of SG on agronomic traits and how the environment and WI, N fertilization, and density influence SG and alter the effect of SG on agronomic traits, we compare a group of four SG genotypes and a group of four NSG genotypes evaluated in four environments under different levels of the abiotic factors using an ANOVA model. The interactions between abiotic factors, SG, and environment were mostly not significant (data not shown). The reduced model without interactions has shown that the differences between the SG and NSG groups (SG factor) were significant ($\alpha \leq 0.05$) for several phenological and agronomic traits (Table 2). The SG group had higher values of DPM, Chlor45, FvFm45, and higher yield and moisture of stover at harvest, cobs, and kernels (SYH, CY, TKW, SMH, CM, and KM) (Supplementary Tables 2–4).

3.2.1 Stover yield

Not only SG but also WI, N fertilization, and PD had significant effects on SYH (Table 2). The magnitude of the effect due to WI was almost twice than SG (Supplementary Table 3). High PD, which means fewer resources, reduced the SYH measured on a plant basis, but not when measured per hectare, because a higher number of plants compensated for less production per plant (Supplementary Table 3). The stover yield at flowering (SYF) averaged over all plots of the experiment was reduced at harvest (SYH). This is indicative

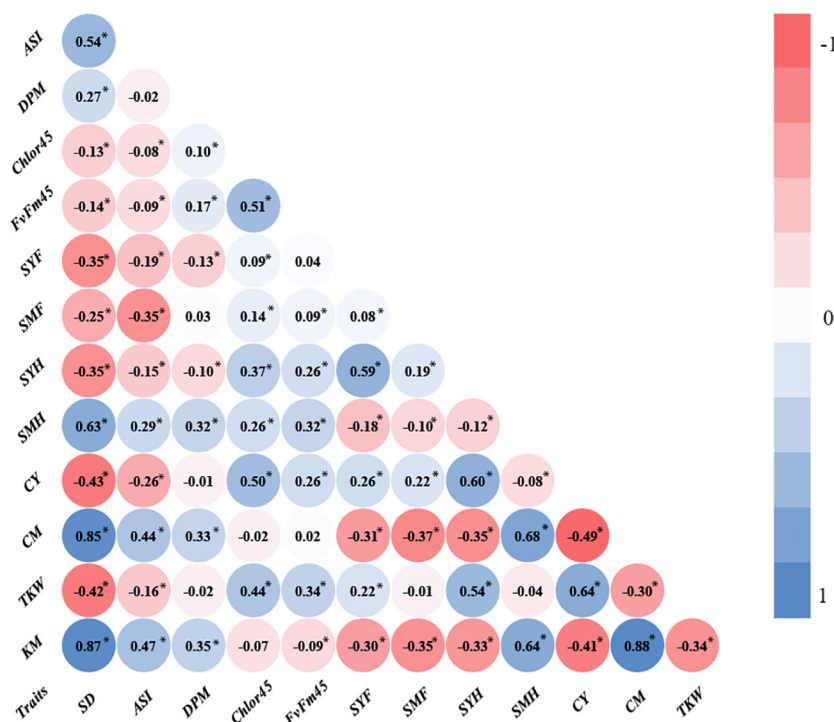
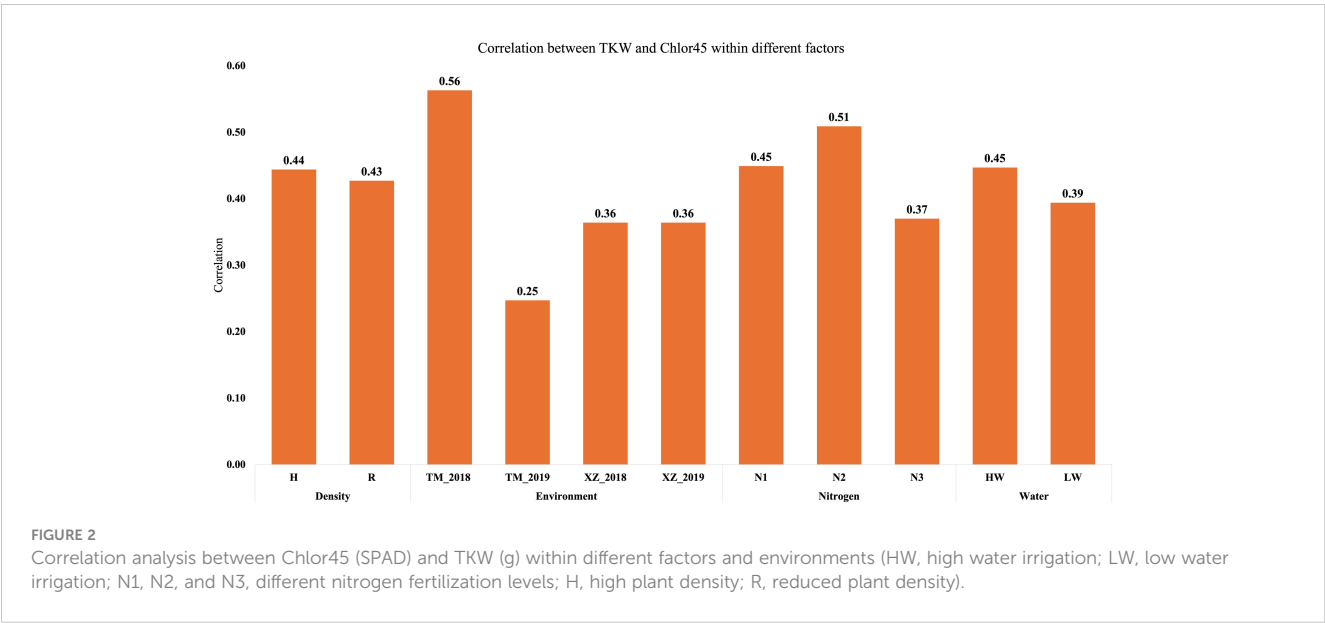


FIGURE 1

Pearson correlation coefficients between traits estimated from all plots of the experiment. SD, days to silking (days); ASI, anthesis silking interval (days); DPM, days to physiological maturity (days); Chlor45, chlorophyll at 45 days after silking; FvFm45, quantum efficiency at 45 days after silking ($\mu\text{mol m}^{-2} \text{s}^{-1}$); SYF, stover yield at flowering (kg/ha); SMF, stover moisture at flowering (%); SYH, stover yield at harvest (kg/ha); SMH, stover moisture at harvest (%); CY, cob yield (kg/ha); CM, cob moisture (%); TKW, thousand kernel weight (g); KM, kernel moisture (%). *, significant at $P \leq 0.05$.



of the translocation of organic matter from the leaves and stems to the kernels during grain filling. Higher WI, higher N fertilization, and lower PD (measured on plant basis) incremented the stover yield at flowering (Supplementary Table 3). The differences were significant or close to significant levels. This suggests that the effects of those factors on stover yield started before flowering. The differences in remobilization from stover to grain ($SYF/SYH \times 100$) among the levels of these factors were low. Therefore, the differences on stover yield at harvest due to those factors were probably generated mostly by differences in the availability of resources for the plant that started before flowering, rather than to differences in remobilization. In contrast, the NSG lines even had more stover at flowering than the SG lines (Supplementary Table 3), but they had 12% more remobilization. Therefore, at difference of

the abiotic factors, the difference in SYH between SG and NSG was mostly due to the differences in remobilization.

3.2.2 Kernel weight and moisture

At difference of SYH, the effect of SG on TKW was higher than the abiotic factors. The only abiotic factor with significant effect on this trait was WI, but the magnitude of the effect of SG on TKW was about twice of the WI (39.3g vs. 14.5g) (Figure 3). The advantage of SG on TKW comes to the cost of a higher KM: SG was the only factor in which significant differences were detected for this variable (Table 2; Figure 3). The SG influenced also more than the other factors the moisture of the stover at harvest and increased the moisture of the cob, although in this case the magnitude was similar to other factors (Supplementary Tables 3, 4). The increment of

TABLE 2 Test of fixed effects for the mixed-model ANOVA combined over environments.

Trait	Effect	WI	NF	PD	SGT	ENV
SD	F-value	0.34	3.66	10.01	1.00	122.08
	Pr > F	0.57	0.03	0.00	0.32	<0.0001
ASI	F-value	2.19	3.20	7.09	1.35	14.07
	Pr > F	0.17	0.05	0.01	0.25	0.00
DPM	F-value	2.39	0.85	0.27	33.77	14.69
	Pr>F	0.15	0.43	0.60	<0.0001	0.00
Chlor45	F-value	8.87	15.01	2.52	95.89	9.67
	Pr > F	0.01	<0.0001	0.12	<0.0001	0.00
FvFm45	F-value	3.49	0.67	0.08	11.55	2.93
	Pr > F	0.09	0.51	0.78	0.00	0.08
SYF	F-value	0.58	0.65	156.01	11.67	9.03
	Pr > F	0.47	0.52	<0.0001	0.00	0.03

(Continued)

TABLE 2 Continued

Trait	Effect	WI	NF	PD	SGT	ENV
SMF	F-value	12.20	11.13	2.10	104.86	30.81
	Pr > F	0.01	<0.0001	0.15	<0.0001	<0.0001
SYH	F-value	13.59	3.83	153.40	9.74	27.88
	Pr > F	0.01	0.03	<0.0001	0.00	0.00
SMH	F-value	0.71	0.40	0.17	31.93	37.73
	Pr>F	0.42	0.67	0.81	<0.0001	<0.0001
TKW	F-value	12.54	2.24	4.67	215.99	69.18
	Pr > F	0.00	0.11	0.03	<0.0001	<0.0001
KM	F-value	0.50	0.48	0.61	12.28	7.26
	Pr > F	0.50	0.62	0.43	0.00	<0.0001
KN	F-value	3.08	0.03	0.39	8.36	15.71
	Pr > F	0.12	0.97	0.54	0.00	0.01
CY	F-value	14.31	3.89	121.68	136.81	54.93
	Pr > F	0.00	0.03	<0.0001	<0.0001	<0.0001
CM	F-value	0.00	3.73	5.96	13.16	97.66
	Pr > F	0.97	0.02	0.01	0.00	<0.0001
SNH	F-value	1.44	8.91	0.33	15.45	4.93
	Pr > F	0.26	0.00	0.57	<0.0001	0.02
SNF	F-value	0.32	20.56	2.54	0.04	5.21
	Pr > F	0.59	<0.0001	0.12	0.84	0.01
SNH	F-value	1.39	9.05	0.48	16.09	4.95
	Pr > F	0.26	0.00	0.49	<0.0001	0.02
TN_Hsoil	F-value	0.09	0.56	0.00	2.46	0.02
	Pr > F	0.76	0.57	0.98	0.11	0.89
NO ₃ _Hsoil	F-value	2.41	2.41	0.04	0.00	6.42
	Pr > F	0.18	0.11	0.84	0.97	0.05
NH ₄ _Hsoil	F-value	0.85	0.99	0.01	0.64	0.05
	Pr >F	0.36	0.38	0.91	0.42	0.85

WI, water condition; NL, nitrogen level; PD, plant density; SGT, stay-green trait; ENV, environment; DS, days to silking; ASI, anthesis silking interval; DPM, days to physiological maturity. Chlor45 (SPAD), chlorophyll at 45 days after silking; FvFm45 ($\mu\text{mol m}^{-2} \text{s}^{-1}$), quantum efficiency at 45 days after silking; SYF(kg/ha), stover yield at flowering (kg/ha); SMF, stover moisture at flowering (%); SYH (kg/ha), stover yield at harvest time (kg/ha); SMH, stover moisture at harvest (%); TKW (g), thousand kernel weight; KM (%), kernel moisture; KN (g kg^{-1}), N-kernel content at harvest time; CY, cob yield (kg/ha); CM, cob moisture (%); SNH, stover N at harvest (g kg^{-1}); SNF, stover N content at flowering time (g kg^{-1}); SNH, stover N at harvest (g kg^{-1}); TN_Hsoil (g kg^{-1}), total N content in soil at harvest time; NO₃_Hsoil (mg kg^{-1}), soil content of NO₃ at harvest time; NH₄_Hsoil (mg kg^{-1}), soil content of NH₄ at harvest time.

kernel weight and moisture in SG genotypes can be partially due to the increment in days from flowering to physiological maturity as DPM was affected by SG more than by other factors (Supplementary Table 2).

3.3 Interaction of SG with abiotic factors and environments

In agreement with the lack of significance between SG and environmental and abiotic factors in the full model ANOVA (data

not shown), the SG group had higher Chlor45 and TKW than the NSG group across specific abiotic factors and across environments (Figures 3, 4). The magnitude of the difference between SG and NSG for Chlor45 and TKW was similar for the different levels of WI, N fertilization, and density within each environment, but the magnitude varied between environments. There were significant differences between environments for most of the traits (Table 2). In Tomeza, the minimum temperatures were higher than in Xinzo along the crop season (Supplementary Figure 1). The lower temperatures that imply lower growing degrees days contributed to later DS and also to shorter DPM, lower SYF and TKW, and

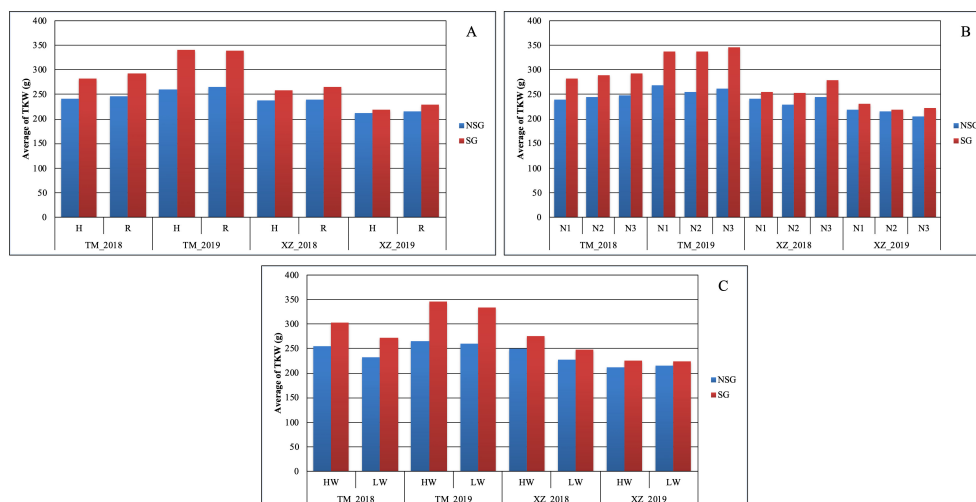


FIGURE 3

Average of thousand kernel weight TKW (g) within each abiotic stress of (A) plant density, (B) nitrogen fertilization, and (C) water irrigation for SG and NSG genotypes (HW, high water irrigation; LW, low water irrigation; N1, N2, and N3, different nitrogen fertilization levels; H, high plant density; R, reduced plant density).

higher KM in Xinzo compared to Tomeza (Table 3). The differences in production between locations were more pronounced in 2019, which had the best (Tomeza 2019) and worst (Xinzo 2019) environment of the experiment. In Tomeza 2019, the average chlorophyll content was still high at 45 days (Chlor45 = 27), indicating a low progress of senescence and a longer period of active photosynthesis compared to Xinzo 2019 (Chlor45 = 18). The difference between SG and NSG on Chlor45 and particularly TKW tended to be higher as the environment was more productive. In other traits related to biomass production (SYH and CY), the SG

lines were consistent across factors and environments, superior to NSG lines (Supplementary Figures 2, 4). For these traits, the magnitude of the difference between SG and NSG tended to be also higher in the more productive environments, particularly Tomeza 2019. The SG lines tended to have higher KM than NSG lines; however, the magnitude of the difference and the consistency across levels of abiotic factors and environments were lower than for yield related traits (Figure 5). Even in Xinzo 2018, the difference between SG and NSG lines for KM had the opposite sign to that in the other environments. The magnitude and consistency across

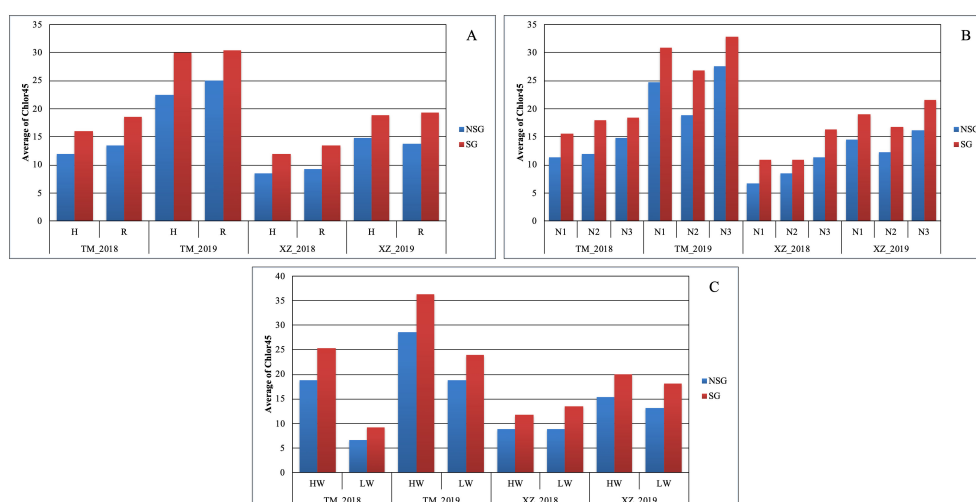


FIGURE 4

Average of chlorophyll content at 45 days after silking (Chlor45) within each abiotic stress of (A) plant density, (B) nitrogen fertilization, and (C) water irrigation for SG and NSG genotypes (HW, high water irrigation; LW, low water irrigation; N1, N2, and N3, different nitrogen fertilization levels; H, high plant density; R, reduced plant density).

TABLE 3 Mean and standard deviation of traits across different environments.

Env	DS Mean \pm SD	DPM Mean \pm SD	SYF Mean \pm SD	TKW Mean \pm SD	KM Mean \pm SD
TM_2018	76.69 \pm 1.24	76.19 \pm 2.47	8,209.68 \pm 2,446.14	265.81 \pm 28.18	18.8 \pm 1.42
TM_2019	81.49 \pm 0.94	75.74 \pm 3.94	8,542.91 \pm 1,654.41	301.22 \pm 40.96	27.23 \pm 1.97
XZ_2018	88.48 \pm 2.07	80.04 \pm 2.68	6,541.52 \pm 1,746.5	250.46 \pm 24.08	38.54 \pm 4.81
XZ_2019	96.4 \pm 1.76	84.2 \pm 2.34	5,788.09 \pm 1,333.6	219.08 \pm 11.84	42.26 \pm 2.41

ENV, environments; SD, standard deviations; DS, days to silking (days); DPM, days to physiological maturity; SYF (kg/ha), stover yield at flowering (kg/ha); TKW (g), thousand kernel weight; KM (%), kernel moisture.

factors and environments of the difference of SG and NSG lines for other moisture related traits (SMH and CM) were similar to those of KM (Supplementary Figures 3, 5).

3.4 Nitrogen assimilation and remobilization

At flowering, the only factor that affected the nitrogen concentration in plants was NF with the highest level of N fertilization having significantly more N concentration in plants than the other two levels (Table 2; Supplementary Table 4). At harvest, the N fertilization also influenced the N concentration in the stover but not in the kernels. The SG lines had higher amount of no remobilized N that remained in the stover at harvest. The concentration of N in the kernels was lower in the SG genotypes, but, taking into account the larger weight of the kernels, the total content of N in the kernels was not reduced compared to that in NSG genotypes. The effect of WI was different to N fertilization as there were not significant differences between levels of irrigation on the concentration of N on stover and grain at harvest. According to the ANOVA analyses, for plant N concentration–related traits, most of the interactions between factors were not significant (data

not shown). However, the differences between SG and NSG were not consistent across levels of factors and environments (Figures 6, 7). The reduced ANOVA did not detect significant differences between SG and between levels of abiotic factor for the concentration of N in the soil (Table 2).

4 Discussion

4.1 Senescence or stay-green: main effects

Considering the general average effect across environments and abiotic factors, the SG genotypes had higher biomass yield at harvest in agreement with different studies (Borrell et al., 2001; Pommel et al., 2006; Christopher et al., 2014). In all levels of factors, there were reduction of biomass from flowering to harvest, indicative of the remobilization of biomass and nutrients from the vegetative parts (leaves and stalks) to the grains (Supplementary Table 3) (He et al., 2004; Ning et al., 2013). Given that the SG genotypes did not produce higher stover yield at flowering, we inferred that the higher stover yield at harvest of the SG genotypes compared to that of NSG genotypes was mainly due to less remobilization of the biomass generated before flowering. The

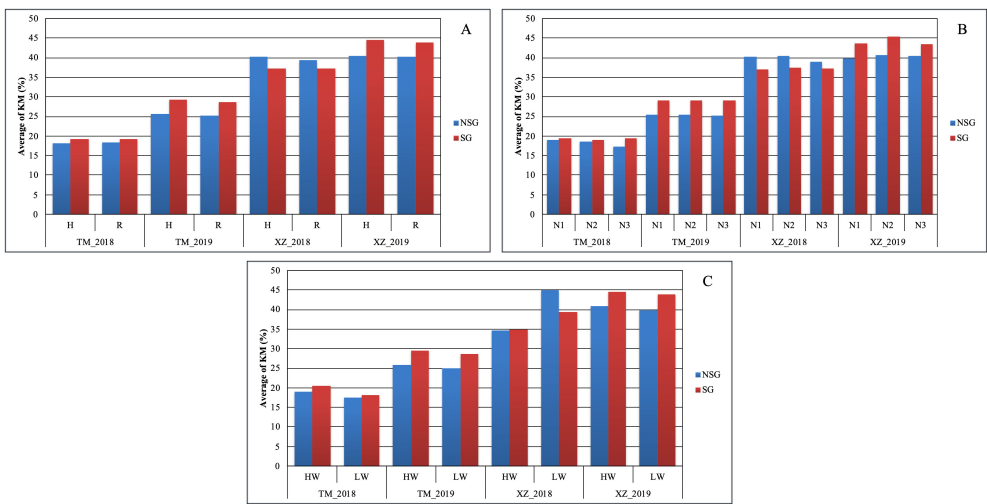


FIGURE 5 Average of kernel moisture (KM %) within each abiotic stresses of (A) plant density, (B) nitrogen fertilization, and (C) water irrigation for SG and NSG genotypes (HW, high water irrigation; LW, low water irrigation; N1, N2, and N3, different nitrogen fertilization levels; H, high plant density; R, reduced plant density).

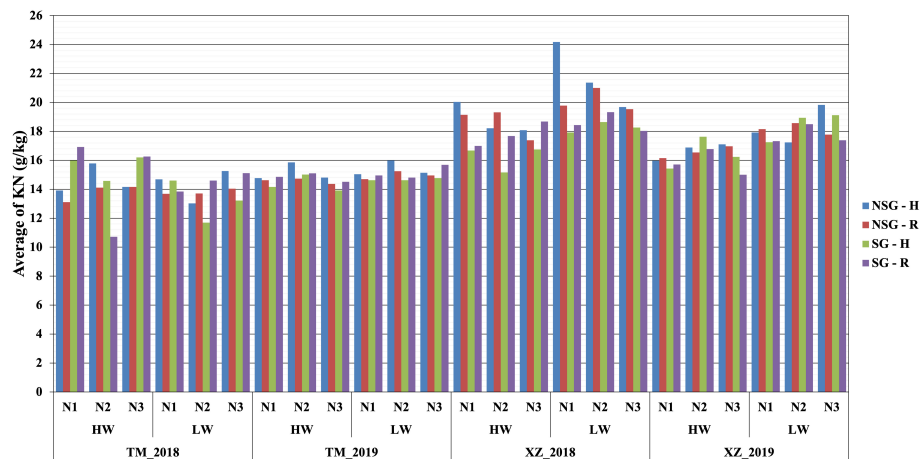


FIGURE 6

Average nitrogen kernel content KN (g/kg) within combined abiotic stresses of water, nitrogen, and high plant density for SG and NSG genotypes (HW, high water irrigation; LW, low water irrigation; N1, N2, and N3, different nitrogen fertilization levels; H, high plant density; R, reduced plant density).

difference in remobilization between SG and NSG (12%) was twice or higher than the differences between the levels of the other factors in this study (Supplementary Table 3). SG genotypes had also, on average, more kernel weight across factors and environments (Figure 3) accordingly to studies of Silva et al. (2003) and Chibane et al. (2021). A comparison of old and new hybrids has shown that SG has contributed to genetic gain in grain yield over the last decades (Pommel et al., 2006; Antonietta et al., 2014), and it is considered an important trait in maize breeding (Gregersen et al., 2008; Gnädinger, 2018; Chibane et al., 2021). Despite the lower remobilization, the weight of the kernels was higher, indicating more post-flowering generation of assimilates and nutrient uptake favored by the elongation of the period with active photosynthesis in leaves and the period of filling in the grain. Other authors have also found higher post flowering uptake and lower remobilization in

SG genotypes (Rajcan and Tollenaar, 1999; Kosgey et al., 2013; Acciaresi et al., 2014; Chibane et al., 2021), which was named “dilemma of senescence” (Bänziger et al., 2000; Wang et al., 2016). Consistently with the biomass remobilization, in the SG genotypes, there was less remobilization of N from stover to grain (Supplementary Table 4), which caused more N content in stover at harvest. This effect is more evident if we consider the absolute value of N content (N per ha) instead of g per Kg because the SG genotypes had higher stover yield at harvest (Supplementary Table 4). The SG genotypes had less N content in grain in percentage or g per kg of the grain (Supplementary Table 4), but, if we adjust for the higher TKW of the SG genotypes, assuming that SG and NG genotypes have the same number of kernels, we found that the absolute N content in grain was also higher in SG genotypes. This is indicative of more N uptake after flowering in

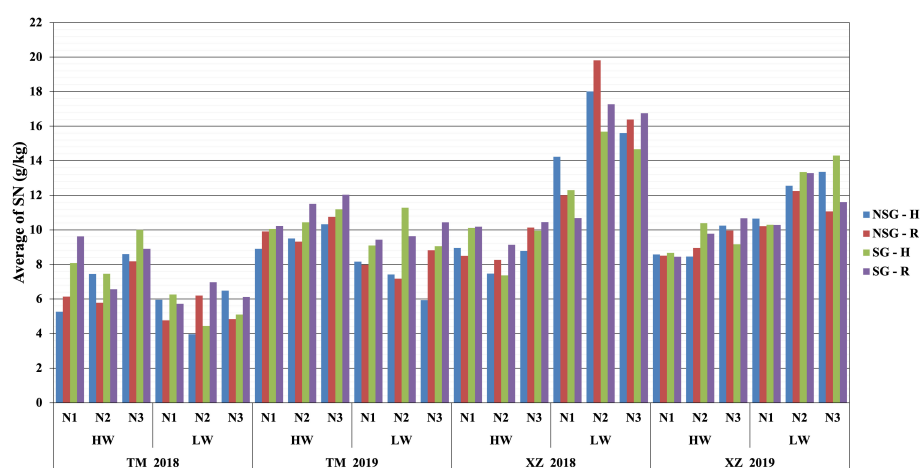


FIGURE 7

Average of nitrogen stover at harvest SNH (g/kg) within combined abiotic stresses of water, nitrogen, and high plant density for SG and NSG genotypes (HW, high water irrigation; LW, low water irrigation; N1, N2, and N3, different nitrogen fertilization levels; H, high plant density; R, reduced plant density).

SG genotypes (Subedi and Ma, 2005). The average favorable effect of SG on yield of stover, cob, and yield was accompanied by an increment in the moisture (Figures 3, 5; Supplementary Tables 3, 4). The trade-off between grain yield and moisture associated with senescence (similar to flowering time) is sometimes neglected: a higher grain yield could not be of value if it was accompanied by excessive moisture. In fact, it is not rational to consider that SG is better than NSG or vice versa but to consider the timing and rate of senescence as relevant traits for adaptation that should be optimized for the specific environment in which the genotypes are going to grow (Munaiz et al., 2020). For the study of senescence to be useful in breeding, it is necessary to integrate it with genotypic and environmental factors, as well as other characteristics that determine the final performance in the target environment. Trachsel et al. (2016b) proposed that reducing flowering time and lengthening senescence, which maintains the duration of the crop, does not increase humidity and increases early vigor to produce greater vegetative biomass that compensates for the shorter time until flowering.

4.2 Senescence or stay-green: interactions with environmental factors

We found large difference between environments, for example, for TKW or KM, indicating that the environments were quite contrasting (Figures 3, 5). The lower levels of the abiotic factors consistently caused ASI lengthening, which is indicative of stressful conditions for the maize plants (Bänziger et al., 2000) (Supplementary Table 2), and appreciable differences among levels of factors were achieved in this experiment. In spite of those differences, the difference in Chlor45 between the SG and NSG genotypes were consistent across environments and levels of abiotic factors (Figure 4). This trait serves to compare the progress of senescence and our data support the notion that the progress of senescence, including timing and progress, is controlled mainly by internal factors in maize, for example, hormone accumulation, which is relatively independent of external signals (Borrás et al., 2003), also found that the progress of senescence is highly conservative and concluded that it is genetically controlled. Differences in senescence had an effect on traits of agronomic relevance, particularly TKW. An interesting question is how extrinsic factors, such as environmental conditions or other biotic factors modify the effects of the differences of senescence on agronomics traits. The abiotic factors that did not alter the progress of senescence did not alter the effect of senescence on traits like TKW or KM (Figures 3, 5). However, the background environment altered the effect of senescence on agronomic traits. Our data suggest that, in the environments that are more productive and where the lines are better adapted, the effect of senescence on agronomic trait is more pronounced. Growing degree days and the total duration of the cultivation cycle are the factors that probably contributed to the effects of the background environments. Analyses of more environments and detailed environmental characterization of them could provide relevant information about the environmental determinants of the effects of the senescence. The relationship between senescence and different factors can be inferred by the analysis of the relative strength of the sources (duration of

photosynthesis activity, availability of water and N, etc.) and sinks (characteristics of the ear and grains, etc.). However, the analyses of the relationship of sources and sinks in relation to senescence provided contradictory results; for example, reducing the sink strength by ear removal or prevention of pollination could accelerate senescence (Rajcan and Tollenaar, 1999) or delay it (Borrás et al., 2003). In a thoughtful analysis of this question, Abeledo et al. (2020), altering the source and sink ratio by pollination prevention, ear removal, and partial defoliation, found that there is no consistent effect of specific environmental changes on the source–sink ratio on senescence. However, similar to other study, the authors found that the response of senescence to changes in the source–sink ratio depends on the background environment. Related to this subject, Martin et al. (2005) raised the interesting question of whether remobilization in leaves started because of the progress of senescence or an increased demand and remobilization of nutrients from leaves triggers the onset of senescence. However, our present and previous research did not allow to resolve this question, and specific designs are needed to answer it. Independent of the internal mechanism of the senescence, the fact that the effect of the senescence on agronomic traits is not altered by abiotic stresses raises doubts about the usefulness of SG as a secondary trait for improving abiotic stress tolerance (Kumar et al., 2022; Ali et al., 2023; Riache et al., 2023; Santos et al., 2023).

4.3 Abiotic factors

Similarly to SG, higher WI resulted in less biomass remobilized to the grains that were, in spite of that, heavier (Supplementary Figures 2, 3). However, at difference of SG, there was not significant difference between levels of irrigation on the concentration of N in the stover at harvest. Corrected by the stover yield, the magnitude of the total content of N in stover at harvest is higher in the low WI level, which suggests that high WI favors N remobilization. There was no difference in the N concentration between levels of irrigation, but, given that the kernels were heavier with high irrigation, the total N content in kernels was not lower or could be even higher if the higher irrigation would have favored a higher number of kernels (Guo et al., 2023; Liu et al., 2024) (Figures 6, 7; Supplementary Table 4). The main effect of N was quite different to SG and WI, as affected only the yield and N concentration of stover but did not have effect on grains.

5 Conclusions

The progress of senescence is very stable across levels of abiotic factors (water, nitrogen, and density) and background environments, supporting the hypothesis that senescence is primarily controlled by internal factors in maize and remains relatively independent of external signals. The effect of stay green on agronomic traits, particularly TKW, is not affected by abiotic factors but is affected by the background environment. Our results have implications for the application of SG as a secondary trait for enhancing abiotic stress tolerance. Future studies could consider a wider range of environmental conditions to assess the performance of SG traits under different climatic and soil conditions.

Data availability statement

The original contributions presented in the study are included in the article/[Supplementary Material](#). Further inquiries can be directed to the corresponding author.

Author contributions

NC: Data curation, Formal analysis, Investigation, Software, Supervision, Visualization, Writing – original draft, Writing – review & editing, Validation. PR: Data curation, Formal analysis, Funding acquisition, Investigation, Methodology, Project administration, Resources, Software, Supervision, Validation, Visualization, Writing – review & editing. VY: Formal analysis, Visualization, Writing – original draft, Writing – review & editing. PM: Methodology, Writing – review & editing. EC: Methodology, Writing – review & editing. BO: Conceptualization, Data curation, Formal analysis, Funding acquisition, Investigation, Methodology, Project administration, Resources, Software, Supervision, Validation, Visualization, Writing – original draft, Writing – review & editing.

Funding

The author(s) declare financial support was received for the research, authorship, and/or publication of this article. This research was funded by the project AGL2016-77628-R, Spain; and IN 607A – Grupos de referencia competitiva (GRC) Xunta de Galicia, Spain.

References

- Abeledo, L. G., Savin, R., and Slafer, G. A. (2020). Maize senescence under contrasting source-sink ratios during the grain filling period. *Environ. Exp. Bot.* 180, 104263. doi: 10.1016/j.envexpbot.2020.104263
- Acciaresi, H. A., Tambussi, E. A., Antonietta, M., Zuluaga, M. S., Andrade, F. H., and Guamét, J. J. (2014). Carbon assimilation, leaf area dynamics, and grain yield in contemporary earlier- and later-senescing maize hybrids. *Eur. J. Agron.* 59, 29–38. doi: 10.1016/j.eja.2014.05.007
- Ali, A., Ullah, Z., Sher, H., Abbas, Z., and Rasheed, A. (2023). Water stress effects on stay green and chlorophyll fluorescence with focus on yield characteristics of diverse bread wheats. *Planta* 257 (6). doi: 10.1007/s00425-023-04140-0
- Antonietta, M., Fanello, D. D., Acciaresi, H. A., and Guamét, J. J. (2014). Senescence and yield responses to plant density in stay green and earlier-senescing maize hybrids from Argentina. *Field Crops Res.* 155, 111–119. doi: 10.1016/j.fcr.2013.09.016
- Asad, M. A. U., Zakari, S. A., Zhao, Q., Zhou, L., Ye, Y., and Cheng, F. (2019). Abiotic stresses intervene with aba signaling to induce destructive metabolic pathways leading to death: Premature leaf senescence in plants. *Int. J. Mol. Sci.* 20, 23. doi: 10.3390/ijms20020256
- Bänziger, M., Edmeades, G. O., Beck, D., and Bellon, M. (2000). *Breeding for Drought and Nitrogen Stress Tolerance in Maize: From Theory to Practice* (Mexico, D.F.: CIMMYT). <https://doi.org/633.1553>
- Borrás, L., Maddonni, G. A., and Otegui, M. E. (2003). Leaf senescence in maize hybrids: Plant population, row spacing and kernel set effects. *Field Crops Res.* 82, 13–26. doi: 10.1016/S0378-4290(03)00002-9
- Borrell, A. K., and Hammer, G. L. (2000). Nitrogen dynamics and the physiological basis of stay-green in sorghum. *Crop Sci.* 40, 1295–1307. doi: 10.2135/cropsci2000.4051295x
- Borrell, A., Hammer, G., and Van Oosterom, E. (2001). Stay-green: A consequence of the balance between supply and demand for nitrogen during grain filling? *Ann. Appl. Biol.* 138, 91–95. doi: 10.1111/j.1744-7348.2001.tb00088.x
- Buchaillot, M. L., Gracia-Romero, A., Vergara-Díaz, O., Zaman-Allah, M. A., Tarekne, A., Cairns, J. E., et al. (2019). Evaluating maize genotype performance under low nitrogen conditions using RGB UAV phenotyping techniques. *Sensors* 19 (8). doi: 10.3390/s19081815
- Burken, D., Harding, J., and McGee, A. (2013). “Effects of Corn Hybrid, Plant Density, and Harvest Time on Yield and Quality of Corn Plants,” in *Nebraska Beef Cattle Report*, 42–43. Available at: http://digitalcommons.unl.edu/animalsci/bcr/719/%5Cnhttps://beef.unl.edu/c/document_library/get_file?uuid=1a52c02a-784b-4318-996b-6777a3f6c78b&groupId=4178167&.pdf.
- Caicedo, B. M. (2018). *Mejora Genética de Maíz para Senescencia Retrasada “STAY GREEN”*. (Santiago de Compostela- Lugo: Universidade de Santiago de Compostela- Lugo).
- Chen, K., Kumudini, S. V., Tollenaar, M., and Vyn, T. J. (2015). Plant biomass and nitrogen partitioning changes between silking and maturity in newer versus older maize hybrids. *Field Crops Res.* 183, 315–328. doi: 10.1016/j.fcr.2015.08.013
- Chibane, N., Caicedo, M., Martinez, S., Marcet, P., Revilla, P., and Ordás, B. (2021). Relationship between delayed leaf senescence (Stay-green) and agronomic and physiological characters in maize (*Zea mays* L.). *Agronomy* 11, 276. doi: 10.3390/agronomy11020276
- Christopher, J. T., Veyradier, M., Borrell, A. K., Harvey, G., Fletcher, S., and Chenu, K. (2014). Phenotyping novel stay-green traits to capture genetic variation in senescence dynamics. *Funct. Plant Biol.* 41, 1035–1048. doi: 10.1071/FP14052
- Clay, S. A., Clay, D. E., Horvath, D. P., Pullis, J., Carlson, C. G., Hansen, S., et al. (2009). Corn response to competition: growth alteration vs. Yield limiting factors. *Agron. J.* 101, 1522–1529. doi: 10.2134/agronj2008.0213x
- Echarte, L., Rothstein, S., and Tollenaar, M. (2008). The response of leaf photosynthesis and dry matter accumulation to nitrogen supply in an older and a newer maize hybrid. *Crop Sci.* 48, 656–665. doi: 10.2135/cropsci2007.06.0366

Acknowledgments

NC would like to thank the Spanish Ministerio de Innovación y Universidades (MCIU), the Agencia Estatal de Investigación (AEI), for FPI scholarship during 4 years. We acknowledge United States Department of Agriculture (USDA) for providing the seeds of the Pioneer ExPVP lines used in the experiment.

Conflict of interest

The authors declare that the research was conducted in the absence of any commercial or financial relationships that could be construed as a potential conflict of interest.

Publisher's note

All claims expressed in this article are solely those of the authors and do not necessarily represent those of their affiliated organizations, or those of the publisher, the editors and the reviewers. Any product that may be evaluated in this article, or claim that may be made by its manufacturer, is not guaranteed or endorsed by the publisher.

Supplementary material

The Supplementary Material for this article can be found online at: <https://www.frontiersin.org/articles/10.3389/fpls.2024.1399072/full#supplementary-material>

- Gnädinger, F. (2018). *High-Throughput Phenotyping the Nitrogen and Carbon Dynamics in Maize at the Reproductive Phase*. Doktorarbeit, Technischen Universität München zur Erlangung des akademischen Grades eines. (Germany: Technischen Universität München).
- Gregersen, P. L., Holm, P. B., and Krupinska, K. (2008). Leaf senescence and nutrient remobilisation in barley and wheat. *Plant Biol.* 10, 37–49. doi: 10.1111/j.1438-8677.2008.00114.x
- Guo, J., Qu, L., Wang, L., Lu, W., and Lu, D. (2023). Effects of post-silking drought stress degree on grain yield and quality of waxy maize. *J. Sci. Food Agric.* 103, 1530–1540. doi: 10.1002/jsfa.12250
- Harris, K. R. (2007). *Genetic Analysis Of The Sorghum Bicolor Stay-Green Drought Tolerance Trait*. Doctor of Philosophy. (Texas: Texas A&M University).
- Havé, M., Marmagne, A., Chardon, F., and Masclaux-Daubresse, C. (2017). Nitrogen remobilization during leaf senescence: Lessons from Arabidopsis to crops. *J. Exp. Bot.* 68, 2513–2529. doi: 10.1093/jxb/erw365
- He, P., Zhou, W., and Jin, J. (2004). Carbon and nitrogen metabolism related to grain formation in two different senescent types of maize. *J. Plant Nutr.* 27, 295–311. doi: 10.1081/PLN-120027655
- Houbav, V. J. G., Temminghoff, E. J. M., Gaikhorst, G. A., and van Vark, W. (2000). Soil analysis procedures using 0.01 M calcium chloride as extraction reagent. *Commun. Soil Sci. Plant Anal.* 31, 1299–1396. doi: 10.1080/00103620009370514
- Jia, Q., Sun, L., Mou, H., Ali, S., Liu, D., Zhang, Y., et al. (2018). Effects of planting patterns and sowing densities on grain-filling, radiation use efficiency and yield of maize (Zea mays L.) in semi-arid regions. *Agric. Water Manage.* 201, 287–298. doi: 10.1016/j.agwat.2017.11.025
- Jiao, B., Meng, Q., and Lv, W. (2020). Roles of stay-green (SGR) homologs during chlorophyll degradation in green plants. *Botanical Stud.* 61, 25. doi: 10.1186/s40529-020-00302-5
- Kamal, N. M., Alnor Gorafi, Y. S. A., Abdelrahman, M., Abdellatif, E., and Tsujimoto, H. (2019). Stay-green trait: A prospective approach for yield potential, and drought and heat stress adaptation in globally important cereals. *Int. J. Mol. Sci.* 20, 5837. doi: 10.3390/ijms20235837
- Kosgey, J. R., Moot, D. J., Fletcher, A. L., and McKenzie, B. A. (2013). Dry matter accumulation and post-silking N economy of “stay-green” maize (Zea mays L.) hybrids. *Eur. J. Agron.* 51, 43–52. doi: 10.1016/j.eja.2013.07.001
- Krotz, L., and Giazzi, G. (2000). Carbon/Nitrogen Ratio in Soils and Plants using The FLASH 2000 Organic Elemental Analyzer. *Milano, Italy: Thermo Fisher Scientific*.
- Kumar, R., Harikrishna, B., Barman, D., Ghimire, O. P., Gurumurthy, S., Singh, P. K., et al. (2022). Stay-green trait serves as yield stability attribute under combined heat and drought stress in wheat (Triticum aestivum L.). *Plant Growth Regul.* 96, 67–78. doi: 10.1007/s10725-021-00758-w
- Liu, G., Yang, Y., Guo, X., Liu, W., Xie, R., Ming, B., et al. (2023). A global analysis of dry matter accumulation and allocation for maize yield breakthrough from 1.0 to 25.0 Mg ha⁻¹. *Resources Conserv. Recycling* 188, 106656. doi: 10.1016/j.RESCONREC.2022.106656
- Liu, X., Chang, X., Wang, Y., Wang, D., Wang, X., Meng, Q., et al. (2024). Adaptation to priming drought at six-leaf stage relieves maize yield loss to individual and combined drought and heat stressors around flowering. *Environ. Exp. Bot.* 224. doi: 10.1016/j.envexpbot.2024.105799
- Lucas, H. D. S., Silva, J. A. G. D., Nörnerberg, R., Zimmer, C. M., Arenhardt, E. G., Caetano, R., et al. (2015). Stay-green effects on adaptability and stability in wheat. *Afr. J. Agric.* 10, 1142–1149. doi: 10.5897/AJAR2013.9308
- Lüdecke, D. (2021). “sjPlot: Data visualization for statistics in social science,” in *R package version, 2.8.16*. Available online at: <https://CRAN.R-project.org/package=sjPlot>.
- Martin, A., Belastegui-Macadam, X., Quilleré, I., Floriot, M., Valadier, M. H., Pommel, B., et al. (2005). Nitrogen management and senescence in two maize hybrids differing in the persistence of leaf greenness: Agronomic, physiological and molecular aspects. *New Phytol.* 167, 483–492. doi: 10.1111/j.1469-8137.2005.01430.x
- Mikel, M. A., and Dudley, J. W. (2006). Evolution of North American dent corn from public to proprietary germplasm. *Crop Sci.* 46, 1193–1205. doi: 10.2135/cropsci2005.10-0371
- Mueller, S. M., Messina, C. D., and Vyn, T. J. (2019). Simultaneous gains in grain yield and nitrogen efficiency over 70 years of maize genetic improvement. *Sci. Rep.* 9 (1). doi: 10.1038/s41598-019-45485-5
- Muniz, E. D., Martínez, S., Kumar, A., Caicedo, M., and Ordás, B. (2020). The senescence (Stay-Green)—an important trait to exploit crop residuals for bioenergy. *Energies* 13, 22. doi: 10.3390/en13040790
- Nasielski, J., Earl, H., and Deen, B. (2019). Luxury vegetative nitrogen uptake in maize buffers grain yield under post-silking water and nitrogen stress: A mechanistic understanding. *Front. Plant Sci.* 10. doi: 10.3389/fpls.2019.00318
- Ning, P., Li, S., Yu, P., Zhang, Y., and Li, C. (2013). Post-silking accumulation and partitioning of dry matter, nitrogen, phosphorus and potassium in maize varieties differing in leaf longevity. *Field Crops Res.* 144, 19–27. doi: 10.1016/j.fcr.2013.01.020
- Ning, P., Yang, L., Li, C., and Fritsch, F. B. (2018). Post-silking carbon partitioning under nitrogen deficiency revealed sink limitation of grain yield in maize. *J. Exp. Bot.* 69, 1707–1719. doi: 10.1093/jxb/erx496
- Ning, P., Fritsch, F. B., and Li, C. (2017). Temporal dynamics of post-silking nitrogen fluxes and their effects on grain yield in maize under low to high nitrogen inputs. *Field Crops Res.* 204, 249–259. doi: 10.1016/j.fcr.2017.01.022
- Pic, E., Teysseier de la Serve, B., Tardieu, F., and Turc, O. (2002). Leaf senescence induced by mild water deficit follows the same sequence of macroscopic, biochemical, and molecular events as monocarpic senescence in pea. *Plant Physiol.* 128, 236–246. doi: 10.1104/pp.010634
- Pommel, B., Gallais, A., Coque, M., Quilleré, I., Hirel, B., Prioul, J. L., et al. (2006). Carbon and nitrogen allocation and grain filling in three maize hybrids differing in leaf senescence. *Eur. J. Agron.* 24, 203–211. doi: 10.1016/j.eja.2005.10.001
- Rajcan, I., and Tollenaar, M. (1999). Source: Sink ratio and leaf senescence in maize: II. Nitrogen metabolism during grain filling. *Field Crops Res.* 60, 255–265. doi: 10.1016/S0378-4290(98)00143-9
- Ramkumar, M. K., Senthil Kumar, S., Gaikwad, K., Pandey, R., Chinnusamy, V., Singh, N. K., et al. (2019). A novel stay-green mutant of rice with delayed leaf senescence and better harvest index confers drought tolerance. *Plants* 8 (10). doi: 10.3390/plants8100375
- R Core Team. (2013). *R: A language and environment for statistical computing*.
- Riache, M., Djemel, A., Revilla, P., Malvar, R. A., and Mefti, M. (2023). Genetic analyses of stay green for tolerance to water stress and nitrogen deficiency in Algerian Saharan maize populations. *Euphytica* 219 (6). doi: 10.1007/s10681-023-03193-2
- Sade, N., Del Mar Rubio-Wilhelmi, M., Umnajkitikorn, K., and Blumwald, E. (2018). Stress-induced senescence and plant tolerance to abiotic stress. *J. Exp. Bot.* 69, 845–853. doi: 10.1093/jxb/erx235
- Sah, R. P., Chakraborty, M., Prasad, K., Pandit, M., Tudu, V. K., Chakravarty, M. K., et al. (2020). Impact of water deficit stress in maize: Phenology and yield components. *Sci. Rep.* 10 (1). doi: 10.1038/s41598-020-59689-7
- Santos, T., de, O., Amaral Junior, A., and Moulin, M. M. (2023). Maize breeding for low nitrogen inputs in agriculture: mechanisms underlying the tolerance to the abiotic stress. *Stresses* 3 (1), 136–152. doi: 10.3390/stresses3010011
- Shafi, M., Bakht, J., Ali, S., Khan, H., Khan, M. A., and Sharif, M. (2012). Effect of planting density on phenology, growth and yield of maize (Zea mays L.). *Pakistan J. Bot.* 44, 691–696.
- Silva, A. S., De Carvalho, F. I. F., Nedel, J. L., Jacinto Cruz, P., Teichert Peske, S., Simioni, D., et al. (2003). Enchimento de sementes em linhas quase-isogênicas de trigo com presença e ausência do caráter “stay-green”. *Pesquisa Agropecuária Brasileira*. 38, 613–618. doi: 10.1590/S0100-204X2003000500009
- Subedi, K. D., and Ma, B. L. (2005). Nitrogen uptake and partitioning in stay-green and leafy maize hybrids. *Crop Sci.* 45, 740–747. doi: 10.2135/cropsci2005.0740
- Thomas, H., Ougham, H., Canter, P., and Donnison, I. (2002). What stay-green mutants tell us about nitrogen remobilization in leaf senescence. *J. Exp. Bot.* 53, 801–808. doi: 10.1093/jxb/53.7.801
- Thomas, H., and Ougham, H. (2014). The stay-green trait. *J. Exp. Bot.* 65, 3889–3900. doi: 10.1093/jxb/eru037
- Tong, T., Gu, W. R., Liu, X. M., and Li, C. F. (2019). Maize yield and leaf photosynthetic characteristics in response to planting densities and application of yuhuangjin, as a new plant growth regulator. *Appl. Ecol. Environ. Res.* 17, 10717–10730. doi: 10.15666/aer/1705_1071710730
- Trachsel, S., Sun, D., Sanvicente, F. M., Zheng, H., Atlin, G. N., Suarez, E. A., et al. (2016a). Identification of QTL for early vigor and stay-green conferring tolerance to drought in two connected advanced backcross populations in tropical maize (Zea mays L.). *PLoS One* 11, 1–22. doi: 10.1371/journal.pone.0149636
- Trachsel, S., Suarez, E. A., San Vicente, F. M., and Dhlwayo, T. (2016b). Interrelations among early vigor, flowering, physiological maturity and grain yield in tropical maize (Zea mays L.) under multiple abiotic stress. *Crop Sci.* 11 (3), 1–22. doi: 10.1371/journal.pone.0149636
- Wang, P., Hou, S. Y., Wen, H. W., Wang, Q. Z., and Li, G. Q. (2021). Chlorophyll retention caused by STAY-GREEN (SGR) gene mutation enhances photosynthetic efficiency and yield in soybean hybrid Z1. *Photosynthetica* 59, 37–48. doi: 10.32615/ps.2020.076
- Wang, X., Wang, L., and Shanguan, Z. (2016). Leaf gas exchange and fluorescence of two winter wheat varieties in response to drought stress and nitrogen supply. *PLoS One* 11, 1–15. doi: 10.1371/journal.pone.0165733
- White, M. R., Mikel, M. A., de Leon, N., and Kaeppler, S. M. (2020). Diversity and heterotic patterns in North American proprietary dent maize germplasm. *Crop Sci.* 60, 100–114. doi: 10.1002/csc2.20050
- Worwu, M., Bänziger, M., Erley, G. S. A. M., Friesen, D., Diallo, A. O., and Horst, W. J. (2007). Nitrogen uptake and utilization in contrasting nitrogen efficient tropical maize hybrids. *Crop Sci.* 47, 519–528. doi: 10.2135/cropsci2005.05.0070
- Wu, Y., Yao, F., Wang, Y., Ma, L., and Li, X. (2023). Association of maize (Zea mays L.) senescence with water and nitrogen utilization under different drip irrigation systems. *Front. Plant Sci.* 14. doi: 10.3389/fpls.2023.1133206
- Yang, J. T., Schneider, H. M., Brown, K. M., and Lynch, J. P. (2019). Genotypic variation and nitrogen stress effects on root anatomy in maize are node specific. *J. Exp. Bot.* 70, 5311–5325. doi: 10.1093/jxb/erz293
- Ye, Y.-x., Wen, Z., Yang, H., Lu, W., and Lu, D. (2020). Effects of post-silking water deficit on the leaf photosynthesis and senescence of waxy maize. *J. Integr. Agric.* 19, 2216–2228. doi: 10.1016/S2095-3119(20)63158-6
- Zhang, L.-L., Zhou, X., Fan, Y., Fu, J., Hou, P., Yang, H., et al. (2019). Post-silking nitrogen accumulation and remobilization are associated with green leaf persistence and plant density in maize. *J. Integr. Agric.* 18, 1882–1892. doi: 10.1016/S2095-3119(18)62087-8
- Zhiipao, R. R., Pooniya, V., Biswakarma, N., Kumar, D., Shivay, Y. S., Dass, A., et al. (2023). Timely sown maize hybrids improve the post-anthesis dry matter accumulation, nutrient acquisition and crop productivity. *Sci. Rep.* 13 (1). doi: 10.1038/s41598-023-28224-9



OPEN ACCESS

EDITED BY

Gustavo A. Slafer,
Catalan Institution for Research and
Advanced Studies (ICREA), Spain

REVIEWED BY

Roberto Tuberosa,
University of Bologna, Italy
Renan Santos Uhdre,
Washington State University, United States

*CORRESPONDENCE

Rosa Ana Malvar

✉ rmalvar@mbg.csic.es

RECEIVED 21 March 2024

ACCEPTED 16 September 2024

PUBLISHED 22 October 2024

CITATION

López-Malvar A, Reséndiz-Ramírez Z,
Butrón A, Jiménez-Galindo JC, Revilla P and
Malvar RA (2024) Validation of QTLs
associated with corn borer resistance and
grain yield: implications in maize breeding.
Front. Plant Sci. 15:1404881.
doi: 10.3389/fpls.2024.1404881

COPYRIGHT

© 2024 López-Malvar, Reséndiz-Ramírez,
Butrón, Jiménez-Galindo, Revilla and Malvar.
This is an open-access article distributed under
the terms of the [Creative Commons Attribution
License \(CC BY\)](#). The use, distribution or
reproduction in other forums is permitted,
provided the original author(s) and the
copyright owner(s) are credited and that the
original publication in this journal is cited, in
accordance with accepted academic
practice. No use, distribution or reproduction
is permitted which does not comply with
these terms.

Validation of QTLs associated with corn borer resistance and grain yield: implications in maize breeding

Ana López-Malvar^{1,2}, Zoila Reséndiz-Ramírez³, Ana Butrón⁴,
Jose Cruz Jiménez-Galindo⁵, Pedro Revilla⁴
and Rosa Ana Malvar^{4*}

¹Facultad, de Biología, Departamento de Biología Vegetal Y Ciencias del Suelo, Universidad de Vigo, Vigo, Spain, ²Agrobiología Ambiental, Calidad de Suelos Y Plantas (UVIGO), Unidad Asociada a La MBG (CSIC), Vigo, Spain, ³Instituto Nacional de Investigaciones Forestales, Agrícolas y Pecuarias, Río Bravo, Tamaulipas, Mexico, ⁴Misión Biológica de Galicia (CSIC), Pontevedra, Spain, ⁵National Institute of Forestry Agriculture and Livestock Research (INIFAP), Cuauhtémoc, Chihuahua, Mexico

Introduction: Validations of previously detected quantitative trait loci (QTLs) to assess their reliability are crucial before implementing breeding programs. The objective of this study was to determine the reliability and practical usefulness of previously reported QTLs for resistance to stem tunneling by the Mediterranean stem borer (MSB) and yield. These authors used approximately 600 recombinant inbred lines (RILs) from a multiparent advanced generation intercross (MAGIC) population to map QTL using a genome-wide association study (GWAS) approach.

Methods: We identified RILs situated at the extremes of resistance and yield distributions within the whole MAGIC, and those QTLs were evaluated *per se* and crossed to a tester (A638) using lattice designs. In each set, a significant single-nucleotide polymorphism (SNP) was considered validated if (1) the same SNP was associated with the trait with a p -value < 0.02 , or (2) within a ± 2 -Mbp interval, an SNP associated with the trait exhibited a p -value < 0.02 and demonstrated linkage disequilibrium ($r^2 > 0.2$) with the SNPs previously reported.

Results and discussion: The novel QTL validation approach was implemented using improved experimental designs that led to higher heritability estimates for both traits compared to those estimated with the whole MAGIC population. The procedure used allowed us to jointly validate several QTL and to ascertain their possible contribution to hybrid improvement. Specifically, nearly three-quarters of the QTLs for tunnel length were confirmed. Notably, QTLs located in the genomic region 6.05–6.07 were consistently validated across different sets and have been previously linked to resistance against stalk tunneling in various mapping populations. For grain yield, approximately 10 out of 16 QTLs were validated. The validation rate for yield was lower than for tunnel length, likely due to the influence of dominance and/or epistatic effects. Overall, 9 out of 21 QTLs for tunnel length and 6 out of 17 QTLs for grain yield identified in our previous research were validated across both validation sets, indicating a moderate genetic correlation between *per se* and testcross performance of inbred lines. These findings offer insights into the reliability of QTL and genomic predictions, both derived from assessments conducted on the entire MAGIC population.

Genomic predictions for tunnel length based on inbred line evaluations could be useful to develop more resistant hybrids; meanwhile, genomic prediction for yield could only be valid in a homozygous background.

KEYWORDS

Mediterranean corn borer, QTL validation, maize breeding, MAGIC population, grain yield, recombinant inbred lines

Introduction

The primary pest affecting maize in Europe is the Mediterranean corn borer (MCB) *Sesamia nonagrioides* (Lef.). Stem corn borer larvae feed on the stem pith of maize producing tunnels that cause yield losses of approximately 30%, equivalent to worldwide losses of 311.3 million tons every year (Meissle et al., 2010). Tunnels produced in the stalk pith interfere with assimilate movement of nutrients toward the developing ear and increase lodging rate (López et al., 2001). One approach to pest control involves the cultivation of resistant and/or tolerant varieties, particularly in regions where the cultivation of transgenic maize is prohibited or heavily regulated, such as in Europe (Farinós et al., 2004). Genetic improvement of pest resistance relies on attaining varieties that experience reduced damage produced by insects. However, the most resistant varieties could not be the most productive in terms of grain yield. Even more, certain materials have shown a negative correlation between resistance to stem borer attack and grain yield (Sandoya et al., 2008; Butrón et al., 2012). In those cases, selection of varieties that are able to produce higher grain yields under high insect pressure could be a better alternative (Butrón et al., 1999; Ordas et al., 2012). However, at a particular site, the pest infestation level is influenced by multiple factors, exhibiting erratic behavior across years, and differences among varieties for grain yield could be highly affected by the infestation rate. Therefore, it is important to assess varieties' performance across different scenarios concerning insect attack intensity in order to select varieties with high stable yield.

In order to optimize the development of varieties with reduced damage by insect attack and/or high yield across different scenarios, it is imperative to comprehend the inheritance of the traits involved and to study the regions of the genome or quantitative trait loci (QTLs) associated with resistance using different mapping populations in order to advance in the complete QTLome knowledge for these highly relevant traits (Salvi and Tuberosa, 2015). Accordingly, we can devise the optimal selection method (whether genomic or phenotypic), determine the feasibility of managing any QTL through marker-assisted selection (MAS), or even investigate genes involved in the inheritance of insect resistance. In the specific case of resistance to corn borers, QTLs have been widely sought using biparental populations and linkage-based QTL mapping (Ordas et al., 2009; Samayoa et al., 2014;

Samayoa et al., 2015a, 2017; Jiménez-Galindo et al., 2017). However, the use of high-density molecular markers is now widespread due to its low cost, and genome-wide association studies (GWAS) are being conducted for a wide range of traits, including maize resistance to insects (Butrón et al., 2018). GWAS for resistance to the MCB have been conducted using diversity panels of inbred lines (Samayoa et al., 2015b) and multiparent advanced generation intercross (MAGIC) populations (Jiménez-Galindo et al., 2019).

Although many QTLs for resistance to stem corn borers have been found, and molecular markers significantly associated to resistance have been identified, MAS (Flint-Garcia et al., 2003; Samayoa et al., 2019) and genomic selection (Gesteiro et al., 2023) have been scarcely used to improve maize resistance to insects. External validations of detected QTL to assess QTL reliability are advisable before implementing MAS. QTL reliability can be affected by a significant QTL \times environment interaction but also by low phenotyping precision.

Phenotyping genetically wide panels of inbred lines or RILs is challenging due to the difficulty of controlling the high experimental error associated with large trials; mostly when evaluations are often done using incomplete block or augmented designs in which most genotypes are assessed only once in each trial. Moreover, assessing plant traits related to performance against pest attack involves managing pest populations that could show variability for survival, voracity, or any other trait that would affect plant performance. Therefore, the high experimental errors associated with these evaluations could greatly interfere with QTL identification.

In addition, reliable additive-effect QTL could not be useful to discriminate among heterozygous genotypes if heterotic effects can counterbalance additive effects. Therefore, QTL validation should be done using inbred lines as well as hybrids to really ascertain the practical value of detected QTLs. Hence, the objective of this study was to determine the reliability and practical usefulness of QTL for resistance and yield reported by Jiménez-Galindo et al. (2019). Identification of QTL was based on a GWAS approach applied to a maize MAGIC population evaluated using augmented designs in a 2-year evaluation. For validation purposes, we selected inbred line sets at the tails of distributions for resistance and yield in the whole MAGIC to maintain genetic variability for both traits. These inbreds were evaluated *per se* and crossed to a tester (A638) using

lattice designs. The results obtained in this study will contribute to expanding the maize QTLome knowledge for traits highly relevant for maize breeding as they are related to pest tolerance and resistance.

Materials and methods

Field experiments

The Maize Genetics and Breeding group of the Misión Biológica de Galicia has developed an eight-way MAGIC population of 608 RILs. This MAGIC population was evaluated for resistance to corn borer attack and grain yield for 2 years (2014 and 2015) using augmented designs (Jiménez-Galindo et al., 2019). Data compiled by these authors are provided in a [Supplementary Table](#).

Based on those evaluations, we selected a group of lines presenting either the longest or shortest tunnels made by MCB attack and/or exhibiting the highest or lowest yield. A collection of 56 RILs [inbred line validation set (IVS)], representing the widest variability for these two traits, was then established as the basis for this study. This set of RILs was crossed with A638 to obtain hybrids to validate QTL in a heterozygous background [hybrid validation set (HVS)]. The tester was chosen to avoid interferences on differences among hybrids due to divergences in heterosis as the inbred A638 belongs to the “Reid” group while RILs are characterized by the lack of Reid material in their pedigrees.

The IVS was evaluated along with the eight inbred checks used in previous evaluations (Jiménez-Galindo et al., 2019). Five of the checks were founders of the MAGIC population (A509, EP125, EP17, EP86, and F473), which are partially resistant to corn borer attack. The other three inbred checks were susceptible inbreds, EP42, EP47, and EP80 (Butrón et al., 2006). The 64 lines were evaluated in Pontevedra, in 2017 and 2018, following simple 8×8 lattice designs in two adjacent trials, one treated with insecticide (INSECT 5G, Chlorpyrifos 5%) (Control) and the other under artificial infestation with *Sesamia nonagrioides* eggs. The first insecticide treatment was applied between the sixth and seventh week after sowing, and treatment was repeated every 3 weeks until harvest.

Before flowering, in the trial under artificial infestation, pest infestation was ensured by placing ~80–120 MCB eggs between the sheath and the stem in one internode below the main ear on five plants per plot. Eggs were obtained from insect rearing in the MBG-CSIC laboratory following the methodology of Eizaguirre and Albajes (1992). In all inbred trials, the elementary plot consisted of 15 plants sown at a density of 70,000 plants/ha.

Fifty-two hybrids (HVS), obtained by crossing 52 out of the 56 selected inbreds with A638, along with four hybrid checks were also evaluated. Evaluations were made in 2017 and 2018 in Pontevedra under insecticide treatment and infestation with MCB eggs, in trials adjacent to those described for inbreds, and in Barrantes (42°29'N; 8°45'O, 115 m above sea level) and Ponte Caldelas (42°23'N 8°30'O, 291 m above sea level) in 2017 under natural infestation conditions. Natural infestation was high in both locations. The experimental design employed was a simple 8×7 lattice, with each elementary

plot consisting of 25 plants and a density of 70,000 plants per hectare.

At harvest, grain yield per plant and plot grain yield were determined and expressed in g plant^{-1} and Mg ha^{-1} at 14% grain moisture content in IVS and HVS, respectively. In the artificial infestation trials, the five infested plants per plot were collected; the stalks were split lengthwise, and the lengths of the tunnels made by the larvae were measured. A similar procedure was used to measure damage by larvae on naturally infested hybrid trials, although it was done on five random plants per plot.

Statistical analysis

Inbred lines

A combined analysis of variance across years and condition (control and infested) was carried out for grain yield and across years at infestation conditions for tunnel length. The inbred lines were considered as fixed factors while the rest of the main factors and interactions were considered as random factors. Comparison of means was done using Fisher's protected LSD.

The best linear unbiased estimators (BLUEs) across environments were calculated for each RIL using the Proc Mixed procedure of SAS, with genotype being considered as a fixed factor and year and block as random factors. Heritabilities on a family mean basis were calculated following Holland et al. (2003). To estimate genotypic, residual, and genotype \times environment variance, we implemented the VARCOMP procedure in SAS considering all factors as random. The phenotypic variance was calculated as the sum of genotypic, residual, and genotype \times environment variance.

Hybrids

A combined analysis across years and conditions was performed for grain yield and tunnel length (excluding protected trial data). Hybrid means were compared using Fisher's protected LSD and BLUEs across environments were estimated for each RIL. Heritabilities and variance components were computed as explained above. All analyses were carried out with SAS software (SAS/STAT, 2007).

Association mapping

GWAS, based on a mixed linear model that includes a genotype–phenotype matrix, was completed with Tassel 5 (Bradbury et al., 2007) on inbred lines and hybrids, separately. Restricted maximum likelihood estimates of variance components were obtained using the “compressed MLM” and “previously determined population parameters” (P3D) methods described by Zhang et al. (2010). The BLUEs comprised the phenotypic matrices while the genotypic matrix consisted of 224,363 single-nucleotide polymorphisms (SNPs), the same matrix employed by Jiménez-Galindo et al. (2019).

In order to validate the SNPs described as significantly associated with grain yield and tunnel length by Jiménez-Galindo et al. (2019), in the current study, the linkage disequilibrium of

significant (p -value < 0.02) marker–phenotype associations with published significant SNPs was studied. In the respective set (inbreds and hybrids), a published significant SNP (from Jiménez-Galindo et al., 2019) was considered validated if (1) the same SNP was associated with the trait with a p -value < 0.02, or (2) within a ± 2 -Mbp interval, there were SNPs associated with the trait at p -value < 0.02 and in linkage disequilibrium ($r^2 > 0.2$) with the SNPs reported by Jiménez-Galindo et al. (2019).

Results

Means, heritability, and variance components

We observed significant differences among inbred checks and among RILs in IVS and HVS (data not shown). BLUE estimates for inbreds and hybrids are shown in Supplementary Tables 2 and 3, respectively. Regarding heritability estimates, we observed an increase in the values obtained using the set of lines showing extreme values for both traits compared to the values obtained

using the whole MAGIC population (Jiménez-Galindo et al., 2019) (Table 1). We studied the decomposition of phenotypic variance in tunnel length and grain yield. Genotype \times environment interaction variance is minimal in both traits, in both magnitude and proportion, though significant in IVS. In tunnel length, genetic variance prevails in IVS, less so in HVS and the entire MAGIC population. In grain yield, genetic variance remains consistent in IVS and HVS but decreases in the whole MAGIC population.

Validation of QTL for tunnel length produced by *Sesamia nonagrioides* larvae

None of the SNPs that showed significant associations with tunnel length in the whole MAGIC (Jiménez-Galindo et al., 2019) showed significant associations ($p < 0.02$) with tunnel length in the IVS and only one in the HVS. However, within both sets, we have pinpointed SNPs that show a significant association with tunnel length falling within the confidence intervals of SNPs significantly linked to the trait across the entire MAGIC population.

TABLE 1 Heritability, means, range, and variance components calculated with the whole MAGIC population, the inbred validation set (IVS), and the hybrid validation set (HVS).

	Tunnel length				Grain yield			
Heritability (h2) ¹								
Whole MAGIC	0.24 ± 0.08*				0.46 ± 0.04*			
IVS	0.74 ± 0.08				0.67 ± 0.08			
HVS	0.52± 0.11				0.74 ± 0.06			
Means								
Whole MAGIC	35 cm				42.4 g/plant			
IVS	25 cm				73.3 g/plant			
HSV	29 cm				7.6 t/ha			
Range								
Whole MAGIC	0–59 cm				0–114 g/plant			
IVS	6–63 cm				20–117 g/plant			
HSV	16–40 cm				4.6–9.4 t/plant			
Variances								
	Vg2	Vgxe3	Vres4	Vp5	Vg	Vgxe	Vres	Vp
Whole MAGIC	21 ± 4	7 ± 5	91 ± 5	119	78 ± 10	3 ± 6	186 ± 9	267
IVS	107 ± 30	38 ± 17	75 ± 12	220	229 ± 70	174 ± 65	582 ± 61	985
HVS	21 ± 9	17 ± 12	119 ± 13	157	118 ± 33	40 ± 31	396 ± 37	555
	Vg/Vp	Vgxe/Vp	Vres/Vp		Vg/Vp	Vgxe/Vp	Vres/Vp	
Whole MAGIC	0.23	0.08	0.76		0.29	0.01	0.70	
IVS	0.49	0.17	0.34		0.23	0.18	0.59	
HVS	0.14	0.11	0.75		0.21	0.07	0.71	

¹Heritability estimated on family basis \pm standard error; 2 Genotypic variance; 3 Genotype \times environment variance; 4 Residual variance; 5 Phenotypic variance. *A variance is significant when it exceeds twice the standard error.

Using the IVS, all of the QTLs detected with the whole MAGIC on chromosomes 5, 6, and 7 were validated. In addition, half of the QTLs on chromosomes 1, 2, and 8 were validated along with one out of three QTLs on chromosome 3. None of the six QTLs on chromosome 4 has been validated in IVS.

Moreover, using HVS, the same SNPs were validated as with the IVS on chromosomes 1, 5, 6, and 7. On chromosome 2, the two

QTLs detected in the full set were confirmed; meanwhile, 2/3 and 2/6 were validated on chromosomes 3 and 4, respectively, although three of them were not validated with the IVS (Tables 2, 3). In summary, out of the 21 QTLs associated with tunnel length in the whole MAGIC population, 14 were validated. Nine were validated using both IVS and HVS, QTL_8_2 with IVS only, and QTL_2_2, QTL_3_3, QTL_4_2, and QTL_4_3 with HVS only (Tables 2, 3).

TABLE 2 Validation of QTL found for tunnel length in the whole MAGIC population (Jiménez-Galindo et al., 2019) using a 56-inbred subset of the MAGIC population (MAGIC subset).

SNP ¹ (Jiménez-Galindo et al., 2019)	QTL ²	p-value ³	SNP ⁴	p-value ⁵	Distance (bp) ⁶	LD r^{27}
Grain yield						
S1_3708430	QTL_1_1	0.01	S1_3708430	0.007	0	Same SNP
S1_199075640	QTL_1_2	0.95	S1_196201034	0.013	2,874,606	0.07
S1_199075673	QTL_1_2	0.95				
S1_199075674	QTL_1_2	0.95				
S1_199075675	QTL_1_2	0.95				
S1_199075677	QTL_1_2	0.95				
S1_199075679	QTL_1_2	0.95				
S1_199075681	QTL_1_2	0.95				
S1_199075682	QTL_1_2	0.95				
S1_199075684	QTL_1_2	0.95				
S1_200077059	QTL_1_3	0.35	S1_201741572	0.013	1,664,513	0.27
S1_200077088	QTL_1_3	0.35				
S1_200408507	QTL_1_3	0.54				
S1_200408528	QTL_1_3	0.47				
S1_200479419	QTL_1_3	0.57				
S1_200801543	QTL_1_3	0.27				
S1_201847366	QTL_1_4	0.32	S1_201741572	0.013	105,794	0.45
S1_201872641	QTL_1_4	0.52				
S1_202160398	QTL_1_4	0.44				
S1_202647745	QTL_1_4	0.49				
S1_279899012	QTL_1_5	0.76	S1_276323139	0.014	3,575,873	0.07
S1_298985014	QTL_1_6	0.63	S1_300073024	0.005	1,088,010	0.37
S1_298986682	QTL_1_6	0.99				
S3_200876919	QTL_3_1	0.22	S3_197019251	0.020	3,857,668	0.13
S3_200876939	QTL_3_1	0.22				
S3_223537342	QTL_3_2	0.19	S3_222132763	0.012	1,404,579	0.22
S3_229992268	QTL_3_3	0.63	S3_223745145	0.016	6,247,123	0.11
S4_235761612	QTL_4_1	0.47	S4_236393647	0.019	632,035	0.28
S5_128333604	QTL_5_1	0.58	S5_133776816	0.016	5,443,212	0.06
S5_128333610	QTL_5_1	0.58				

(Continued)

TABLE 2 Continued

SNP ¹ (Jiménez-Galindo et al., 2019)	QTL ²	p-value ³	SNP ⁴	p-value ⁵	Distance (bp) ⁶	LD r^{27}
Grain yield						
S7_33885476	QTL_7_1	0.10	S7_34480421	0.012	594,945	0.76
S8_171634738	QTL_8_1	0.32	S8_173704033	0.002	2,069,295	0.17
S9_5656122	QTL_9_1	0.21	S9_5656939	0.004	817	No
S9_5656138	QTL_9_1	0.21				
S9_9966270	QTL_9_2	0.08	S9_13495777	0.008	3,529,507	0.23
S9_9966272	QTL_9_2	0.08				
S9_9966291	QTL_9_2	0.08				
S9_11084679	QTL_9_3	0.09	S9_13495777	0.0080057	2,411,098	0.15
S9_11746822	QTL_9_4	0.52	S9_11564902	0.005	181,920	No

SNPs highlighted in green are validated following the two criteria previously described, i.e., the same SNP was associated with the trait or an SNP within an interval was associated with the trait.

¹SNP identified by Jiménez-Galindo et al. (2019) as associated with grain yield. The number before the underscores indicates the chromosome number and the number after the underscore indicates the physical position in bp within the chromosome.

²QTL code from the whole MAGIC population (Jiménez-Galindo et al., 2019). The number before the underscores indicates the chromosome and the number after the underscores indicates the QTL within the chromosome.

³p-value of the significant SNP using the whole MAGIC (Jiménez-Galindo et al., 2019) in the GWAS of the MAGIC subset.

⁴Significant SNP at $p < 0.02$ in the GWAS of the MAGIC subset and located within the confidence interval of a significant SNP in the whole MAGIC (Jiménez-Galindo et al., 2019). The number before the underscores indicates the chromosome number and the number after the underscore indicates the physical position in bp within the chromosome.

⁵p-value of the significant SNP at $p < 0.02$ in the GWAS of the MAGIC subset.

⁶Distance in bp from the SNP described in Jiménez-Galindo et al. (2019) and the one found in the current study using the MAGIC subset.

⁷Linkage disequilibrium between the SNP described in Jiménez-Galindo et al. (2019) and the one in the current study using the MAGIC subset.

TABLE 3 Validation of significant QTL found for tunnel length in the whole MAGIC population (Jiménez-Galindo et al. 2019) in a hybrid background.

SNP ¹ (Jiménez-Galindo et al., 2019)	QTL ²	p-value ³	SNP ⁴	p-value ⁵	Distance (bp) ⁶	LD r^{27}
Tunnel length						
S1_19252698	QTL_1_1	0.25	S1_18200092	0.002	1,052,606	0.22
S1_290934634	QTL_1_2	0.60	S1_290306138	0.004	628,496	0.01
S2_14798875	QTL_2_1	0.01	S2_14798875	0.009	0	Same SNP
S2_179803199	QTL_2_2	0.09	S2_180155965	0.015	352,766	0.77
S3_191332395	QTL_3_1	0.94	S3_190325618	0.018	1,006,777	0.45
S3_212770896	QTL_3_2	0.74	S3_212771115	0.004	219	0.15
S3_218807815	QTL_3_3	0.99	S3_218835769	0.018	27,954	0.31
S3_218807820	QTL_3_3	0.99				
S4_127856740	QTL_4_1	0.59	S4_131837902	0.014	3,981,162	0.11
S4_127955231	QTL_4_1	0.69				
S4_155128691	QTL_4_2	0.87	S4_154625109	0.003	503,582	0.21
S4_155830369	QTL_4_3	0.20	S4_154625109	0.003	1,205,260	0.39
S4_155830370	QTL_4_3	0.20				
S4_155830400	QTL_4_3	0.20				
S4_156193095	QTL_4_4	0.32	S4_156023370	0.006	169,725	0.02
S4_181340312	QTL_4_5	0.22	S4_201364747	0.016	20,024,435	0.21
S4_221752511	QTL_4_6	0.10	S4_222702242	0.019	949,731	No
S5_24771445	QTL_5_1	0.18	S5_33610351	0.016	8,838,906	0.38

(Continued)

TABLE 3 Continued

SNP ¹ (Jiménez-Galindo et al., 2019)	QTL ²	p-value ³	SNP ⁴	p-value ⁵	Distance (bp) ⁶	LD r ²⁷
Tunnel length						
S6_147725553	QTL_6_1	0.17	S6_147968131	0.011	242,578	1.00
S6_150800759	QTL_6_2	0.07	S6_150889722	0.011	88,963	0.68
S6_156035854	QTL_6_3	0.47	S6_156282464	0.017	246,610	0.69
S6_164776991	QTL_6_4	0.28	S6_160234735	0.013	4,542,256	0.33
S7_109722251	QTL_7_1	0.15	S7_112215633	0.005	2,493,382	0.42
S8_24527783	QTL_8_1	0.40	S8_26089118	0.016	1,561,335	0.01
S8_28525990	QTL_8_2	0.81	S8_26089118	0.016	2,436,872	0.03

SNPs highlighted in green are validated following the two criteria previously described, i.e., the same SNP was associated with the trait or an SNP within an interval was associated with the trait.

¹SNP identified by Jiménez-Galindo et al. (2019) as associated with tunnel length. The number before the underscores indicates the chromosome number and the number after the underscore indicates the physical position in bp within the chromosome.

²QTL code from the whole MAGIC population (Jiménez-Galindo et al., 2019). The number before the underscores indicates the chromosome and the number after the underscores indicates the QTL within the chromosome.

³p-value of the significant SNP using the whole MAGIC (Jiménez-Galindo et al., 2019) in the GWAS of the MAGIC subset.

⁴Significant SNP at p < 0.02 in the GWAS of the MAGIC subset and located within the confidence interval of a significant SNP in the whole MAGIC (Jiménez-Galindo et al., 2019). The number before the underscores indicates the chromosome number and the number after the underscore indicates the physical position in bp within the chromosome.

⁵p-value of the significant SNP at p < 0.02 in the GWAS of the MAGIC subset.

⁶Distance in bp from the SNP described in Jiménez-Galindo et al. (2019) and the one found in the current study using the MAGIC subset.

Current GWAS was done on hybrids developed by crossing a 52-inbred subset of the MAGIC population (MAGIC subset) with A638.

TABLE 4 Validation of QTL found for grain yield in the whole MAGIC population (Jiménez-Galindo et al. 2019) using a 56-inbred subset of the MAGIC population (MAGIC subset).

SNP ¹ (Jiménez-Galindo et al., 2019)	QTL ²	p-value ³	SNP ⁴	p-value ⁵	Distance (bp) ⁶	LD r ²⁷
S1_3708430	QTL_1_1	0.007	S1_3197323	0.014	511,107	0.39
S1_199075640	QTL_1_2	0.953	S1_200288001	0.014	1,212,361	0.37
S1_199075673	QTL_1_2	0.953				
S1_199075674	QTL_1_2	0.953				
S1_199075675	QTL_1_2	0.953				
S1_199075677	QTL_1_2	0.953				
S1_199075679	QTL_1_2	0.953				
S1_199075681	QTL_1_2	0.953				
S1_199075682	QTL_1_2	0.953				
S1_199075684	QTL_1_2	0.953				
S1_200077059	QTL_1_3	0.353	S1_200288001	0.014	210,942	0.46
S1_200077088	QTL_1_3	0.353				
S1_200408507	QTL_1_3	0.545				
S1_200408528	QTL_1_3	0.471				
S1_200479419	QTL_1_3	0.572				
S1_200801543	QTL_1_3	0.270				
S1_201847366	QTL_1_4	0.319	S1_201872818	0.008	25,452	0.68
S1_201872641	QTL_1_4	0.521				
S1_202160398	QTL_1_4	0.440				
S1_202647745	QTL_1_4	0.490				
S1_279899012	QTL_1_5	0.762	S1_280826390	0.017	927,378	0.07

(Continued)

TABLE 4 Continued

SNP ¹ (Jiménez-Galindo et al., 2019)	QTL ²	p-value ³	SNP ⁴	p-value ⁵	Distance (bp) ⁶	LD r ²⁷
S1_298985014	QTL_1_6	0.628	S1_299470567	0.008	483,885	0.12
S1_298986682	QTL_1_6	0.985				
S3_200876919	QTL_3_1	0.220	S3_199293659	0.010	1,583,260	0.10
S3_200876939	QTL_3_1	0.220				
S3_223537342	QTL_3_2	0.192	S3_225038503	0.004	1,501,161	0.459
S3_229992268	QTL_3_3	0.634	S3_228983201	0.009	1,009,067	0.133
S4_235761612	QTL_4_1	0.466	S4_235381320	0.020	380,292	0.531
S5_128333604	QTL_5_1	0.583	S5_135433904	0.018	7,100,300	0.537
S5_128333610	QTL_5_1	0.583				
S7_33885476	QTL_7_1	0.101	S7_23960799	0.016	9,924,677	0.227
S8_171634738	QTL_8_1	0.323	S8_171625362	0.013	9,376	0.06
S9_5656122	QTL_9_1	0.207	S9_8039883	0.011	2,383,761	No
S9_5656138	QTL_9_1	0.207				
S9_9966270	QTL_9_2	0.082	S9_8039883	0.011	1,926,387	0.1
S9_9966272	QTL_9_2	0.082				
S9_9966291	QTL_9_2	0.082				
S9_11084679	QTL_9_3	0.086	S9_13662469	0.011	2,577,790	0.32
S9_11746822	QTL_9_4	0.525	S9_12599906	0.00696272	853,084	No

Current GWAS was done on hybrids developed by crossing a 52-inbred subset of the MAGIC population (MAGIC subset) with A638.
SNP highlighted in green are validated following the two criteria previously described, i.e. the same SNP was associated with the trait or a SNP within an interval was associated with the trait
¹SNP identified by Jiménez-Galindo et al. (2019) as associated with grain yield. The number before the underscores indicates the chromosome number and the number after the underscore indicates the physical position in bp within the chromosome.
²QTL code from the whole MAGIC population (Jiménez-Galindo et al. 2019). The number before the underscores indicates the chromosome and the number after the underscores indicates the QTL within the chromosome.
³p-value of the significant SNP using the whole MAGIC (Jiménez-Galindo et al. 2019) in the GWAS of the MAGIC subset
⁴Significant SNP at $p < 0.02$ in the GWAS of the MAGIC subset and located within the confidence interval of a significant SNP in the whole MAGIC (Jiménez-Galindo et al. 2019). The number before the underscores indicates the chromosome number and the number after the underscore indicates the physical position in bp within the chromosome.
⁵p-value of the significant SNP at $p < 0.02$ in the GWAS of the MAGIC subset
⁶Distance in bp from the SNP described in Jiménez-Galindo et al. 2019 and the one found in the current study using the MAGIC subset
⁷Linkage disequilibrium between the SNP described in Jiménez-Galindo et al. 2019 and the one in the current study using the MAGIC subset7: Linkage disequilibrium between the SNP described in Jiménez-Galindo et al. 2019 and the one in the current study using the MAGIC subset

Validation of QTL for grain yield

The SNP S1_3708430 that was described as significantly associated with grain yield in the complete set of RILs (Jiménez-Galindo et al., 2019) also showed a significant association ($p < 0.02$) with yield in the current study using the IVS. In addition, three out of the six QTLs for yield found on chromosome 1 using the complete MAGIC population (Jiménez-Galindo et al., 2019) were validated using both validation sets, IVS and HVS (QTL_1_1; QTL_1_3 and QTL_1_4). QTL_1_6 was only validated in the IVS and QTL_1_2 was only validated using the HVS (Tables 4, 5). Notably, QTL_1_2 and QTL_1_3 exhibited a high degree of linkage disequilibrium ($r^2 = 0.80$) and are situated at a distance of 1,001,419 base pairs (Figure 1). Similarly, the linkage between QTL_1_3 and QTL_1_4 is substantial ($r^2 = 0.72$), with a genomic separation of 1,770,307 base pairs. This observation suggests the potential categorization of these adjacent QTLs as a single QTL encompassing the QTL_1_2, QTL_1_3, and QTL_1_4 reported by Jiménez-Galindo et al. (2019).

One out of the three QTLs for yield was found on chromosome 3 using the whole MAGIC, and the QTL on chromosome 7 and the QTL on chromosome 4 were validated using both validation sets. The QTL on chromosome 5 and one out of four QTLs on chromosome 9 were validated in HVS. Finally, one out of four QTLs on chromosome 9 was validated in the IVS. To summarize, out of the 39 SNPs, corresponding to 17 QTLs, associated with grain yield in the whole MAGIC population, 11 were validated. Six were validated using IVS and HVS, two with IVS only, and three with HVS only (Tables 4, 5).

Discussion

The experimental design used in Jiménez-Galindo et al., 2019 was an augmented design, originally conceived to evaluate a large number of genotypes with the objective of discarding those that presented poor performances. In this study, we have selected a reduced set of

TABLE 5 Validation of significant QTL found for grain yield in the whole MAGIC population (MAGIC) and published in Jiménez-Galindo et al. (2019) in a hybrid background.

SNP ¹ (Jiménez-Galindo et al., 2019)	QTL ²	p-value ³	SNP ⁴	p-value ⁴	Distance (bp) ⁶	LD r ²⁷
Tunnel length						
S1_19252698	QTL_1_1	0.12	S1_18978470	0.013	274,228	0.26
S1_290934634	QTL_1_2	0.13	S1_292415110	0.004	1,480,476	0.06
S2_14798875	QTL_2_1	0.15	S2_15140966	0.016	342,091	0.65
S2_179803199	QTL_2_2	0.68	S2_185171168	0.011	5,367,969	0.18
S3_191332395	QTL_3_1	0.16	S3_191368808	0.017	36,413	0.65
S3_212770896	QTL_3_2	0.86	S3_212502290	0.003	268,606	0.08
S3_218807815	QTL_3_3	0.66	S3_216256039	0.008	2,551,776	0.20
S3_218807820	QTL_3_3	0.66				
S4_127856740	QTL_4_1	0.35	S4_111050431	0.018	16,806,309	0.61
S4_127955231	QTL_4_1	0.38				
S4_155128691	QTL_4_2	0.94	S4_158606264	0.007	3,477,573	0.02
S4_155830369	QTL_4_3	0.37	S4_153520875	0.014	2,309,494	0.02
S4_155830370	QTL_4_3	0.37				
S4_155830400	QTL_4_3	0.37				
S4_156193095	QTL_4_4	0.27	S4_156718547	0.018	525,452	0.09
S4_181340312	QTL_4_5	0.86	S4_181696701	0.007	356,389	0.12
S4_221752511	QTL_4_6	0.73	S4_222716155	0.014	963,644	0.04
S5_24771445	QTL_5_1	0.09	S5_23764335	0.011	1,007,110	0.40
S6_147725553	QTL_6_1	0.93	S6_148774898	0.009	1,049,345	0.21
S6_150800759	QTL_6_2	0.15	S6_150697524	0.006	103,235	0.34
S6_156035854	QTL_6_3	0.14	S6_155739471	0.019	296,383	0.23
S6_164776991	QTL_6_4	0.85	S6_166815163	0.011	2,038,172	0.23
S7_109722251	QTL_7_1	0.87	S7_112219931	0.008	2,497,680	0.32
S8_24527783	QTL_8_1	0.96	S8_27642137	0.011	3,114,354	0.13
S8_28525990	QTL_8_2	0.66	S8_27642137	0.018	883,853	0.23

SNPs highlighted in green are validated following the two criteria previously described, i.e., the same SNP was associated with the trait or an SNP within an interval was associated with the trait.

¹SNP identified by Jiménez-Galindo et al. (2019) as associated with tunnel length. The number before the underscores indicates the chromosome number and the number after the underscore indicates the physical position in bp within the chromosome.

²QTL code from the whole MAGIC population (Jiménez-Galindo et al., 2019). The number before the underscores indicates the chromosome and the number after the underscores indicates the QTL within the chromosome.

³p-value of the significant SNP using the whole MAGIC (Jiménez-Galindo et al., 2019) in the GWAS of the MAGIC subset.

⁴Significant SNP at $p < 0.02$ in the GWAS of the MAGIC subset and located within the confidence interval of a significant SNP in the whole MAGIC (Jiménez-Galindo et al., 2019).

⁵p-value of the significant SNP at $p < 0.02$ in the GWAS of the MAGIC subset.

⁶Distance in bp from the SNP described in Jiménez-Galindo et al. (2019) and the one found in the current study using the MAGIC subset.

⁷Linkage disequilibrium between the SNP described in Jiménez-Galindo et al. (2019) and the one in the current study using the MAGIC subset.

inbred lines (IVS) at the tails of distributions for resistance and yield in the whole MAGIC population in order to maintain trait variability but limiting the number of individuals. This allowed us to improve the phenotyping reliability as the new set could be evaluated using an α -lattice design with two replications instead of an augmented design. The α -lattice experimental design provides enhanced control over experimental variability among replications and blocks, improving phenotyping precision and repeatability and increasing the genotypic/phenotypic variation ratio. As a result of the improved experimental design and more accurate phenotyping, we observed a

gain in heritability values in both validations sets, inbred lines and hybrids, compared to heritability estimates in the whole MAGIC population (Jiménez et al., 2019). The increased inheritance estimates for tunnel length and yield in the IVS seemed to be a consequence of higher observed genetic variability; meanwhile, observed genetic variance was not increased in the HVS but the higher number of evaluations reduced the variability of hybrid means. As expected, owing to the reduced importance of additive genetic effects in a heterozygous background, we found that hybrids presented half or less than a half of the genotypic variation of the *per se* inbreds

agreeing with (Michel et al., 2022). The reduction of genetic variance in the HVS compared to IVS was significant only for tunnel length because additive effects are the only significant genetic effects for this trait and, consequently, dominance and/or epistasis effects would not contribute to increase genotypic variability among hybrids as it could happen for yield (Butrón et al., 1999; Cartea et al., 1999).

The QTL validation approach used in the current study greatly differed from approaches used in other works, as those studies usually restringed genetic variation to a particular genomic region (single QTL) using near-isogenic inbred lines (NIL) or heterogeneous inbred families (HIF) (Huo et al., 2016; Jiménez-Galindo et al., 2018; Zhao et al., 2022; Yang et al., 2017). Evaluation of NIL and HIF genotypes is very valuable to advance in the isolation and cloning of the genes involved in the inheritance of a particular trait, but is not useful to validate the genetic weight of a particular QTL in a more real scenario in which variation for the trait is not limited. Conversely, results derived from the current validations could provide information of the usefulness of QTL and genomic predictions, both based on the evaluation of the whole MAGIC population, for implementing marker-assisted or/and genomic selection. In addition, the validation of additive-effect

QTL detected by Jiménez-Galindo et al. (2019) has been done in homozygous and heterozygous backgrounds, which would allow us to assess the value of these QTLs for improved hybrid development. For validation in a heterozygous background, IVS inbreds were crossed to the Reid inbred line A638. It has been previously shown that using testers from complementary heterotic groups to the heterotic group or groups of the evaluated inbreds is superior for detecting/validating additive-effect QTLs than testers more genetically related to the inbreds (Frascaroli et al., 2009).

In the present study, almost three-fourths of QTLs found as associated to tunnel length by Jiménez-Galindo et al. (2019) were validated. However, the *p*-values of current associations were high, excluding the suitability of these QTLs for performing MAS but emphasizing that genomic predictions based on genotype-phenotype associations in the whole MAGIC population could be valuable for genomic selection. QTLs in the region 6.05–6.07 were validated in both sets, and this genomic region has also been associated with resistance to stalk tunneling in different mapping populations and environments. In addition, this region encompasses several QTLs for cell wall digestibility (Ralph et al., 2004) and, consequently, deserves to be deeply studied to identify the genes behind those associations.

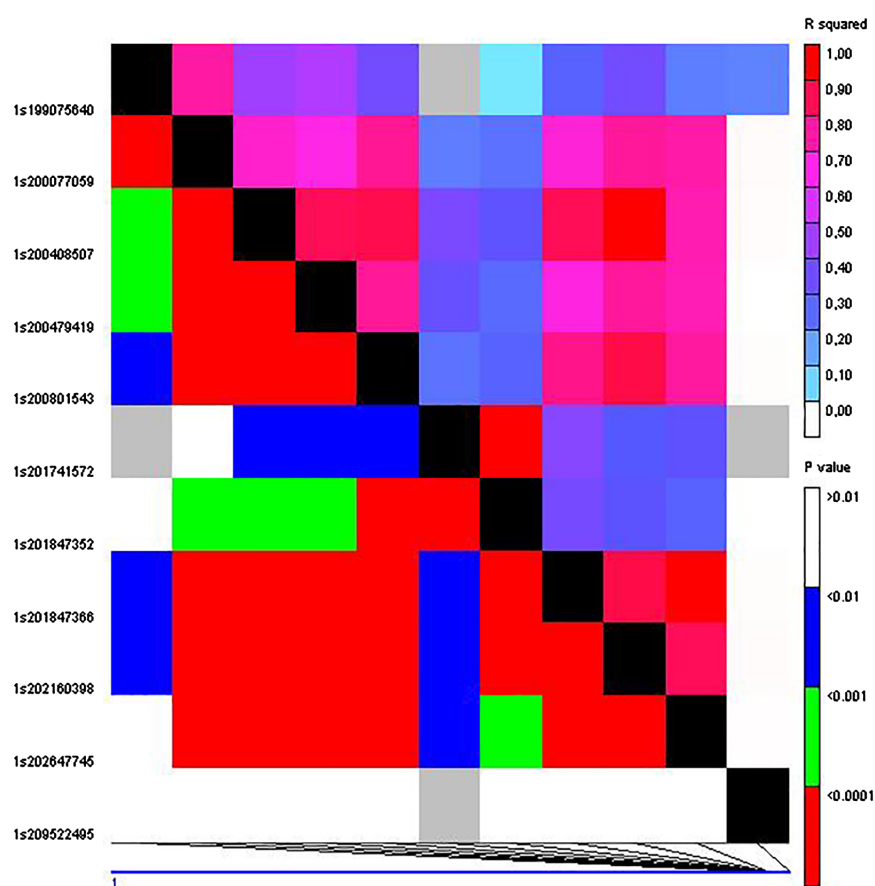


FIGURE 1

Linkage disequilibrium among the 23 SNPs on chromosome 1 significantly associated with grain yield using the whole MAGIC population (Jiménez-Galindo et al., 2019).

Ten out of 16 (approximately ⅔) QTLs for grain yield found in the whole MAGIC population were validated. The QTL validation ratio was inferior for yield than for tunnel length as expected because dominance and/or epistatic effects are equally or more important than additive effects for yield and could mask additive effects (Butrón et al., 2009). Interestingly, the additive-effect QTL on the long arm of chromosome 8 detected by Jiménez-Galindo et al. (2019) could not be validated in any validation set and, in the same chromosome arm, several authors have found significant QTLs for mid-parent heterosis for yield (Schön et al., 2010; Tang et al., 2010; Larièpe et al., 2012; Samayoa et al., 2017). Again, *p*-values of associations found in the current study between markers linked to QTLs detected by Jiménez-Galindo et al. (2019) and grain yield were high, suggesting that genomic prediction based on the evaluation of the whole MAGIC population could be suitable to improve yield. Gesteiro et al. (2023) have already shown that genotypic selection for yield surpassed phenotypic selection, although genotypic and phenotypic selection for reducing tunnel lengths could be preferred to improve yield and resistance simultaneously.

Nine out of 21 and 6 out of 17 QTLs identified for tunnel length and grain yield, respectively, by Jiménez-Galindo et al. (2019) were validated across both validation sets, suggesting a moderate genetic correlation between *per se* and testcross performance of inbred lines. However, Zhang et al. (2011), although having estimated moderate to high genetic correlations between *per se* and testcross evaluations for plant and ear heights, showed that few QTLs were detected in both genetic backgrounds. In any case, the validation of a moderate proportion of QTL for tunnel length in both validation sets suggested that genomic predictions for tunnel length based on inbred line evaluations could be useful to develop improved hybrids (Ma et al., 2022). Michel et al. (2022) already estimated promising genomic value predictive abilities between $r = 0.49$ and $r = 0.55$ for models predicting maize hybrid traits that were trained with *per se* data.

Conclusions

In this study, we have used a novel validation QTL approach together with improved experimental designs that led to higher heritability estimates for both traits compared to the whole MAGIC population. A substantial proportion of QTLs associated with tunnel length and grain yield were validated across both sets. The current validations offer insights for guiding the implementation of marker-assisted or genomic selection strategies. Moreover, the study indicates the potential value of utilizing genomic predictions based on inbred line assessments to enhance the development of superior hybrid varieties.

Phenotyping genetically-wide panels of inbred lines or RILs is challenging due to the difficulty of controlling the high experimental error associated with large trials. Therefore, the high experimental errors associated with these evaluations could greatly interfere with QTL identification making necessary to validate those QTL before implementing any marker-assisted or genomic selection program. In

such scenario, a novel validation approach has been used that allows to ascertain the reliability of QTL as well as its practical value to contribute to hybrid improvement.

Data availability statement

The original contributions presented in the study are included in the article/Supplementary Material. Further inquiries can be directed to the corresponding author.

Ethics statement

The manuscript presents research on animals that do not require ethical approval for their study.

Author contributions

AL-M: Data curation, Formal Analysis, Investigation, Methodology, Writing – original draft, Writing – review & editing. ZR-R: Data curation, Investigation, Methodology, Writing – review & editing. AB: Data curation, Funding acquisition, Investigation, Methodology, Project administration, Resources, Supervision, Writing – review & editing. JJ-G: Data curation, Investigation, Methodology, Writing – review & editing. PR: Investigation, Resources, Supervision, Writing – review & editing. RM: Conceptualization, Data curation, Formal Analysis, Funding acquisition, Investigation, Methodology, Project administration, Resources, Supervision, Validation, Visualization, Writing – review & editing.

Funding

The author(s) declare financial support was received for the research, authorship, and/or publication of this article. This research was funded by subsequent projects financed by MCIU/AEI/FEDER, UE (RTI2018-096776-B-C21 and PID2021-122196OB-C21).

Acknowledgments

We thank the technical staff for their support in the experimental trials. AL-M thanks her postdoctoral contract granted by Xunta de Galicia. JJ-G thanks a PhD scholarship #314685 from the National Council for Science and Technology (CONACYT), Mexico. ZR-R thanks a Scholarship from the National Council of Science and Technology (CONACYT) to carry out Postdoctoral studies.

Conflict of interest

The authors declare that the research was conducted in the absence of any commercial or financial relationships that could be construed as a potential conflict of interest.

The author(s) declared that they were an editorial board member of Frontiers, at the time of submission. This had no impact on the peer review process and the final decision.

Publisher's note

All claims expressed in this article are solely those of the authors and do not necessarily represent those of their affiliated organizations, or those of the publisher, the editors and the

reviewers. Any product that may be evaluated in this article, or claim that may be made by its manufacturer, is not guaranteed or endorsed by the publisher.

Supplementary material

The Supplementary Material for this article can be found online at: <https://www.frontiersin.org/articles/10.3389/fpls.2024.1404881/full#supplementary-material>

References

- Bradbury, P. J., Zhang, Z., Kroon, D. E., Casstevens, T. M., Ramdoss, Y., and Buckler, E. S. (2007). TASSEL: software for association mapping of complex traits in diverse samples. *Bioinformatics* 23, 2633–2635. doi: 10.1093/BIOINFORMATICS/BTM308
- Butrón, A., Malvar, R. A., Velasco, P., Vales, M. I., and Ordás, A. (1999). Combining abilities for maize stem antibiosis, yield loss, and yield under infestation and non infestation with pink stem borer. *Crop Sci.* 39, 691–696. doi: 10.2135/cropsci1999.0011183X003900020015x
- Butrón, A., Romay, M. C., Peña-Asín, J., Alvarez, A., and Malvar, R. A. (2012). Genetic relationship between maize resistance to corn borer attack and yield. *Crop Sci.* 52, 1176–1180. doi: 10.2135/cropsci2011.11.0584
- Butrón, A., Samayoa, L. F., Santiago, R., Ordás, B., and Malvar, R. A. (2018). “Genomics of insect resistance,” in *The Maize Genome*. Eds. J. T. R. Bennetzen, S. Flint-Garcia and C. Hirsch (Springer Nature, Switzerland), 163–183.
- Butrón, A., Sandoya, G., Revilla, P., and Malvar, R. A. (2009). Genetics of resistance to the pink stem borer (*Sesamia nonagrioides*) in maize (*Zea mays*). *Ann. Appl. Biol.* 154, 205–217. doi: 10.1111/j.1744-7348.2008.00284.x
- Butrón, A., Sandoya, G., Santiago, R., Ordás, A., Rial, A., and Malvar, R. A. (2006). Searching for new sources of pink stem borer resistance in maize (*Zea mays* L.). *Genetic Resources Crop Evol.* 53, 1455–1462.
- Cartea, M. E., Malvar, R. A., Butrón, A., Vales, M. I., and Ordás, A. (1999). Inheritance of antibiosis to *Sesamia nonagrioides* (Lepidoptera: Noctuidae) in maize. *J. Economic Entomol.* 92 (4), 994–998.
- Eizaguirre, M., and Albajes, R. (1992). Diapause induction in the stem corn borer, *Sesamia nonagrioides* (Lepidoptera: Noctuidae). *Entomologia Generalis* 17 (4), 277–283. doi: 10.1127/entom.gen/17/1992/277
- Farinós, G. P., de la Poza, M., Hernández-Crespo, P., Ortego, F., and Castañera, P. (2004). Resistance monitoring of field populations of the corn borers *Sesamia nonagrioides* and *Ostrinia nubilalis* after 5 years of Bt maize cultivation in Spain. *Entomologia Experimentalis et Applicata*, 110 (1), 23–30. doi: 10.1111/j.0013-8703.2004.00116.x
- Flint-Garcia, S. A., Jampatong, C., Darrah, L. L., and McMullen, M. D. (2003). Quantitative trait locus analysis of stalk strength in four maize populations. *Crop Sci.* 43, 13–22. doi: 10.2135/cropsci2003.0013
- Frascaroli, E., Canè, M. A., Pè, M. E., Pea, G., Morgante, M., and Landi, P. (2009). QTL detection in maize testcross progenies as affected by related and unrelated testers. *Theor. Appl. Genet.* 118, 993–1004. doi: 10.1007/s00122-008-0956-3
- Gesteiro, N., Ordás, B., Butrón, A., de la Fuente, M., Jiménez-Galindo, J. C., Samayoa, L. F., et al. (2023). Genomic versus phenotypic selection to improve corn borer resistance and grain yield in maize. *Front. Plant Sci.* 14. doi: 10.3389/fpls.2023.1162440
- Holland, J. B., Nyquist, W. E., and Cervantes-Martínez, C. T. (2003). Estimated and interpreting heritability for plant breeding: An update. *Plant Breed Rev.* 22, 9–122. doi: 10.1002/9780470650202
- Huo, D., Ning, Q., Shen, X., Liu, L., and Zhang, Z. (2016). QTL mapping of kernel number-related traits and validation of one major QTL for ear length in maize. *PLoS One* 11 (5), e0155506. doi: 10.1371/journal.pone.0155506
- Jiménez-Galindo, J. C., Malvar, R. A., Butrón, A., Caicedo, M., and Ordás, B. (2018). Fine analysis of a genomic region involved in resistance to Mediterranean corn borer. *BMC Plant Biol.* 18, 1–13. doi: 10.1186/s12870-018-1385-3
- Jiménez-Galindo, J. C., Malvar, R. A., Butrón, A., Santiago, R., Samayoa, L. F., Caicedo, M., et al. (2019). Mapping of resistance to corn borers in a MAGIC population of maize. *BMC Plant Biol.* 19, 1–17. doi: 10.1186/s12870-019-2052-z
- Jiménez-Galindo, J. C., Ordás, B., Butrón, A., Samayoa, L. F., and Malvar, R. A. (2017). QTL mapping for yield and resistance against Mediterranean corn borer in maize. *Front. Plant Sci.* 8, 698.
- Lariépe, A., Mangin, B., Jasson, S., Combes, V., Dumas, F., Jamin, P., et al. (2012). The genetic basis of heterosis: multiparental quantitative trait loci mapping reveals contrasted levels of apparent overdominance among traits of agronomical interest in maize (*Zea mays* L.). *Genetics*. 190 (2), 795–811. doi: 10.1534/genetics.111.133447
- López, C., Sans, A., Asin, L., and EizaGuirre, M. (2001). Phenological model for *Sesamia nonagrioides* (Lepidoptera: noctuidae). *Environ. Entomol.* 30, 23–30. doi: 10.1603/0046-225X-30.1.23
- Ma, Y., Li, D., Xu, Z., Gu, R., Wang, P., Fu, J., et al. (2022). Dissection of the genetic basis of yield traits in line per se and testcross populations and identification of candidate genes for hybrid performance in maize. *Int. J. Mol. Sci.* 23 (9), 5074. doi: 10.3390/ijms23095074
- Meissle, M., Mouron, P., Musa, T., Bigler, F., Pons, X., Vasileiadis, V. P., et al. (2010). Pests, pesticide use and alternative options in European maize production: Current status and future prospects. *J. Appl. Entomology* 134, 357–375. doi: 10.1111/j.1439-0418.2009.01491.x
- Michel, K. J., Lima, D. C., Hundley, H., Singan, V., Yoshinaga, Y., Daum, C., et al. (2022). Genetic mapping and prediction of flowering time and plant height in a maize Stiff Stalk MAGIC population. *Genetics*. 221 (2), iyac063. doi: 10.1093/genetics/iyac063
- Ordas, B., Butron, A., Alvarez, A., Revilla, P., and Malvar, R. A. (2012). Comparison of two methods of reciprocal recurrent selection in maize (*Zea mays* L.). *Theor. Appl. Genet.* 124, 1183–1191. doi: 10.1007/s00122-011-1778-2/TABLES/5
- Ordas, B., Malvar, R. A., Santiago, R., Sandoya, G., Romay, M. C., and Butron, A. (2009). Mapping of QTL for resistance to the Mediterranean corn borer attack using the intermated B73 × Mo17 (IBM) population of maize. *Theor. Appl. Genet.* 119, 1451–1459. doi: 10.1007/s00122-009-1147-6
- Ralph, J., Guillaumie, S., Grabber, J. H., Lapierre, C., and Barrière, Y. (2004). Genetic and molecular basis of grass cell-wall biosynthesis and degradability. III. Towards a forage grass ideotype. *C R Biol.* 327, 467–479. doi: 10.1016/j.crv.2004.03.004
- Salvi, S., and Tuberosa, R. (2015). The crop QTLome comes of age. *Curr. Opin. Biotechnol.* 32, 179–185. doi: 10.1016/j.copbio.2015.01.001
- Samayoa, L. F., Butron, A., and Malvar, R. A. (2014). QTL mapping for maize resistance and yield under infestation with *Sesamia nonagrioides*. *Mol. Breed.* 34, 1331–1344. doi: 10.1007/s11032-014-0119-y
- Samayoa, L. F., Butrón, A., and Malvar, R. A. (2019). Usefulness of marker-assisted selection to improve maize for increased resistance to *Sesamia nonagrioides* attack with no detrimental effect on yield. *Annals Applied Biol.* 174 (2), 219–222. doi: 10.1111/aab.12480
- Samayoa, L. F., Malvar, R. A., and Butrón, A. (2017). QTL for maize midparent heterosis in the heterotic pattern American dent × European flint under corn borer pressure. *Front. Plant Sci.* 8. doi: 10.3389/fpls.2017.00573
- Samayoa, L. F., Malvar, R. A., McMullen, M. D., and Butrón, A. (2015a). Identification of QTL for resistance to Mediterranean corn borer in a maize tropical line to improve temperate germplasm. *BMC Plant Biol.* 15. doi: 10.1186/s12870-015-0652-9
- Samayoa, L. F., Malvar, R. A., Olukolu, B. A., Holland, J. B., and Butrón, A. (2015b). Genome-wide association study reveals a set of genes associated with resistance to the Mediterranean corn borer (*Sesamia nonagrioides* L.) in a maize diversity panel. *BMC Plant Biol.* 15, 1–15. doi: 10.1186/s12870-014-0403-3
- Sandoya, G., Butrón, A., Alvarez, A., Ordás, A., and Malvar, R. A. (2008). Direct response of a maize synthetic to recurrent selection for resistance to stem borers. *Crop Sci.* 48, 113–118. doi: 10.2135/CROPSCI2007.02.0084
- SAS/STAT (2007) (Cary, NC: SAS Institute Inc).
- Schön, C. C., Baldev, D. S., Friedrich Utz, H., and Melchinger, A. E. (2010). High congruency of QTL positions for heterosis of grain yield in three crosses of maize. doi: 10.1007/s00122-009-1209-9
- Tang, J., Yan, J., Ma, X., Teng, W., Wu, W., Dai, J., et al. (2010). Dissection of the genetic basis of heterosis in an elite maize hybrid by QTL mapping in an immortalized F 2 population. doi: 10.1007/s00122-009-1213-0

Yang, Z., Li, X., Zhang, N., Wang, X., Zhang, Y., Ding, Y., et al. (2017). Mapping and validation of the quantitative trait loci for leaf stay-green-associated parameters in maize. *Plant Breed.* 136, 188–196. doi: 10.1111/pbr.12451

Zhang, Y., Li, Y., Wang, Y., Peng, B., Liu, C., Liu, Z., et al. (2011). Correlations and QTL detection in maize family per se and testcross progenies for plant height and ear height. *Plant Breed.* 130, 617–624. doi: 10.1111/J.1439-0523.2011.01878.X

Zhang, Z., Ersoz, E., Lai, C. Q., Todhunter, R. J., Tiwari, H. K., Gore, M. A., et al. (2010). Mixed linear model approach adapted for genome-wide association studies. *Nature Genetics*. 42 (4), 355–360.

Zhao, Y., Ma, X., Zhou, M., Wang, J., Wang, G., and Su, C. (2022). validating a major quantitative trait locus and predicting candidate genes associated with kernel width through qtl mapping and RNA-sequencing technology using near-isogenic lines in maize. *Front. Plant Sci.* 13. doi: 10.3389/fpls.2022.935654



OPEN ACCESS

EDITED BY

Iker Aranjuelo,
Institute of Agrobiotechnology, Spanish
National Research Council (CSIC), Spain

REVIEWED BY

Jordi Voltas,
Universitat de Lleida, Spain
Sumeet Mankar,
Donald Danforth Plant Science Center,
United States

*CORRESPONDENCE

Ana M. Casas
✉ acasas@eead.csic.es

RECEIVED 27 March 2024

ACCEPTED 13 November 2024

PUBLISHED 02 December 2024

CITATION

Cabeza A, Casas AM, Larruy B, Costar MA,
Martínez V, Contreras-Moreira B and
Igartua E (2024) Genetic control of root/
shoot biomass partitioning in barley seedlings.
Front. Plant Sci. 15:1408043.
doi: 10.3389/fpls.2024.1408043

COPYRIGHT

© 2024 Cabeza, Casas, Larruy, Costar,
Martínez, Contreras-Moreira and Igartua. This is
an open-access article distributed under the
terms of the [Creative Commons Attribution
License \(CC BY\)](https://creativecommons.org/licenses/by/4.0/). The use, distribution or
reproduction in other forums is permitted,
provided the original author(s) and the
copyright owner(s) are credited and that the
original publication in this journal is cited, in
accordance with accepted academic
practice. No use, distribution or reproduction
is permitted which does not comply with
these terms.

Genetic control of root/shoot biomass partitioning in barley seedlings

Alejandra Cabeza, Ana M. Casas*, Beatriz Larruy,
María Asunción Costar, Vanesa Martínez,
Bruno Contreras-Moreira and Ernesto Igartua

Aula Dei Experimental Station, EEAD, CSIC, Zaragoza, Spain

The process of allocating resources to different plant organs in the early stage of development can affect their adaptation to drought conditions, by influencing water uptake, transpiration, photosynthesis, and carbon storage. Early barley development can affect the response to drought conditions and mitigate yield losses. A distinct behavior of biomass partitioning between two Spanish barley landraces (SBCC073 and SBCC146) was observed in a previous rhizotron experiment. An RIL population of approximately 200 lines, derived from the cross of those lines, was advanced using speed breeding. We devised an experiment to test if seedling biomass partitioning was under genetic control, growing the seedlings in pots filled with silica sand, in a growth chamber under controlled conditions. After 1 week, the shoot and root were separated, oven dried, and weighted. There were genotypic differences for shoot dry weight, root dry weight, and root-to-shoot ratio. The population was genotyped with a commercial 15k SNP chip, and a genetic map was constructed with 1,353 SNP markers. A QTL analysis revealed no QTL for shoot or root dry weight. However, a clear single QTL for biomass partitioning (RatioRS) was found, in the long arm of chromosome 5H. By exploring the high-confidence genes in the region surrounding the QTL peak, five genes with missense mutations between SBCC146 and SBCC073, and differential expression in roots compared to other organs, were identified. We provide evidence of five promising candidate genes with a role in biomass partitioning that deserve further research.

KEYWORDS

barley, seedling, biomass partitioning, carbon allocation, plant architecture

1 Introduction

Photosynthate allocation and partitioning encompass the regulatory processes governing the distribution of fixed carbon within plants. These regulatory mechanisms dictate the allocation of carbon toward storage, intracellular metabolism, or immediate transport to sink tissues. In sink tissues, sugars are allocated toward growth processes of

different plant organs (Taiz et al., 2015). On the other hand, partitioning refers to the selective distribution of photosynthates throughout the entire plant. Partitioning mechanisms dictate the amounts of fixed carbon directed toward specific sink tissues. Processes, such as phloem loading and unloading, alongside photosynthate allocation and partitioning, are subjects of significant research interest due to their pivotal roles in enhancing crop productivity (Slafer et al., 2023).

Over the life cycle of the plants, the dynamics of photosynthate allocation result in allometric growth of plant tissues, with an effect on the relative size of the organs and, hence, on the ability to capture the resources from the surrounding environment. Plants devoting more growth to roots invest more in foraging for water and nutrients, whereas plants investing more on shoots and leaves maximize radiation and CO₂ capture (Siddiqui et al., 2021). Then, to have reproductive and agronomic success, plants must be able to derive an important part of resources toward the reproductive organs, to produce healthy seeds in the largest number possible.

To identify bottlenecks limiting growth and yield, plant physiologists classically take a source-sink perspective. This is a view of growth at the whole-plant scale incorporating mechanistic interactions between physiology, resource allocation, and plant development (White et al., 2016). Sink strength can be defined as the ability of a sink tissue to mobilize photosynthate by itself. It depends on two components: the sink size (total weight of sink tissue) and the sink activity (rate of uptake photosynthates per unit weight of sink tissue). Tissues can be simultaneously source and sink (roots are a source for nitrogen and a sink for carbon). The pull strength of sinks determines the allometric growth. Biomass partitioning between roots and shoots has been identified as an adaptive factor in tree species (Aranda et al., 2010; Voltas et al., 2024), even at seedling stage (Corcuera et al., 2012), with intraspecific variation. In general, populations coming from arid environments show a larger investment in roots than populations coming from humid environments (Lombardi et al., 2021). This feature confers a higher capacity to scavenge for water, thus becoming advantageous for the plants in water-limited environments. Several studies have already looked into biomass partitioning between root and shoot in barley (Bertholdsson and Kolodinska Brantestam, 2009), in some cases finding phenotypic diversity (Voss-Fels et al., 2018; Wang et al., 2021). Some studies looked for QTL in different populations involving a cross of wild and cultivated barley (Arifuzzaman et al., 2014), a wide panel of wild and cultivated barley (Reinert et al., 2016), spring cultivars (Abdel-Ghani et al., 2019), or spring landraces (Khodaeiaminjan et al., 2023). In all these cases, a few QTL for root-to-shoot ratio (calculated in different manners) were found. There are no studies, however, focusing on winter landraces, which make the most abundant barley landrace groups in Spain (Yahiaoui et al., 2008).

Three lines of the Spanish Barley Core Collection (SBCC042, SBCC073, and SBCC146) and three cultivars (Cierzo, Orria, and Scarlett) were tested previously under control and drought conditions for root and shoot growth (Boudiar et al., 2020). This experiment was carried out for 4 weeks using the rhizotrons of the GrowScreen-Rhizo phenotyping platform (Nagel et al., 2012) from the Plant Sciences, Forschungszentrum Jülich GmbH, Germany. It was found that

SBCC073 devoted relatively more resources to roots, whereas SBCC146 devoted relatively more resources to shoots. These two lines also showed good field performance, particularly SBCC073, which was the best line of a large set of landraces and modern cultivars tested in a field network in Spain (Yahiaoui et al., 2014).

Our research question is to find out whether genetic variation for biomass partitioning between roots and shoots exists in winter barley landraces from Spain, and to discover QTL that may underlie its genetic control. We will use a biparental barley RIL population that, based on earlier evidence, has the potential to show differences in early allometric growth.

2 Materials and methods

2.1 Plant material development

The population was developed from an F1 cross between inbred lines SBCC073 and SBCC146. These lines were developed by single seed descent from two Spanish six-rowed landraces, belonging to the two main germplasm groups detected in the Spanish Barley Core Collection (SBCC), using molecular markers (Yahiaoui et al., 2008). SBCC073 comes from the southern part of the country, with warm temperatures and high evapotranspiration, and SBCC146 from cooler areas in the central plateau region. The original cross was performed in 2016. The F1 was multiplied in the field the following year, and the F2 was sown in a growth chamber in the 2018–2019 season. A total of 232 spikes from individual plants were harvested in the F3 plot, to start producing a recombinant inbred line population by single seed descent (SSD). The seed was advanced from F3 to F5 by two generations of speed breeding in a growth chamber following the protocols of Ghosh et al. (2018). The F5 plants were then multiplied in the field in the season 2019–2020. At the end of this process, 195 families were left, which were field multiplied and/or tested in the ensuing seasons. The remaining F6 lines were sown in the field in the 2020–2021 season, for seed multiplication, in plots of two rows, 1-m long, without replication, at the experimental fields of EEAD-CSIC.

2.2 Phenotyping test

One hundred and ninety-three genotypes derived from the cross of SBCC073 and SBCC146, and the parents, were tested for root dry weight (RDW), shoot dry weight (SDW), total dry weight (TDW), and root/shoot ratio (RatioRS). Five varieties were used as fillers. We devised a bespoke phenotyping test, for which several sand substrates were evaluated in several tests, until an appropriate type was found. The sand chosen produced barley plants of normal aspect and development and allowed easy washing of the roots. The particularity of this phenotyping test lies in the choice of substrate; since one of the main drawbacks of using commercial substrates is the impossibility of eliminating all traces of soil adhered to the root.

Seeds were pre-germinated in Petri dishes. After 72 h, five similar size germinated seeds of each line were transferred to pots (18-cm high, 15-cm outer diameter) filled with 2 L of silica sand

(0.4–0.8 mm) and irrigated with 100 ml of Hoagland nutrient solution 0.2× (Figure 1A). For 1 week, plants developed in a growth chamber under 16-h light/8-h night photoperiod, at 22°C/18°C, 70% humidity, and 250 $\mu\text{mol m}^{-2} \text{s}^{-1}$. Pots were irrigated with 50 ml of Hoagland 0.2× twice during the experiment. After 1 week, plants were extracted from pots, and roots were cleaned using low-pressure tap water, carefully (Figure 1B). Roots and shoots were air dried during a few hours (Figure 1C) and then transferred to paper envelopes. All plants from each pot were kept together in the same envelope (five plants per pot were the experimental unit). Seedlings with abnormal root or shoot development were discarded. Abnormal plants were discarded visually after extracting and cleaning the roots. Extremely short shoot and/or root compared to the other plants of the same genotype were discarded. Roots and shoots were oven dried for 72 h at 70°C (Figure 1D) and weighted in a precision scale (Ohaus PR223/E).

The experiment comprised four replications of 200 genotypes each. Four rounds, being 50 genotypes studied in each round, formed each replication. Each round (50 pots, in five trays) was planted and transferred to the growth chamber in a single day. Two or three sowing dates were performed per week. Each genotype was replicated four times (four pots), so a total of 800 pots were used in the experiment. The experimental unit for each genotype was the aggregated value of five seedlings planted in a single pot. Recombinant inbred lines (RIL), checks, and parents (200 genotypes in total) were randomized in five trays, with 10 pots on each tray. Four rounds of five trays conformed one repetition of the whole experiment. Trays were numbered, and their positions inside the growth chamber were consistent across the experiment. When abnormally developed plants were discarded, the data taken from the remaining four plants were multiplied by the appropriate factor to equalize them to the other observations.

2.3 Statistical analysis

Statistical analyses were performed, considering growth chamber position, round, repetition, and round nested within repetition as random effects. The variance components for the population and parents were obtained using dummy variables for RILs vs. parents, parents, and RILs as in Piepho et al. (2006). Best

linear unbiased estimations (BLUEs) for each RIL were obtained considering genotype as fixed effect. To control for the possible influence of seed size on the traits measured, additional analyses were run with thousand kernel weight (TKW) as covariate. All models were run using ASReml-R (Butler et al., 2017). Means and confidence intervals were obtained using the R package “predictmeans” (Luo et al., 2018).

2.4 QTL analysis

DNA was extracted from 7-day-old individual seedlings using the EchoLUTION Plant DNA kit (BioEcho, GmbH). Genotyping was performed with a proprietary 15k Barley Infinium SNP array by SGS Institute Fresenius GmbH, TraitGenetics Section. A genetic map was then constructed for 193 F5 RIL lines with JoinMap 4, assigning 3,566 SNP markers to seven linkage groups. After filtering co-segregating markers, 1,353 SNPs with unique map position were used for QTL analysis (Supplementary Table S1), with the software Genstat Release 22.1 (VSN International, 2022). For each trait, QTL analysis was carried out using composite interval mapping, calculating genetic predictors every 3 cM, setting the minimum distance for QTL peaks to 20 cM, and the minimum distance between cofactors to 30 cM. The procedure was run iteratively until the number of QTLs detected stabilized. The Li and Ji (2005) method was used to estimate a 5% genome-wide significance threshold for the $-\log_{10}$ p-values. For each marker, physical position in the Morex V3 reference genome (Mascher et al., 2021) was retrieved from Barleymap (Cantalapiedra et al., 2015).

2.5 Searching for candidate genes

Gene models in the reference genome Morex V3 (Mascher et al., 2021), within the QTL confidence interval, were retrieved using Barleymap (Cantalapiedra et al., 2015). Then, genes were classified into high- (HC) or low-confidence classes, and the HC genes with design of exome capture targets were identified in BARLEX (Colmsee et al., 2015). The subset of exome-captured HC genes was further reduced to those genes showing SNP polymorphisms between exome capture data of the parents, which



FIGURE 1

Development of the different experimental phases. (A) Pre-germinated seedlings just transplanted to the pot. (B) Root extraction. (C) Roots and shoot air dried. (D) Shoots and roots oven dried.

was available in-house (Casas et al., 2018). Exome sequencing was performed previously according to the methods described by Mascher et al. (2013). DNA sequencing, made at CNAG (Centro Nacional de Análisis Genómico, Barcelona), and data analysis were performed as described by Cantalapiedra et al. (2016). Expression data from a selected set of genes was retrieved from the Barley Expression Database (Li et al., 2023). The selected genes were clustered according to their expression in informative experiments and tissues from the expression database using R function `heatmap.2` in package `gplots` (Warnes et al., 2016). Presence of the identified polymorphisms was validated by comparison to the SBCC073 transcriptome (Cantalapiedra et al., 2017) and the barley pangenome (Jayakodi et al., 2020). SIFT scores of non-synonymous protein mutations were retrieved from Ensembl Plants using recipe 8 from Contreras-Moreira et al. (2022). Collinear pangene clusters containing gene models of interest from MorexV3 and the other accessions in the pangenome, built with version 11012024 of GET_PANGENES (Contreras-Moreira et al., 2023), were retrieved from https://eead-csic-compbio.github.io/barley_pangenes. Alignment of amino acid sequences of candidate genes were plotted with NCBI MSA Viewer 1.25.0. We used the Frequency-Based Differences method, which assigns scores to bases based on their representation in the column's frequency profile.

3 Results

3.1 Genotypic differences in seedling growth

The two parents showed quite divergent values for all traits, and the distributions of the variables for the population showed a smooth quantitative variation, when lines were ordered from lowest to highest values, for all four traits considered (Figure 2, Supplementary Table S2).

The analyses of variance revealed significant genotypic differences for all four traits considered, for the population lines, and for parents (Table 1). Parent SBCC073 showed higher RDW and SDW than SBCC146, although the difference was not significant. SBCC073 turned out to present the highest RDW mean value of the whole experiment. The parents of the population only showed differences in RatioRS, even when TKW was used as a covariate (Supplementary Figure S1), confirming the results of Boudiar et al. (2020). Considering these traits, SBCC073 exhibits more RDW, SDW, TDW, and RatioRS; therefore, it appears to be a genotype that invests more photosynthetic assimilates in both parts when compared to the other parent of the population, SBCC146.

3.2 QTL analysis

A single QTL was detected for the RatioRS trait, located on the long arm of chromosome 5H at 66.6 cM (400,664,453 bp) (Figure 3), explaining 15.2% of the phenotypic variance. The

allele of SBCC073 led to increasing the ratio by 0.062. This QTL was independent of seed size, as it was also detected when TKW was used as covariate. Interestingly, no other QTL was detected for any other traits, although there were genotypic differences for all of them (Table 1) suggesting that the partitioning QTL detected was instrumental in the phenotypic differences found for seedling architecture.

3.3 Candidate genes

The peak marker for the RatioRS QTL was BOPA2_12_10725 located within gene HORVU.MOREX.r3.5HG0475170. The QTL confidence interval ranged from 62.6 to 66.9 cM, or 350,508,439 to 403,211,990 bp in the reference genome. The region contains 589 gene models, with 270 HC genes, including 189 with exome capture data. For each of those genes, inspection of putative variants between SBCC146 and SBCC073 recognized 102 genes without variants, 43 genes with polymorphisms outside the coding region, 22 genes with synonymous SNPs, and 22 genes with non-synonymous SNPs. We examined the annotated gene descriptions and constructed a heat map, based on expression data, for 24 genes, including those with non-synonymous SNPs (Supplementary Tables S3 and S4; Supplementary Figure S2). SBCC073 displayed missense mutations in four genes that showed higher expression in roots than in other tissues making them good candidate genes (Supplementary Table S5). Alignment of amino acid sequences for the candidate genes in the barley pangenome revealed natural variation for all of them (Supplementary Figure S3). Thus, five polymorphisms were found in gene HORVU.MOREX.r3.5HG0473970, Glycosyltransferase (D344V, R362Q, R413H, K430E, and V469A). The variants identified in SBCC073 were also found in pangenome genotypes, such as HOR13942 or RGT Planet, so they are likely true variants. Also, seven polymorphisms were found in model HORVU.MOREX.r3.5HG0474460, Protein kinase, putative (G14A, W147R, H149S, S159L, V184A, F281L, and G757S). The same variants were identified in the pangenome genotype HOR13942. Nine polymorphisms were identified in gene HORVU.MOREX.r3.5HG0474880, Leguminosin group485 secreted peptide (Y25H, G26C, I46L, V63A, V64M, A68T, V90L, R138P, and E153A), all of them in common with pangenome genotype HOR13942. It is worth mentioning another gene (HORVU.MOREX.r3.5HG0471560, Receptor kinase), in which SBCC073 showed a missense polymorphism (F7L), although in this case, our results do not cover the complete sequence of the gene. The other parent of the population, SBCC146, had missense polymorphisms in another gene, HORVU.MOREX.r3.5HG0474810, Receptor-like protein kinase, which showed lower expression in roots than in other tissues. SBCC146 and SBCC073 differed in three polymorphisms (P204T, P277L, and A422V), and both genotypes carried the alternative allele in two other cases (S324P and N599T). Those five variants, identified in SBCC146, were all present in pangenome genotype Igri. Therefore, this gene is also a good candidate yielding in total five candidates.

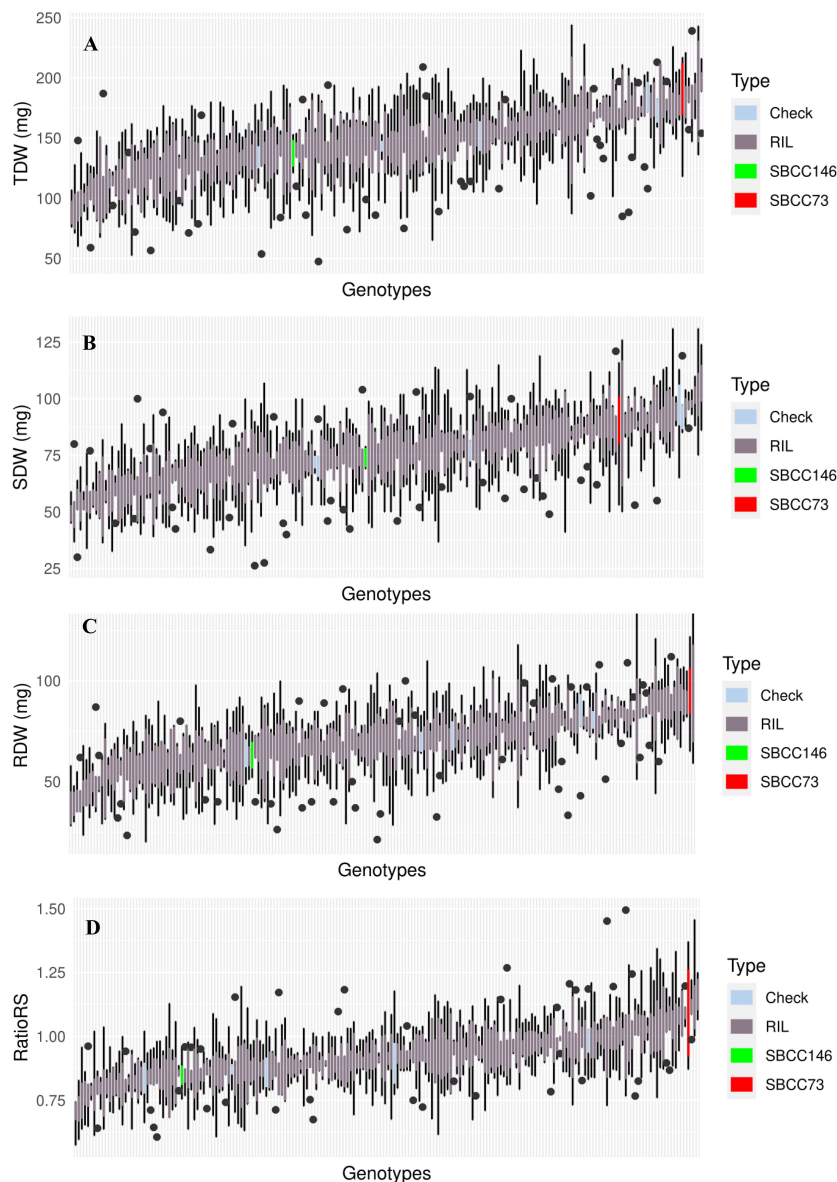


FIGURE 2

Boxplot representing median, minimum, and maximum of (A) TDW, (B) SDW, (C) RDW, and (D) RatioRS of the whole set of genotypes tested in the experiment. In red, parent SBCC073; in green, parent SBCC0146; in dark gray, a set of RIL; and in light blue, five genotypes as checks.

4 Discussion

The results found in this experiment indicate a difference in assimilate partitioning in young seedlings of the RIL population between two Spanish landraces belonging to different genetic groups, which prevailed in areas with contrasting agro-climatic conditions. The parents follow a similar root growth trend as reported by Boudiar et al. (2020), with more vigorous root growth for SBCC073, but not for shoot growth, which was similar for the two genotypes. The differences in experimental set up and

duration of the experiment are likely causing this discrepancy. Both experiments support that SBCC073 allocates more biomass to root tissue.

Is it more beneficial for a plant to invest more carbon resources to root tissue or to an aerial part at the first stage of development? During the first stages of development, crops need to be well established acquiring enough water and nutrients, and the root system is one of the main organs that requires carbon investment. On the other hand, plants need to produce energy through photosynthesis, so increasing shoots will derive into more

TABLE 1 Analyses of variance results.

Wald statistic	Source of variation		
	Parents	RILS vs. parents	RILS
DF	1	1	192
TDW	1.43	1.73	323.82***
SDW	0.26	0.93	318.92***
RDW	3.14	2.42	328.87***
RatioRS	6.21*	1.64	346.13***
TDW_SS	0.30	0.01	267.48***
SDW_SS	0.11	0.037	267.23***
RDW_SS	0.66	0.048	264.33***
RatioRS_SS	4.38*	0.50	336.02***

The genotype source of variation was broken down into the corresponding terms for population RILs, parents, and the contrast between RILs and parents. _SS, analyses taking into account seed size (thousand kernel weight) as covariate. p-value < 0.05 *, 0.01 **, 0.001 ***.

photosynthetic tissue and a more vigorous canopy development. The difference found between these landraces actually bodes well with their geographic origin. SBCC073 is representative of a genetic group coming from dryer and warmer areas than those where the group of SBCC146 was established (Contreras-Moreira et al., 2019). We hypothesize that the presence of an allele favoring biomass allocation to roots in a barley from dry areas can be an adaptive trait. This hypothesis should be tested in more landrace materials of known origins. Studies comparing root system architecture at seedling and adult stages suggested that the root system architecture does not correlate well at both developmental phases (Maccaferri et al., 2016; Williams et al., 2022). This means that the root architecture traits observed at seedling stage are not expected to carry over at adult stage and that it is necessary to confirm the biomass partitioning trait detected in this population at adult stage.

Moreover, it will be interesting to test how this population modulates biomass allocation under drought stress, at seedling and adult stages, since plants are able to modify its phenotype in response to biotic and abiotic environmental signals (Poorter et al., 2012). A previous study (Boudiar et al., 2020) suggested that SBCC073 decreased RDW by 43% and SBCC146 by only 16%, under drought, in a 4-week experiment in rhizotrons.

A QTL for the root/shoot ratio was identified on chromosome 5H, with SBCC073 contributing the favorable allele. The QTL peak marker was at 66.6 cM (400.66 Mb), with a confidence interval ranging from 350.50 to 403.21 Mbp in the reference genome. This region is proximal to the one (between 68.78 and 320.04 Mbp on chromosome 5H) identified by Wonneberger et al. (2023) in modern European spring two-rowed barleys. The authors suggested that this haplotype probably originated from Northern Africa. Indeed, the six-rowed Spanish landrace SBCC073 mostly

shared the RGT Planet haplotype in that region (132 identical SNPs out of 137, from 67.6 to 319.9 Mbp), but was different at the QTL region. Different genome-wide association studies have searched for QTL for root-to-shoot ratio in barley using plastic pots (Reinert et al., 2016), filter rolls (Abdel-Ghani et al., 2019), or germination pouches (Khodaeiaminjan et al., 2023). Those studies looked at biomass partitioning in plants older than ours, and identified QTL for this trait on chromosome 5H but distal to our QTL region (475–495 Mbp), pointing to a different region in the genome.

We searched for putative candidate genes in the region, focusing on those with differential expression between roots and shoots in other transcriptomic studies, and containing SNP polymorphisms in the coding region. Two of them, a UDP-glycosyltransferase (HORVU.MOREX.r3.5HG0473970), and a gene annotated as Leguminosin group485 secreted peptide (HORVU.MOREX.r3.5HG0474880) showed higher expression in root samples, and both of them accumulated several missense variants between the parents of the population. SBCC073 shared those variants with the pangenome genotype “HOR13942,” a landrace originating from Baeza, Southern Spain, close to the collection site of SBCC073. UDP-glycosyltransferases glycosylate small molecules such as phytohormones, secondary metabolites, and xenobiotics (Gharabli et al., 2023). A rice UDP-glycosyltransferase was identified as QTL regulating grain size by modulating cell proliferation and expansion indirectly affecting auxin levels (Dong et al., 2020). Cytokinin glucosyltransferases have also been identified as key regulators of cytokinin homeostasis, with potential value for wheat breeding (Chen et al., 2021). A gene annotated as Leguminosin group458 secreted protein was the most upregulated gene in barley leaves during the recovery phase after a drought treatment (Paul et al., 2023). Nevertheless, that gene is located in a different position on chromosome 5H (539.41 Mbp). We did not identify orthologs in *Arabidopsis* or rice, but a BLASTp of the transcript corresponding to the gene identified in this study had its best match [100% identity, expected value (E-value) of 3e–93] to a protein PELPK1-like from barley (XP_044947259.1). An *Arabidopsis thaliana* PELPK1 is a cell wall protein required for normal germination and growth (Rashid and Deyholos, 2011). Other gene annotated as Protein kinase, putative (HORVU.MOREX.r3.5HG0474460), an LRR receptor-like protein kinase, was highly expressed in root samples of different transcriptomic studies. Li et al. (2020), investigating the dynamics of C/N-nutrient-related phosphorylation signals in *A. thaliana*, identified related proteins. A Brassinosteroid-like receptor kinase (BRL1-like, HORVU.MOREX.r3.5HG0471560) was also included in the confidence interval of the QTL, although we only identified a tolerated missense variant in that gene. Therefore, we have less evidence in this case to be declared as a candidate gene, although it is still worth mentioning due to the relevance of the gene family. It has been shown that

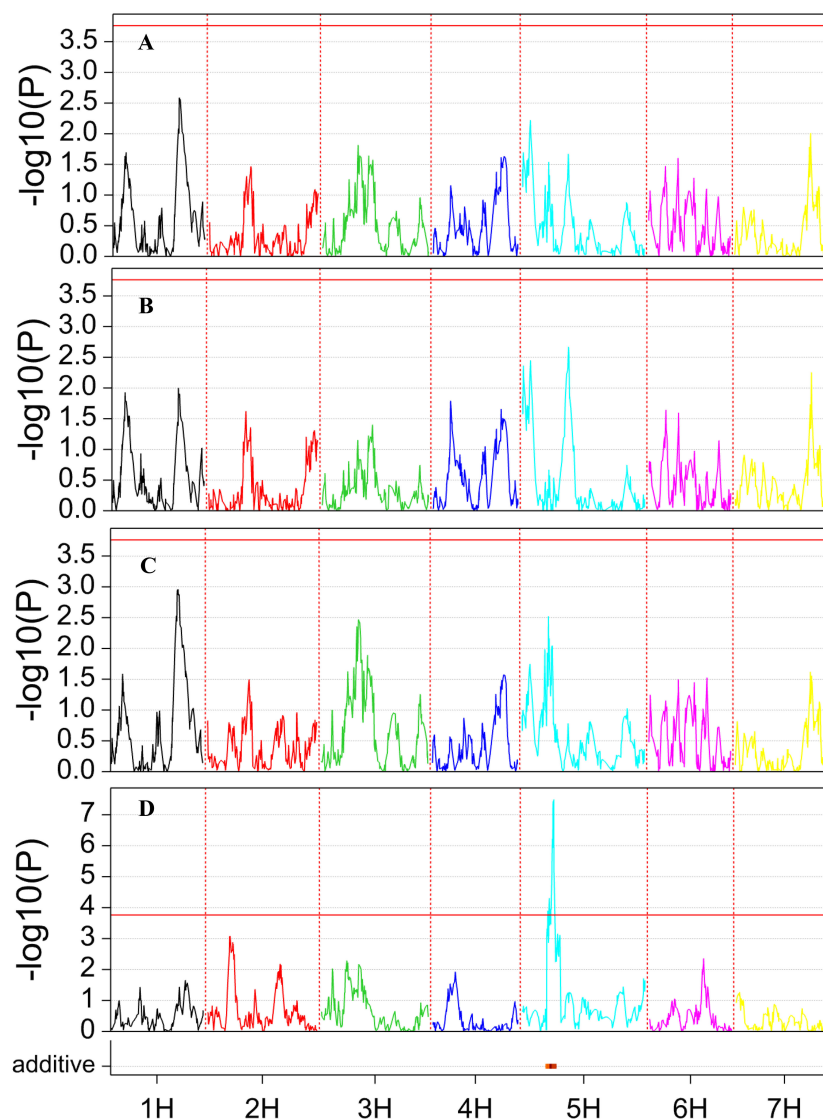


FIGURE 3

QTL scan for the traits recorded in this study. (A) TDW, (B) SDW, (C) RDW, and (D) RatioRS. At the bottom of the graphs, a red dash indicates the presence of a QTL for which SBCC073 contributes the allele with the larger value.

brassinosteroids affect barley root growth (Kartal et al., 2009), and a missense mutation in a BR receptor protein is associated with the semi-dwarf “uzu” mutation in barley (Chono et al., 2003). In rice, Nakamura et al. (2006) observed a high expression of the *OsBRL1* and *OsBRL3* genes in roots and suggested that they may be involved in BR perception in the roots. SBCC146 showed two missense variants in another gene, annotated as Receptor-like protein kinase (HORVU.MOREX.r3.5HG04 74810), highly expressed in shoots. Receptor-like kinases are signaling proteins implicated in the regulation of development and stress responses (Morillo and Tax, 2006; Vij et al., 2008; Gish and Clark, 2011). Nevertheless, we cannot rule out that other

genes in the interval are responsible for the trait. The results should be confirmed performing the experiment for a longer period validating the polymorphisms identified and testing gene expression of the candidate genes in this population.

We have identified genetic diversity for biomass partitioning between shoots and roots at the seedling stage in barley landraces coming from distinct agro-ecological regions, with potential adaptive meaning. The genetic control of partitioning seems to be a single gene, and we provide genomic evidence for five possible candidate genes that deserve further research, evaluating the performance of contrasting genotypes at seedling stage extending to the growth period, and at adult stage in the field.

Data availability statement

The exome capture dataset utilized in this study is available at the European Nucleotide Archive, accession PRJEB73755.

Author contributions

AC: Conceptualization, Data curation, Formal analysis, Investigation, Methodology, Visualization, Writing – original draft, Writing – review & editing. AMC: Conceptualization, Formal analysis, Funding acquisition, Supervision, Writing – original draft, Writing – review & editing. BL: Investigation, Methodology, Writing – review & editing, Writing – original draft. MC: Investigation, Methodology, Writing – review & editing, Writing – original draft. VM: Investigation, Methodology, Writing – review & editing, Writing – original draft. BC-M: Formal analysis, Visualization, Writing – review & editing, Writing – original draft. EI: Conceptualization, Formal analysis, Funding acquisition, Supervision, Writing – original draft, Writing – review & editing.

Funding

The author(s) declare financial support was received for the research, authorship, and/or publication of this article. Funding of this research was provided by project AGL2016-80967-R (MINECO/AEI) 10.13039/501100011033 and by “ERDF A way of making Europe,” project PID2019-111621RB-I00 (MCIN/AEI) 10.13039/501100011033, project PID2022-142116OB-I00 (MCIN/AEI) 10.13039/501100011033, and by “ERDF A way of making Europe,” grant A08_23R (Government of Aragón).

References

- Abdel-Ghani, A. H., Sharma, R., Wabila, C., Dhanagond, S., Owais, S. J., Duwayri, M. A., et al. (2019). Genome-wide association mapping in a diverse spring barley collection reveals the presence of QTL hotspots and candidate genes for root and shoot architecture traits at seedling stage. *BMC Plant Biol.* 19, 216. doi: 10.1186/s12870-019-1828-5
- Aranda, I., Alía, R., Ortega, U., Dantas, ÂK., and Majada, J. (2010). Intra-specific variability in biomass partitioning and carbon isotopic discrimination under moderate drought stress in seedlings from four *Pinus pinaster* populations. *Tree Genet. Genomes.* 6, 169–178. doi: 10.1007/s11295-009-0238-5
- Arifuzzaman, M., Sayed, M. A., Muzammil, S., Pillen, K., Schumann, H., Naz, A. A., et al. (2014). Detection and validation of novel QTL for shoot and root traits in barley (*Hordeum vulgare* L.). *Mol. Breed.* 34, 1373–1387. doi: 10.1007/s11032-014-0122-3
- Bertholdsson, N., and Kolodinska Brantestam, A. (2009). A century of Nordic barley breeding—Effects on early vigour root and shoot growth, straw length, harvest index and grain weight. *Eur. J. Agron.* 30, 266–274. doi: 10.1016/j.eja.2008.12.003
- Boudiar, R., Casas, A. M., Gioia, T., Fiorani, F., Nagel, K. A., and Igartua, E. (2020). Effects of low water availability on root placement and shoot development in landraces and modern barley cultivars. *Agronomy-Basel.* 10, 134. doi: 10.3390/agronomy10010134
- Butler, D. G., Cullis, B. R., Gilmour, A. R., Gogel, B. J., and Thompson, R. (2017). *ASReml-R reference manual version 4* (Hemel Hempstead, HP1 1ES, UK: VSN International Ltd).
- Cantalapiedra, C. P., Boudiar, R., Casas, A. M., Igartua, E., and Contreras-Moreira, B. (2015). BARLEYMAP: physical and genetic mapping of nucleotide sequences and annotation of surrounding loci in barley. *Mol. Breed.* 35, 13. doi: 10.1007/s11032-015-0253-1
- Cantalapiedra, C. P., Contreras-Moreira, B., Silvar, C., Perovic, D., Ordon, F., Gracia, M. P., et al. (2016). A cluster of nucleotide-binding site-leucine-rich repeat genes resides in a barley powdery mildew resistance quantitative trait loci on 7HL. *Plant Genome.* 9, 1–14. doi: 10.3835/plantgenome2015.10.0101
- Cantalapiedra, C. P., Garcia-Pereira, M. J., Gracia, M. P., Igartua, E., Casas, A. M., and Contreras-Moreira, B. (2017). Large differences in gene expression responses to drought and heat stress between elite barley cultivar scarlett and a spanish landrace. *Front. Plant Sci.* 8. doi: 10.3389/fpls.2017.00647
- Casas, A. M., Contreras-Moreira, B., Cantalapiedra, C. P., Sakuma, S., Gracia, M. P., Moralejo, M., et al. (2018). Resequencing the Vrs1 gene in Spanish barley landraces revealed reversion of six-rowed to two-rowed spike. *Mol. Breed.* 38, 51. doi: 10.1007/s11032-018-0816-z
- Chen, L., Zhao, J., Song, J., and Jameson, P. E. (2021). Cytokinin glucosyl transferases, key regulators of cytokinin homeostasis, have potential value for wheat improvement. *Plant Biotechnol. J.* 19, 878–896. doi: 10.1111/pbi.13595
- Chono, M., Honda, I., Zeniya, H., Yoneyama, K., Saisho, D., Takeda, K., et al. (2003). A semidwarf phenotype of barley uzu results from a nucleotide substitution in the gene encoding a putative brassinosteroid receptor. *Plant Physiol.* 133, 1209–1219. doi: 10.1104/103.026195
- Colmsee, C., Beier, S., Himmelsbach, A., Schmutzer, T., Stein, N., Scholz, U., et al. (2015). BARLEX- the barley draft genome explorer. *Mol. Plant* 8, 964–966. doi: 10.1016/j.molp.2015.03.009

Computing hardware was funded by grant FAS2022_052 from CSIC. AC was supported by the FPI grant BES-2017-082746 (MCIN/AEI) 10.13039/501100011033, and by “ESF investing in your future.”

Acknowledgments

The authors acknowledge the support of Francesc Montardit for bioinformatics analysis and of Antonio Pérez-Torres for support in the experimental set-up.

Conflict of interest

The authors declare that the research was conducted in the absence of any commercial or financial relationships that could be construed as a potential conflict of interest.

Publisher's note

All claims expressed in this article are solely those of the authors and do not necessarily represent those of their affiliated organizations, or those of the publisher, the editors and the reviewers. Any product that may be evaluated in this article, or claim that may be made by its manufacturer, is not guaranteed or endorsed by the publisher.

Supplementary material

The Supplementary Material for this article can be found online at: <https://www.frontiersin.org/articles/10.3389/fpls.2024.1408043/full#supplementary-material>

- Contreras-Moreira, B., Naamati, G., Rosello, M., Allen, J. E., Hunt, S. E., Muffato, M., et al. (2022). Scripting analyses of genomes in ensembl plants. *Methods Mol. Biol.*, 2443, 27–55. doi: 10.1007/978-1-0716-2067-0_2
- Contreras-Moreira, B., Saraf, S., Naamati, G., Casas, A. M., Amberkar, S. S., Flicek, P., et al. (2023). GET_PANGENES: calling pangenes from plant genome alignments confirms presence-absence variation. *Genome Biol.* 24, 223. doi: 10.1186/s13059-023-03071-z
- Contreras-Moreira, B., Serrano-Notivol, R., Mohammed, N. E., Cantalapiedra, C. P., Begueria, S., Casas, A. M., et al. (2019). Genetic association with high-resolution climate data reveals selection footprints in the genomes of barley landraces across the Iberian Peninsula. *Mol. Ecol.* 28, 1994–2012. doi: 10.1111/mec.15009
- Corcuera, L., Gil-Pelegrin, E., and Notivol, E. (2012). Differences in hydraulic architecture between mesic and xeric *Pinus pinaster* populations at the seedling stage. *Tree Physiol.* 32, 1442–1457. doi: 10.1093/treephys/tps103
- Dong, N., Sun, Y., Guo, T., Shi, C., Zhang, Y., Kan, Y., et al. (2020). UDP-glucosyltransferase regulates grain size and abiotic stress tolerance associated with metabolic flux redirection in rice. *Nat. Commun.* 11, 2629. doi: 10.1038/s41467-020-16403-5
- Gharabli, H., Della Gala, V., and Welner, D. H. (2023). The function of UDP-glucosyltransferases in plants and their possible use in crop protection. *Biotechnol. Adv.* 67, 108182. doi: 10.1016/j.biotechadv.2023.108182
- Ghosh, S., Watson, A., Gonzalez-Navarro, O. E., Ramirez-Gonzalez, R. H., Yanes, L., Mendoza-Suarez, M., et al. (2018). Speed breeding in growth chambers and glasshouses for crop breeding and model plant research. *Nat. Protoc.* 13, 2944–2963. doi: 10.1038/s41596-018-0072-z
- Gish, L. A., and Clark, S. E. (2011). The RLK/Pelle family of kinases. *Plant J.* 66, 117–127. doi: 10.1111/j.1365-313X.2011.04518.x
- Jayakodi, M., Padmarasu, S., Haber, G., Bonthala, V. S., Gundlach, H., Monat, C., et al. (2020). The barley pan-genome reveals the hidden legacy of mutation breeding. *Nature*. 588, 284–289. doi: 10.1038/S41586-020-2947-8
- Kartal, G., Temel, A., Arican, E., and Gozukirmizi, N. (2009). Effects of brassinosteroids on barley root growth, antioxidant system and cell division. *Plant Growth Regul.* 58, 261–267. doi: 10.1007/s10725-009-9374-z
- Khodaeiamanjan, M., Knoch, D., Ndella Thiaw, M. R., Marchetti, C. F., Kořínková, N., Techer, A., et al. (2023). Genome-wide association study in two-row spring barley landraces identifies QTL associated with plantlets root system architecture traits in well-watered and osmotic stress conditions. *Front. Plant Sci.* 4. doi: 10.3389/fpls.2023.1125672
- Li, J., and Ji, L. (2005). Adjusting multiple testing in multilocus analyses using the eigenvalues of a correlation matrix. *Heredity* 95, 221–227. doi: 10.1038/sj.hdy.6800717
- Li, T., Li, Y., Shanguan, H., Bian, J., Luo, R., Tian, Y., et al. (2023). BarleyExpDB: an integrative gene expression database for barley. *BMC Plant Biol.* 23, 170. doi: 10.1186/s12870-023-04193-z
- Li, X., Sanagi, M., Lu, Y., Nomura, Y., Stolze, S. C., Yasuda, S., et al. (2020). Protein phosphorylation dynamics under carbon/nitrogen-nutrient stress and identification of a cell death-related receptor-like kinase in arabidopsis. *Front. Plant Sci.* 11. doi: 10.3389/fpls.2020.00377
- Lombardi, E., Ferrio, J. P., Rodríguez-Robles, U., Resco de Dios, V., and Voltas, J. (2021). Ground-Penetrating Radar as phenotyping tool for characterizing intraspecific variability in root traits of a widespread conifer. *Plant Soil* 468, 319–336. doi: 10.1007/s11104-021-05135-0
- Luo, D., Ganesh, S., Koolaard, J., and Luo, M. D. (2018). *Package predictmeans* (Comprehensive R Archive Network). Available online at: <https://CRAN.R-project.org/package=predictmeans>.
- Maccaferri, M., El-Feki, W., Nazemi, G., Salvi, S., Cane, M. A., Colalongo, M. C., et al. (2016). Prioritizing quantitative trait loci for root system architecture in tetraploid wheat. *J. Exp. Bot.* 67, 1161–1178. doi: 10.1093/jxb/erw039
- Mascher, M., Richmond, T. A., Gerhardt, D. J., Himmelbach, A., Clissold, L., Sampath, D., et al. (2013). Barley whole exome capture: a tool for genomic research in the genus *Hordeum* and beyond. *Plant J.* 76, 494–505. doi: 10.1111/tpj.12294
- Mascher, M., Wicker, T., Jenkins, J., Plott, C., Lux, T., Koh, C. S., et al. (2021). Long-read sequence assembly: a technical evaluation in barley. *Plant Cell*. 33, 1888–1906. doi: 10.1093/plcell/koab077
- Morillo, S. A., and Tax, F. E. (2006). Functional analysis of receptor-like kinases in monocots and dicots. *Curr. Opin. Plant Biol.* 9, 460–469. doi: 10.1016/j.pbi.2006.07.009
- Nagel, K. A., Putz, A., Gilmer, F., Heinz, K., Fischbach, A., Pfeifer, J., et al. (2012). GROWSCREEN-Rhizo is a novel phenotyping robot enabling simultaneous measurements of root and shoot growth for plants grown in soil-filled rhizotrons. *Funct. Plant Biol.* 39, 891–904. doi: 10.1071/FP12023
- Nakamura, A., Fujioka, S., Sunohara, H., Kamiya, N., Hong, Z., Inukai, Y., et al. (2006). The role of osBRL1 and its homologous genes, osBRL1 and osBRL3, in rice. *Plant Physiol.* 140, 580–590. doi: 10.1104/105.072330
- Paul, M., Tanskanen, J., Jääskeläinen, M., Chang, W., Dalal, A., Moshelion, M., et al. (2023). Drought and recovery in barley: key gene networks and retrotransposon response. *Front. Plant Sci.* 14. doi: 10.3389/fpls.2023.1193284
- Piepho, H. P., Williams, E. R., and Fleck, M. (2006). A note on the analysis of designed experiments with complex treatment structure. *Hortscience*. 41, 446–452. doi: 10.21273/HORTSCI.41.2.446
- Poorter, H., Niklas, K. J., Reich, P. B., Oleksyn, J., Poot, P., and Mommer, L. (2012). Biomass allocation to leaves, stems and roots: meta-analyses of interspecific variation and environmental control. *New Phytol.* 193, 30–50. doi: 10.1111/j.1469-8137.2011.03952.x
- Rashid, A., and Deyholos, M. K. (2011). PELPK1 (At5g09530) contains a unique pentapeptide repeat and is a positive regulator of germination in *Arabidopsis thaliana*. *Plant Cell Rep.* 30, 1735–1745. doi: 10.1007/s00299-011-1081-3
- Reinert, S., Kortz, A., Léon, J., and Naz, A. A. (2016). Genome-wide association mapping in the global diversity set reveals new QTL controlling root system and related shoot variation in barley. *Front. Plant Sci.* 7. doi: 10.3389/fpls.2016.01061
- Siddiqui, M. N., Léon, J., Naz, A. A., and Ballvora, A. (2021). Genetics and genomics of root system variation in adaptation to drought stress in cereal crops. *J. Exp. Bot.* 72, 1007–1019. doi: 10.1093/jxb/eraa487
- Slafer, G. A., Foulkes, M. J., Reynolds, M. P., Murchie, E. H., Carmo-Silva, E., Flavell, R., et al. (2023). A ‘wiring diagram’ for sink strength traits impacting wheat yield potential. *J. Exp. Bot.* 74, 40–71. doi: 10.1093/jxb/erac410
- Taiz, L., Zeiger, E., Møller, I. M., and Murphy, A. (2015). *Plant physiology and development* Vol. 6 (Sunderland (USA: Sinauer Associates Incorporated), 761.
- Vij, S., Giri, J., Dansana, P. K., Kapoor, S., and Tyagi, A. K. (2008). The receptor-like cytoplasmic kinase (OsRLCK) gene family in rice: organization, phylogenetic relationship, and expression during development and stress. *Mol. Plant* 1, 732–750. doi: 10.1093/mp/ssn047
- Voltas, J., Amigó, R., Shestakova, T. A., Matteo, G., Diaz, R., and Zas, R. (2024). Phylogeography and climate shape the quantitative genetic landscape and range-wide plasticity of a prevalent conifer. *Ecol. Monogr.* 94, e1596. doi: 10.1002/ecm.1596
- Voss-Fels, K. P., Robinson, H., Mudge, S. R., Richard, C., Newman, S., Wittkop, B., et al. (2018). VERNALIZATION1 modulates root system architecture in wheat and barley. *Mol. Plant* 11, 226–229. doi: 10.1016/j.molp.2017.10.005
- VSN International (2022). *Genstat for windows, 22nd Edition*. Hemel Hempstead, UK
- Wang, J., Chen, Y., Zhang, Y., Zhang, Y., Ai, Y., Feng, Y., et al. (2021). Phenotyping and validation of root morphological traits in barley (*Hordeum vulgare* L.). *Agronomy-Basel*. 11, 1583. doi: 10.3390/agronomy11081583
- Warnes, M. G. R., Bolker, B., Bonebakker, L., Gentleman, R., Huber, W., and Liaw, A. (2016). *Package gplots*. Available online at: <https://CRAN.R-project.org/package=gplots>.
- White, A. C., Rogers, A., Rees, M., and Osborne, C. P. (2016). How can we make plants grow faster? A source-sink perspective on growth rate. *J. Exp. Bot.* 67, 31–45. doi: 10.1093/jxb/erv447
- Williams, J. L., Sherman, J. D., Lamb, P., Cook, J., Lachowicz, J. A., and Bourgault, M. (2022). Relationships between roots, the stay-green phenotype, and agronomic performance in barley and wheat grown in semi-arid conditions. *Plant Phenome J.* 5, e220050. doi: 10.1002/ppj2.20050
- Wonneberger, R., Schreiber, M., Haaning, A., Muehlbauer, G. J., Waugh, R., and Stein, N. (2023). Major chromosome 5H haplotype switch structures the European two-rowed spring barley germplasm of the past 190 years. *Theor. Appl. Genet.* 136, 174. doi: 10.1007/s00122-023-04418-7
- Yahiaoui, S., Cuesta-Marcos, A., Gracia, M. P., Medina, B., Lasa, J. M., Casas, A. M., et al. (2014). Spanish barley landraces outperform modern cultivars at low-productivity sites. *Plant Breed.* 133, 218–226. doi: 10.1111/pbr.12148
- Yahiaoui, S., Igartua, E., Moralejo, M., Ramsay, L., Molina-Cano, J. L., Ciudad, F. J., et al. (2008). Patterns of genetic and eco-geographical diversity in Spanish barleys. *Theor. Appl. Genet.* 116, 271–282. doi: 10.1007/s00122-007-0665-3

Frontiers in Plant Science

Cultivates the science of plant biology and its applications

The most cited plant science journal, which advances our understanding of plant biology for sustainable food security, functional ecosystems and human health.

Discover the latest Research Topics

[See more →](#)

Frontiers

Avenue du Tribunal-Fédéral 34
1005 Lausanne, Switzerland
frontiersin.org

Contact us

+41 (0)21 510 17 00
frontiersin.org/about/contact

